Performance Evaluation of Inverted Tee (IT) Bridge System

Garret Martindale
Graduate Research Assistant
Department of Civil Engineering
University of Nebraska-Lincoln

Daniel Watson
Graduate Research Assistant
Department of Civil Engineering
University of Nebraska-Lincoln

Antony Mohsen Kamal Masoud Kodsy
Graduate Research Assistant
Department of Construction Engineering
University of Nebraska-Lincoln

Mostafa Abo El-Khier
Graduate Research Assistant
Department of Construction Engineering
University of Nebraska-Lincoln

Richard L. Wood, Ph. D.
Assistant Professor
Department of Civil Engineering
University of Nebraska-Lincoln

George Morcous, Ph.D., P.E.
Professor
Department of Construction Engineering
University of Nebraska-Lincoln

A Report on Research Sponsored by

Nebraska Department of Transportation

University of Nebraska-Lincoln

August 2019

Technical Report Documentation Page

1. Report No	2. Government Accession No.	3. Recipient's Catalog No.	
4. Title and Subtitle Performance Evaluation of Inverted Tee (IT) Bridge System		5. Report Date August 2019	
		6. Performing Organization Code	
7. Author(s) Garret Martindale, Daniel Watson, Antony Mohsen Kamal Masoud Kodsy, Mostafa Abo El-Khier, Richard L. Wood, and George Morcous		8. Performing Organization Report No. 2611214037-001	
9. Performing Organization Name and Address University of Nebraska – Lincoln 1400 R Street Lincoln, NE 68588		10. Work Unit No. (TRAIS)	
		11. Contract or Grant No.	
12. Sponsoring Organization Name and Address Nebraska Department of Transportation 1500 Highway 2 Lincoln, NE 68502		13. Type of Report and Period Covered July 2016 – May 2019	
		14. Sponsoring Agency Code	
15. Supplementary Notes			
16. Abstract The Inverted Tee (IT) girder bridge system was originally developed in 1996 by the University of Nebraska–Lincoln (UNL) researchers and Nebraska Department of Transportation (NDOT) engineers. This bridge system currently accounts for over 110 bridges in Nebraska used for both state highways and local county roads. Extensive longitudinal and transverse deck cracking have been observed and noted in numerous bridge inspection reports. Since the IT girder bridge system is relatively new, limited data and knowledge exist on its structural performance and behavior. This study evaluates the IT girder bridge system by conducting twenty field observations as well as recording accelerometer, strain gauge, and LVDT time histories and lidar scans for a selected subset of these bridges and then a three-dimensional finite element analysis (FEA) was conducted. The field observations included visual inspection for damage and developing deck crack maps to identify a trend for the damage. System identification of the bridge deck and girders helped investigate the global and local structural responses, respectively. Operational modal analysis quantified the natural frequencies, damping ratios, and operational deflected shapes for the instrumented IT girder bridges. These results helped diagnose the reason for the longitudinal deck cracking. The IT girders respond non-uniformly for the first operational deflected shape and independently for higher modes. Two comparable bridges, namely one slab and one NU girder bridge, were instrumented to verify and demonstrate that the IT girder behavior is unique. An advanced geospatial analysis was conducted for the IT girder bridges to develop lidar depth maps of the deck and girders elevations. These depth maps help identify locations of potential water/chloride penetration and girders set at various elevations and/or where the deck thickness is non-uniform. Live load tests helped quantify the transverse dynamic behavior of the bridge girders. Quantifying the transverse dynamic behavior helped validate the source of longitudinal deck cracking in IT girder bridges, which was determined to be the differential deflection between adjacent IT girders. The FEA analysis was conducted to evaluate the live load moment and shear distribution factors and compare that to the predicted values calculated from the AASHTO Standard and LRFD bridge design specifications. The comparison indicated that the predicted distribution factors were conservative. Also, interviews with IT bridge producers and contractors were conducted to determine production and construction advantages and challenges of this bridge system.			
17. Key Words Inverted tee girder, bridge assessment, differential deflection, system identification, finite element analysis, distribution factor	18. Distribution Statement		
19. Security Classification (of this report) Unclassified	20. Security Classification (of this page) Unclassified	21. No. Of Pages 416	22. Price

TABLE OF CONTENTS

LIST OF FIGURES

LIST OF TABLES

ACKNOWLEDGEMENTS

Funding for this project was provided by the Nebraska Department of Transportation (NDOT) under project number SG-04 – Performance Evaluation of Inverted Tee (IT) Bridge System. The authors would like to express their gratitude for the support and guidance provided by the NDOT Technical Advisory Committee as well as graduate research assistants Dr. Mohammad Ebrahim Mohammadi and Ms. Yijun Liao for assisting in the field lidar scanning and instrumentation and removal of bridge accelerometers, graduate research assistant Mr. Kanchan Devkota for leading the lidar scan processing used with the advanced geospatial analysis techniques, and Mr. Peter Hilsabeck of the UNL Structural Laboratory. Findings and conclusions of this project are of the authors and do not reflect the sponsor agencies and collaborators.

DISCLAIMER

The contents of this report reflect the views of the authors, who are responsible for the facts and the accuracy of the information presented herein. The opinions, findings, and conclusions expressed in this publication are those of the authors and not necessarily those of the sponsors. This report does not constitute a standard, specification, or regulation.

ABSTRACT

The Inverted Tee (IT) girder bridge system was originally developed in 1996 by the University of Nebraska–Lincoln (UNL) researchers and Nebraska Department of Transportation (NDOT) engineers. This bridge system currently accounts for over 110 bridges in Nebraska used for both state highways and local county roads. Extensive longitudinal and transverse deck cracking have been observed and noted in numerous bridge inspection reports. Since the IT girder bridge system is relatively new, limited data and knowledge exist on its structural performance and behavior. This study evaluates the IT girder bridge system by conducting twenty field observations as well as recording accelerometer, strain gauge, and LVDT time histories and lidar scans for a selected subset of these bridges and then a three-dimensional finite element analysis (FEA) was conducted. The field observations included visual inspection for damage and developing deck crack maps to identify a trend for the damage. System identification of the bridge deck and girders helped investigate the global and local structural responses, respectively. Operational modal analysis quantified the natural frequencies, damping ratios, and operational deflected shapes for the instrumented IT girder bridges. These results helped diagnose the reason for the longitudinal deck cracking. The IT girders respond non-uniformly for the first operational deflected shape and independently for higher modes. Two comparable bridges, namely one slab and one NU girder bridge, were instrumented to verify and demonstrate that the IT girder behavior is unique. An advanced geospatial analysis was conducted for the IT girder bridges to develop lidar depth maps of the deck and girders elevations. These depth maps help identify locations of potential water/chloride

penetration and girders set at various elevations and/or where the deck thickness is non-uniform. Live load tests helped quantify the transverse dynamic behavior of the bridge girders. Quantifying the transverse dynamic behavior helped validate the source of longitudinal deck cracking in IT girder bridges, which was determined to be the differential deflection between adjacent IT girders. The FEA analysis was conducted to evaluate the live load moment and shear distribution factors and compare that to the predicted values calculated from the AASHTO Standard and LRFD bridge design specifications. The comparison indicated that the predicted distribution factors were conservative. Also, interviews with IT bridge producers and contractors were conducted to determine production and construction advantages and challenges of this bridge system.

CHAPTER 1 – INTRODUCTION

1.1 PROJECT OVERVIEW

The purpose of this research project is to evaluate the structural serviceability, durability, and performance of the Inverted Tee (IT) girder bridge system. To accomplish this task, the bridge property information and current inspection reports were collected for all state and local county IT girder bridges. A well-diversified group of 20 IT girder bridges across the state of Nebraska were selected for visual inspection. Ten IT girder bridges, one slab bridge, and one NU girder bridge were instrumented with accelerometers to quantify the vibrational properties. These vibrational properties, namely the natural frequencies and operational deflected shapes, were used to investigate the likelihood for cracking in the IT girder bridge deck. The local dynamic behavior of the IT girder bridge system was compared to one bridge for each alternative system. An advanced geospatial analysis was performed using lidar scans of 11 IT girder bridges to develop depth maps of the deck and girder elevations. Live load tests were conducted by instrumenting 4 IT girder bridges with LVDT's, 3 bridges with strain gauges, and 1 bridge with lidar scans to quantify the transverse dynamic behavior. A finite element analysis was conducted to evaluate the parameters that impact the live load moment and shear distribution factors for IT girder bridges and how they compare to AASHTO Standard and LRFD specifications. The results from these assessments will help recommend further enhancements that are needed to improve the structural durability and performance of the IT girder bridge system.

1.2 MOTIVATIONS & OBJECTIVES OF RESEARCH

The IT bridge system has a unique design and beneficial construction procedure for short to medium spans ranging from 30 to 80 feet. The cast-in-place deck acts as the composite top flange of the IT girders. This efficient use of material reduces the bridge weight and increases the span-to-depth ratio. The IT girder bridge system is an effective design when superstructure depth is a constraint. Since temporary formwork is not required, the construction process is quick with fewer roadway downtimes and closures. However, there are several challenges that exist for the relatively new IT girder bridge system due to the limited performance data and knowledge. This project is an opportunity to employ state-of-the-art nondestructive and non-contact testing and assessment techniques along with the visual inspections. These advanced assessment techniques include system identification and advanced geospatial analysis utilizing accelerometer time histories and lidar scans, respectively. The primary objective is to perform these assessment techniques to evaluate the structural durability and performance of the IT girder system, as well as compare the dynamic behavior of the bridges to other competitive systems. The goal is to identify the deficiencies of the IT girder bridge system and recommend further design enhancements to become even more competitive with alternative designs.

1.3 PROJECT OUTLINE & SCOPE

The evaluation of the structural durability and performance for the IT girder bridge system is presented within the scope of the following chapters and appendices:

Chapter 2 presents a literature review on the history and description of the IT girder bridge system, system identification, modal analysis techniques, and example case

studies that guide this project. This chapter also summarizes interviews with IT bridge producers and contractors.

Chapter 3 summarizes the field assessments of the 20 selected IT girder bridges with representative photos of common damage and an example bridge deck crack. This chapter mentions the likely cause and time of occurrence for each type of commonly observed damage.

Chapter 4 explains the general instrumentation setups, system identification process, and operational modal analysis techniques used to obtain the structural dynamic properties of the global and local responses for the bridges. This complete process is elucidated for one of the instrumented IT girder bridges. The dynamic behavior of this IT girder bridge is compared to the response of two comparable bridges, namely one slab and one NU girder bridge, with similar traffic characteristics. Evaluating these dynamic properties helps indicate the causes of the commonly observed damage for the IT girder bridges.

Chapter 5 describes the advanced geospatial analysis used to develop depth maps of the deck and girders from lidar scans. These depth maps provide the relative deck and girder elevations for the scanned IT girder bridges.

Chapter 6 presents the instrumentation setup of LVDT's, strain gauges, and lidar scans to quantify the transverse dynamic behavior for IT girder bridges under live loads. Quantifying the transverse dynamic behavior helped assess the potential cause for longitudinal deck cracking in IT girder bridges.

Chapter 7 evaluates the live load moment and shear distribution factors for IT girder bridges using three-dimensional finite element analysis (FEA) and AASHTO live

loads. FEA results were compared to those predicted using AASHTO Standard and LRFD bridge design specifications. This chapter then performs a parametric study to determine the effect span length, skew angles, number of lanes loaded, deck slab thickness, and intermediate diaphragm type have on the structural performance of the system.

Chapter 8 summarizes the project conclusions and recommendations as well as states potential future research topics for the IT girder bridge system.

Appendix A contains photos of observed damage for the IT girder bridges that were field assessed.

Appendix B consists of the deck crack maps for the IT girder bridges that were field assessed.

Appendix C details the system identification results for the instrumented bridges.

Appendix D includes the plots from the field assessment analysis for the instrumented IT girder bridges.

Appendix E contains the deck and girder lidar depth maps for the scanned IT girder bridges.

Appendix F consists of the LVDT and strain gauge results for the instrumented bridges.

Appendix G contains the contractor interview responses.

Appendix H includes plots comparing NBI condition ratings to the age of the bridge at the time of inspection and a table summarizing the condition ratings for all IT girder bridges.

CHAPTER 2 – LITERATURE REVIEW

2.1 HISTORY AND DESCRIPTION OF THE IT GIRDER BRIDGE SYSTEM

The University of Nebraska–Lincoln (UNL) researchers and Nebraska Department of Transportation (NDOT) engineers originally developed the IT girder bridge system in 1996 (Kamel and Tadros, 1996; Jaber, 2013). There currently are over 110 IT girder bridges used for both state highway and local county bridges in Nebraska (Figure 2.1). Most of these bridges are located in the eastern part of the state, as illustrated in the figure. The bridge system is considered as a type of accelerated bridge construction (ABC), which provides a competitive design for short to medium spans ranging from 30 to 80 feet. There are several advantages of the IT girder bridge system compared to other competitive systems. A few of the advantages include no required temporary formwork, quick construction process, shorter road closures, reduced bridge weight, and efficient material usage. The reduced girder weight increases the ease of construction for the IT girder bridge system, especially for areas not easily accessible for large cranes. Also, the high span-to-depth ratio provides an adequate design for superstructure bridge replacements, especially when depth is a constraint (e.g., hydraulic clearance).

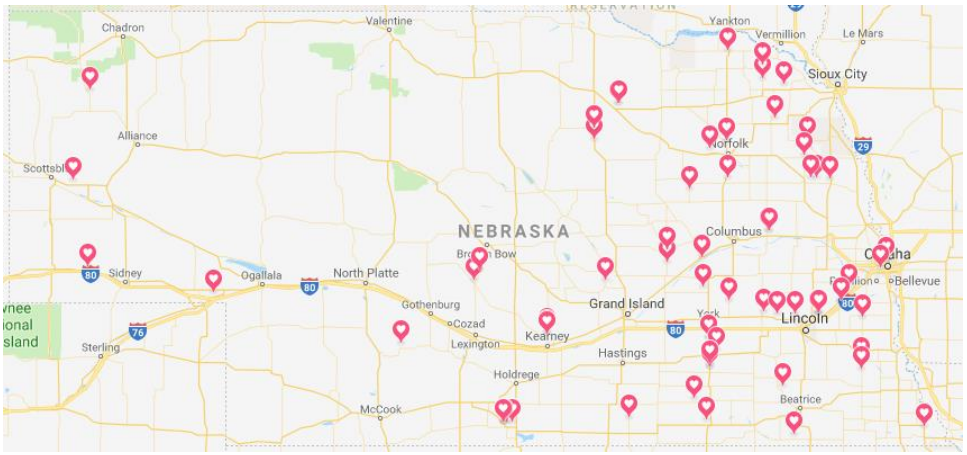

Figure 2.1: Locations of IT girder bridges in Nebraska (courtesy of Google Maps).

The cross-sectional properties of the prestressed IT girders are provided in Table 2.1. Drawings of the dimensions, reinforcement, and strand layout for a typical IT-400 girder is displayed in Figure 2.2. The IT girder heights range from 13.3 to 36.9 inches (IT-300 to IT-900). All IT girders have a consistent web width of 6.38 inches (162 mm), flange width of 23.63 inches (600 mm), and flange thickness of 5.50 inches (140 mm). Each girder has a maximum of 22 – 0.5 inch prestressing strands. Figure 2.3 shows an example IT girder formwork and reinforcement scheme. The girder spacing ranges from 25 to 37 inches (635 to 940 mm). Concrete with a 28-day compressive strength of 8,000 psi is most commonly used for the girders.

Table 2.1: Cross-sectional properties of the IT girders (NDOT 2014).

Girder	Height* (in)	Web Width (in)	Flange Thickness (in)	Flange Width (in)	Area (in^2)	Centroid** (in)	Inertia (in^4)	Weight (lb/ft)
IT-300	13.31	6.38	5.50	23.63	178.9	4.50	2,034	186.4
IT-400	17.25	6.38	5.50	23.63	204.0	5.81	4,468	212.5
IT-500	21.19	6.38	5.50	23.63	229.1	7.25	8,331	238.6
IT-600	25.13	6.38	5.50	23.63	254.2	8.75	13,866	264.8
IT-700	29.06	6.38	5.50	23.63	279.3	10.38	21,293	290.9
IT-800	33.00	6.38	5.50	23.63	304.4	12.06	30,827	317.1
IT-900	36.94	6.38	5.50	23.63	329.5	13.75	42,674	343.2

* Height is based on the actual geometry and include a 1.5-inch notch
** Measured from the bottom of the girder

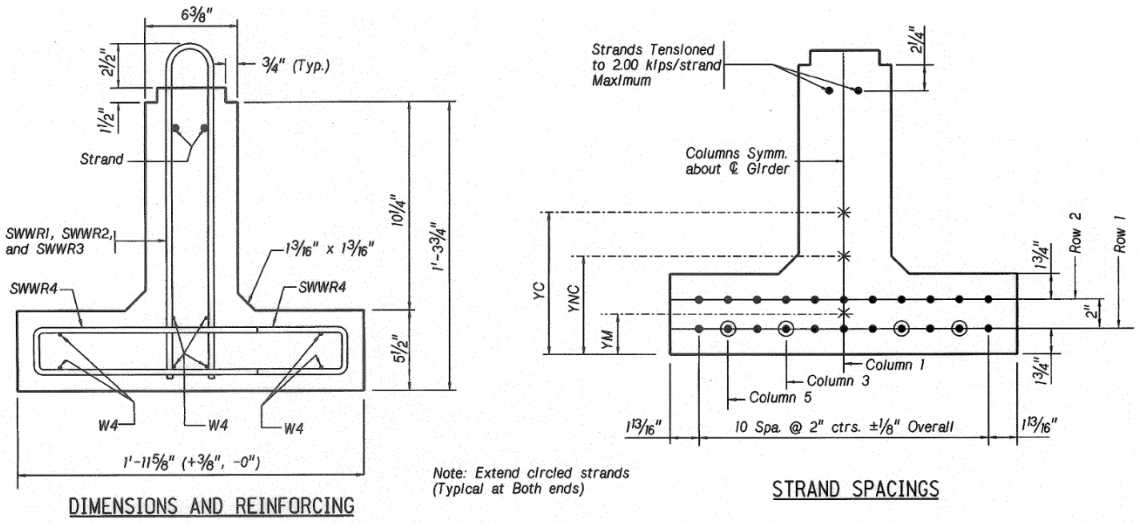

Figure 2.2: Drawing of the dimensions, reinforcement, and strand layout for a typical IT-400 girder (courtesy of NDOT).

Figure 2.3: Example IT girder formwork and reinforcement scheme (courtesy of NDOT).

Before pouring the cast-in-place deck, stay-in-place forms made from ¾ inch plywood sheets are installed spanning between girder to girder, as shown in Figure 2.4. The cast-in-place deck is six inches thick with a single reinforcement layer for typical highway and local road IT girder bridges. For IT girder bridges on the interstate or with a 42-inch NU rail, the cast-in-place deck is eight inches thick with two reinforcement layers. The thicker concrete deck is to account for larger bridge rail capacity under a collision (TL-4). The transverse and longitudinal reinforcement is #5 rebar at 6-inch and 10-inch spacing,

respectively. The deck is continuous over the piers. Concrete with a 28-day compressive strength of 4,000 psi is typically used for the deck.

(a) (b)

Figure 2.4: Stay-in-place plywood forms spanning between girders.

Several challenges exist for the relatively new IT girder bridge system due to the limited performance data and knowledge. The live load distribution factors have not been fully explored or determined for the IT girder bridge system. This is particularly true with varying span lengths, skew angles, deck thicknesses, diaphragm types, girder sizes, and girder spacing. Furthermore, one construction challenge is handling the flexible girders before the cast-in-place deck is poured. Intermediate concrete or steel diaphragms are sometimes used to help stabilize the outside girders of the bridge during the construction process, as illustrated in Figure 2.5. Excessive transverse and longitudinal deck cracking has been observed and noted in numerous bridge inspection reports, even at an early age. The transverse cracking occurs in the negative moment region over the piers, where the

spans are continuous for the live load (Ambare and Peterman, 2006; Larson et al., 2013). The Kansas DOT introduced a design update that included post-tensioning of the IT girders to help improve the durability of the bridge (Nayal et al., 2006). A draped post-tensioning duct was added to every IT girder stem to better control the unpredictable camber and stresses throughout the bridge. When the post-tensioning is applied after the concrete diaphragms and deck are cured, the transverse cracking in the deck is significantly reduced over the piers.

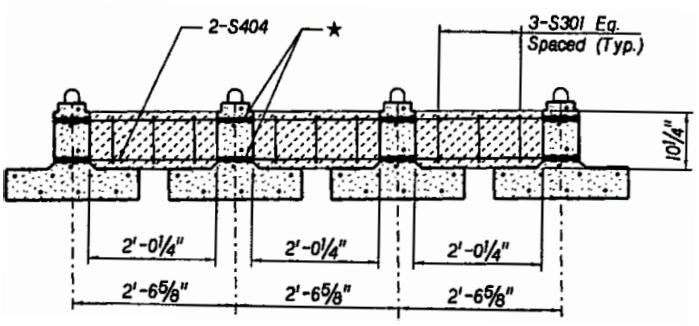

(a)

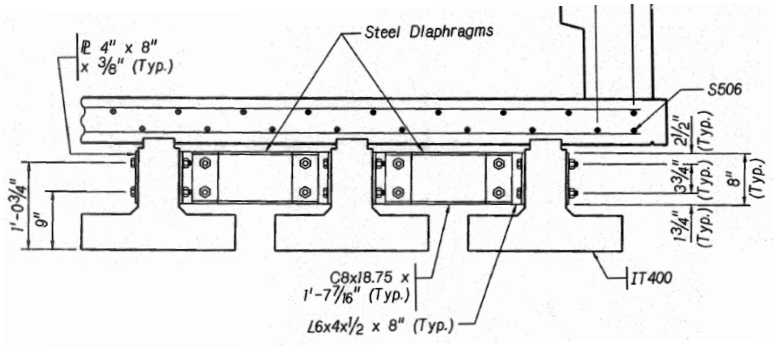

(b)

Figure 2.5: Drawings of an example intermediate diaphragm layout for an IT girder bridge: (a) concrete and (b) steel (courtesy of NDOT).

2.2 SYSTEM IDENTIFICATION AND MODAL ANALYSIS

System identification of the IT girder bridges will aid in investigating a connection between the dynamic behavior of the bridges and the possible damage mechanisms that

create longitudinal deck cracks in the bridge decks. System identification is the process of developing a mathematical model based on measured data from a structure (Peeters and Roeck, 2001). Accelerometers record the vibrations of the structure, and this data is used for system identification. An understanding of structural dynamics and accelerometer data processing is important when performing system identification. Bore (2014) presents a basic introduction to digital signal processing that can be applied to acceleration time histories. He and Fu (2001) explain modal analysis in full detail including its various applications, mathematics, frequency and time domain analysis methods, and processing examples on real-world structures. Experimental modal analysis (EMA) or operational modal analysis (OMA) is performed to determine the dynamic characteristics of a structure using frequency or time domain techniques. EMA explores the transfer of the measured input signal through the structure to the measured output signal. An impulse hammer or portable shaker is typically used as the input excitation. OMA considers only the output vibrations and assumes the unknown input is random (Brincker and Ventura, 2015). The method is typically performed on larger structures, such as building or bridges, operating under ambient conditions excited by live and wind loads.

Modal analysis can be performed in the frequency or time domain to obtain the modal properties of a structure, namely the natural frequencies, damping ratios, and mode shapes. A natural frequency is the frequency of vibration that a structure will tend towards and is a function of the mass and stiffness distributions. A damping ratio is a decay of vibration for a given frequency of a system expressed in percent of critical damping. Damping ratios are not completely reliable under ambient loads due to the low level of excitation. A mode shape is a relative vibration pattern of a structure for a given frequency.

Example mode shapes for an idealized two-dimensional four-story frame structure is shown in Figure 2.6.

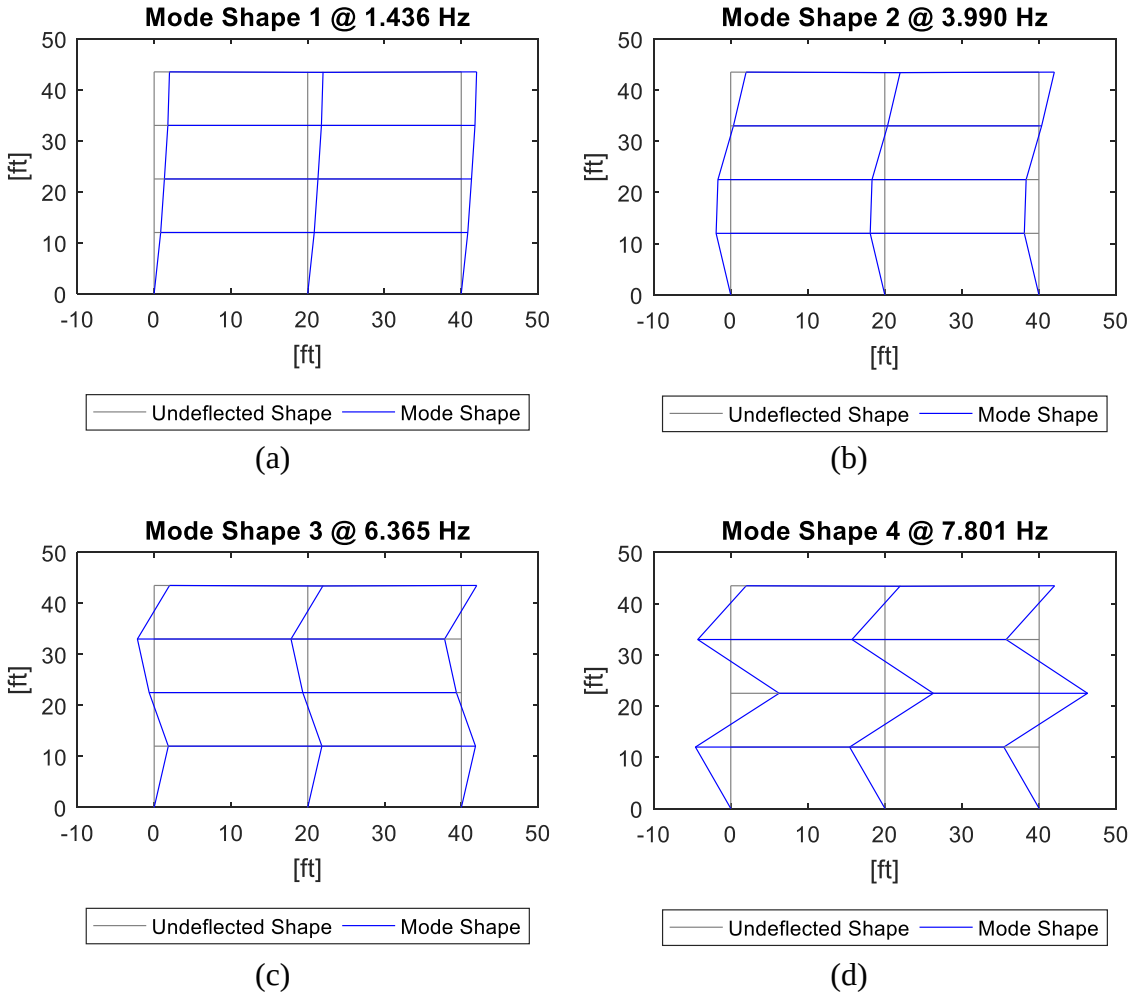

Figure 2.6: Modes shapes in the horizontal x-direction degree-of-freedom for an example two-dimensional four-story frame.

The peak-picking method is an approximate and quick way to determine the modal properties based on the peak value of the fast Fourier transform (FFT) signal plots. An FFT is an algorithm to convert the signal from the time domain into the frequency domain (Welch, 1967). Figure 2.7 illustrates an example of peak-picking frequency domain analysis for a structural assessment using ambient vibrations. The frequency domain

decomposition (FDD) method is commonly performed for EMA to determine estimates of the modal properties based on cross-correlation spectra (Brincker et al., 2000).

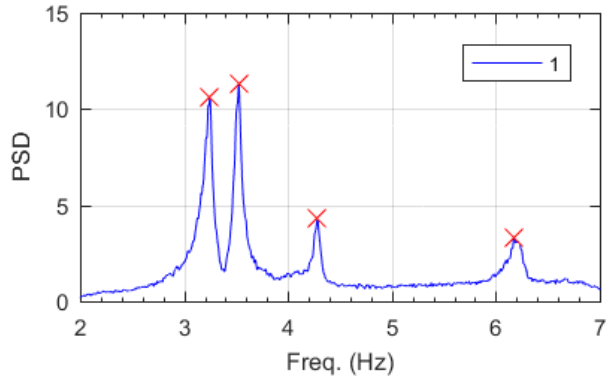

Figure 2.7: Example of peak-picking frequency domain analysis.

Stochastic Subspace Identification (SSI) is known as the most powerful and reliable time domain operational modal analysis technique (Brincker and Anderson, 2006). The SSI technique is a significantly more complicated algorithm that minimizes the error between the mathematical model and measured system response by adjusting various parameters. Herlufsen et al. (2005) and Structural Vibrations Solutions (2017) introduces the multiple implementations of the SSI technique. Two popular implementations are the Unweighted Principal Component (SSI-UPC) and the Extended Unweighted Principal Component (SSI-UPCX), which generates stabilization diagrams with confidence bounds and removes potential modes with high values of uncertainty (Mellinger et al., 2016). Figure 2.8 provides an example stabilization diagram utilizing the SSI-UPCX technique.

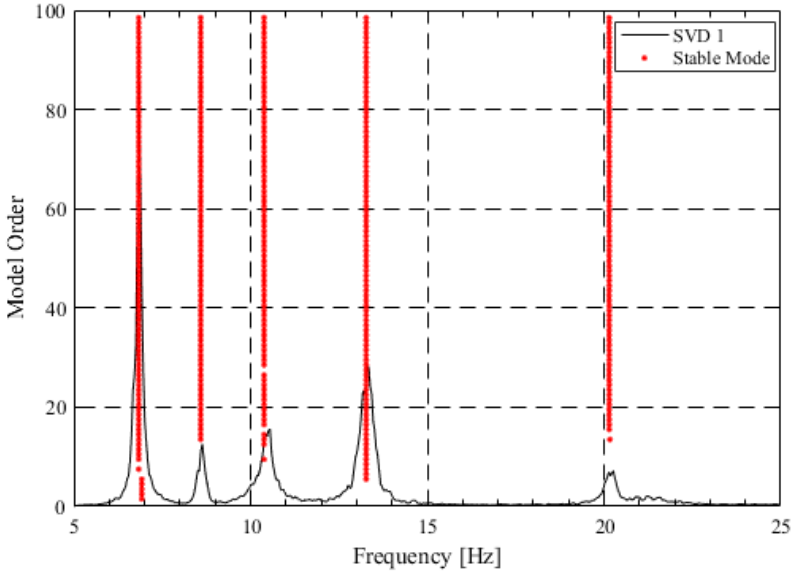

Figure 2.8: Example SSI-UPCX stabilization diagram.

2.3 SYSTEM IDENTIFICATION CASE STUDY EXAMPLES

System identification of civil engineering infrastructure has been a popular research topic over the past few decades. Several case studies have applied EMA and OMA methods for various applications and investigations. Khalil et al. (1998) investigated the deck rehabilitation of the Boone River bridge on Iowa State Highway 17 by comparing the before and after modal properties. Modal analysis was used as a nondestructive evaluation technique that can be used in conjunction with visual inspections for a more effective bridge assessment. As bridges deteriorate or are retrofitted, the dynamic properties change. The computed natural frequencies and mode shapes were used to obtain the current stiffness and mass properties of the bridge. Ren et al. (2004) performed output-only modal identification using the peak-picking and SSI methods on a steel girder arch bridge. The ambient vibrations excited by traffic and wind were collected by triaxial accelerometers. The natural frequencies, damping ratios, and mode shapes were generated for the three-

dimensional motion of the bridge. Cunha and Caetano (2006) implemented EMA on the Jindo cable-stayed bridge and the Norsjö dam using portable shakers and OMA on the Heritage Court Tower and the Guadiana cable-stayed bridge.

2.4 INTERVIEWS

Three bridge contractors responded to a questionnaire assessing the performance of the IT Bridge System during construction in the regional area. Combined the contractors have completed over 40 IT bridges with an average of 3 or 4 per year (all in Nebraska). In this report, the contractor's responses are anonymous to obscure their identity. When comparing IT to slab bridges, they said the total costs of construction are relatively comparable, but the IT bridge is faster, easier, and requires a smaller crew to construct. According to one contractor, the typical three span slab bridge would take approximately one month longer to build than the same sized IT girder bridge. Also, IT bridges are safer to construct due to not requiring falsework and eliminating many fall hazards when decking (excluding exterior girders). They also reduce the need to access the waterway due to the longer spans.

Overall, the contractors had positive experiences with IT bridge construction due to the ease of construction and not needing a large crane due to the lightweight girders. The main problem the contractors had with IT bridge construction is the deflection and camber of girders during deck construction. One contractor stated that the over-camber of IT girders may cause the deck to be poured thicker than the design plans. Thicker decks are especially problematic because one or more contractors said girder deflection during deck placement is a problem. For example, one contractor believes the thicker 8-inch deck is the

reason the Interstate 80 bridges "over deflected". Additionally, the exterior girder deflection must be more carefully monitored both during the placement of the deck and anytime there are machine loads near the edge of the bridge. A suggestion to attempt to reduce the cost of IT bridge construction is to do a cost analysis trying to reduce the number of girders by increasing girder spacing but utilizing larger girders. However, the contractors say stay in place forms are essential, so if the spacing is too large a light stay-in-place metal decking may be required instead of plywood. A suggestion to improve construction is to minimize the overhang which would reduce the live load impact on the exterior girder during deck placement. Also, one contractor suggests trying to bring the picking eyes (for erection) closer to the midpoint, so the sling angle is reduced when picking with one crane. To speed up construction and save money, one or more contractors suggest that any intermediate diaphragms be made of steel. One contractor says that it takes a crew of 3-4 people approximately two and a half days for the forming, pouring, and stripping of concrete whereas a steel diaphragm will take the same group a few hours to complete. If concrete intermediate diaphragms are used, one contractor suggests making the diaphragms consistent, allowing tolerance in formwork at the base, and allowing them to be poured before the deck. Details of contractor responses can be found in Appendix G.

Also, two bridge producers were interviewed to get their insights about the challenges in the production of IT girders. Table 2.2 summarizes the questions asked to each producer and their answers. Based on their responses, the producers recommended eliminating the use of partially bonded top strands and suggested increasing girder spacing to be more competitive to slab bridges.

Table 2.2: Producer Interviews.

Question/Item	Producer 1	Producer 2
IT Project owners	NDOR, Iowa counties, private Kansas	NDOR only
Range of sizes	IT 400-800 (few IT300, no IT900)	IT 400-800 (few IT300, no IT900)
Difference from NU girder production	Use of 0.5 in. diameter straight strands	No draping, a lot of debonding, and use of two fully tensioned top strands
Shipping	As many as possible with total weight limit of 45,000 lb. Challenging when truck is moving backward	As many as possible with total weight limit of 45,000 lb.
Recommendations to reduce production cost	Allow using mild reinforcement as alternative to WWR	Reduce release strength and debonded strands, eliminate partially bonded top strands
Rejected IT	3, cutting top strands resulted in significant cracking	None
Reasons for less IT bridges	Not true. More repair than new construction recently	General observation in new bridge construction
Increasing IT girder spacing	Good idea that makes it more competitive than slab bridges	Good idea and can make it more competitive than slab bridges

2.5 APPLICATION TO THE PROJECT

The literature review helped establish a plan to successfully guide and ultimately accomplish this research project. The project goals and achievement strategy were developed subsequent to the literature review. The history and description of the IT girder bridge system provided insights on the design goals, construction procedures, and numerous challenges. The study on system identification and modal analysis aided in understanding the multiple techniques of obtaining the modal properties of structures by using accelerometer time history data. The system identification methods used for this research project is a combination of the techniques discussed in the system identification case study examples. These case studies demonstrate that the system identification process is applicable to civil engineering infrastructure and the results are comprehensible. The interviews with the contractors and producers responsible for building the IT girder bridge system gave a unique perspective of the advantages and disadvantages associated with construction. They also suggested ways that an IT girder bridge may be able to be built more efficiently.

CHAPTER 3 – FIELD OBSERVATIONS

3.1 INTRODUCTION

There are over 110 IT girder bridges throughout Nebraska with most of them located in the eastern part of the state. Multiple parameters were considered to select a well-diversified subset of bridges for field observations. These parameters include year constructed, average daily truck traffic (ADTT), maximum span length, skew, deck rating, superstructure rating, girder size, deck thickness, and girder spacing. Histograms were created to help visualize the distribution of data for the Nebraska IT girder bridges during the field observation selection process. Figure 3.1 provides a few relevant histograms indicating the selected bridges for field observation are a diverse representation of the entire population. Twenty IT girder bridges, listed in Table 3.1, were selected for field observations. This chapter provides an overview of commonly found damage and observations of a recently constructed IT girder bridge. An assembly of the photos of observed damage and the deck crack maps for each bridge are compiled in Appendix A and Appendix B, respectively.

3.2 COMMON OBSERVATIONS OF DAMAGE

The commonly found damage for these 20 IT girder bridges is grouped into five categories: deck cracking, damaged abutment caps, damaged pier caps, damaged girders, and cracked bridge rail. Table 3.2 provides a summary of the observations from the bridge field visits. There are no noticeable relationships between the severity of damage and the year constructed, IT girder size, maximum span length, nor skew angle.

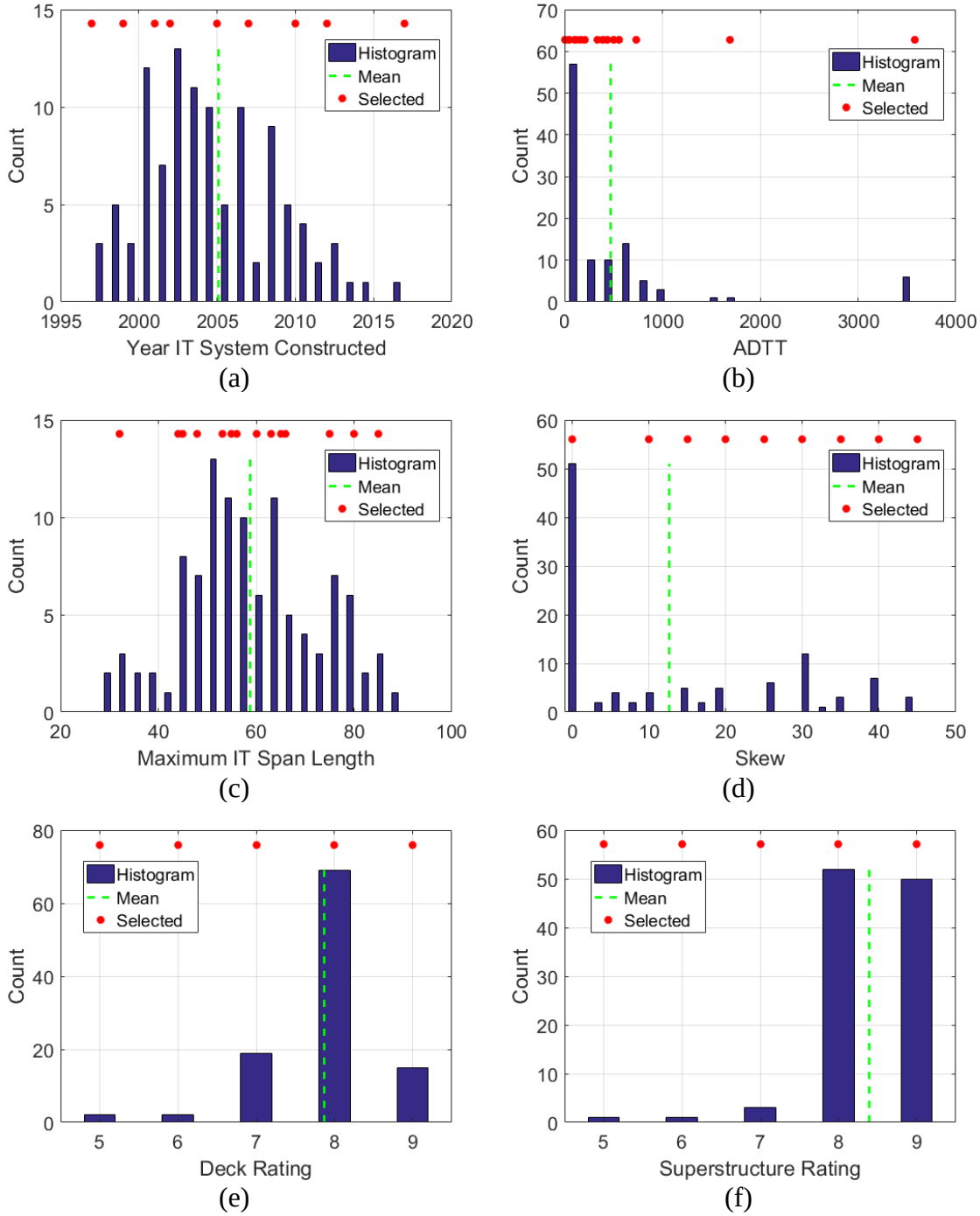

Figure 3.1: Histograms for bridge field observation selection.

Table 3.1: Bridges selected for field observations.

Bridge ID	County	Year Built	IT Height		Girder Spacing		Deck Thickness		No. of Girders	Interior Diaphragm	No. of Spans	Max. Span Length (ft.)	Width (ft.)	Skew Angle (°)	Inspection Date	Inspection Rating		
			mm	in	mm	in	mm	in								Deck	Super	Sub
S006 26001	Fillmore	1999	300	11.81	738	29.06	150	5.91	19	None	3	32.50	45.6	20	7/6/2015	8	8	7
S006 34277	Sarpy	2002	300	11.81	730	28.75	152	6.00	19	None	3	40.00	46.3	40	1/6/2016	7	7	8
S009 00888	Cuming	2002	400	15.75	711	28.00	152	6.00	18	None	3	44.00	42.4	45	5/20/2015	8	8	7
S020 32260	Holt	2012	400	15.75	699	27.50	152	6.00	20	C8x18.75	4	46.00	46.3	40	3/24/2015	7	7	7
S034 31644	Lancaster	2005	400	15.75	724	28.50	152	6.00	42	C8x18.75	3	48.00	99.9	30	2/11/2015	7	9	8
S050 04149	Johnson	1997	600	23.62	650	25.59	150	5.91	19	Concrete	3	67.25	41.7	10	7/13/2016	7	8	7
S050 06686	Cass	2007	700	27.56	730	28.75	152	6.00	24	C12x30	3	75.00	58.8	0	6/9/2016	7	8	8
S058 00994	Howard	2001	300	11.81	670	26.38	150	5.91	18	None	3	45.00	40.0	0	12/2/2014	6	8	8
S080 40872R	Lancaster	2010	400	15.75	756	29.75	178	7.00	25	C8x18.75	3	53.50	62.8	0	1/29/2015	8	9	9
S080 40927R	Lancaster	2010	400	15.75	756	29.75	178	7.00	25	C8x18.75	3	53.50	62.8	0	1/29/2015	8	9	9
S081 05152L	York	1999	400	15.75	660	25.98	150	5.91	19	Concrete	3	56.00	40.7	10	12/19/2014	7	8	7
S089 06047	Harlan	2007	300	11.81	724	28.50	152	6.00	16	Concrete	3	45.00	38.4	0	4/21/2015	8	9	9
S089 06062	Harlan	2007	400	15.75	778	30.63	152	6.00	15	Concrete	6	55.00	36.4	25	4/21/2015	8	9	9
S103 02465	Gage	1999	900	35.43	905	35.63	150	5.91	4	Concrete	5	85.00	41.7	0	7/10/2014	7	7	7
S275 18587	Douglas	1997	500	19.69	660	25.98	150	5.91	34	Concrete	3	60.00	74.3	0	2/9/2016	7	8	7
SS66C00220	Otoe	2001	700	27.56	740	29.13	150	5.91	15	Concrete	1	80.00	37.7	25	2/11/2015	8	9	8
C002408505	Dawson	2005	600	23.63	721	28.375	152	6.00	13	C8x18.75	1	65.00	30.4	35	10/8/2015	5	9	9
C008504145	Thayer	2007	600	23.63	737	29.00	150	5.91	12	C10x15.3	3	63.50	30.4	0	11/14/2014	5	5	6
M011022220	Sherman	2012	600	23.63	721	28.375	152	6.00	13	C8x18.75	1	65.00	30.4	15	11/23/2016	6	6	7
C004931110	Johnson	2017	600	23.63	762	30.00	152	6.00	12	C12x30	4	75.00	27.5	20	--	9	9	9

Table 3.2: Summary of the bridge field observations.

Bridge ID	Year IT Constructed	IT Size	Max. Span Length (ft.)	Skew Angle (°)	Location									
					Deck				Abutment Cap		Pier Cap	Girders		Rails
					Longitudinal Cracks	Transverse Cracks	Diagonal Cracks	Gravel Covered	Chipped	Cracked	Damaged	Chipped	Patched	Cracked
S006 26001	1999	300	32.50	20	Full length	Partial width			1	1				Yes
S006 34277	2002	300	40.00	40	Full length				1			2		Yes
S009 00888	2002	400	44.00	45	Partial length		Yes			2	Yes	1		Yes
S020 32260	2012	400	46.00	40	Partial length	Full width								Yes
S034 31644	2005	400	48.00	30	Full length	Partial width	Yes		1			1	2	Yes
S050 04149	1997	600	67.25	10	Full length	Full width			1	1				Yes
S050 06686	2007	700	75.00	0	Full length	Partial width			2	1		5	1	Yes
S058 00994	2001	300	45.00	0	Full length	Full width			2		Yes		1	Yes
S080 40872R	2010	400	53.50	0	Full length	Partial width	Yes		2					Yes
S080 40927R	2010	400	53.50	0	Full length	Partial width	Yes							Yes
S081 05152L	1999	400	56.00	10	Full length	Partial width	Yes							Yes
S089 06047	2007	300	45.00	0	Full length	Partial width	Yes							Yes
S089 06062	2007	400	55.00	25	Full length	Full width	Yes							Yes
S103 02465	1999	900	85.00	0	Partial length	Full width				2	Yes			Yes
S275 18587	1997	500	60.00	0	Full length		Yes		1					Yes
SS66C00220	2001	700	80.00	25	Partial length		Yes			2				Yes
C002408505	2005	600	65.00	35	Full length		Yes	Partially		2			1	Yes
C008504145	2007	600	63.50	0	Partial length			Partially		2		1		Yes
M011022220	2012	600	65.00	15				Fully						Yes
C004931110	2017	600	75.00	20		Partial width								Yes

3.2.1 Deck Cracking

The deck cracking is documented in an idealized crack map for each bridge. For example, Figure 3.2 shows the deck crack map for bridge S080 40872R. Longitudinal, transverse, and diagonal cracks are found on all IT girder bridges, as observed by visual assessment. Longitudinal cracks (Figure 3.3) are found on each of the 20 IT girder bridges at almost every girder for the full length of the bridge. Despite this common occurrence in IT bridge systems, longitudinal cracking is not commonly found on other types of bridges. Transverse cracks (Figure 3.4) are commonly found over the bridge piers due to the negative moment. Diagonal cracks (Figure 3.5) are typically found near the bridge abutments, particularly in moderate to larger skew angles. There was no observable benefit to the reduction of deck cracking when increasing the deck thickness from six to eight inches (for the two interstate highway bridges). Three out of the four county bridges that were visited had fully or partially gravel covered decks, which is the reason for the low deck rating of five or six. Deck cracking may be caused by numerous factors. In this case, the longitudinal deck cracking is speculated to be a cause of the inefficient transverse load distribution. This hypothesis will be assessed furthermore in Chapters 4 and 6.

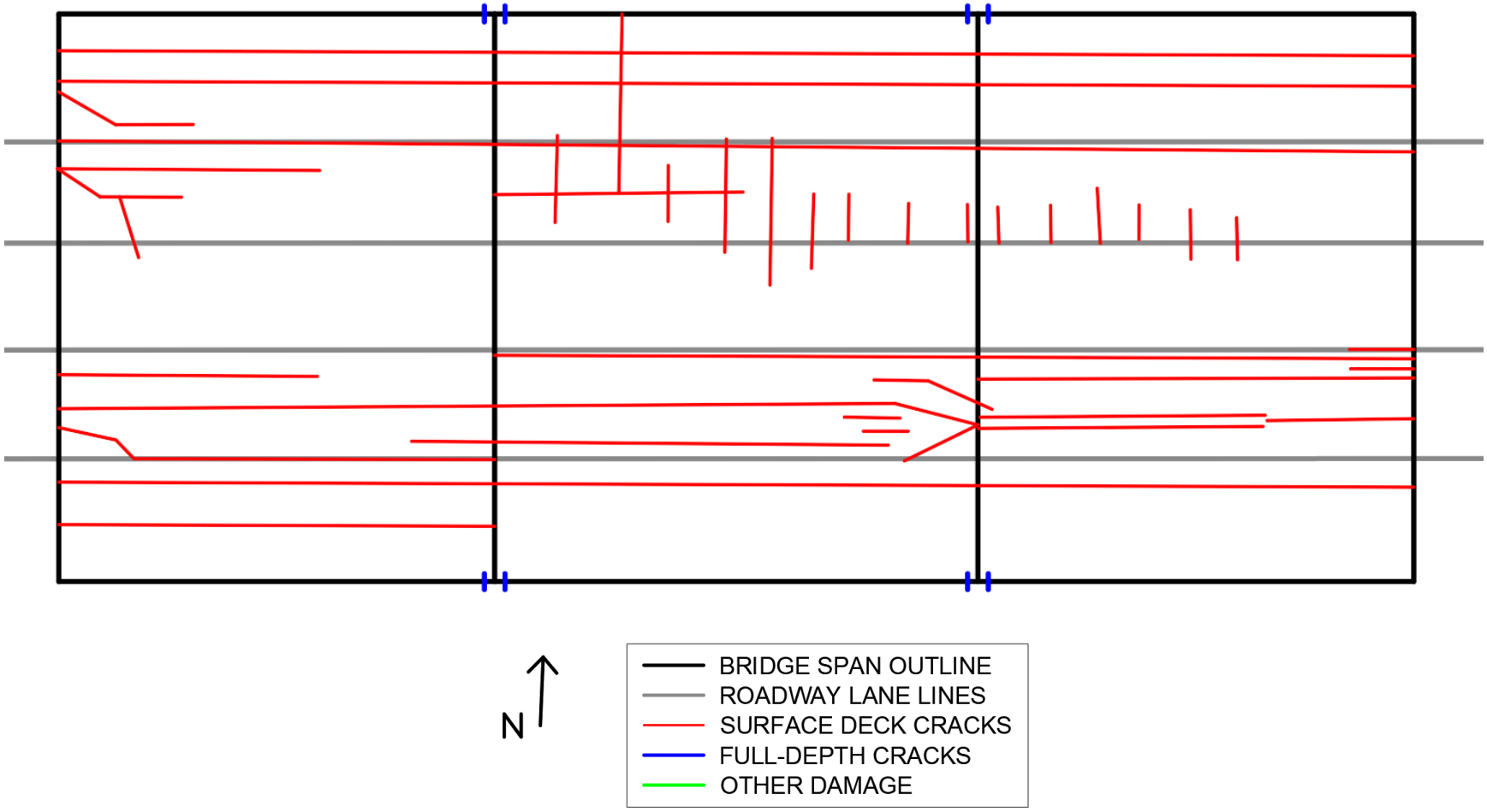

Figure 3.2: Deck crack map for bridge S080 40872R.

(a) (b)

Figure 3.3: Examples of longitudinal deck cracking.

(a) (b)

Figure 3.4: Examples of transverse deck cracking.

Figure 3.5: Example of diagonal deck cracking.

3.2.2 Damaged Abutment Caps

Several IT girder bridges have chipped or cracked abutment caps (Figure 3.6 & Figure 3.7). However, this type of damage is not unique to IT girder bridges. Damaged abutment caps are commonly found on other types of bridges. This damage is may be caused by concrete shrinkage, successive freeze-thaw cycles in the expansion joint, and salt deteriorating the concrete.

(a) (b)

Figure 3.6: Examples of chipped abutment caps.

(a) (b)

Figure 3.7: Examples of cracked abutment caps.

3.2.3 Damaged Pier Caps

A few IT girder bridges have chipped or cracked pier caps (Figure 3.8). However, this type of damage is not unique to IT girder bridges. Damaged pier caps are commonly found on other types of bridges. Concrete shrinkage and expansion joint placement over the piers are may be the reason for the pier cap damage.

(a) (b)

Figure 3.8: Examples of damaged pier caps.

3.2.4 Damaged Girders

Poor construction practices (e.g., quality control or installation techniques) are likely the primary reason for the damaged girders. This damage is not likely caused by the structural performance of the bridge. Some IT girder bridges have chipped girders (Figure 3.9), and a few girders have been patched (Figure 3.10). Bridges S006 34277 and S058

00994 have a damaged girder bottom flange due to water entrapment in the concrete formwork (Figure 3.11).

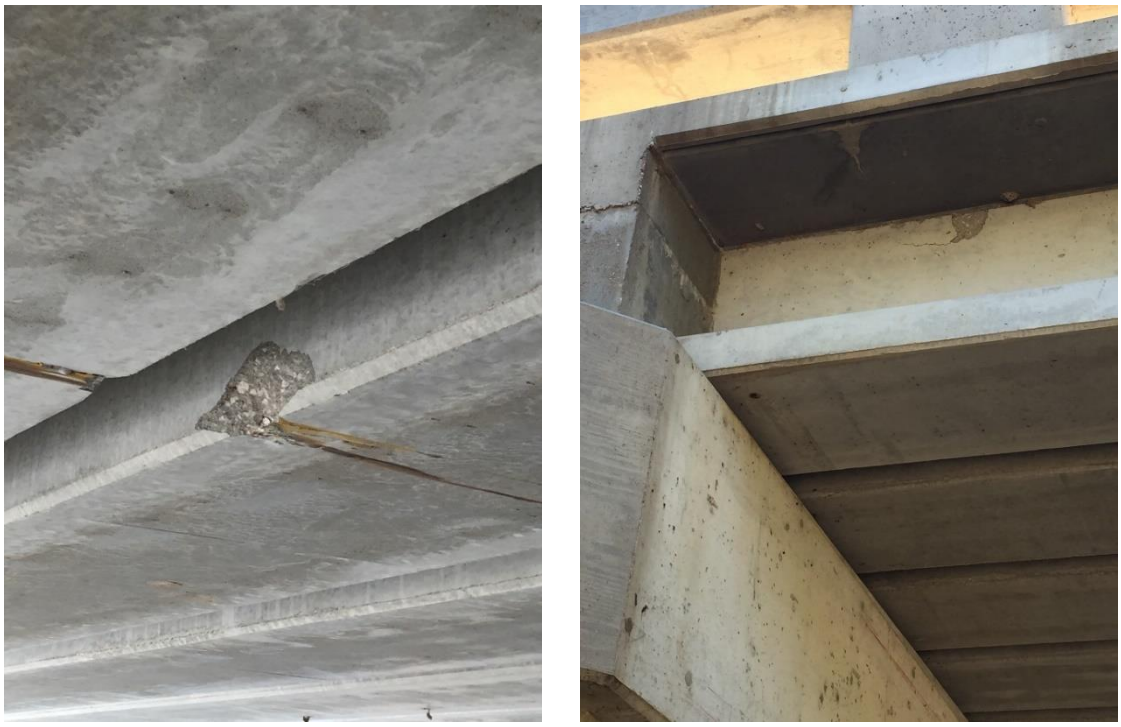

(a) (b)

Figure 3.9: Examples of chipped girders.

(a) (b)

Figure 3.10: Examples of patched girders.

(a) (b)

Figure 3.11: Examples of girder damage due to water entrapment in the concrete forms.

3.2.5 Cracked Bridge Rails

All IT girder bridges have cracked bridge rails (Figure 3.12). However, this type of damage is not unique to IT girder bridges. Cracked bridge rails are commonly found on other types of bridges. This damage is may be caused by concrete shrinkage.

(a) (b)

Figure 3.12: Examples of cracked bridge rails.

3.3 OBSERVATION OF A RECENTLY CONSTRUCTED BRIDGE

Bridge C004931110 located in Sterling, NE was visited for visual observation on 9/4/2017 because construction was recently completed in the spring of 2017. A deck crack map (Figure 3.13) is documented for the bridge. During this field visit, no longitudinal cracks were found on the bridge deck. This suggests that longitudinal deck cracking does not occur during construction, but rather is caused by heavy live loads. Full-depth transverse cracks are found beginning on the outsides of the bridge deck over the piers.

Most of the transverse cracks are around three feet long and proceed towards the center-line of the bridge. Also, several cracks are found on the bridge rail which may have occurred during construction. The bridge was revisited on 4/4/2018, where no additional damage was identified, likely due to its very low ADTT.

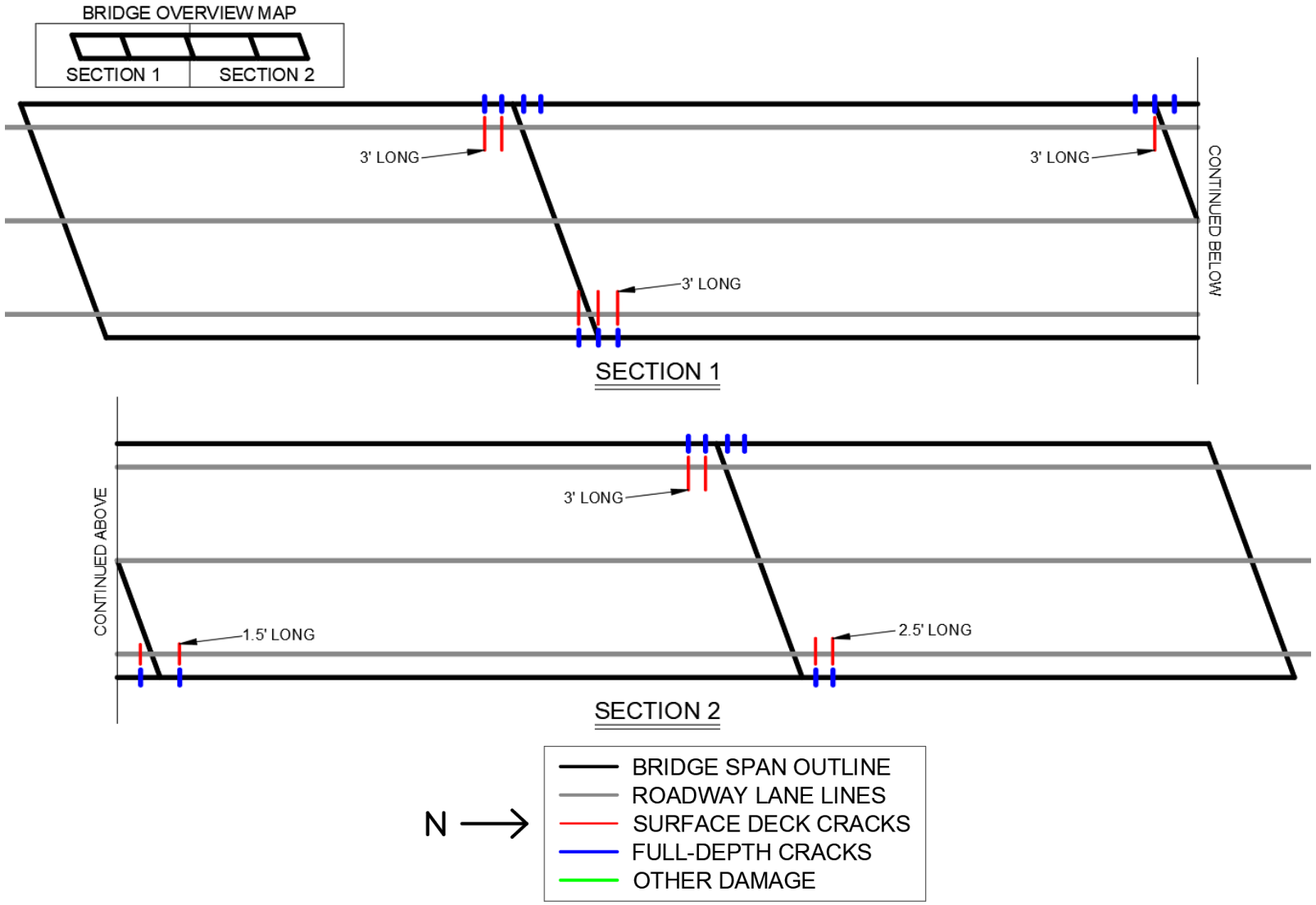

Figure 3.13: Deck crack map for bridge C004931110.

3.4 CONCLUSIONS

The following conclusions are made based on the field observations of the 20 IT girder bridges:

1. IT girder bridges have longitudinal deck cracking, which is not commonly found on other types of bridges.
2. Longitudinal deck cracking does not occur during construction and is likely due to heavy live loads.
3. Transverse deck cracking and bridge rail cracking are found in recently constructed bridges and may occur during construction.
4. There is no observable benefit to the reduction of deck cracking when increasing the deck thickness from six to eight inches.

CHAPTER 4 – SYSTEM IDENTIFICATION

4.1 INTRODUCTION

System identification is a method to develop a mathematical model representation for a dynamic system based on its input and output accelerations (e.g., Peeters and Roeck, 2001). This can either be classified as experimental (EMA, input-output) or operational (OMA, output-only) modal analysis. Within this work, the focus is on OMA, this is performed on bridges under random live loads due to traffic and human activities as well as wind loads. System identification of the IT girder bridges will aid in investigating a connection between the dynamic behavior of the bridges and the possible mechanisms that create longitudinal deck cracking in the bridge decks. Furthermore, system identification results can also be used to calibrate and refine finite element models. Histograms were created to help visualize the distribution of data for the Nebraska IT girder bridges during the instrumented bridge selection process. Figure 4.1 provides a few relevant histograms indicating the selected bridges for instrumentation are a diverse representation of the entire population. Accelerometer data were collected on ten IT girder bridges along with two comparable bridges (one slab and one NU girder bridge), as shown in Table 4.1. This chapter will explain the general process of data collection, processing, and analysis used for the instrumented bridges along with a detailed example for bridge S080 40872R. A complete set of system identification results is compiled in Appendix C. Information and properties for bridge S080 40872R is given in Table 4.2. The approximate location and a photo of bridge S080 40872R are illustrated in Figure 4.2 and Figure 4.3, respectively.

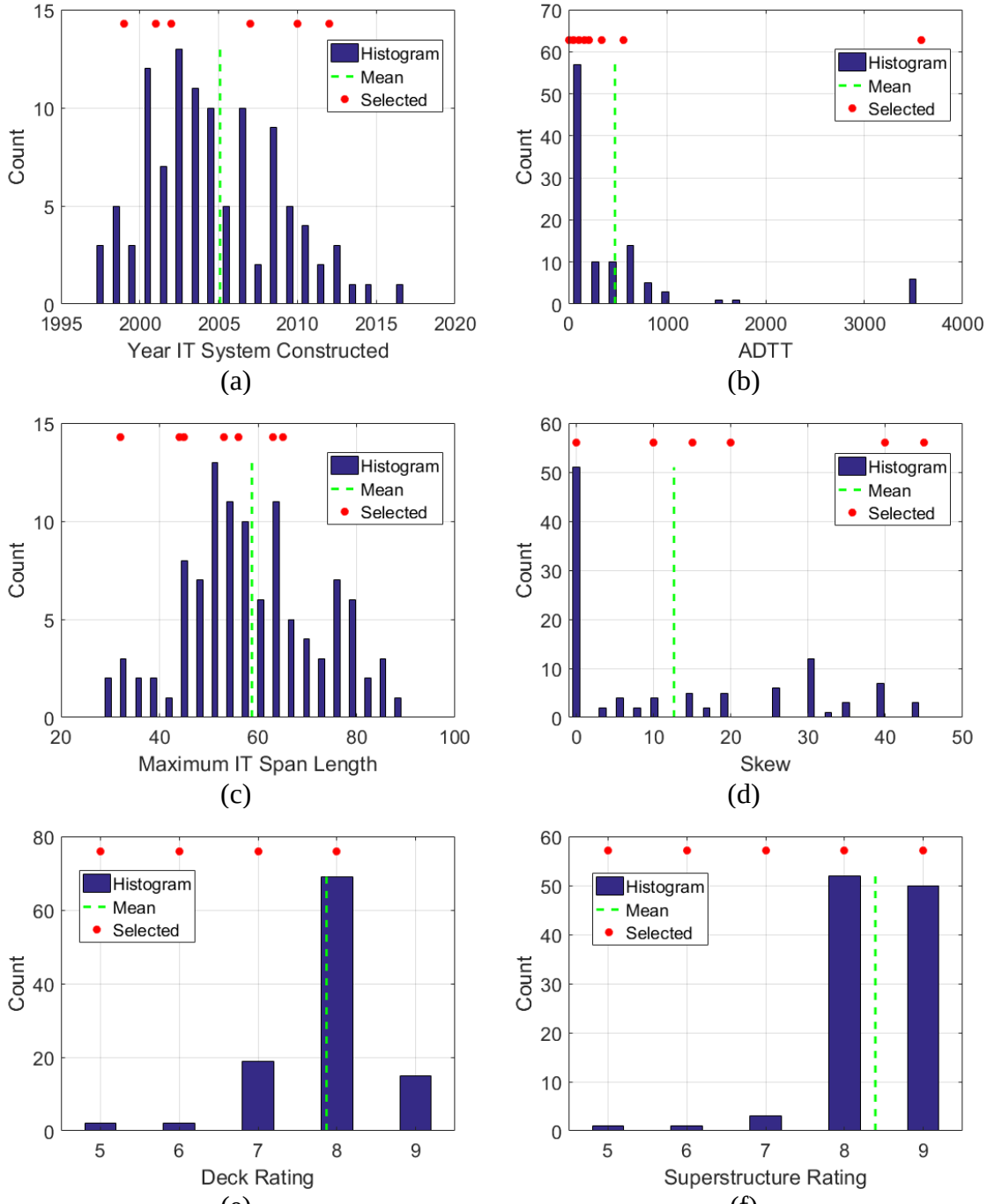

Figure 4.1: Histograms for bridge instrumentation selection.

Table 4.1: Instrumented bridges for system identification.

Bridge ID	Bridge Type	Deck Setup	Girder Setup
S006 26001	IT Girder	X	X
S009 00888	IT Girder	X	
S020 32260	IT Girder	X	
S058 00994	IT Girder	X	
S080 40872R	IT Girder	X	X
S080 40927R	IT Girder		X
S081 05152L	IT Girder	X	
S089 06047	IT Girder	X	X
C008504145	IT Girder	X	
M011022220	IT Girder	X	
S080 38614R	Slab	X	
S080 40797R	NU Girder		X

Table 4.2: Information summary for bridge S080 40872R.

Bridge ID	S080 40872R	**Girder Height (in [mm])**	15.75 [400]
County	Lancaster	**Girder Width (in [mm])**	23.63 [600]
Year Built	2010	**Girder Spacing (in [mm])**	29.75 [756]
No. of Spans	3	**Deck Thickness (in [mm])**	8 [203]
Length Span 1 (ft)	48.25	**No. of Girders**	25
Length Span 2 (ft)	53.50	**Diaphragm**	C8x18.75
Length Span 3 (ft)	48.25	**Deck Rating**	8
Bridge Width (ft)	62.80	**Superstructure Rating**	9
Skew Angle (°)	0	**Substructure Rating**	9

Figure 4.2: Location of bridge S080 40872R (courtesy of Google Maps).

Figure 4.3: Photo of bridge S080 40872R.

4.2 INSTRUMENTATION SETUP

Two different types of accelerometer networks were used to record the bridge ambient vibrations. The uniaxial PCB sensors are wired piezoelectric accelerometers, shown in Figure 4.4(a). The PCB accelerometers have a measurement range of ±5g and a broadband resolution of 3x10 µg root mean square (RMS). The triaxial WSN sensors are wireless MEMS accelerometers, shown in Figure 4.4(b). The WSN accelerometers have a measurement range of ±2g and a sensitivity of 61 µg/digit. The different accelerometers complemented each other due to the restriction of no cables on the roadway surface. Bridge ambient vibrations are recorded using two types of accelerometer setups as described below.

(a) (b)

Figure 4.4: Photos of the two types of accelerometers: (a) PCB and (b) WSN.

4.2.1 Deck Setup (Global Response)

The deck setup quantifies the global response of the bridge under random ambient loads. This type of setup was performed on nine IT girder bridges and one slab bridge. Figure 4.5(a) shows an example field instrumentation of the deck accelerometer setup. For this type of setup, WSN accelerometers are typically placed in pairs on the deck shoulder near the rails. The deck accelerometer setup for bridge S080 40872R is shown in Figure 4.6 and Table 4.3.

4.2.2 Girder Setup (Local Response)

The girder setup quantifies the local response of the bridge under random ambient loads, at the girder level. This setup indicates the response of each girder under the live loads and is indicative of the potential independent girder response (due to insufficient transverse load distribution). This type of setup was performed on four IT girder bridges and one NU girder bridge. Figure 4.5(b) shows an example field instrumentation of the girder accelerometer setup. For this type of setup, PCB accelerometers are typically placed on the bottoms of the girder flanges near midspan. The girder accelerometer setup for bridge S080 40872R is shown in Figure 4.7 and Table 4.4.

(a)

(b)

Figure 4.5: Field accelerometer instrumentation of the (a) deck setup for bridge S089 06047 and (b) girder setup for bridge S080 40872R.

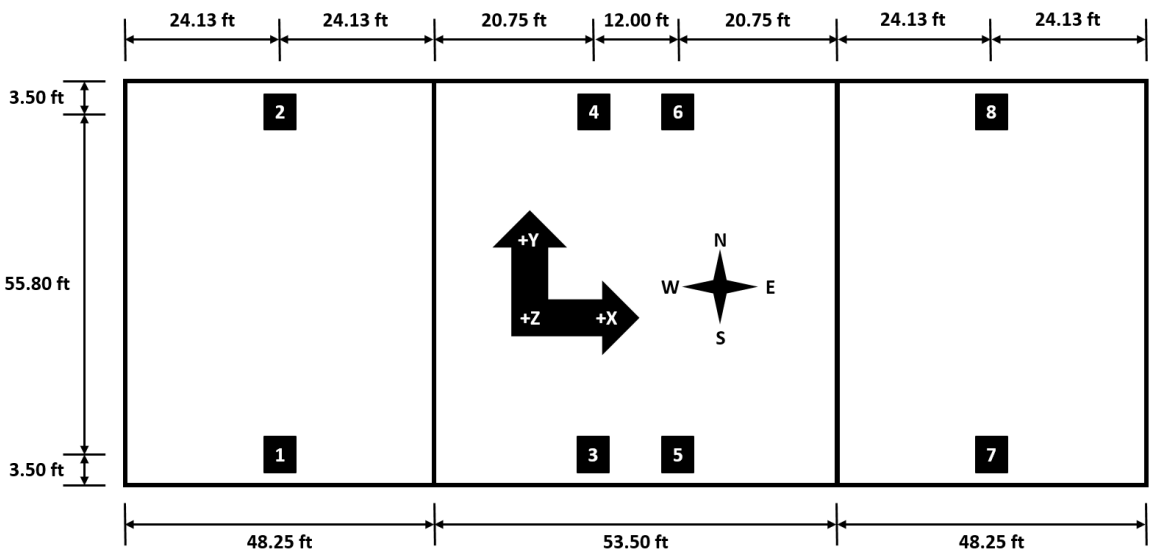

Figure 4.6: Sensor locations capturing the global response for bridge S080 40872R.

Table 4.3: Sensor information of the global response setup for bridge S080 40872R.

Sensor Location	Sensor Type	Sensor Id	Calibration Factor (mV/g)
1	WSN	848Z	--
2	WSN	997Z	--
3	WSN	968Z	--
4	WSN	99CZ	--
5	WSN	995Z	--
6	WSN	99DZ	--
7	WSN	996Z	--
8	WSN	99FZ	--

Date of Collection	10/17/2016
Length of Data (min)	74.53
Sampling Rate (Hz)	256

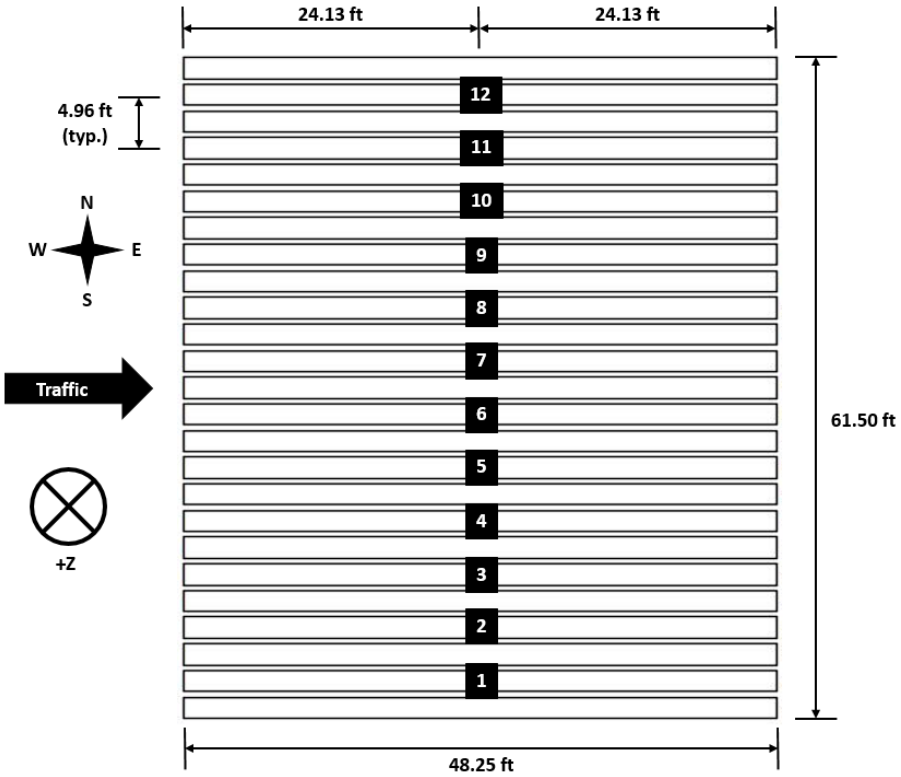

Figure 4.7: Sensor locations capturing the local response for bridge S080 40872R.

Table 4.4: Sensor information of the local response setup for bridge S080 40872R.

Sensor Location	Sensor Type	Sensor Id	Calibration Factor (mV/g)
1	PCB	N1	1001
2	PCB	N2	997
3	PCB	N3	1019
4	PCB	N4	1065
5	PCB	N9	1000
6	PCB	N10	977
7	PCB	N11	987
8	PCB	N12	1027
9	PCB	N5	1006
10	PCB	N6	993
11	PCB	N7	986
12	PCB	N8	998

Date of Collection	3/21/2017
Length of Data (min)	58.89
Sampling Rate (Hz)	2048

4.3 OPERATIONAL MODAL ANALYSIS

Operational modal analysis is performed to determine the dynamic characteristics and responses of the bridges under random traffic loads. This section will explain the general process of operational modal analysis used for the instrumented bridges along with a detailed example for bridge S080 40872R. All figures and tables in this section are from data processed for both the deck and girder setups at bridge S080 40872R.

4.3.1 DATA FILTERING

The raw acceleration time histories are filtered initially before any further processing or analysis. This is done to remove any bias in the collected data due to bracket installation or electronic shorts. First, a Hampel identifier outlier removal is used to remove unrepresentative spikes in the data based on an input parameter of filter order (Table 4.5). Second, a finite impulse response (FIR) bandpass filter is used to remove unwanted frequencies outside of the specified range. This filter requires input parameters of filter order, lower cutoff frequency, and upper cutoff frequency (Table 4.5). The cutoff frequencies are set to acquire approximately the first five natural frequencies of the bridge. After applying these data filters, the filtered acceleration time histories (Figure 4.8 & Figure 4.9) can be analyzed in the frequency and time domain. The root mean square (RMS) values for each sensor are calculated for the filtered acceleration data (Table 4.6 & Table 4.7).

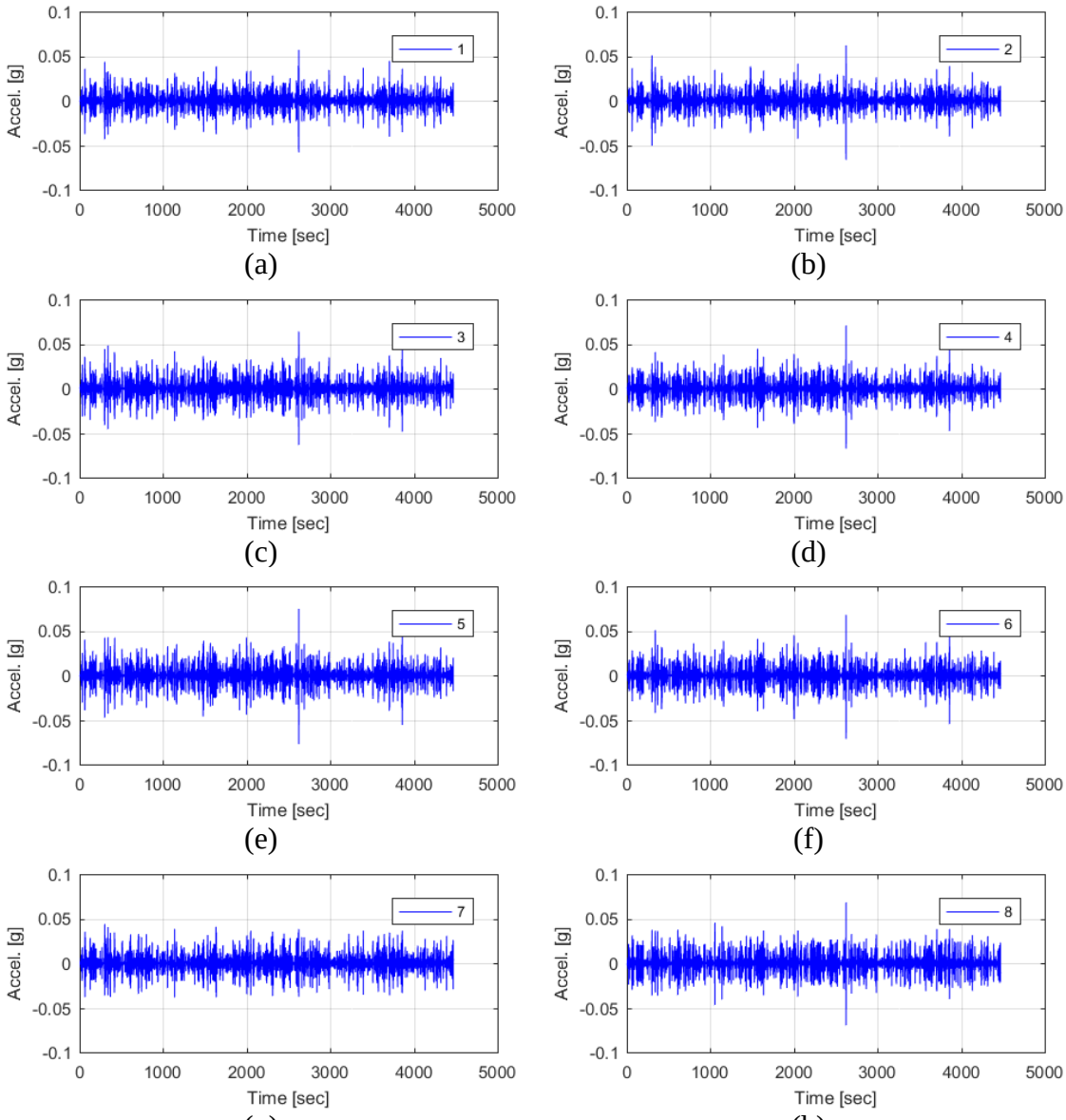

Figure 4.8: Filtered acceleration data of the global response for bridge S080 40872R.

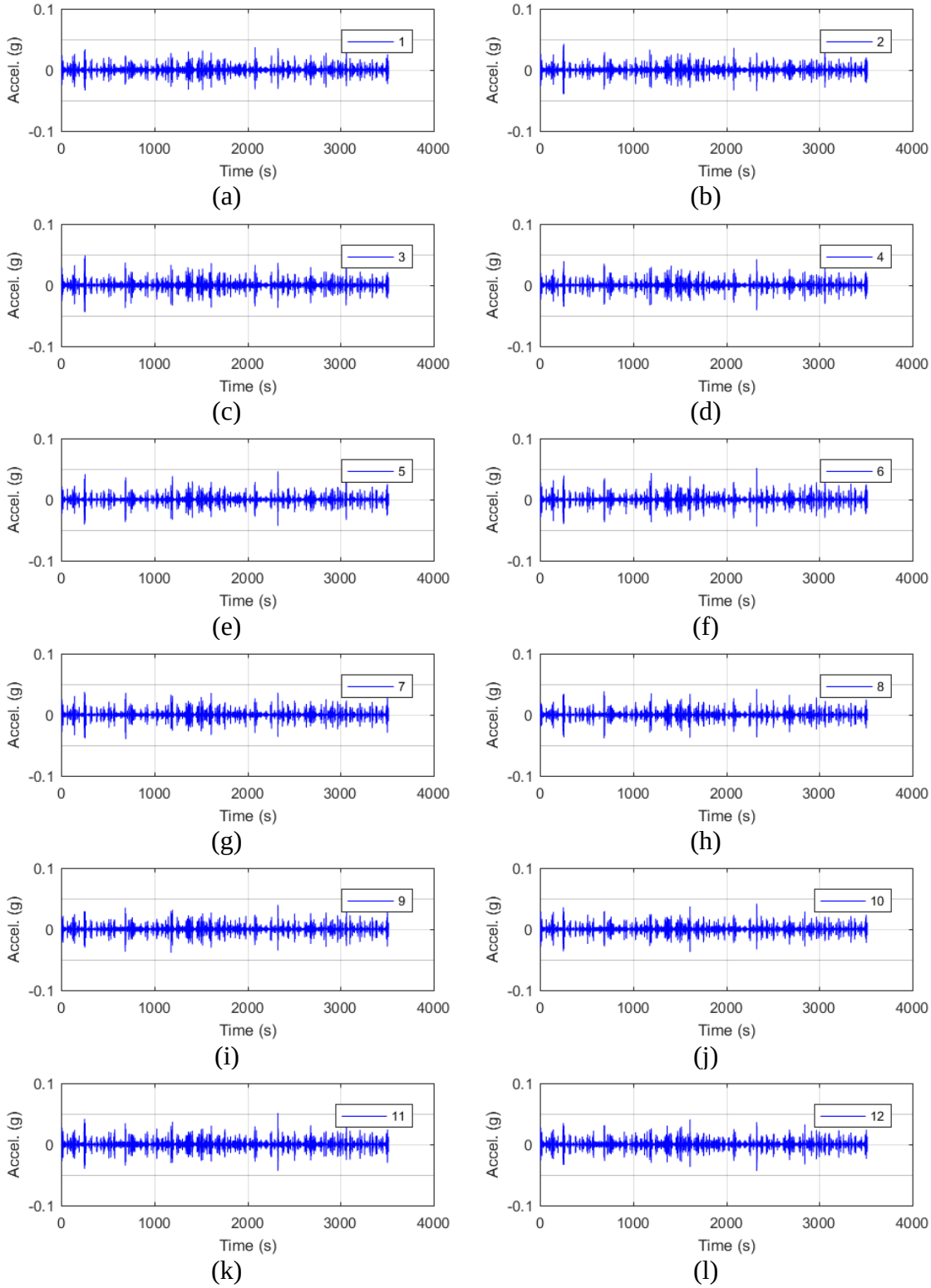

Figure 4.9: Filtered acceleration data of the local response for bridge S080 40872R.

Table 4.5: Filter parameters of the global and local responses for bridge S080 40872R.

Filter Parameter	Value
Hampel Identifier Order	10
FIR Bandpass Filter Order (for global response only)	3072
FIR Bandpass Filter Order (for local response only)	24576
FIR Bandpass Filter Lower Cutoff Frequency (Hz)	7
FIR Bandpass Filter Upper Cutoff Frequency (Hz)	19
Tukey Averaging Window (min)	1.5

Table 4.6: Filtered acceleration RMS values of the global response for bridge S080 40872R.

Sensor	Filtered a_{RMS} (μg)
1	2900
2	2822
3	3211
4	3081
5	3358
6	3291
7	3002
8	3192

Table 4.7: Filtered acceleration RMS values of the local response for bridge S080 40872R.

Sensor	Filtered a_{RMS} (μg)
1	2140
2	2175
3	2324
4	2156
5	2129
6	2385
7	2198
8	2109
9	2201
10	2167
11	2399
12	2226

4.3.2 FREQUENCY DOMAIN ANALYSIS

A fast Fourier transform (FFT) is used to convert the filtered acceleration time history for a single sensor into the frequency domain. Multiple FFTs of the segmented time history data are averaged using Tukey windows to produce the power spectral density (PSD) versus frequency plots (Figure 4.10 & Figure 4.11). An estimation technique called the peak-picking method selects localized maxima in the frequency plots to provide approximate natural frequency values (Table 4.8 & Table 4.9). Natural frequencies are the frequencies of vibration that a structure will tend towards and a function of the mass and stiffness distributions in the bridge system. Peak-picking is performed only to provide a quick estimate of the frequencies of the bridge system. This will provide guidance when performing the time domain system identification analysis.

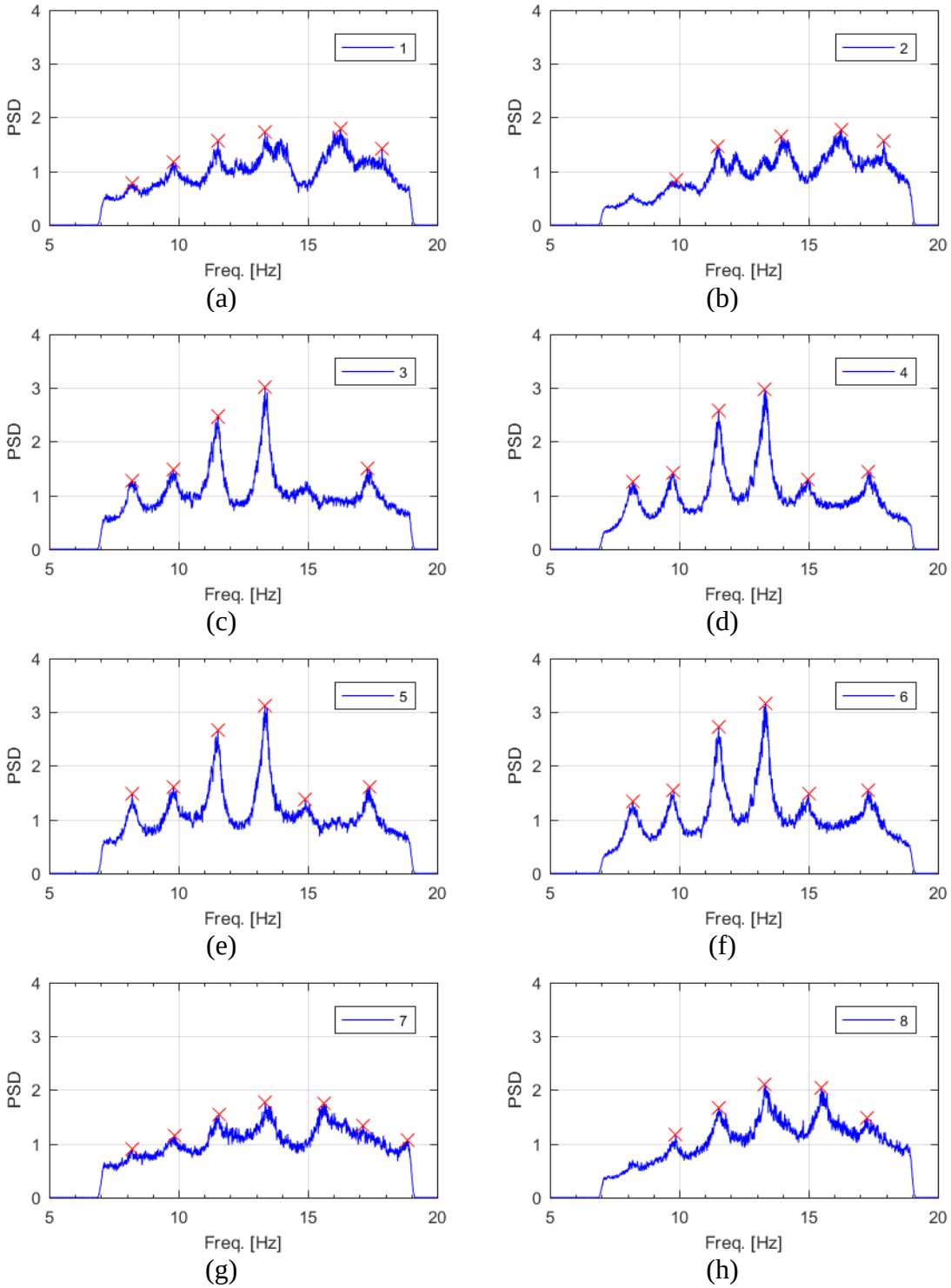

Figure 4.10: Frequency content of the filtered acceleration data and peak-picking frequencies of the global response for bridge S080 40872R.

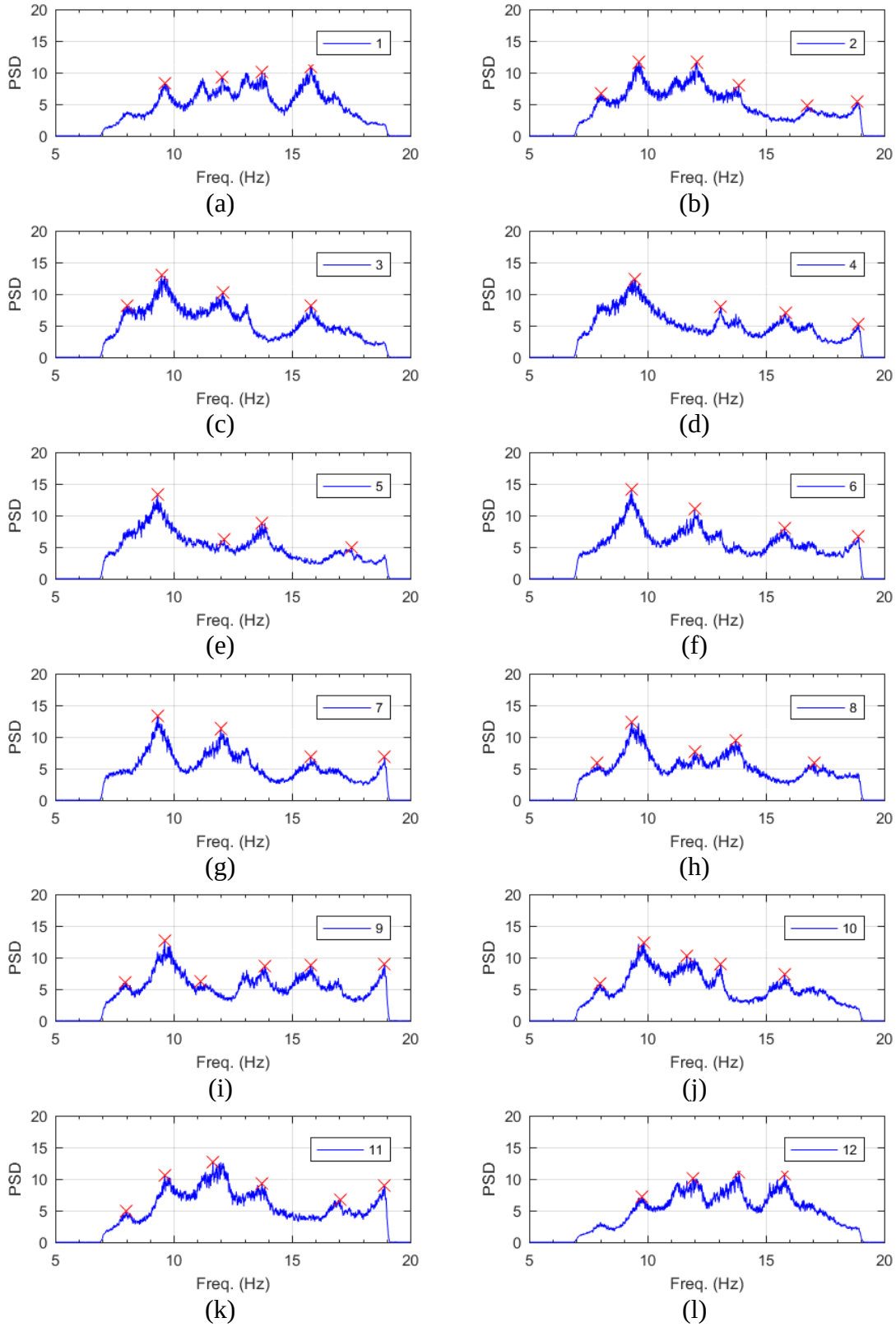

Figure 4.11: Frequency content of the filtered acceleration data and peak-picking frequencies of the local response for bridge S080 40872R.

Table 4.8: Peak-picking frequencies of the global response for bridge S080 40872R.

Mode	Individual Sensor Frequencies (Hz)							
	1	**2**	**3**	**4**	**5**	**6**	**7**	**8**
1	8.20	--	8.21	8.21	8.21	8.21	8.20	--
2	9.80	9.89	9.79	9.77	9.81	9.78	9.86	9.87
3	11.52	--	11.52	11.52	11.52	11.52	11.56	11.53
4	13.35	--	13.35	13.32	13.35	13.35	13.36	13.32
5	--	13.95	--	--	--	--	--	--

Table 4.9: Peak-picking frequencies of the local response for bridge S080 40872R.

Mode	Individual Sensor Frequencies (Hz)					
	1	**2**	**3**	**4**	**5**	**6**
$1_{midspan}$	--	8.05	8.05	--	--	--
1	--	--	9.49	9.46	9.32	9.32
2	9.64	9.64	--	--	--	--
3	12.05	12.08	12.08	--	12.14	11.99
4	13.73	13.85	--	13.09	13.74	--
5	15.78	--	15.78	15.82	--	15.79

Mode	Individual Sensor Frequencies (Hz)					
	7	**8**	**9**	**10**	**11**	**12**
$1_{midspan}$	--	7.88	7.97	8.02	8.02	--
1	9.32	9.35	--	--	--	--
2	--	--	9.62	9.86	9.62	9.74
3	11.99	11.98	11.13	11.66	11.66	11.92
4	--	13.74	13.85	13.09	13.74	13.85
5	15.79	--	15.78	15.79	--	15.79

4.3.3 TIME DOMAIN ANALYSIS

A time domain analysis called the Stochastic Subspace Identification (SSI) technique with the Extended Unweighted Principal Component (UPCX) implementation type generates a stabilization diagram (Figure 4.12 & Figure 4.13). The stabilization diagram helps determine the appropriate vibrational properties of the IT girder bridges, with much greater confidence than the peak-picking technique. These vibrational properties include the natural frequencies, damping ratios, operational deflection shapes

(ODS), and ODS complexity factors (Table 4.10 & Table 4.11). A damping ratio is a decay of vibration for a given frequency of a system expressed in percent of critical damping. A disclaimer is that the damping ratios are not completely reliable under ambient loads, due to the low level of excitation. An ODS is a relative vibration pattern of a structure for a given frequency under operating loads. In many scenarios, an ODS is equivalent to a mode shape. An ODS complexity factor is a relation to a real-valued classically damped mode. An ODS complexity factor of 0% corresponds to a real mode and 100% corresponds to an imaginary mode. ODS complexity factors will also increase when the modes demonstrate a “wave-like” or non-synchronized response, which can be existent in torsional responses.

The ODS coordinates and illustrations for the global and local response of bridge S080 40872R are shown in Table 4.12 & Table 4.13 and Figure 4.14 & Figure 4.15, respectively. The first ODS of the local response for bridge S080 40872R shows a nonuniform vertical deflection response along the bridge cross-section. When the coordinate value of the center girder is 1.00, the farthest out girders are at 0.31 and 0.21. This differential response between adjacent IT girders observed within the ODS is noteworthy and likely contributes to the longitudinal deck cracking. The local bridge response has an unusual wave-like motion due to the phase delay. This phase delay is the reason for the high ODS complexity factor for the fundamental mode.

Modal Assurance Criterion (MAC) values are computed to compare two ODS. The two ODS are consistent when MAC values equal one and inconsistent when MAC values equal zero. The MAC values for bridge S080 40872R (Table 4.14 & Table 4.15 and Figure 4.16 & Figure 4.17) are low, which means the ODS are unique (inconsistent), well-separated, and independent of each other, as anticipated for most civil infrastructure.

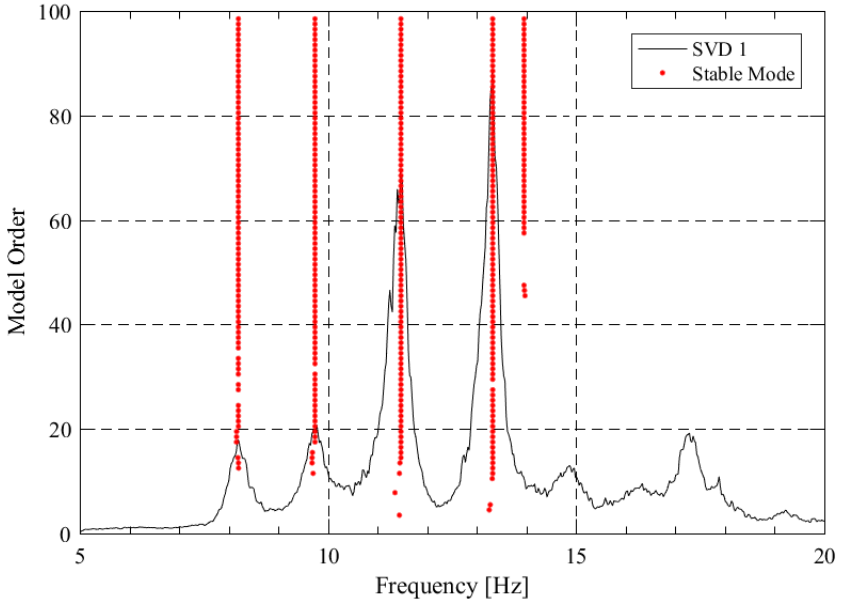

Figure 4.12: SSI-UPCX method stabilization diagram of the global response for bridge S080 40872R.

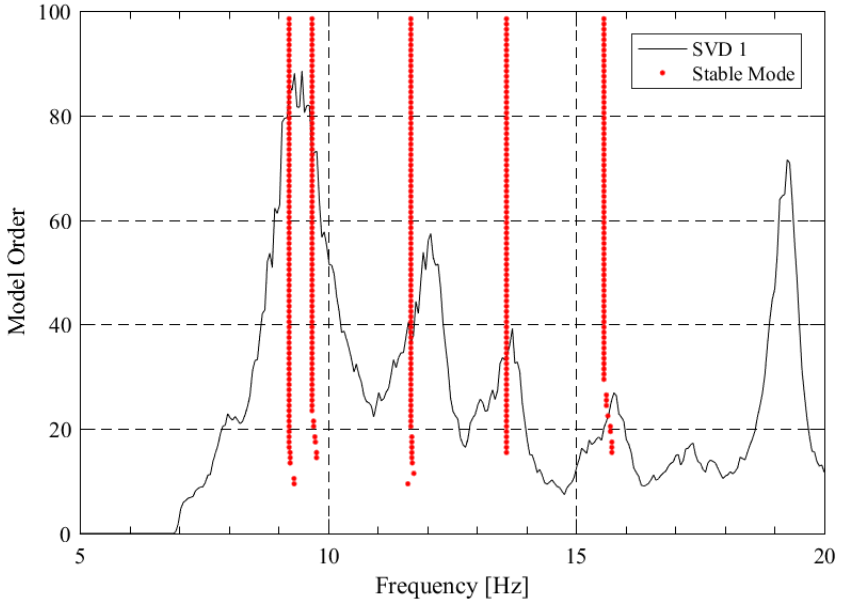

Figure 4.13: SSI-UPCX method stabilization diagram of the local response for bridge S080 40872R.

Table 4.10: SSI-UPCX method dynamic properties of the global response for bridge S080 40872R.

Mode	Frequency (Hz)	Damping (%)	Complexity (%)
1	8.18	2.90	20.90
2	9.73	3.07	13.00
3	11.47	2.00	12.99
4	13.31	1.63	16.72
5	13.95	2.80	40.17

Table 4.11: SSI-UPCX method dynamic properties of the local response for bridge S080 40872R.

Mode	Frequency (Hz)	Damping (%)	Complexity (%)
1	9.22	5.70	33.07
2	9.69	7.19	5.79
3	11.67	5.53	3.08
4	13.60	7.63	12.20
5	15.57	7.43	28.45

Table 4.12: Operational deflected shape coordinates of the global response for bridge S080 40872R.

Sensor	ODS Coordinates				
	Mode 1	**Mode 2**	**Mode 3**	**Mode 4**	**Mode 5**
1	-0.23	-0.42	-0.38	-0.37	1.00
2	0.21	-0.25	0.32	-0.21	-0.84
3	0.86	0.91	0.92	0.93	-0.15
4	-0.68	0.90	-0.86	0.87	0.42
5	1.00	1.00	1.00	1.00	0.03
6	-0.66	0.91	-0.91	0.92	0.42
7	-0.22	-0.51	-0.33	-0.26	0.39
8	0.19	-0.37	0.30	-0.23	-0.39

Table 4.13: Operational deflected shape coordinates of the local response for bridge S080 40872R.

Sensor	ODS Coordinates				
	Mode 1	Mode 2	Mode 3	Mode 4	Mode 5
1	0.31	-0.40	0.62	0.90	1.00
2	0.61	-0.62	0.84	1.00	0.10
3	0.80	-0.62	0.74	0.44	-0.86
4	0.93	-0.40	0.22	-0.46	-0.71
5	0.96	-0.16	-0.37	-0.78	0.19
6	0.99	0.13	-0.76	-0.32	0.88
7	1.00	0.47	-0.82	0.38	0.59
8	0.87	0.71	-0.39	0.94	-0.32
9	0.76	0.91	0.26	0.72	-0.90
10	0.60	1.00	0.83	-0.18	-0.60
11	0.39	0.83	1.00	-1.00	0.37
12	0.21	0.51	0.70	-0.88	0.97

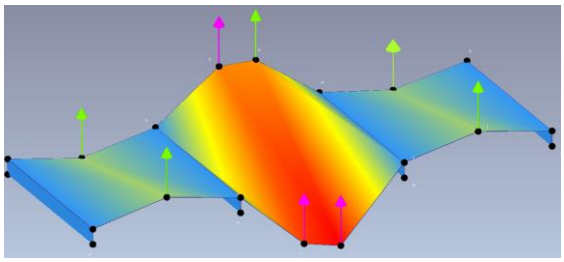

(a) Mode 1

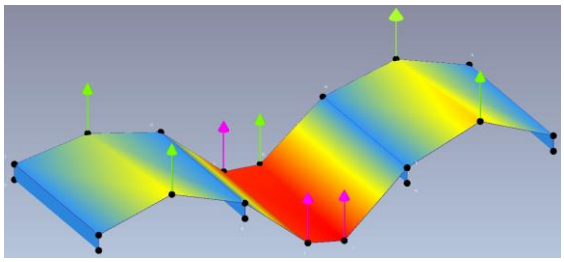

(b) Mode 2

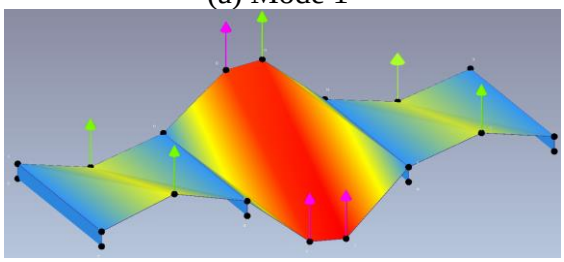

(c) Mode 3

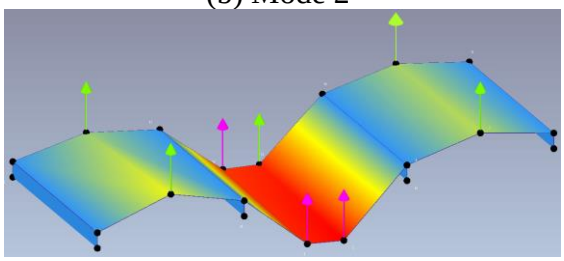

(d) Mode 4

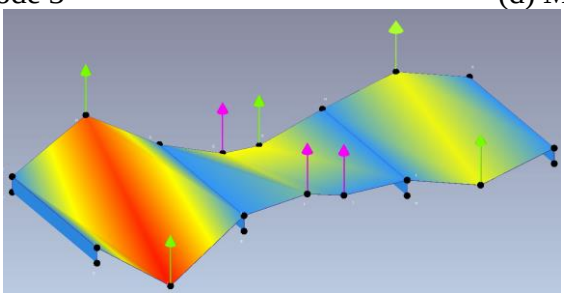

(e) Mode 5

Figure 4.14: Operational deflected shapes of the global response for bridge S080 40872R.

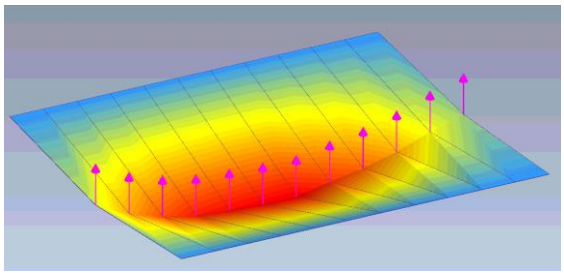

(a) Mode 1

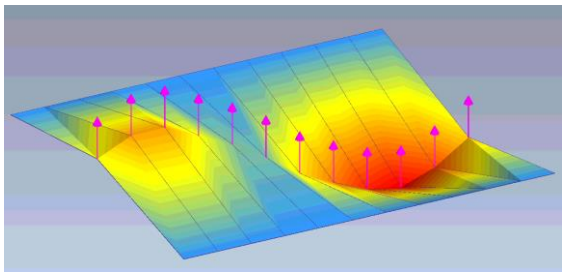

(b) Mode 2

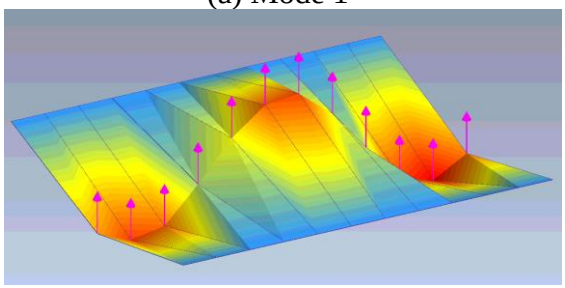

(c) Mode 3

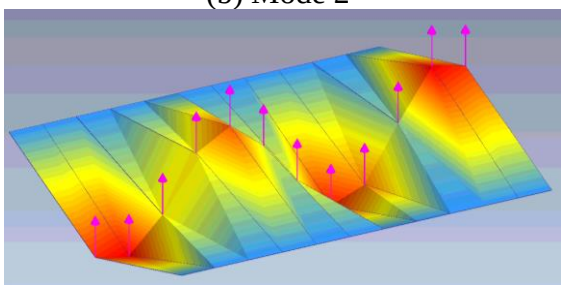

(d) Mode 4

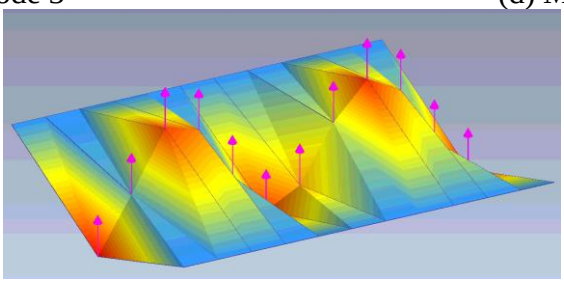

(e) Mode 5

Figure 4.15: Operational deflected shapes of the local response for bridge S080 40872R.

Table 4.14: MAC values of the global response for bridge S080 40872R.

MAC	Mode 1	Mode 2	Mode 3	Mode 4	Mode 5
Mode 1	1.000	0.052	0.953	0.060	0.220
Mode 2	0.052	1.000	0.018	0.979	0.026
Mode 3	0.953	0.018	1.000	0.015	0.312
Mode 4	0.060	0.979	0.015	1.000	0.030
Mode 5	0.220	0.026	0.312	0.030	1.000

Table 4.15: MAC values of the local response for bridge S080 40872R.

MAC	Mode 1	Mode 2	Mode 3	Mode 4	Mode 5
Mode 1	1.000	0.081	0.005	0.067	0.006
Mode 2	0.081	1.000	0.038	0.005	0.020
Mode 3	0.005	0.038	1.000	0.034	0.080
Mode 4	0.067	0.005	0.034	1.000	0.042
Mode 5	0.006	0.020	0.080	0.042	1.000

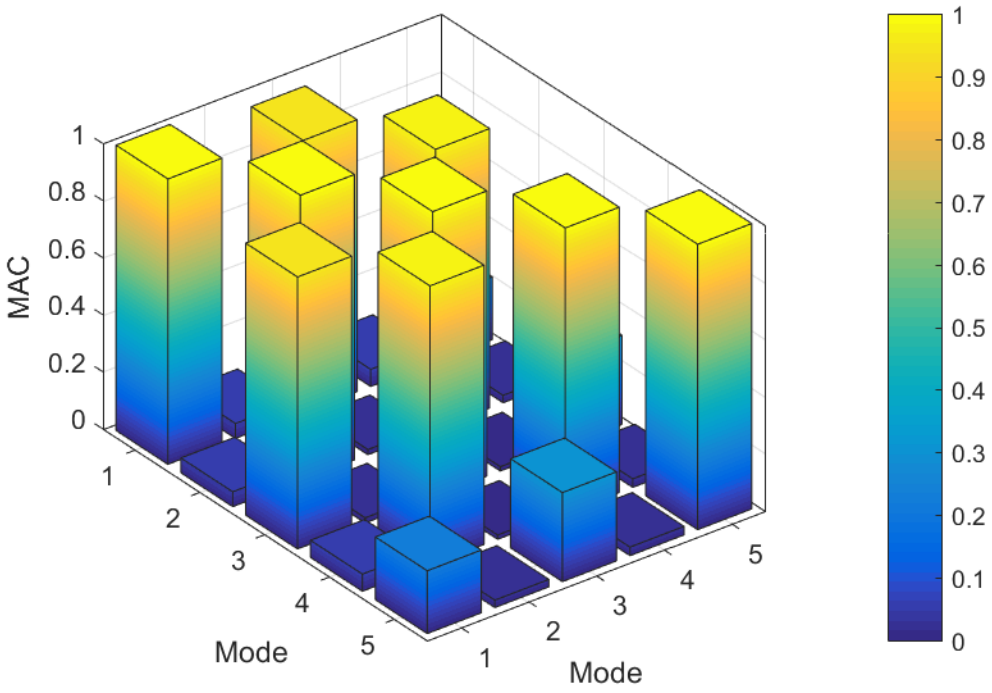

Figure 4.16: MAC values of the global response for bridge S080 40872R.

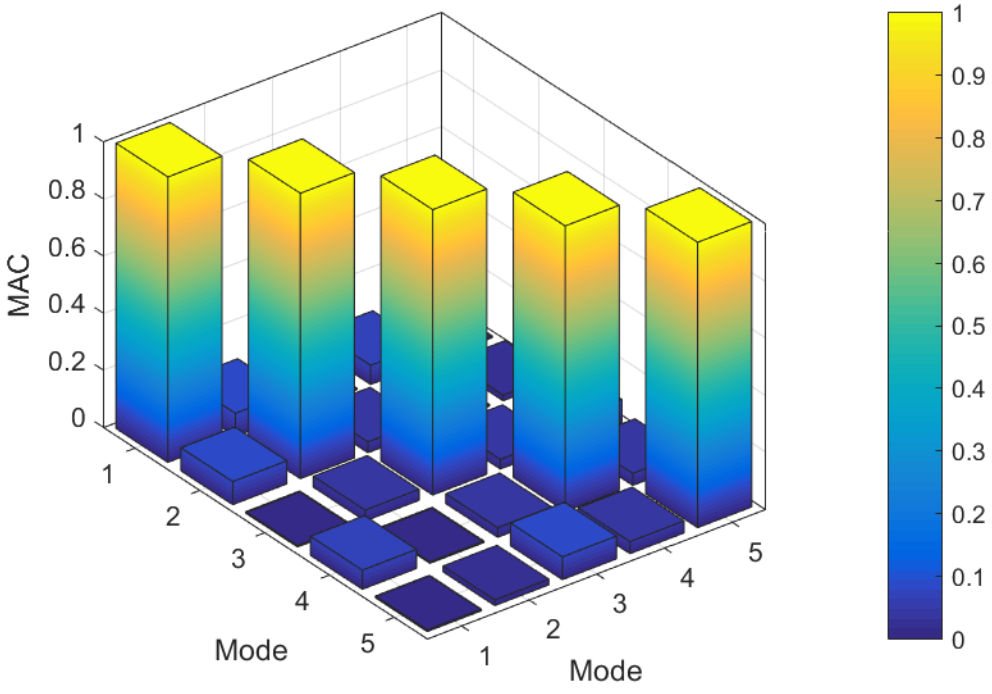

Figure 4.17: MAC values of the local response for bridge S080 40872R.

4.4 SUMMARY OF FIELD ASSESSMENTS FOR ALL IT BRIDGES

Operational modal analysis was performed for the remaining instrumented IT girder bridges. Table 4.16 summarizes the key variables for data filtering and processing. Table 4.17 presents the identified natural frequencies for the instrumented IT girder bridges. After processing and evaluating the field assessments, the results suggest that live loads contribute to the predominate independent response of the girders and corresponding deck cracking. The excitation due to the live loads dominantly resonates higher modes ranging from around 10 to 15 Hz for a typical IT girder bridge system. The independent response of the IT girders is contributing to the longitudinal deck cracking. There is no significant benefit to the bridge dynamic response when increasing the deck thickness from six to eight inches. Figure 4.18 shows the first ODS of the local response, with noticeable gradients between girders, for bridges S089 06047 (6-inch deck), S080 40872R (8-inch deck), and S080 40927R (8-inch deck) along the cross-section at midspan. These three ODS were linearly interpolated to compute the MAC values between them. The MAC values are provided in Table 4.18.

Table 4.16: Summary of the data filtering and processing variables for the instrumented IT girder bridges.

Bridge ID	Setup Type	Hampel Identifier Order	FIR Bandpass Filter			Tukey Averaging Window (min)
			Order	Lower Cutoff Frequency (Hz)	Upper Cutoff Frequency (Hz)	
S006 26001	Deck (Global)	--	2048	8	28	1.5
S009 00888		--	2048	10	28	1.5
S020 32260		8	4096	8	28	1.5
S058 00994		--	4096	5	28	1.5
S080 40872R		10	3072	7	19	1.5
S081 05152L		--	2048	5	25	1.5
S089 06047		--	2048	6	18	1.5
C008504145		--	4096	5	37	1.5
M011022220		--	4096	4	37	1.5
S006 26001	Girder (Local)	--	4096	8	23	1.5
S080 40872R		10	24576	7	19	1.5
S080 40927R		10	24576	7	19	1.5
S089 06047		--	8192	6	18	1.5

Table 4.17: Summary of the identified natural frequencies for the instrumented IT girder bridges.

Bridge ID	Setup Type	Identified Frequency (Hz)						
		Mode 1	Mode 2	Mode 3	Mode 4	Mode 5	Mode 6	Mode 7
S006 26001	Deck (Global)	10.64	12.49	12.89	14.09	15.27	15.99	--
S009 00888		11.44	13.69	15.71	17.75	--	--	--
S020 32260		8.96	11.10	13.02	15.89	20.28	26.28	--
S058 00994		7.85	10.23	12.87	13.47	14.03	17.09	17.34
S080 40872R		8.18	9.73	11.47	13.31	13.95	--	--
S081 05152L		6.05	7.82	9.91	11.90	--	--	--
S089 06047		7.37	9.79	12.55	14.79	15.28	--	--
C008504145		6.83	8.59	10.38	13.27	20.15	--	--
M011022220		5.46	7.66	10.41	14.31	20.23	--	--
S006 26001	Girder (Local)	10.65	12.28	12.64	15.24	16.92	--	--
S080 40872R		9.22	9.69	11.67	13.60	15.57	--	--
S080 40927R		9.25	9.74	11.67	13.63	15.59	--	--
S089 06047		7.34	9.42	11.67	12.67	15.33	--	--

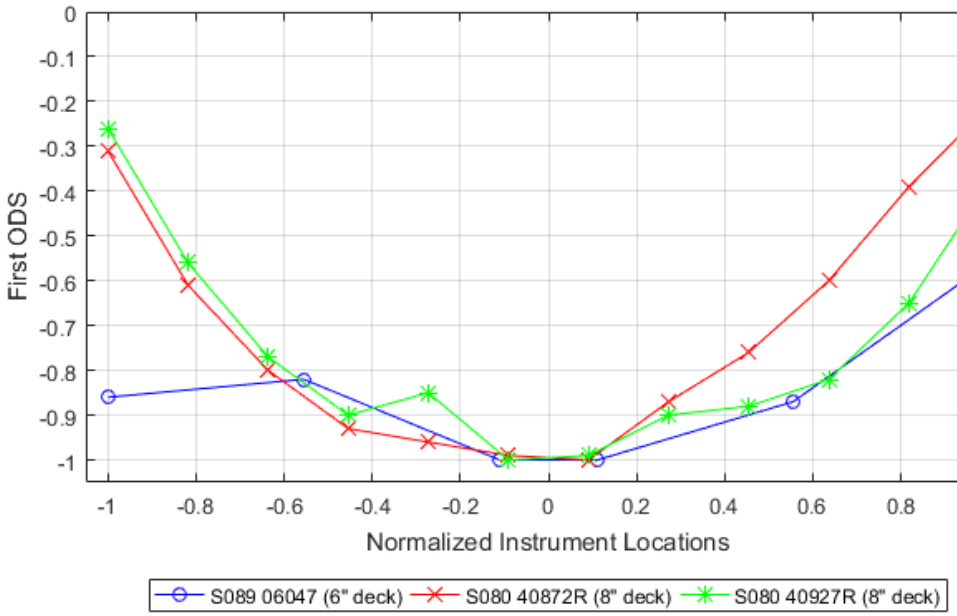

Figure 4.18: First ODS of the local response for the three IT girder bridges along the cross-section at midspan with normalized instrument locations.

Table 4.18: MAC values for the first ODS of the local response for the three IT girder bridges with normalized instrument locations.

Bridge	**S089 06047 (6" deck)**	**S080 40872R (8" deck)**	**S080 40927R (8" deck)**
S089 06047 (6" deck)	1.000	0.906	0.918
S080 40872R (8" deck)	0.906	1.000	0.976
S080 40927R (8" deck)	0.918	0.976	1.000

4.5 FIELD ASSESSMENT ANALYSIS

An analysis of the factors that influence the dynamic characteristics of a bridge is performed. These trends are constructed to guide the parametric analytical studies and future work. Comparison plots are created to seek linear or higher-order relationships between the first two natural frequencies with the various bridge parameters. Linear trends are found in the following bridge parameters: first three modal frequencies (Figure 4.19), maximum span length (Figure 4.20), mean span length (Figure 4.21), minimum clear span length (Figure 4.22), and mean clear span length (Figure 4.23). The most reliable trend for a bridge parameter is the mean clear span length plotted against the first two natural frequencies with R-squared values of 0.751 and 0.785, respectively. The following bridge parameters are also considered; however, no trends are found: maximum clear span length, girder height, number of girders, girder spacing, width of bridge, and bridge skew angle. Plots for these parameters can be found in Appendix D.

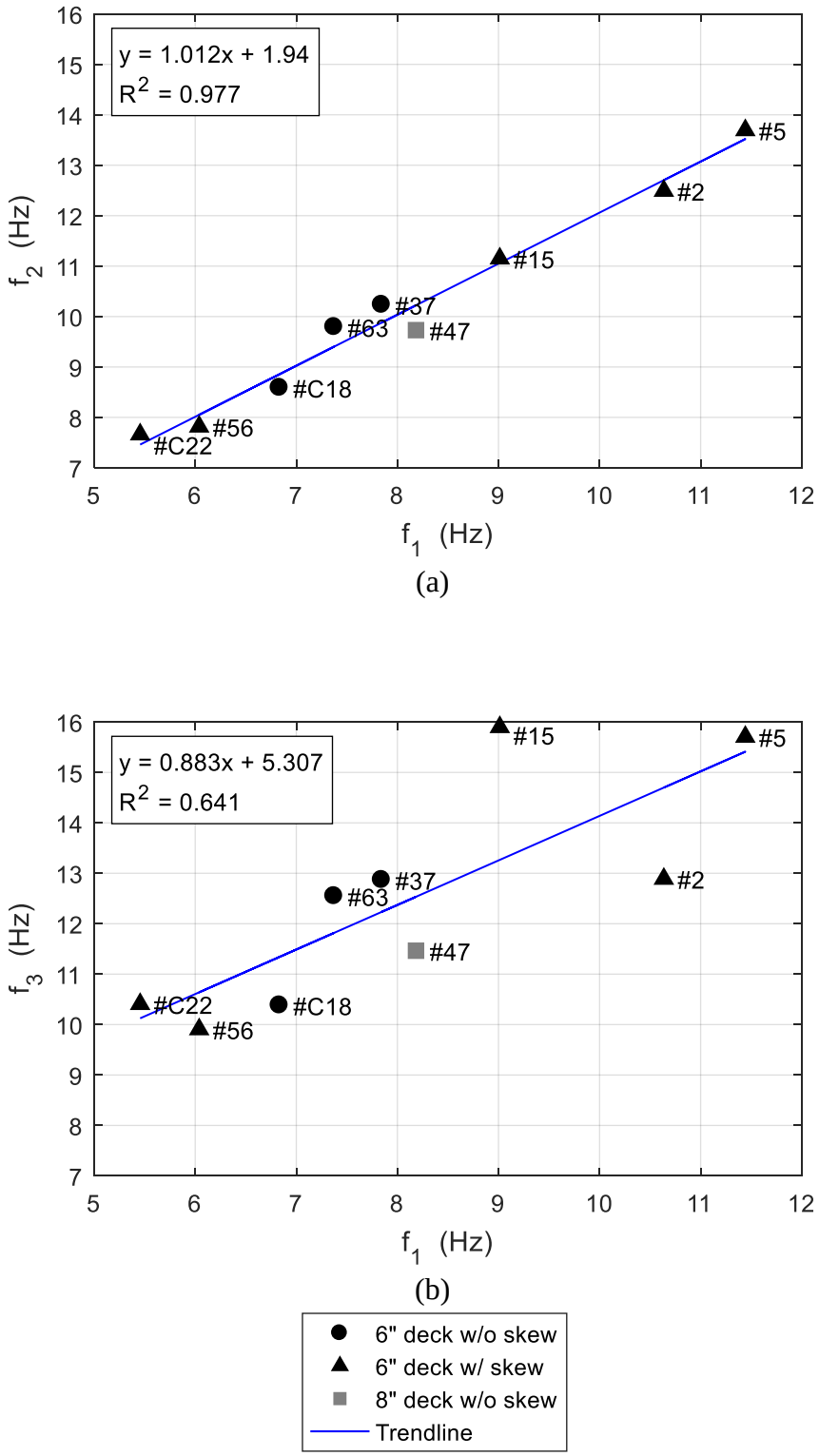

Figure 4.19: System identification comparison of the modal frequencies with a trendline for the instrumented IT bridges.

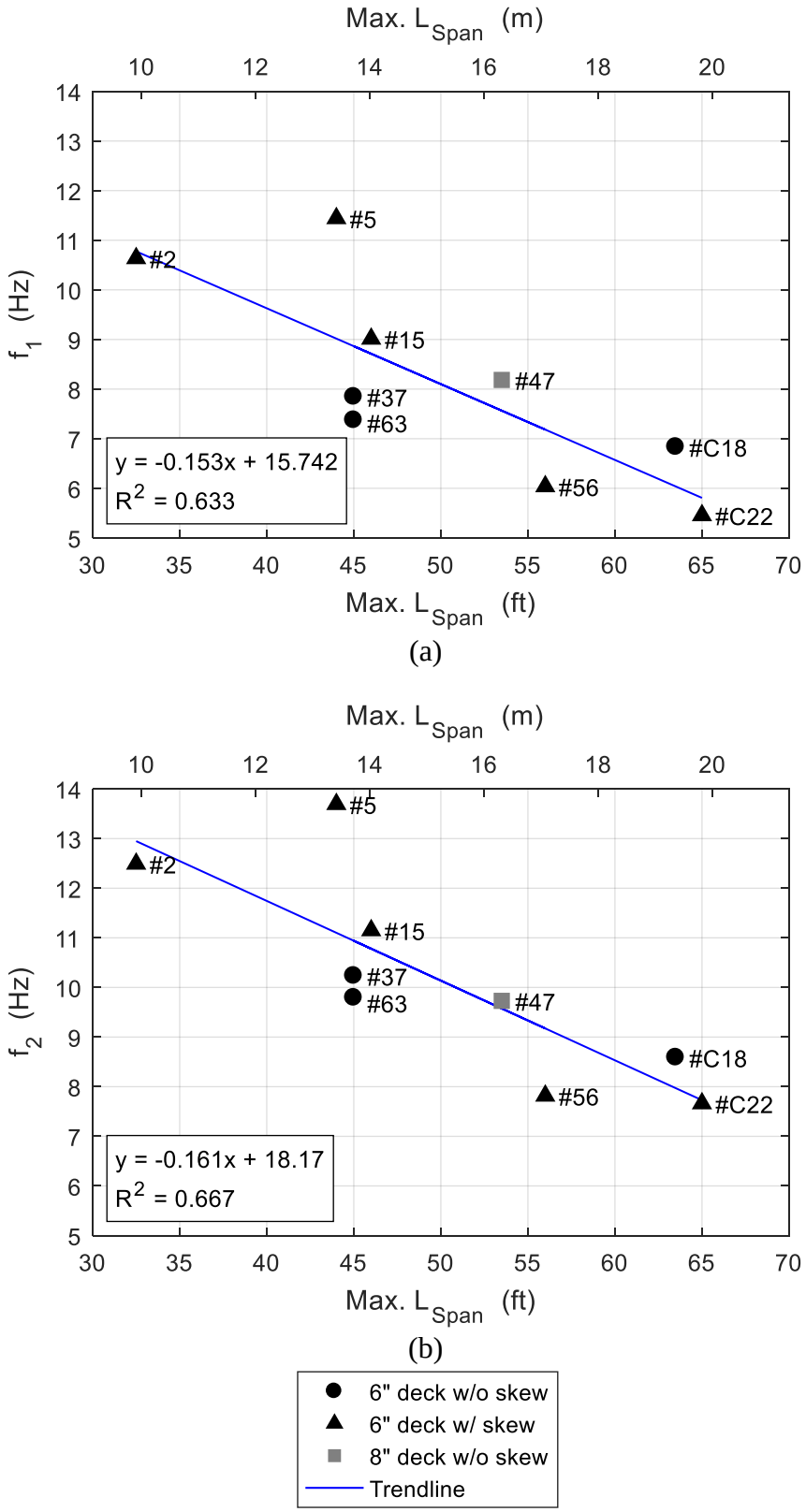

Figure 4.20: System identification comparison of the maximum span length with a trendline for the instrumented IT bridges.

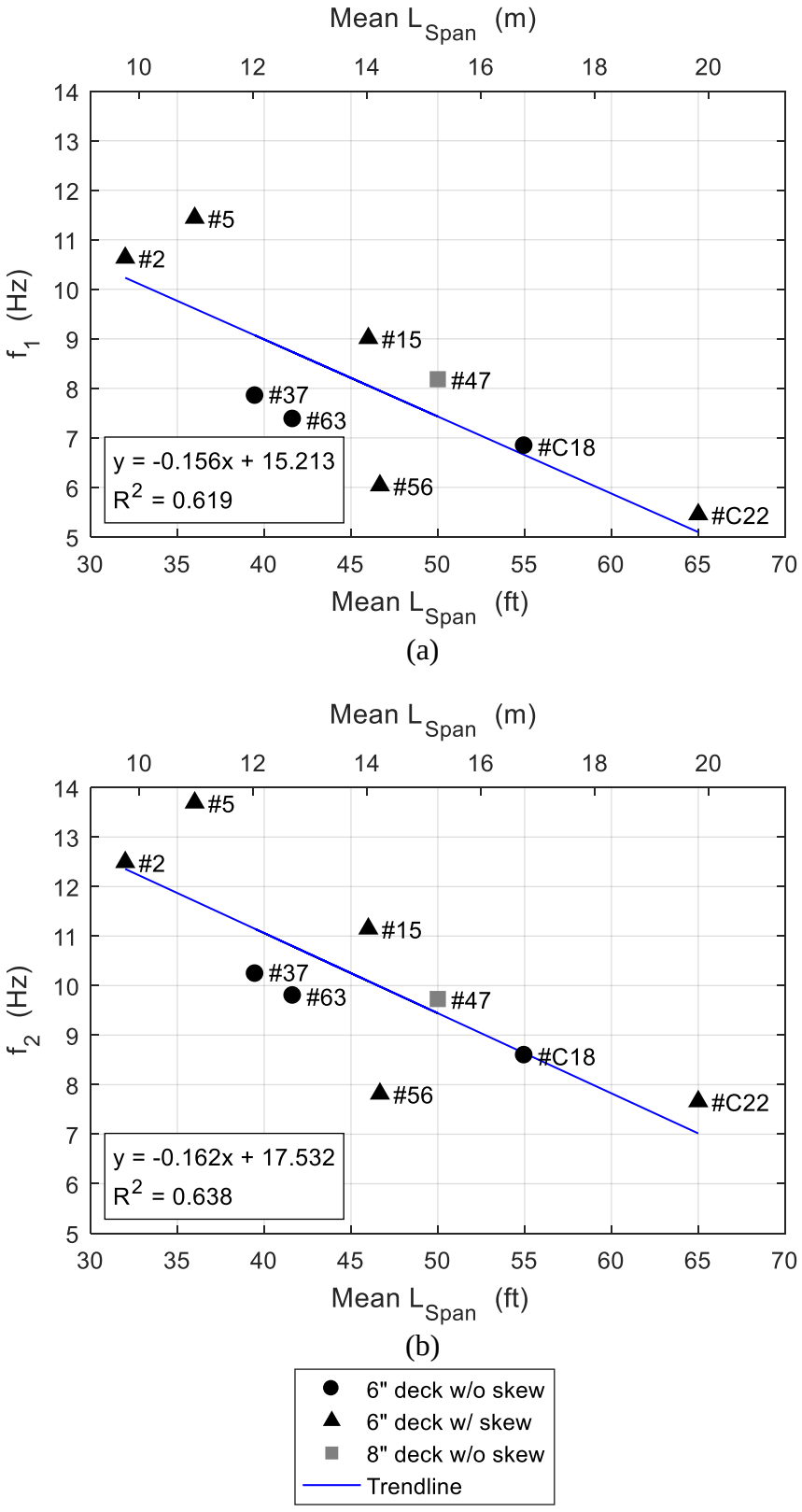

Figure 4.21: System identification comparison of the mean span length with a trendline for the instrumented IT bridges.

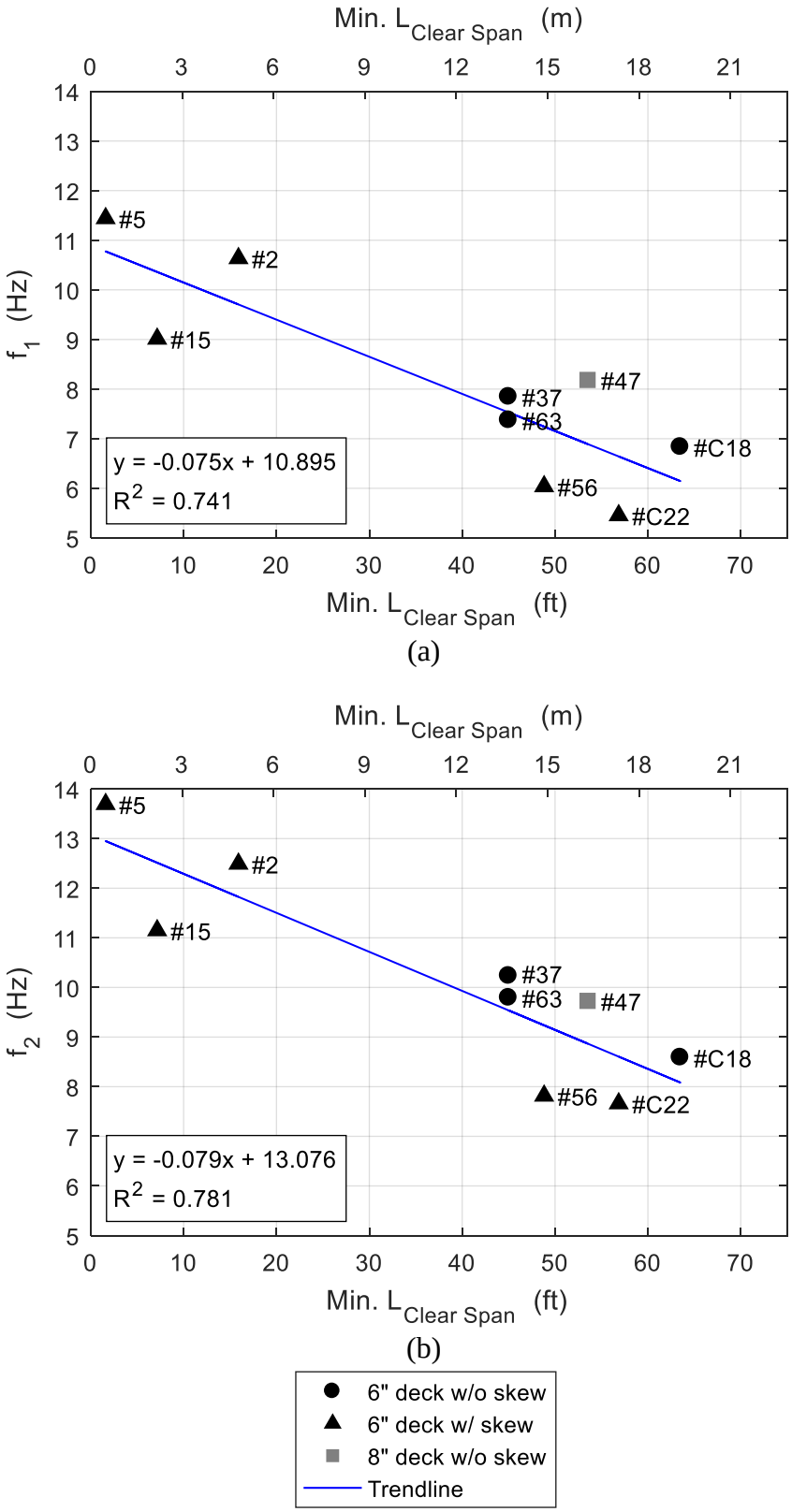

Figure 4.22: System identification comparison of the minimum clear span length with a trendline for the instrumented IT bridges.

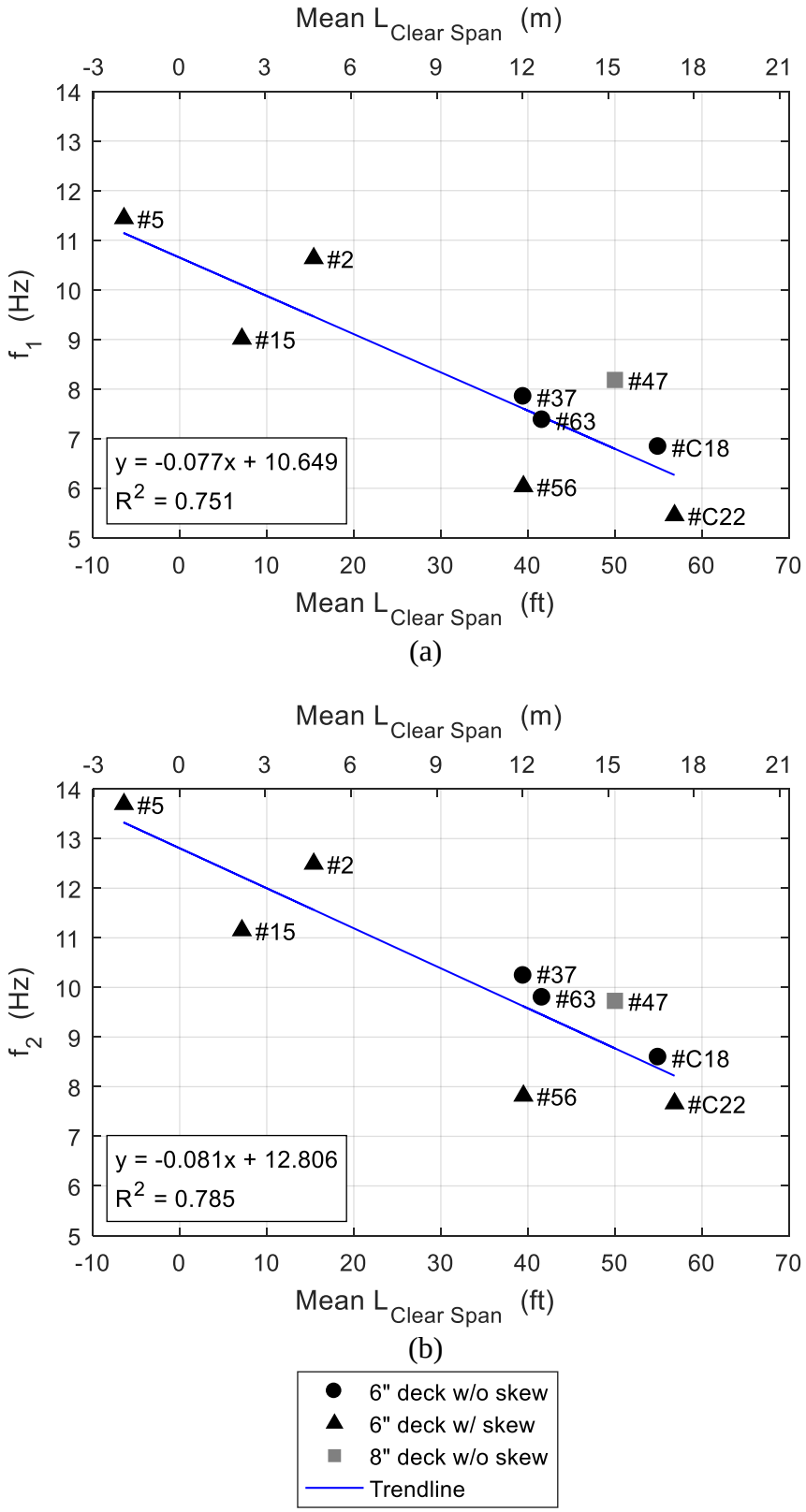

Figure 4.23: System identification comparison of the mean clear span length with a trendline for the instrumented IT bridges.

4.6 COMPARISON TO OTHER SYSTEMS

To demonstrate if the IT girder bridge system behavior was unique in comparison to other bridge systems, two comparable bridges were instrumented for verification. One slab bridge (S080 38614R) and one NU girder bridge (S080 40797R) were instrumented to compare the responses to the local response of an IT girder bridge (S080 40872R). The results and conclusions presented within this section may not represent all slab and NU girder bridges. These three bridges are located on I-80 eastbound lanes near Lincoln and have similar traffic patterns (as well as similar collection times of day). The IT girder bridge and the NU girder bridge are located within 1 mile of each other. The IT girder bridge and the slab bridge are approximately 22.5 miles apart.

4.6.1 SLAB BRIDGE

Operational modal analysis was performed for slab bridge S080 38614R. Information and properties of this bridge are given in Table 4.19. Four PCB accelerometers were placed on the bottom side of the slab on the westmost span. The sensor setup is shown in Figure 4.24 and Table 4.20. The slab bridge is similar in stiffness compared to a typical IT girder bridge since modal frequencies are within the same range (Table 4.21). The ODS coordinates and illustrations for the response of the slab bridge are shown in Table 4.22 and Figure 4.25, respectively. The first ODS shows a more uniform and dependent response across the bridge compared to the IT girder bridge. When the coordinate value of the center of the slab is 1.00, the outsides of the slab are at 0.81 and 0.82.

Table 4.19: Information summary for bridge S080 38614R.

Bridge ID	S080 38614R	**Girder Height (in [mm])**	--
County	Seward	**Girder Width (in [mm])**	--
Year Built	1980	**Girder Spacing (in [mm])**	--
No. of Spans	3	**Deck Thickness (in [mm])**	16.25 [413]
Length Span 1 (ft)	32.00	**No. of Girders**	--
Length Span 2 (ft)	44.00	**Diaphragm**	--
Length Span 3 (ft)	32.00	**Deck Rating**	6
Bridge Width (ft)	37.00	**Superstructure Rating**	6
Skew Angle (°)	0	**Substructure Rating**	7

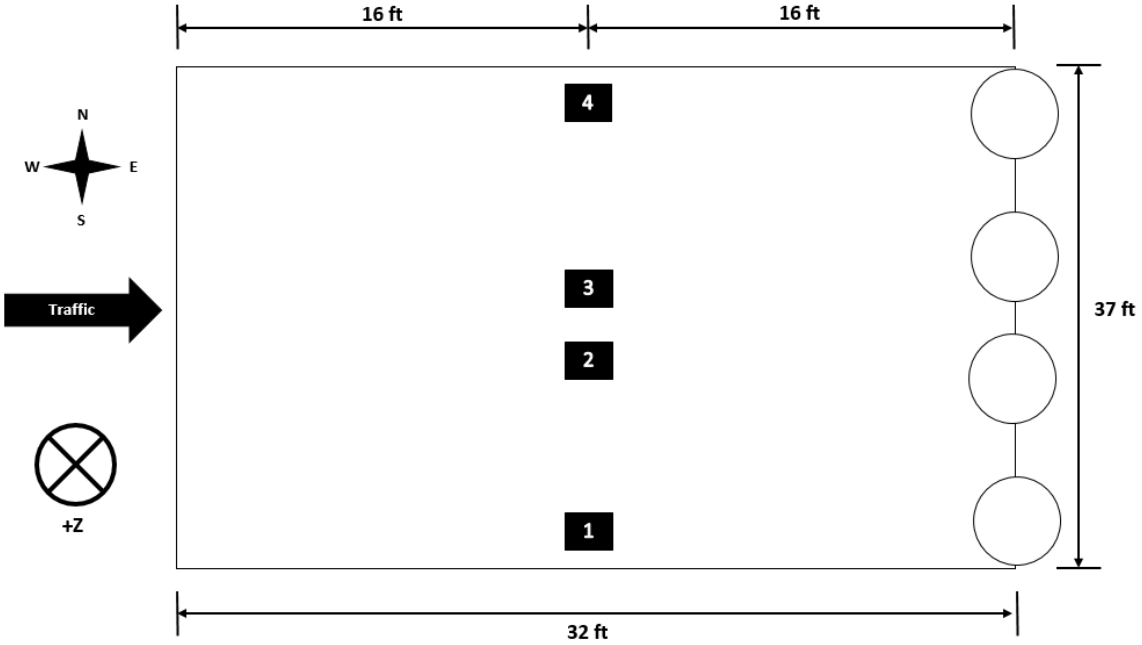

Figure 4.24: Sensor locations capturing the global response for bridge S080 38614R.

Table 4.20: Sensor information of the global response setup for bridge S080 38614R.

Sensor Location	Sensor Type	Sensor Id	Calibration Factor (mV/g)
1	PCB	N1	1001
2	PCB	N2	997
3	PCB	N3	1019
4	PCB	N4	1065

Date of Collection	3/31/2017
Length of Data (min)	67.38
Sampling Rate (Hz)	2048

Table 4.21: SSI-UPCX method dynamic properties of the global response for bridge S080 38614R.

Mode	Frequency (Hz)	Damping (%)	Complexity (%)
1	9.21	9.81	3.54
2	13.66	4.58	3.42
3	17.28	8.07	2.88

Table 4.22: Operational deflected shape coordinates of the global response for bridge S080 38614R.

Sensor	ODS Coordinates		
	Mode 1	Mode 2	Mode 3
1	0.81	0.59	0.66
2	0.98	0.90	1.00
3	1.00	1.00	0.98
4	0.82	0.76	0.53

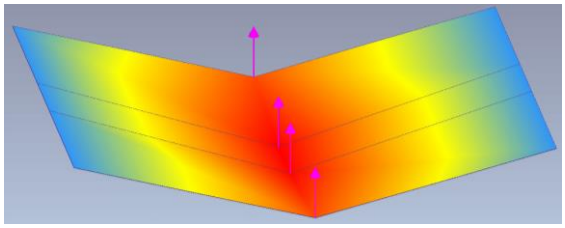

(a) Mode 1

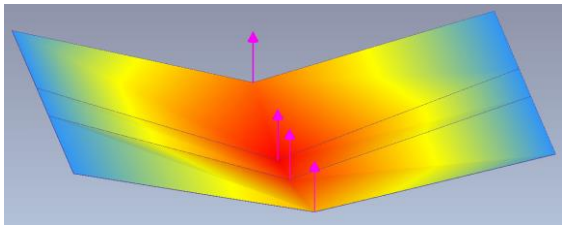

(b) Mode 2

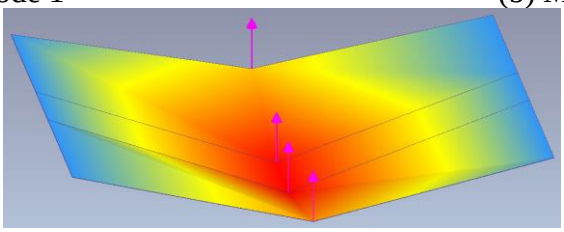

(c) Mode 3

Figure 4.25: Operational deflected shapes of the global response for bridge S080 38614R.

4.6.2 NU GIRDER BRIDGE

Operational modal analysis was performed for NU girder bridge S080 40797R. Information and properties of this bridge are given in Table 4.23. The selected NU girder bridge has interior steel diaphragms at midspan and a 29° skew angle. One PCB accelerometer was placed on the bottom side of each girder (six in total) on the westmost span. The sensor setup is shown in Figure 4.26 and Table 4.24. The 95 ft. NU girder bridge span is a lot more flexible compared to a typical IT girder bridge, resulting in lower modal frequencies (Table 4.25). The ODS coordinates and illustrations for the response of the NU girder bridge are shown in Table 4.26 and Figure 4.27, respectively. The first ODS shows a more uniform and dependent response of the NU bridge girder compared to the IT bridge girders. When the coordinate value of the center girder is 1.00, the farthest out girders are at 0.80 and 0.94.

Table 4.23: Information summary for bridge S080 40797R.

Bridge ID	S080 40797R	**Girder Height (in [mm])**	78.75 [2000]
County	Lancaster	**Girder Width (in [mm])**	38.38 [975]
Year Built	2010	**Girder Spacing (in [mm])**	132 [3353]
No. of Spans	3	**Deck Thickness (in [mm])**	8 [203]
Length Span 1 (ft)	95.00	**No. of Girders**	6
Length Span 2 (ft)	165.00	**Diaphragm**	Steel
Length Span 3 (ft)	95.00	**Deck Rating**	8
Bridge Width (ft)	62.67	**Superstructure Rating**	9
Skew Angle (°)	29	**Substructure Rating**	8

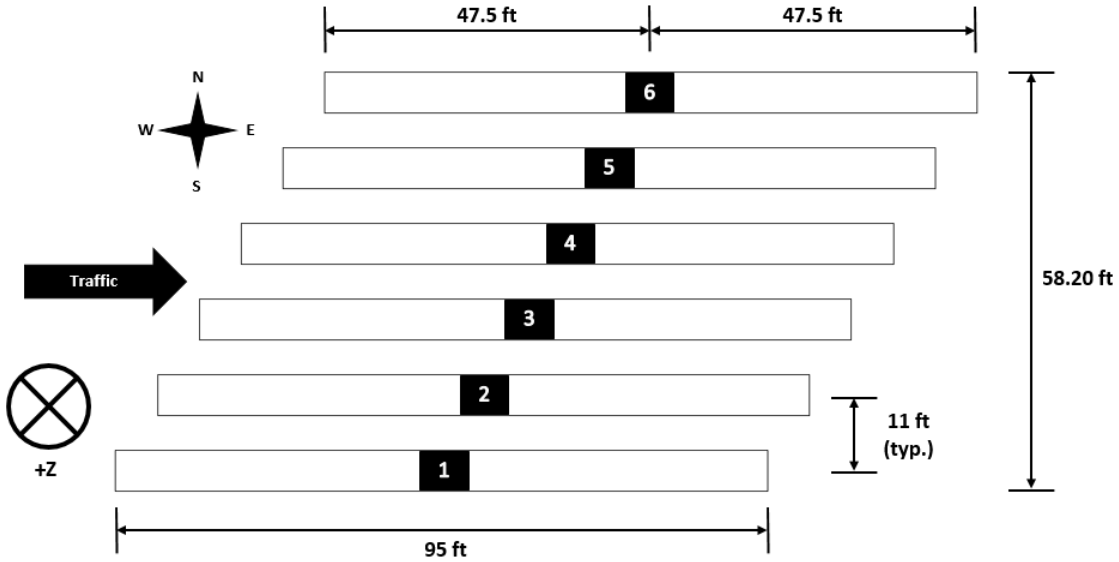

Figure 4.26: Sensor locations capturing the local response for bridge S080 40797R.

Table 4.24: Sensor information of the local response setup for bridge S080 40797R.

Sensor Location	Sensor Type	Sensor Id	Calibration Factor (mV/g)
1	PCB	N1	1001
2	PCB	N2	997
3	PCB	N3	1019
4	PCB	N4	1065
5	PCB	N5	1006
6	PCB	N6	993

Date of Collection	3/22/2017
Length of Data (min)	61.52
Sampling Rate (Hz)	2048

Table 4.25: SSI-UPCX method dynamic properties of the local response for bridge S080 40797R.

Mode	Frequency (Hz)	Damping (%)	Complexity (%)
1	3.23	1.33	0.29
2	3.50	0.89	1.30
3	4.26	1.73	7.85

Table 4.26: Operational deflected shape coordinates of the local response for bridge S080 40797R.

Sensor	ODS Coordinates		
	Mode 1	Mode 2	Mode 3
1	0.80	-0.96	1.00
2	0.85	-0.64	0.19
3	0.98	-0.35	-0.39
4	1.00	0.13	-0.94
5	0.97	0.57	-0.46
6	0.94	1.00	0.83

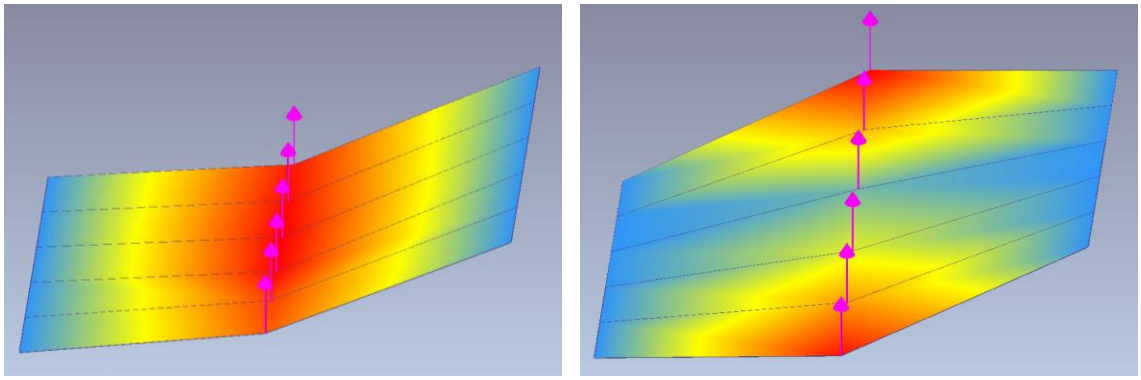

(a) Mode 1 (b) Mode 2

(c) Mode 3

Figure 4.27: Operational deflected shapes of the local response for bridge S080 40797R.

4.6.3 IT GIRDER BRIDGE COMPARISON

The slab and NU girder bridge both respond more uniformly along the bridge cross-section compared to the IT girder bridge. Figure 4.28 shows the first ODS of the local response for the slab, NU girder, and IT girder bridges along the cross-section at midspan. These ODS were linearly interpolated to compute the MAC values between them. The corresponding MAC values are provided in Table 4.27. The differential response between adjacent IT girders is causing the longitudinal deck cracking. Figure 4.29 compares all the midspan ODS cross-sections of the local response for the IT girder bridge and slab bridge within the 9 to 18 Hz frequency range. The corresponding MAC values are provided in Table 4.28. The IT girder bridge and slab bridge have similar stiffnesses, but the IT girders respond more independently of each other, as demonstrated by some sharp gradients. The IT girder ODS moderately resembles the buckling modes of a simply-supported beam due to the lack of transverse rigidity within the system.

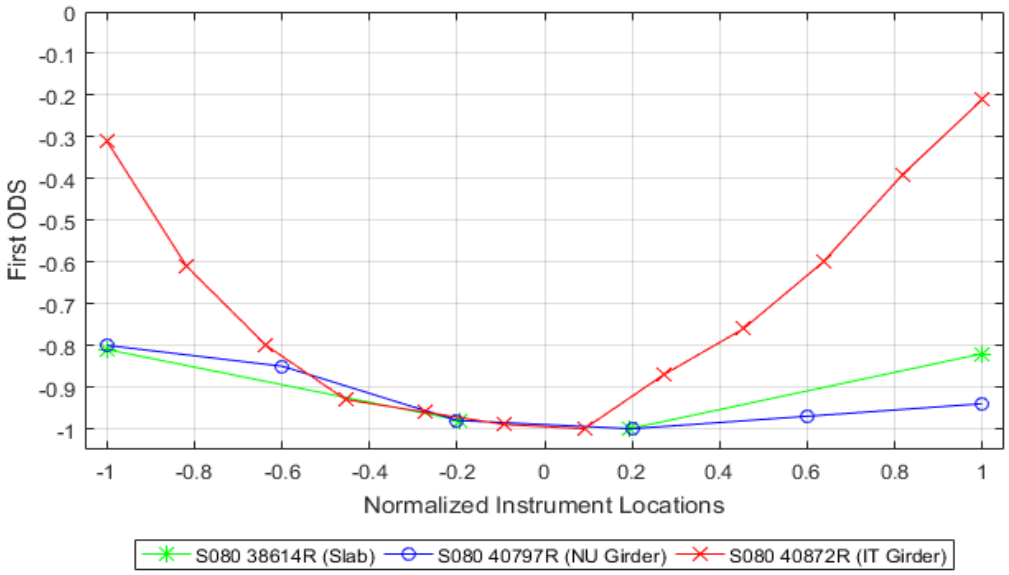

Figure 4.28: First ODS of the local response for the slab, NU girder, and IT girder bridges along the cross-section at midspan with normalized instrument locations.

Table 4.27: MAC values for the ODS of the local response for the slab, NU girder, and IT girder bridges with normalized instrument locations.

Bridge	S080 38614R (Slab)	S080 40797R (NU Girder)	S080 40872R (IT Girder)
S080 38614R (Slab)	1.000	0.997	0.827
S080 40797R (NU Girder)	0.997	1.000	0.851
S080 40872R (IT Girder)	0.827	0.851	1.000

Table 4.28: MAC values for the ODS of the local response for the IT girder bridge and slab bridge with normalized instrument locations.

		S080 38614R (Slab)			S080 40872R (IT Girder)				
		Mode 1	**Mode 2**	**Mode 3**	**Mode 1**	**Mode 2**	**Mode 3**	**Mode 4**	**Mode 5**
S080 38614R (Slab)	**Mode 1**	1.000	0.978	0.992	0.827	0.172	0.000	0.002	0.651
	Mode 2	0.978	1.000	0.990	0.864	0.245	0.007	0.000	0.566
	Mode 3	0.992	0.990	1.000	0.926	0.154	0.027	0.008	0.516
S080 40872R (IT Girder)	**Mode 1**	0.827	0.864	0.926	1.000	0.081	0.005	0.067	0.006
	Mode 2	0.172	0.245	0.154	0.081	1.000	0.038	0.005	0.020
	Mode 3	0.000	0.007	0.027	0.005	0.038	1.000	0.034	0.080
	Mode 4	0.002	0.000	0.008	0.067	0.005	0.034	1.000	0.042
	Mode 5	0.651	0.566	0.516	0.006	0.020	0.080	0.042	1.000

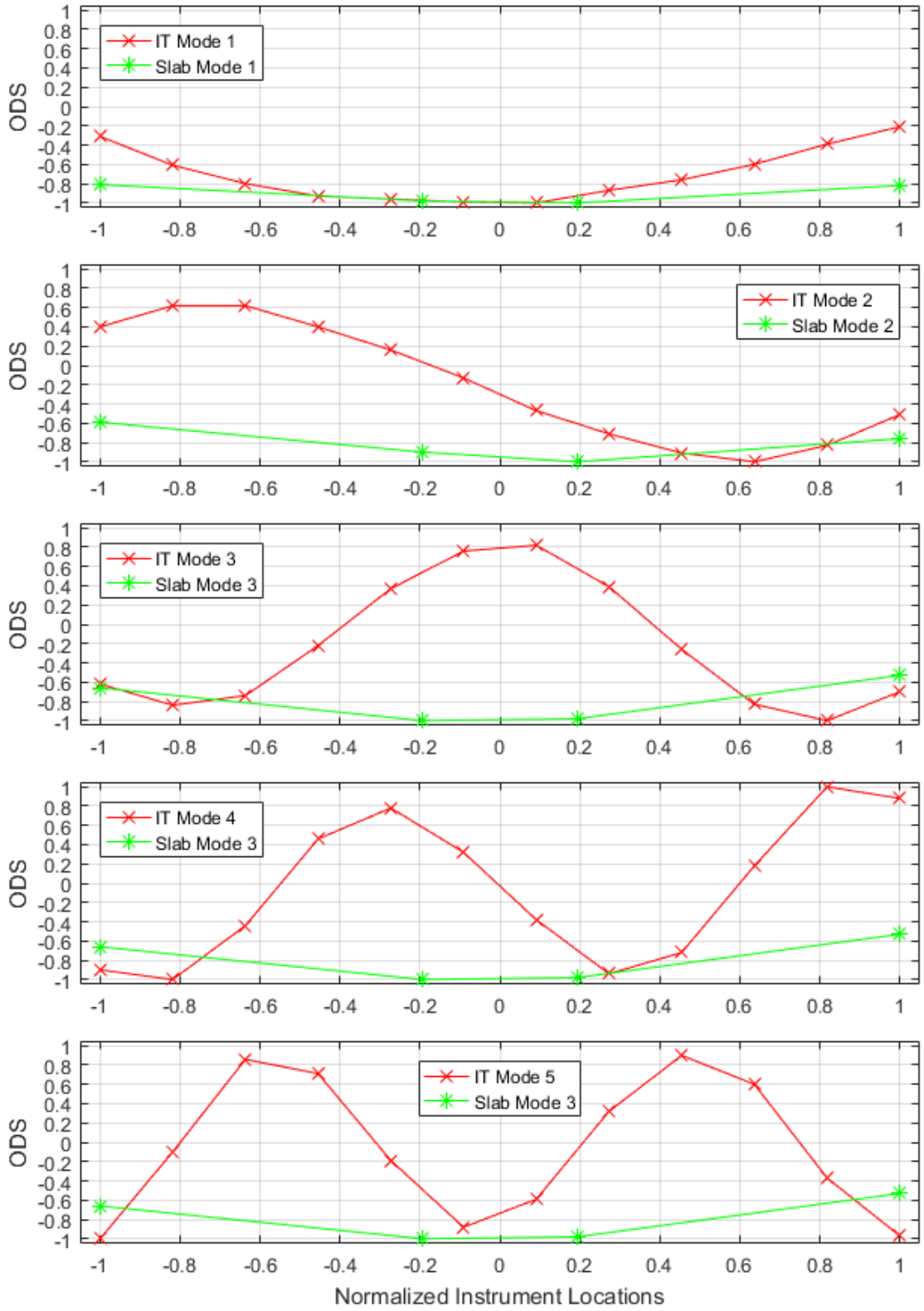

Figure 4.29: ODS of local response for the IT girder bridge and slab bridge along the cross-section at midspan with normalized instrument locations.

4.7 CONCLUSIONS

The following conclusions are made based on the system identification of the instrumented bridges:

1. Live loads contribute to the predominate independent response of the girders. The excitation due to the live loads dominantly resonates higher modes ranging from around 10 to 15 Hz for a typical IT girder bridge. The independent response of the IT girders is very likely contributing to the longitudinal deck cracking.
2. The instrumented slab bridge and NU girder bridge respond more uniformly along the bridge cross-section compared to the IT girder bridge. The distinct differential response between adjacent IT girders observed within the ODS is very likely the cause of the longitudinal deck cracking.
3. Increasing the transverse stiffeners between the IT girders by modifying or adding diaphragms may decrease the differential response between adjacent girders.
4. There is no significant benefit to the bridge dynamic performance nor a reduction in the differential girder response when increasing the deck thickness from six to eight inches.

CHAPTER 5 – ADVANCED GEOSPATIAL ANALYSIS

5.1 INTRODUCTION

Light detection and ranging (lidar) is a remote-sensing technique that records distances of objects that reflects the emitted laser light pulses from the scanner. The distances are documented as (x,y,z) points in a three-dimensional coordinate system to create a 3D point cloud geospatial representation of the scan. This chapter provides an overview of creating the lidar point clouds of the IT girder bridges and then generating the deck and girder depth maps. Deck depth maps were developed for eleven IT girder bridges, and girder depth maps were also produced for seven of these bridges (Table 5.1). The deck and girder depth maps are compiled in Appendix E.

Table 5.1: Scanned IT girder bridge with deck and girder depth maps.

Bridge ID	Deck Depth Map	Girder Depth Map
S006 26001	X	X
S009 00888	X	X
S050 04149	X	
S058 00994	X	
S080 40872R	X	X
S080 40927R	X	
S081 05152L	X	X
S089 06047	X	X
SS66C00220	X	X
M011022220	X	
C004931110	X	X

5.2 LIDAR POINT CLOUDS

The Faro Focus^{3D} X130 lidar or laser scanner was utilized during the site investigations of the IT girder bridges. Important performance specifications for the Faro

laser scanner are provided in Table 5.2 (Faro 2011). For terrestrial-based scanning, multiple scans at various locations with adequate overlap are required to create a dense point cloud, reduce areas of occlusions, and improve the alignment accuracy. Areas of occlusions are caused by beam divergence since the laser scanner only records points in its line of sight as well as undesirable objects (vehicles, vegetation, etc.). Figure 5.1 shows the laser scanner being setup for a deck scan of an IT girder bridge.

Table 5.2: Performance specifications for the Faro Focus^{3D} X130 laser scanner[1].

Specification	Value
Wavelength	1550 nm
Maximum Recording Rate	976,000 pts/sec
Range	130 m
Error (Points @ 10 to 25 m)	± 2 mm
Vertical Field of View	300º
Horizontal Field of View	360º
Minimum Angular Resolution	0.009º

Figure 5.1: Deck scan setup for bridge S058 00994.

[1] Note: 1 meter = 3.281 feet and 1 mm = 0.039 inches.

The scan files are uploaded into computer software, such as Faro Scene or CloudCompare, for point cloud processing. Each individual scan will contain several occasions of noise and unnecessary points. Most of these points are removed with segmentation and filtering techniques. Segmentation is used to remove the majority of the noise and unnecessary points manually. This process consists of drawing a polyline area to enclose points to be segmented in or out of the cloud. Point clouds can be subsampled to increase the processing speed during filtering. Statistical outlier removal (S.O.R.) is used to eliminate most of the noise and erroneous points, especially those caused by sharp object edges. This filter estimates the mean distance between the inputted number of random points and removes the points outside of the specified standard deviation threshold.

The method of aligning multiple scans to a common coordinate system is called scan registration or alignment. With multiple scans per data set, one point cloud will be the reference while the other point clouds will be individually aligned to it. A transformation matrix describes the translation and rotation for the alignment of one point cloud to another. There are two different registration techniques when aligning point clouds: point-to-point and cloud-to-cloud. Both methods have multiple techniques that can be combined or performed separately. Normally, point-to-point alignment is used first to obtain an initial approximate alignment. The user manually chooses at least four points in the reference cloud and selects those same exact locations in the cloud being aligned. The associated transformation error and root mean square (RMS) are calculated for the point pairs. Cloud-to-cloud alignment is conducted for a more precise point cloud alignment and performed for all of these bridge systems. This method iteratively shifts the point cloud being aligned to find the location which minimizes the RMS or mean scan point tension value. The final

alignment statistics for the deck and girder point clouds are given in Table 5.3. The mean scan point tension values range between 0.90 to 7.49 mm, and the percentage of points within 4 mm ranges between 30.2 to 85.6%.

Table 5.3: Final alignment statistics for the deck and girder point clouds.

Bridge ID	Deck Depth Map		Girder Depth Map	
	Mean Scan Point Tension (mm)	Points within 4 mm (%)	Mean Scan Point Tension (mm)	Points within 4 mm (%)
S006 26001	n/a	n/a	n/a	n/a
S009 00888	2.509	74.5	n/a	n/a
S050 04149	7.490	30.2	--	--
S058 00994	2.242	67.5	--	--
S080 40872R	2.562	68.1	0.904	85.6
S080 40927R	2.760	66.1	--	--
S081 05152L	2.660	73.0	n/a	n/a
S089 06047	1.503	81.2	n/a	n/a
SS66C00220	1.880	74.3	n/a	n/a
M011022220	n/a	n/a	--	--
C004931110	6.117	44.9	n/a	n/a

5.3 DECK AND GIRDER DEPTH MAPS

Depth maps are generated for the processed 3D point clouds. The maximum and minimum elevation (z-coordinate) is found for a point cloud, and then equal relative elevation ranges are determined for the specified number of bins. The points are separated by elevation into the corresponding bin number. Each bin is assigned a distinct color for the points. The color-coded points are projected to the 2D (x,y) plot to create the depth map. The legend provides the elevation ranges and color for each bin.

Existing conditions of bridges such as relative deck and girder elevations are determined by lidar depth mapping. Deck depth maps can identify possible areas of water

ponding for increased water and/or chloride penetration as well as unintended final elevations. Girder depth maps can provide differential placement heights of the girders.

The deck and girder depth maps for bridge S080 40872R are displayed in Figure 5.2 and Figure 5.3, respectively. For bridge S080 40872R, the bridge crown is approximately at 11 meters (36 ft) from the south side of the bridge and the computed cross-slopes are 2.1% on the left of the crown and 2.1% on the right side of the crown. The bridge crown and cross slopes found with the deck depth map are consistent with the design drawings. The design drawings have a 2.0% cross slope on both sides of the bridge crown located at 11.0 meters (36 ft) from the south side and 7.3 meters (24 ft) from the north side of the bridge. Likewise, for bridge S080 40872R, the elevations of the underside of the girders partially match the crown location and slopes of the deck. A few girder depth maps, namely for bridges S089 06047, SS66C00220, and C004931110, suggest that some IT girders are either set at various elevations and/or the resulting deck thickness is nonuniform. The largest elevation difference found was 5 cm (1.97 inches) between the center and adjacent girders of bridge SS66C00220. The unpredictable camber errors may contribute to the inconsistent thickness, stiffness irregularities, and torsional global response of the bridge deck. The deck and girder depth maps for all the IT girder bridges listed in Table 5.1 are compiled in Appendix E.

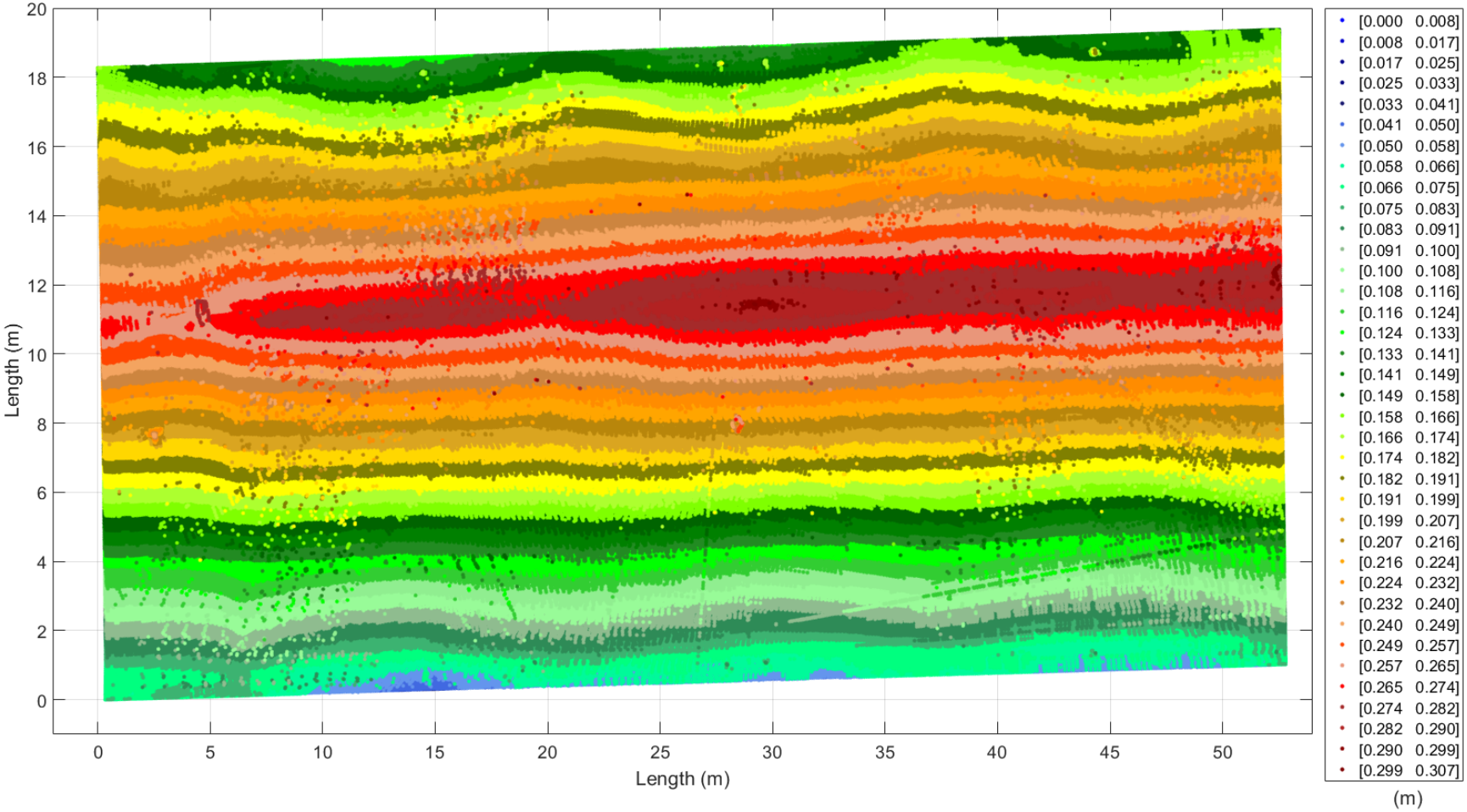

Figure 5.2: Deck depth map for bridge S080 40872R.

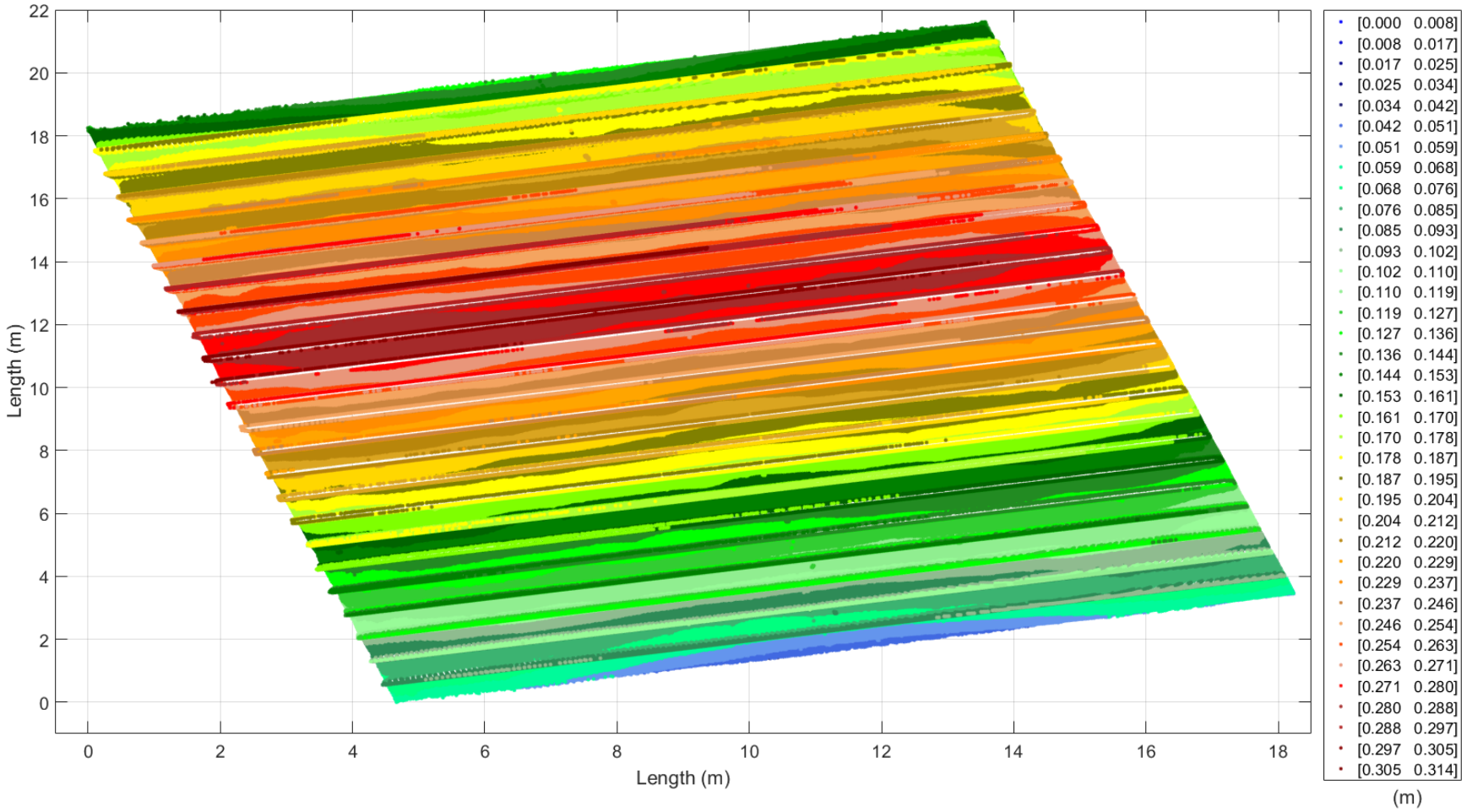

Figure 5.3: Girder depth map for bridge S080 40872R.

5.4 CONCLUSIONS

The following conclusions are made based on the advanced geospatial analysis of the IT girder bridges:

1. Existing conditions of bridges such as relative deck and girder elevations are determined by lidar depth mapping.
2. For the IT girder bridges, the deck depth maps have consistent cross slopes compared to the drawings and identify no significant locations of potential water ponding for increased water and/or chloride penetration.
3. The girder depth maps suggest that some IT girders are either set at various elevations and/or the resulting deck thickness is nonuniform.
4. The unpredictable camber variability may contribute to the inconsistent thickness, stiffness irregularities, and global torsional response of the bridge deck.

CHAPTER 6 – LIVE LOAD TESTS

6.1 INTRODUCTION

This section will quantify the differential deflection and strain between adjacent girders using strain gauges, Linear Variable Differential Transforms (LVDTs), and lidar to help quantifiably explain the longitudinal deck cracking in the bridge deck. It will also investigate the impact of span-to-depth ratio, skew angle, deck thickness, and intermediate diaphragms on the differential deflection between adjacent girders. Table 6.1 shows which bridges were monitored and with what equipment. In this section, the strain gauge and LVDT process for bridge S006 26001 will be outlined, while the complete set is compiled and detailed in Appendix F. The live load (LL) test using lidar was done for one IT girder bridge, C002408505. The creating, filtering, and aligning point clouds will use the same process as that outlined in Chapter 4.1 through 4.3. However, this time it will compare the girder depth map under the influence of a static live loads.

Table 6.1: Instrumented bridges for LL tests

Bridge ID	**LVDT**	**Strain**	**Lidar**
S080 40927R	X	X	
S006 26001	X	X	
S050 04149	X		
S089 06047	X	X	
C002408505			X

6.2 INSTRUMENT SETUP

As shown in Table 6.2, the S006 26001 bridge structural system consists of 19 precast IT300 girders with a 31.7 feet span for the instrumented span. Girders were simply supported along the instrumented span. The bridge does not contain any intermediate diaphragms. Six intermediate girders were instrumented using LVDTs to measure deflection, in addition to six strain gauges at the bottom flange of each girder. Figure 6.3 shows the position of the instrumented girders and sensor positions. Figure 6.1 shows LVDTs and strain gauges setup under the instrumented girders. Figure 6.2 shows sensor installation under one of the six instrumented bridge girders.

Table 6.3 shows that the C002408505 bridge consists of 13 IT600 girders with a single, 65-foot span. As in Chapter 4.2, the Faro Focus3D X130 lidar or laser scanner was set up underneath the bridge to create the girder point clouds. Figure 6.4 shows where the DL and LL scans were taken and where the truck was located for each LL scans. Notice that a scan for the DL case was taken at each end but only one scan was taken for each LL scan. This is to limit the amount of time that the bridge is closed to traffic. The first LL scan was with the triaxial truck placed on the center of the roadway while the second LL scan had the triaxial truck placed as close to the parapet as possible. The midspan of the bridge is located between the two back tires where the force is the greatest. Figure 6.5 shows the truck position during the first load case.

Table 6.2: Bridge information summary for bridge S006 26001.

Bridge ID	S006 26001	**Girder Height (in [mm])**	11.81 [300]
County	Fillmore	**Girder Width (in [mm])**	23.63 [600]
Year Built	1999	**Girder Spacing (in [mm])**	29.06 [738]
No. of Spans	3	**Deck Thickness (in [mm])**	6 [152]
Length Span 1 (ft)	31.70	**No. of Girders**	19
Length Span 2 (ft)	32.50	**Diaphragm**	None
Length Span 3 (ft)	31.70	**Deck Rating**	8
Bridge Width (ft)	45.60	**Superstructure Rating**	8
Skew Angle (°)	20	**Substructure Rating**	7

Figure 6.1: LVDT and strain gauge setup for bridge S006 26001.

Figure 6.2: Accelerometer, LVDT, and strain gauge installation for bridge S006 26001.

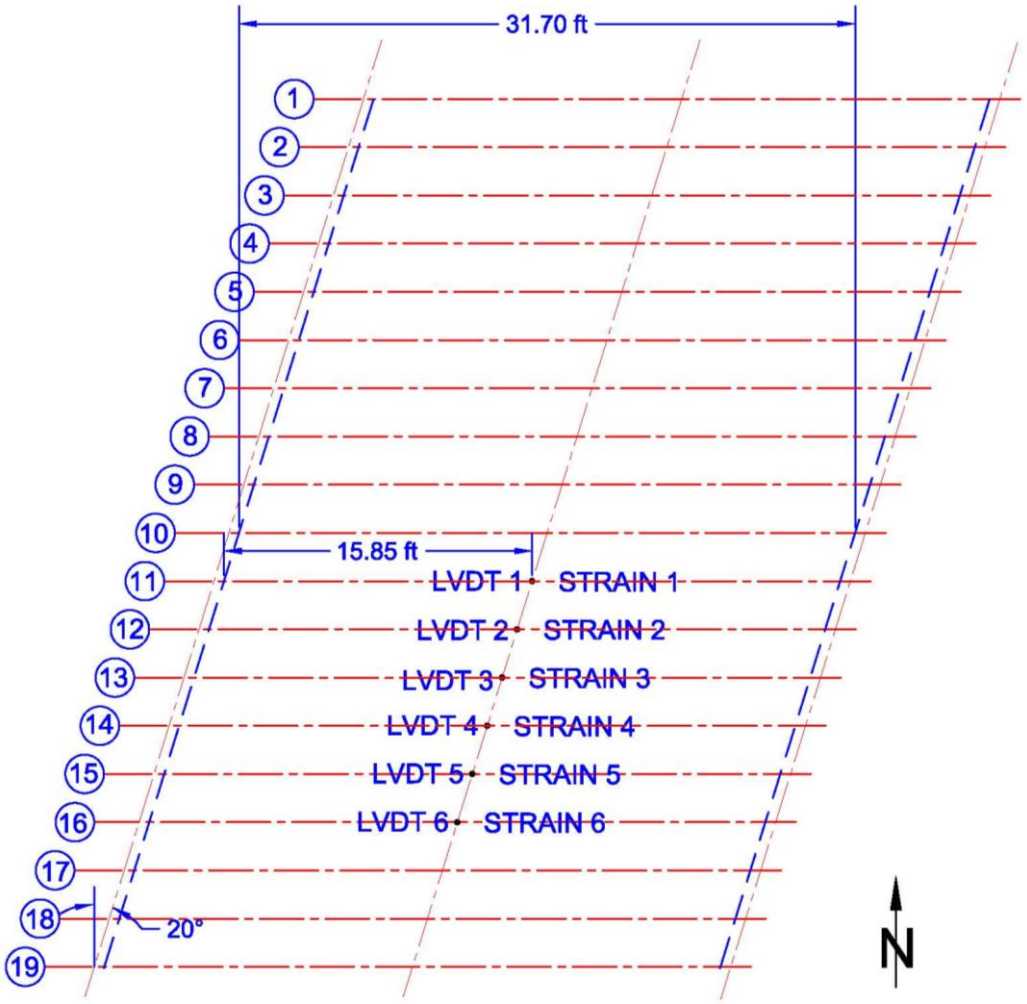

Figure 6.3: LVDT and strain gauge positions for bridge S006 26001.

Table 6.3: Bridge information summary for bridge C002408505.

Bridge ID	C002408505	**Girder Height (in [mm])**	23.63 [600]
County	Dawson	**Girder Width (in [mm])**	23.63 [600]
Year Built	2005	**Girder Spacing (in [mm])**	28.38 [721]
No. of Spans	1	**Deck Thickness (in [mm])**	6 [152]
Length Span 1 (ft)	65.00	**No. of Girders**	13
Length Span 2 (ft)	--	**Diaphragm**	C8x18.75
Length Span 3 (ft)	--	**Deck Rating**	5
Bridge Width (ft)	30.40	**Superstructure Rating**	9
Skew Angle (°)	35	**Substructure Rating**	9

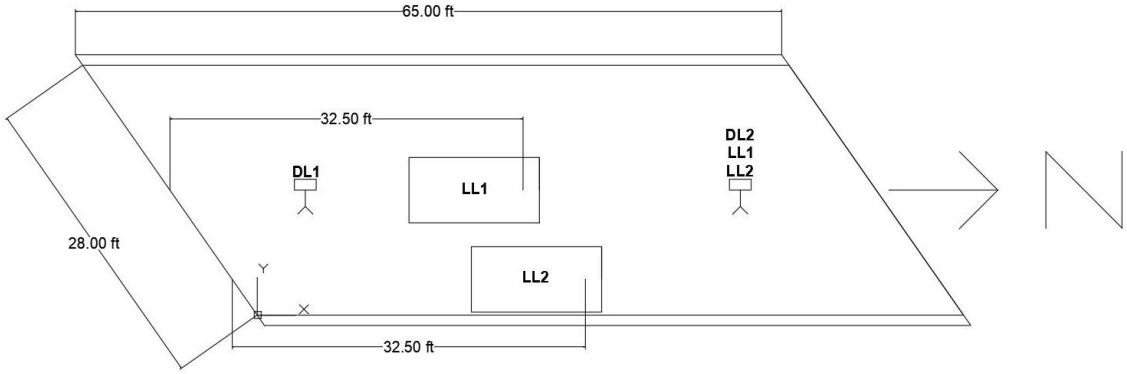

Figure 6.4: Laser scanner and truck locations for bridge C002408505.

Figure 6.5: Photo of load case I for bridge C002408505.

6.3 SUMMARY OF FIELD ASSESSMENTS FOR ALL IT BRIDGES

For the bridges instrumented with strain gauges and LVDTs, the data was plotted for each girder. Then the peak values were zoomed in on to produce plots as shown in Figure 6.6 and Figure 6.7. Notice that the deflection at girder 11 is the greatest and each girder after that has a significant drop in deflection. The same trend is seen in the strain results. Then the peak values are compared at the specific peak time and plotted as displayed in Figure 6.8. This plot again shows that girder 16 barely deflects while girder 11 deflects significantly. The most critical differential deflection and the corresponding maximum deflection values for each monitored bridge are summarized in Table 6.4 along with the bridge's IT height, deck thickness, span, span-to–depth ratio, skew, and the intermediate diaphragm details. The corresponding maximum strain and differential strain are also presented in Table 6.4. There does not appear to be any significant impact by any of those on the differential deflection.

The results from the lidar scans for bridge C002408505 are also displayed in Table 6.4 and the process to obtain those results will be outlined in the rest of this section. The distance between the DL lidar generated point cloud and the DL plus LL point clouds can be calculated using a cloud-to-cloud distance tool. The DL only cloud is used as the reference cloud because it has a higher cloud density. The DL plus LL clouds will be the compared clouds which means that each of their points will be compared to the nearest point in the reference cloud by the z-dimension value only. The cloud-to-cloud distances for the two load cases are shown in Figure 6.9 and Figure 6.10. Blue represents the greatest downward differential deflection between the DL cloud and the DL plus LL clouds. For both load cases, the location of the truck corresponds to the greatest LL deflection.

Figure 6.9 and Figure 6.10 can be difficult to visualize, therefore, to obtain a better understanding of the deflection, cross-sections at midspan perpendicular to the bridge were segmented out. These cross-sections were plotted as shown in Figure 6.11 and Figure 6.12. These plots show the elevations of individual points in the DL only and the DL plus LL clouds. Near the truck wheel lines, the girders deflect substantially but as they get farther away the girders quickly return to the same elevation. This confirms the results for differential deflections as seen in the LDTVs.

To turn this deflection information into results that can be more easily compared, Figure 6.14 was made to show the LL deflections at the center of the girder. Figure 6.13 shows an example calculation for girder #8 under central LL. It shows that a linear best fit line in the form of y=m*x+b was created using the data. In this equation, the arctangent of m is the girders rotation in radians and the relative midpoint depth is calculated by plugging in half the girder width in as x. Note that 5% of points were removed from each edge of the girder prior to linear fitting to reduce the error potentially introduced by noisy or stray points. These noisy edge points or edge artifacts happen primarily due to beam scattering.

The differential deflection between adjacent girders is shown in Figure 6.15. The max differential deflections occur just outside of the wheel lines with a critical max values 0.0298 and 0.0300 inches for center LL and offset LL, respectively. Looking closely at Figure 6.11 and Figure 6.12, it was noticed that the girders were not only deflecting, but they were also rotating. Figure 6.16 was created to display the differential in LL rotation. This is the change in radians of rotation between DL and DL plus LL for each of the girders. Over the section of loading, the girders go from clockwise rotation to counterclockwise

rotation. The rotating of the girders may be slightly magnifying the differential deflection and may contribute to longitudinal deck cracking.

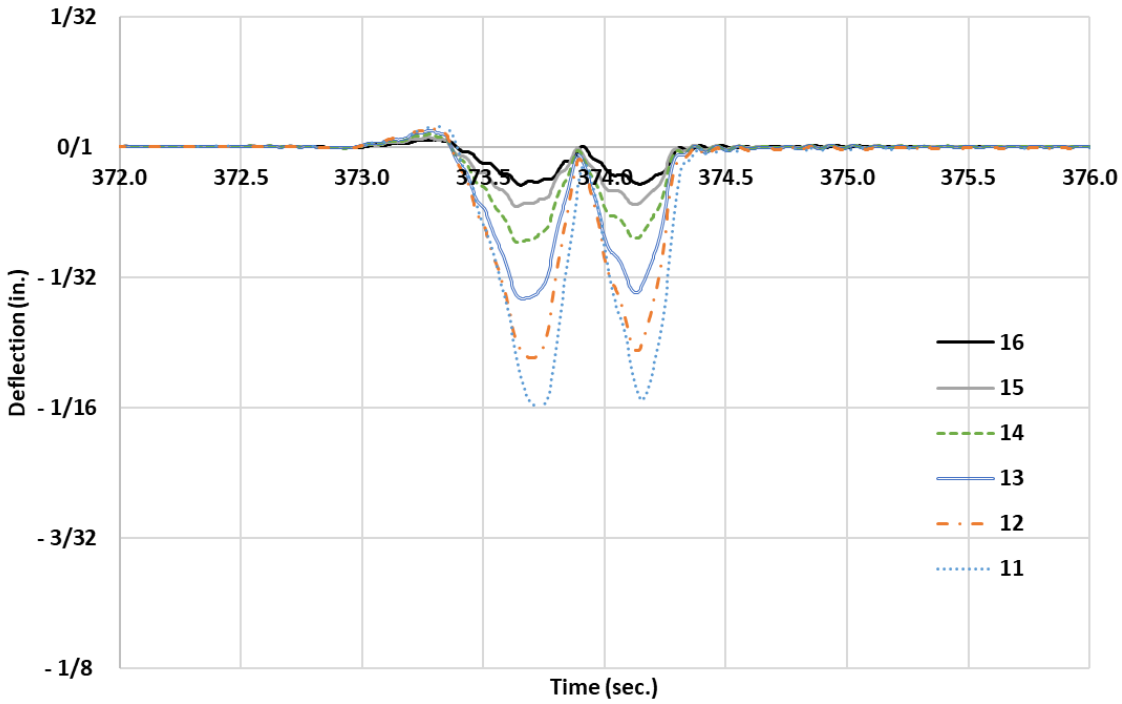

Figure 6.6: Deflection-time plot for the peak truck loading for bridge S006 26001.

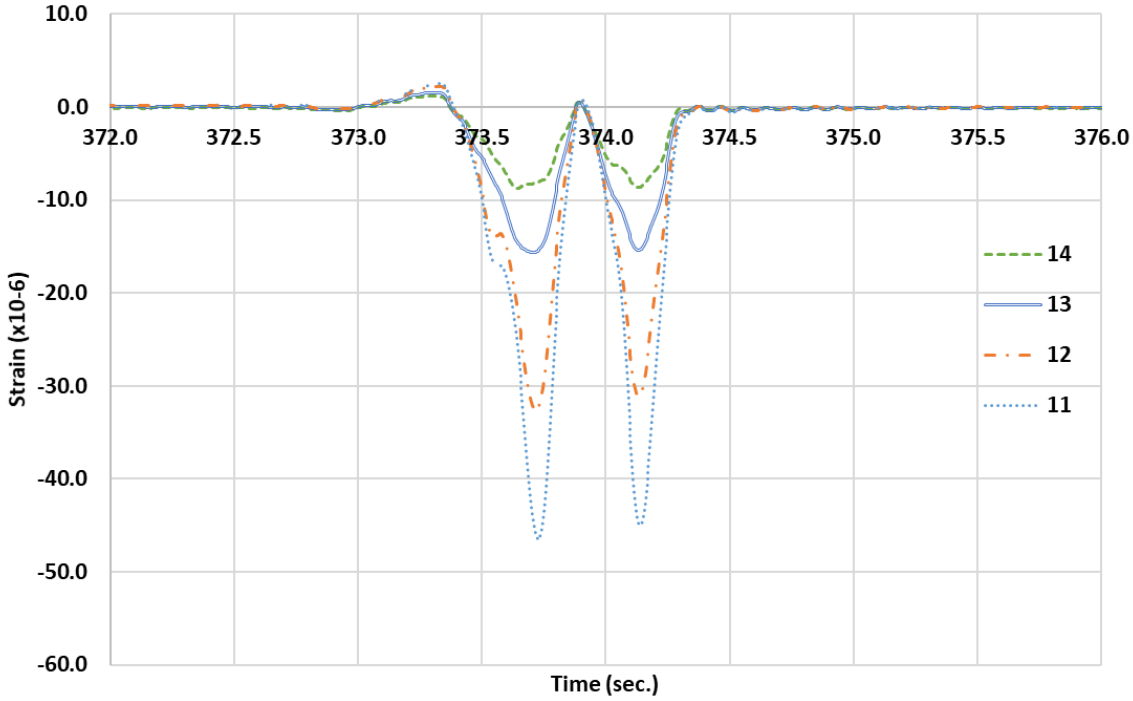

Figure 6.7: Strain-time plot for the peak truck loading for bridge S006 26001.

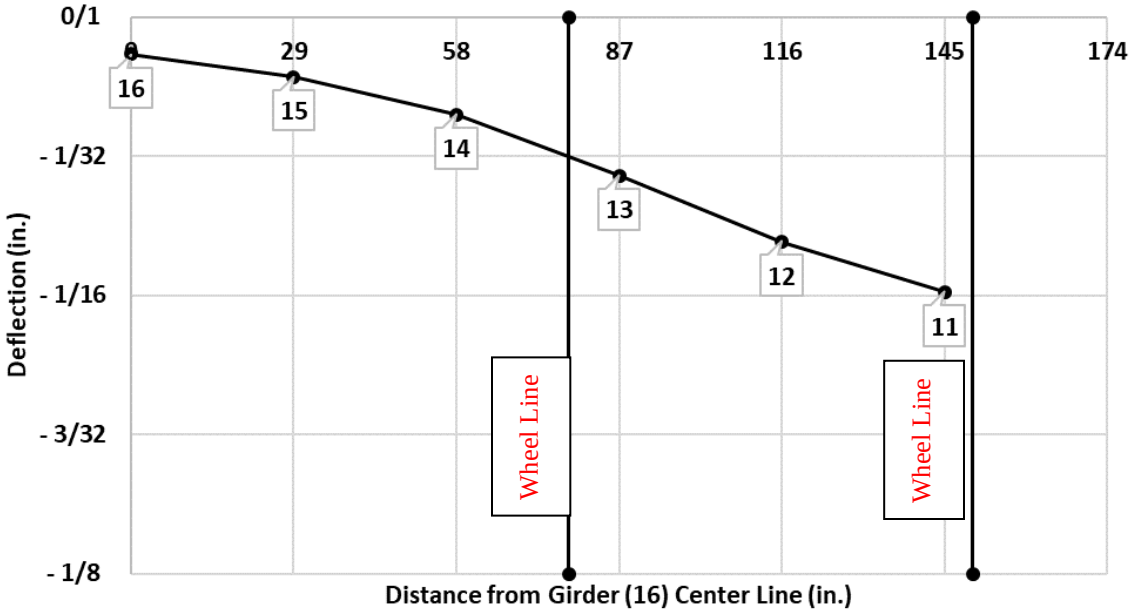

Figure 6.8: Girder deflection profile at t = 373.708 seconds for bridge S006 26001.

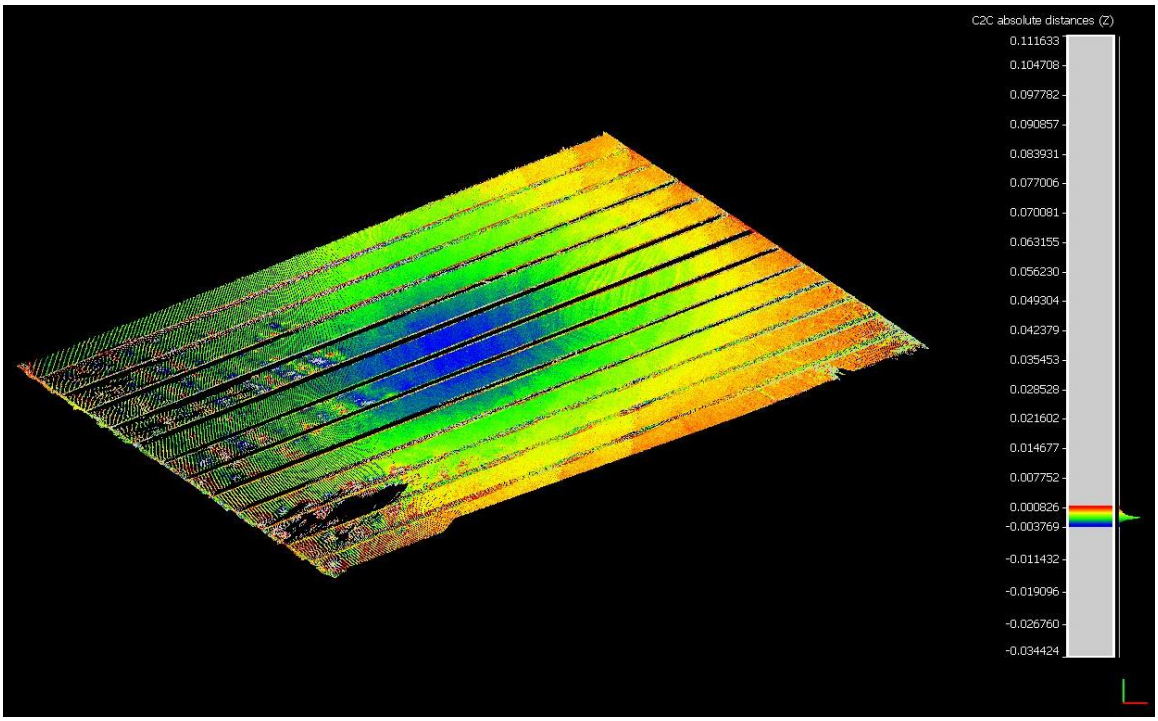

Figure 6.9: Cloud-to-cloud distance between DL only and DL plus central LL (meters).

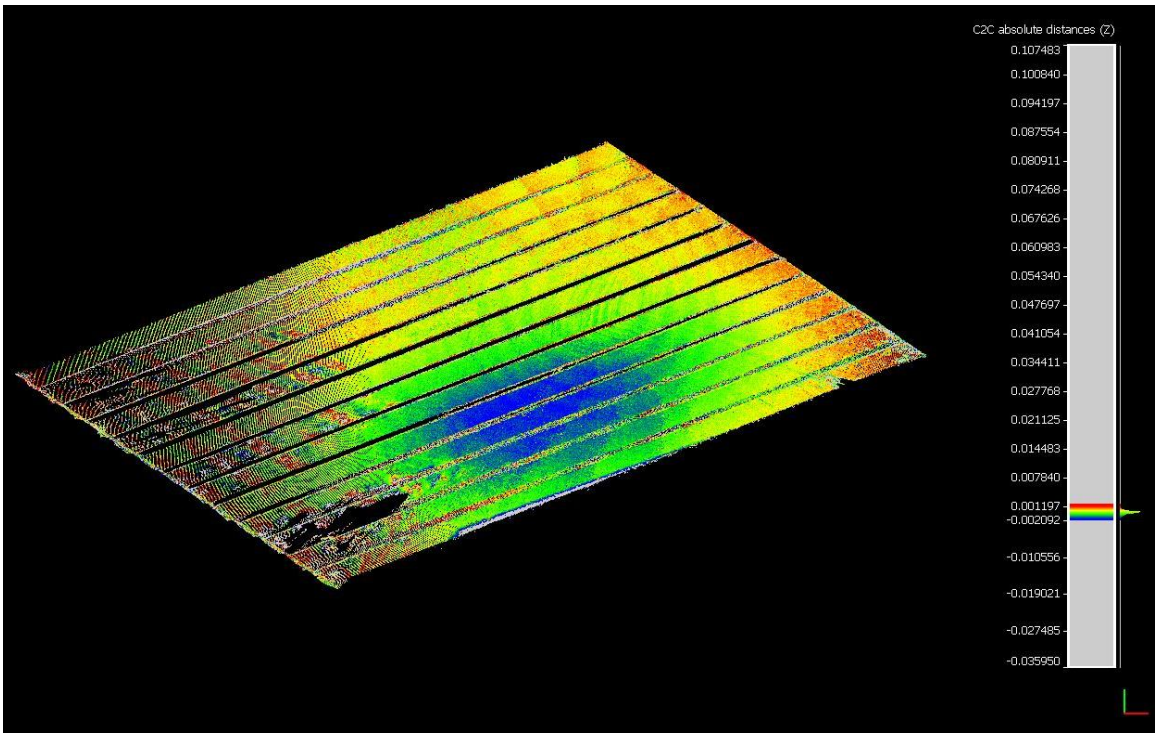

Figure 6.10: Cloud-to-Cloud distance between DL only and DL plus offset LL (meters).

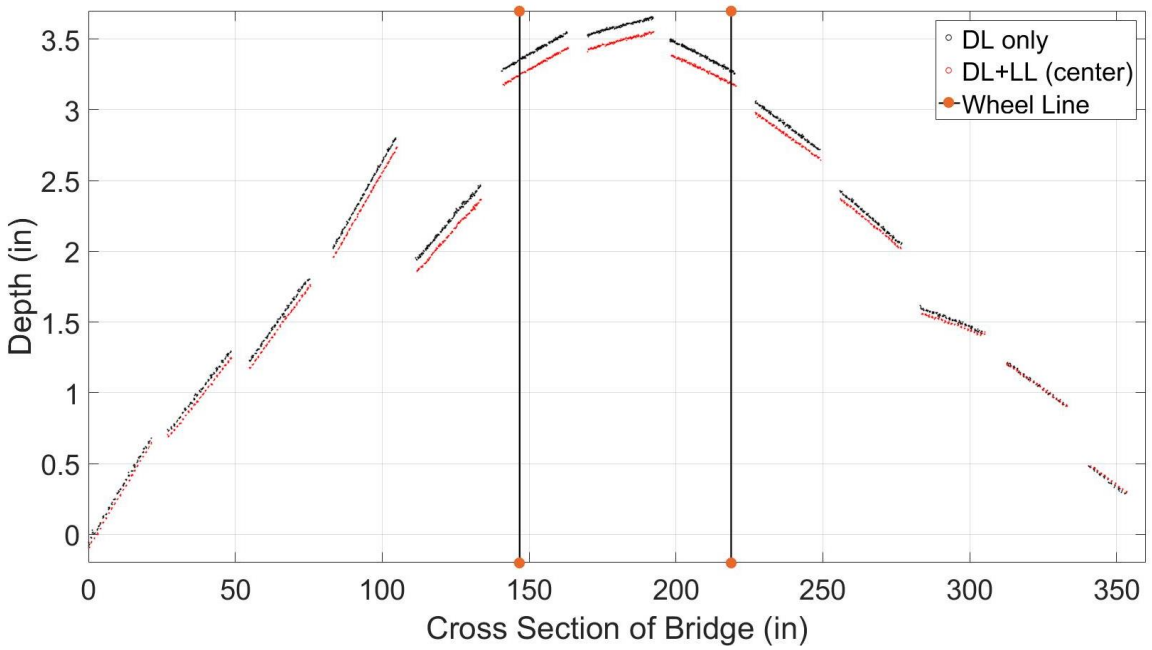

Figure 6.11: Girder depth at midspan perpendicular to the girders: DL only versus DL plus central LL.

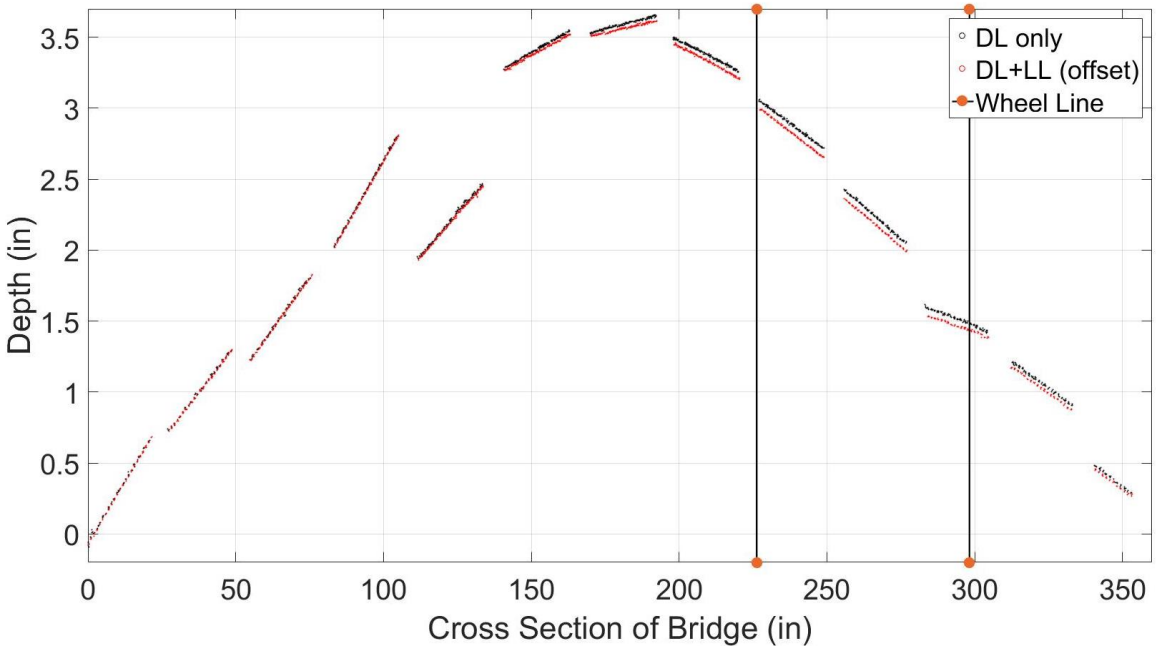

Figure 6.12: Girder depth at midspan perpendicular to the girders: DL only versus DL plus offset LL.

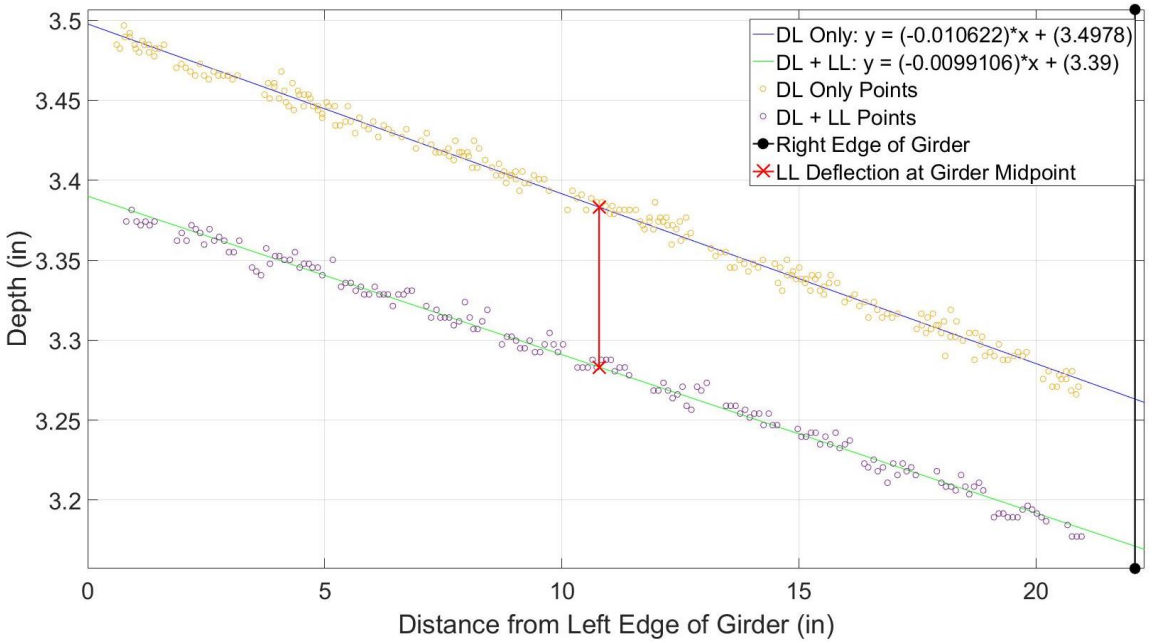

Figure 6.13: Example of calculations for girder #8 under central LL.

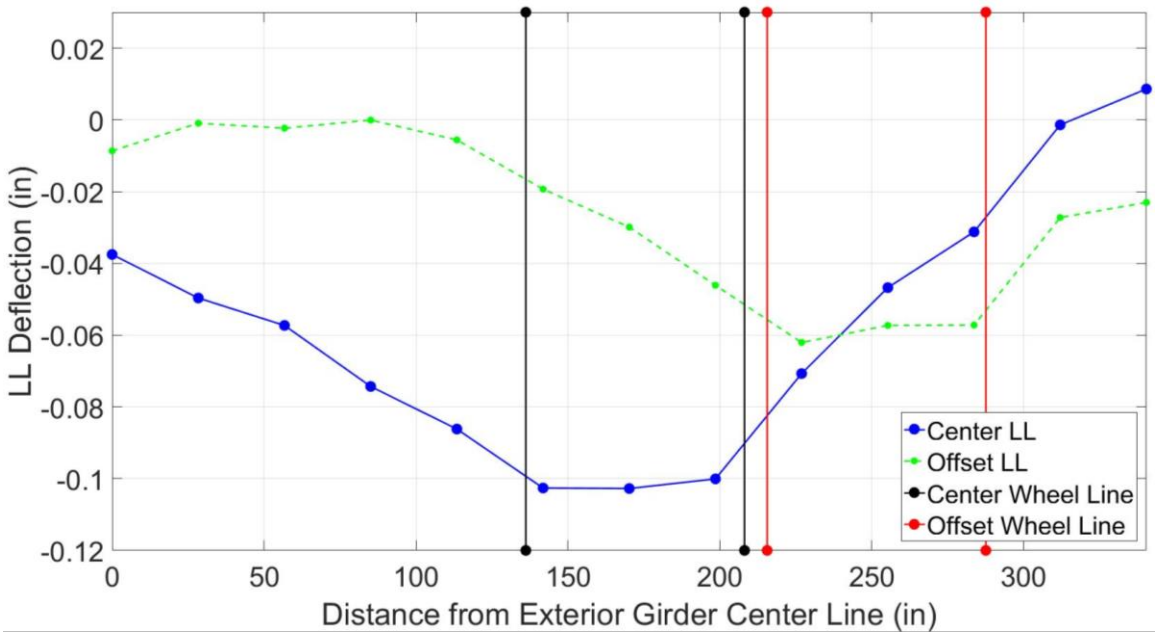

Figure 6.14: LL deflection at girder midpoints.

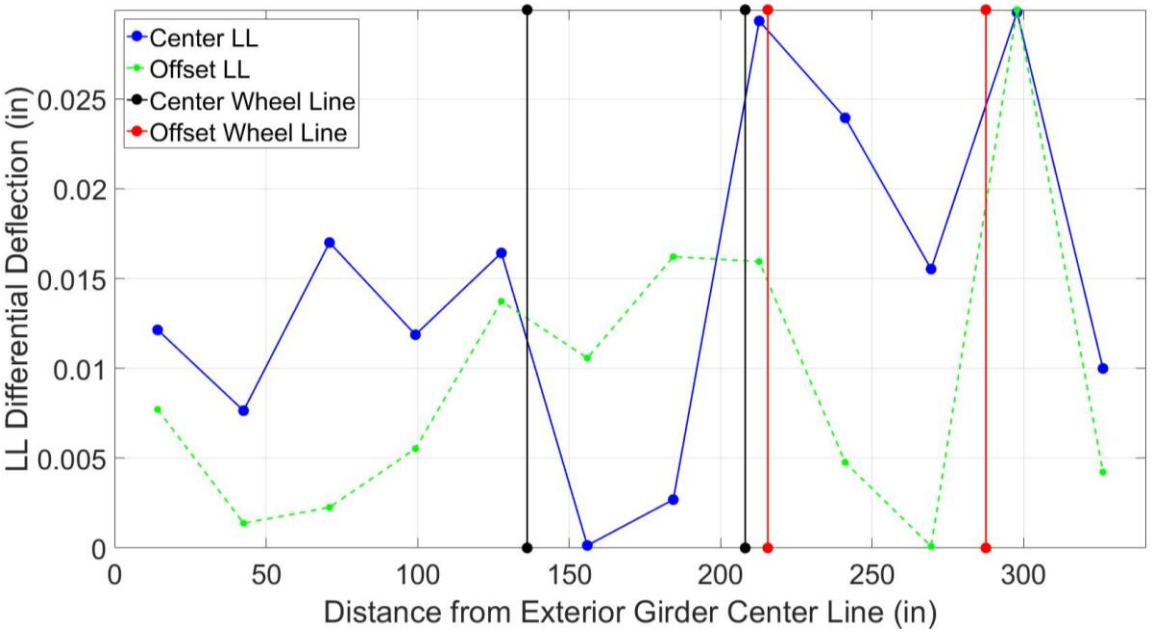

Figure 6.15: LL differential deflection between adjacent girders (in).

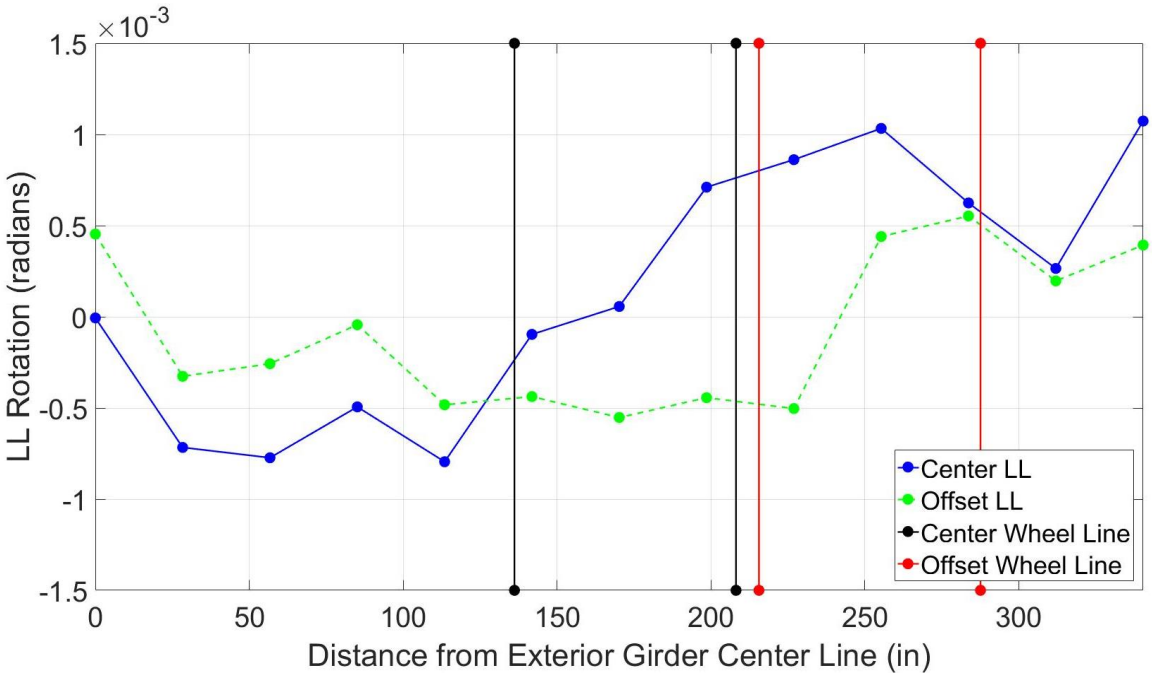

Figure 6.16: LL rotation between adjacent girders.

Table 6.4: Summary of results for all instrumented bridges.

Bridge # (ID)	IT Height (in)	Deck Thickness (in)	Span (ft)	Span-to-Depth Ratio	Skew	Intermediate Diaphragm	Continuity	Highest Recorded Differential Deflection (in)	Corresponding Deflection (in)	Corresponding Recorded Differential Strain (micro)	Corresponding Strain (micro)
S080 40872R	15.75	8	48.25	36.8	0	Steel (3 exterior girders)	Continuous (one end)	0.017	0.065	9.2	31
S006 26001	11.81	6	31.7	32.2	20^0	None	Simple	0.015	0.050	16.7	32.4
S050 04149	23.63	6	66.5	33.8	10^0	Concrete (all girders)	Continuous (one end)	0.017	0.067	X	X
S089 06047	11.81	6	40	40.6	0	Concrete (4 exterior girders)	Continuous (one end)	0.007	0.039	25.9	66.1
C002408505	23.63	6	65	33.0	35^0	Steel (3 exterior girders)	Simple	0.030 (static loading)	0.103 (static loading)	X	X

6.4 CONCLUSIONS

Based on the live load tests, the following conclusions can be made:

1. The girders experience noticeably larger deflections and strain under LL where the wheel line is, but the deflection and strain quickly reduce at adjacent girders.
2. The differences in deflections between adjacent girders show that the girders are responding independently despite their narrow spacing, which may result in the longitudinal deck cracking in the IT girder bridge system.
3. The girders are also rotating under live load, which may be contributing to longitudinal deck cracking.
4. Span-to-depth ratio, skew angle, and deck thickness did not show a significant effect on differential deflections.
5. The currently used intermediate diaphragms did not demonstrate a significant effect on reducing differential deflections.

CHAPTER 7 – LIVE LOAD DISTRIBUTION FACTORS

7.1 INTRODUCTION

Live load distribution factors are used as a simplified way to determine the live load moment and shear forces acting on each girder of the bridge when one or more lanes are loaded. These factors are dependent on the superstructure type, girder spacing, and girder and deck stiffness. Current AASHTO LRFD bridge design specifications section 4.6.2.2.2 divides bridges into several categories for distribution factor calculations (AASHTO 2014). Since the IT bridge system is a relatively new system and not yet considered in any of these categories, the distribution factors of Category K, which consists of cast-in-place concrete slab on multi-girder systems, could be used for IT girders after ignoring the spacing condition.

NDOR Bridge Office Policies and Procedures (BOPP) manual recommended the use of the distribution factors of the AASHTO Standard Specification for IT girder bridges. A grid analysis was performed to evaluate these factors, and the results confirmed their adequacy (Kamel and Tadros 1996). These distribution factors are S/5.5 per wheel load and S/11 per lane load for interior girders, where S is the IT girder spacing in feet (BOPP 2016). Analysis results also indicated that intermediate diaphragm did not affect the live load distribution factors.

Finite element analysis (FEA) was also conducted on bridges with different spans, widths, and skew angles to develop wheel load distribution expressions for interior and exterior girders on simply supported skewed I-beam composite bridges (Bishara et al. 1993). The three-dimensional interaction of all bridge members was considered in the

analysis. Wheel load distribution equations were developed for exterior and interior girders. These equations gave distribution factors, which were 20 to 80% of the AASHTO distribution factor (S/5.5). A two-dimensional grillage model and three-dimensional finite element model were developed to evaluate the live load distribution factors for IT bridges in Kansas (Ambare and Peterman 2006). A parametric study was also conducted to determine the effect of span length, superstructure width, skew angle, the number of lanes loaded, end support conditions and overhang width on the distribution factors. The live load moment distribution factors obtained from AASHTO were close to those obtained from refined models. Simple equations were developed based on this study. Three-dimensional FE models were developed to simulate reinforced concrete slab bridges that were simply supported, single span, multilane, and skewed (Menassa et al. 2007). The concrete deck slabs were simulated as quadrilateral shell elements with linearly elastic behavior. Based on this study, a comparison between straight and skewed bridges was conducted. This study recommended that a three-dimensional finite-element analysis be performed when the skew angle is greater than 20˚.

7.2 FINITE ELEMENT ANALYSIS (FEA)

AASHTO LRFD bridge design specifications permit the use of finite element methods to determine the live load distribution factors. Three-dimensional finite element modeling allows the designer to better simulate bridge components and connections between the girder and slab. Several models were created using SAP2000 v18 to study the effect of design parameters on the system performance. These parameters are span length, skew angle, number of lanes loaded, deck thickness and addition of diaphragms. The deck

slabs were modeled as shell elements, as shown in Figure 7.1, meshed into a reasonable number of elements to obtain accurate results in an efficient manner (CSI 2011). The girders were modeled as frame elements placed eccentrically below the shell elements, as shown in Figure 7.1, to achieve the composite section. The FE model was loaded with a load combination of a moving truckload (HL-93) and a uniformly distributed load of 9.34 KN/m (0.64 klf) according to AASHTO LRFD design specifications. The truckload was applied on paths with a maximum discretization length of 152 mm (6 in.) to obtain accurate results. This study is performed on three constructed IT girder bridges with 55.2 MPa (8 ksi) concrete strength for the prestressed IT girders and 27.6 MPa (4 ksi) concrete strength for deck slab. The investigated IT concrete girder bridges properties are shown in Table 7.1.

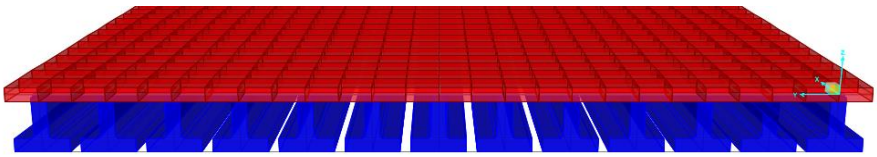

Figure 7.1: Finite element cross-section.

Table 7.1: Investigated IT concrete girder bridge properties.

Bridge ID	S080 40927R	M011022220	SS66C00220
County	Lancaster	Sherman	Otoe
Span	Three spans 14.7 m, 16.3 m, and 14.8 m (48.25 ft., 53.50 ft., and 48.25 ft)	One span 19.8 m (65.0 ft)	One span 24 m (78.9 ft)
Skew Angle	Straight (0˚)	15˚	25˚
No. of IT Girders	25	13	15
Girders Spacing, m (ft.)	0.76 (2.48)	0.72 (2.37)	0.74 (2.43)
IT Section	IT-400	IT-600	IT-700
Section Height, mm (in.)	400 (15.75)	600 (23.63)	700 (27.56)
Centroid, mm (in.)	148 (5.81)	222 (8.75)	264 (10.38)

Slab Thickness, mm (in.)	203 (8)	152 (6)	152 (6)
Diaphragm Section	steel channel (C8x18.75)		concrete 203 mm (8 in.) width
Diaphragm Location	mid-span at the exterior three girders from both sides		two full-width at 5.6 m and 13.6 m (220 in.& 535 in.)

Figure 7.2 summarizes the parametric study conducted on the three constructed IT girder bridges. The three-span lengths and the corresponding IT girder sizes of these bridges are used assuming the current skew angle as well as a zero skew angle and 45-degree skew angle. The current diaphragm of the constructed bridges is considered as a reference and two additional cases are studied. The first case is using the current steel diaphragm but for the full-width of the bridge instead of the exterior girders only. The second case replaces the steel diaphragm with concrete diaphragm for the full width of the bridge as shown in Figure 7.2. Also, 152 mm (6 in.) and 203 mm (8 in.) thick deck slabs are considered for the two loading conditions: one-lane loading, and two-lane loading.

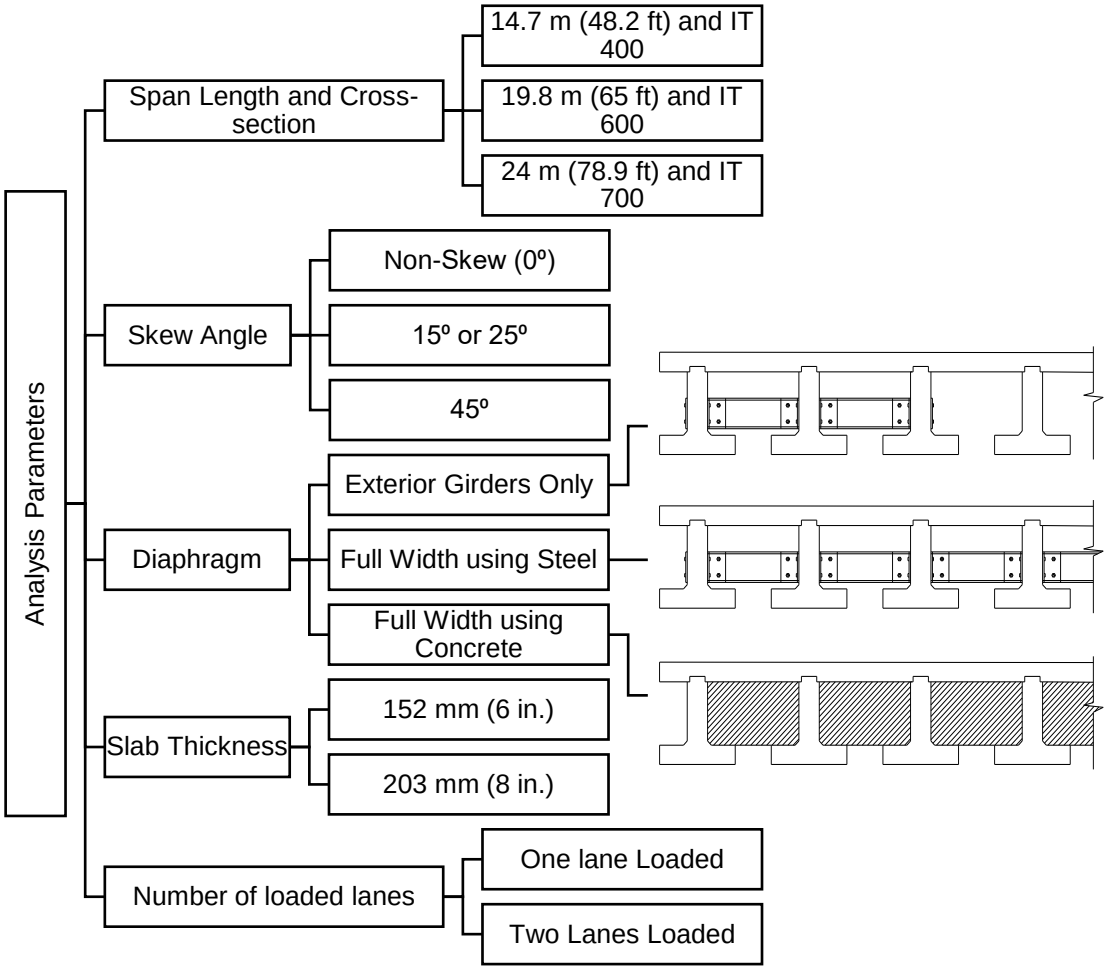

Figure 7.2: Parametric analysis matrix.

There are two types of live load distribution factors depending on the truck wheel load location, as shown in Figure 7.3: exterior girder distribution factors when the truck wheel is placed on the exterior girder, and interior girder distribution factors when the wheel load is placed on the interior girders. Figure 7.3 shows that because the truck wheel cannot be placed closer than 0.61 m (2.0 ft) from the bridge rail, the two loading conditions are almost the same. Therefore, the parametric study is conducted using the truck wheel placed at the first interior girder only as it will yield the highest distribution factors in comparison to others.

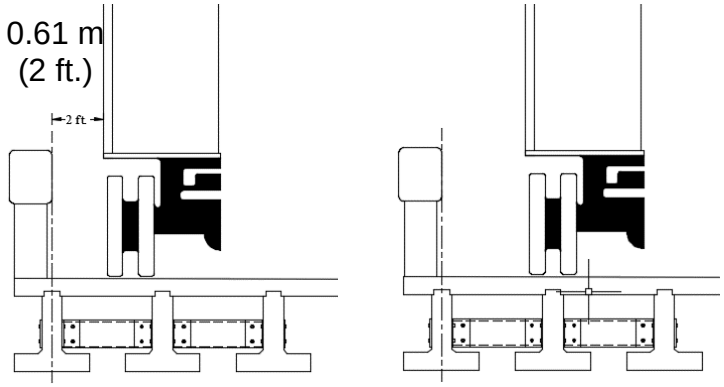

(a) Exterior Girder (b) First Interior Girder

Figure 7.3: Truck load location for exterior and interior girders.

7.3 DISTRIBUTION FACTOR ANALYSIS RESULTS

Figure 7.4 shows the live load moment and shear distribution factors for bridge S080 40927R with different skew angles. This figure indicates that the skew angle has a negligible effect on the live load moment and shear distribution factors. It also indicates that the values obtained from the FE model are in a good agreement with those predicted by the BOPP manual.

Figure 7.5 shows the live load moment and shear distribution factors for bridge S080 40927R with different diaphragm systems. This figure also indicates that the diaphragm system has a negligible effect on the live load moment and shear distribution factors. In addition, it confirms that the values obtained from the FE model are close to those predicted by the BOPP manual.

Figure 7.6 shows the live load moment and shear distribution factors for the bridge S080 40927R with different deck slab thickness. This figure indicates that there is a slight decrease in the live load moment and shear distribution factors with the increase of deck

slab thickness from 152 mm (6 in.) to 203 mm (8 in.) as expected due to the increase in the deck stiffness. The figure also shows that the BOPP manual provides conservative predictions for the distribution factors.

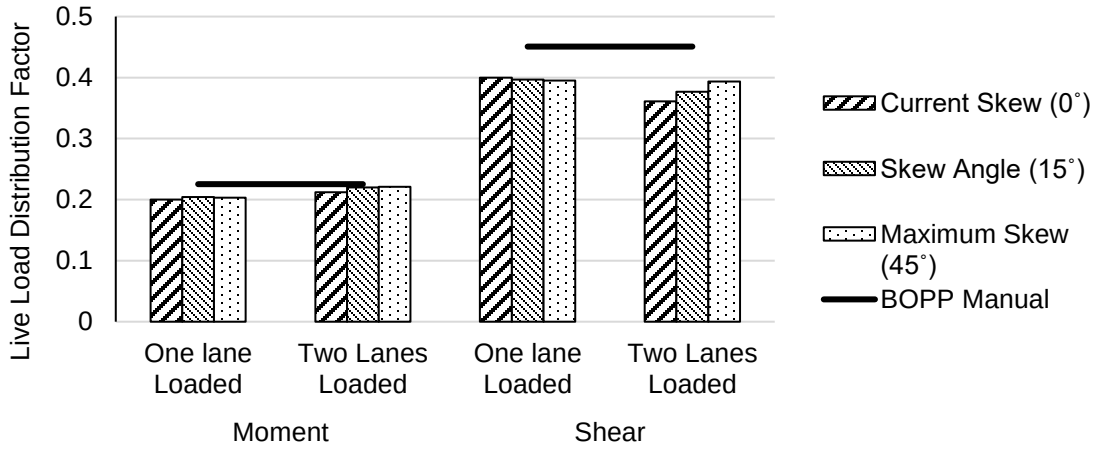

Figure 7.4: Effect of skew angle on LLMDFs and LLSDFs for bridge S080 40927R.

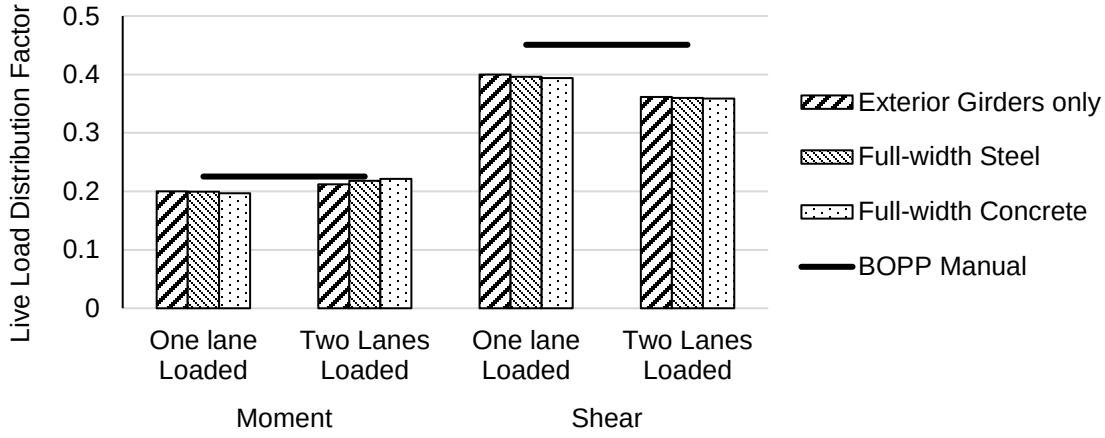

Figure 7.5: Effect of the diaphragm on LLMDFs and LLSDFs for bridge S080 40927R.

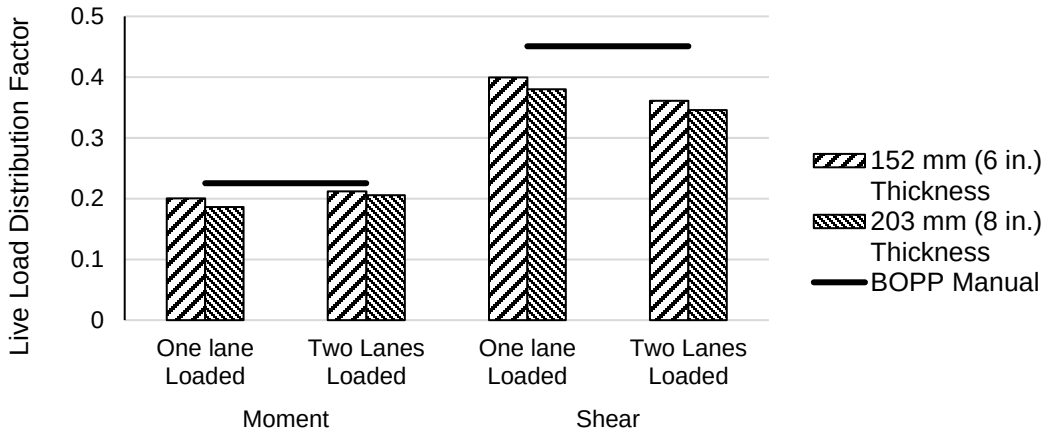

Figure 7.6: Effect of slab thickness on LLMDFs and LLSDFs for bridge S080 40927R.

7.4 COMPARING DISTRIBUTION FACTOR PREDICTION METHODS

Figure 7.7 shows a comparison of the live load distribution factors predicted by AASHTO LRFD, BOPP, and FEA for the skewed bridge M011022220. For the one lane loaded case, the moment distribution factors obtained from AASHTO LRFD and BOPP are higher than those obtained from FEA by 5.4% and 16.7%, respectively. However, for the two-lane loaded case, the moment distribution factors obtained from BOPP and FEA are the same, while those obtained from AASHTO LRFD are 37.4% higher. The shear distribution factors predicted by AASHTO LRFD and BOPP are about 14.6% to 28.5% higher than those predicted by the FEA. Also, The LLDFs obtained from the FEA of the skewed bridge SS66C00220 were compared to predicted factors by AASHTO LRFD, BOPP and it follows the same aspect as bridge M01102220 as shown in Figure 7.8.

Figure 7.9 shows a comparison of the live load distribution factors predicted by AASHTO LRFD, BOPP, and FEA for the continuous bridge S080 40927R. Both moment and shear live load distribution factors predicted by AASHTO LRFD and BOPP are

conservative compared to those obtained from FEA in both one-lane and two-lane loading cases.

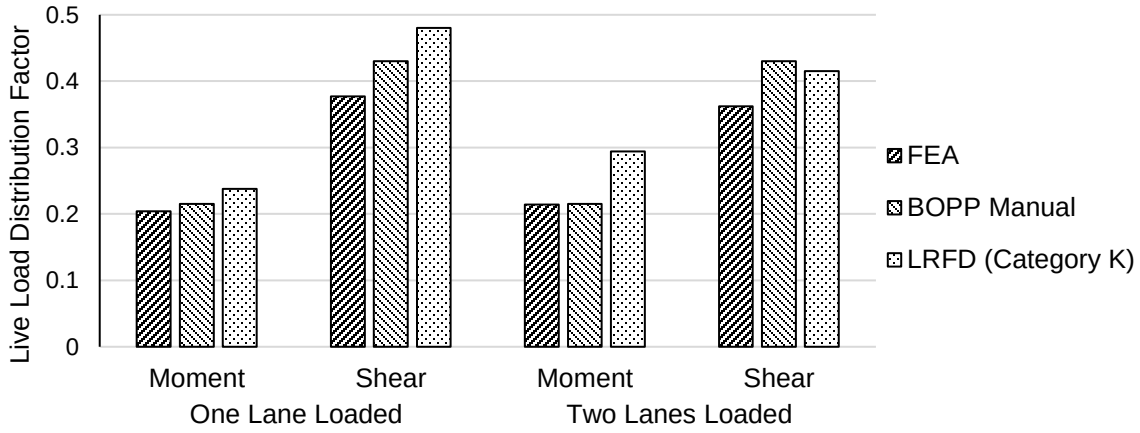

Figure 7.7: Live load distribution factors for the skewed bridge M01102220.

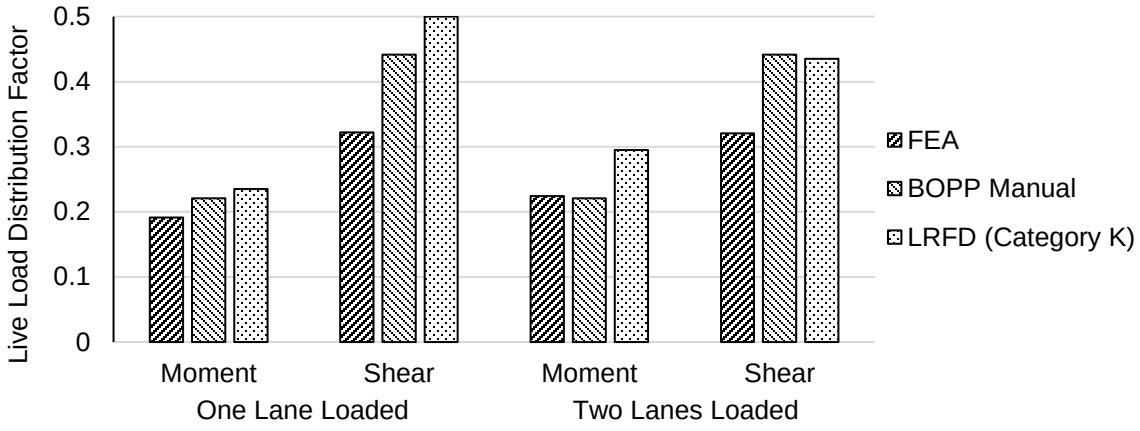

Figure 7.8: Live load distribution factors for the skewed bridge SS66C00220.

Figure 7.9: Live load distribution factors for the straight bridge S080 40927R.

7.5 EFFECT OF DIAPHRAGM TYPE AND SLAB THICKNESS ON IT GIRDER DEFLECTIONS

In this study, the three cases of diaphragm type shown in Figure 7.2 were studied for two different design truck locations. First, two trucks were placed asymmetrically in the transverse direction at the mid-span section as shown in Figure 7.10. Second, one truck was placed symmetrically in the transverse direction at the mid-span section as shown in Figure 7.11. Third, two trucks were placed symmetrically in the transverse direction at the mid-span section as shown in Figure 7.12. These figures indicate that the type of diaphragm has slight to moderate effect on the deflection of bridge girders and differential deflections between adjacent girders. Full-width uncracked concrete intermediate diaphragms transversely distribute the live loads better than other types, which results in smaller differential deflections than the other two diaphragm types. The relative deflection between adjacent girders is decreased by 25% when using the concrete diaphragms, which reduces

deck cracking. Also, the full-width uncracked concrete intermediate diagram reduces the maximum bridge deflection by 15.46% and 8.37% lower than the current diaphragm for one lane loaded and two lanes loaded respectively.

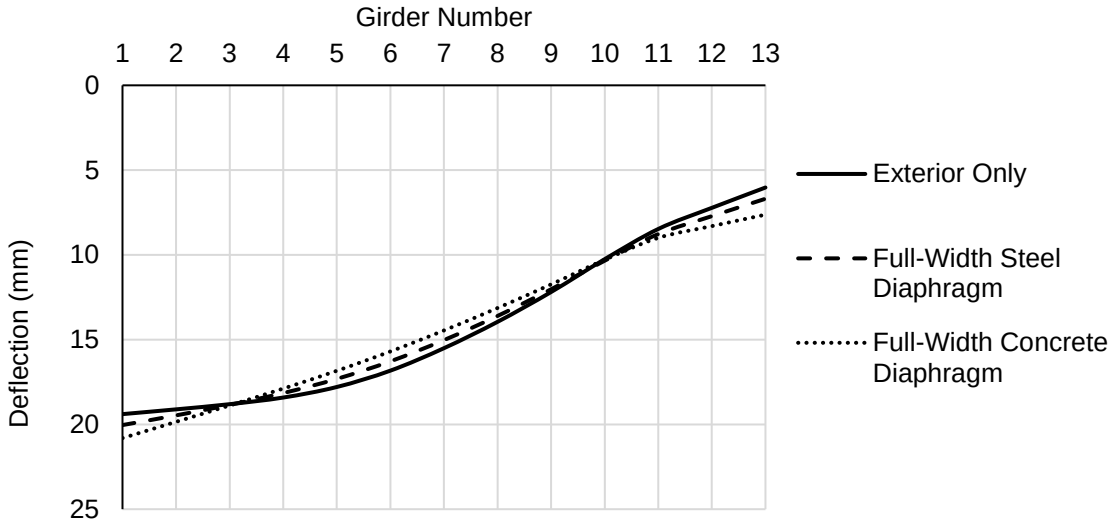

Figure 7.10: Bridge deflection at mid-span for two trucks placed asymmetrically in the transverse direction for different types of the diaphragm.

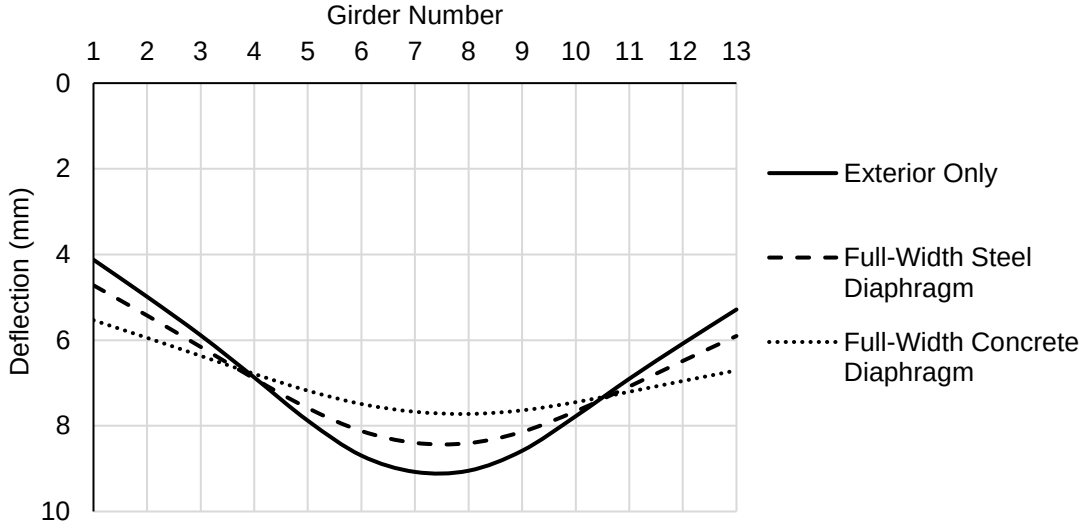

Figure 7.11: Bridge deflection at mid-span for one truck placed symmetrically in the transverse direction for different types of the diaphragm.

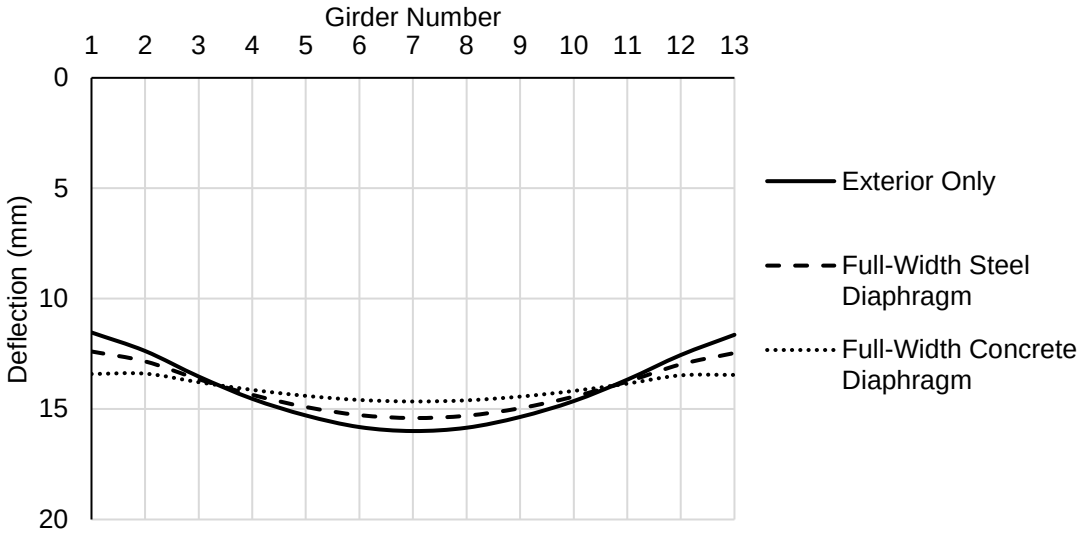

Figure 7.12: Bridge deflection at mid-span for two trucks placed symmetrically in the transverse direction for different types of the diaphragm.

Four different combinations of slab thickness and diaphragm type were studied using FEA of bridge M01102220. These four combinations are 152 mm (6 in.) slab without a diaphragm, 152 mm (6 in.) slab with a full-width uncracked concrete intermediate diaphragm, 203 mm (8 in.) slab without a diaphragm and 203 mm (8 in.) slab with a full-width uncracked concrete intermediate diaphragm. Figure 7.13 shows the deflected shape of the bridge in the transverse direction for all four cases when loaded asymmetrically with two trucks. This plot indicates that the deflection values decrease significantly with the increase in slab thickness. It also shows that the differential deflections decrease significantly with the addition of a full-width uncracked concrete intermediate diaphragm. Therefore, the combination of the 203 mm (8 in.) slab thickness and a full-width uncracked concrete intermediate diaphragm results in the highest stiffness in the transverse direction.

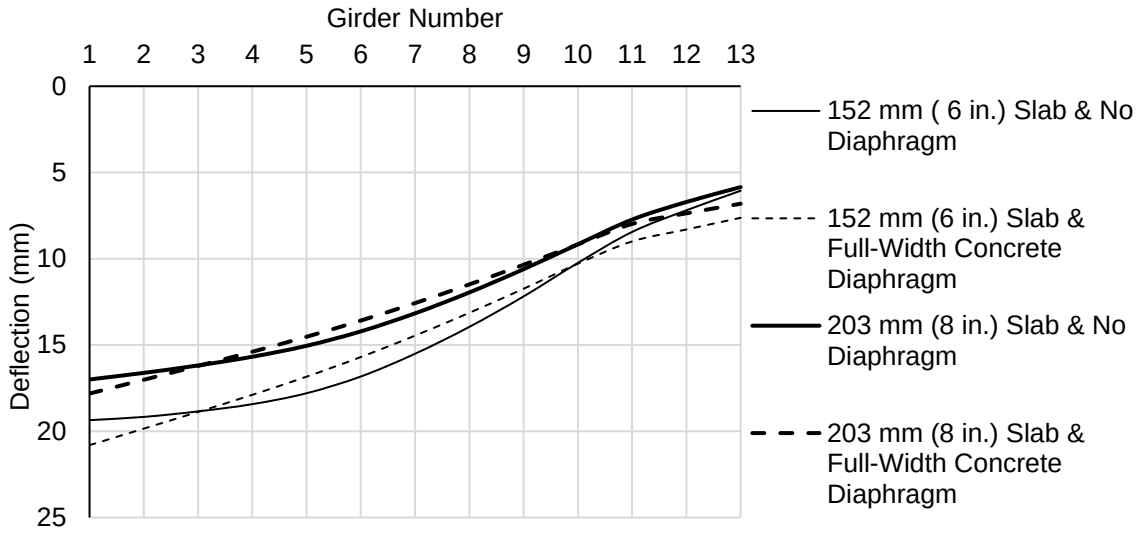

Figure 7.13: Mid-span bridge deflection for two trucks placed asymmetrically in the transverse direction for different slab thicknesses w/ and w/o a diaphragm.

7.6 EFFECT OF DIAPHRAGM TYPE AND SLAB THICKNESS ON SLAB TRANSVERSE STRESSES

During the field inspections of several IT bridges, longitudinal cracks over girder lines were observed. To determine the effect of diaphragm type and slab thickness in reducing transverse deck stresses that cause these cracks, a single wheel load of AASHTO HL-93 design truck and tandem (plus 75% dynamic load allowance) were applied to the developed FE models. For each model, un-cracked section analysis procedures were used, and wheel loads were placed over girder lines and between girder lines as point loads. FEA results indicated that tandem wheel loads placed over the middle girder line resulted in the highest stresses for all cases of mid-span diaphragm. The maximum transverse tensile stresses occurred at the second interior girder, which is typically where the longitudinal cracks are observed. Using a full-width uncracked concrete intermediate diaphragm

reduced deck transverse tensile stresses significantly from 2.07 MPa (0.3 ksi) (when no diaphragm was used) to 0.21 MPa (0.03 ksi). Also, using a full-width steel diaphragm reduced deck transverse tensile stresses from 1.38 MPa (0.2 ksi) (when steel diaphragms were used at exterior girders only) to 0.48 MPa (0.07 ksi). Two different slab thicknesses (152 mm (6 in.) and 203 mm (8 in.)) were also investigated and indicated that increasing the deck slab thickness has a slight effect in reducing transverse tensile stresses from 2.07 MPa (0.3 ksi) to 1.52 MPa (0.22 ksi).

7.7 CONCLUSIONS

Based on the results of the analytical investigation conducted in this chapter, the following conclusions can be made:

1. Skew angle and deck slab thickness have a negligible effect on live load distribution factors for IT bridges.
2. Live load distribution factors obtained from the AASHTO LRFD bridge design specifications and BOPP manual are conservative compared to those obtained from FEA.
3. The maximum transverse tensile stress in the deck slab occurs at the second interior girder line and results in the longitudinal cracks observed during field inspections. The wheel load of the AASHTO design tandem creates higher transverse stresses in the deck than the HL-93 truck wheel load for IT Bridges.
4. Using a full-width uncracked concrete intermediate diaphragm (e.g., transversely prestressed diaphragm) reduces IT bridge deflection at mid-span by 15.5% compared to using only a steel diaphragm at the exterior girders. It also

reduces the differential deflection between adjacent girders by 25% and the deck transverse tensile stresses significantly, which could help minimize the longitudinal deck cracking.

CHAPTER 8– CONCLUSIONS

8.1 CONCLUSIONS

Previous chapters have summarized numerous conclusions supported by the visual and quantified findings from the field observations, system identification, and advanced geospatial analysis of the IT girder bridge system. These conclusions indicate that despite the structural adequacy of the IT girder system, closely spaced girders are responding nonuniformly and independently, which may contribute to the longitudinal deck cracking.

The field observations of the 20 IT girder bridges identified five main categories of common damage. These categories include deck cracking, damaged abutment caps, damaged pier caps, damaged girders, and cracked bridge rails. The most surprising discovery is that longitudinal deck cracking occurs between most adjacent IT girders. In comparison, this damage is not commonly found on alternative bridge types. For the IT girder bridge system, longitudinal deck cracking does not occur during construction and is likely caused by heavy live loads. To the contrary, transverse deck cracking and bridge rail cracking are found in recently constructed bridges and may initiate during construction. When increasing the deck thickness from six to eight inches, observations indicated no reduction of deck cracking and therefore no impact to the serviceability of the bridge decks.

The system identification results demonstrated that the instrumented slab bridge and NU girder bridge both respond more uniformly along their cross-section compared to the IT girder bridge. Consequently, one key conclusion made here is that the differential response between adjacent IT girders observed within the ODS is very likely the cause of the longitudinal deck cracking. Increasing the transverse stiffeners between the IT girders

by modifying or adding full-width intermediate diaphragms may decrease the differential response between adjacent girders. To further exacerbate the deck cracking, excitations due to live loads dominantly resonates higher modes ranging between 10 to 15 Hz for a typical IT girder bridge. The girders respond independently of each other within these higher modes, which is likely contributing to the longitudinal deck cracking. When increasing the deck thickness from six to eight inches, there is no significant benefit to the bridge dynamic performance nor a reduction in the differential girder response as demonstrated by the instrumented bridge responses.

Advanced geospatial analysis of the IT girder bridges determined the relative deck and girder elevations by lidar depth mapping. The deck depth maps identify no significant locations of potential water ponding for increased water and/or chloride penetration. The computed cross slopes are consistent compared to the design specifications. However, the girder depth maps suggest that some IT girders were either set at various elevations and/or the resulting deck thickness is nonuniform. The unpredictable camber variation may contribute to the inconsistent thickness, stiffness irregularities, and global torsional response of the bridge deck.

The live load tests using LVDT's, strain gauges, and lidar determined that the girders near the load will have significant deflection and strain, but girders a few places over will have very low deflection and strain values. This results in significant differential deflections and strains, which are contributing to the longitudinal deck cracking. Span-to-depth ratio, skew angle, deck thickness, and current intermediate diaphragms did not have a significant impact on the differential deflection values. Finding a way to increase the

transverse stiffness to stop the girders from acting independently would reduce the amount of longitudinal deck cracking.

The FEA determined that the live load distribution factors obtained from the AASHTO LRFD bridge design specifications and BOPP manual are conservative. It also determined that the skew angle and deck slab thickness have a negligible effect on the live load distribution factors. The maximum transverse tensile stress in the deck slab occurs at the second interior girder line which matches up with the longitudinal cracking observed in the field. This max stress was caused by the wheel load of the AASHTO design tandem and not that of the HL-93 truck wheel load. The use of uncracked full-width concrete diaphragm (e.g., transversely prestressed intermediate diaphragm) reduces IT bridge deflection at mid-span by 15.5% compared to using only a steel diaphragm on the exterior girders. It also reduces the differential deflection between adjacent girders by 25% and the deck transverse tensile stresses significantly, which could help minimize the longitudinal deck cracking.

8.2 RECOMMENDATIONS

Although the longitudinal deck cracking is unique to the IT bridge system, the structural performance of the system is adequate with no signs of premature deterioration. Therefore, it is recommended to continue to use the system while monitoring its long-term durability. There are no noticeable trends between the severity of deck cracking and the year constructed, IT girder size, maximum span length, nor skew angle. This indicates that the cracking does not seem to progress with age and use, but this is only observable over a few decades due to their recent construction. Any girder damage observed did not appear

to be caused by the structural performance of the bridge but from construction practices or water entrapment. The findings here indicate that the LL differential deflection of the girders is likely the cause of the longitudinal deck cracking. Note, that the total deflection is not large enough to cause concern and is within normal working limits. One potential solution to combat the serviceability issue of deck cracking is to use a waterproof membrane with an asphalt overlay.

The IT girder bridges should continue to be looked at as a competitive design for short to medium length spans ranging from 30 to 80 feet. The system continues to offer many benefits including no required temporary formwork, quick and easy construction process, shorter road closures, reduced bridge weight, and efficient material usage. The longitudinal cracking should be kept in mind, but it is a minor serviceability concern and not a performance concern. The FEA results showed that using full-width prestressed concrete diaphragms will slightly increase the transverse stiffness helping reduce that differential deflection between girders which might not be a very cost-effective solution.

8.3 FUTURE WORK

The conclusions identified a few deficiencies of the IT girder bridge system that requires future research work to further understand and improve. The next step is to explore ways to reduce and preferably minimize the longitudinal deck cracking. A future research topic would be to find an effective method to increase the transverse stiffness of the IT girder bridge system. The IT girders need to respond more uniformly and consistently along the bridge cross-section with less differential response between adjacent girders. The

following research topics are suggested to further study the longitudinal deck cracking problem for the IT girder bridge system:

1. Develop a feasible method of post tensioning to reduce longitudinal deck cracking, similar to the design modifications by the Kansas DOT to prevent transverse deck cracking over the piers (Nayal et al., 2006).
2. Investigate utilizing high-performance concrete (HPC), or even ultra-high performance concrete (UHPC) for the deck.
3. Determine if there is deterioration of the reinforcing steel due to the longitudinal deck cracking. If there is deterioration, investigate the use of an asphalt overlay with membrane or fiberglass reinforcement.
4. Conduct lidar scans to compare LL deflection for bridges with and without diaphragms.

REFERENCES

AASHTO (2014). LRFD Bridge Design Specifications; Seventh Edition. American Association of State Highway and Transportation Officials, Washington, D.C.

AASHTO (1996). Standard Specifications for Highway Bridges; Sixteenth Edition. American Association of State Highway and Transportation Officials, Washington, D.C.

Ambare, S., and Peterman, R. J. (2006). Evaluation of the inverted Tee shallow bridge system for use in Kansas. (No. K-TRAN: KSU-00-1). Kansas Department of Transportation.

Bishara, A. G., Liu, M. C. and Ali, N.D. (1993). "Wheel Load Distribution on Simply Supported Skew I-Beam Composite Bridges." Journal of Structural Engineering, 119(2), 399-419.

Bore, C. (2014). DSP Without Math: A Brief Introduction. BORES Signal Processing.

Brincker, R. and Anderson, P. (2006). "Understanding Stochastic Subspace Identification." Proceedings of the 24th International Modal Analysis Conference, St. Louis, MO.

Brincker, R. and Ventura, C. (2015). Introduction to Operational Modal Analysis.

Brincker, R., Zhang, L., and Anderson, P. (2000). “Modal Identification from Ambient Responses using Frequency Domain Decomposition.” Proceedings of the 18th International Modal Analysis Conference, San Antonio, TX.

CSI (2011). Analysis Reference Manual for SAP2000, ETABS, SAFE and CSiBridge. Computer & Structures Inc, Berkeley, California.

Cunha, A. and Caetano E. (2006). “Experimental Modal Analysis of Civil Engineering Structures.” Journal of Sound and Vibration.

Faro (2011). Faro laser scanner Focus 3D: features, benefits & technical specifications. FARO Technologies, Lake Mary, FL.

He, J. and Fu, Z-F. (2001). Modal Analysis. Butterworth-Heinemann: Woburn, MA.

Herlufsen, H., Kjær, B., and Andersen, P. (2005). “Identification Techniques for Operational Modal Analysis – An Overview and Practical Experiences.”

Jaber, F. (2013). “Nebraska’s Inverted Tee Short-Span Bridge System.” PCI ASPIRE, Spring 2013, 34-35.

Kamel, M.R. and Tadros, M.K. (1996). “The Inverted Tee Shallow Bridge System for Rural Areas.” PCI Journal, 41(5), 28-43.

Khalil, A., Greimann, L., Wipf, T.J., and Wood, D. (1998). “Modal Testing for Nondestructive Evaluation of Bridges: Issues.” Proceedings of the Transportation Conference, Ames, IA.

Larson, N., Gomez, E. F., Garber, D., Bayrak, O., and Ghannoum, W. (2013). Strength and Serviceability Design of Reinforced Concrete Inverted-T Beams. (No. FHWA/TX-13/0-6416-1).

Mellinger, P., Döhler, M., and Mevel, L. (2016). “Variance estimation of modal parameters from output-only and input/output subspace-based system identification.” Journal of Sound and Vibration. Elsevier, 379, 1-27. <10.1016/j.jsv.2016.05.037>. <hal-01328435>

Menassa, C., Mabsout, M., Tarhini, K. and Frederick, G. (2007). “Influence of Skew Angle on Reinforced Concrete Slab Bridge.” Journal of Bridge Engineering, 12(2), 205-21.

Nayal, R.M.N., Peterman, R.J., and Esmaeily, A. (2006). Post-Tensioning the Inverted T-Bridge System for Improved Durability and Increased Span-to-Depth Ratio. (No. K-TRAN: KSU-03-5) Kansas Department of Transportation.

Nebraska Department of Roads (NDOR) (2014). Bridge Office Policies and Procedures. BOPP 2014, Nebraska Department of Roads, Bridge Division.

Peeters, B. and Roeck, G.D. (2001). "Stochastic System Identification for Operational Modal Analysis: A Review." Journal of Dynamic Systems Measurement and Control, 123(4).

Ren, W., Zhao, T., and Harik, I.E. (2004). "Experimental and Analytical Modal Analysis of Steel Arch Bridge." J. Struct. Eng., 130(7), 1022-1031.

Structural Vibrations Solutions. (2017). "SSI-UPCX." <http://www.svibs.com/resources/ARTeMIS_Modal_Help/SSI-UPCX.html > (March 11, 2018).

Tadros, M. K. and Kamel, M. R. (1996). "The Inverted Tee Shallow Bridge System for Rural Areas." PCI Journal, 41(5).

Welch, P.D. (1967). "The Use of Fast Fourier Transform for the Estimation of Power Spectra: A Method Based on Time Averaging Over Short, Modified Periodograms." IEEE Transactions on Audio and Electroacoustics, 15(2), 70-73.

APPENDIX A

IT Girder Bridge S006 26001:

Figure A.1: Location of bridge S006 26001 (courtesy of Google Maps).

Table A.1: Bridge information summary for bridge S006 26001.

Bridge ID	S006 26001	**Girder Height (in [mm])**	11.81 [300]
County	Fillmore	**Girder Width (in [mm])**	23.63 [600]
Year Built	1999	**Girder Spacing (in [mm])**	29.06 [738]
No. of Spans	3	**Deck Thickness (in [mm])**	6 [152]
Length Span 1 (ft)	31.70	**No. of Girders**	19
Length Span 2 (ft)	32.50	**Diaphragm**	None
Length Span 3 (ft)	31.70	**Deck Rating**	8
Bridge Width (ft)	45.60	**Superstructure Rating**	8
Skew Angle (°)	20	**Substructure Rating**	7

Figure A.2: Photo of bridge S006 26001.

(a) (b)

Figure A.3: Deck cracks on bridge S006 26001.

Figure A.4: Full-depth deck crack on bridge S006 26001.

Figure A.5: Damaged southwest abutment on bridge S006 26001.

Figure A.6: Damaged southeast abutment on bridge S006 26001.

Figure A.7: Damaged northwest abutment on bridge S006 26001.

Figure A.8: Damaged northeast abutment on bridge S006 26001.

IT Girder Bridge S006 34277:

Figure A.9: Location of bridge S006 34277 (courtesy of Google Maps).

Table A.2: Bridge information summary for bridge S006 34277.

Bridge ID	S006 34277	**Girder Height (in [mm])**	11.81 [300]
County	Sarpy	**Girder Width (in [mm])**	23.63 [600]
Year Built	2002	**Girder Spacing (in [mm])**	28.75 [730]
No. of Spans	3	**Deck Thickness (in [mm])**	6 [152]
Length Span 1 (ft)	35.00	**No. of Girders**	19
Length Span 2 (ft)	40.00	**Diaphragm**	None
Length Span 3 (ft)	35.00	**Deck Rating**	7
Bridge Width (ft)	46.30	**Superstructure Rating**	7
Skew Angle (°)	40	**Substructure Rating**	8

Figure A.10: Photo of bridge S006 34277.

Figure A.11: Deck cracks on bridge S006 34277.

(a) (b)

Figure A.12: Chips in the deck on bridge S006 34277.

(a) (b)

Figure A.13: Damaged east abutment on bridge S006 34277.

(a) (b)

Figure A.14: Damaged girder at west abutment on bridge S006 34277.

(a) (b)

Figure A.15: Damaged girder at south abutment on bridge S006 34277.

Figure A.16: Damaged north abutment on bridge S006 34277.

(a) (b)

Figure A.17: Damaged girder flange caused by water entrapment in concrete forms on bridge S006 34277.

Figure A.18: Washout under south abutment on bridge S006 34277.

Figure A.19: Cracked rail on bridge S006 34277.

IT Girder Bridge S009 00888:

Figure A.20: Location of bridge S009 00888 (courtesy of Google Maps).

Table A.3: Bridge information summary for bridge S009 00888.

Bridge ID	S009 00888	**Girder Height (in [mm])**	15.75 [400]
County	Cuming	**Girder Width (in [mm])**	23.63 [600]
Year Built	2002	**Girder Spacing (in [mm])**	28.00 [711]
No. of Spans	3	**Deck Thickness (in [mm])**	6 [152]
Length Span 1 (ft)	32.00	**No. of Girders**	18
Length Span 2 (ft)	44.00	**Diaphragm**	None
Length Span 3 (ft)	32.00	**Deck Rating**	8
Bridge Width (ft)	42.40	**Superstructure Rating**	8
Skew Angle (°)	45	**Substructure Rating**	7

Figure A.21: Photo of bridge S009 00888.

Figure A.22: Deck crack on bridge S009 00888.

Figure A.23: Small deck potholes on bridge S009 00888.

(a) (b)

Figure A.24: Cracked abutment cap on bridge S009 00888.

(a) (b)

Figure A.25: Damaged southeast abutment on bridge S009 00888.

(a) (b)

Figure A.26: Damaged southwest and northwest abutment on bridge S009 00888.

Figure A.27: Chipped girder on bridge S009 00888.

(a) (b)

Figure A.28: Rusted piles on bridge S009 00888.

IT Girder Bridge S034 31644:

Figure A.29: Location of bridge S034 31644 (courtesy of Google Maps).

Table A.4: Bridge information summary for bridge S034 31644.

Bridge ID	S034 31644	**Girder Height (in [mm])**	15.75 [400]
County	Lancaster	**Girder Width (in [mm])**	23.63 [600]
Year Built	2005	**Girder Spacing (in [mm])**	28.50 [724]
No. of Spans	3	**Deck Thickness (in [mm])**	6 [152]
Length Span 1 (ft)	46.00	**No. of Girders**	42
Length Span 2 (ft)	48.00	**Diaphragm**	C8x18.75
Length Span 3 (ft)	46.00	**Deck Rating**	7
Bridge Width (ft)	99.90	**Superstructure Rating**	9
Skew Angle (°)	30	**Substructure Rating**	8

Figure A.30: Photo of bridge S034 31644.

(a) (b)

Figure A.31: Deck cracks on bridge S034 31644.

Figure A.32: Longitudinal and diagonal deck cracks on bridge S034 31644.

(a) (b)

Figure A.33: Damaged abutments on bridge S034 31644.

Figure A.34: Chipped and patched girder on bridge S034 31644.

Figure A.35: Cracked rail on bridge S034 31644.

IT Girder Bridge S050 04149:

Figure A.36: Location of bridge S050 04149 (courtesy of Google Maps).

Table A.5: Bridge information summary for bridge S050 04149.

Bridge ID	S050 04149	**Girder Height (in [mm])**	23.63 [600]
County	Johnson	**Girder Width (in [mm])**	23.63 [600]
Year Built	1997	**Girder Spacing (in [mm])**	25.59 [650]
No. of Spans	3	**Deck Thickness (in [mm])**	6 [152]
Length Span 1 (ft)	66.50	**No. of Girders**	19
Length Span 2 (ft)	67.25	**Diaphragm**	Concrete
Length Span 3 (ft)	66.50	**Deck Rating**	7
Bridge Width (ft)	41.70	**Superstructure Rating**	8
Skew Angle (°)	10	**Substructure Rating**	7

Figure A.37: Photo of bridge S050 04149.

(a) (b)

Figure A.38: Deck cracks on bridge S050 04149.

(a) (b)

Figure A.39: Damaged abutments on bridge S050 04149.

Figure A.40: Cracked rail on bridge S050 04149.

IT Girder Bridge S050 06686:

Figure A.41: Location of bridge S050 06686 (courtesy of Google Maps).

Table A.6: Bridge information summary for bridge S050 06686.

Bridge ID	S050 06686	**Girder Height (in [mm])**	27.56 [700]
County	Cass	**Girder Width (in [mm])**	23.63 [600]
Year Built	2007	**Girder Spacing (in [mm])**	28.75 [730]
No. of Spans	3	**Deck Thickness (in [mm])**	6 [152]
Length Span 1 (ft)	62.50	**No. of Girders**	24
Length Span 2 (ft)	75.00	**Diaphragm**	C12x30
Length Span 3 (ft)	62.50	**Deck Rating**	7
Bridge Width (ft)	58.80	**Superstructure Rating**	8
Skew Angle (°)	0	**Substructure Rating**	8

Figure A.42: Photo of bridge S050 06686.

(a) (b)

Figure A.43: Deck cracks on bridge S050 06686.

(a) (b)

Figure A.44: Damaged abutments on bridge S050 06686.

Figure A.45: Cracked abutment cap on bridge S050 06686.

(a) (b)

Figure A.46: Washout under abutments on bridge S050 06686.

(a) (b)

Figure A.47: Chipped girders on bridge S050 06686.

Figure A.48: Cracked rail on bridge S050 06686.

IT Girder Bridge S058 00994:

Figure A.49: Location of bridge S058 00994 (courtesy of Google Maps).

Table A.7: Bridge information summary for bridge S058 00994.

Bridge ID	S058 00994	**Girder Height (in [mm])**	11.81 [300]
County	Howard	**Girder Width (in [mm])**	23.63 [600]
Year Built	2001	**Girder Spacing (in [mm])**	26.38 [670]
No. of Spans	3	**Deck Thickness (in [mm])**	6 [152]
Length Span 1 (ft)	36.75	**No. of Girders**	18
Length Span 2 (ft)	45.00	**Diaphragm**	None
Length Span 3 (ft)	36.75	**Deck Rating**	6
Bridge Width (ft)	40.00	**Superstructure Rating**	8
Skew Angle (°)	0	**Substructure Rating**	8

Figure A.50: Photo of bridge S058 00994.

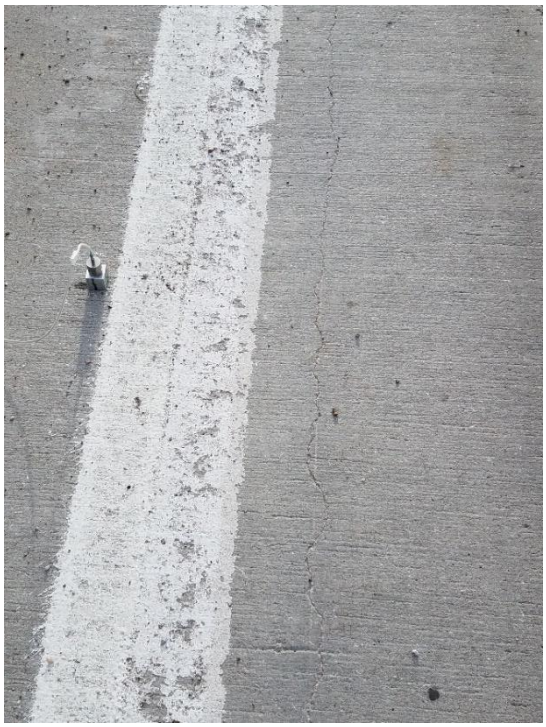

(a)

(b)

Figure A.51: Deck cracks on bridge S058 00994.

(a)

(b)

Figure A.52: Damaged south abutment on bridge S058 00994.

Figure A.53: Damaged east abutment on bridge S058 00994.

(a) (b)

Figure A.54: Damaged expansion joints on bridge S058 00994.

Figure A.55: Damaged girder flange caused by water entrapment in concrete forms on bridge S058 00994.

IT Girder Bridge S080 40872R:

Figure A.56: Location of bridge S080 40872R (courtesy of Google Maps).

Table A.8: Bridge information summary for bridge S080 40872R.

Bridge ID	S080 40872R	**Girder Height (in [mm])**	15.75 [400]
County	Lancaster	**Girder Width (in [mm])**	23.63 [600]
Year Built	2010	**Girder Spacing (in [mm])**	29.75 [756]
No. of Spans	3	**Deck Thickness (in [mm])**	8 [203]
Length Span 1 (ft)	48.25	**No. of Girders**	25
Length Span 2 (ft)	53.50	**Diaphragm**	C8x18.75
Length Span 3 (ft)	48.25	**Deck Rating**	8
Bridge Width (ft)	62.80	**Superstructure Rating**	9
Skew Angle (°)	0	**Substructure Rating**	9

Figure A.57: Photo of bridge S080 40872R.

(a) (b)

Figure A.58: Deck cracks on bridge S080 40872R.

(a) (b)

Figure A.59: Damaged southeast abutment on bridge S080 40872R.

(a) (b)

Figure A.60: Damaged northwest abutment on bridge S080 40872R.

Figure A.61: Cracked rail on bridge S080 40872R.

IT Girder Bridge S080 40927R:

Figure A.62: Location of bridge S080 40927R (courtesy of Google Maps).

Table A.9: Bridge information summary for bridge S080 40927R.

Bridge ID	S080 40927R	**Girder Height (in [mm])**	15.75 [400]
County	Lancaster	**Girder Width (in [mm])**	23.63 [600]
Year Built	2010	**Girder Spacing (in [mm])**	29.75 [756]
No. of Spans	3	**Deck Thickness (in [mm])**	8 [203]
Length Span 1 (ft)	48.25	**No. of Girders**	25
Length Span 2 (ft)	53.50	**Diaphragm**	C8x18.75
Length Span 3 (ft)	48.25	**Deck Rating**	8
Bridge Width (ft)	62.80	**Superstructure Rating**	9
Skew Angle (°)	0	**Substructure Rating**	9

Figure A.63: Photo of bridge S080 40927R.

(a) (b)

Figure A.64: Deck cracks on bridge S080 40927R.

Figure A.65: Cracked rail on bridge S080 40927R.

IT Girder Bridge S081 05152L:

Figure A.66: Location of bridge S081 05152L (courtesy of Google Maps).

Table A.10: Bridge information summary for bridge S081 05152L.

Bridge ID	S081 05152L	**Girder Height (in [mm])**	15.75 [400]
County	York	**Girder Width (in [mm])**	23.63 [600]
Year Built	1999	**Girder Spacing (in [mm])**	25.98 [660]
No. of Spans	3	**Deck Thickness (in [mm])**	6 [152]
Length Span 1 (ft)	42.00	**No. of Girders**	19
Length Span 2 (ft)	56.00	**Diaphragm**	Concrete
Length Span 3 (ft)	42.00	**Deck Rating**	7
Bridge Width (ft)	40.70	**Superstructure Rating**	8
Skew Angle (°)	10	**Substructure Rating**	7

Figure A.67: Photo of bridge S081 05152L.

(a) (b)

Figure A.68: Deck cracks on bridge S081 05152L.

Figure A.69: Cracked rail on bridge S081 05152L.

IT Girder Bridge S089 06047:

Figure A.70: Location of bridge S089 06047 (courtesy of Google Maps).

Table A.11: Bridge information summary for bridge S089 06047.

Bridge ID	S089 06047	**Girder Height (in [mm])**	11.81 [300]
County	Harlan	**Girder Width (in [mm])**	23.63 [600]
Year Built	2007	**Girder Spacing (in [mm])**	28.50 [724]
No. of Spans	3	**Deck Thickness (in [mm])**	6 [152]
Length Span 1 (ft)	40.00	**No. of Girders**	16
Length Span 2 (ft)	45.00	**Diaphragm**	Concrete
Length Span 3 (ft)	40.00	**Deck Rating**	8
Bridge Width (ft)	38.40	**Superstructure Rating**	9
Skew Angle (°)	0	**Substructure Rating**	9

Figure A.71: Photo of bridge S089 06047.

Figure A.72: Deck cracks on bridge S089 06047.

Figure A.73: Cracked rail on bridge S089 06047.

IT Girder Bridge S089 06062:

Figure A.74: Location of bridge S089 06062 (courtesy of Google Maps).

Table A.12: Bridge information summary for bridge S089 06062.

Bridge ID	S089 06062	**Girder Height (in [mm])**	15.75 [400]
County	Harlan	**Girder Width (in [mm])**	23.63 [600]
Year Built	2007	**Girder Spacing (in [mm])**	30.63 [778]
No. of Spans	6	**Deck Thickness (in [mm])**	6 [152]
Length Span 1/6 (ft)	50.00	**No. of Girders**	15
Length Span 2/3 (ft)	55.00	**Diaphragm**	Concrete
Length Span 4/5 (ft)	55.00	**Deck Rating**	8
Bridge Width (ft)	36.40	**Superstructure Rating**	9
Skew Angle (°)	25	**Substructure Rating**	9

Figure A.75: Photo of bridge S089 06062.

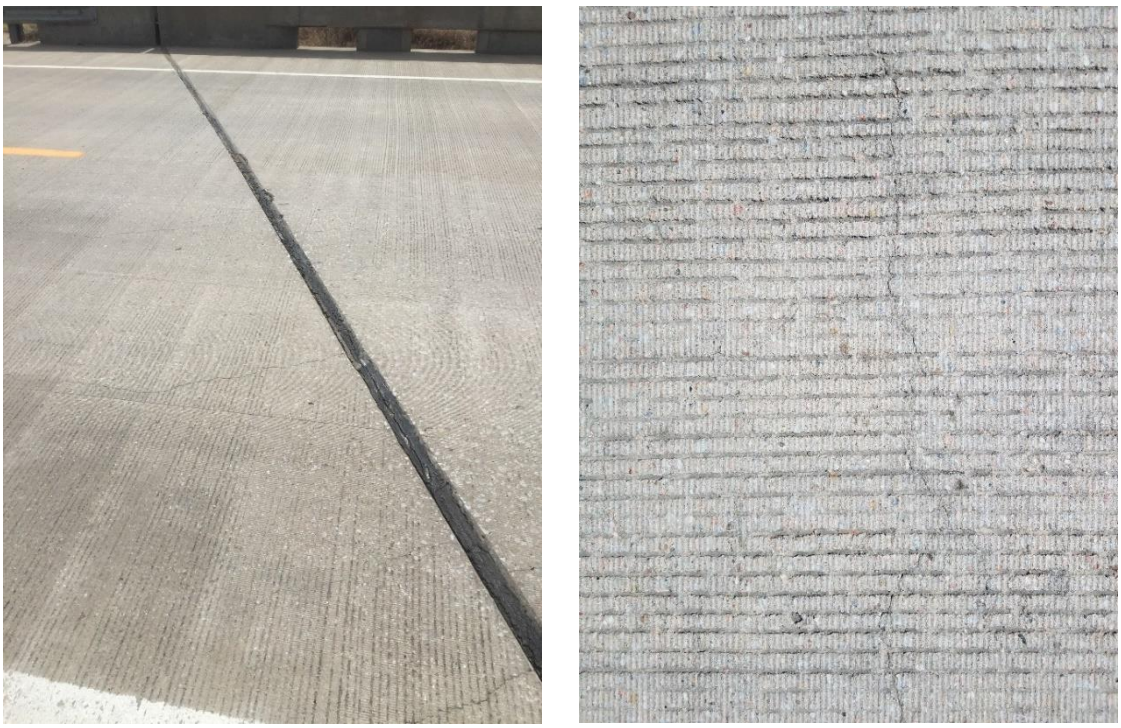

(a) (b)

Figure A.76: Deck cracks on bridge S089 06062.

IT Girder Bridge S103 02465:

Figure A.77: Location of bridge S103 02465 (courtesy of Google Maps).

Table A.13: Bridge information summary for bridge S103 02465.

Bridge ID	S103 02465	**Girder Height (in [mm])**	35.43 [900]
County	Gage	**Girder Width (in [mm])**	23.63 [600]
Year Built	1999	**Girder Spacing (in [mm])**	35.63 [905]
No. of Spans	5	**Deck Thickness (in [mm])**	6 [152]
Length Span 1/6 (ft)	45.00	**No. of Girders**	4 (expansion)
Length Span 2/5 (ft)	55.00	**Diaphragm**	Concrete
Length Span 3 (ft)	85.00	**Deck Rating**	7
Bridge Width (ft)	41.70	**Superstructure Rating**	7
Skew Angle (°)	0	**Substructure Rating**	7

Figure A.78: Photo of bridge S103 02465.

Figure A.79: Full-depth deck crack on bridge S103 02465.

Figure A.80: Damaged abutment on bridge S103 02465.

(a) (b)

Figure A.81: Damaged east pier cap on bridge S103 02465.

(a) (b)

Figure A.82: Damaged west pier cap on bridge S103 02465.

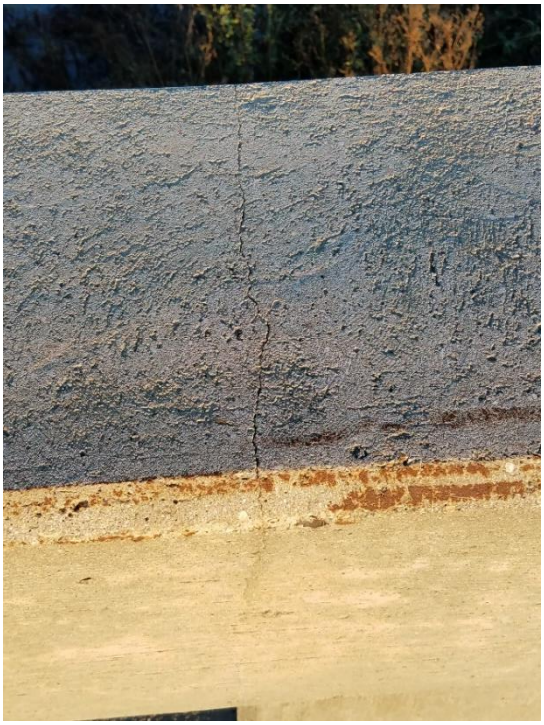

Figure A.83: Cracked rail on bridge S103 02465.

IT Girder Bridge S275 18587:

Figure A.84: Location of bridge S275 18587 (courtesy of Google Maps).

Table A.14: Bridge information summary for bridge S275 18587.

Bridge ID	S275 18587	**Girder Height (in [mm])**	19.69 [500]
County	Douglas	**Girder Width (in [mm])**	23.63 [600]
Year Built	1997	**Girder Spacing (in [mm])**	25.98 [660]
No. of Spans	3	**Deck Thickness (in [mm])**	6 [152]
Length Span 1 (ft)	54.50	**No. of Girders**	34
Length Span 2 (ft)	60.00	**Diaphragm**	Concrete
Length Span 3 (ft)	45.00	**Deck Rating**	7
Bridge Width (ft)	74.30	**Superstructure Rating**	8
Skew Angle (°)	0	**Substructure Rating**	7

Figure A.85: Photo of bridge S275 18587.

Figure A.86: Deck cracks on bridge S275 18587.

Figure A.87: Damaged abutment on bridge S275 18587.

IT Girder Bridge SS66C00220:

Figure A.88: Location of bridge SS66C00220 (courtesy of Google Maps).

Table A.15: Bridge information summary for bridge SS66C00220.

Bridge ID	SS66C00220	**Girder Height (in [mm])**	27.56 [700]
County	Otoe	**Girder Width (in [mm])**	23.63 [600]
Year Built	2001	**Girder Spacing (in [mm])**	29.13 [740]
No. of Spans	1	**Deck Thickness (in [mm])**	6 [152]
Length Span 1 (ft)	80.00	**No. of Girders**	15
Length Span 2 (ft)	--	**Diaphragm**	Concrete
Length Span 3 (ft)	--	**Deck Rating**	8
Bridge Width (ft)	37.70	**Superstructure Rating**	9
Skew Angle (°)	25	**Substructure Rating**	8

Figure A.89: Photo of bridge SS66C00220.

Figure A.90: Deck cracks on bridge SS66C00220.

(a) (b)

Figure A.91: Damaged abutment on bridge SS66C00220.

IT Girder Bridge C002408505:

Figure A.92: Location of bridge C002408505 (courtesy of Google Maps).

Table A.16: Bridge information summary for bridge C002408505.

Bridge ID	C002408505	**Girder Height (in [mm])**	23.63 [600]
County	Dawson	**Girder Width (in [mm])**	23.63 [600]
Year Built	2005	**Girder Spacing (in [mm])**	28.38 [721]
No. of Spans	1	**Deck Thickness (in [mm])**	6 [152]
Length Span 1 (ft)	65.00	**No. of Girders**	13
Length Span 2 (ft)	--	**Diaphragm**	C8x18.75
Length Span 3 (ft)	--	**Deck Rating**	5
Bridge Width (ft)	30.40	**Superstructure Rating**	9
Skew Angle (°)	35	**Substructure Rating**	9

Figure A.93: Photo of bridge C002408505.

Figure A.94: Gravel covered deck on bridge C002408505.

(a) (b)

Figure A.95: Damaged southeast abutment on bridge C002408505.

Figure A.96: Concrete patches on bridge C002408505.

Figure A.97: Cracked rail on bridge C002408505.

IT Girder Bridge C008504145:

Figure A.98: Location of bridge C008504145 (courtesy of Google Maps).

Table A.17: Bridge information summary for bridge C008504145.

Bridge ID	C008504145	**Girder Height (in [mm])**	23.63 [600]
County	Thayer	**Girder Width (in [mm])**	23.63 [600]
Year Built	2007	**Girder Spacing (in [mm])**	29.00 [737]
No. of Spans	3	**Deck Thickness (in [mm])**	6 [152]
Length Span 1 (ft)	50.75	**No. of Girders**	12
Length Span 2 (ft)	63.50	**Diaphragm**	C10x15.3
Length Span 3 (ft)	50.75	**Deck Rating**	5
Bridge Width (ft)	30.40	**Superstructure Rating**	5
Skew Angle (°)	0	**Substructure Rating**	6

Figure A.99: Photo of bridge C008504145.

(a) (b)

Figure A.100: Damaged north abutment on bridge C008504145.

Figure A.101: Chipped girder on bridge C008504145.

Figure A.102: Cracked rail on bridge C008504145.

IT Girder Bridge M011022220:

Figure A.103: Location of bridge M011022220 (courtesy of Google Maps).

Table A.18: Bridge information summary for bridge M011022220.

Bridge ID	M011022220	**Girder Height (in [mm])**	23.63 [600]
County	Sherman	**Girder Width (in [mm])**	23.63 [600]
Year Built	2012	**Girder Spacing (in [mm])**	28.38 [721]
No. of Spans	1	**Deck Thickness (in [mm])**	6 [152]
Length Span 1 (ft)	65.00	**No. of Girders**	13
Length Span 2 (ft)	--	**Diaphragm**	C8x18.75
Length Span 3 (ft)	--	**Deck Rating**	6
Bridge Width (ft)	30.40	**Superstructure Rating**	6
Skew Angle (°)	15	**Substructure Rating**	7

Figure A.104: Photo of bridge M011022220.

Figure A.105: Gravel covered deck on bridge M011022220.

Figure A.106: Cracked rail on bridge M011022220.

Figure A.107: Concrete patched rail on bridge M011022220.

IT Girder Bridge C004931110:

Figure A.108: Location of bridge C004931110 (courtesy of Google Maps).

Table A.19: Bridge information summary for bridge C004931110.

Bridge ID	C004931110	**Girder Height (in [mm])**	23.63 [600]
County	Johnson	**Girder Width (in [mm])**	23.63 [600]
Year Built	2017	**Girder Spacing (in [mm])**	30.00 [762]
No. of Spans	4	**Deck Thickness (in [mm])**	6 [152]
Length Span 1 (ft)	57.50	**No. of Girders**	12
Length Span 2/3 (ft)	75.00	**Diaphragm**	C12x30
Length Span 4 (ft)	57.50	**Deck Rating**	9
Bridge Width (ft)	27.50	**Superstructure Rating**	9
Skew Angle (°)	20	**Substructure Rating**	9

Figure A.109: Photo of bridge C004931110.

(a) (b)

Figure A.110: Transverse deck cracks on bridge C004931110.

Figure A.111: Cracked rail on bridge C004931110.

APPENDIX B

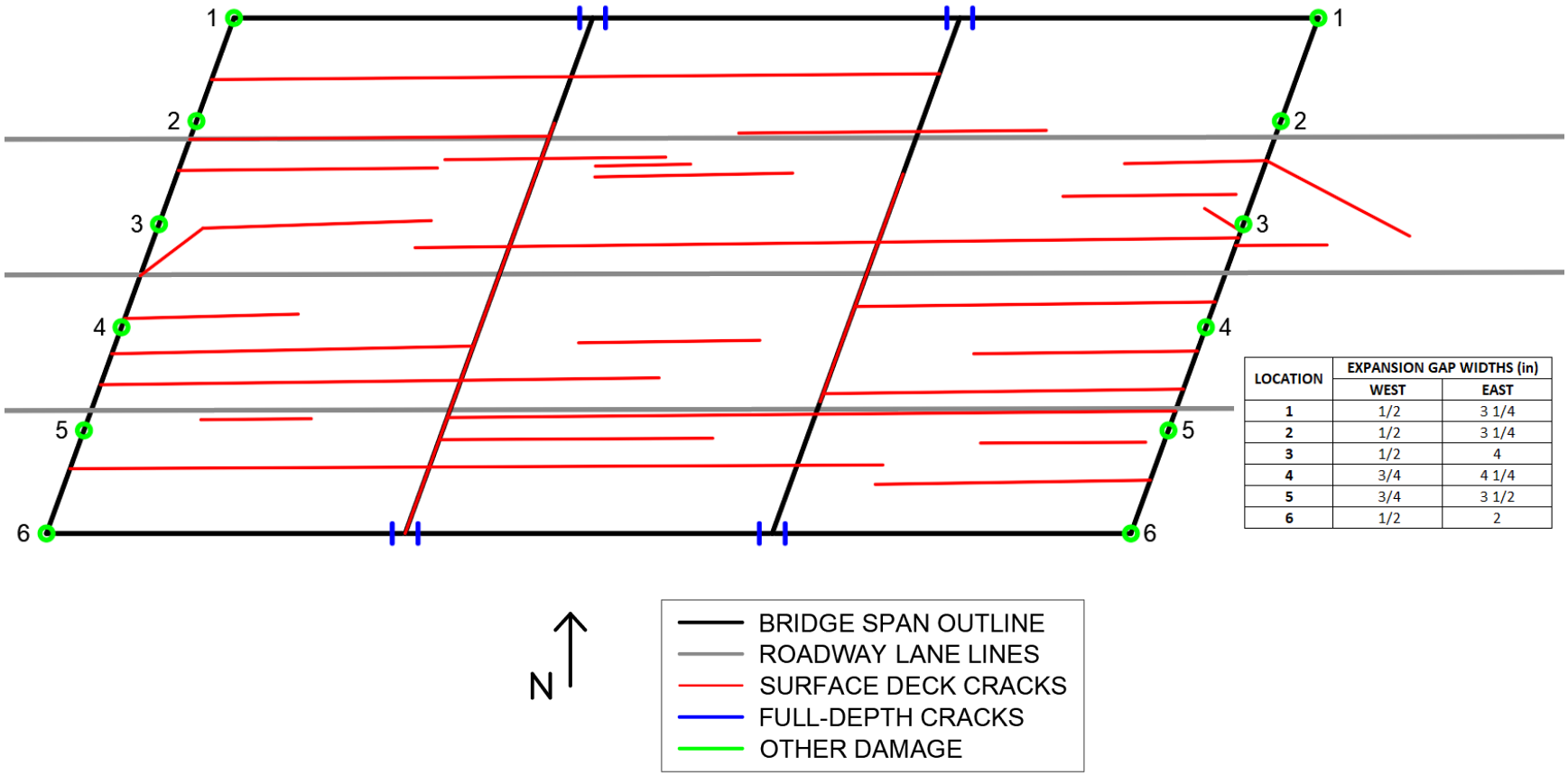

LOCATION	EXPANSION GAP WIDTHS (in)	
	WEST	EAST
1	1/2	3 1/4
2	1/2	3 1/4
3	1/2	4
4	3/4	4 1/4
5	3/4	3 1/2
6	1/2	2

Figure B.1: Deck crack map for bridge S006 26001.

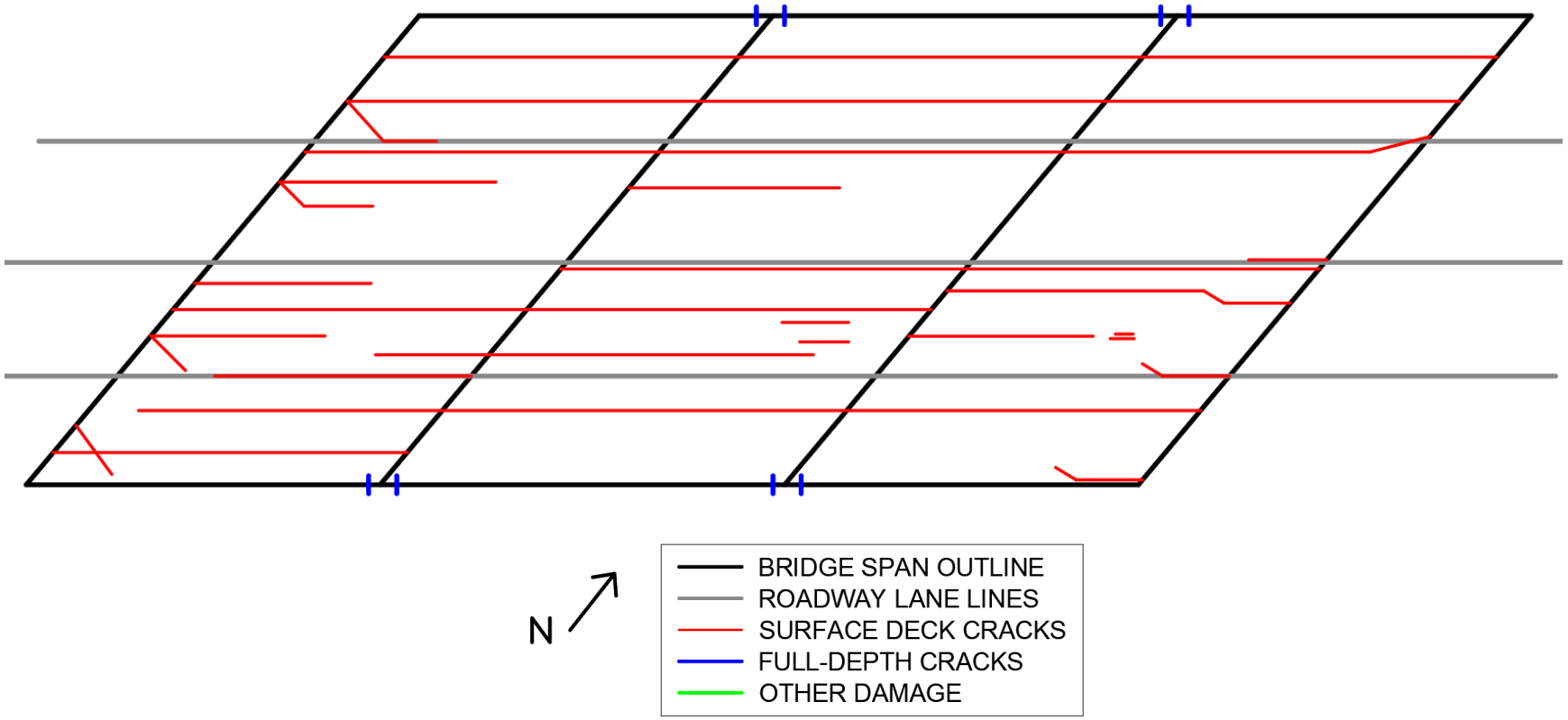

Figure B.2: Deck crack map for bridge S006 34277.

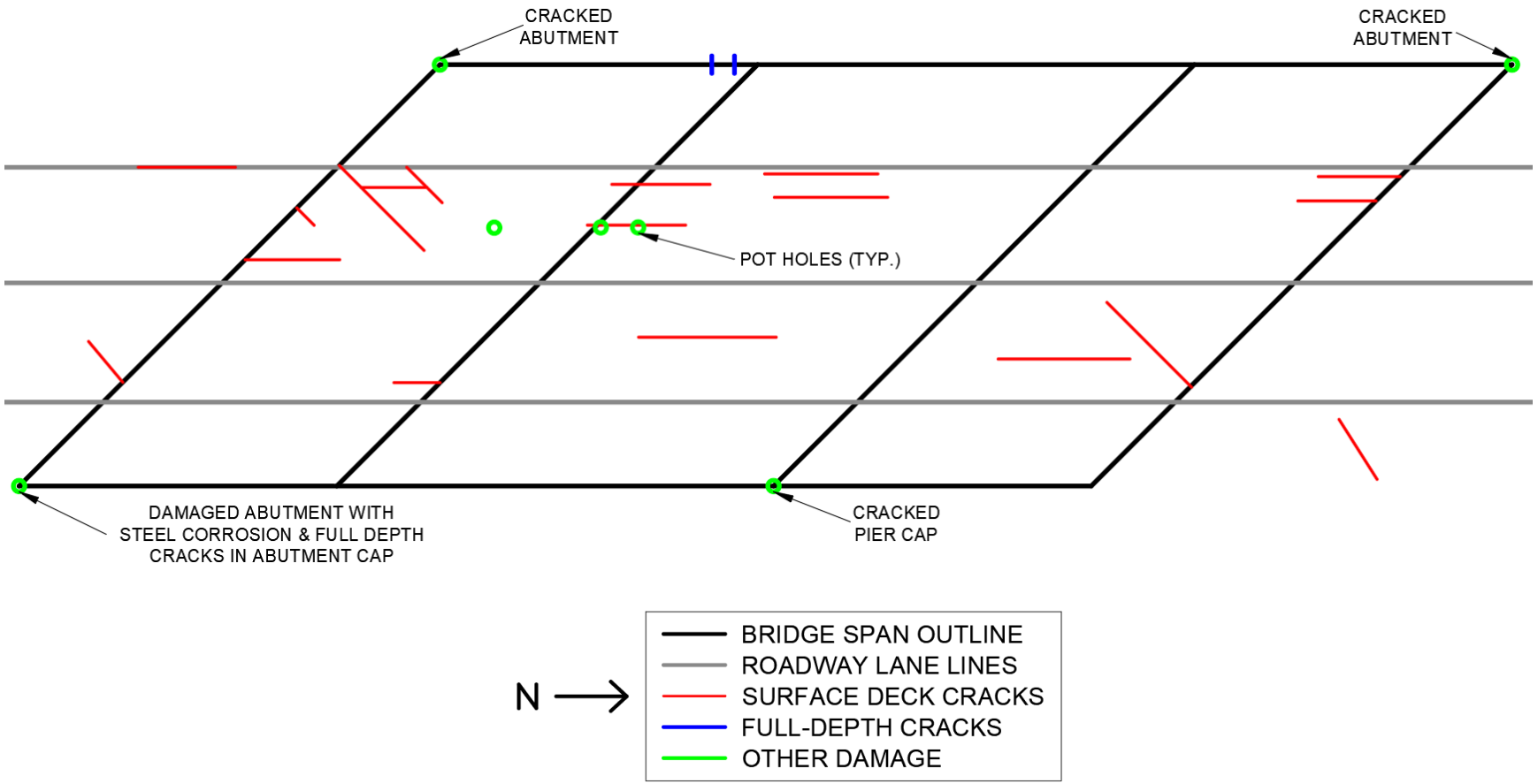

Figure B.3: Deck crack map for bridge S009 00888.

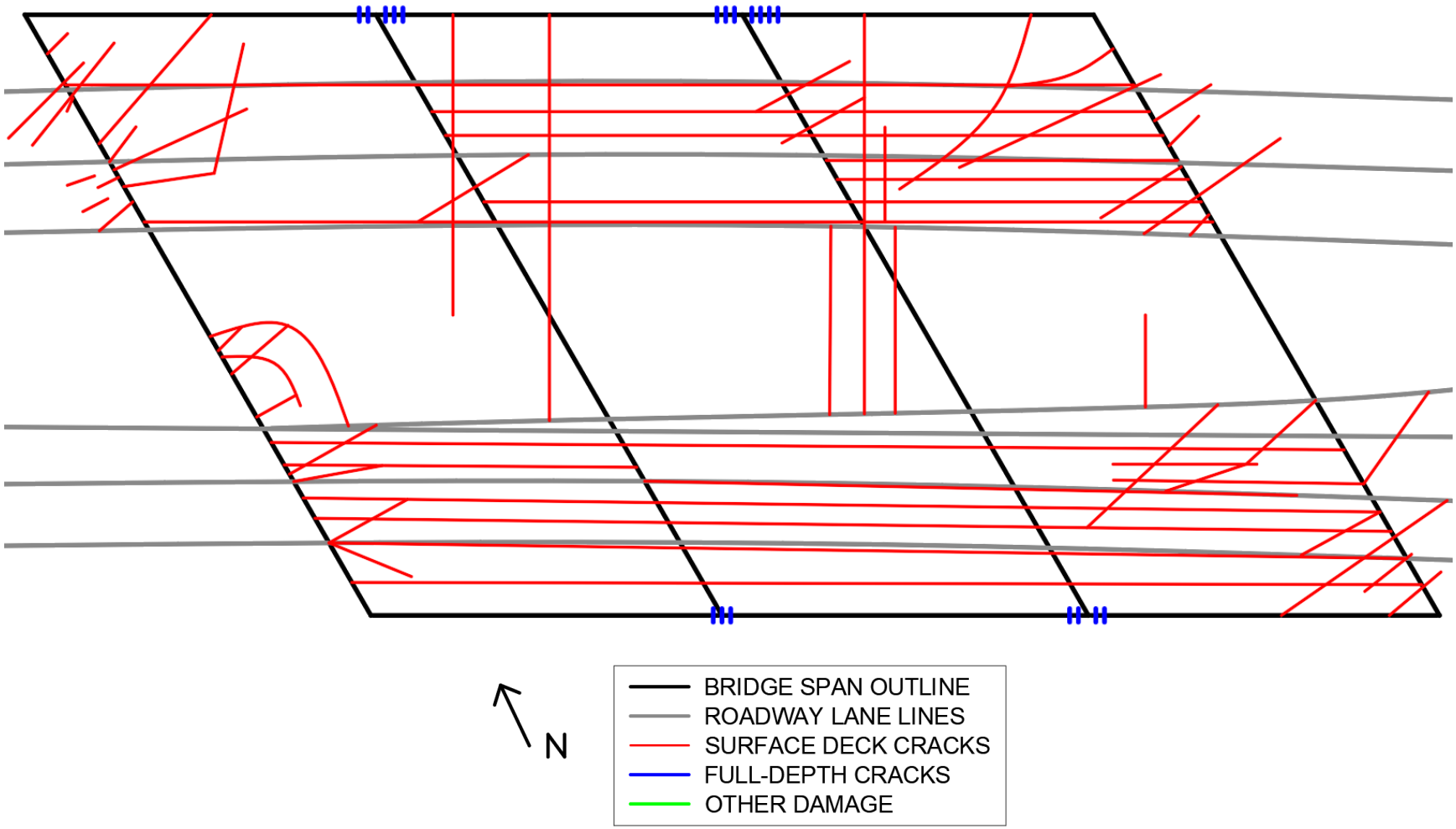

Figure B.4: Deck crack map for bridge S034 31644.

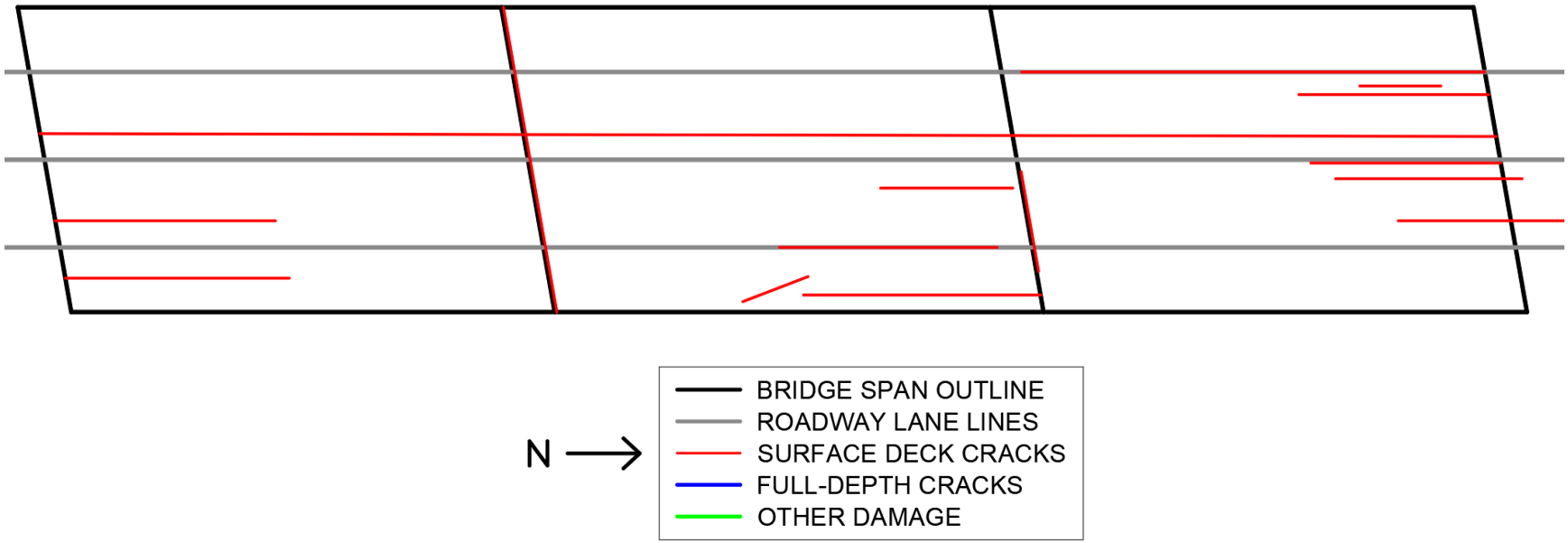

Figure B.5: Deck crack map for bridge S050 04149.

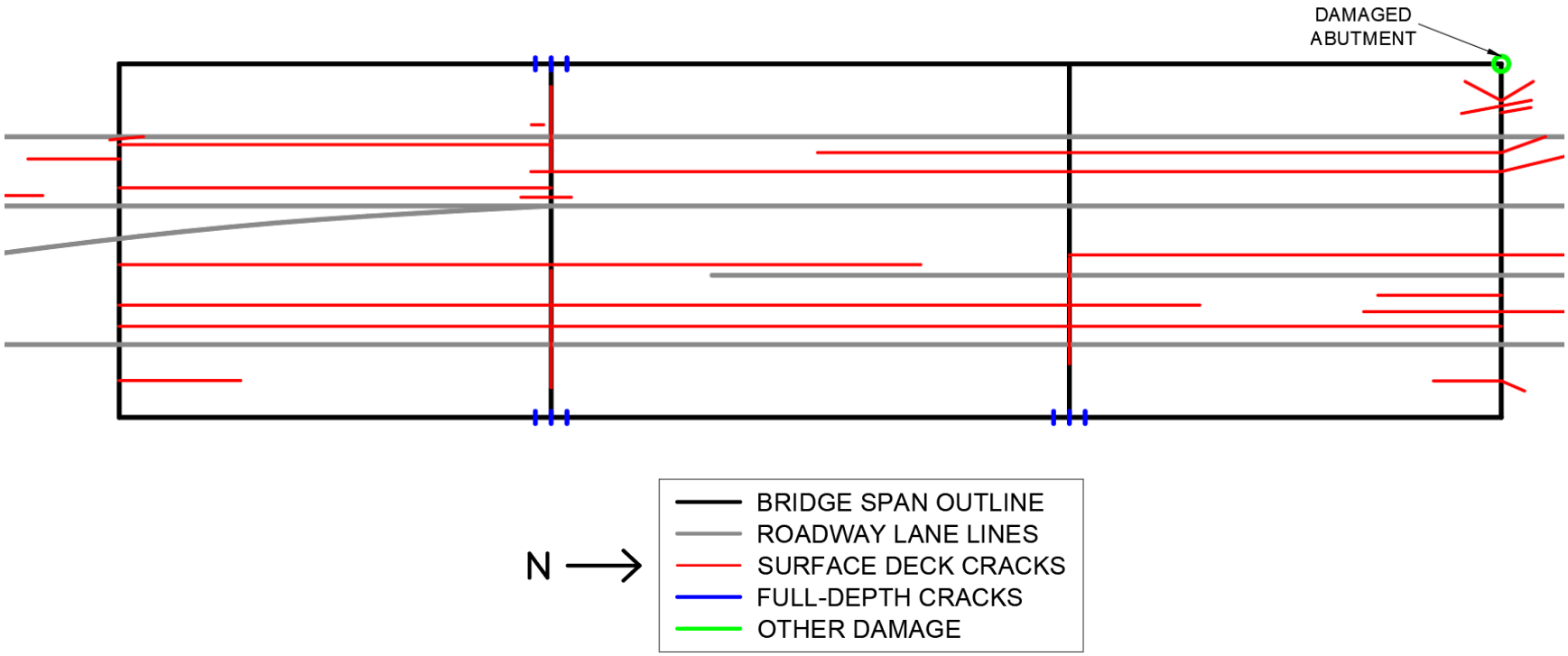

Figure B.6: Deck crack map for bridge S050 06686.

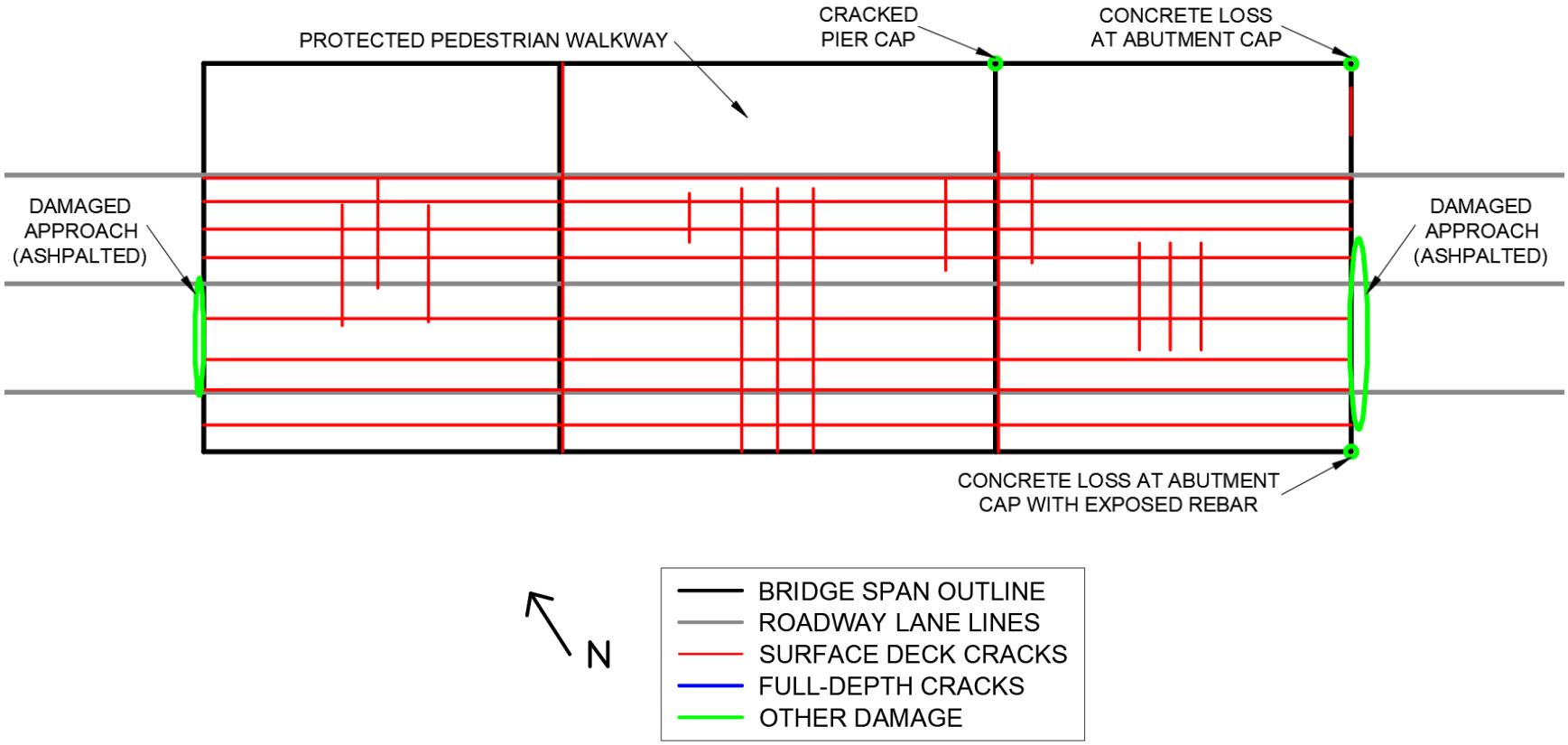

Figure B.7: Deck crack map for bridge S058 00994.

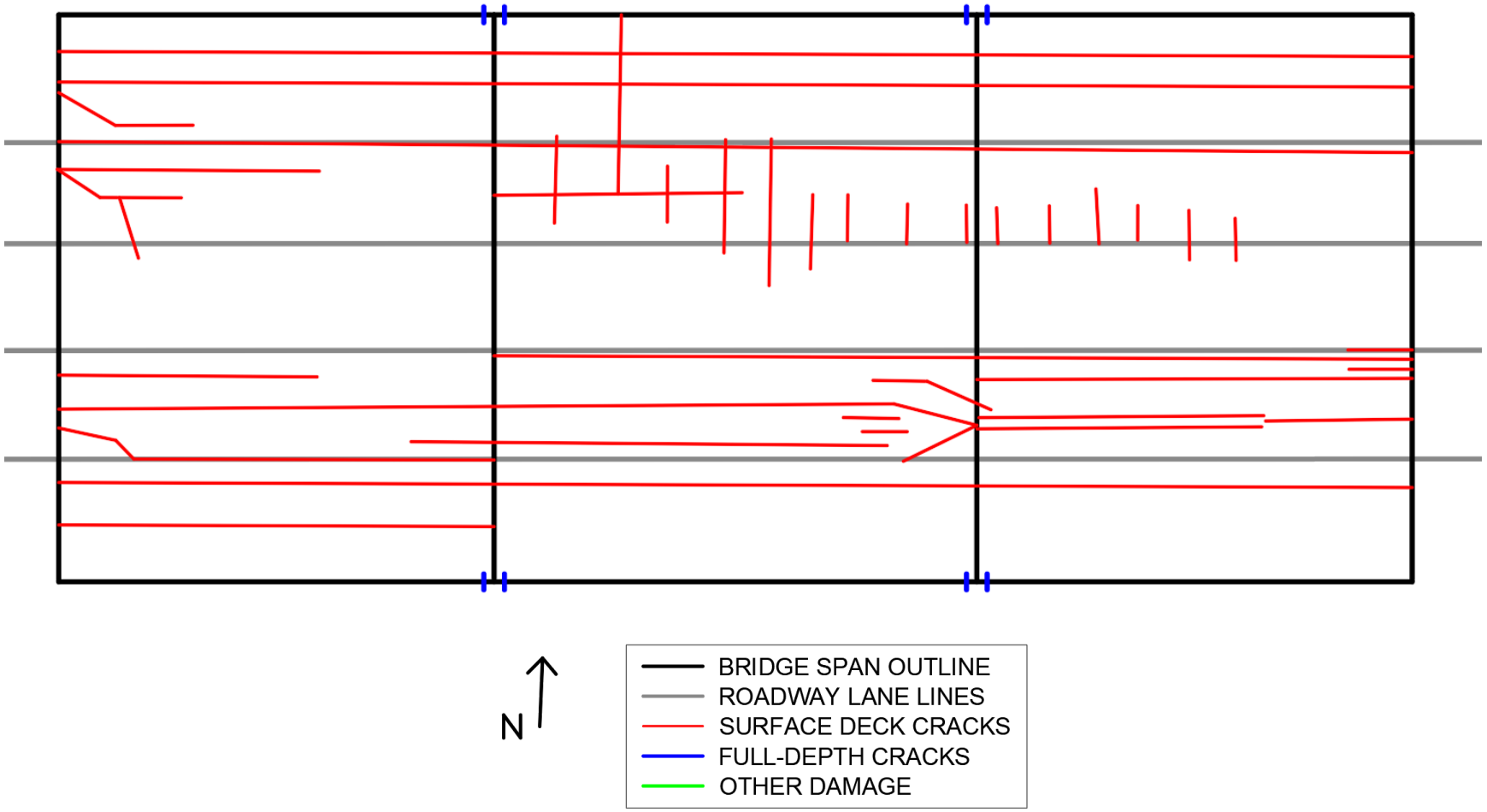

Figure B.8: Deck crack map for bridge S080 40872R.

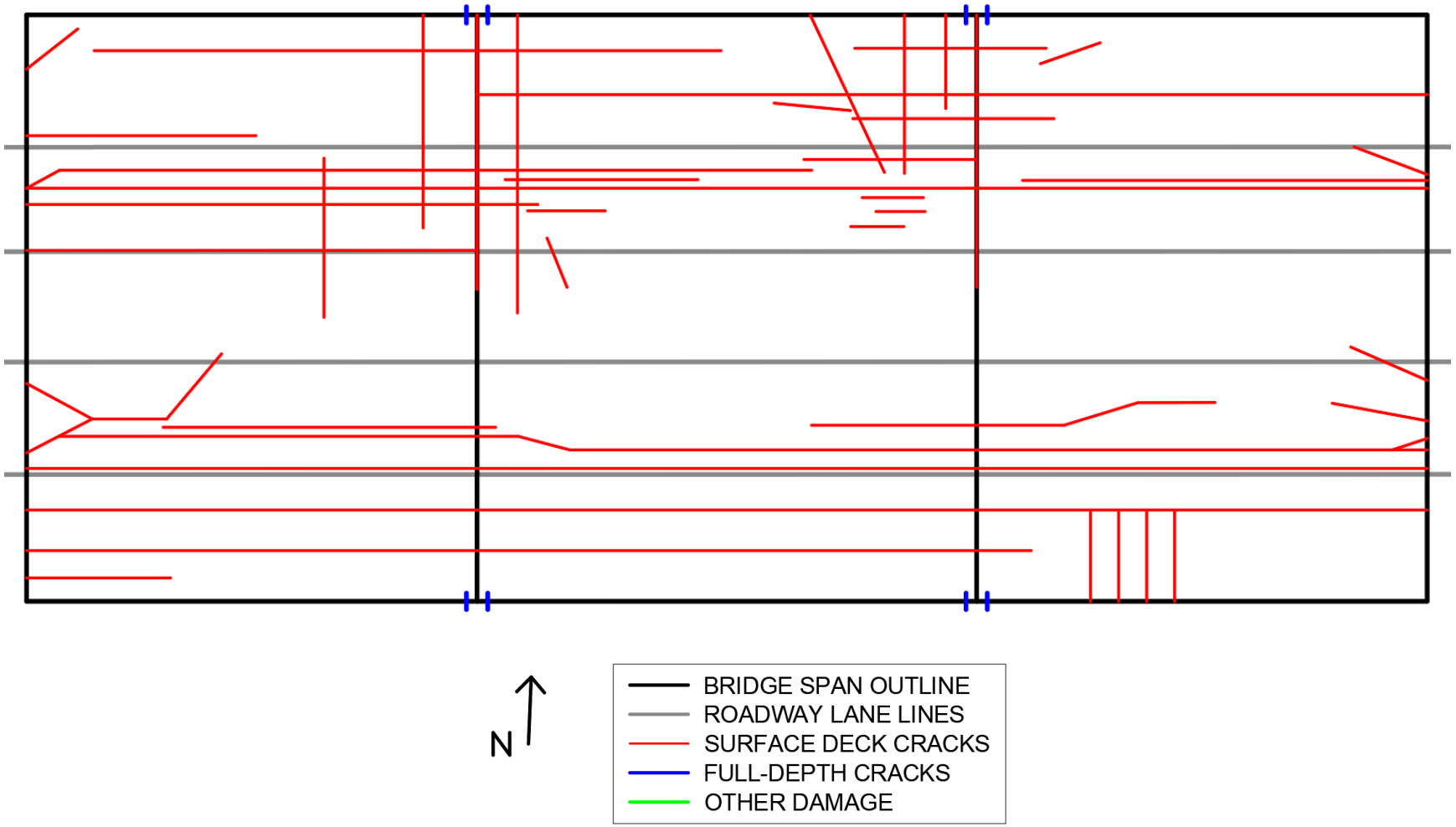

Figure B.9: Deck crack map for bridge S080 40927R.

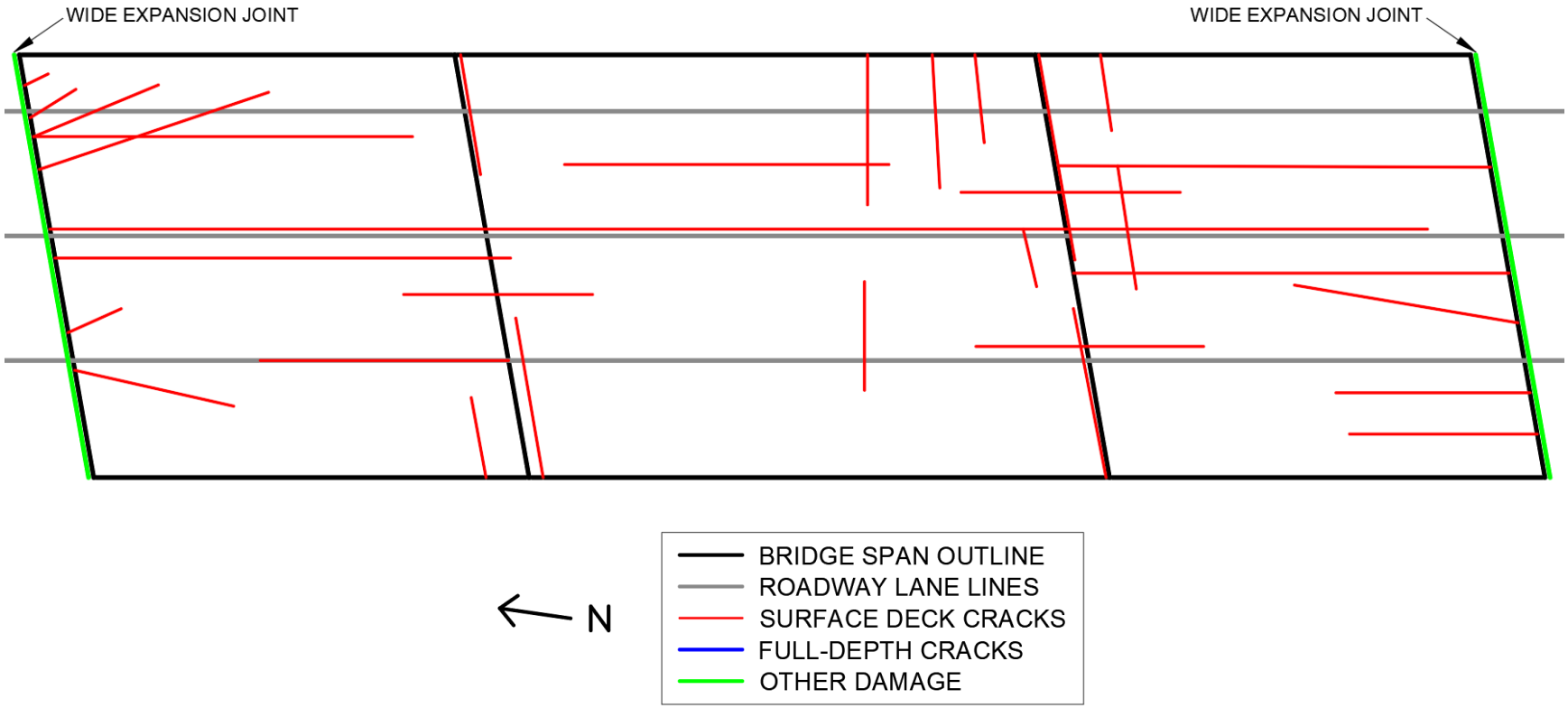

Figure B.10: Deck crack map for bridge S081 05152L.

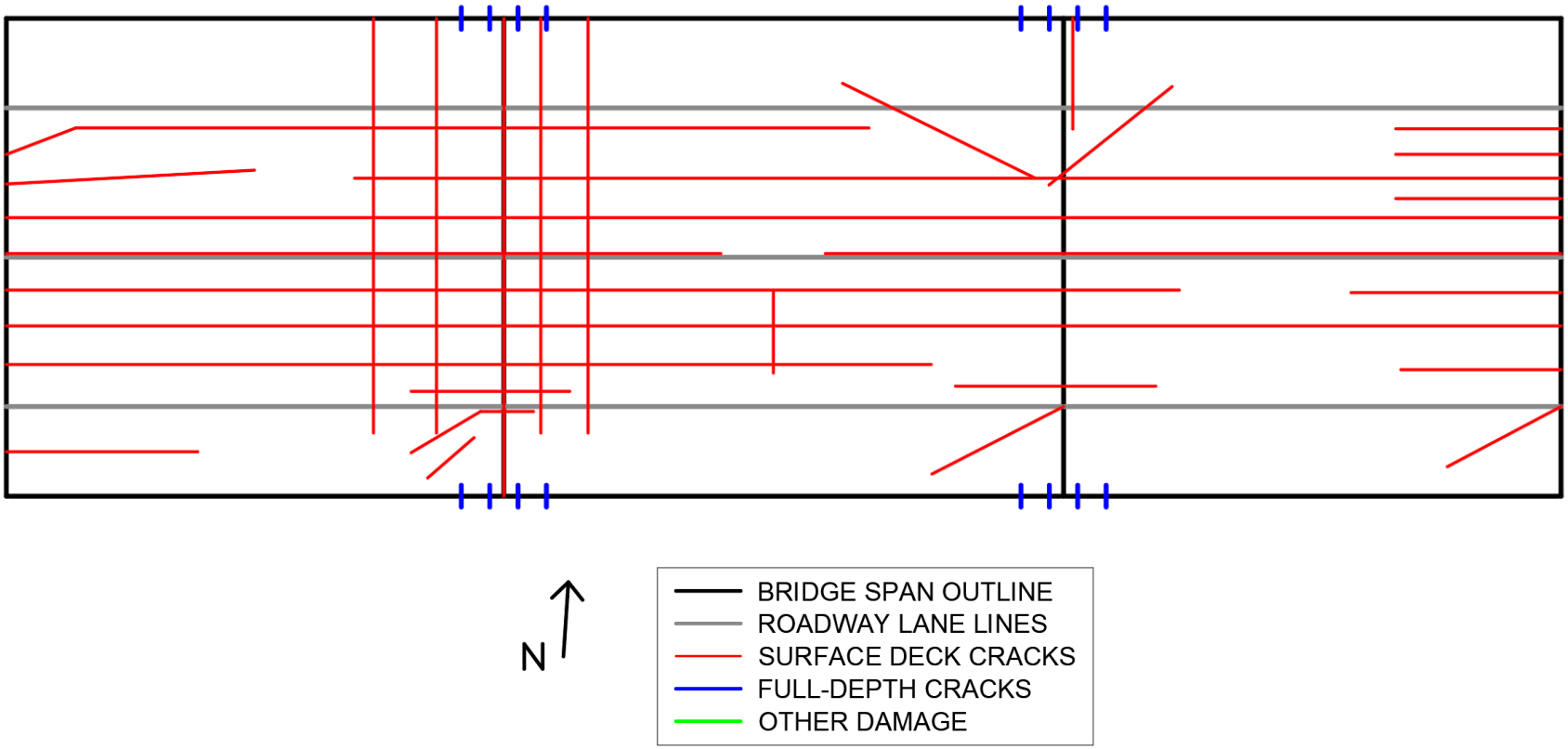

Figure B.11: Deck crack map for bridge S089 06047.

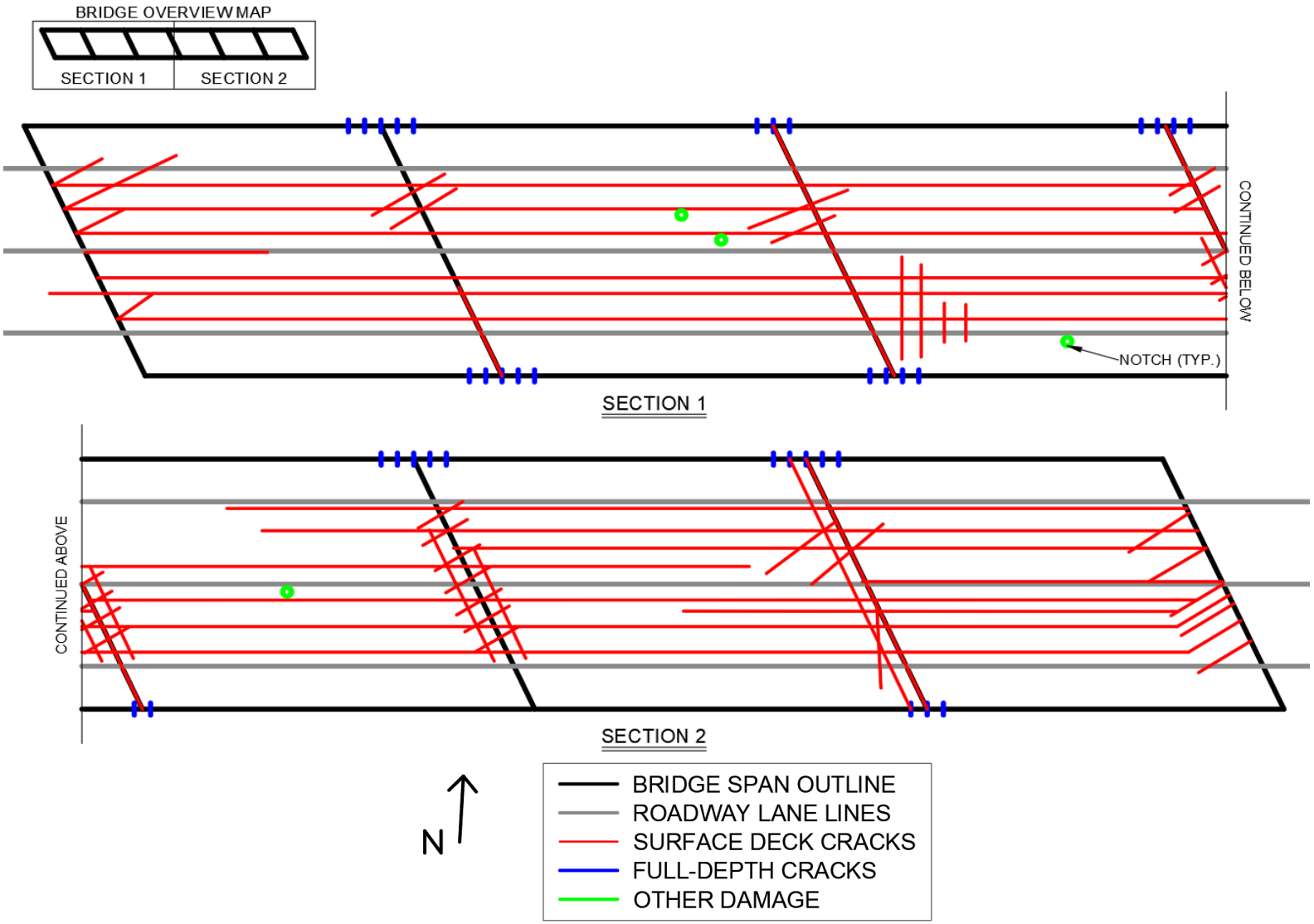

Figure B.12: Deck crack map for bridge S089 06062.

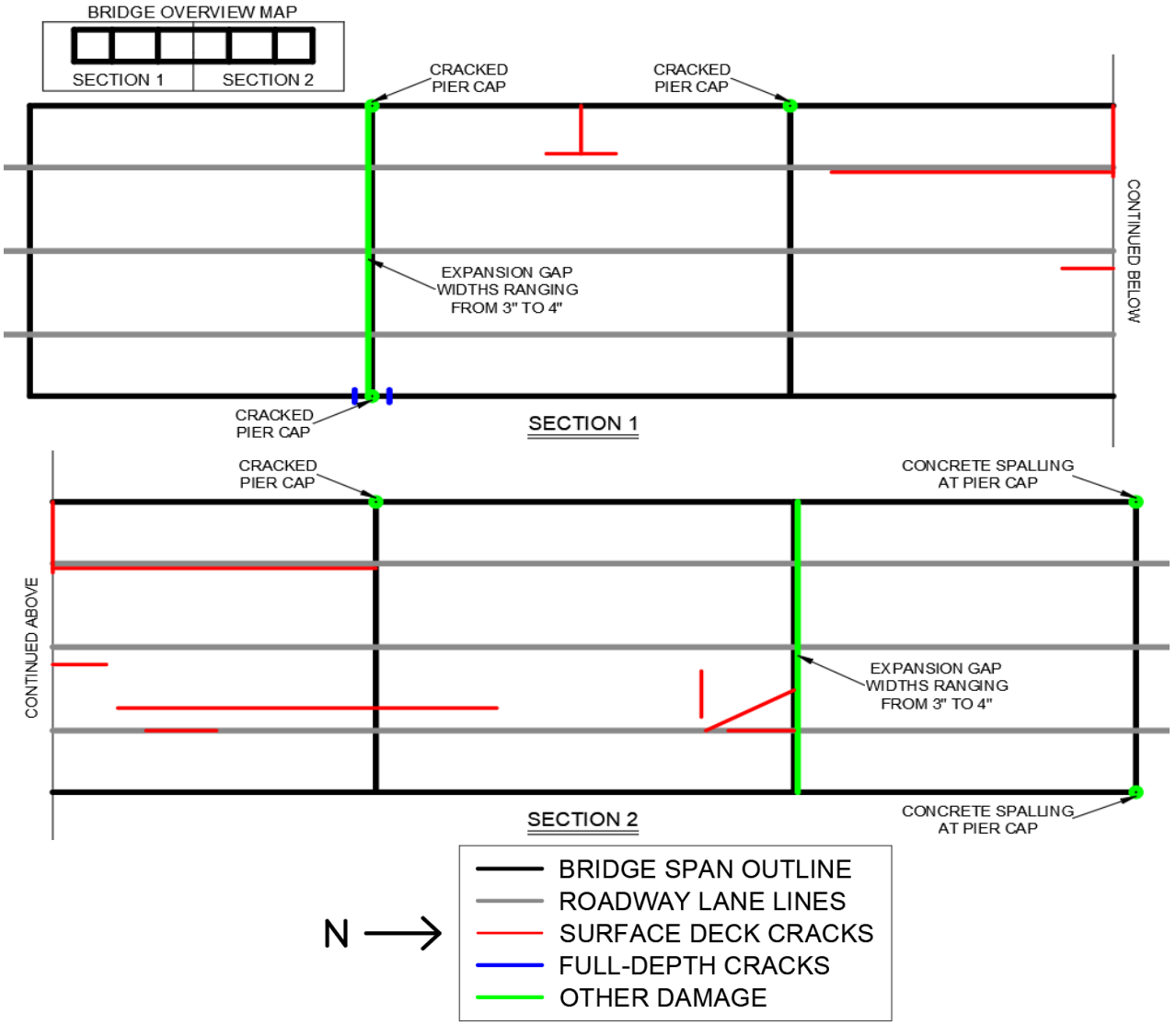

Figure B.13: Deck crack map for bridge S103 02465.

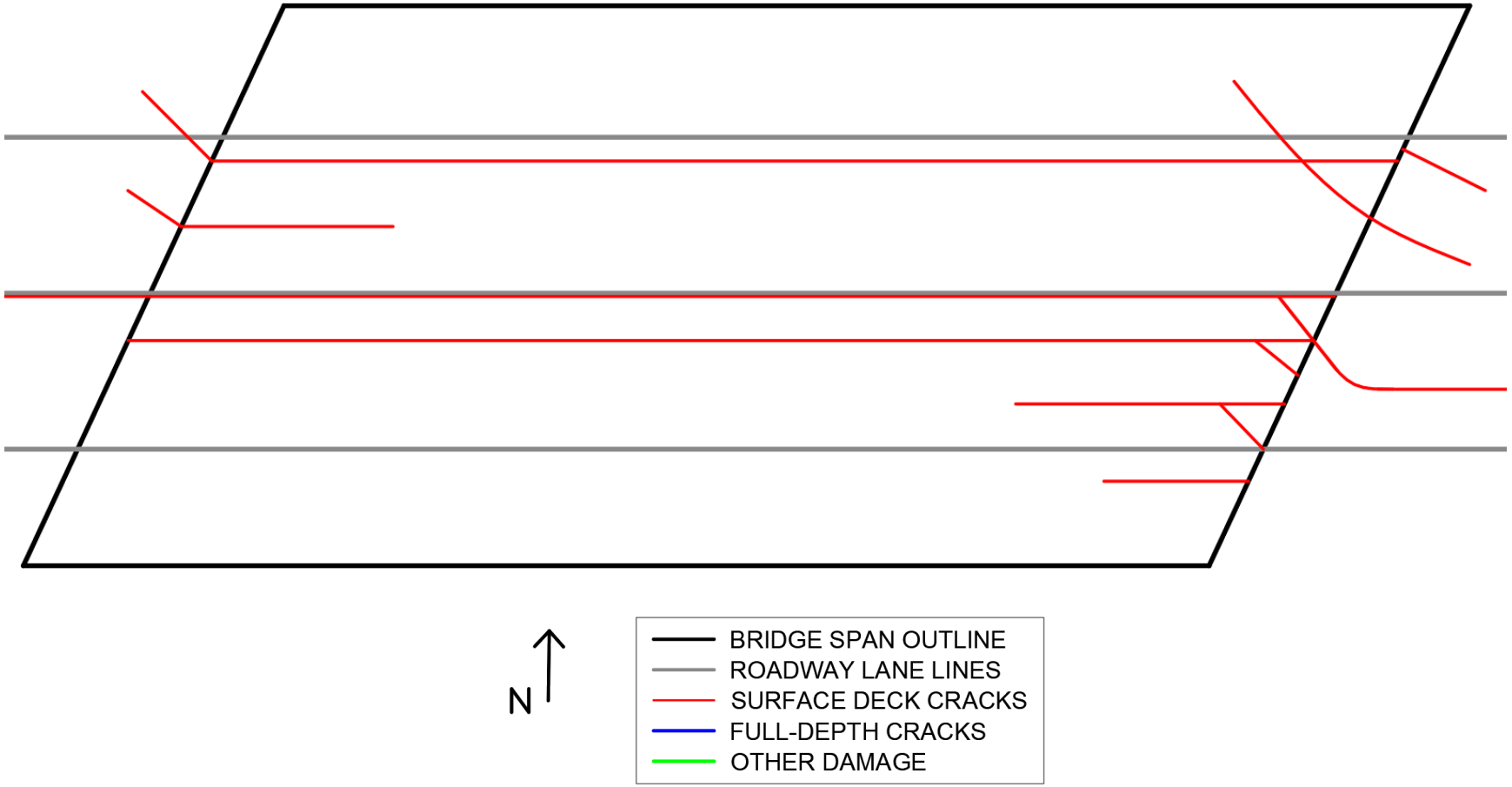

Figure B.14: Deck crack map for bridge SS66C00220.

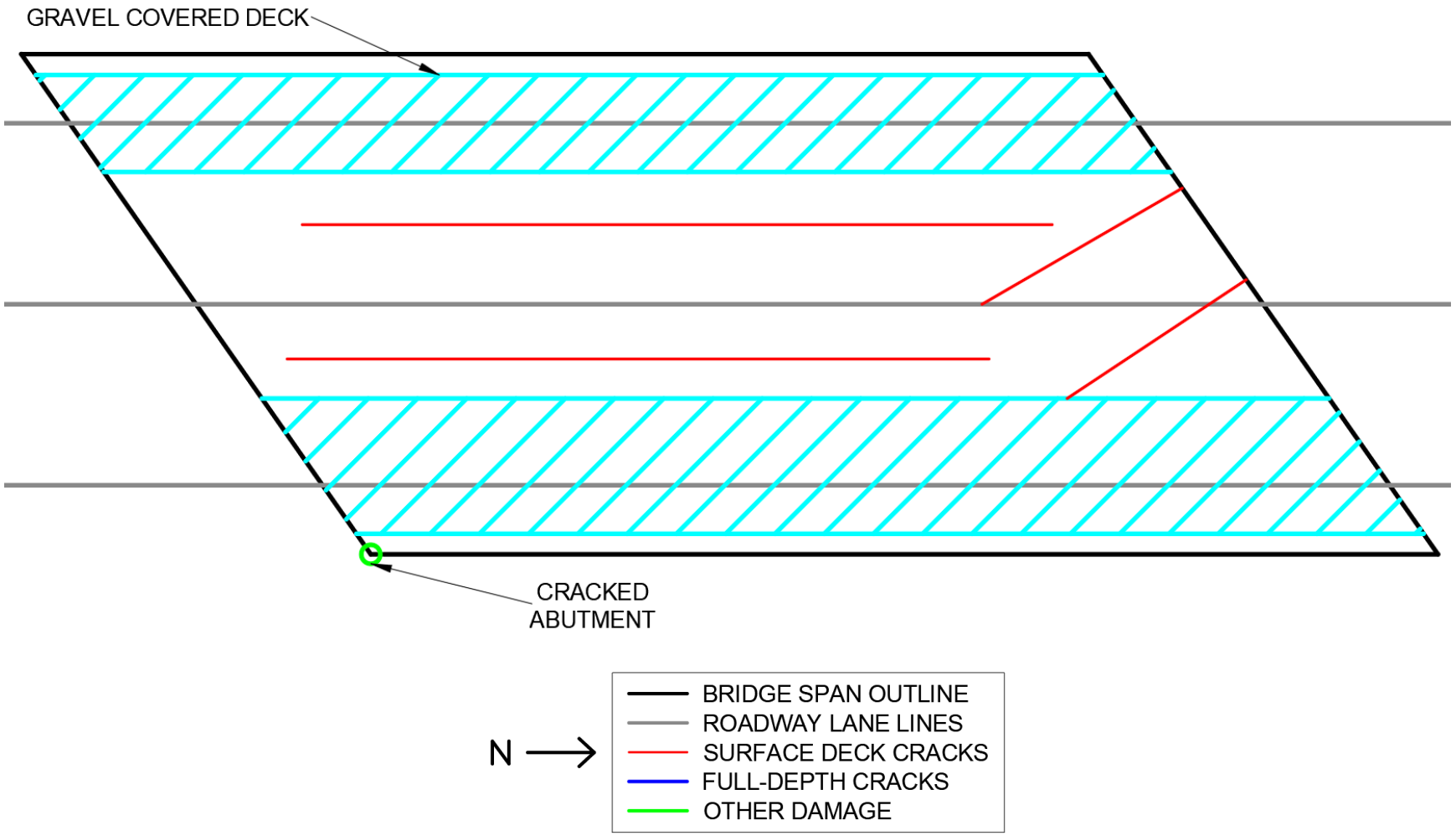

Figure B.15: Deck crack map for bridge C002408505.

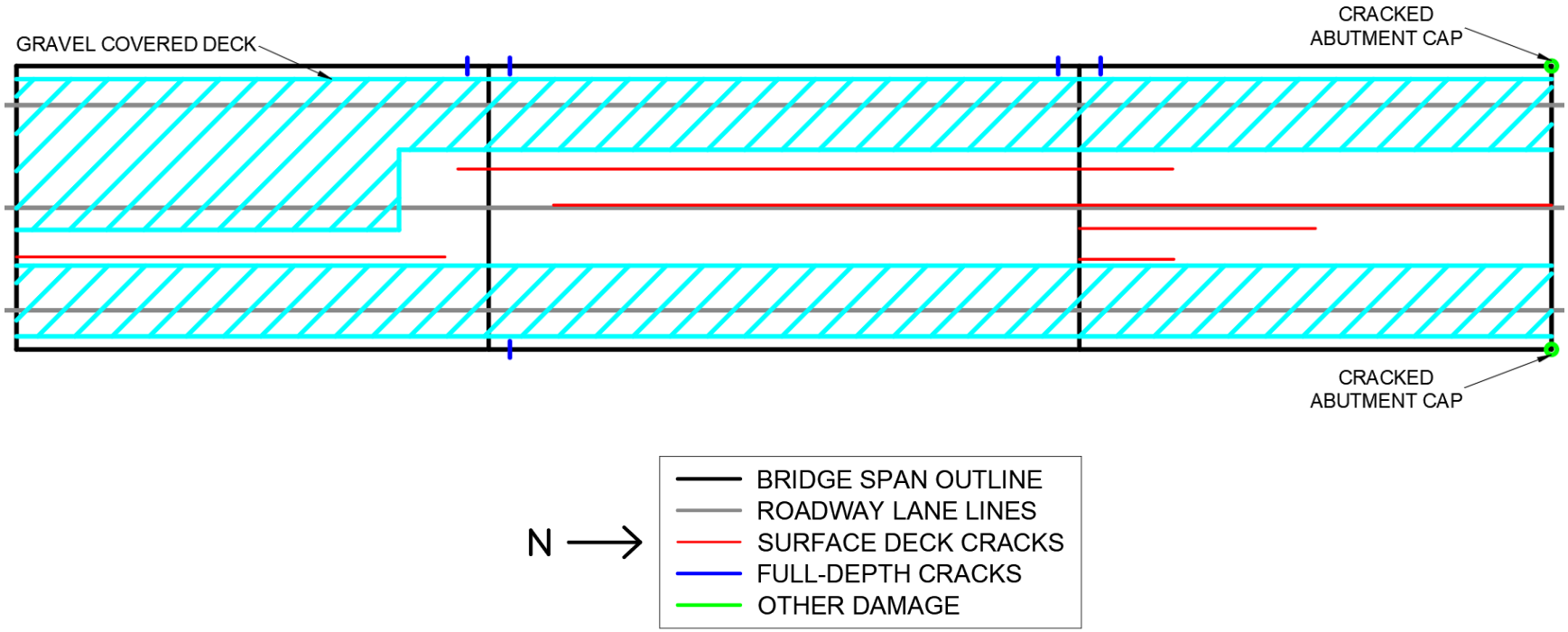

Figure B.16: Deck crack map for bridge C008504145.

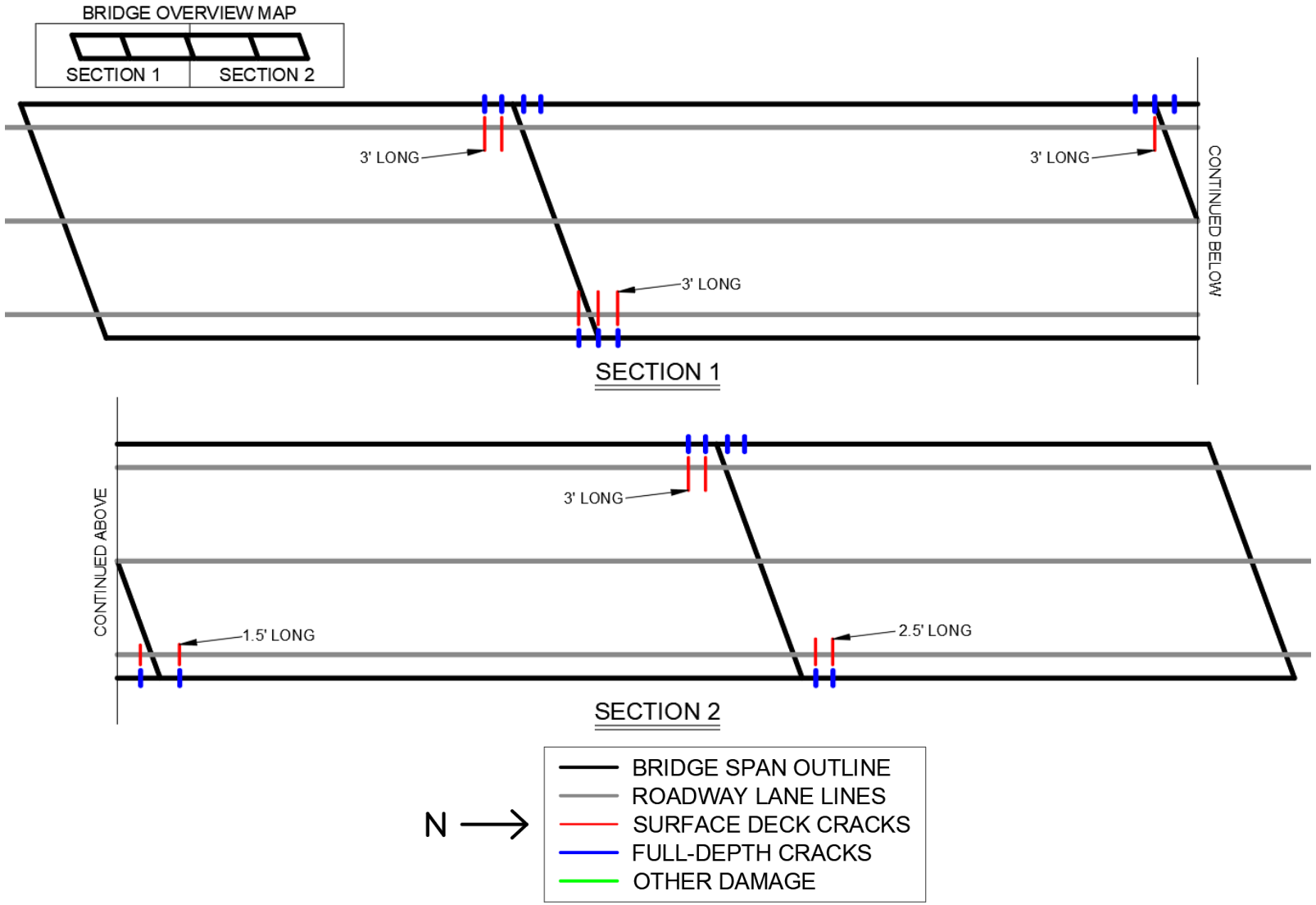

Figure B.17: Deck crack map for bridge C004931110.

APPENDIX C

IT Girder Bridge S006 26001:

Figure C.1: Location of bridge S006 26001 (courtesy of Google Maps).

Table C.1: Bridge information summary for bridge S006 26001.

Bridge ID	S006 26001	**Girder Height (in [mm])**	11.81 [300]
County	Fillmore	**Girder Width (in [mm])**	23.63 [600]
Year Built	1999	**Girder Spacing (in [mm])**	29.06 [738]
No. of Spans	3	**Deck Thickness (in [mm])**	6 [152]
Length Span 1 (ft)	31.70	**No. of Girders**	19
Length Span 2 (ft)	32.50	**Diaphragm**	None
Length Span 3 (ft)	31.70	**Deck Rating**	8
Bridge Width (ft)	45.60	**Superstructure Rating**	8
Skew Angle (°)	20	**Substructure Rating**	7

Figure C.2: Photo of bridge S006 26001.

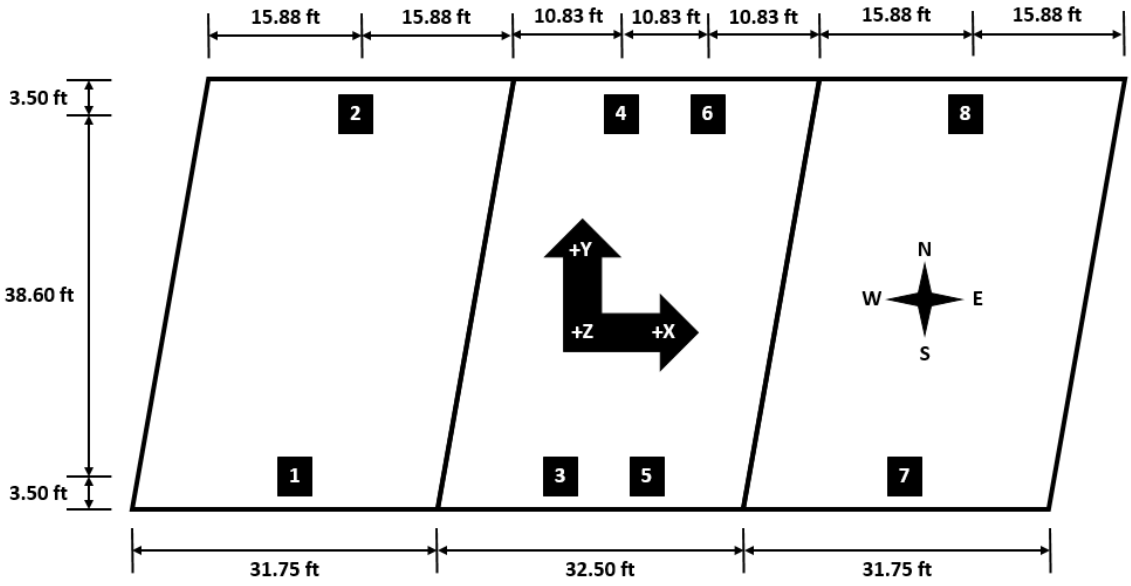

Figure C.3: Sensor locations capturing the global response for bridge S006 26001.

Table C.2: Sensor information of the global response setup for bridge S006 26001.

Sensor Location	Sensor Type	Sensor Id	Calibration Factor (mV/g)
1	WSN	99FZ	--
2	WSN	996Z	--
3	WSN	99DZ	--
4	WSN	995Z	--
5	WSN	99CZ	--
6	WSN	968Z	--
7	WSN	997Z	--
8	WSN	848Z	--

Date of Collection	10/7/2016
Length of Data (min)	51.58
Sampling Rate (Hz)	256

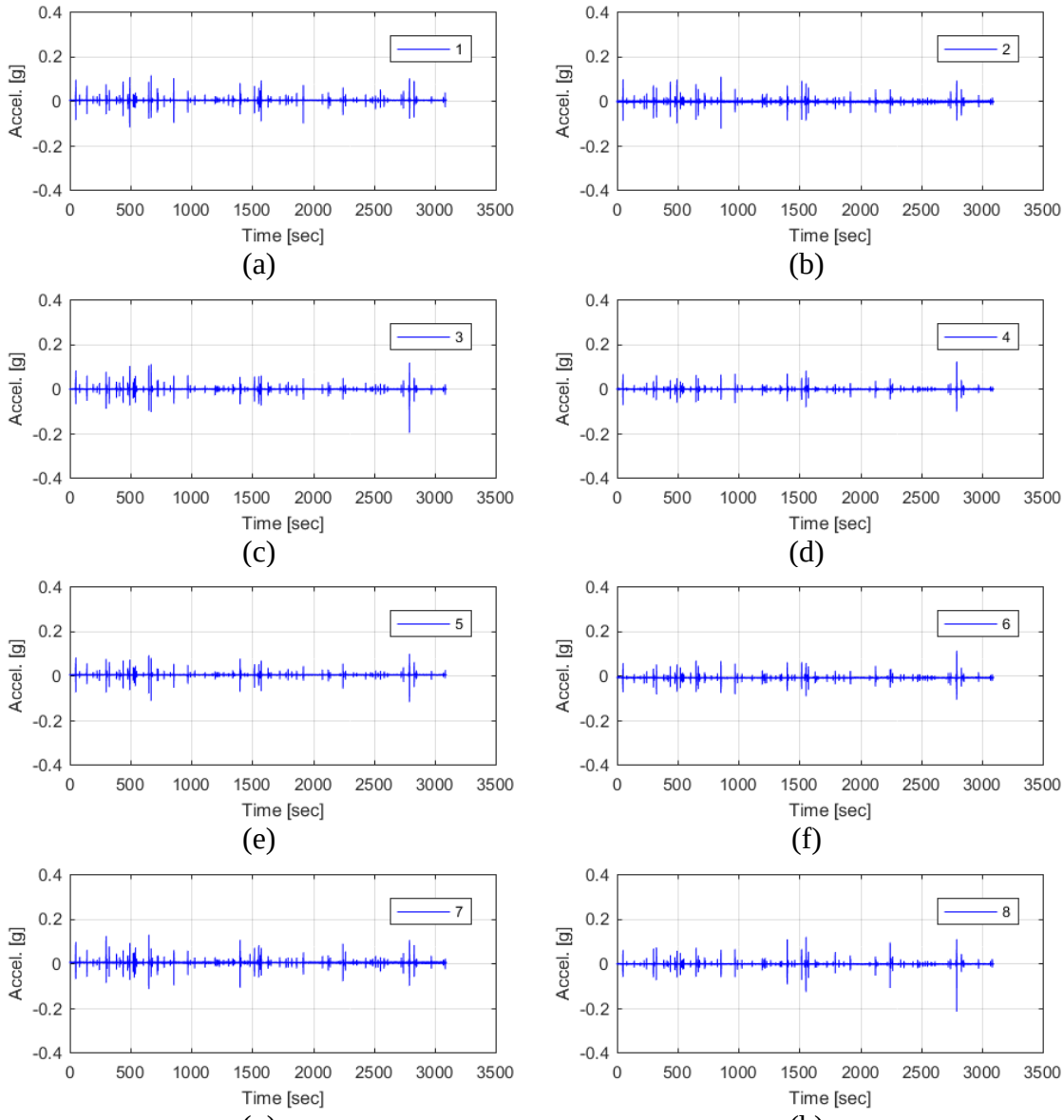

Figure C.4: Raw acceleration data of the global response for bridge S006 26001.

Table C.3: Filter parameters of the global response for bridge S006 26001.

Filter Parameter	Value
Hampel Identifier Order	--
FIR Bandpass Filter Order	2048
FIR Bandpass Filter Lower Cutoff Frequency (Hz)	8
FIR Bandpass Filter Upper Cutoff Frequency (Hz)	28
Tukey Averaging Window (min)	1.5

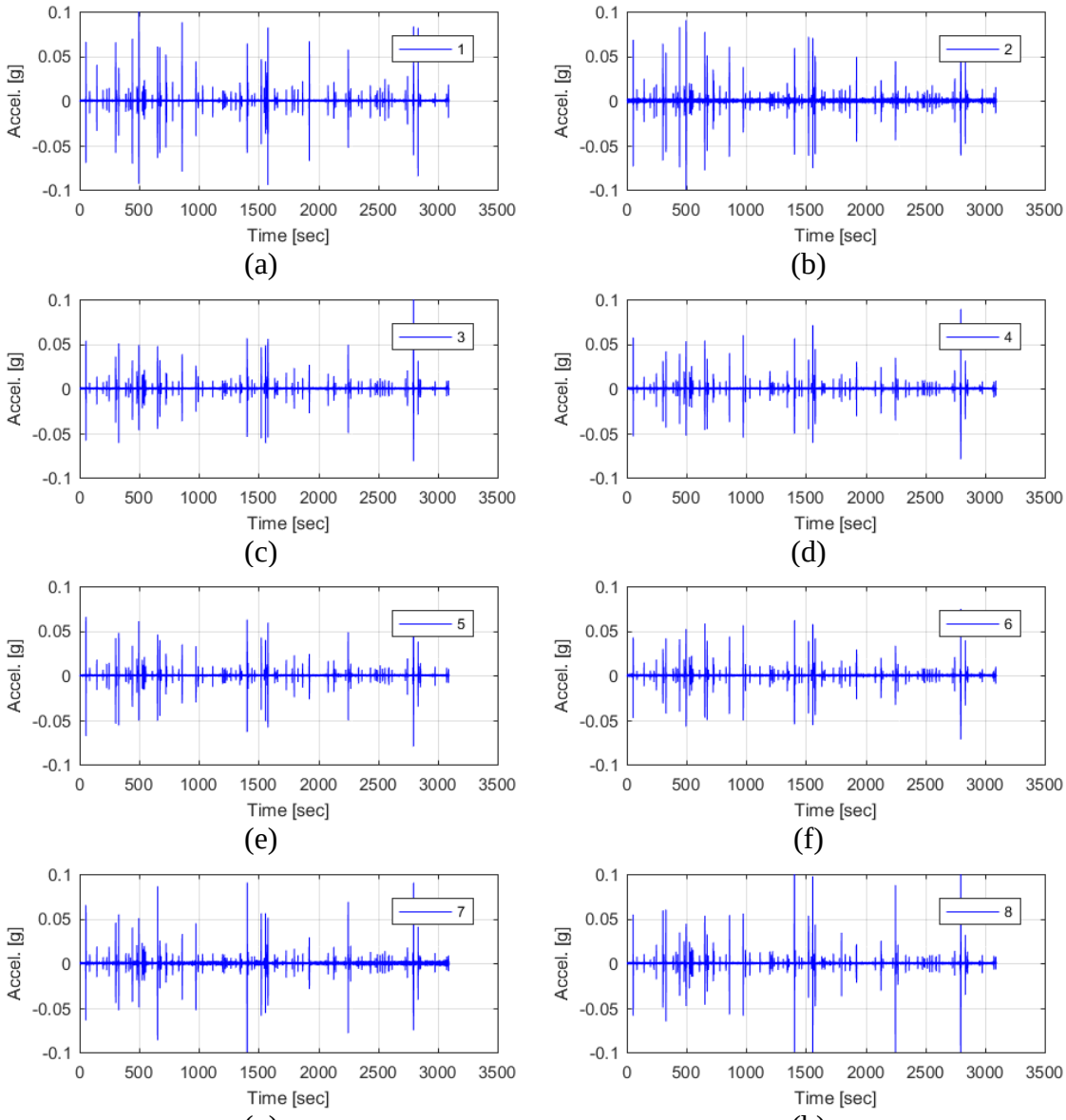

Figure C.5: Filtered acceleration data of the global response for bridge S006 26001.

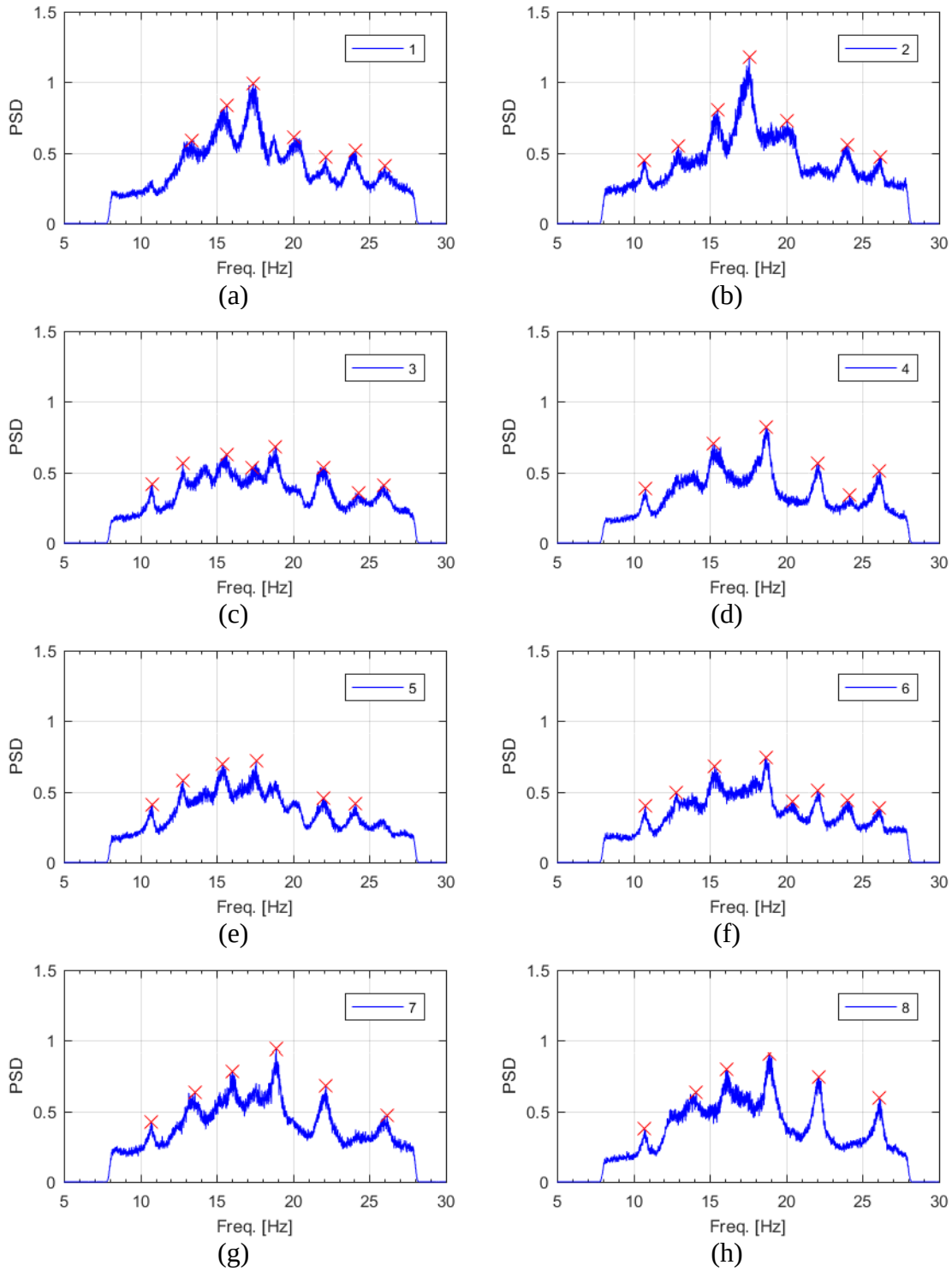

Figure C.6: Frequency content of the filtered acceleration data and peak-picking frequencies of the global response for bridge S006 26001.

Table C.4: Filtered acceleration RMS values of the global response for bridge S006 26001.

Sensor	Filtered a_{RMS} (µg)
1	2177
2	2230
3	1728
4	1750
5	1768
6	1733
7	2038
8	2174

Table C.5: Peak-picking frequencies of the global response for bridge S006 26001.

Mode	Individual Sensor Frequencies (Hz)							
	1	**2**	**3**	**4**	**5**	**6**	**7**	**8**
1	--	10.74	10.79	10.79	10.79	10.79	10.74	10.74
2	--	--	--	--	--	--	--	--
3	--	12.93	12.78	--	12.80	12.80	--	--
4	13.37	--	--	--	--	--	13.57	14.12
5	15.66	15.50	15.66	15.20	15.41	15.33	--	--
6	--	--	--	--	--	--	16.04	16.09

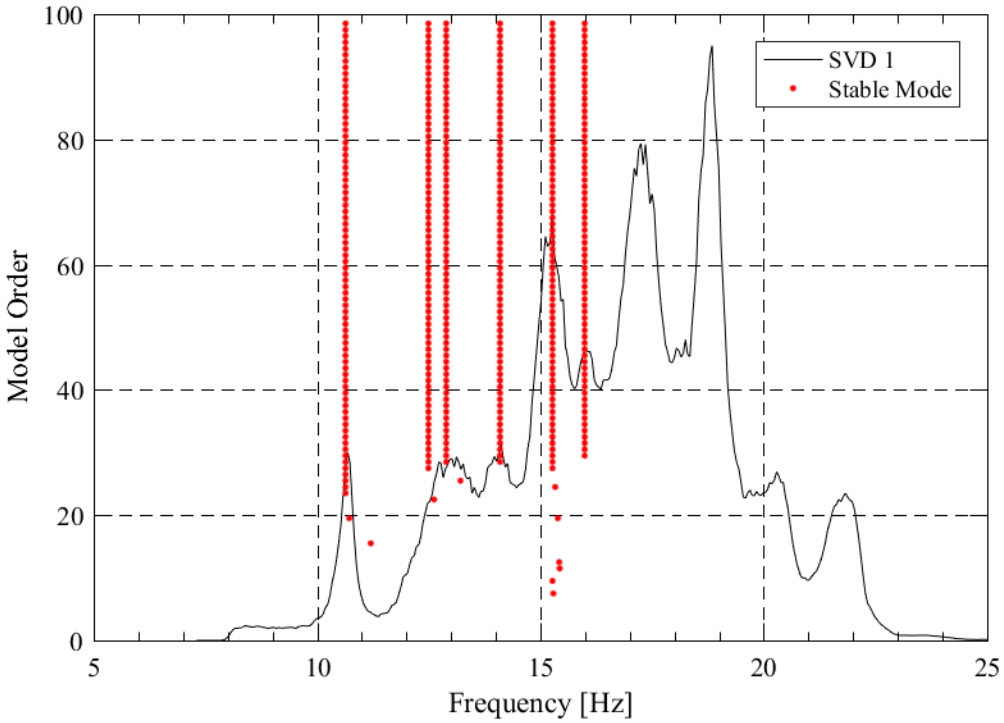

Figure C.7: SSI-UPCX method stabilization diagram of the global response for bridge S006 26001.

Table C.6: SSI-UPCX method dynamic properties of the global response for bridge S006 26001.

Mode	Frequency (Hz)	Damping (%)	Complexity (%)
1	10.64	2.86	13.68
2	12.49	4.91	58.94
3	12.89	5.98	44.81
4	14.09	4.63	56.81
5	15.27	2.42	27.82
6	15.99	3.40	83.97

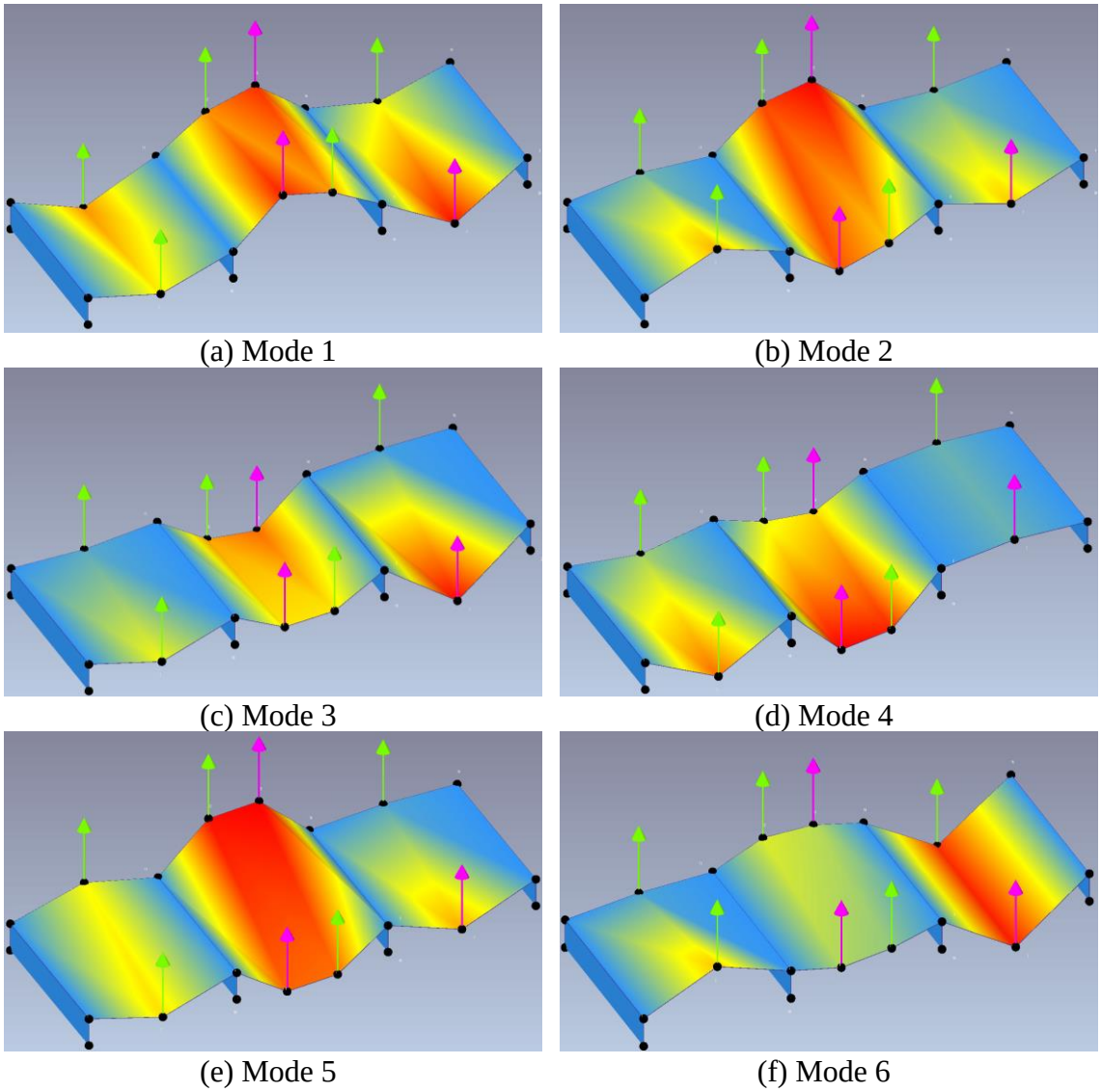

(a) Mode 1 (b) Mode 2

(c) Mode 3 (d) Mode 4

(e) Mode 5 (f) Mode 6

Figure C.8: Operational deflected shapes of the global response for bridge S006 26001.

Table C.7: Operational deflected shape coordinates of the global response for bridge S006 26001.

Sensor	ODS Coordinates					
	Mode 1	Mode 2	Mode 3	Mode 4	Mode 5	Mode 6
1	0.45	0.59	0.38	0.74	-0.47	-0.57
2	0.68	0.10	0.08	0.22	0.40	-0.06
3	-0.96	-0.97	0.46	1.00	-0.77	0.27
4	-0.67	0.91	0.62	0.36	0.96	-0.35
5	-0.65	-0.69	0.46	0.92	-0.74	0.21
6	-0.92	1.00	0.75	0.49	1.00	-0.29
7	1.00	-0.77	1.00	-0.11	-0.60	1.00
8	0.40	-0.31	-0.04	-0.11	0.06	0.95

Table C.8: MAC values of the global response for bridge S006 26001.

MAC	Mode 1	Mode 2	Mode 3	Mode 4	Mode 5	Mode 6
Mode 1	1.000	0.043	0.073	0.215	0.046	0.198
Mode 2	0.043	1.000	0.026	0.044	0.591	0.280
Mode 3	0.073	0.026	1.000	0.233	0.055	0.159
Mode 4	0.215	0.044	0.233	1.000	0.039	0.027
Mode 5	0.046	0.591	0.055	0.039	1.000	0.311
Mode 6	0.198	0.280	0.159	0.027	0.311	1.000

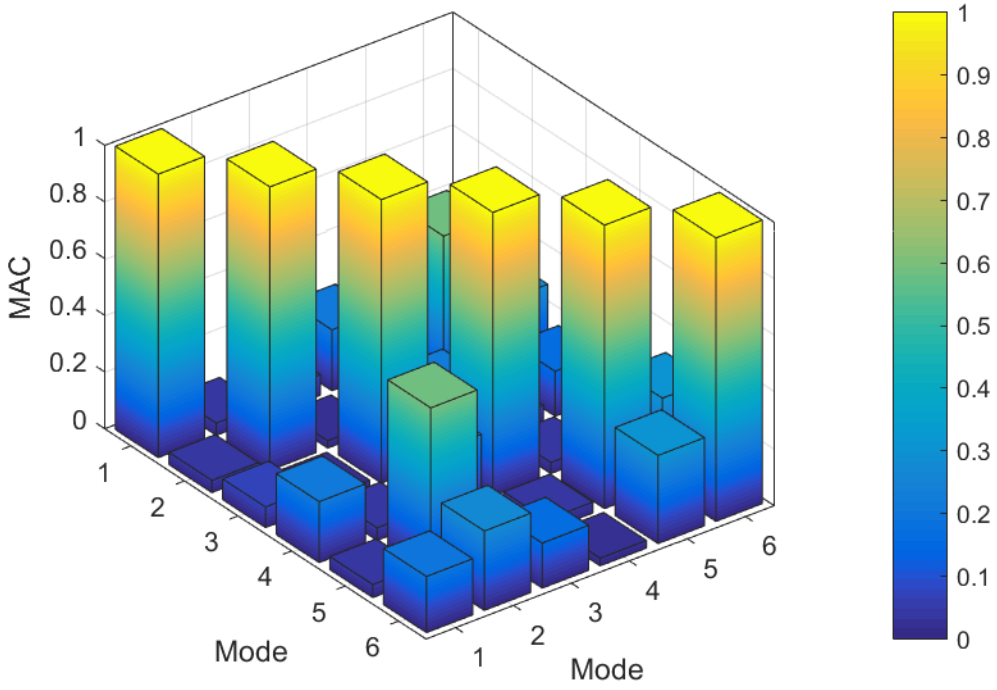

Figure C.9: MAC values of the global response for bridge S006 26001.

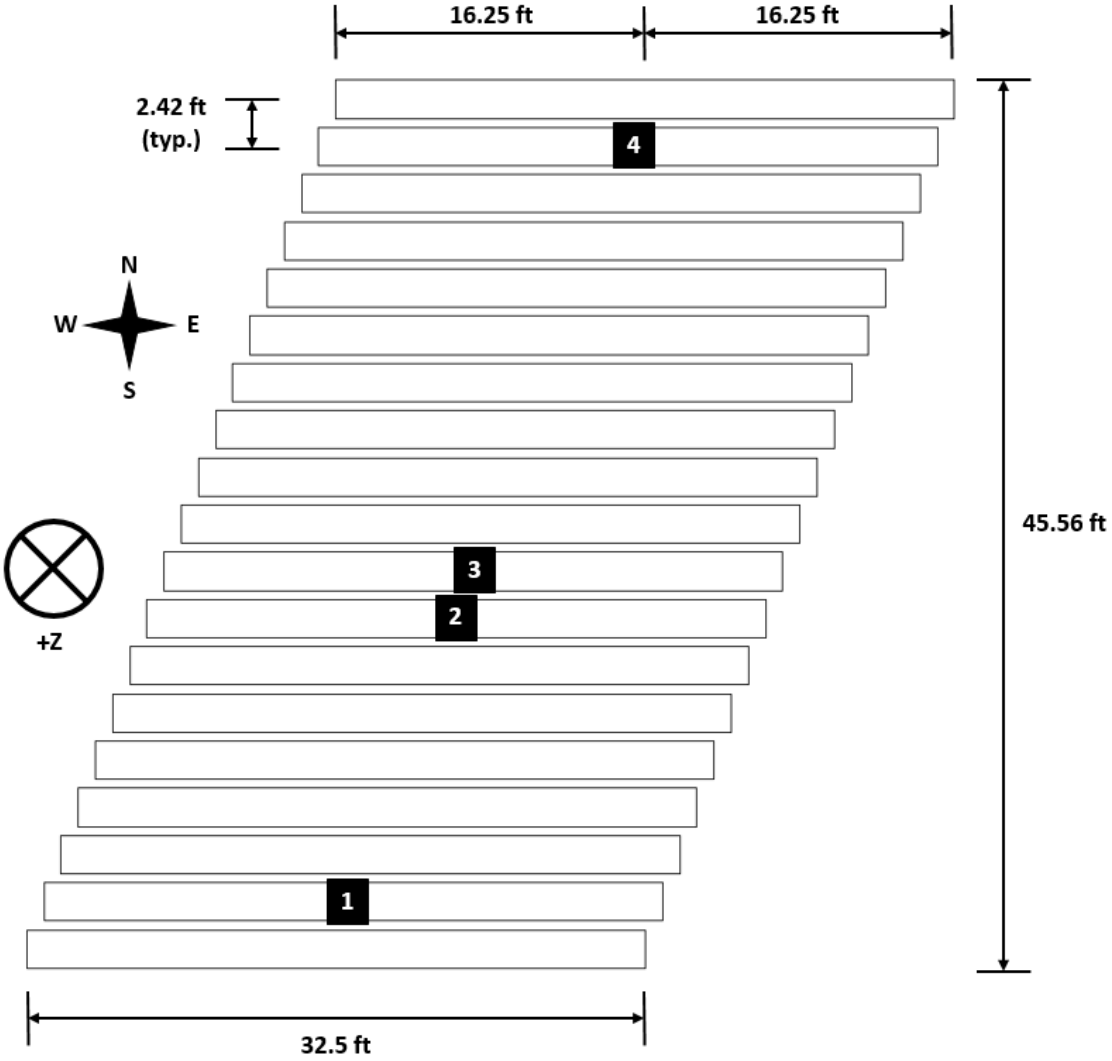

Figure C.10: Sensor locations capturing the local response for bridge S006 26001.

Table C.9: Sensor information of the local response setup for bridge S006 26001.

Sensor Location	Sensor Type	Sensor Id	Calibration Factor (mV/g)
1	PCB	N1	1001
2	PCB	N2	997
3	PCB	N3	1019
4	PCB	N4	1065

Date of Collection	10/7/2016
Length of Data (min)	52.73
Sampling Rate (Hz)	2048

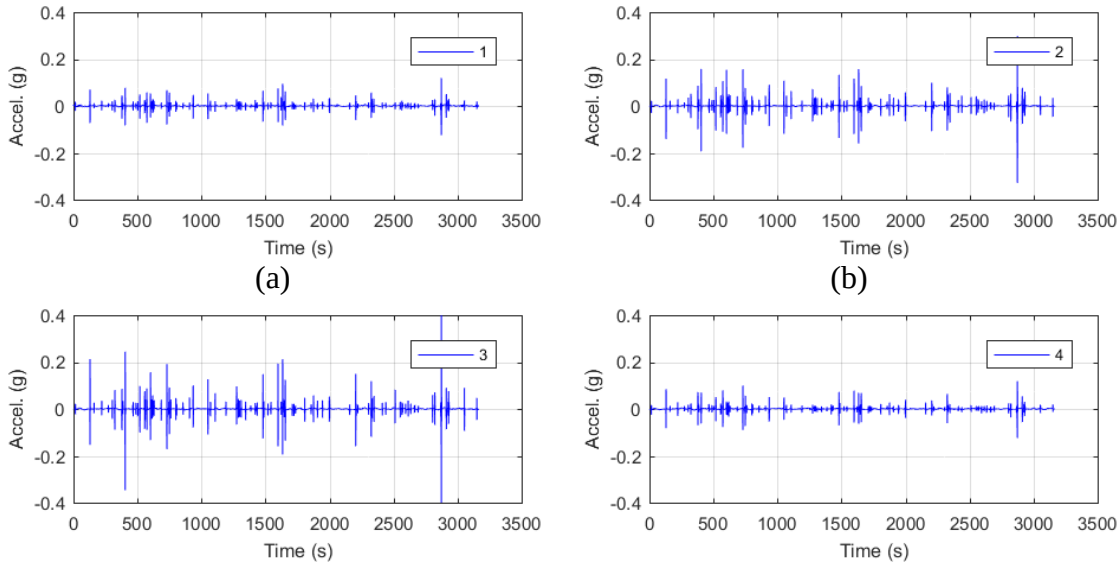

Figure C.11: Raw acceleration data of the local response for bridge S006 26001.

Table C.10: Filter parameters of the local response for bridge S006 26001.

Filter Parameter	Value
Hampel Identifier Order	--
FIR Bandpass Filter Order	4096
FIR Bandpass Filter Lower Cutoff Frequency (Hz)	8
FIR Bandpass Filter Upper Cutoff Frequency (Hz)	23
Tukey Averaging Window (min)	1.5

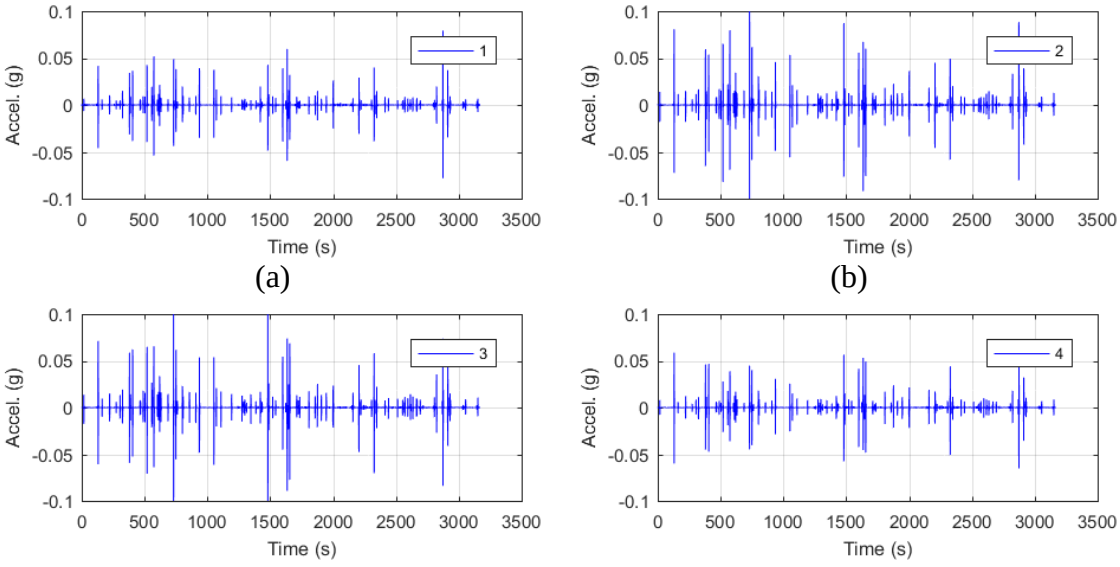

Figure C.12: Filtered acceleration data of the local response for bridge S006 26001.

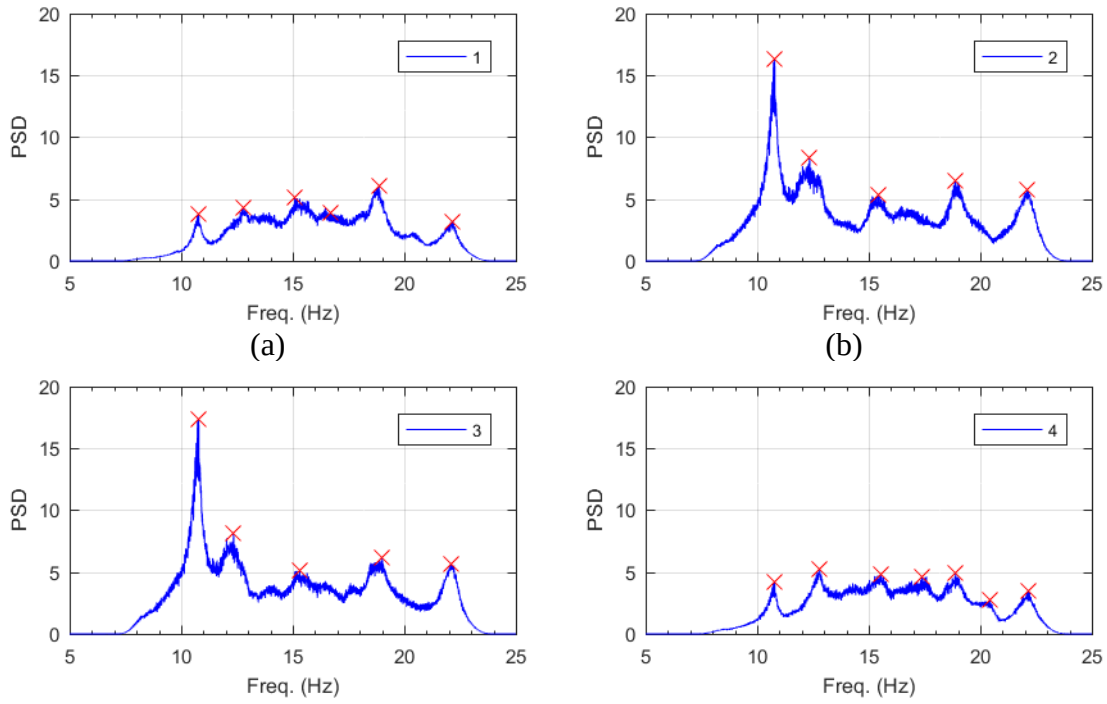

Figure C.13: Frequency content of the filtered acceleration data and peak-picking frequencies of the local response for bridge S006 26001.

Table C.11: Filtered acceleration RMS values of the local response for bridge S006 26001.

Sensor	**Filtered a_{RMS} (μg)**
1	1518
2	2508
3	2599
4	1534

Table C.12: Peak-picking frequencies of the local response for bridge S006 26001.

Mode	**Individual Sensor Frequencies (Hz)**			
	1	**2**	**3**	**4**
1	10.78	10.78	10.79	10.79
2	--	12.35	12.35	--
3	12.80	--	--	12.80
4	15.10	15.42	15.31	15.52
5	16.71	--	--	--

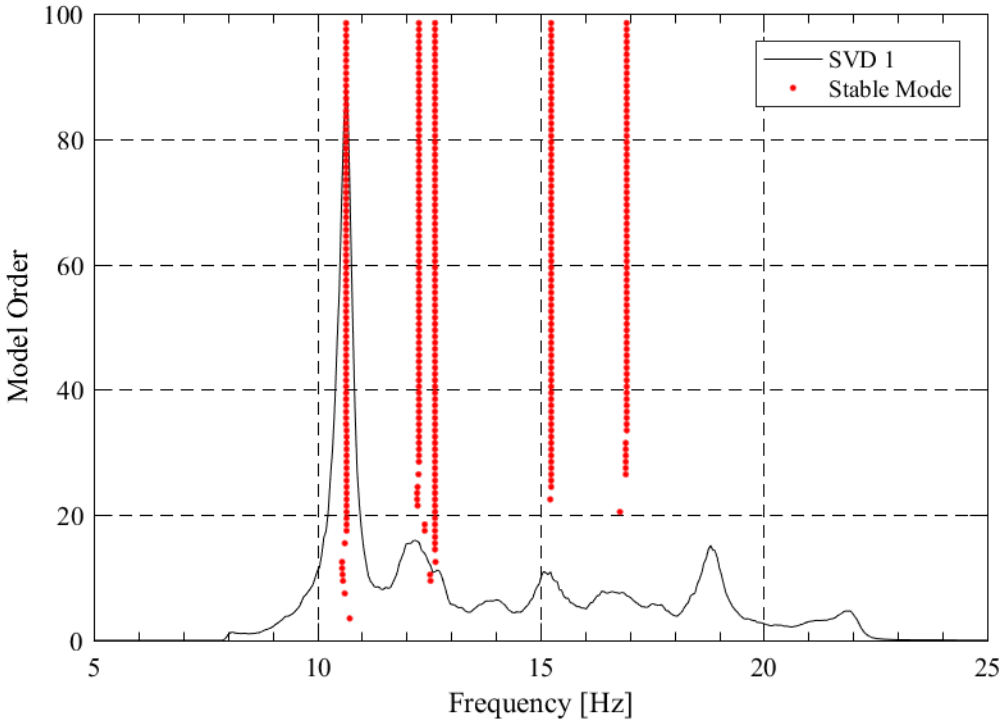

Figure C.14: SSI-UPCX method stabilization diagram of the local response for bridge S006 26001.

Table C.13: SSI-UPCX method dynamic properties of the local response for bridge S006 26001.

Mode	Frequency (Hz)	Damping (%)	Complexity (%)
1	10.65	1.97	0.55
2	12.28	3.81	2.37
3	12.64	4.62	53.47
4	15.24	1.67	5.96
5	16.92	4.01	22.78

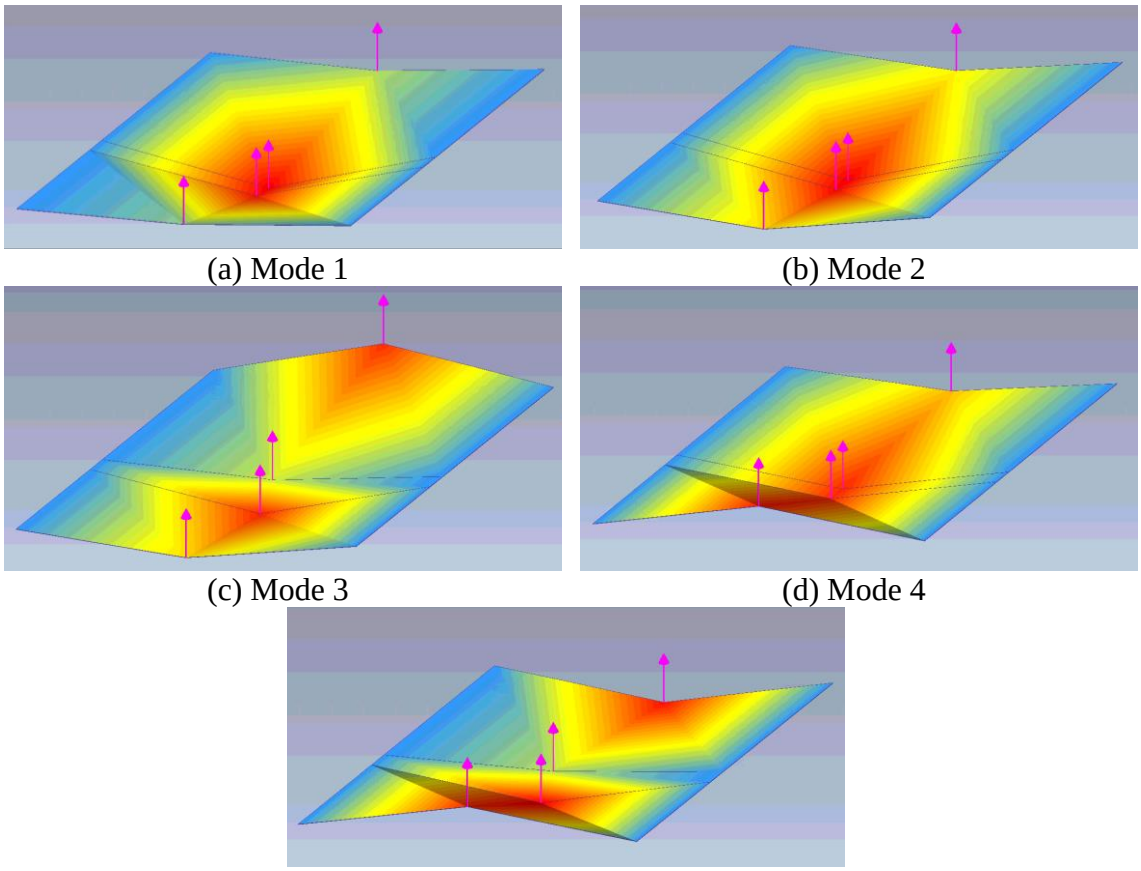

(a) Mode 1 (b) Mode 2

(c) Mode 3 (d) Mode 4

(e) Mode 5

Figure C.15: Operational deflected shapes of the local response for bridge S006 26001.

Table C.14: Operational deflected shape coordinates of the local response for bridge S006 26001.

Sensor	**ODS Coordinates**				
	Mode 1	**Mode 2**	**Mode 3**	**Mode 4**	**Mode 5**
1	0.25	0.43	-0.76	-0.55	0.95
2	1.00	1.00	0.38	-0.98	0.27
3	0.94	0.98	1.00	-0.90	1.00
4	0.18	0.50	0.62	1.00	-0.90

Table C.15: MAC values of the local response for bridge S006 26001.

MAC	**Mode 1**	**Mode 2**	**Mode 3**	**Mode 4**	**Mode 5**
Mode 1	1.000	0.968	0.541	0.237	0.366
Mode 2	0.968	1.000	0.689	0.236	0.257
Mode 3	0.541	0.689	1.000	0.325	0.053
Mode 4	0.237	0.236	0.325	1.000	0.610
Mode 5	0.366	0.257	0.053	0.610	1.000

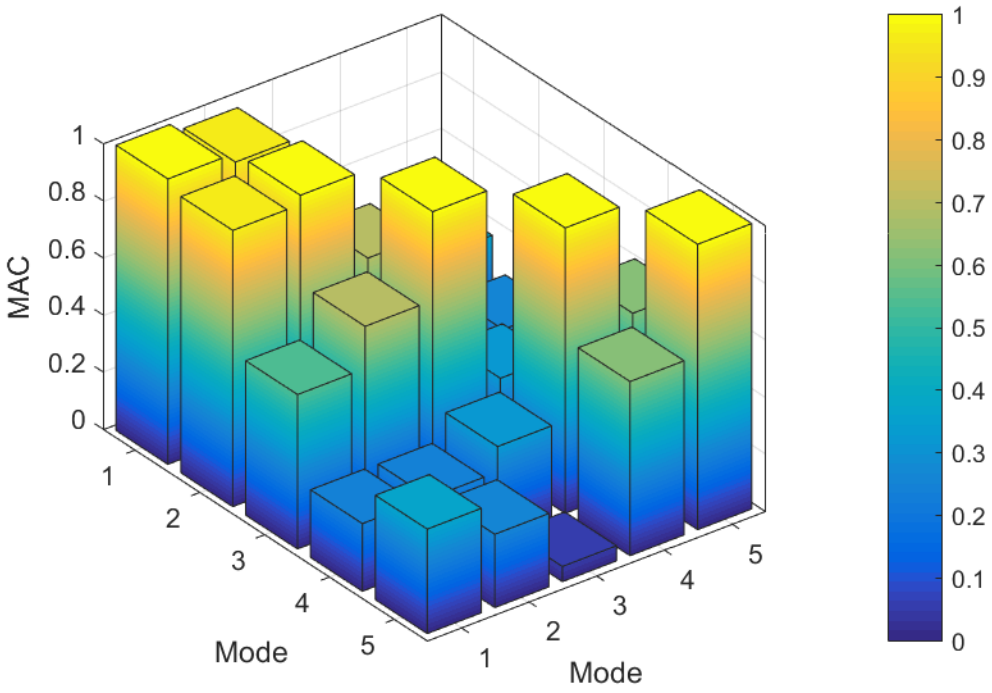

Figure C.16: MAC values of the local response for bridge S006 26001.

IT Girder Bridge S009 00888:

Figure C.17: Location of bridge S009 00888 (courtesy of Google Maps).

Table C.16: Bridge information summary for bridge S009 00888.

Bridge ID	S009 00888	**Girder Height (in [mm])**	15.75 [400]
County	Cuming	**Girder Width (in [mm])**	23.63 [600]
Year Built	2002	**Girder Spacing (in [mm])**	28.00 [711]
No. of Spans	3	**Deck Thickness (in [mm])**	6 [152]
Length Span 1 (ft)	32.00	**No. of Girders**	18
Length Span 2 (ft)	44.00	**Diaphragm**	None
Length Span 3 (ft)	32.00	**Deck Rating**	8
Bridge Width (ft)	42.40	**Superstructure Rating**	8
Skew Angle (°)	45	**Substructure Rating**	7

Figure C.18: Photo of bridge S009 00888.

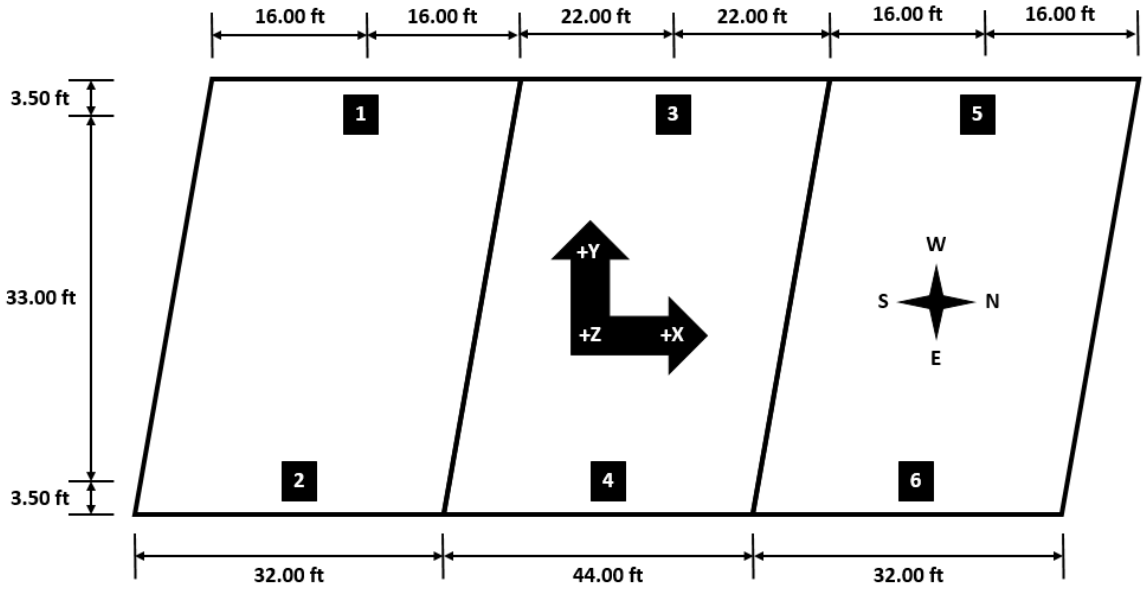

Figure C.19: Sensor locations capturing the global response for bridge S009 00888.

Table C.17: Sensor information of the global response setup for bridge S009 00888.

Sensor Location	Sensor Type	Sensor Id	Calibration Factor (mV/g)
1	WSN	996Z	--
2	WSN	99FZ	--
3	WSN	995Z	--
4	WSN	99CZ	--
5	WSN	848Z	--
6	WSN	997Z	--

Date of Collection	10/14/2016
Length of Data (min)	52.43
Sampling Rate (Hz)	256

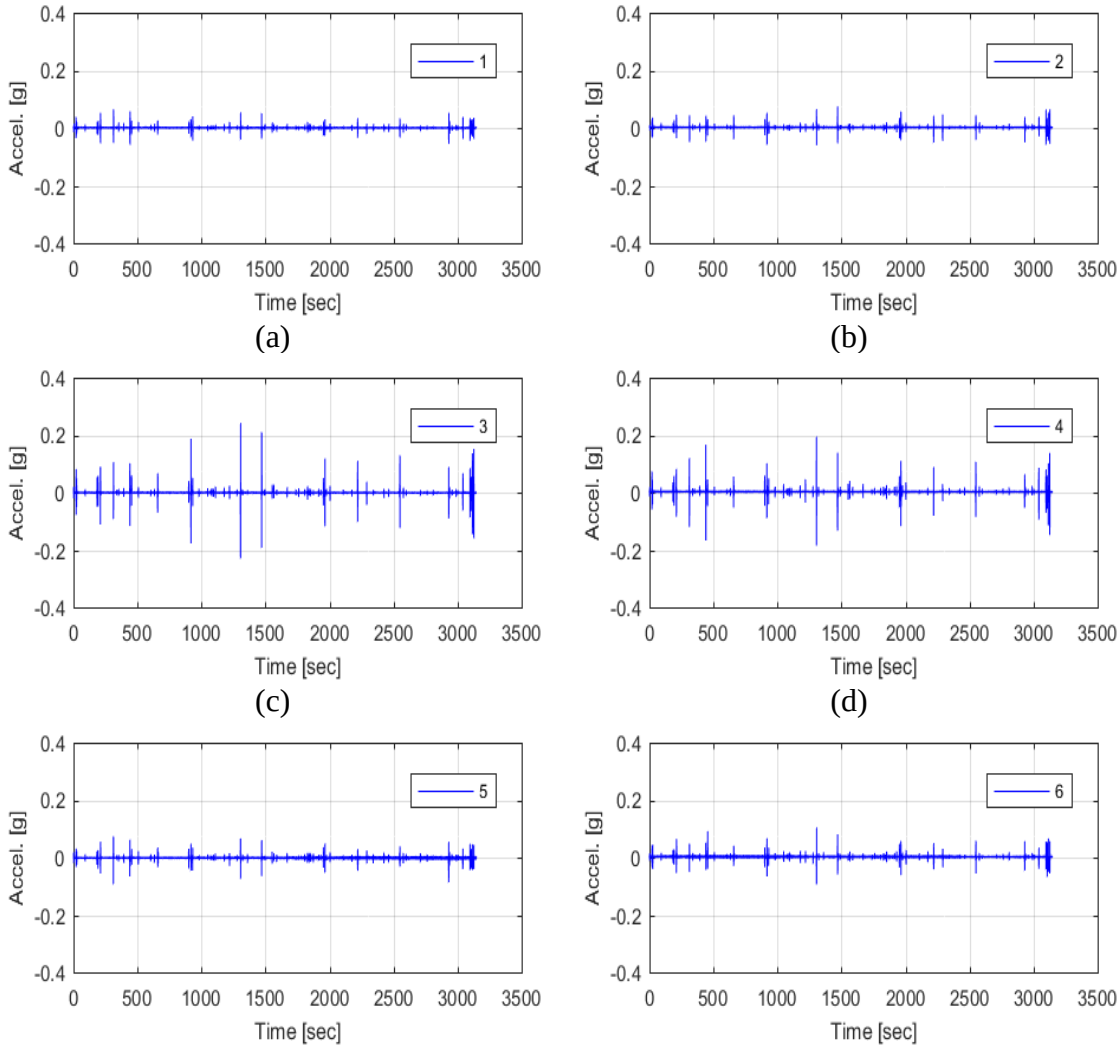

Figure C.20: Raw acceleration data of the global response for bridge S009 00888.

Table C.18: Filter parameters of the global response for bridge S009 00888.

Filter Parameter	Value
Hampel Identifier Order	--
FIR Bandpass Filter Order	2048
FIR Bandpass Filter Lower Cutoff Frequency (Hz)	10
FIR Bandpass Filter Upper Cutoff Frequency (Hz)	28
Tukey Averaging Window (min)	1.5

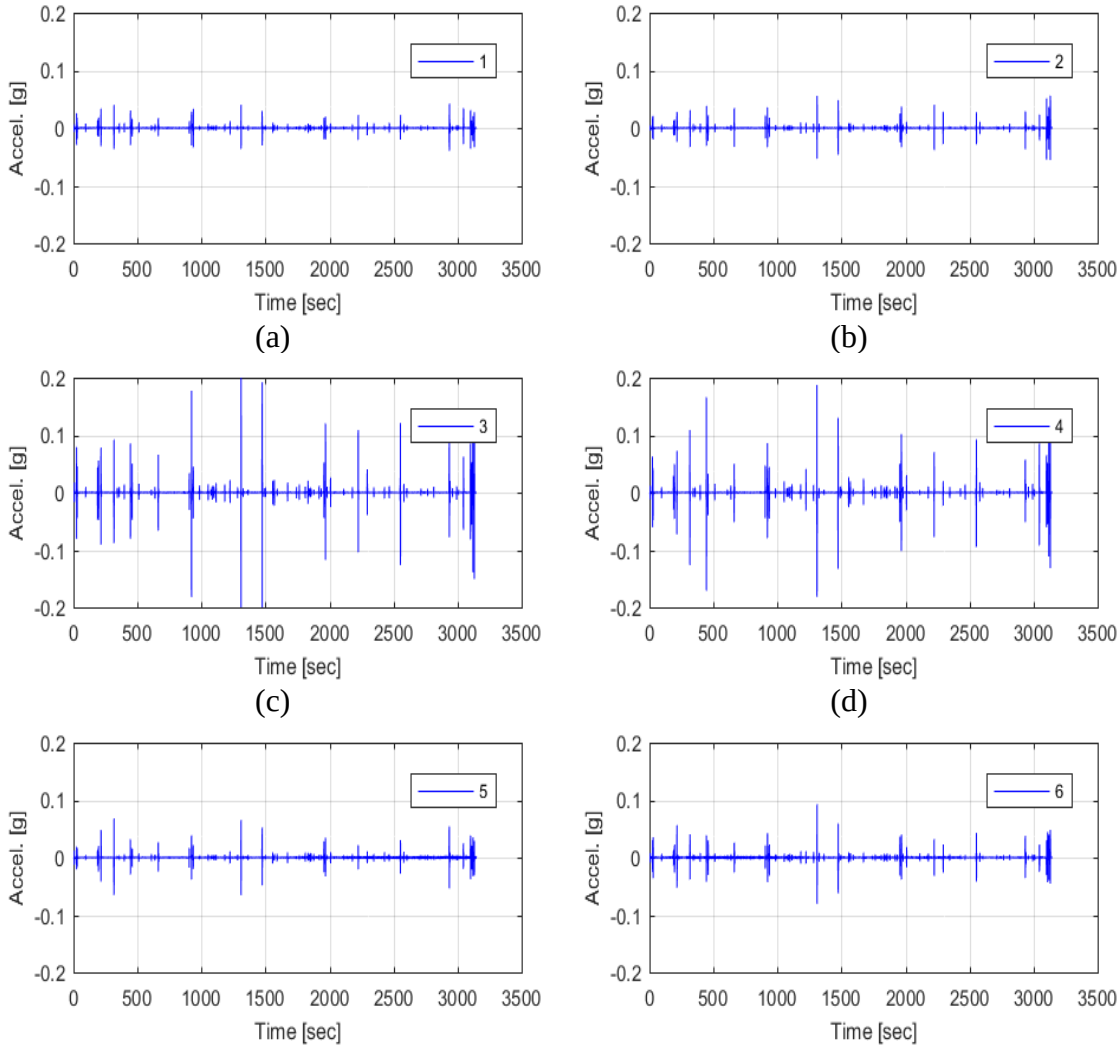

Figure C.21: Filtered acceleration data of the global response for bridge S009 00888.

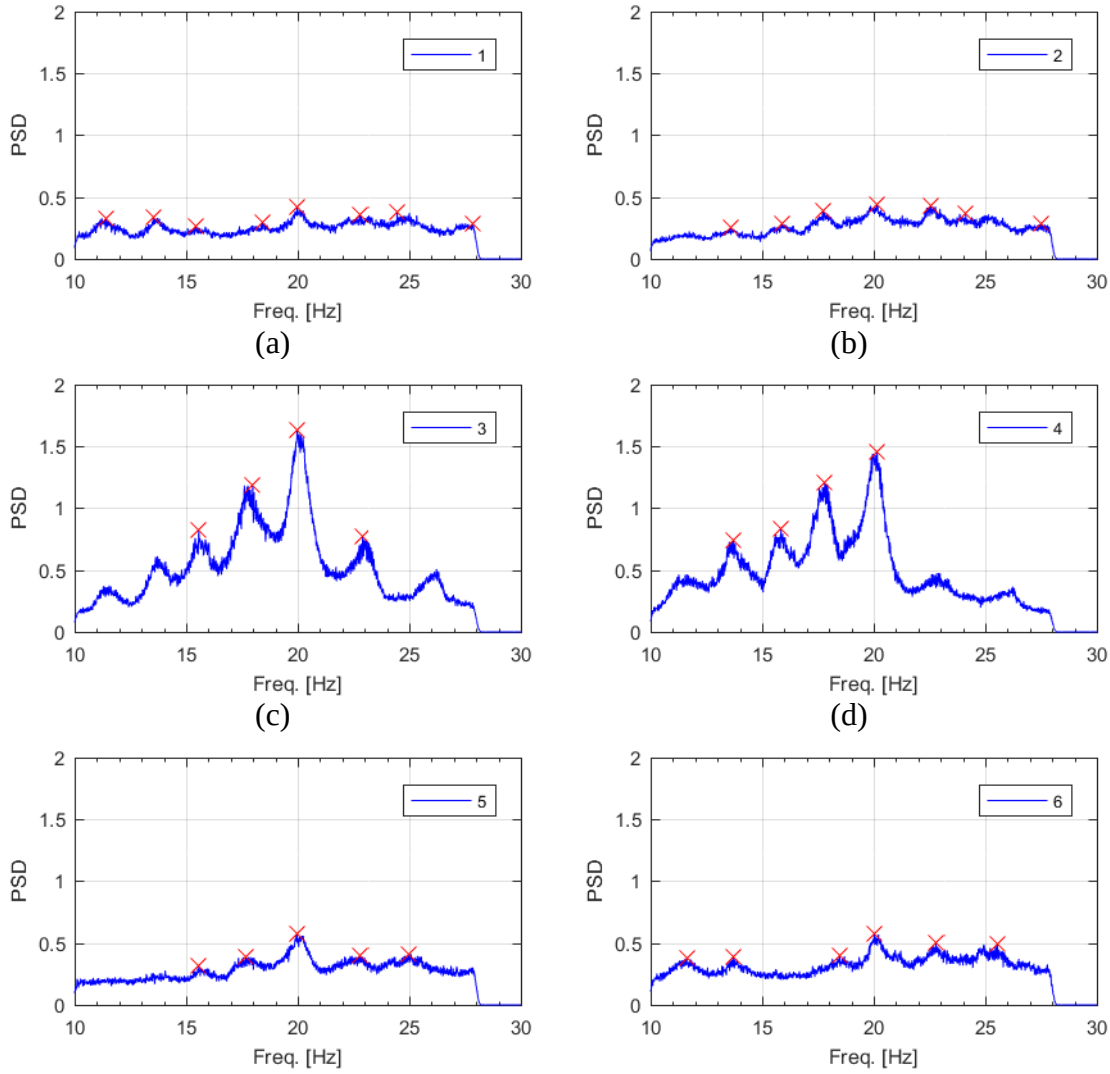

Figure C.22: Frequency content of the filtered acceleration data and peak-picking frequencies of the global response for bridge S009 00888.

Table C.19: Filtered acceleration RMS values of the global response for bridge S009 00888.

Sensor	**Filtered a_{RMS} (µg)**
1	1174
2	1335
3	3594
4	3334
5	1387
6	1565

Table C.20: Peak-picking frequencies of the global response for bridge S009 00888.

Mode	Individual Sensor Frequencies (Hz)					
	1	**2**	**3**	**4**	**5**	**6**
1	11.42	--	--	--	--	11.62
2	13.56	13.58	--	13.71	--	13.71
3	15.41	15.90	15.56	15.84	15.57	--
4	--	17.72	17.98	17.80	17.68	--

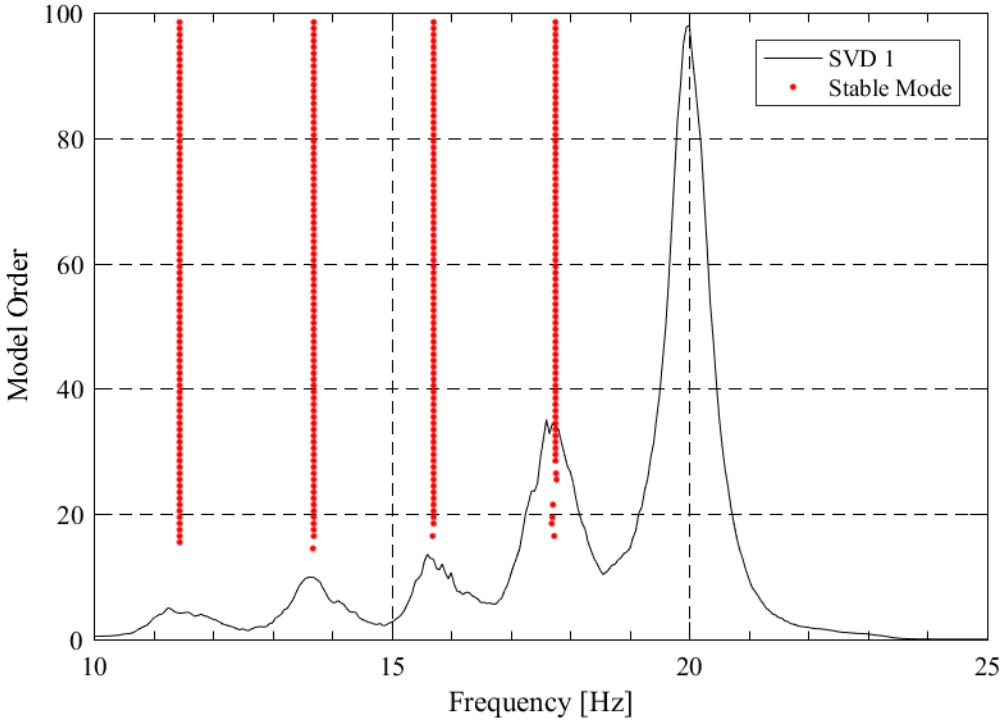

Figure C.23: SSI-UPCX method stabilization diagram of the global response for bridge S009 00888.

Table C.21: SSI-UPCX method dynamic properties of the global response for bridge S009 00888.

Mode	Frequency (Hz)	Damping (%)	Complexity (%)
1	11.44	0.98	7.24
2	13.69	0.84	34.15
3	15.71	2.07	22.23
4	17.75	0.45	38.63

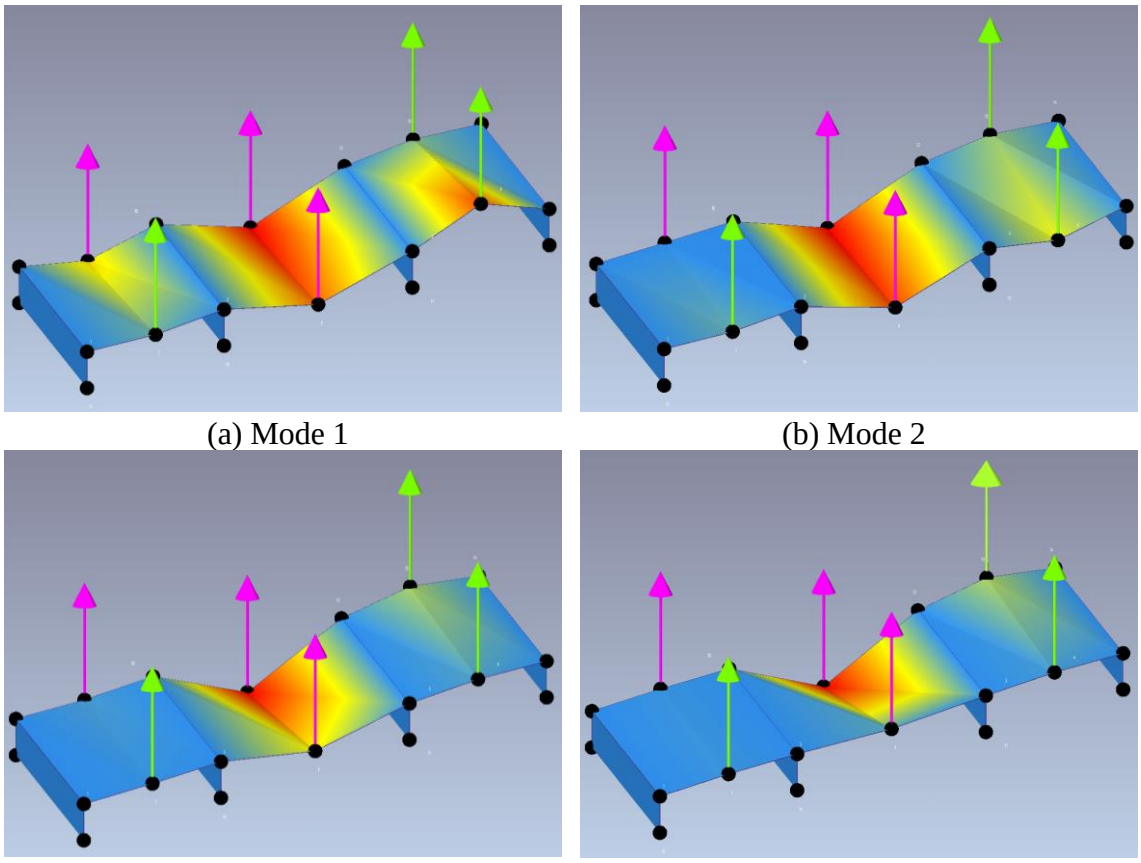

(a) Mode 1 (b) Mode 2

(c) Mode 3 (d) Mode 4

Figure C.24: Operational deflected shapes of the global response for bridge S009 00888.

Table C.22: Operational deflected shape coordinates of the global response for bridge S009 00888.

Sensor	ODS Coordinates			
	Mode 1	Mode 2	Mode 3	Mode 4
1	0.48	0.00	0.05	-0.02
2	0.13	0.11	0.02	-0.02
3	1.00	1.00	1.00	1.00
4	0.75	0.84	0.41	0.09
5	-0.17	-0.20	-0.23	-0.24
6	-0.82	0.36	-0.07	-0.04

Table C.23: MAC values of the global response for bridge S009 00888.

MAC	Mode 1	Mode 2	Mode 3	Mode 4
Mode 1	1.000	0.387	0.638	0.515
Mode 2	0.387	1.000	0.675	0.571
Mode 3	0.638	0.675	1.000	0.878
Mode 4	0.515	0.571	0.878	1.000

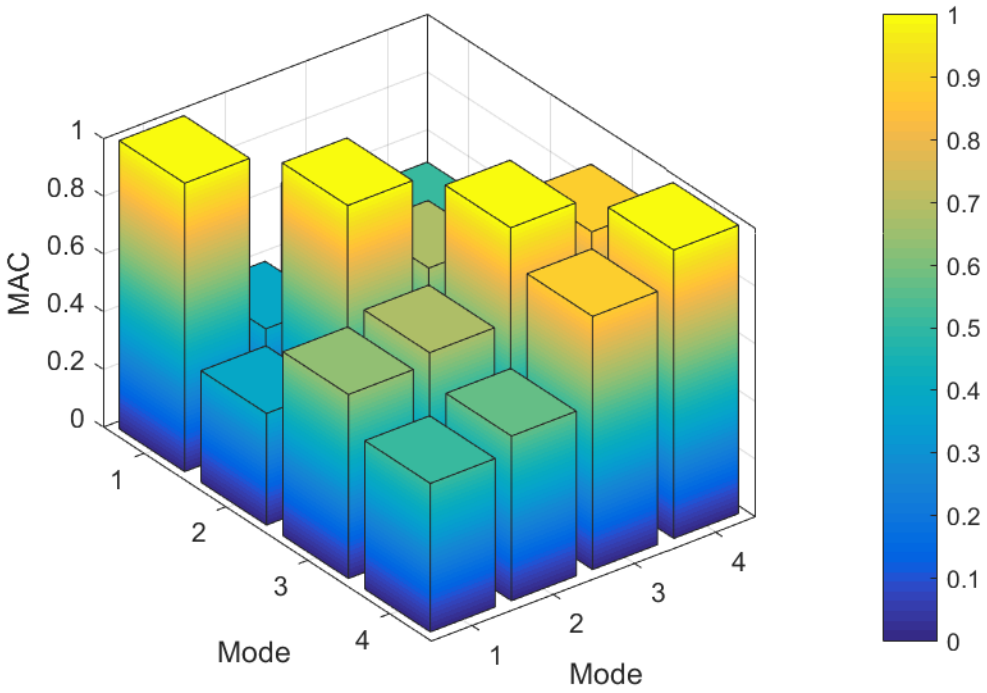

Figure C.25: MAC values of the global response for bridge S009 00888.

IT Girder Bridge S020 32260:

Figure C.26: Location of bridge S020 32260 (courtesy of Google Maps).

Table C.24: Bridge information summary for bridge S020 32260.

Bridge ID	S020 32260	**Girder Height (in [mm])**	15.75 [400]
County	Holt	**Girder Width (in [mm])**	23.63 [600]
Year Built	2012	**Girder Spacing (in [mm])**	27.50 [699]
No. of Spans	4	**Deck Thickness (in [mm])**	6 [152]
Length Span 1 (ft)	46.00	**No. of Girders**	20
Length Span 2 (ft)	--	**Diaphragm**	C8x18.75
Length Span 3 (ft)	--	**Deck Rating**	7
Bridge Width (ft)	46.30	**Superstructure Rating**	7
Skew Angle (°)	40	**Substructure Rating**	7

Figure C.27: Photo of bridge S020 32260.

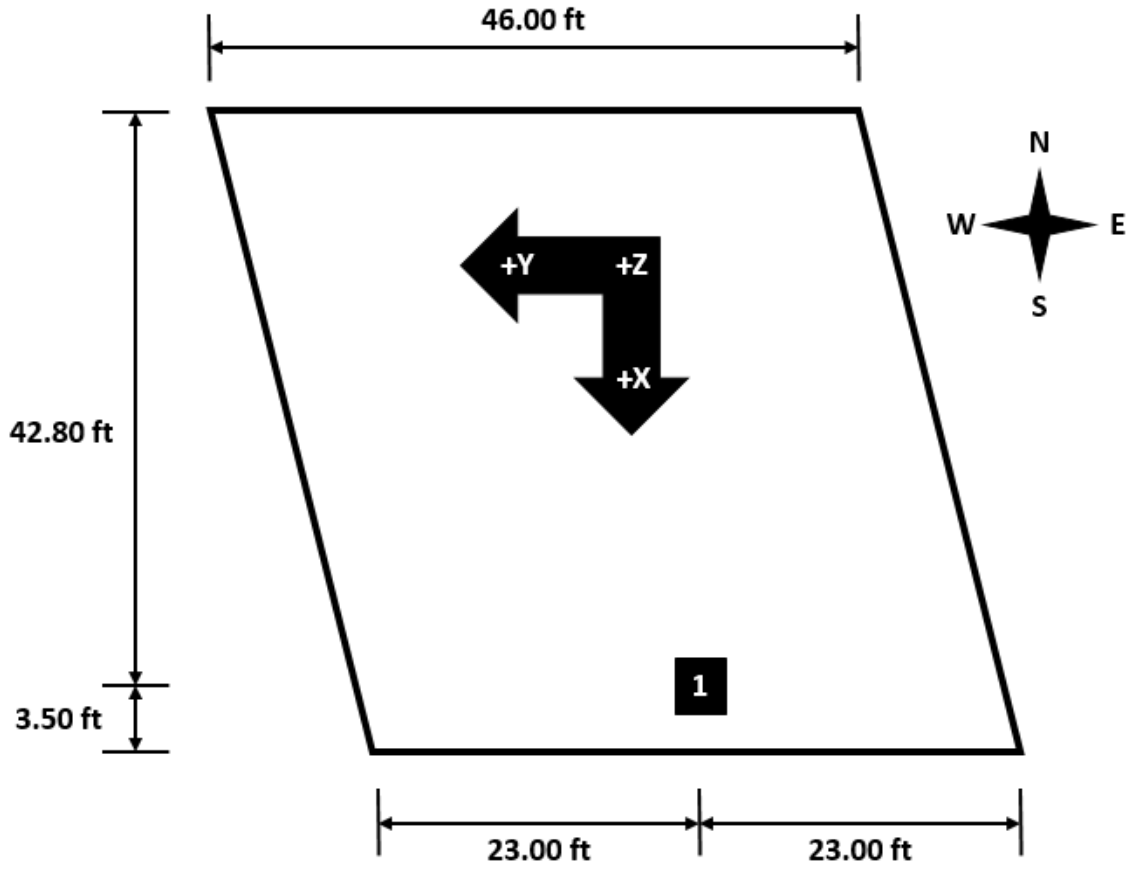

Figure C.28: Sensor locations capturing the global response for bridge S020 32260.

Table C.25: Sensor information of the global response setup for bridge S020 32260.

Sensor Location	Sensor Type	Sensor Id	Calibration Factor (mV/g)
1 Z	PCB	N2	997
1 X	PCB	N3	1019

Date of Collection	1/4/2017
Length of Data (min)	8.79
Sampling Rate (Hz)	2048

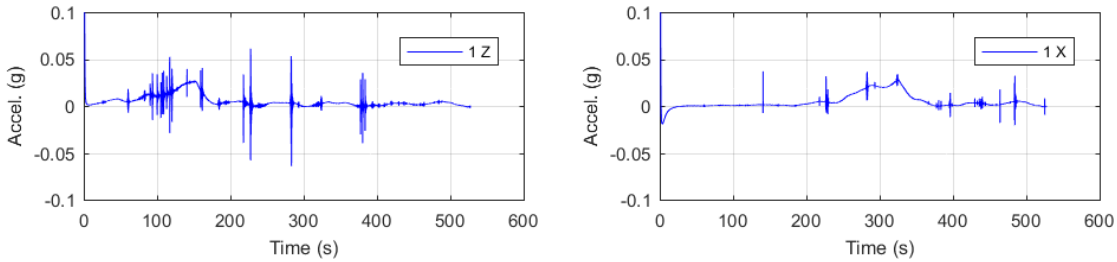

(a) (b)

Figure C.29: Raw acceleration data of the global response for bridge S020 32260.

Table C.26: Filter parameters of the global response for bridge S020 32260.

Filter Parameter	Value
Hampel Identifier Order	8
FIR Bandpass Filter Order	4096
FIR Bandpass Filter Lower Cutoff Frequency (Hz)	8
FIR Bandpass Filter Upper Cutoff Frequency (Hz)	28
Tukey Averaging Window (min)	1.5

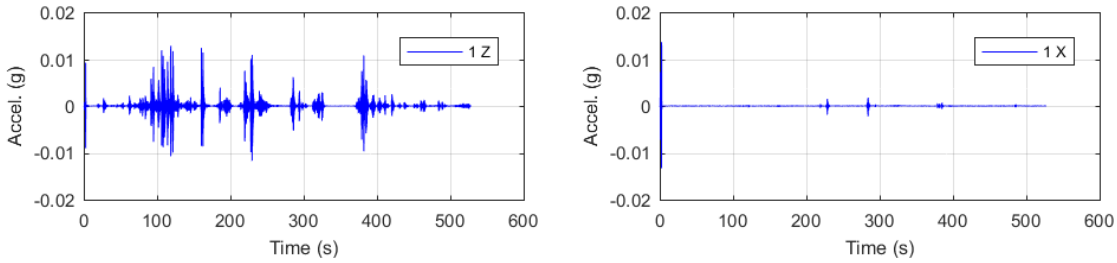

(a) (b)

Figure C.30: Filtered acceleration data of the global response for bridge S020 32260.

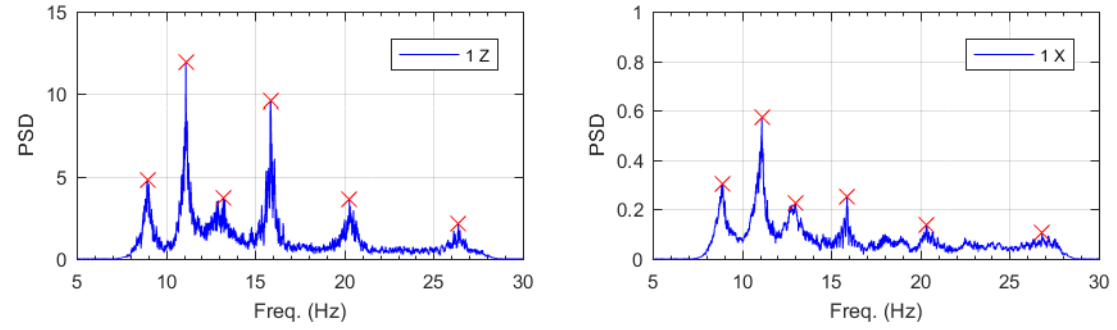

(a) (b)

Figure C.31: Frequency content of the filtered acceleration data and peak-picking frequencies of the global response for bridge S020 32260.

Table C.27: Filtered acceleration RMS values of the global response for bridge S020 32260.

Sensor	Filtered a_{RMS} (μg)
1 Z	828
1 X	140

Table C.28: Peak-picking frequencies of the global response for bridge S020 32260.

Mode	Individual Sensor Frequencies (Hz)	
	1 Z	**1 X**
1	8.97	8.94
2	11.12	11.12
3	13.22	13.00
4	15.85	15.89
5	20.28	20.33
6	26.39	26.83

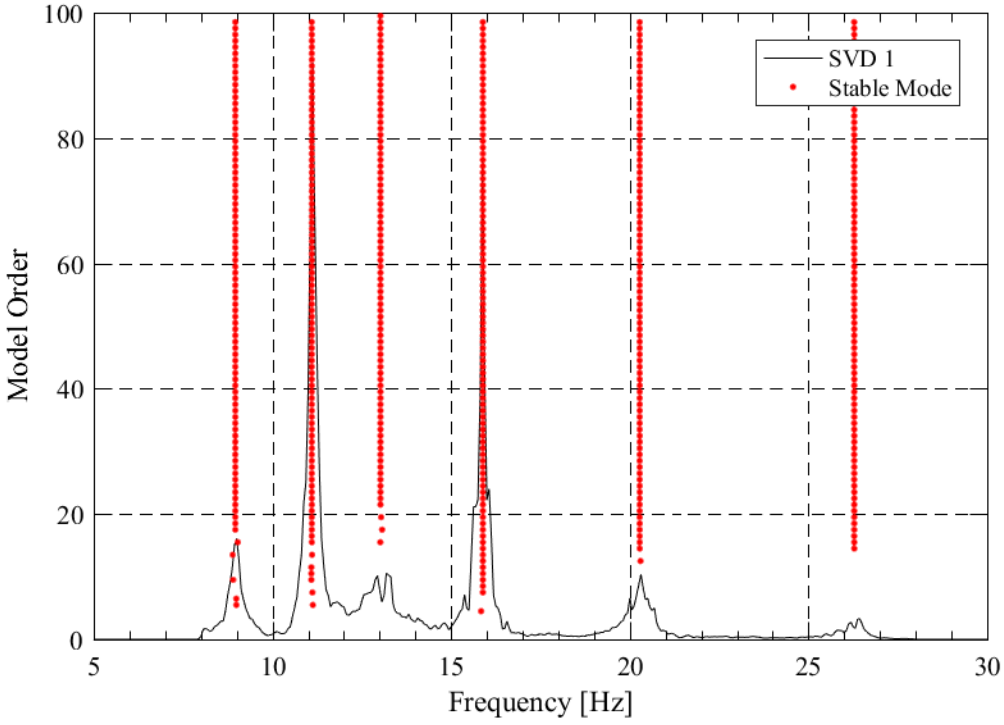

Figure C.32: SSI-UPCX method stabilization diagram of the global response for bridge S020 32260.

Table C.29: SSI-UPCX method dynamic properties of the global response for bridge S020 32260.

Mode	Frequency (Hz)	Damping (%)	Complexity (%)
1	8.96	2.58	4.11
2	11.10	0.91	0.10
3	13.02	6.80	0.10
4	15.89	0.87	0.01
5	20.28	1.76	0.12
6	26.28	1.16	0.22

IT Girder Bridge S058 00994:

Figure C.33: Location of bridge S058 00994 (courtesy of Google Maps).

Table C.30: Bridge information summary for bridge S058 00994.

Bridge ID	S058 00994	**Girder Height (in [mm])**	11.81 [300]
County	Howard	**Girder Width (in [mm])**	23.63 [600]
Year Built	2001	**Girder Spacing (in [mm])**	26.38 [670]
No. of Spans	3	**Deck Thickness (in [mm])**	6 [152]
Length Span 1 (ft)	36.75	**No. of Girders**	18
Length Span 2 (ft)	45.00	**Diaphragm**	None
Length Span 3 (ft)	36.75	**Deck Rating**	6
Bridge Width (ft)	40.00	**Superstructure Rating**	8
Skew Angle (°)	0	**Substructure Rating**	8

Figure C.34: Photo of bridge S058 00994.

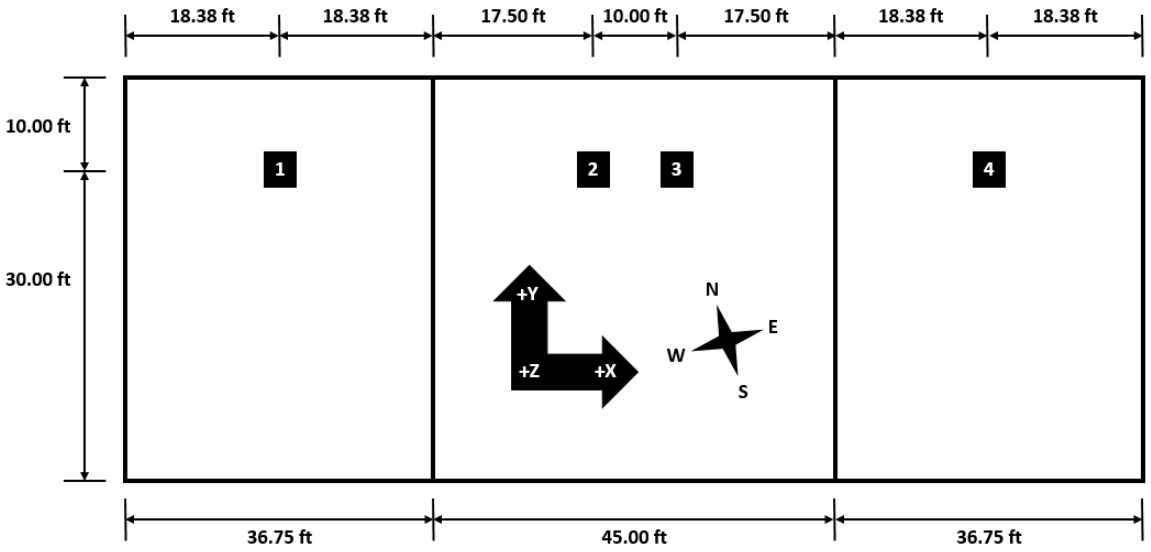

Figure C.35: Sensor locations capturing the global response for bridge S058 00994.

Table C.31: Sensor information of the global response setup for bridge S058 00994.

Sensor Location	Sensor Type	Sensor Id	Calibration Factor (mV/g)
1	PCB	N1	1001
2	PCB	N2	997
3	PCB	N3	1019
4	PCB	N4	1065

Date of Collection	10/21/2016
Length of Data (min)	64.45
Sampling Rate (Hz)	2048

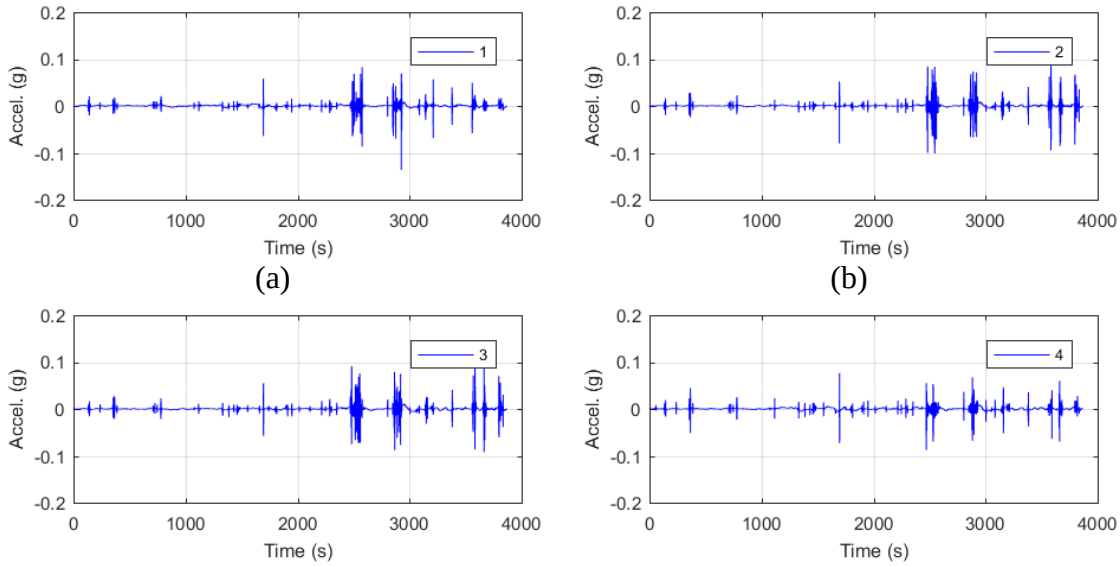

Figure C.36: Raw acceleration data of the global response for bridge S058 00994.

Table C.32: Filter parameters of the global response for bridge S058 00994.

Filter Parameter	Value
Hampel Identifier Order	--
FIR Bandpass Filter Order	4096
FIR Bandpass Filter Lower Cutoff Frequency (Hz)	5
FIR Bandpass Filter Upper Cutoff Frequency (Hz)	28
Tukey Averaging Window (min)	1.5

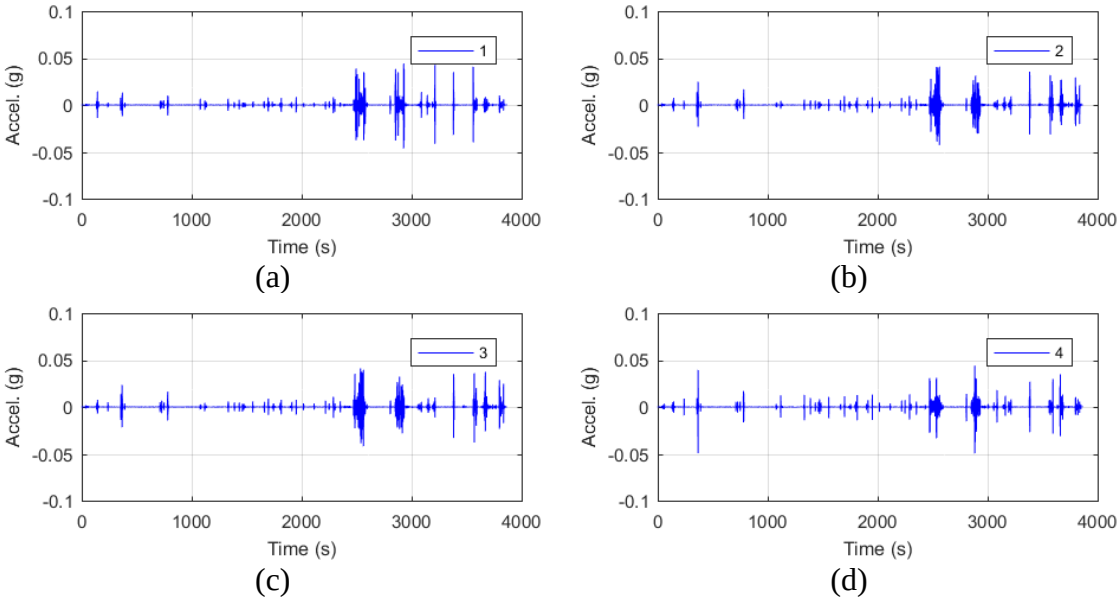

Figure C.37: Filtered acceleration data of the global response for bridge S058 00994.

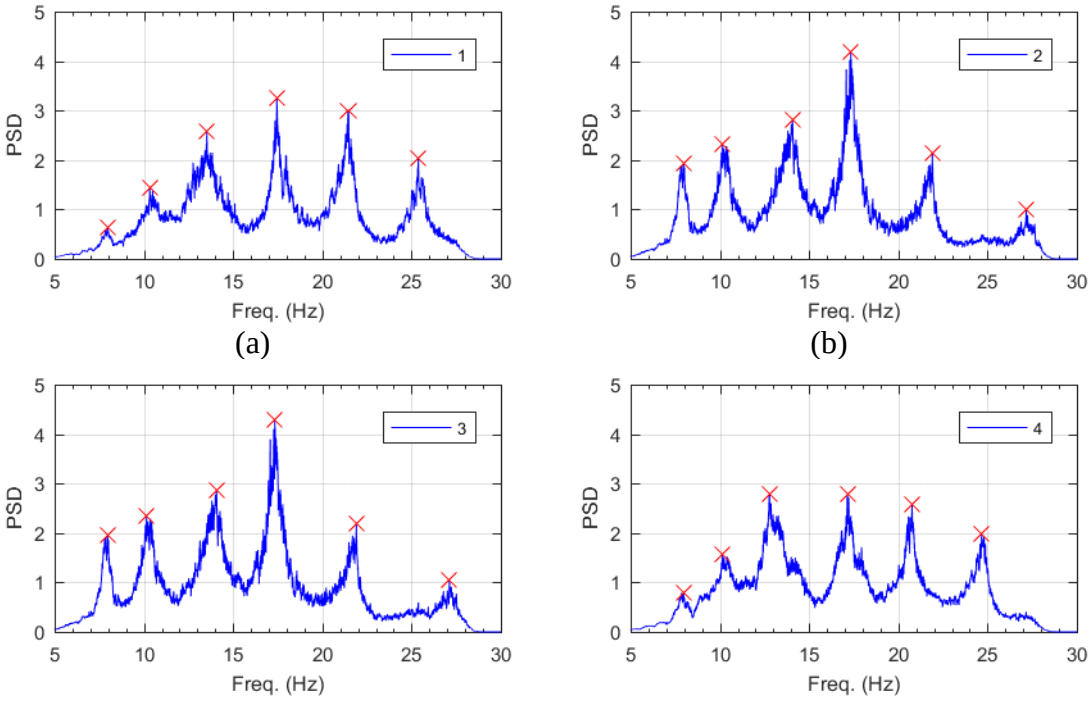

Figure C.38: Frequency content of the filtered acceleration data and peak-picking frequencies of the global response for bridge S058 00994.

Table C.33: Filtered acceleration RMS values of the global response for bridge S058 00994.

Sensor	**Filtered a_{RMS} (μg)**
1	832
2	930
3	944
4	815

Table C.34: Peak-picking frequencies of the global response for bridge S058 00994.

Mode	**Individual Sensor Frequencies (Hz)**			
	1	**2**	**3**	**4**
1	7.96	7.97	7.97	7.96
2	10.33	10.15	10.15	10.15
3	--	--	--	12.78
4	13.53	--	--	--
5	--	14.07	14.07	--
6	--	--	--	17.14
7	17.45	17.34	17.34	--

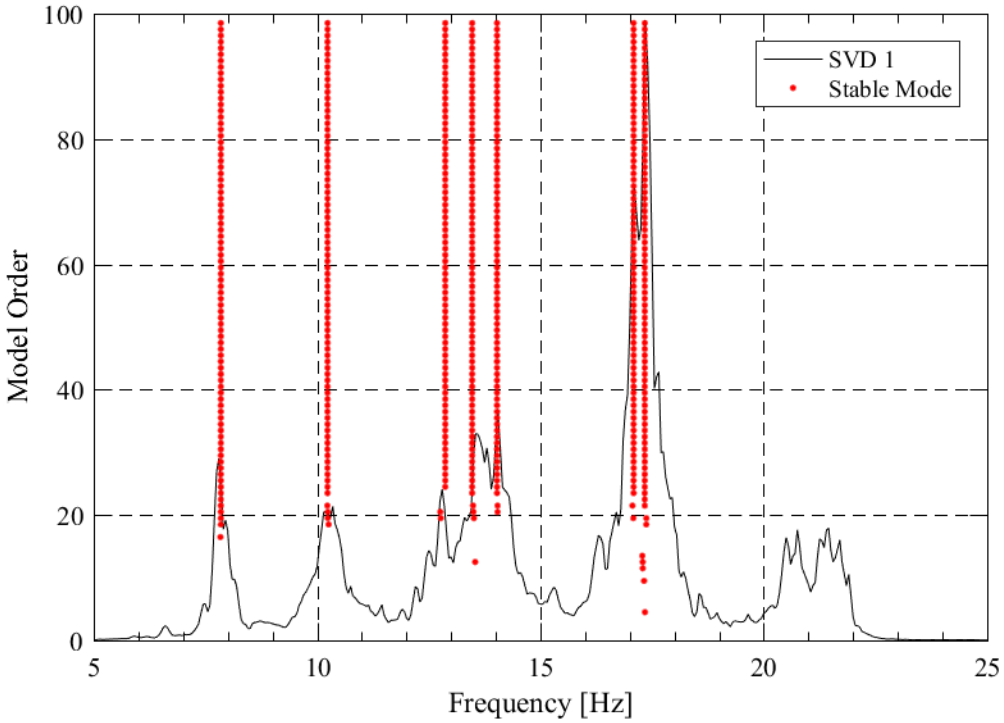

Figure C.39: SSI-UPCX method stabilization diagram of the global response for bridge S058 00994.

Table C.35: SSI-UPCX method dynamic properties of the global response for bridge S058 00994.

Mode	Frequency (Hz)	Damping (%)	Complexity (%)
1	7.85	2.26	1.62
2	10.23	3.86	20.02
3	12.87	3.90	16.15
4	13.47	3.63	29.28
5	14.03	2.49	0.28
6	17.09	1.51	2.52
7	17.34	1.48	8.64

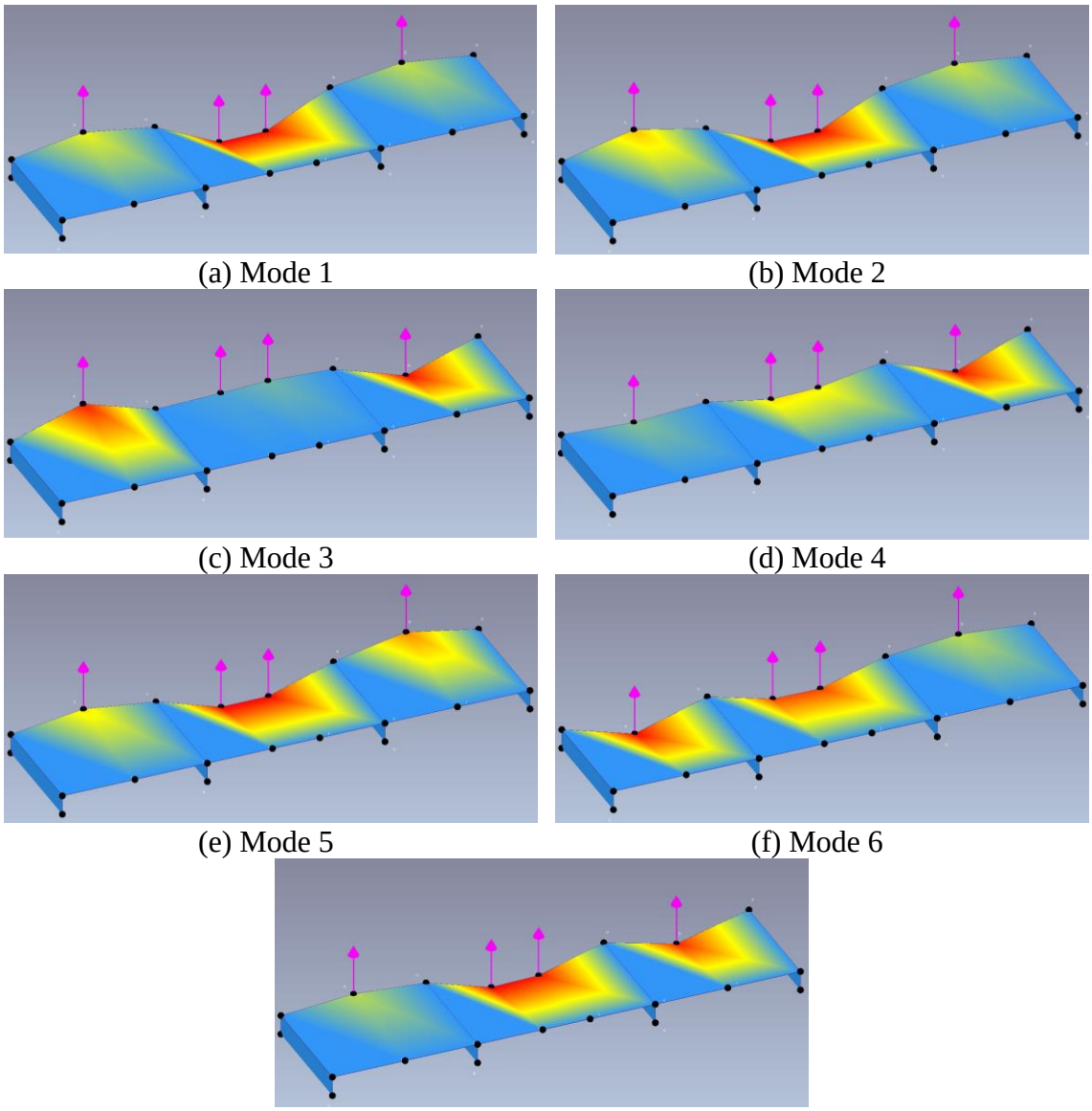

(a) Mode 1 (b) Mode 2

(c) Mode 3 (d) Mode 4

(e) Mode 5 (f) Mode 6

(g) Mode 7

Figure C.40: Operational deflected shapes of the global response for bridge S058 00994.

Table C.36: Operational deflected shape coordinates of the global response for bridge S058 00994.

Sensor	**ODS Coordinates**						
	Mode 1	**Mode 2**	**Mode 3**	**Mode 4**	**Mode 5**	**Mode 6**	**Mode 7**
1	-0.37	-0.54	-0.95	0.16	-0.45	1.00	-0.26
2	1.00	0.98	-0.06	0.47	1.00	0.82	1.00
3	0.99	1.00	-0.13	0.43	0.99	0.84	0.95
4	-0.29	-0.31	1.00	1.00	-0.67	-0.28	0.92

Table C.37: MAC values of the global response for bridge S058 00994.

MAC	Mode 1	Mode 2	Mode 3	Mode 4	Mode 5	Mode 6	Mode 7
Mode 1	1.000	0.960	0.026	0.706	0.989	0.339	0.983
Mode 2	0.960	1.000	0.124	0.777	0.929	0.290	0.970
Mode 3	0.026	0.124	1.000	0.347	0.026	0.573	0.055
Mode 4	0.706	0.777	0.347	1.000	0.607	0.711	0.815
Mode 5	0.989	0.929	0.026	0.607	1.000	0.279	0.946
Mode 6	0.339	0.290	0.573	0.711	0.279	1.000	0.417
Mode 7	0.983	0.970	0.055	0.815	0.946	0.417	1.000

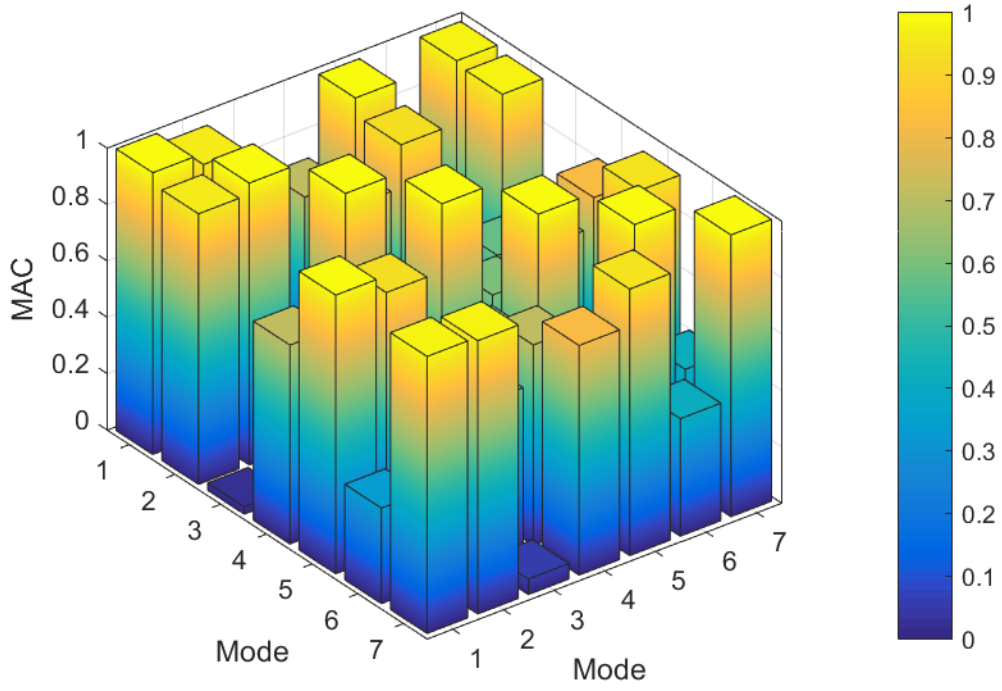

Figure C.41: MAC values of the global response for bridge S058 00994.

Slab Bridge S080 38614R:

Figure C.42: Location of bridge S080 38614R (courtesy of Google Maps).

Table C.38: Bridge information summary for bridge S080 38614R.

Bridge ID	S080 38614R	**Girder Height (in [mm])**	--
County	Seward	**Girder Width (in [mm])**	--
Year Built	1980	**Girder Spacing (in [mm])**	--
No. of Spans	3	**Deck Thickness (in [mm])**	16.25 [413]
Length Span 1 (ft)	32.00	**No. of Girders**	--
Length Span 2 (ft)	44.00	**Diaphragm**	--
Length Span 3 (ft)	32.00	**Deck Rating**	6
Bridge Width (ft)	37.00	**Superstructure Rating**	6
Skew Angle (°)	0	**Substructure Rating**	7

Figure C.43: Photo of bridge S080 38614R.

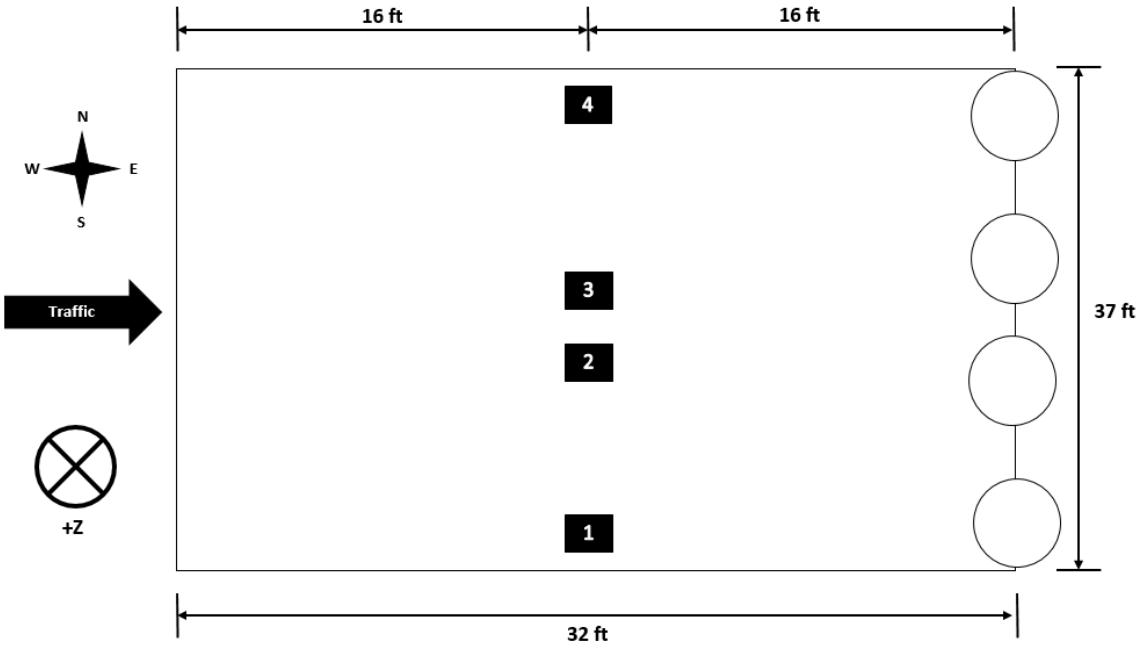

Figure C.44: Sensor locations capturing the global response for bridge S080 38614R.

Table C.39: Sensor information of the global response setup for bridge S080 38614R.

Sensor Location	Sensor Type	Sensor Id	Calibration Factor (mV/g)
1	PCB	N1	1001
2	PCB	N2	997
3	PCB	N3	1019
4	PCB	N4	1065

Date of Collection	3/31/2017
Length of Data (min)	67.38
Sampling Rate (Hz)	2048

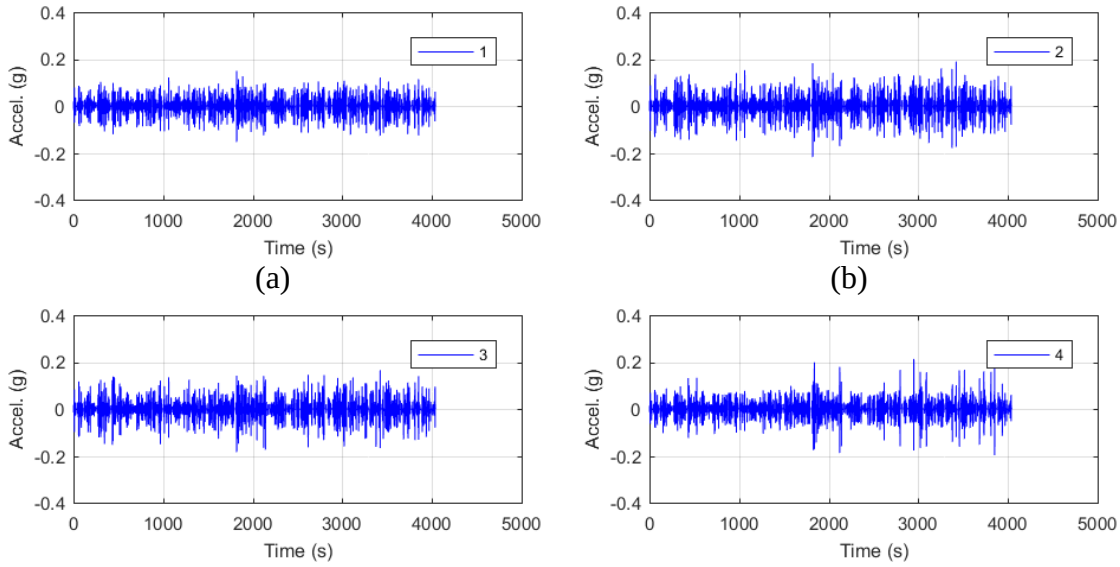

Figure C.45: Raw acceleration data of the global response for bridge S080 38614R.

Table C.40: Filter parameters of the global response for bridge S080 38614R.

Filter Parameter	Value
Hampel Identifier Order	--
FIR Bandpass Filter Order	8192
FIR Bandpass Filter Lower Cutoff Frequency (Hz)	6
FIR Bandpass Filter Upper Cutoff Frequency (Hz)	25
Tukey Averaging Window (min)	1.5

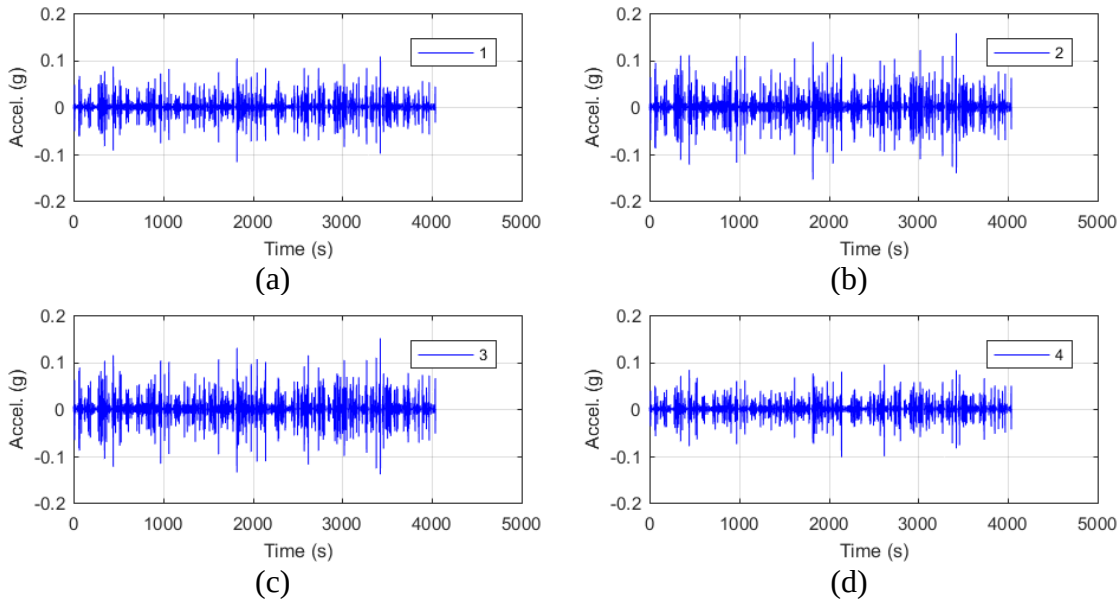

Figure C.46: Filtered acceleration data of the global response for bridge S080 38614R.

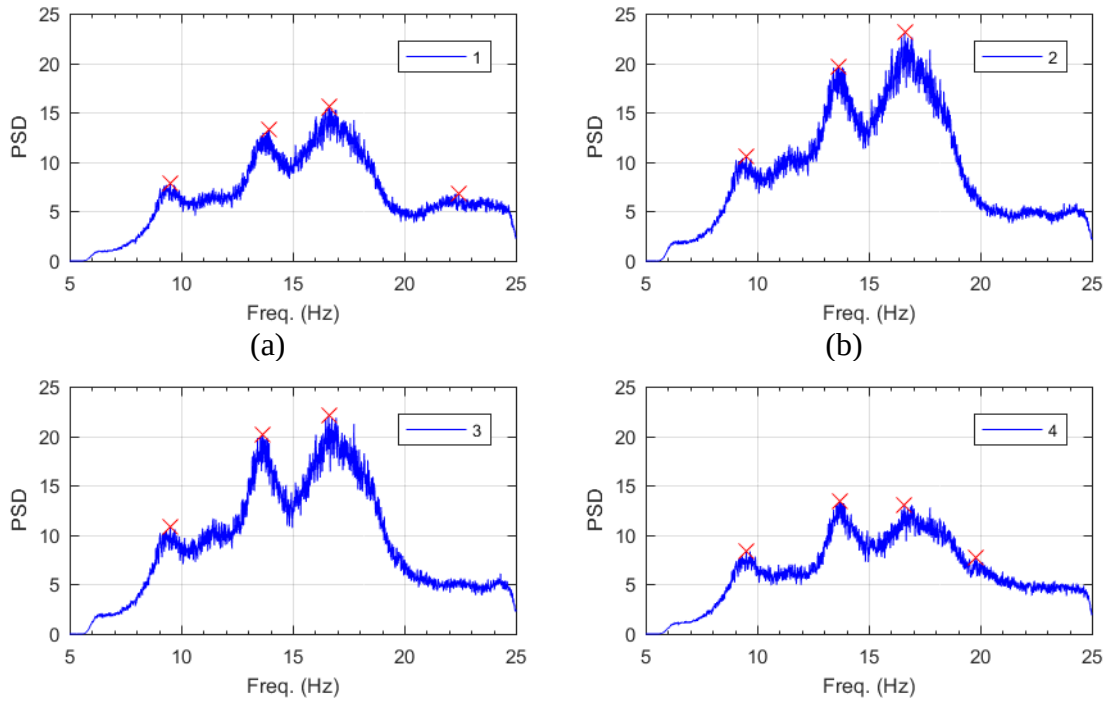

Figure C.47: Frequency content of the filtered acceleration data and peak-picking frequencies of the global response for bridge S080 38614R.

Table C.41: Filtered acceleration RMS values of the global response for bridge S080 38614R.

Sensor	**Filtered a_{RMS} (μg)**
1	3503
2	4944
3	4921
4	3310

Table C.42: Peak-picking frequencies of the global response for bridge S080 38614R.

Mode	**Individual Sensor Frequencies (Hz)**			
	1	**2**	**3**	**4**
1	9.51	9.51	9.51	9.51
2	13.94	13.67	13.64	13.71
3	16.61	16.61	16.61	16.61

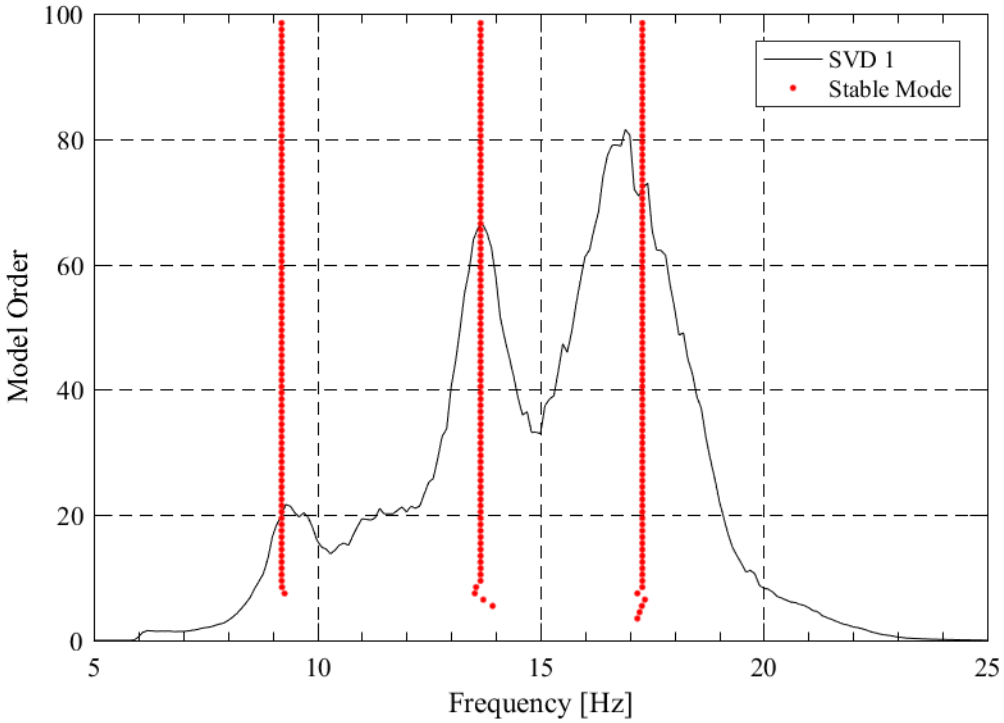

Figure C.48: SSI-UPCX method stabilization diagram of the global response for bridge S080 38614R.

Table C.43: SSI-UPCX method dynamic properties of the global response for bridge S080 38614R.

Mode	Frequency (Hz)	Damping (%)	Complexity (%)
1	9.21	9.81	3.54
2	13.66	4.58	3.42
3	17.28	8.07	2.88

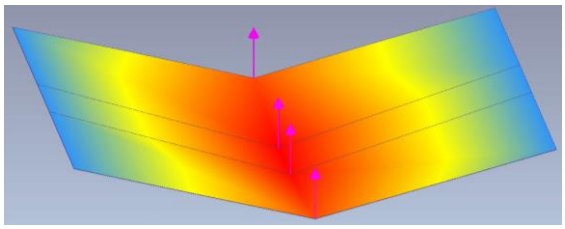

(a) Mode 1

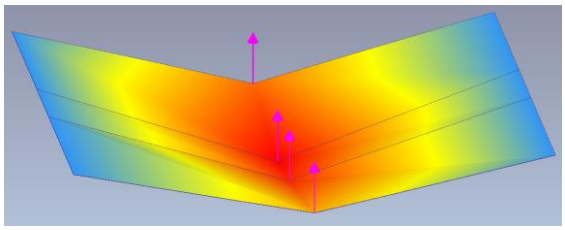

(b) Mode 2

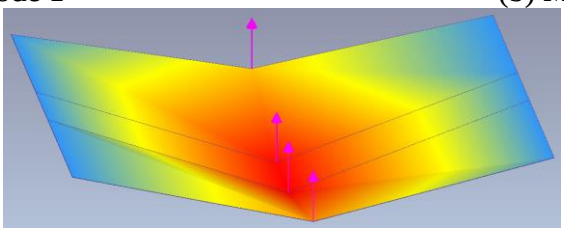

(c) Mode 3

Figure C.49: Operational deflected shapes of the global response for bridge S080 38614R.

Table C.44: Operational deflected shape coordinates of the global response for bridge S080 38614R.

Sensor	**ODS Coordinates**		
	Mode 1	**Mode 2**	**Mode 3**
1	0.81	0.59	0.66
2	0.98	0.90	1.00
3	1.00	1.00	0.98
4	0.82	0.76	0.53

Table C.45: MAC values of the global response for bridge S080 38614R.

MAC	**Mode 1**	**Mode 2**	**Mode 3**
Mode 1	1.000	0.978	0.992
Mode 2	0.978	1.000	0.990
Mode 3	0.992	0.990	1.000

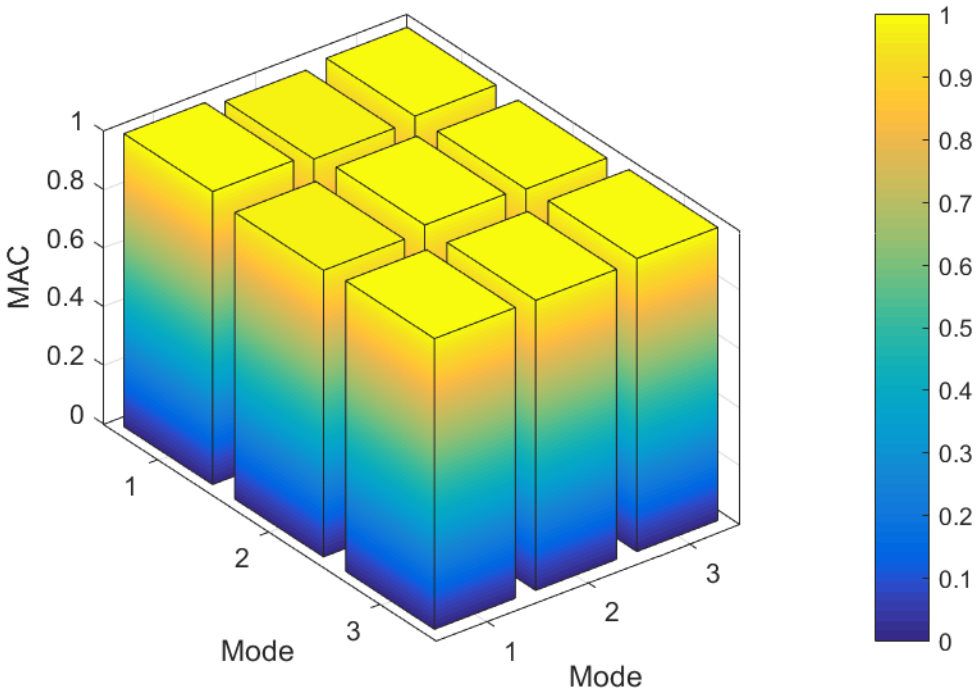

Figure C.50: MAC values of the global response for bridge S080 38614R.

NU Girder Bridge S080 40797R:

Figure C.51: Location of bridge S080 40797R (courtesy of Google Maps).

Table C.46: Bridge information summary for bridge S080 40797R.

Bridge ID	S080 40797R	**Girder Height (in [mm])**	78.75 [2000]
County	Lancaster	**Girder Width (in [mm])**	38.38 [975]
Year Built	2010	**Girder Spacing (in [mm])**	132 [3353]
No. of Spans	3	**Deck Thickness (in [mm])**	8 [203]
Length Span 1 (ft)	95.00	**No. of Girders**	6
Length Span 2 (ft)	165.00	**Diaphragm**	Steel
Length Span 3 (ft)	95.00	**Deck Rating**	8
Bridge Width (ft)	62.67	**Superstructure Rating**	9
Skew Angle (°)	29	**Substructure Rating**	8

Figure C.52: Photo of bridge S080 40797R.

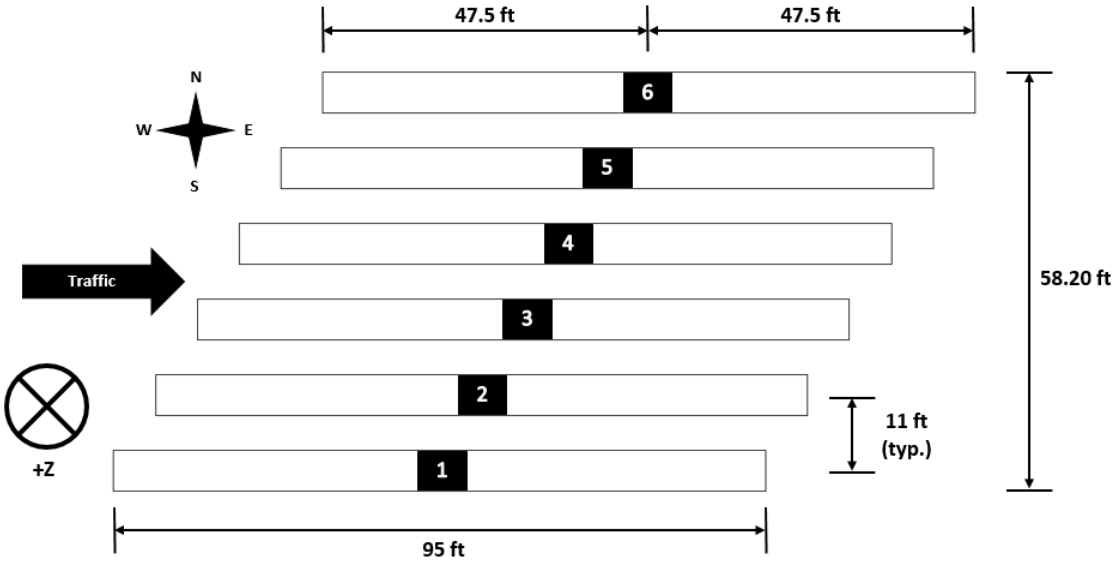

Figure C.53: Sensor locations capturing the local response for bridge S080 40797R.

Table C.47: Sensor information of the local response setup for bridge S080 40797R.

Sensor Location	Sensor Type	Sensor Id	Calibration Factor (mV/g)
1	PCB	N1	1001
2	PCB	N2	997
3	PCB	N3	1019
4	PCB	N4	1065
5	PCB	N5	1006
6	PCB	N6	993

Date of Collection	3/22/2017
Length of Data (min)	61.52
Sampling Rate (Hz)	2048

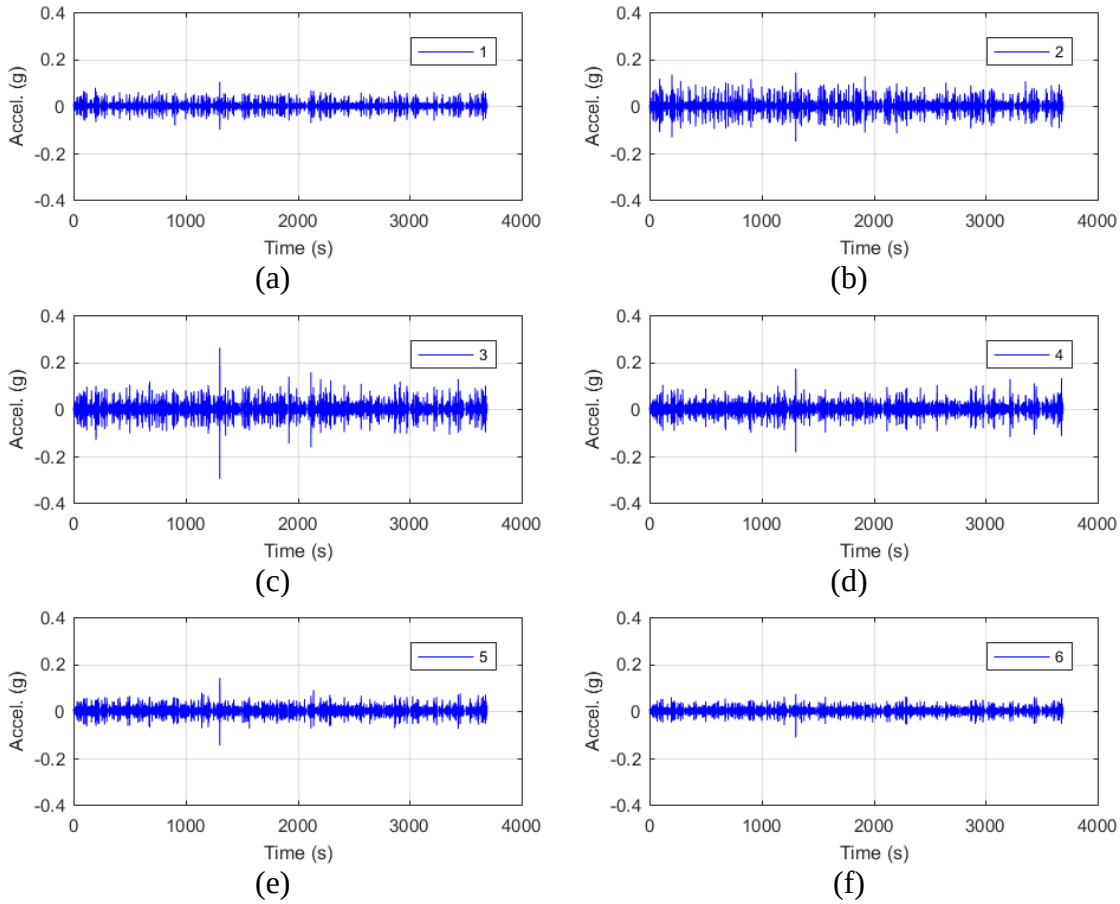

Figure C.54: Raw acceleration data of the local response for bridge S080 40797R.

Table C.48: Filter parameters of the local response for bridge S080 40797R.

Filter Parameter	Value
Hampel Identifier Order	10
FIR Bandpass Filter Order	8192
FIR Bandpass Filter Lower Cutoff Frequency (Hz)	2
FIR Bandpass Filter Upper Cutoff Frequency (Hz)	7
Tukey Averaging Window (min)	1.5

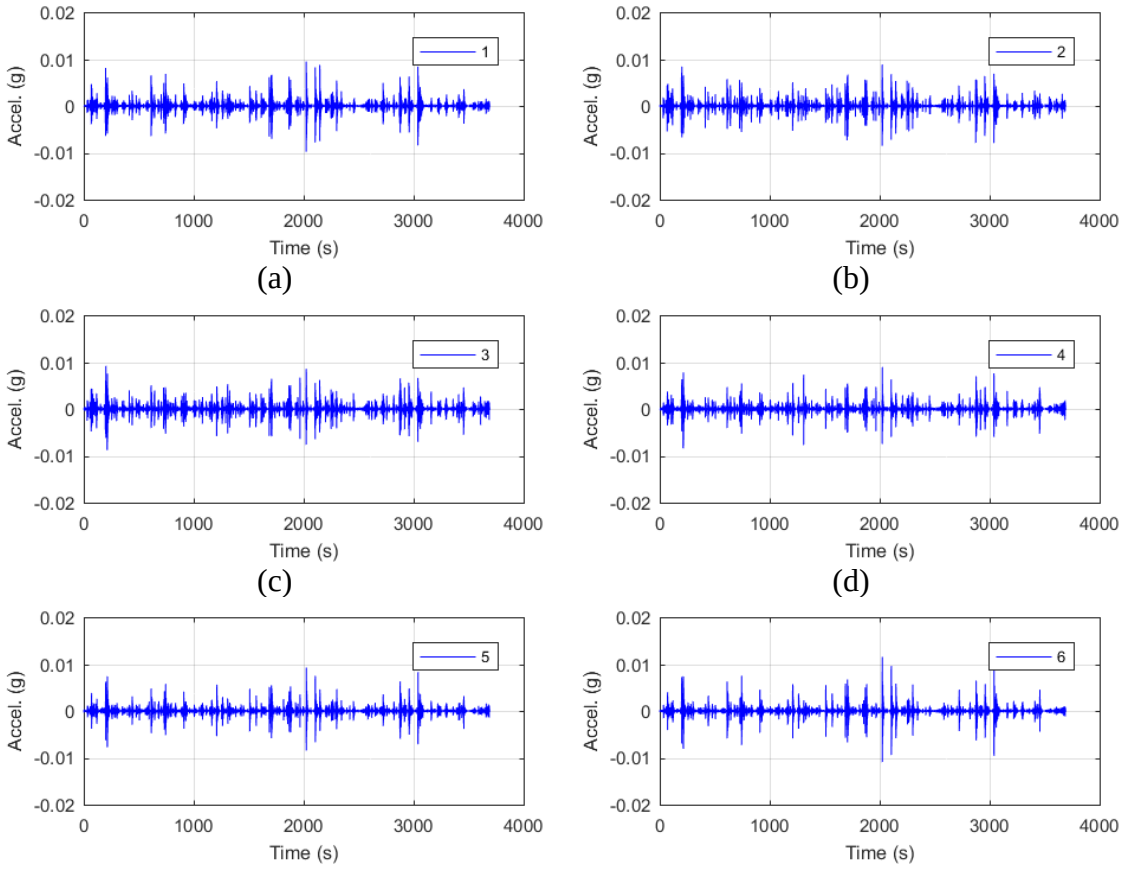

Figure C.55: Filtered acceleration data of the local response for bridge S080 40797R.

Table C.49: Filtered acceleration RMS values of the local response for bridge S080 40797R.

Sensor	**Filtered a_{RMS} (μg)**
1	631
2	619
3	624
4	591
5	596
6	680

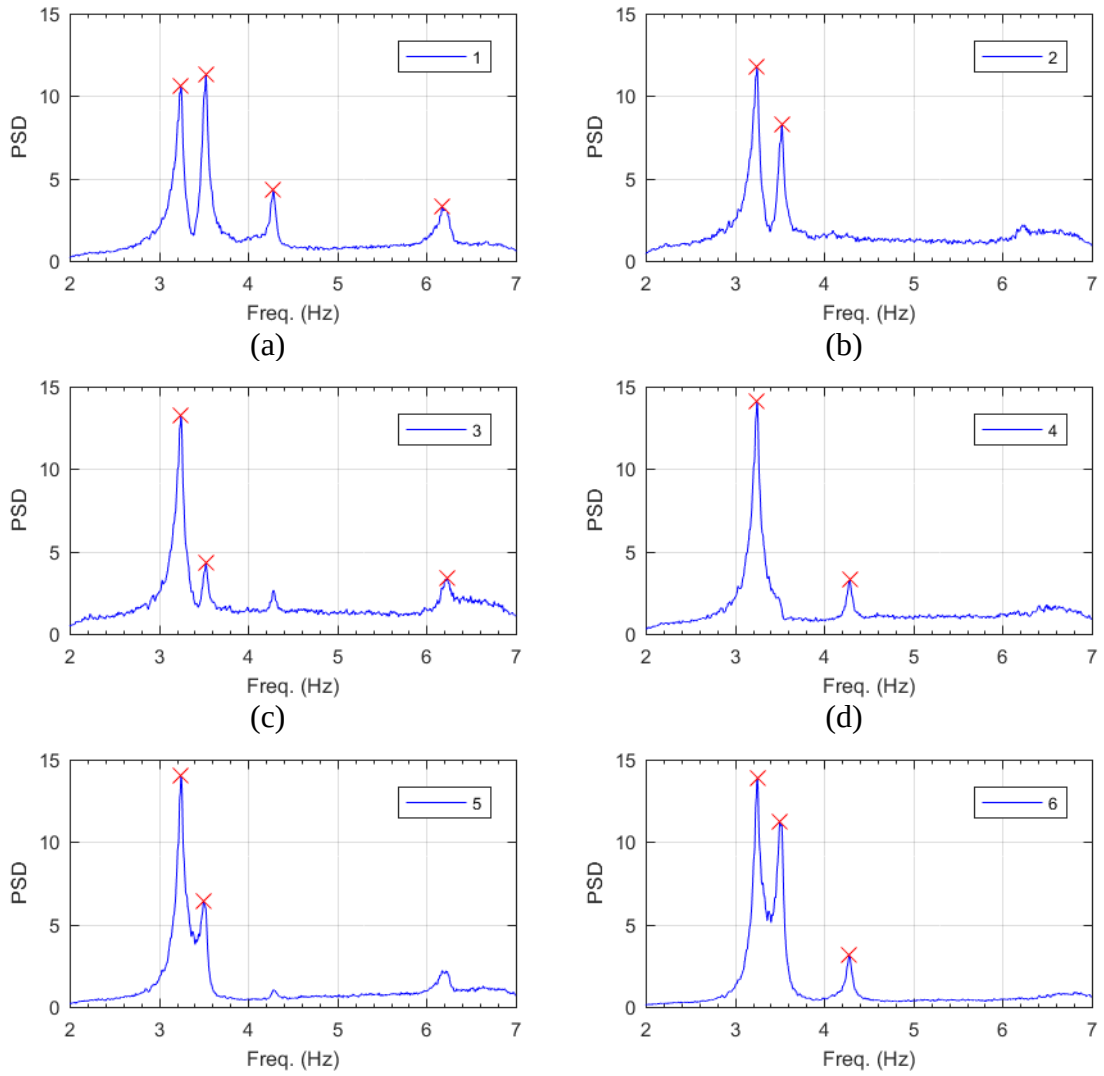

Figure C.56: Frequency content of the filtered acceleration data and peak-picking frequencies of the local response for bridge S080 40797R.

Table C.50: Peak-picking frequencies of the local response for bridge S080 40797R.

Mode	**Individual Sensor Frequencies (Hz)**					
	1	**2**	**3**	**4**	**5**	**6**
1	3.25	3.25	3.25	3.25	3.25	3.25
2	3.53	3.53	3.53	--	3.50	3.50
3	4.28	--	--	4.28	--	4.28
4	6.18	--	6.23	--	--	--

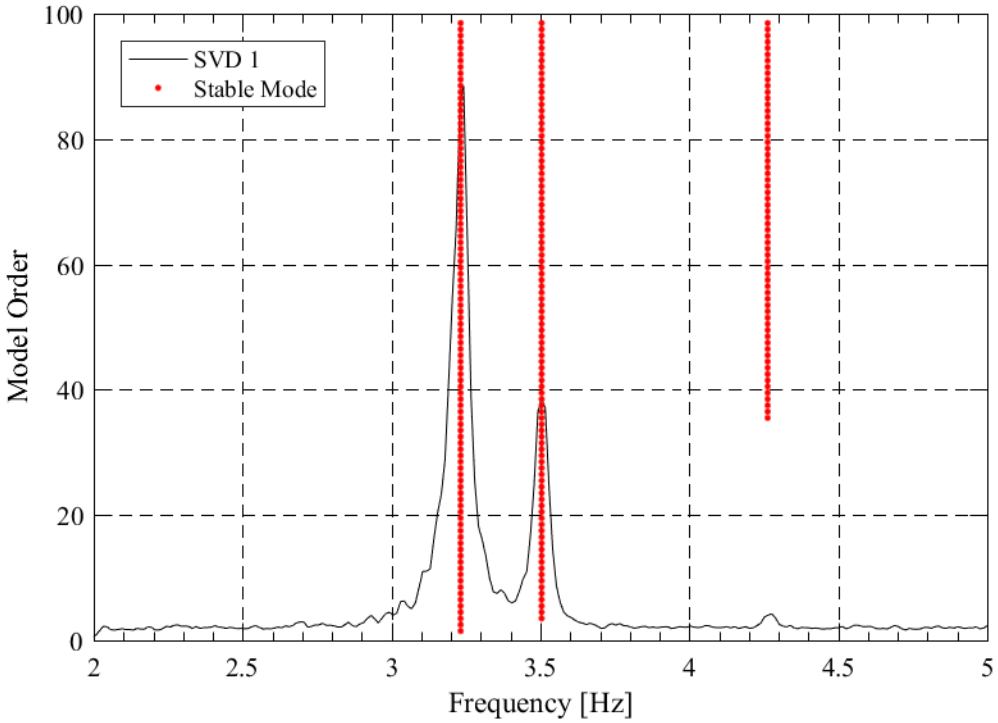

Figure C.57: SSI-UPCX method stabilization diagram of the local response for bridge S080 40797R.

Table C.51: SSI-UPCX method dynamic properties of the local response for bridge S080 40797R.

Mode	Frequency (Hz)	Damping (%)	Complexity (%)
1	3.23	1.33	0.29
2	3.50	0.89	1.30
3	4.26	1.73	7.85

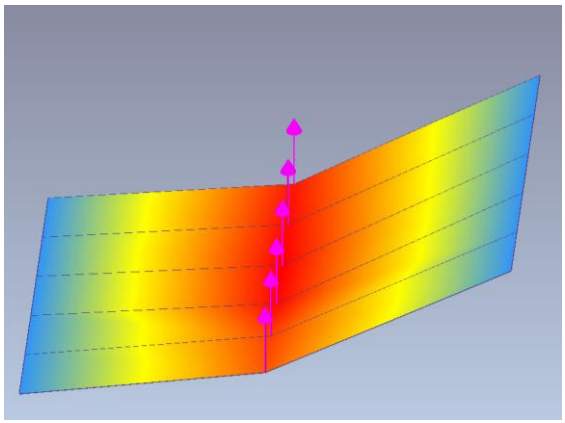

(a) Mode 1

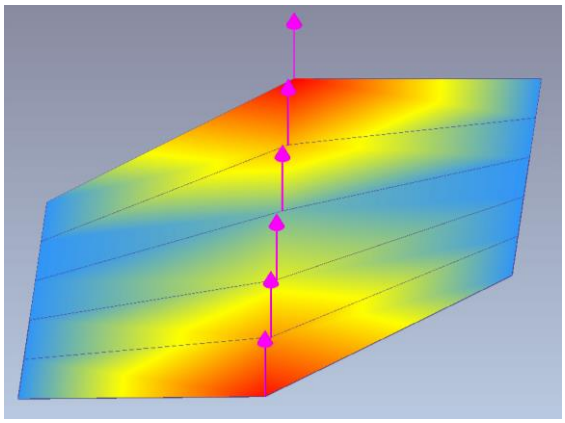

(b) Mode 2

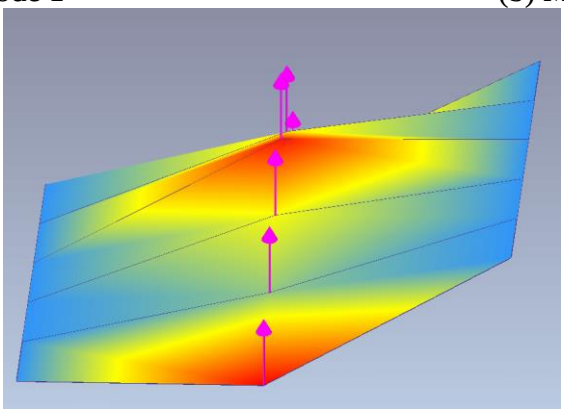

(c) Mode 3

Figure C.58: Operational deflected shapes of the local response for bridge S080 40797R.

Table C.52: Operational deflected shape coordinates of the local response for bridge S080 40797R.

Sensor	**ODS Coordinates**		
	Mode 1	**Mode 2**	**Mode 3**
1	0.80	-0.96	1.00
2	0.85	-0.64	0.19
3	0.98	-0.35	-0.39
4	1.00	0.13	-0.94
5	0.97	0.57	-0.46
6	0.94	1.00	0.83

Table C.53: MAC values of the local response for bridge S080 40797R.

MAC	**Mode 1**	**Mode 2**	**Mode 3**
Mode 1	1.000	0.124	0.091
Mode 2	0.124	1.000	0.411
Mode 3	0.091	0.411	1.000

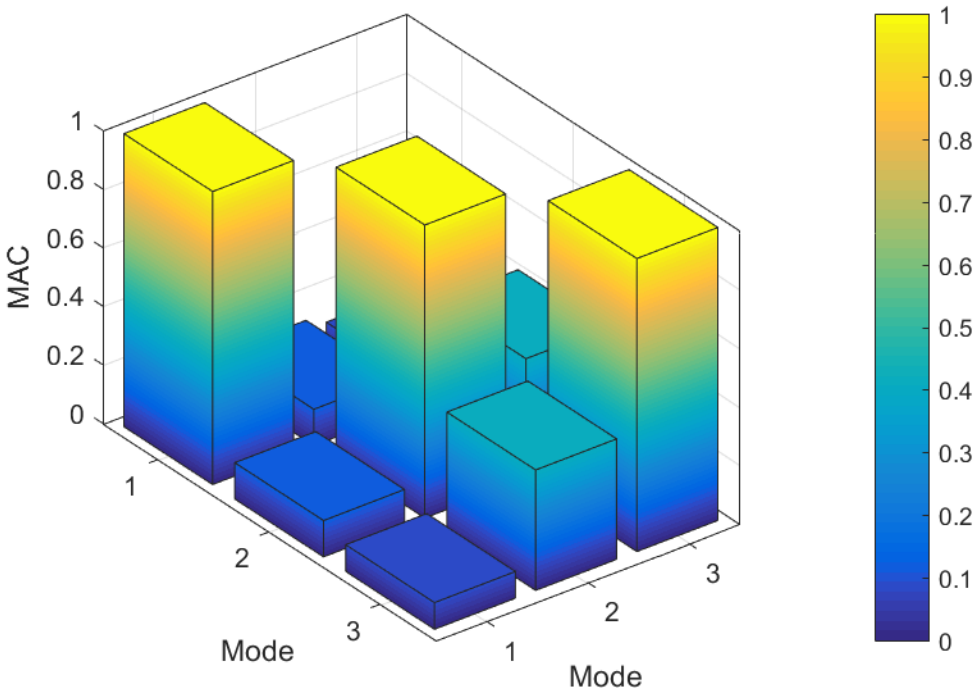

Figure C.59: MAC values of the local response for bridge S080 40797R.

IT Girder Bridge S080 40872R:

Figure C.60: Location of bridge S080 40872R (courtesy of Google Maps).

Table C.54: Bridge information summary for bridge S080 40872R.

Bridge ID	S080 40872R	**Girder Height (in [mm])**	15.75 [400]
County	Lancaster	**Girder Width (in [mm])**	23.63 [600]
Year Built	2010	**Girder Spacing (in [mm])**	29.75 [756]
No. of Spans	3	**Deck Thickness (in [mm])**	8 [203]
Length Span 1 (ft)	48.25	**No. of Girders**	25
Length Span 2 (ft)	53.50	**Diaphragm**	C8x18.75
Length Span 3 (ft)	48.25	**Deck Rating**	8
Bridge Width (ft)	62.80	**Superstructure Rating**	9
Skew Angle (°)	0	**Substructure Rating**	9

Figure C.61: Photo of bridge S080 40872R.

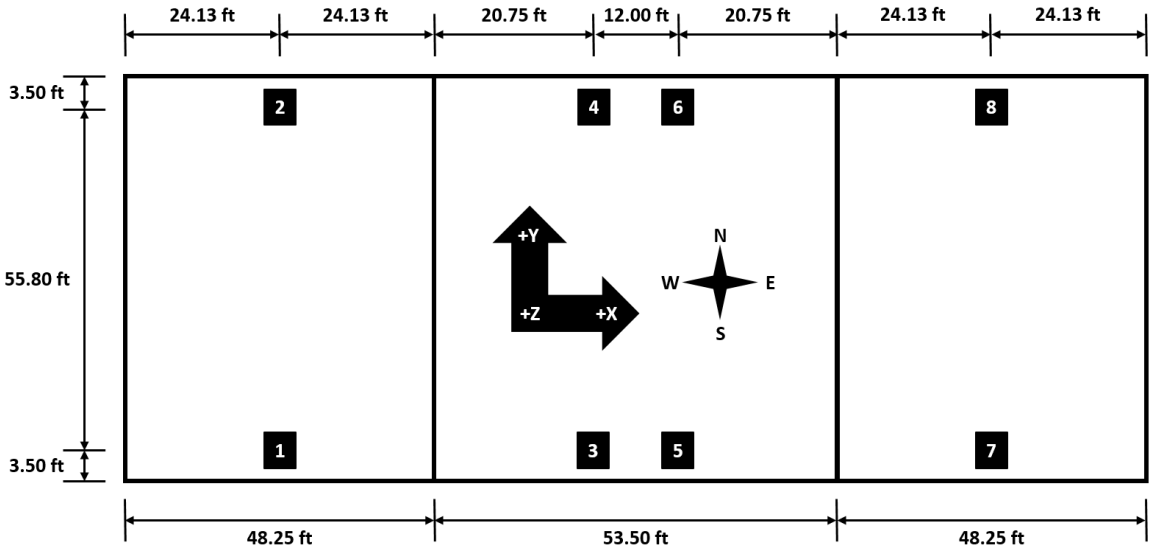

Figure C.62: Sensor locations capturing the global response for bridge S080 40872R.

Table C.55: Sensor information of the global response setup for bridge S080 40872R.

Sensor Location	Sensor Type	Sensor Id	Calibration Factor (mV/g)
1	WSN	848Z	--
2	WSN	997Z	--
3	WSN	968Z	--
4	WSN	99CZ	--
5	WSN	995Z	--
6	WSN	99DZ	--
7	WSN	996Z	--
8	WSN	99FZ	--

Date of Collection	10/17/2016
Length of Data (min)	74.53
Sampling Rate (Hz)	256

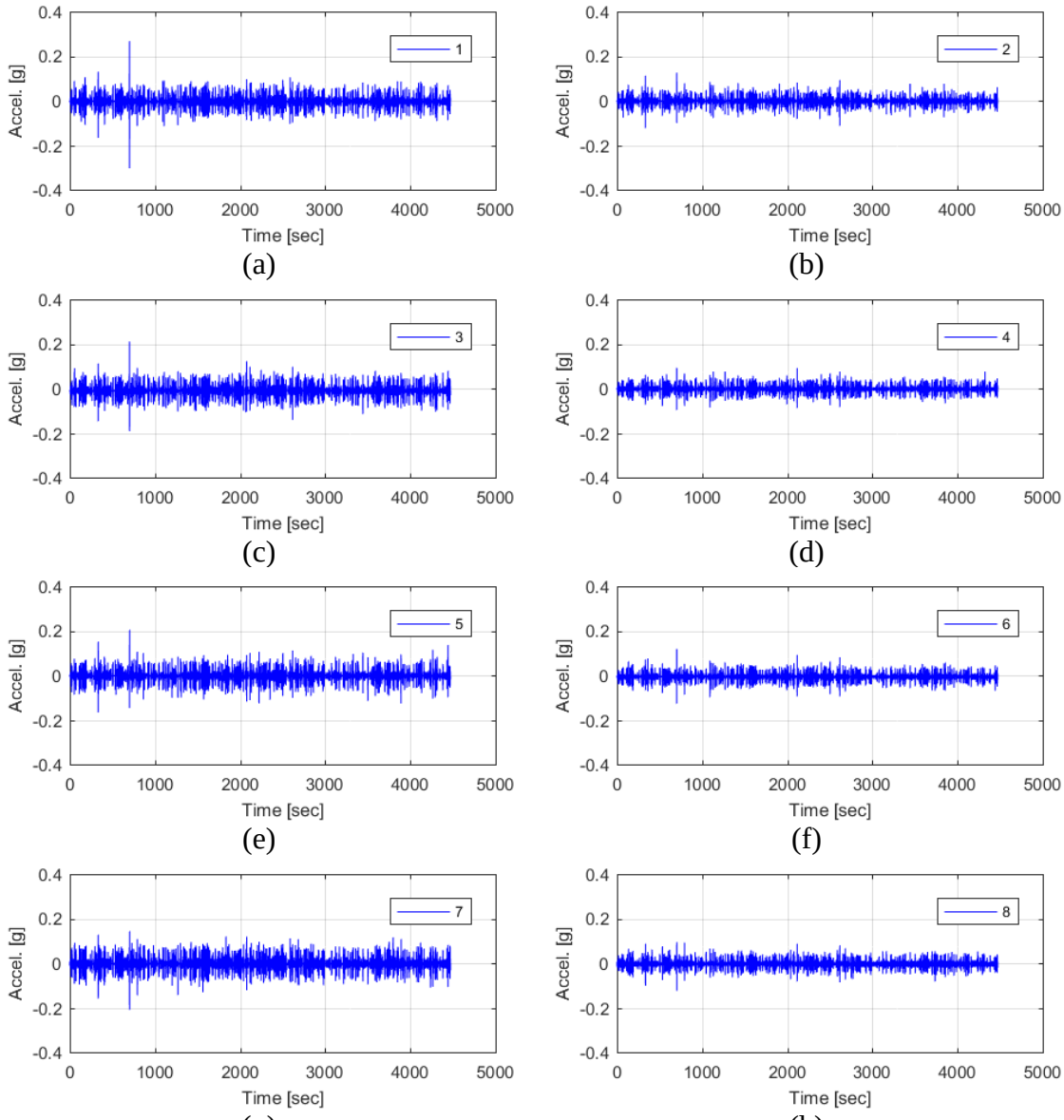

Figure C.63: Raw acceleration data of the global response for bridge S080 40872R.

Table C.56: Filter parameters of the global response for bridge S080 40872R.

Filter Parameter	Value
Hampel Identifier Order	10
FIR Bandpass Filter Order	3072
FIR Bandpass Filter Lower Cutoff Frequency (Hz)	7
FIR Bandpass Filter Upper Cutoff Frequency (Hz)	19
Tukey Averaging Window (min)	1.5

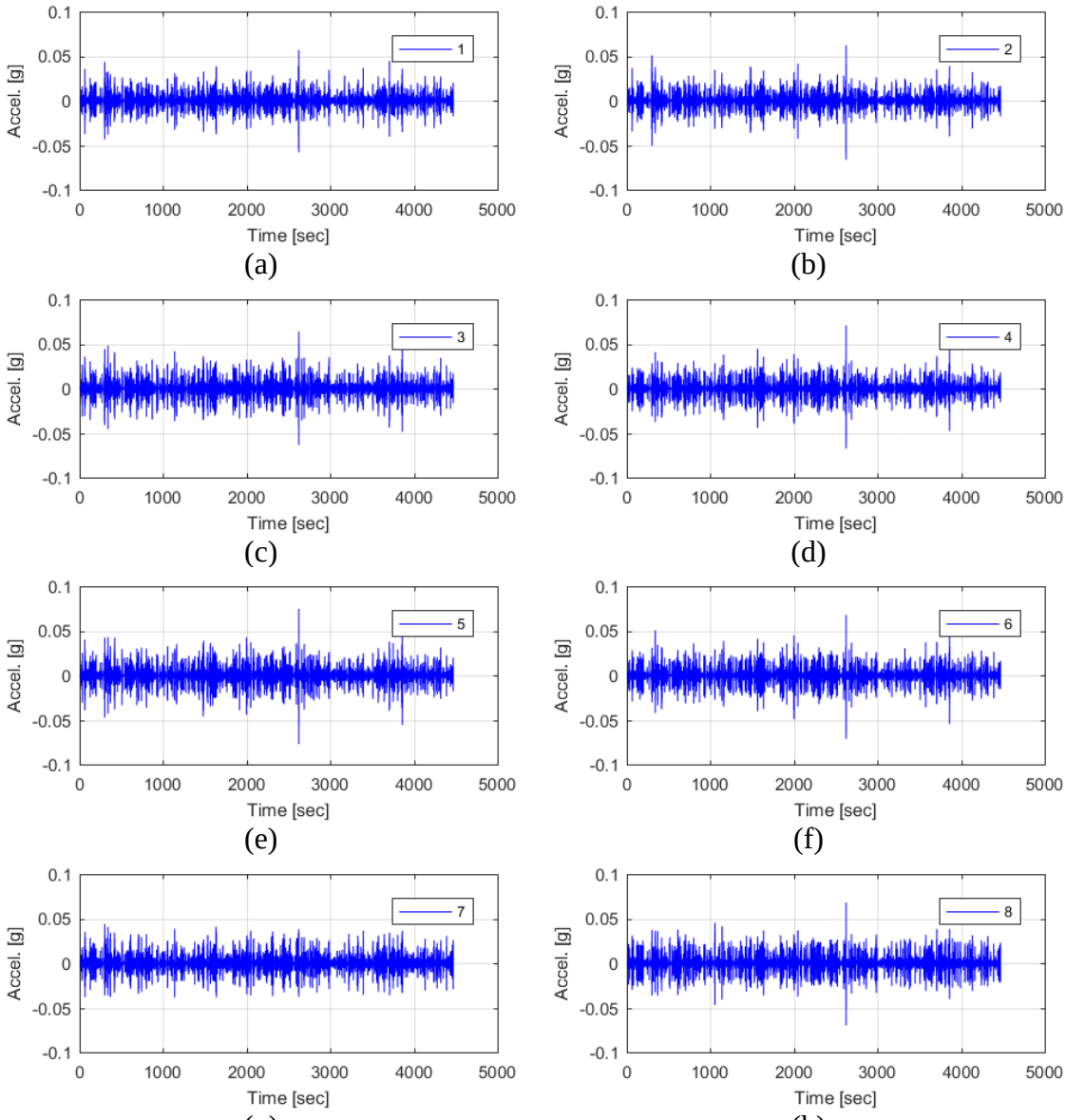

Figure C.64: Filtered acceleration data of the global response for bridge S080 40872R.

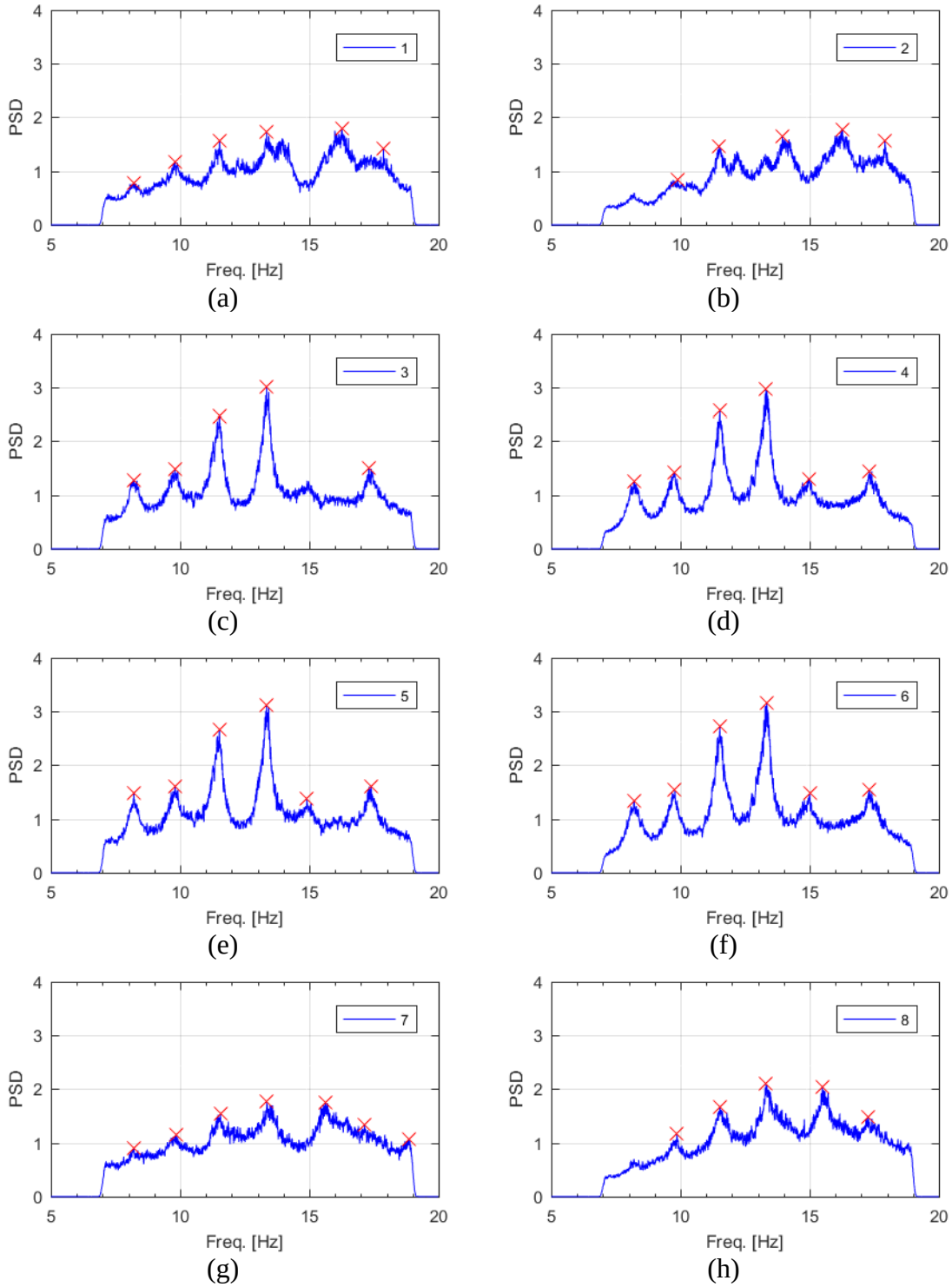

Figure C.65: Frequency content of the filtered acceleration data and peak-picking frequencies of the global response for bridge S080 40872R.

Table C.57: Filtered acceleration RMS values of the global response for bridge S080 40872R.

Sensor	Filtered a_{RMS} (µg)
1	2900
2	2822
3	3211
4	3081
5	3358
6	3291
7	3002
8	3192

Table C.58: Peak-picking frequencies of the global response for bridge S080 40872R.

Mode	Individual Sensor Frequencies (Hz)							
	1	**2**	**3**	**4**	**5**	**6**	**7**	**8**
1	8.20	--	8.21	8.21	8.21	8.21	8.20	--
2	9.80	9.89	9.79	9.77	9.81	9.78	9.86	9.87
3	11.52	--	11.52	11.52	11.52	11.52	11.56	11.53
4	13.35	--	13.35	13.32	13.35	13.35	13.36	13.32
5	--	13.95	--	--	--	--	--	--

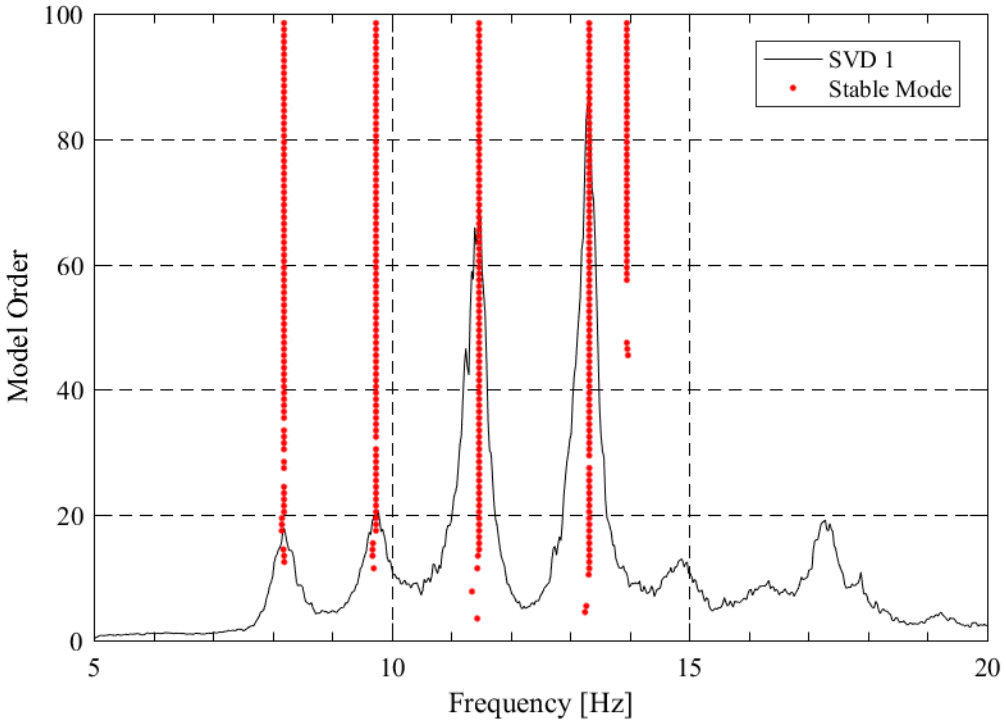

Figure C.66: SSI-UPCX method stabilization diagram of the global response for bridge S080 40872R.

Table C.59: SSI-UPCX method dynamic properties of the global response for bridge S080 40872R.

Mode	Frequency (Hz)	Damping (%)	Complexity (%)
1	8.18	2.90	20.90
2	9.73	3.07	13.00
3	11.47	2.00	12.99
4	13.31	1.63	16.72
5	13.95	2.80	40.17

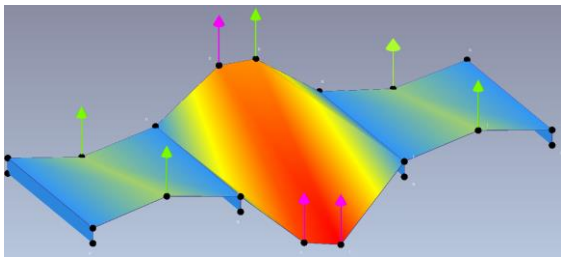

(a) Mode 1

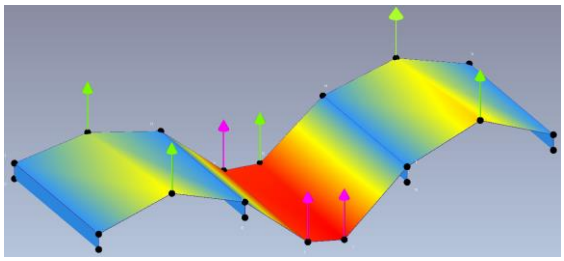

(b) Mode 2

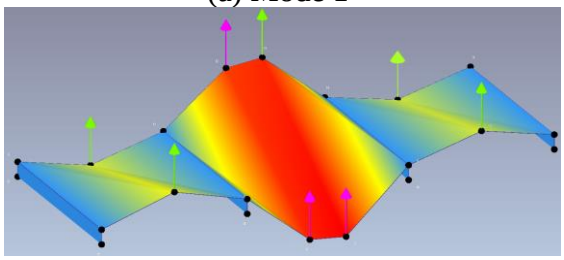

(c) Mode 3

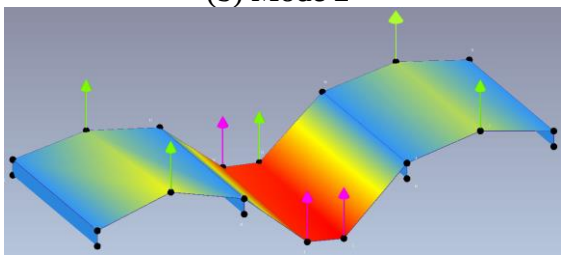

(d) Mode 4

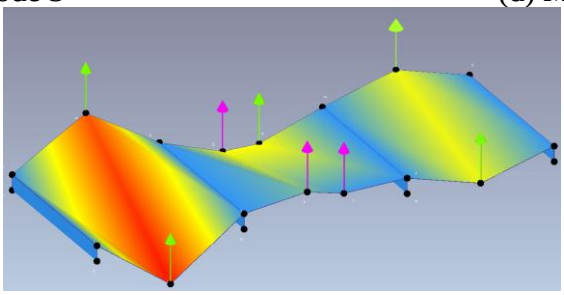

(e) Mode 5

Figure C.67: Operational deflected shapes of the global response for bridge S080 40872R.

Table C.60: Operational deflected shape coordinates of the global response for bridge S080 40872R.

Sensor	ODS Coordinates				
	Mode 1	Mode 2	Mode 3	Mode 4	Mode 5
1	-0.23	-0.42	-0.38	-0.37	1.00
2	0.21	-0.25	0.32	-0.21	-0.84
3	0.86	0.91	0.92	0.93	-0.15
4	-0.68	0.90	-0.86	0.87	0.42
5	1.00	1.00	1.00	1.00	0.03
6	-0.66	0.91	-0.91	0.92	0.42
7	-0.22	-0.51	-0.33	-0.26	0.39
8	0.19	-0.37	0.30	-0.23	-0.39

Table C.61: MAC values of the global response for bridge S080 40872R.

MAC	Mode 1	Mode 2	Mode 3	Mode 4	Mode 5
Mode 1	1.000	0.052	0.953	0.060	0.220
Mode 2	0.052	1.000	0.018	0.979	0.026
Mode 3	0.953	0.018	1.000	0.015	0.312
Mode 4	0.060	0.979	0.015	1.000	0.030
Mode 5	0.220	0.026	0.312	0.030	1.000

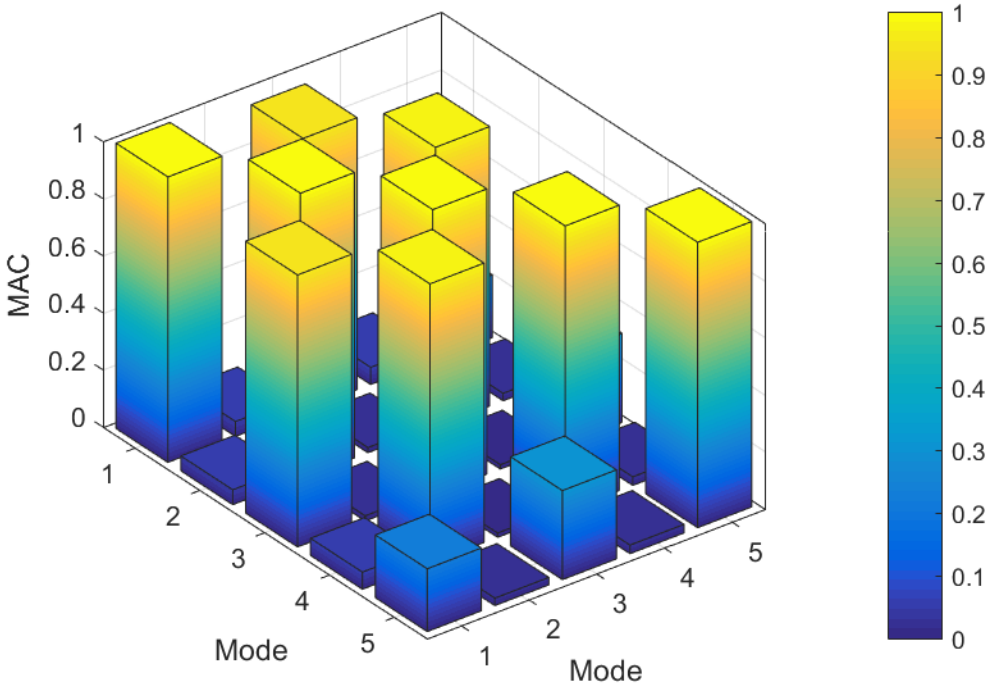

Figure C.68: MAC values of the global response for bridge S080 40872R.

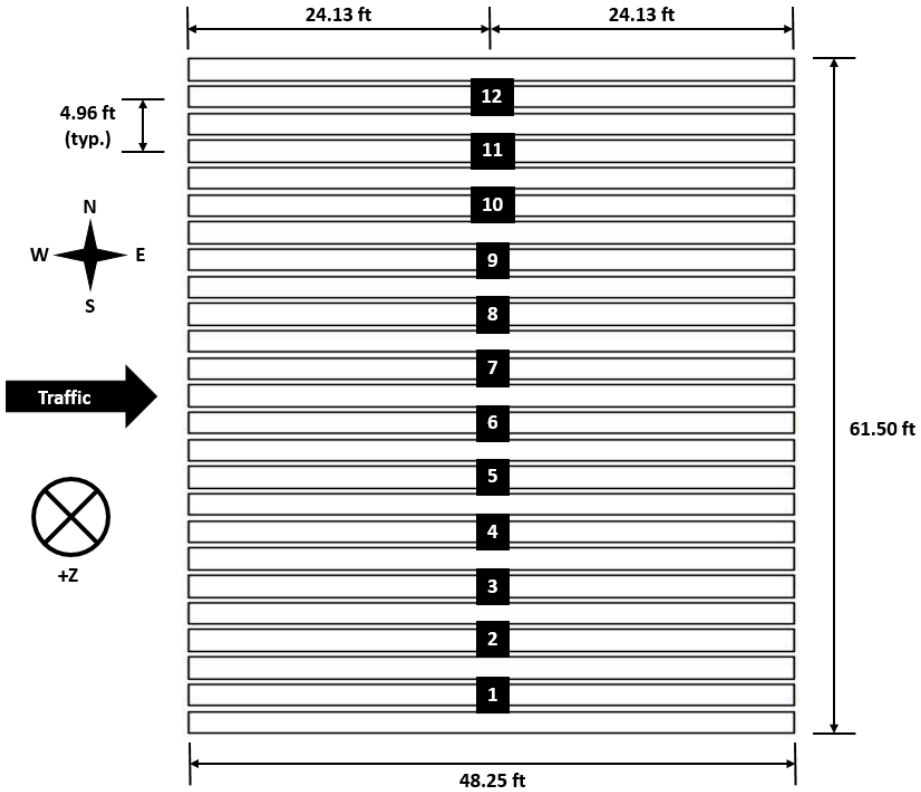

Figure C.69: Sensor locations capturing the local response for bridge S080 40872R.

Table C.62: Sensor information of the local response setup for bridge S080 40872R.

Sensor Location	Sensor Type	Sensor Id	Calibration Factor (mV/g)
1	PCB	N1	1001
2	PCB	N2	997
3	PCB	N3	1019
4	PCB	N4	1065
5	PCB	N9	1000
6	PCB	N10	977
7	PCB	N11	987
8	PCB	N12	1027
9	PCB	N5	1006
10	PCB	N6	993
11	PCB	N7	986
12	PCB	N8	998

Date of Collection	3/21/2017
Length of Data (min)	58.89
Sampling Rate (Hz)	2048

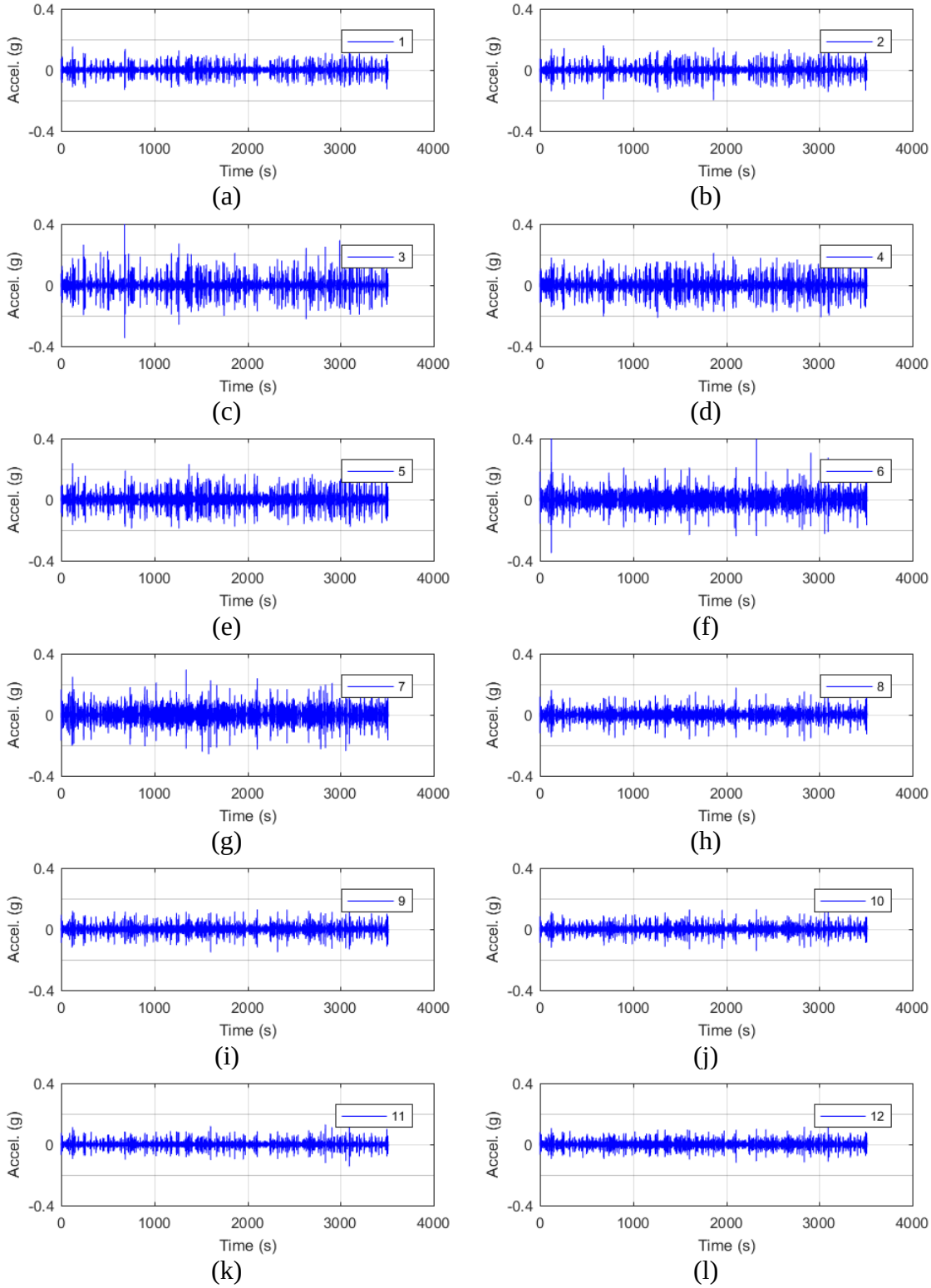

Figure C.70: Raw acceleration data of the local response for bridge S080 40872R.

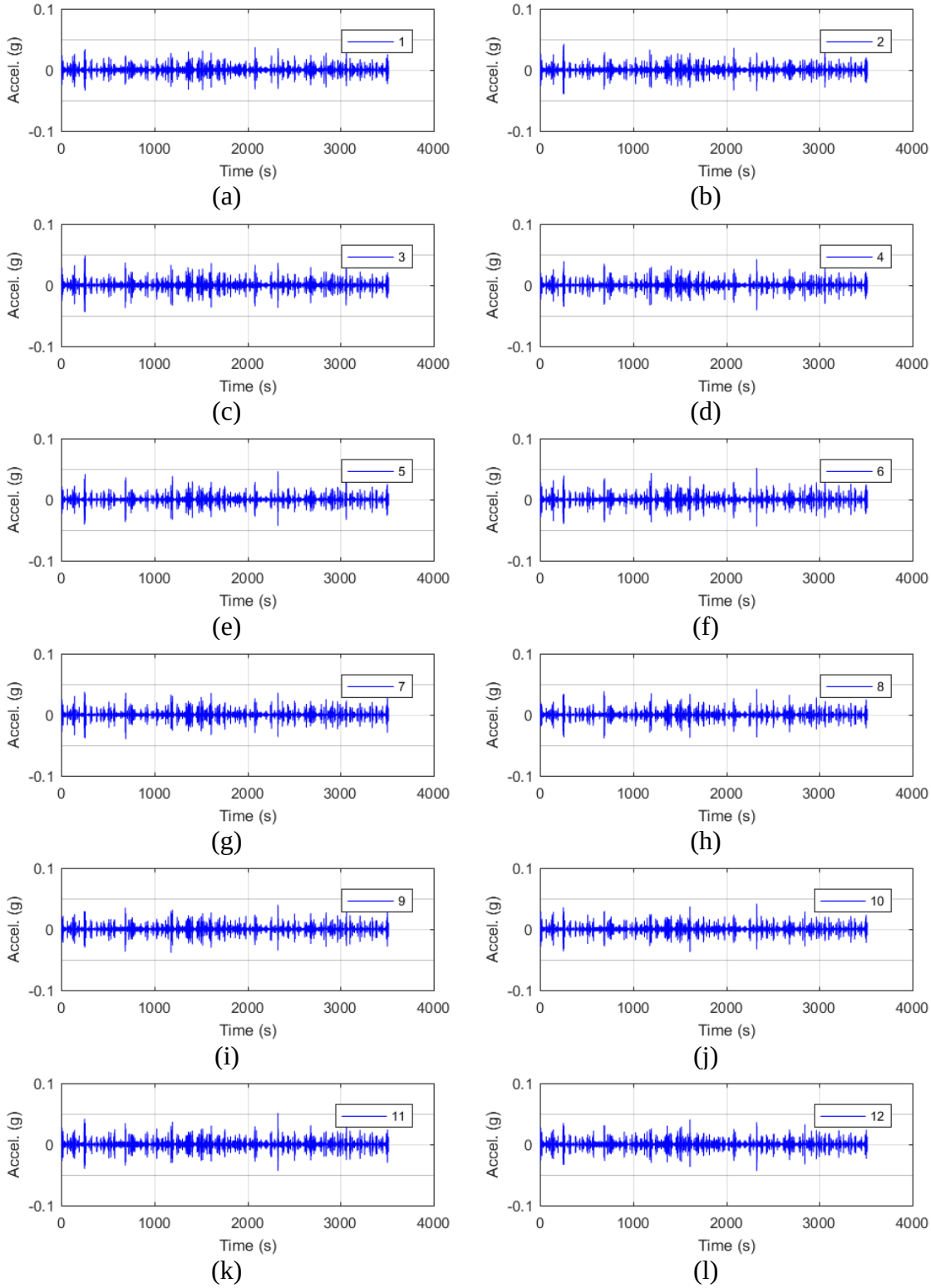

Figure C.71: Filtered acceleration data of the local response for bridge S080 40872R.

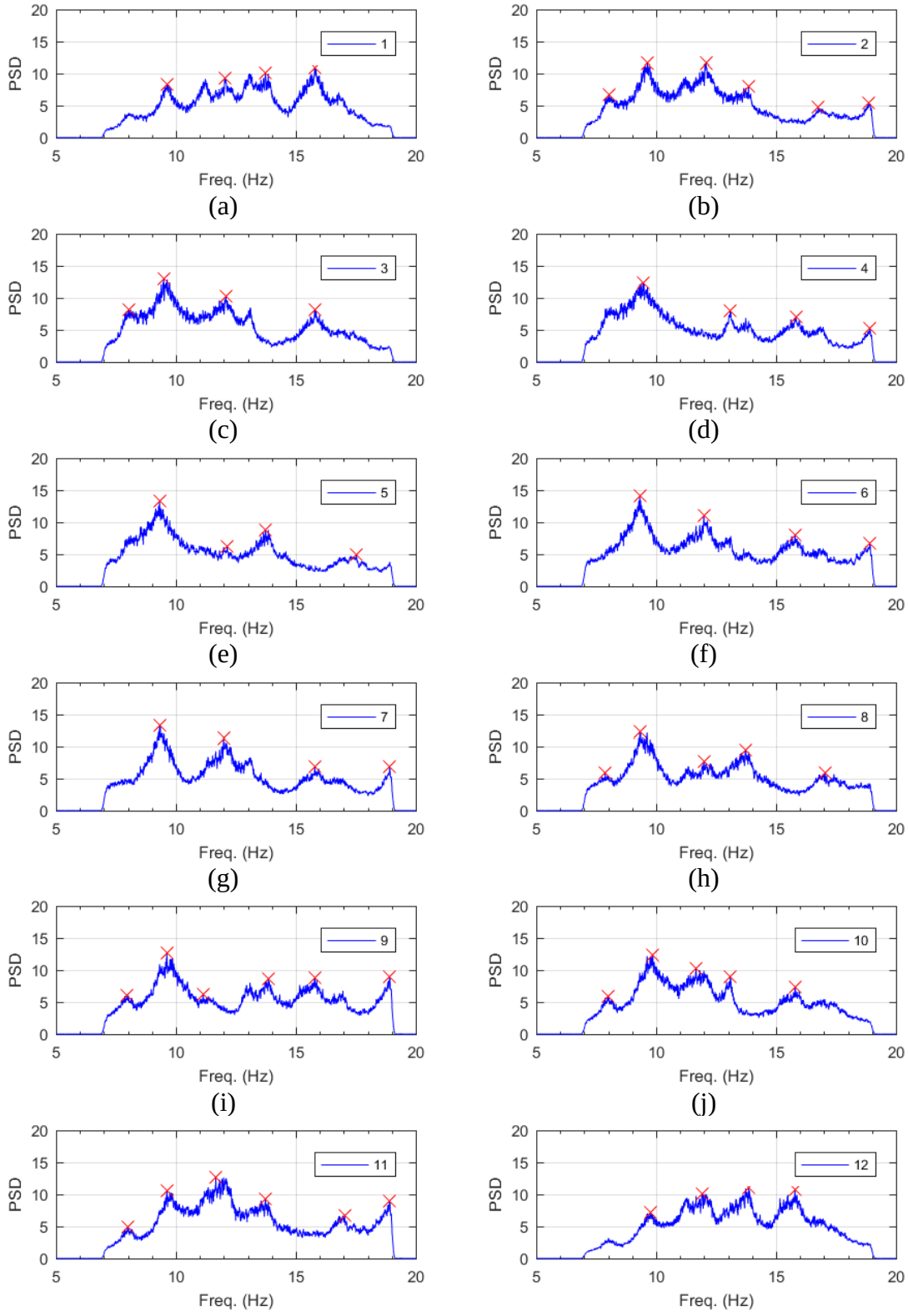

Figure C.72: Frequency content of the filtered acceleration data and peak-picking frequencies of the local response for bridge S080 40872R.

Table C.63: Filter parameters of the local response for bridge S080 40872R.

Filter Parameter	Value
Hampel Identifier Order	10
FIR Bandpass Filter Order	24576
FIR Bandpass Filter Lower Cutoff Frequency (Hz)	7
FIR Bandpass Filter Upper Cutoff Frequency (Hz)	19
Tukey Averaging Window (min)	1.5

Table C.64: Filtered acceleration RMS values of the local response for bridge S080 40872R.

Sensor	Filtered a_{RMS} (µg)
1	2140
2	2175
3	2324
4	2156
5	2129
6	2385
7	2198
8	2109
9	2201
10	2167
11	2399
12	2226

Table C.65: Peak-picking frequencies of the local response for bridge S080 40872R.

Mode	Individual Sensor Frequencies (Hz)					
	1	**2**	**3**	**4**	**5**	**6**
$\mathbf{1_{midspan}}$	--	8.05	8.05	--	--	--
1	--	--	9.49	9.46	9.32	9.32
2	9.64	9.64	--	--	--	--
3	12.05	12.08	12.08	--	12.14	11.99
4	13.73	13.85	--	13.09	13.74	--
5	15.78	--	15.78	15.82	--	15.79

Mode	Individual Sensor Frequencies (Hz)					
	7	**8**	**9**	**10**	**11**	**12**
$\mathbf{1_{midspan}}$	--	7.88	7.97	8.02	8.02	--
1	9.32	9.35	--	--	--	--
2	--	--	9.62	9.86	9.62	9.74
3	11.99	11.98	11.13	11.66	11.66	11.92
4	--	13.74	13.85	13.09	13.74	13.85
5	15.79	--	15.78	15.79	--	15.79

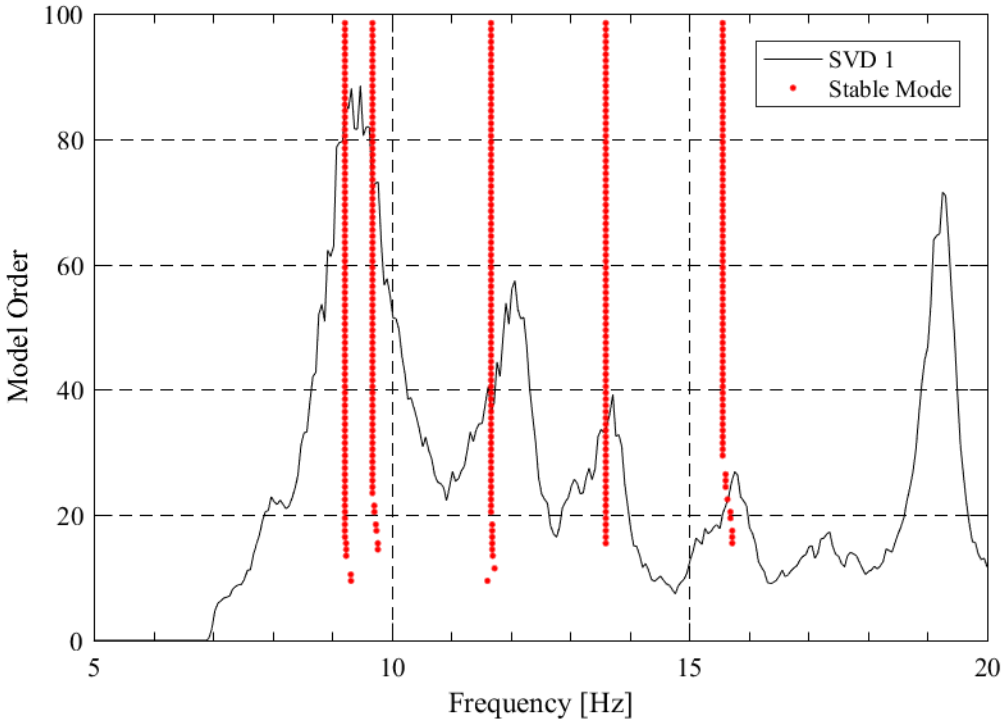

Figure C.73: SSI-UPCX method stabilization diagram of the local response for bridge S080 40872R.

Table C.66: SSI-UPCX method dynamic properties of the local response for bridge S080 40872R.

Mode	Frequency (Hz)	Damping (%)	Complexity (%)
1	9.22	5.70	33.07
2	9.69	7.19	5.79
3	11.67	5.53	3.08
4	13.60	7.63	12.20
5	15.57	7.43	28.45

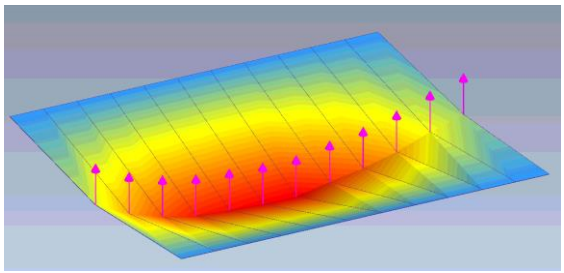

(a) Mode 1

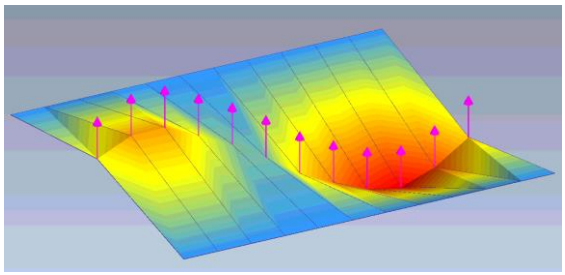

(b) Mode 2

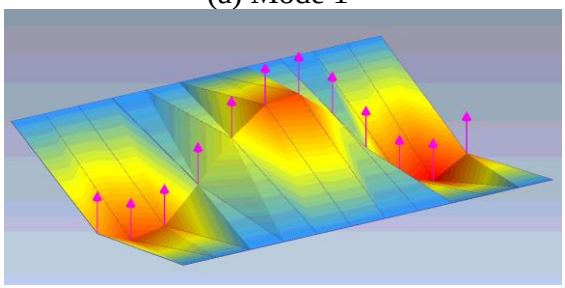

(c) Mode 3

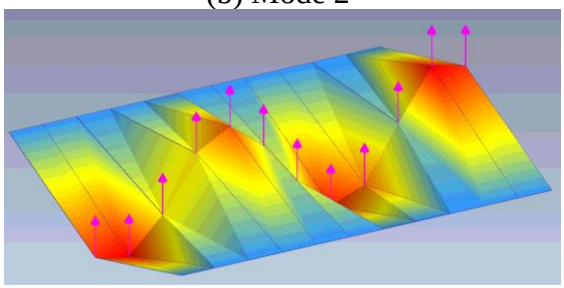

(d) Mode 4

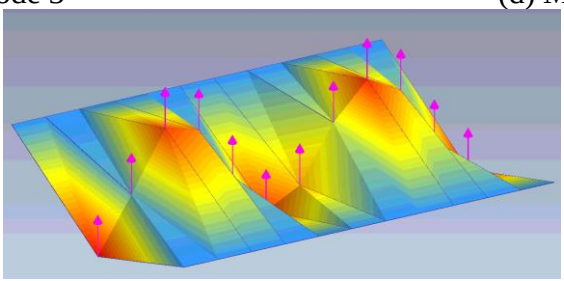

(e) Mode 5

Figure C.74: Operational deflected shapes of the local response for bridge S080 40872R.

Table C.67: Operational deflected shape coordinates of the local response for bridge S080 40872R.

Sensor	**ODS Coordinates**				
	Mode 1	**Mode 2**	**Mode 3**	**Mode 4**	**Mode 5**
1	0.31	-0.40	0.62	0.90	1.00
2	0.61	-0.62	0.84	1.00	0.10
3	0.80	-0.62	0.74	0.44	-0.86
4	0.93	-0.40	0.22	-0.46	-0.71
5	0.96	-0.16	-0.37	-0.78	0.19
6	0.99	0.13	-0.76	-0.32	0.88
7	1.00	0.47	-0.82	0.38	0.59
8	0.87	0.71	-0.39	0.94	-0.32
9	0.76	0.91	0.26	0.72	-0.90
10	0.60	1.00	0.83	-0.18	-0.60
11	0.39	0.83	1.00	-1.00	0.37
12	0.21	0.51	0.70	-0.88	0.97

Table C.68: MAC values of the local response for bridge S080 40872R.

MAC	Mode 1	Mode 2	Mode 3	Mode 4	Mode 5
Mode 1	1.000	0.081	0.005	0.067	0.006
Mode 2	0.081	1.000	0.038	0.005	0.020
Mode 3	0.005	0.038	1.000	0.034	0.080
Mode 4	0.067	0.005	0.034	1.000	0.042
Mode 5	0.006	0.020	0.080	0.042	1.000

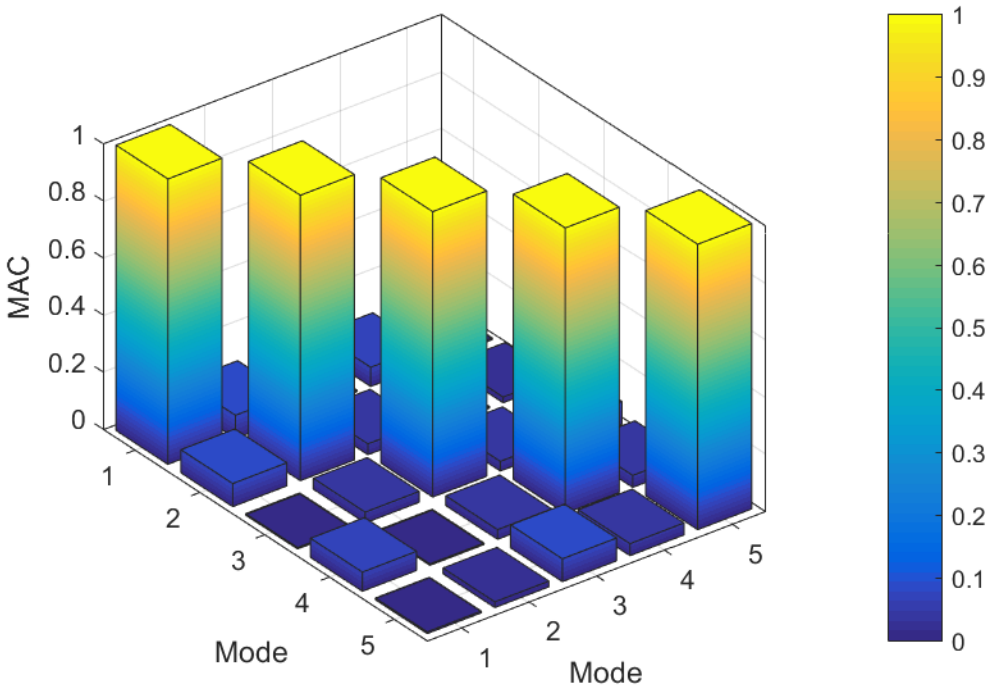

Figure C.75: MAC values of the local response for bridge S080 40872R.

IT Girder Bridge S080 40927R:

Figure C.76: Location of bridge S080 40927R (courtesy of Google Maps).

Table C.69: Bridge information summary for bridge S080 40927R.

Bridge ID	S080 40927R	**Girder Height (in [mm])**	15.75 [400]
County	Lancaster	**Girder Width (in [mm])**	23.63 [600]
Year Built	2010	**Girder Spacing (in [mm])**	29.75 [756]
No. of Spans	3	**Deck Thickness (in [mm])**	8 [203]
Length Span 1 (ft)	48.25	**No. of Girders**	25
Length Span 2 (ft)	53.50	**Diaphragm**	C8x18.75
Length Span 3 (ft)	48.25	**Deck Rating**	8
Bridge Width (ft)	62.80	**Superstructure Rating**	9
Skew Angle (°)	0	**Substructure Rating**	9

Figure C.77: Photo of bridge S080 40927R.

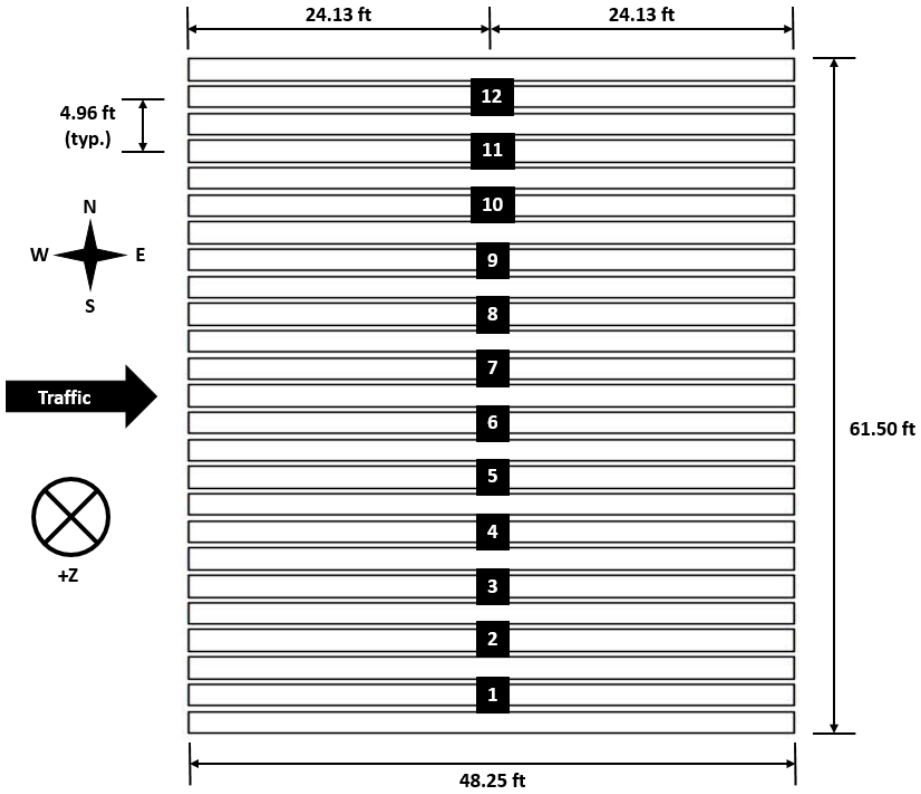

Figure C.78: Sensor locations capturing the local response for bridge S080 40927R.

Table C.70: Sensor information of the local response setup for bridge S080 40927R.

Sensor Location	Sensor Type	Sensor Id	Calibration Factor (mV/g)
1	PCB	N1	1001
2	PCB	N2	997
3	PCB	N3	1019
4	PCB	N4	1065
5	PCB	N9	1000
6	PCB	N10	977
7	PCB	N11	987
8	PCB	N12	1027
9	PCB	N5	1006
10	PCB	N6	993
11	PCB	N7	986
12	PCB	N8	998

Date of Collection	6/30/2017
Length of Data (min)	76.17
Sampling Rate (Hz)	2048

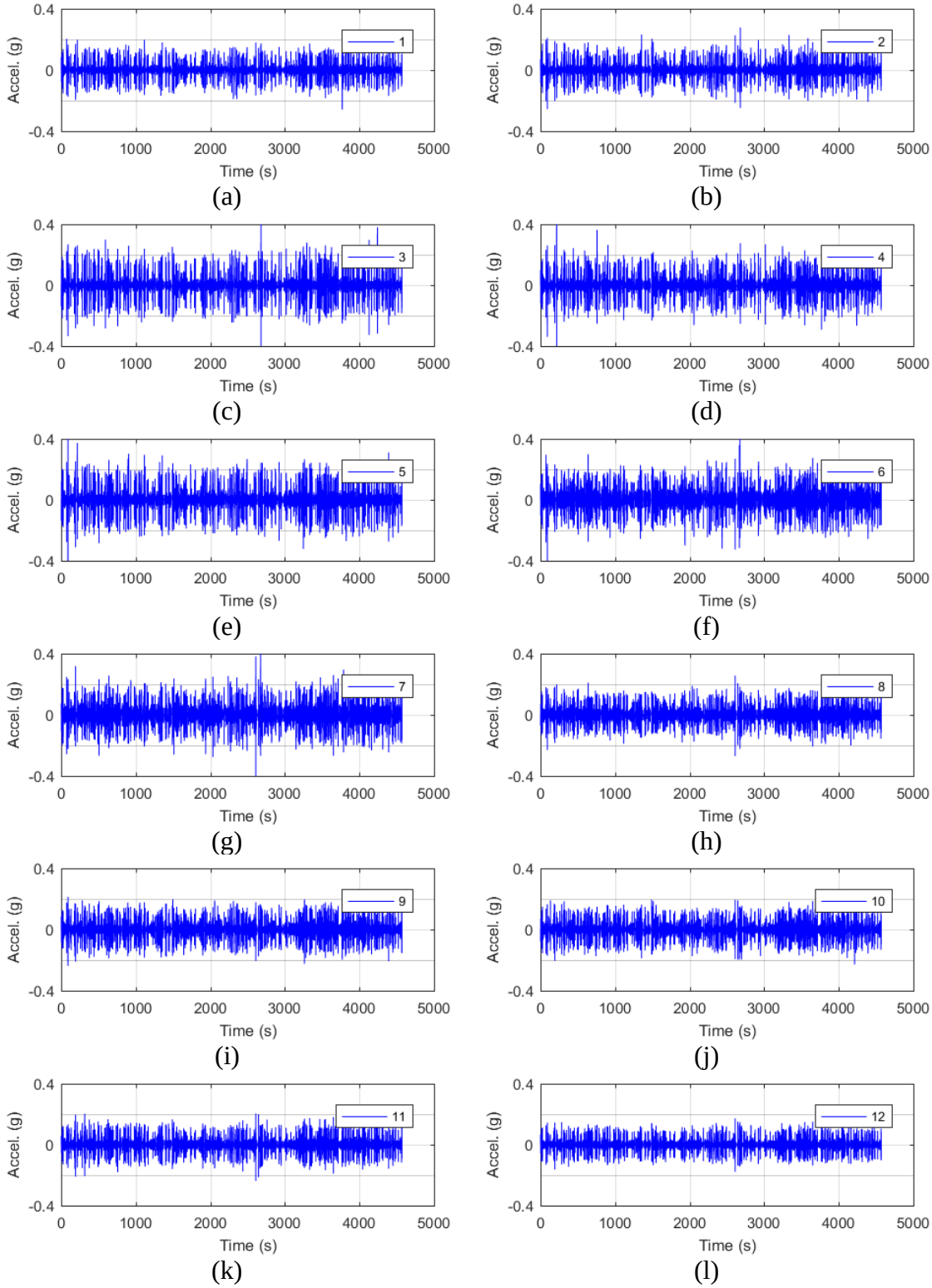

Figure C.79: Raw acceleration data of the local response for bridge S080 40927R.

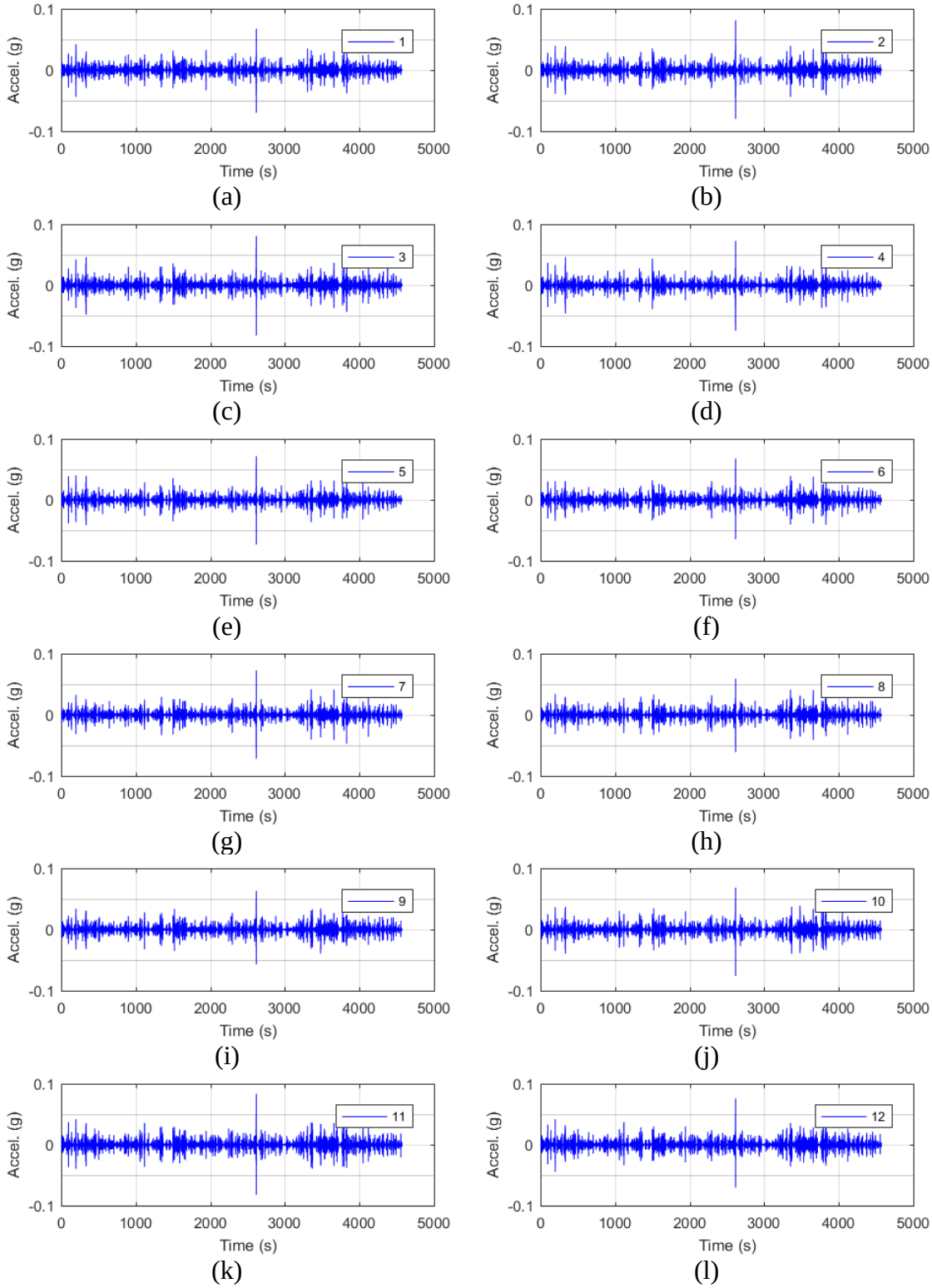

Figure C.80: Filtered acceleration data of the local response for bridge S080 40927R.

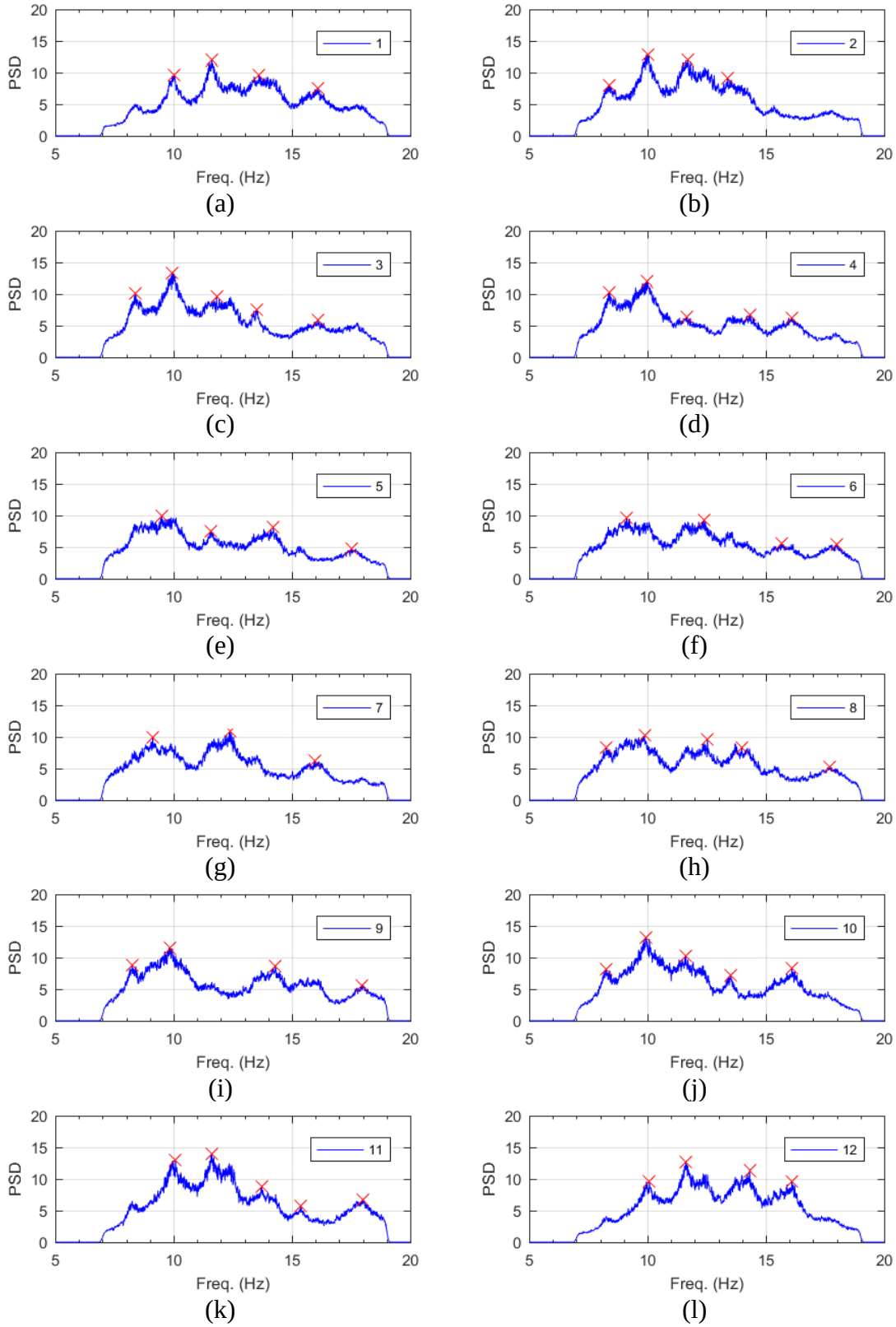

Figure C.81: Frequency content of the filtered acceleration data and peak-picking frequencies of the local response for bridge S080 40927R.

Table C.71: Filter parameters of the local response for bridge S080 40927R.

Filter Parameter	Value
Hampel Identifier Order	10
FIR Bandpass Filter Order	24576
FIR Bandpass Filter Lower Cutoff Frequency (Hz)	7
FIR Bandpass Filter Upper Cutoff Frequency (Hz)	19
Tukey Averaging Window (min)	1.5

Table C.72: Filtered acceleration RMS values of the local response for bridge S080 40927R.

Sensor	Filtered a_{RMS} (µg)
1	2266
2	2453
3	2392
4	2171
5	2078
6	2203
7	2204
8	2272
9	2240
10	2414
11	2625
12	2460

Table C.73: Peak-picking frequencies of the local response for bridge S080 40927R.

Mode	Individual Sensor Frequencies (Hz)					
	1	**2**	**3**	**4**	**5**	**6**
$\mathbf{1_{midspan}}$	--	8.36	8.41	8.40	--	--
1	--	--	--	--	9.50	9.12
2	10.03	10.03	9.96	9.96	--	--
3	11.62	11.70	11.82	11.67	11.58	12.41
4	13.61	13.40	13.52	14.35	14.22	--
5	16.08	--	16.08	16.08	--	15.67

Mode	Individual Sensor Frequencies (Hz)					
	7	**8**	**9**	**10**	**11**	**12**
$\mathbf{1_{midspan}}$	--	8.25	8.25	8.24	--	--
1	9.12	--	--	--	--	--
2	--	9.87	9.86	9.95	10.08	10.08
3	12.41	12.54	--	11.62	11.62	11.62
4	--	13.98	14.30	13.52	13.72	14.32
5	15.97	--	--	16.10	15.38	16.10

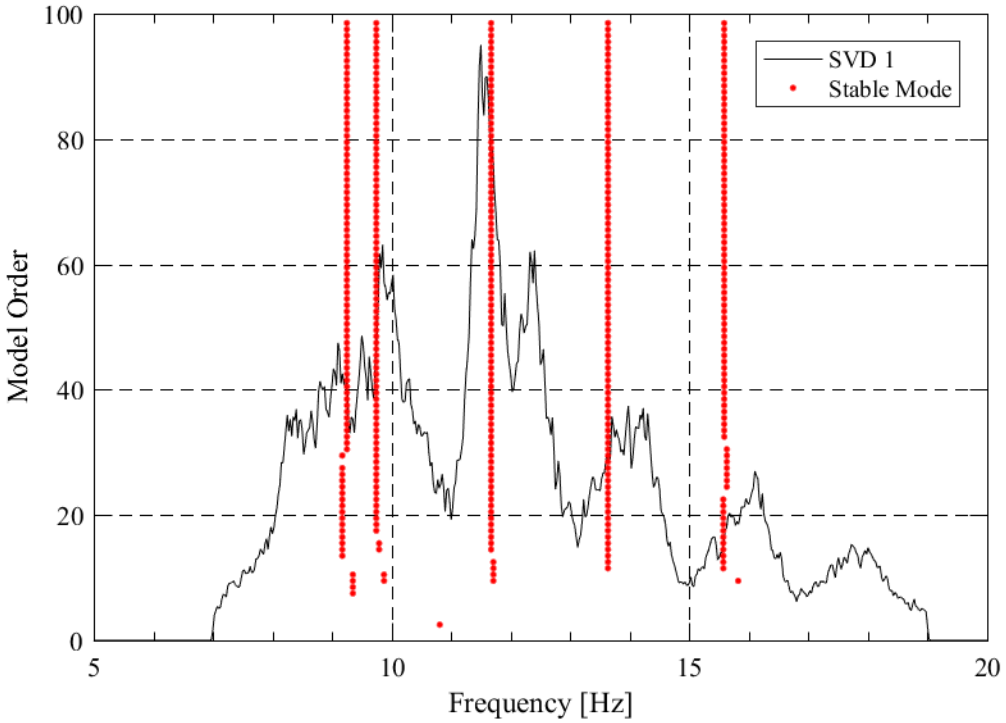

Figure C.82: SSI-UPCX method stabilization diagram of the local response for bridge S080 40927R.

Table C.74: SSI-UPCX method dynamic properties of the local response for bridge S080 40927R.

Mode	Frequency (Hz)	Damping (%)	Complexity (%)
1	9.25	6.55	21.51
2	9.74	5.38	5.55
3	11.67	5.60	6.24
4	13.63	6.99	22.74
5	15.59	4.93	12.79

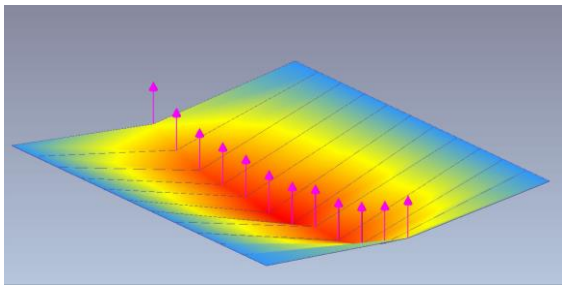

(a) Mode 1

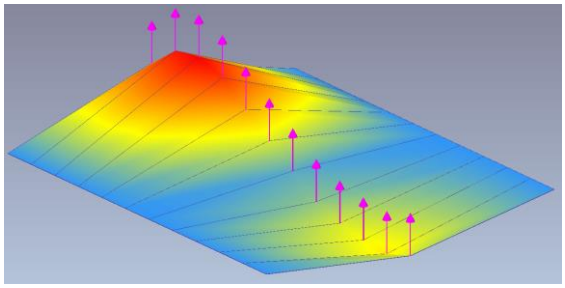

(b) Mode 2

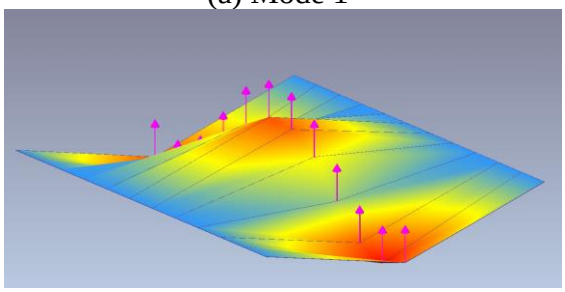

(c) Mode 3

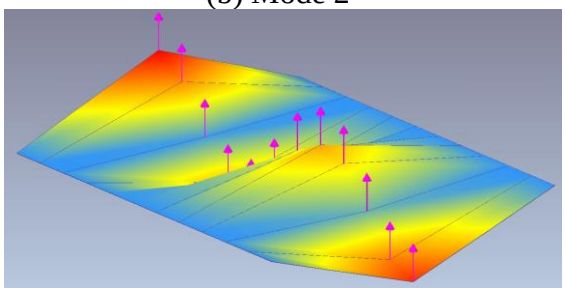

(d) Mode 4

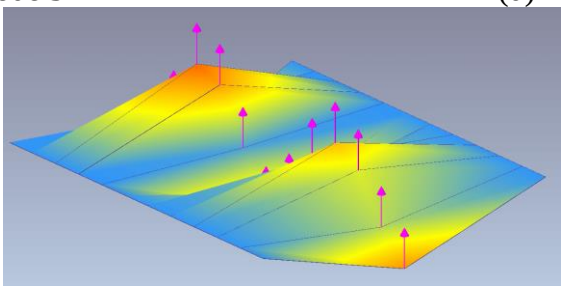

(e) Mode 5

Figure C.83: Operational deflected shapes of the local response for bridge S080 40927R.

Table C.75: Operational deflected shape coordinates of the local response for bridge S080 40927R.

Sensor	**ODS Coordinates**				
	Mode 1	**Mode 2**	**Mode 3**	**Mode 4**	**Mode 5**
1	0.26	-0.31	0.79	-0.90	0.65
2	0.56	-0.44	0.98	-0.71	0.25
3	0.77	-0.40	0.79	-0.12	-0.34
4	0.90	-0.32	0.20	0.47	-0.55
5	0.85	-0.18	-0.43	0.60	-0.21
6	1.00	0.08	-0.75	0.37	0.37
7	0.99	0.33	-0.80	-0.19	0.67
8	0.90	0.60	-0.51	-0.66	0.05
9	0.88	0.87	0.13	-0.58	-0.62
10	0.82	1.00	0.75	-0.03	-0.75
11	0.65	0.94	1.00	0.66	-0.01
12	0.38	0.63	0.81	1.00	1.00

Table C.76: MAC values of the local response for bridge S080 40927R.

MAC	Mode 1	Mode 2	Mode 3	Mode 4	Mode 5
Mode 1	1.000	0.120	0.003	0.012	0.003
Mode 2	0.120	1.000	0.011	0.024	0.013
Mode 3	0.003	0.011	1.000	0.045	0.034
Mode 4	0.012	0.024	0.045	1.000	0.001
Mode 5	0.003	0.013	0.034	0.001	1.000

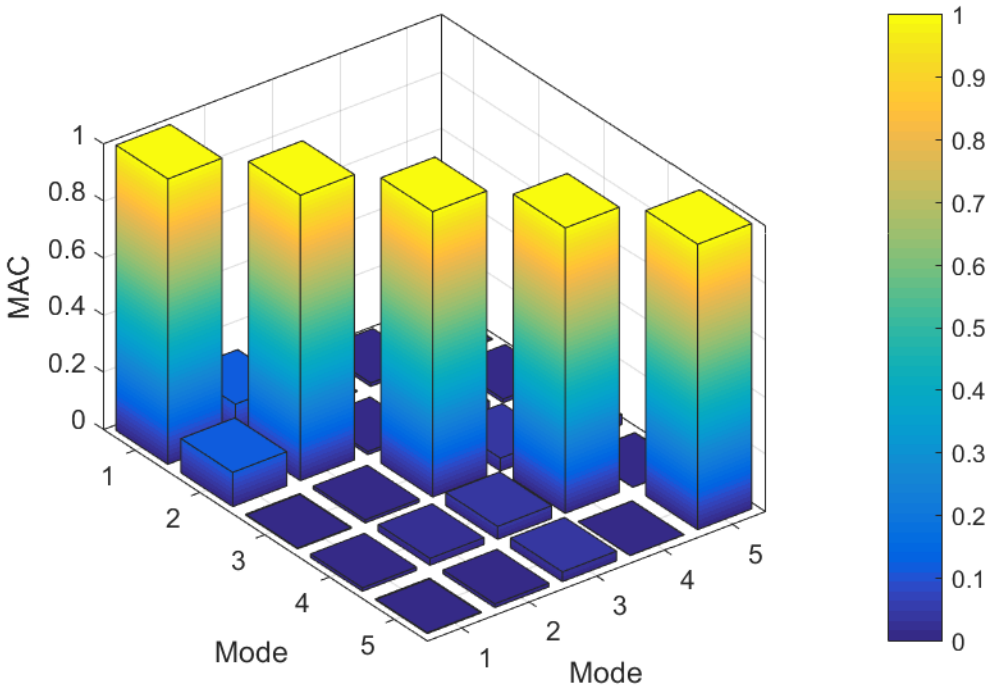

Figure C.84: MAC values of the local response for bridge S080 40927R.

IT Girder Bridge S081 05152L:

Figure C.85: Location of bridge S081 05152L (courtesy of Google Maps).

Table C.77: Bridge information summary for bridge S081 05152L.

Bridge ID	S081 05152L	**Girder Height (in [mm])**	15.75 [400]
County	York	**Girder Width (in [mm])**	23.63 [600]
Year Built	1999	**Girder Spacing (in [mm])**	25.98 [660]
No. of Spans	3	**Deck Thickness (in [mm])**	6 [152]
Length Span 1 (ft)	42.00	**No. of Girders**	19
Length Span 2 (ft)	56.00	**Diaphragm**	Concrete
Length Span 3 (ft)	42.00	**Deck Rating**	7
Bridge Width (ft)	40.70	**Superstructure Rating**	8
Skew Angle (°)	10	**Substructure Rating**	7

Figure C.86: Photo of bridge S081 05152L.

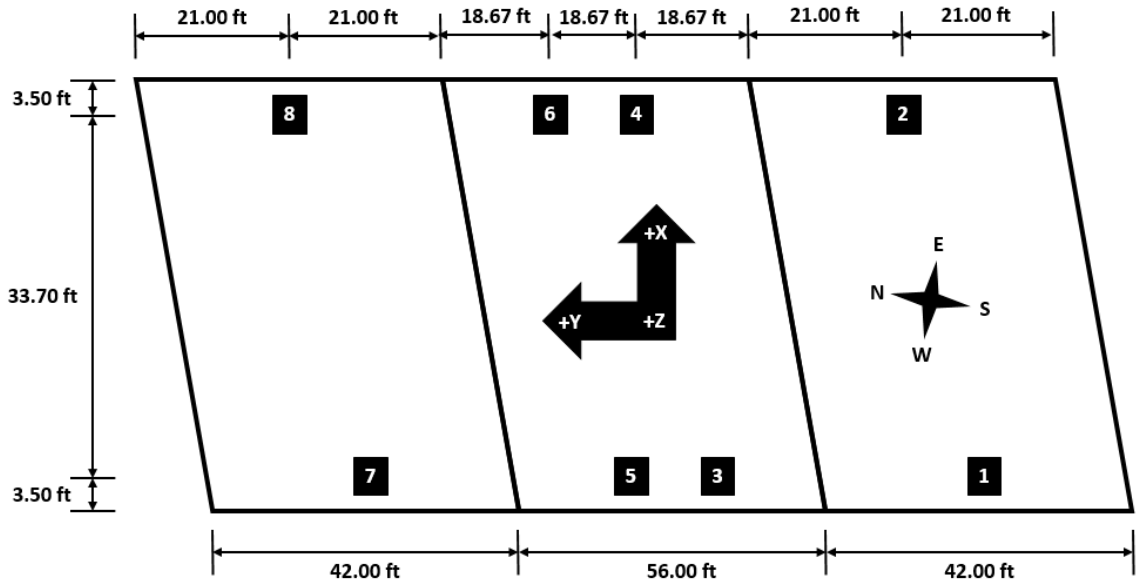

Figure C.87: Sensor locations capturing the global response for bridge S081 05152L.

Table C.78: Sensor information of the global response setup for bridge S081 05152L.

Sensor Location	Sensor Type	Sensor Id	Calibration Factor (mV/g)
1	WSN	996Z	--
2	WSN	99CZ	--
3	WSN	848Z	--
4	WSN	99FZ	--
5	WSN	968Z	--
6	WSN	99DZ	--
7	WSN	997Z	--
8	WSN	995Z	--

Date of Collection	9/30/2016
Length of Data (min)	46.59
Sampling Rate (Hz)	256

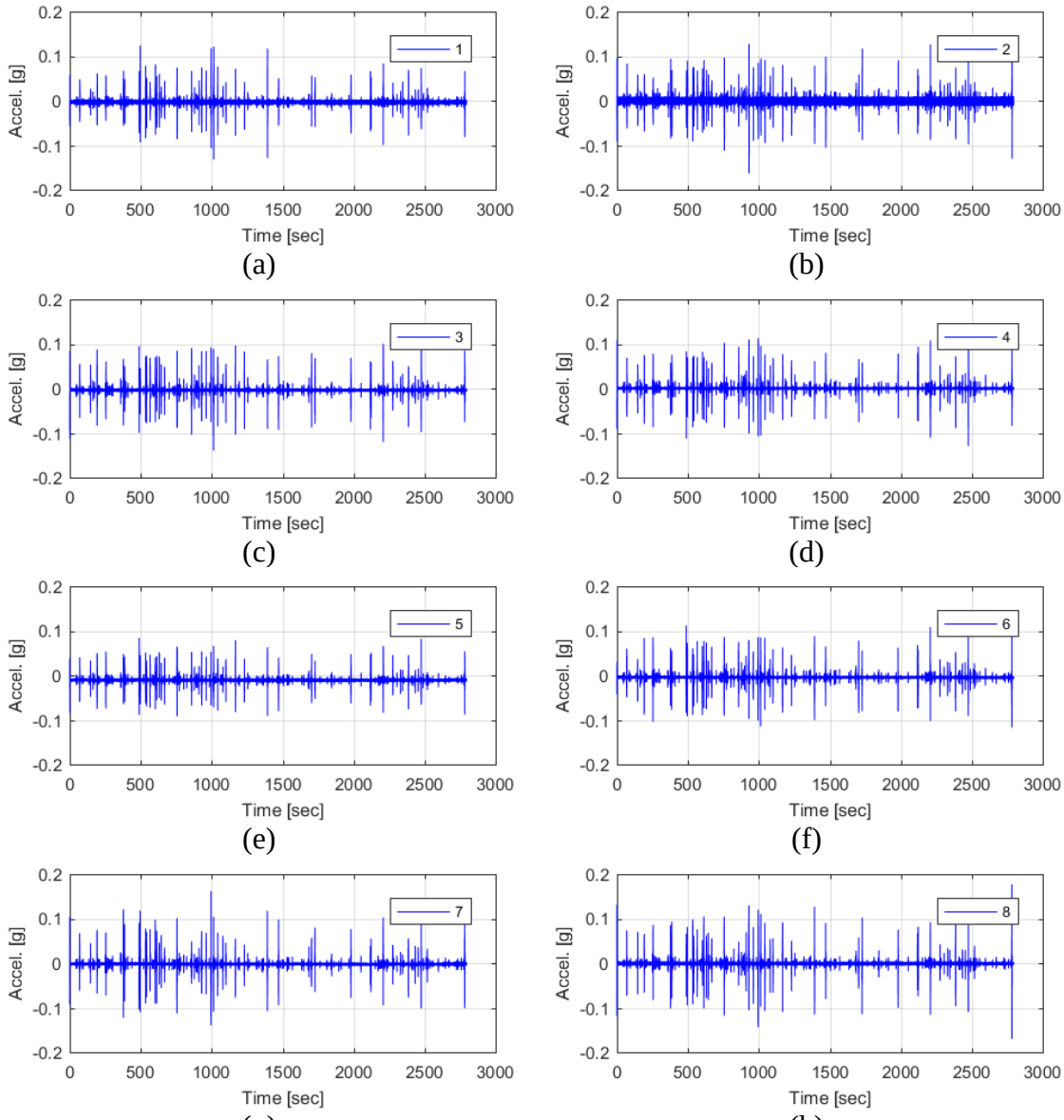

Figure C.88: Raw acceleration data of the global response for bridge S081 05152L.

Table C.79: Filter parameters of the global response for bridge S081 05152L.

Filter Parameter	Value
Hampel Identifier Order	--
FIR Bandpass Filter Order	2048
FIR Bandpass Filter Lower Cutoff Frequency (Hz)	5
FIR Bandpass Filter Upper Cutoff Frequency (Hz)	25
Tukey Averaging Window (min)	1.5

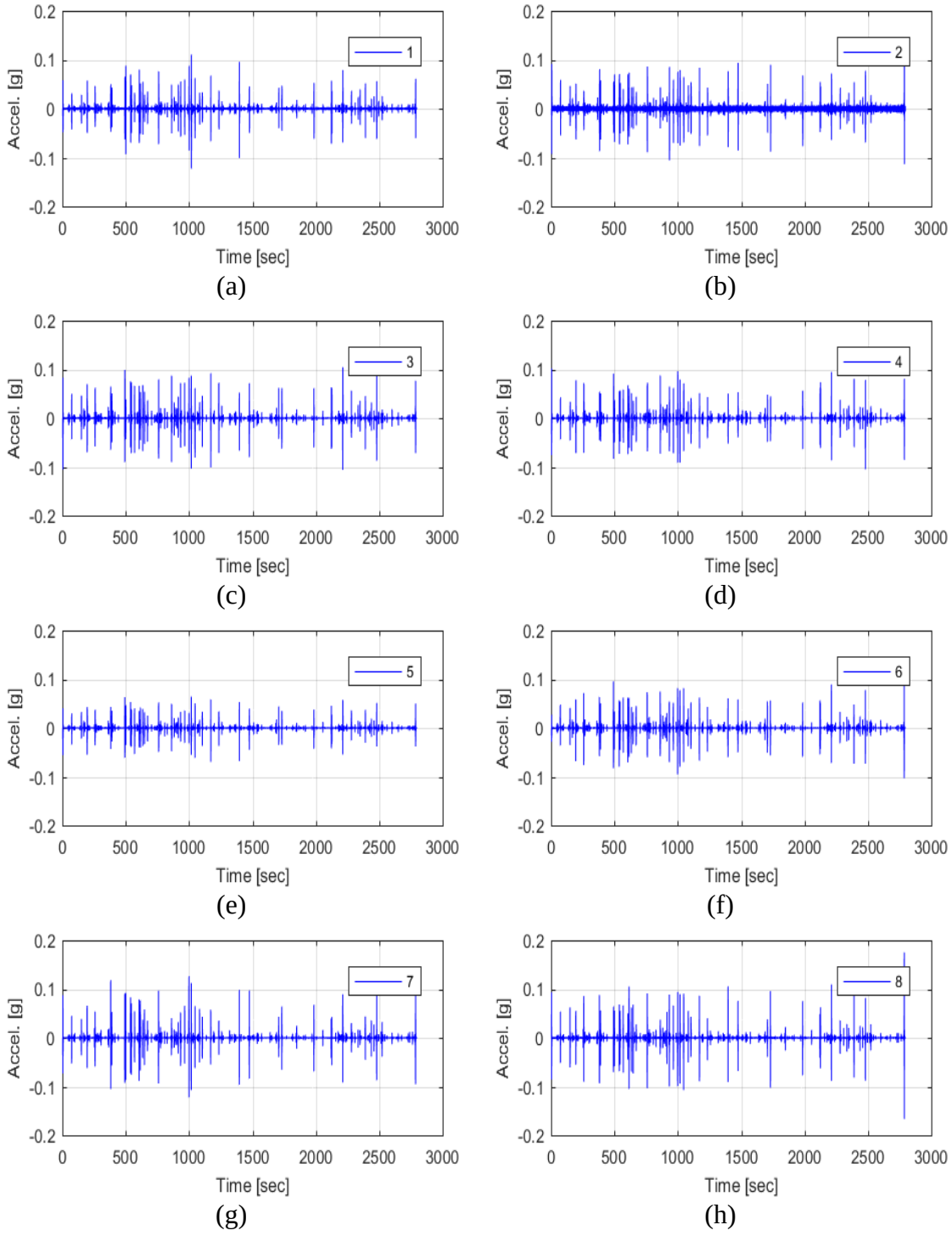

Figure C.89: Filtered acceleration data of the global response for bridge S081 05152L.

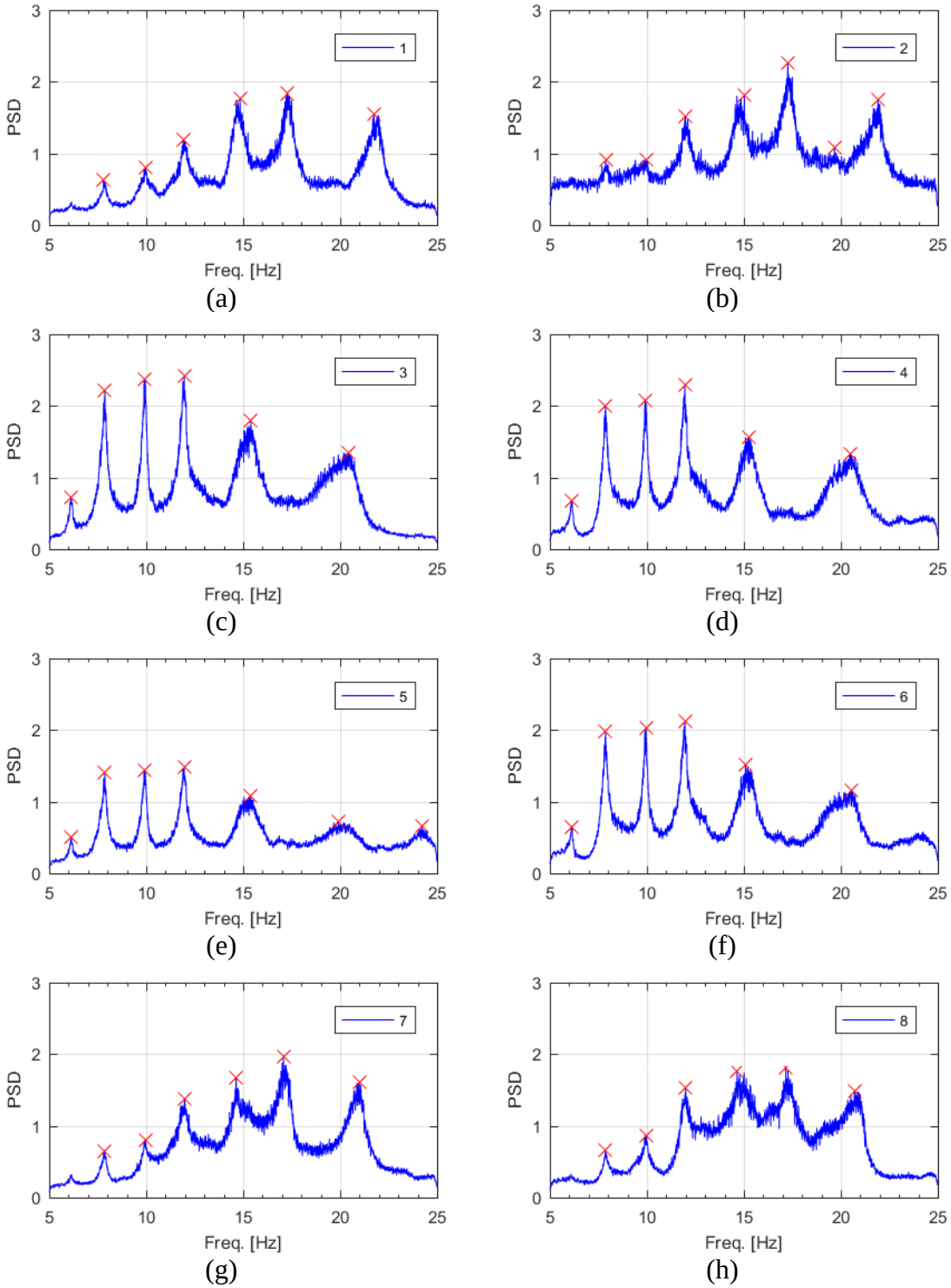

Figure C.90: Frequency content of the filtered acceleration data and peak-picking frequencies of the global response for bridge S081 05152L.

Table C.80: Filtered acceleration RMS values of the global response for bridge S081 05152L.

Sensor	Filtered a_{RMS} (µg)
1	3280
2	3842
3	3920
4	3626
5	2448
6	3359
7	3601
8	3893

Table C.81: Peak-picking frequencies of the global response for bridge S081 05152L.

Mode	Individual Sensor Frequencies (Hz)							
	1	**2**	**3**	**4**	**5**	**6**	**7**	**8**
1	--	--	6.14	6.13	6.14	6.11	--	--
2	7.80	7.87	7.87	7.87	7.87	7.87	7.87	7.87
3	9.98	9.96	9.89	9.92	9.89	9.95	9.95	9.96
4	11.91	11.98	11.96	11.96	11.96	11.96	11.98	12.00

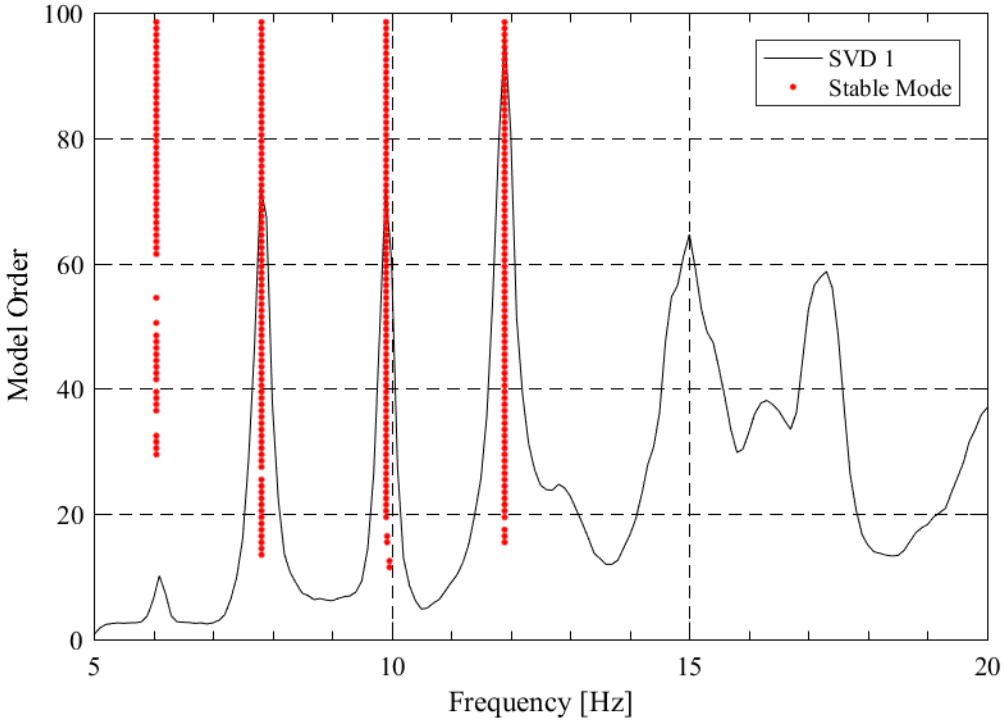

Figure C.91: SSI-UPCX method stabilization diagram of the global response for bridge S081 05152L.

Table C.82: SSI-UPCX method dynamic properties of the global response for bridge S081 05152L.

Mode	Frequency (Hz)	Damping (%)	Complexity (%)
1	6.05	2.46	0.70
2	7.82	1.93	1.24
3	9.91	1.14	1.55
4	11.90	1.61	10.04

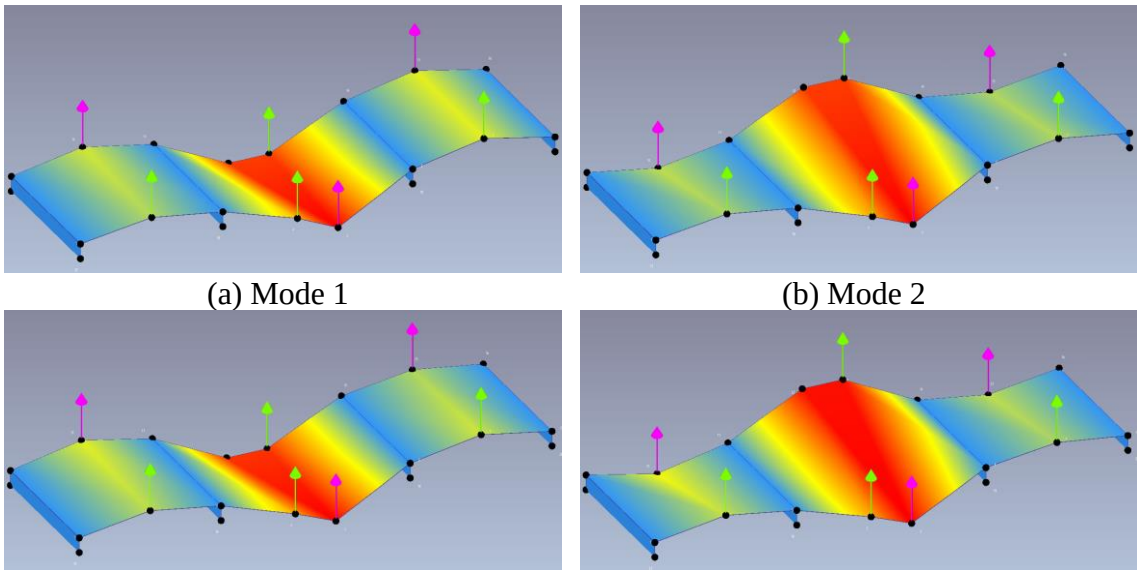

(a) Mode 1 (b) Mode 2

(c) Mode 3 (d) Mode 4

Figure C.92: Operational deflected shapes of the global response for bridge S081 05152L.

Table C.83: Operational deflected shape coordinates of the global response for bridge S081 05152L.

Sensor	ODS Coordinates			
	Mode 1	**Mode 2**	**Mode 3**	**Mode 4**
1	-0.35	-0.25	-0.31	-0.24
2	-0.35	0.25	-0.25	0.28
3	1.00	1.00	1.00	1.00
4	0.86	-0.85	0.88	-0.96
5	0.56	0.60	0.60	0.60
6*	--	--	--	--
7	-0.25	-0.24	-0.27	-0.28
8	-0.31	0.28	-0.35	0.38

* Sensor removed for being out of phase

Table C.84: MAC values of the global response for bridge S081 05152L.

MAC	Mode 1	Mode 2	Mode 3	Mode 4
Mode 1	1.000	0.086	0.993	0.056
Mode 2	0.086	1.000	0.079	0.981
Mode 3	0.993	0.079	1.000	0.047
Mode 4	0.056	0.981	0.047	1.000

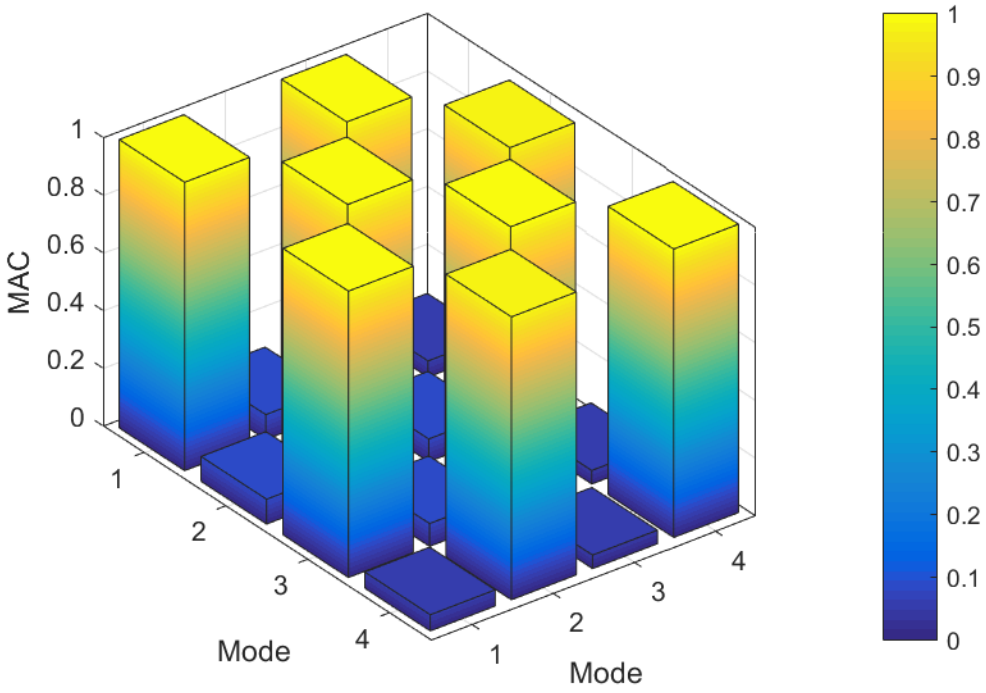

Figure C.93: MAC values of the global response for bridge S081 05152L.

IT Girder Bridge S089 06047:

Figure C.94: Location of bridge S089 06047 (courtesy of Google Maps).

Table C.85: Bridge information summary for bridge S089 06047.

Bridge ID	S089 06047	**Girder Height (in [mm])**	11.81 [300]
County	Harlan	**Girder Width (in [mm])**	23.63 [600]
Year Built	2007	**Girder Spacing (in [mm])**	28.50 [724]
No. of Spans	3	**Deck Thickness (in [mm])**	6 [152]
Length Span 1 (ft)	40.00	**No. of Girders**	16
Length Span 2 (ft)	45.00	**Diaphragm**	Concrete
Length Span 3 (ft)	40.00	**Deck Rating**	8
Bridge Width (ft)	38.40	**Superstructure Rating**	9
Skew Angle (°)	0	**Substructure Rating**	9

Figure C.95: Photo of bridge S089 06047.

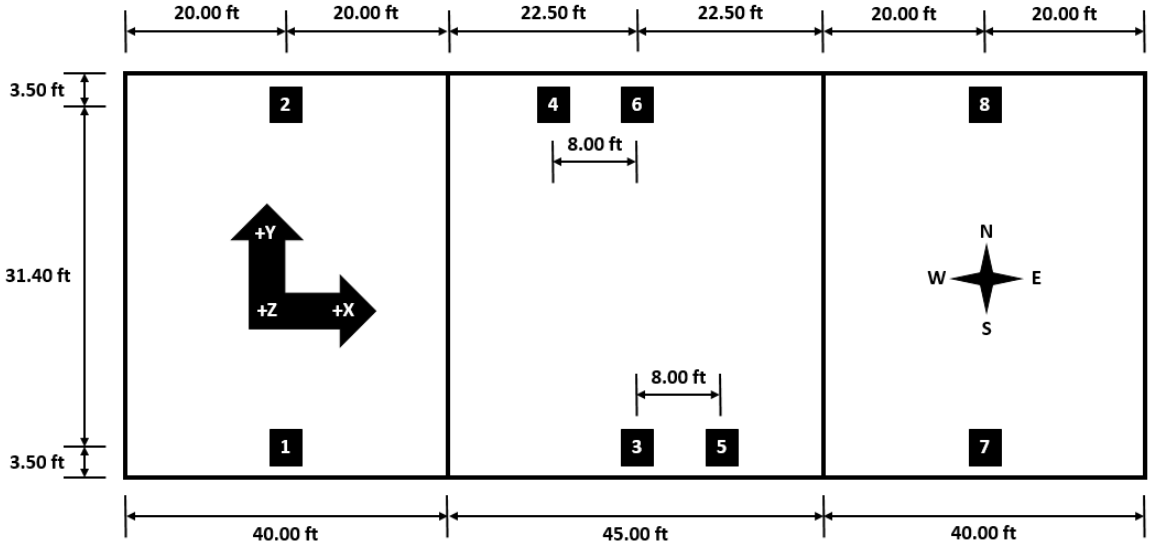

Figure C.96: Sensor locations capturing the global response for bridge S089 06047.

Table C.86: Sensor information of the global response setup for bridge S089 06047.

Sensor Location	Sensor Type	Sensor Id	Calibration Factor (mV/g)
1	WSN	997Z	--
2	WSN	848Z	--
3	WSN	99CZ	--
4	WSN	968Z	--
5	WSN	99DZ	--
6	WSN	995Z	--
7	WSN	99FZ	--
8	WSN	996Z	--

Date of Collection	3/20/2017
Length of Data (min)	51.63
Sampling Rate (Hz)	256

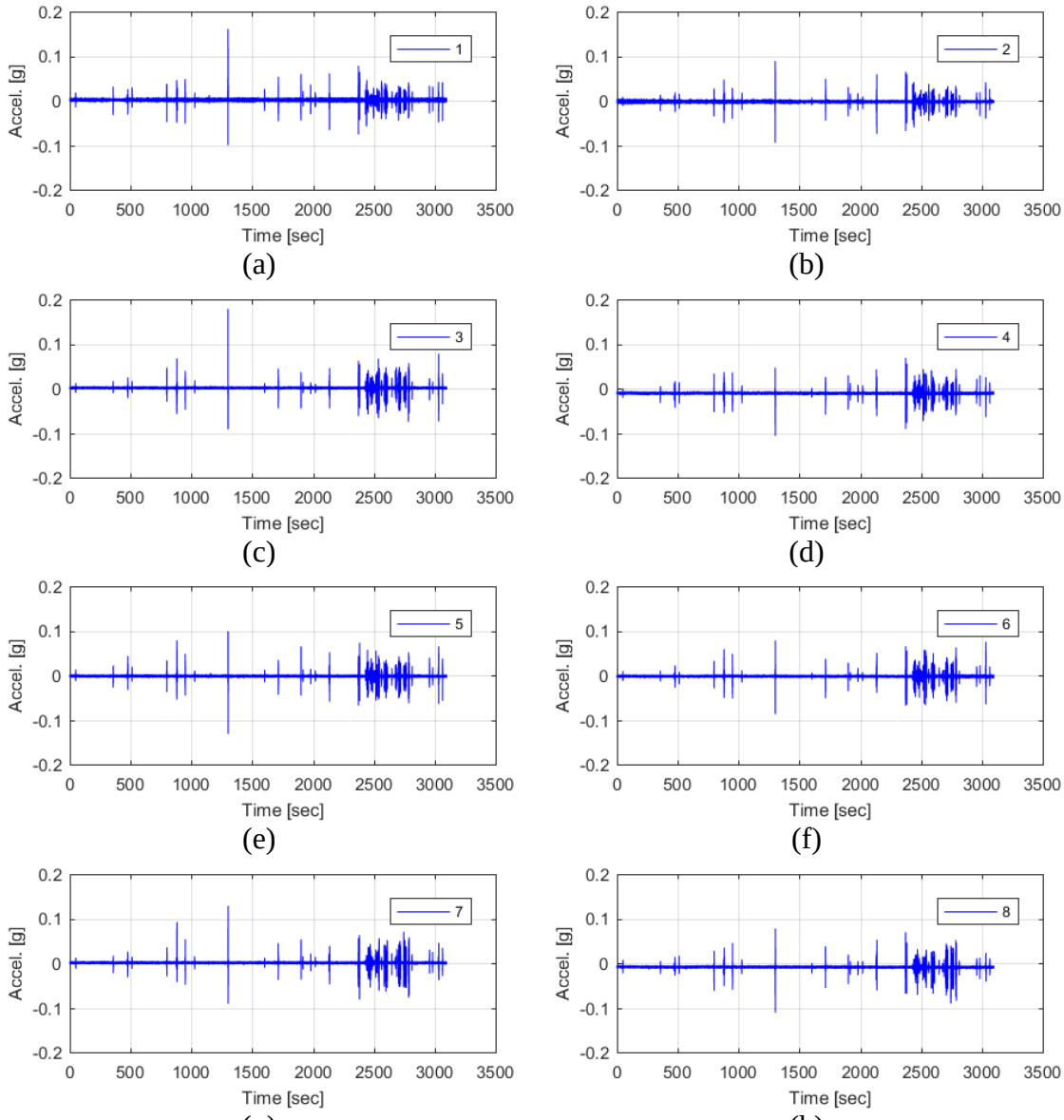

Figure C.97: Raw acceleration data of the global response for bridge S089 06047.

Table C.87: Filter parameters of the global response for bridge S089 06047.

Filter Parameter	Value
Hampel Identifier Order	--
FIR Bandpass Filter Order	2048
FIR Bandpass Filter Lower Cutoff Frequency (Hz)	6
FIR Bandpass Filter Upper Cutoff Frequency (Hz)	18
Tukey Averaging Window (min)	1.5

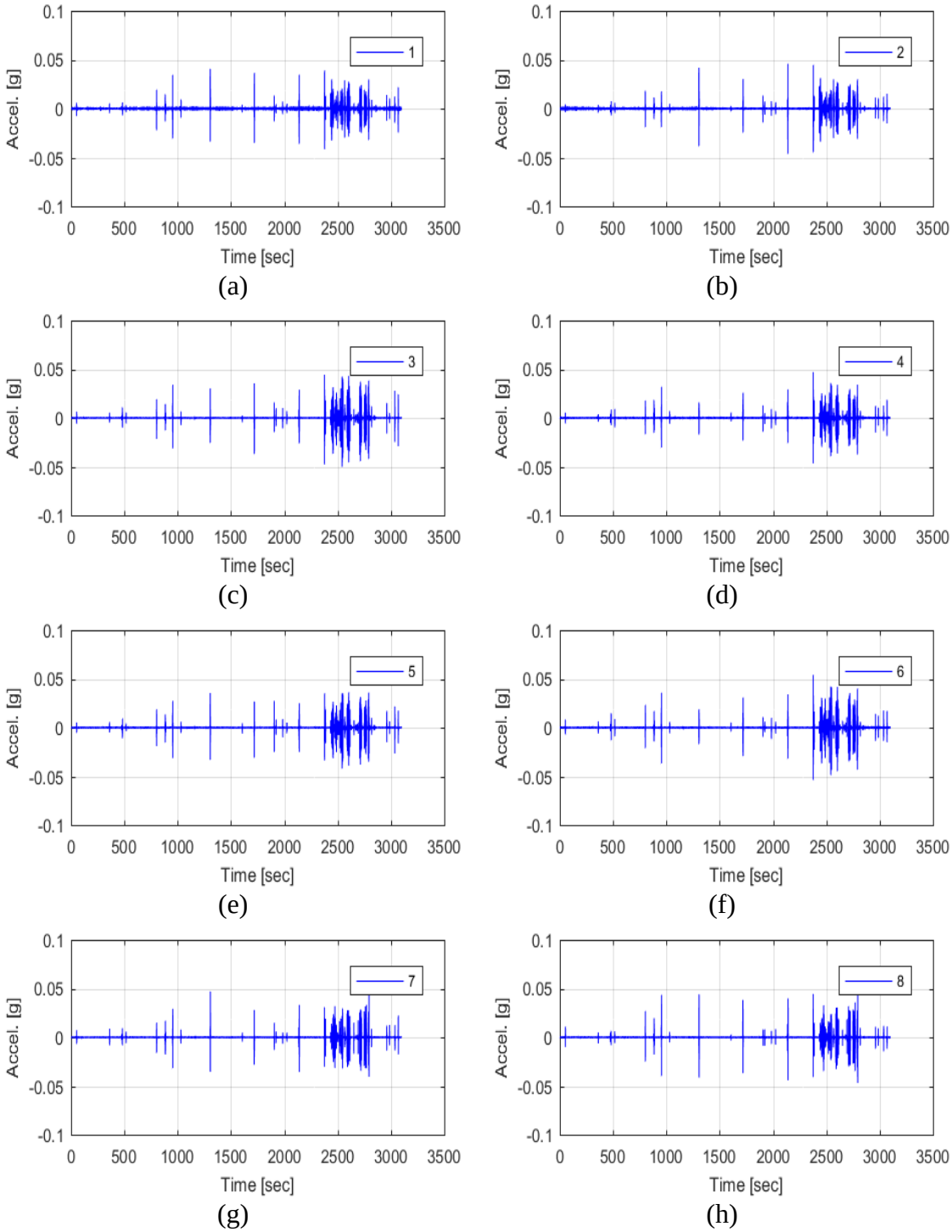

Figure C.98: Filtered acceleration data of the global response for bridge S089 06047.

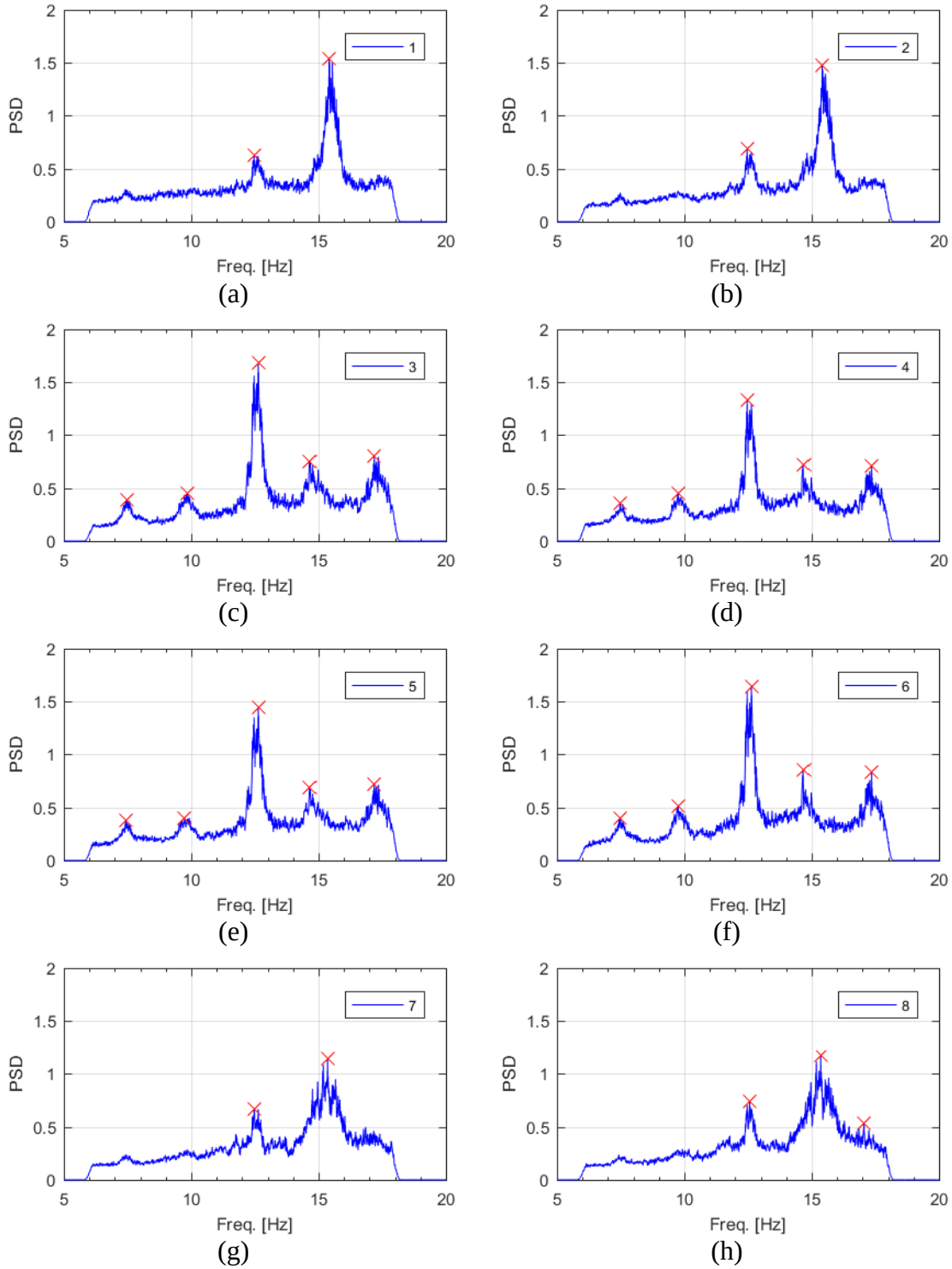

Figure C.99: Frequency content of the filtered acceleration data and peak-picking frequencies of the global response for bridge S089 06047.

Table C.88: Filtered acceleration RMS values of the global response for bridge S089 06047.

Sensor	Filtered a_{RMS} (µg)
1	1642
2	1623
3	1992
4	1633
5	1735
6	1949
7	1634
8	1670

Table C.89: Peak-picking frequencies of the global response for bridge S089 06047.

Mode	Individual Sensor Frequencies (Hz)							
	1	**2**	**3**	**4**	**5**	**6**	**7**	**8**
1	--	--	7.49	7.48	7.43	7.49	--	--
2	--	--	9.85	9.75	9.74	9.75	--	--
3	12.47	12.47	12.63	12.47	12.63	12.63	12.47	12.56
4	--	--	14.65	14.66	14.65	14.66	--	--
5	15.41	15.41	--	--	--	--	15.35	15.35

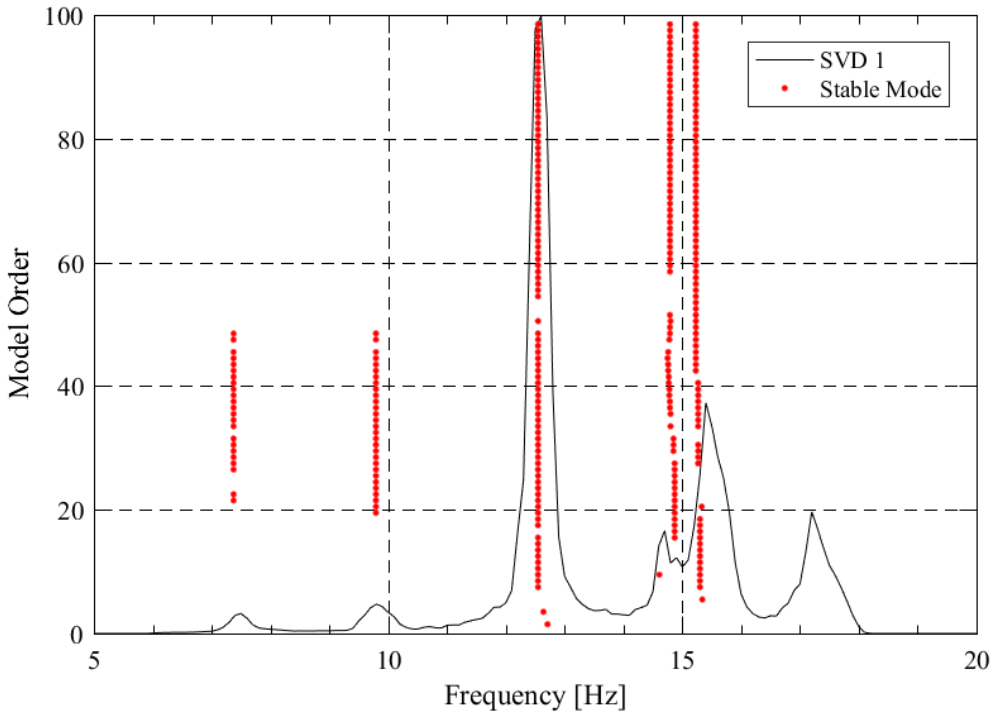

Figure C.100: SSI-UPCX method stabilization diagram of the global response for bridge S089 06047.

Table C.90: SSI-UPCX method dynamic properties of the global response for bridge S089 06047.

Mode	Frequency (Hz)	Damping (%)	Complexity (%)
1	7.37	3.62	27.29
2	9.79	3.53	23.02
3	12.55	1.23	37.90
4	14.79	2.23	32.32
5	15.28	1.47	90.26

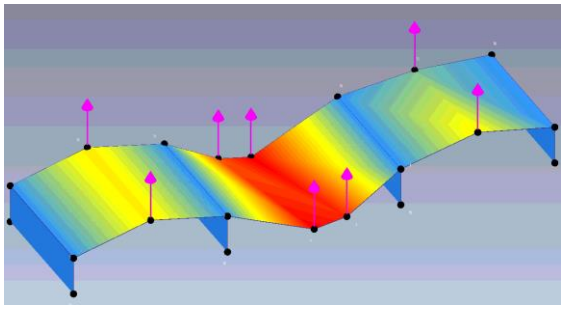

(a) Mode 1

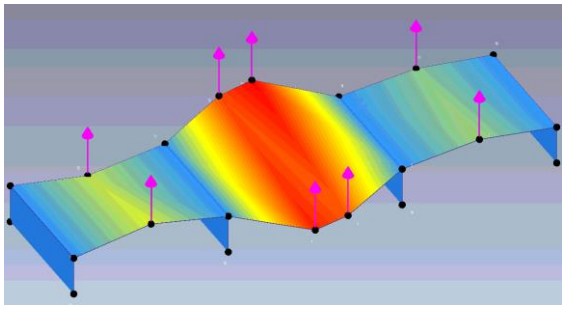

(b) Mode 2

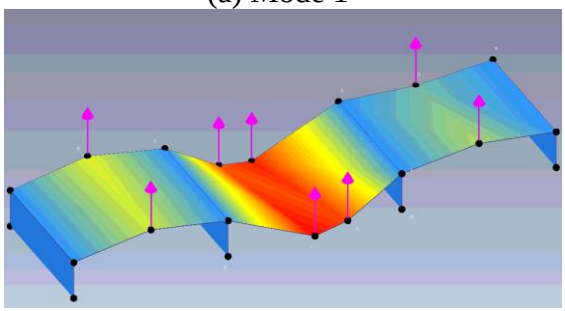

(c) Mode 3

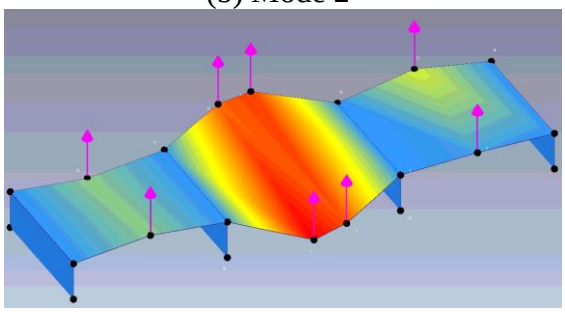

(d) Mode 4

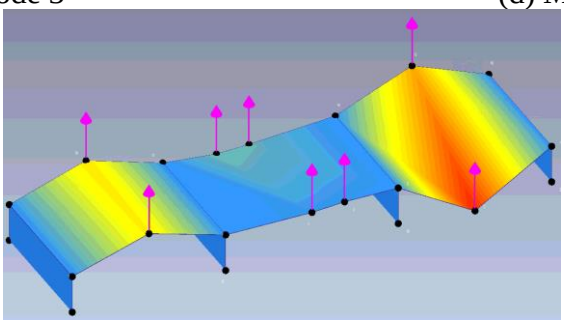

(e) Mode 5

Figure C.101: Operational deflected shapes of the global response for bridge S089 06047.

Table C.91: Operational deflected shape coordinates of the global response for bridge S089 06047.

Sensor	ODS Coordinates				
	Mode 1	Mode 2	Mode 3	Mode 4	Mode 5
1	-0.46	0.33	-0.30	-0.18	-0.51
2	-0.47	-0.27	-0.34	0.18	-0.53
3	0.99	-0.93	1.00	1.00	0.02
4	0.80	0.83	0.81	-0.76	0.13
5	0.89	-0.79	0.83	0.81	-0.02
6	1.00	1.00	0.93	-0.85	0.11
7	-0.43	0.22	-0.24	-0.04	1.00
8	-0.15	0.17	0.13	-0.32	-0.67

Table C.92: MAC values of the global response for bridge S089 06047.

MAC	Mode 1	Mode 2	Mode 3	Mode 4	Mode 5
Mode 1	1.000	0.002	0.963	0.017	0.004
Mode 2	0.002	1.000	0.009	0.960	0.039
Mode 3	0.963	0.009	1.000	0.006	0.007
Mode 4	0.017	0.960	0.006	1.000	0.033
Mode 5	0.004	0.039	0.007	0.033	1.000

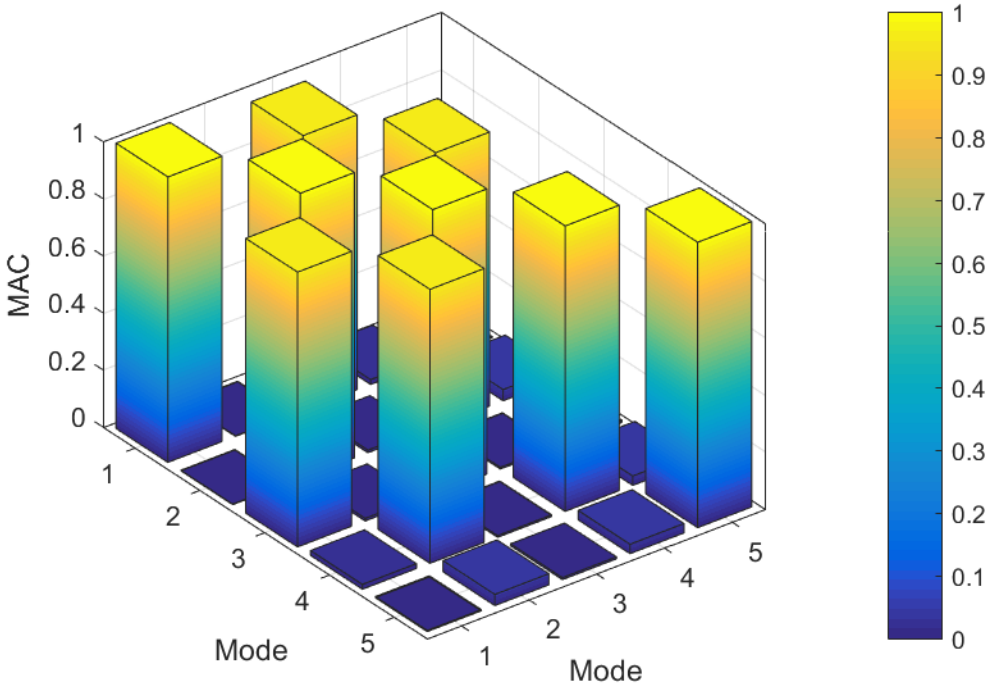

Figure C.102: MAC values of the global response for bridge S089 06047.

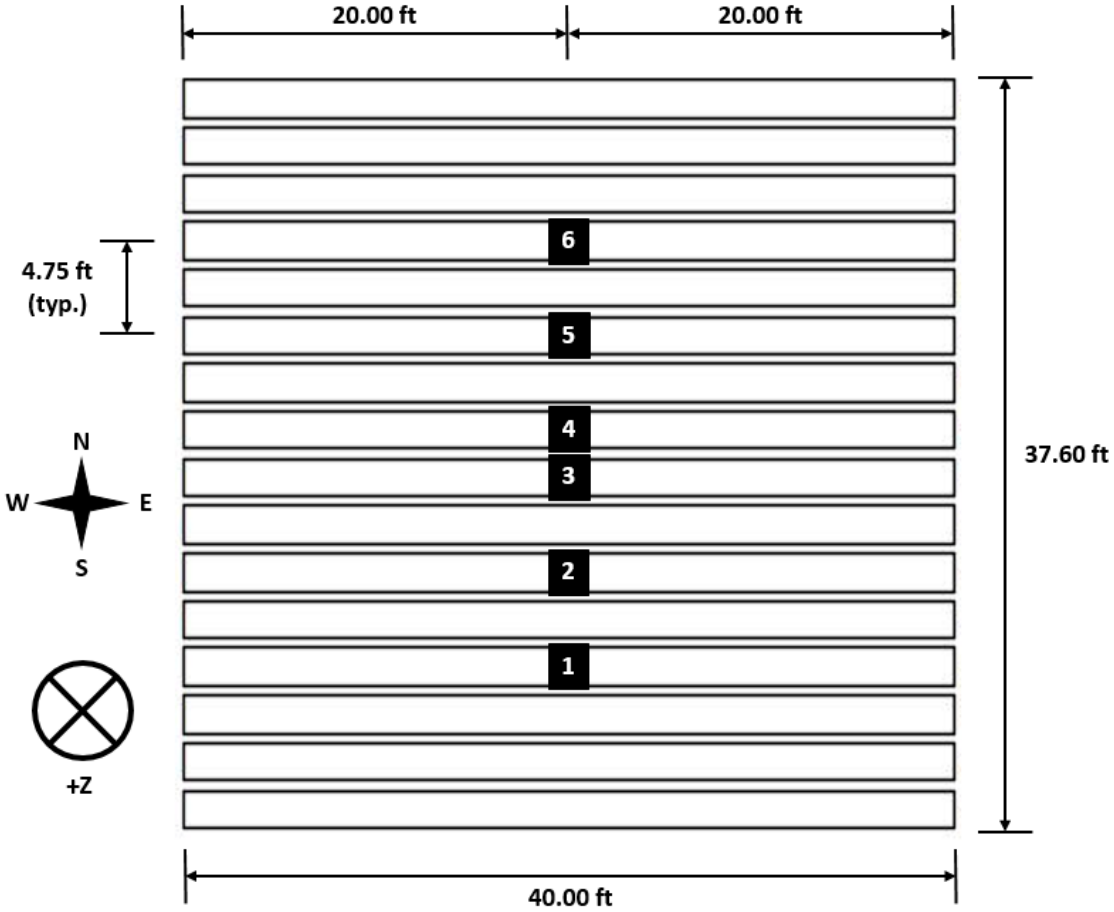

Figure C.103: Sensor locations capturing the local response for bridge S089 06047.

Table C.93: Sensor information of the local response setup for bridge S089 06047.

Sensor Location	Setup Number	Sensor Type	Sensor Id	Calibration Factor (mV/g)
1	2	PCB	N4	1065
2	1	PCB	N4	1065
3	1 & 2	PCB	N2	997
4	1 & 2	PCB	N1	1001
5	1	PCB	N3	1019
6	2	PCB	N3	1019

Date of Collection	3/20/2017
Length of Data Setup 1 (min)	29.30
Length of Data Setup 2 (min)	29.30
Sampling Rate (Hz)	2048

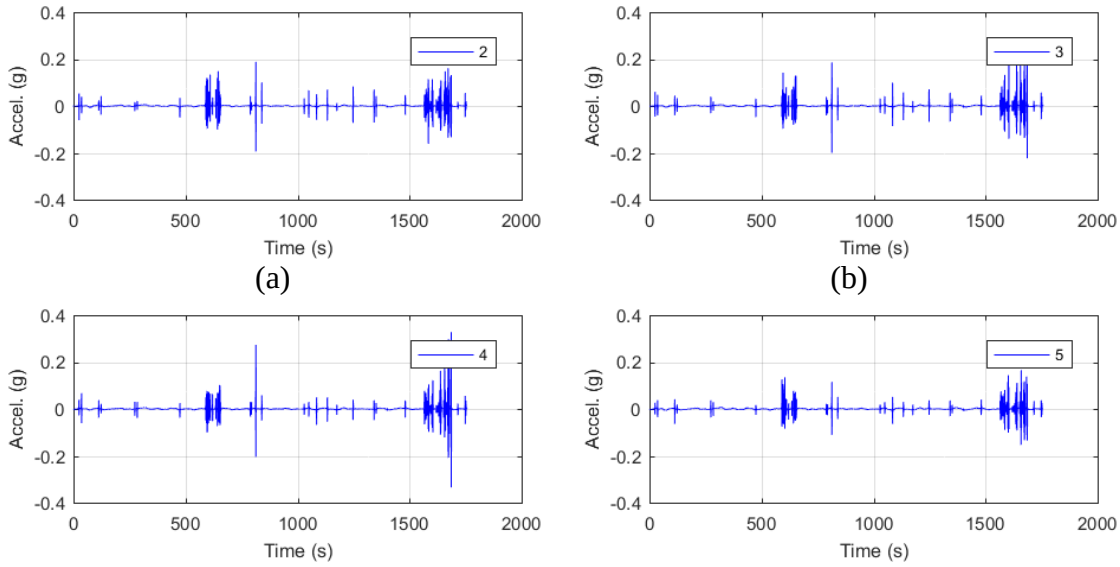

Figure C.104: Raw acceleration data of the local response setup 1 for bridge S089 06047.

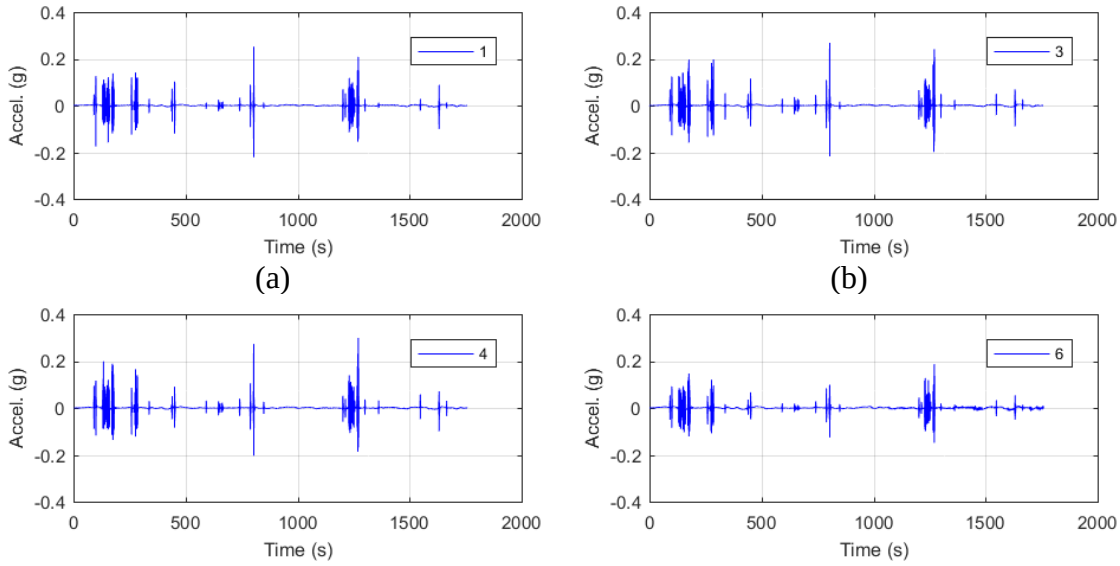

Figure C.105: Raw acceleration data of the local response setup 2 for bridge S089 06047.

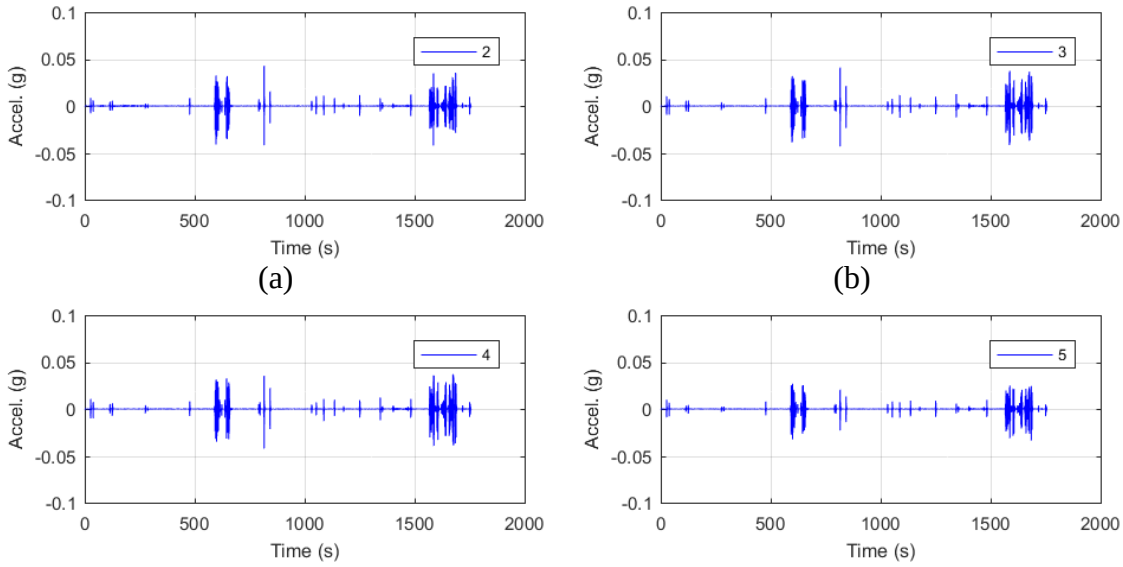

Figure C.106: Filtered acceleration data of the local response setup 1 for bridge S089 06047.

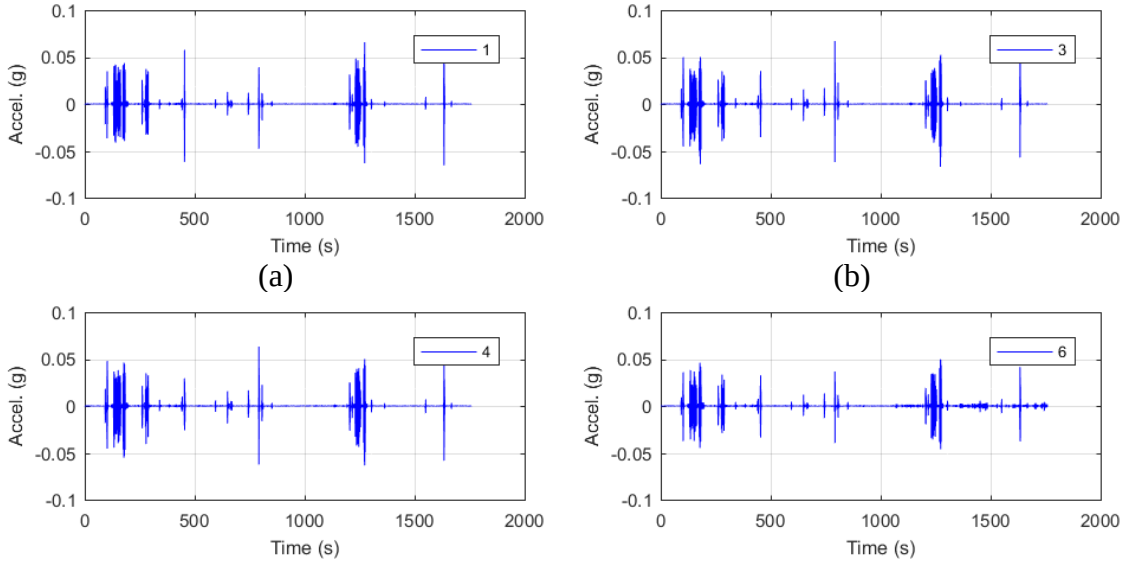

Figure C.107: Filtered acceleration data of the local response setup 2 for bridge S089 06047.

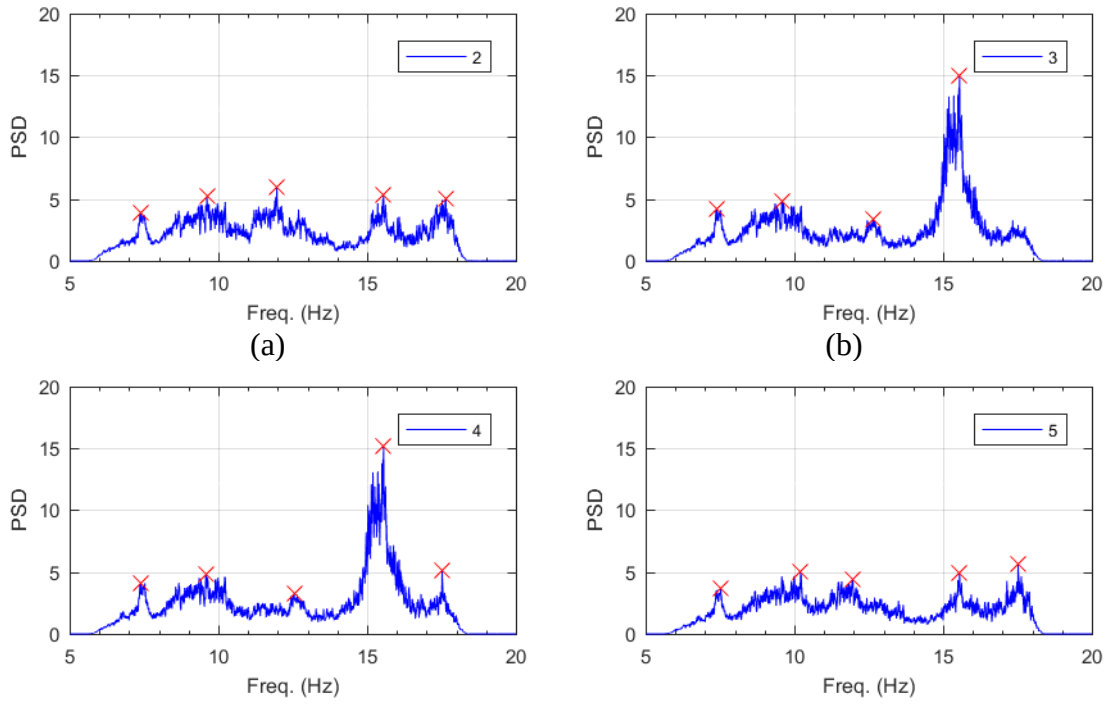

Figure C.108: Frequency content of the filtered acceleration data and peak-picking frequencies of the local response setup 1 for bridge S089 06047.

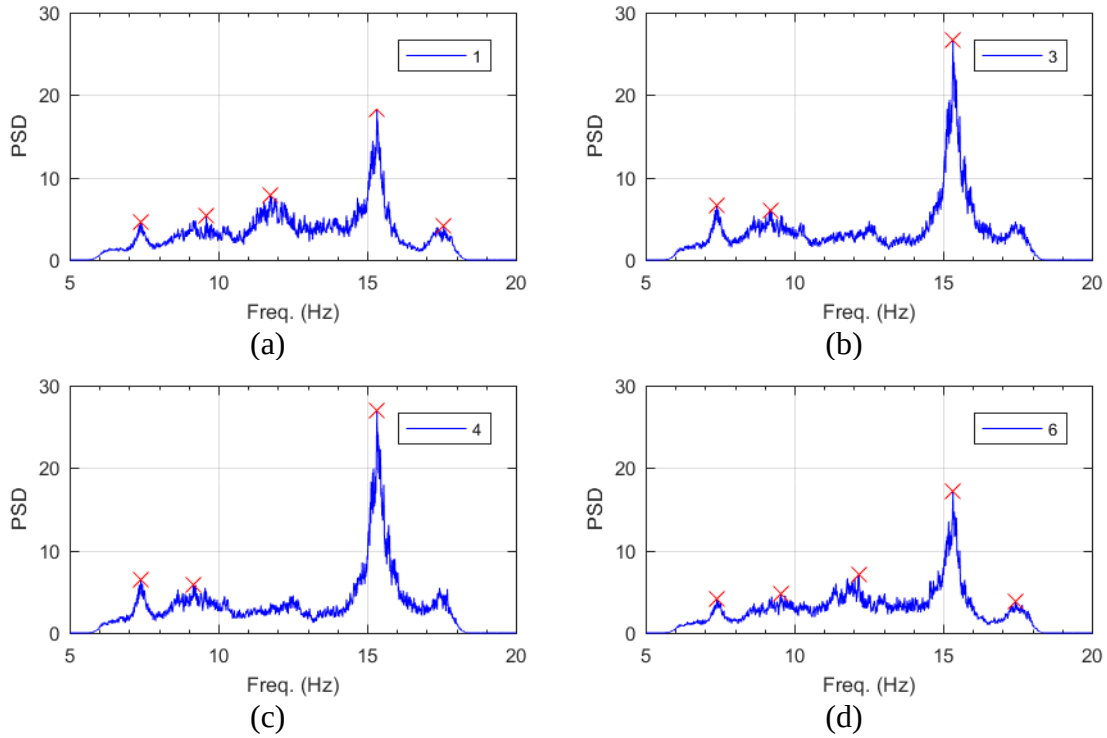

Figure C.109: Frequency content of the filtered acceleration data and peak-picking frequencies of the local response setup 2 for bridge S089 06047.

Table C.94: Filter parameters of the local response for bridge S089 06047.

Filter Parameter	Value
Hampel Identifier Order	--
FIR Bandpass Filter Order	8192
FIR Bandpass Filter Lower Cutoff Frequency (Hz)	6
FIR Bandpass Filter Upper Cutoff Frequency (Hz)	18
Tukey Averaging Window (min)	1.5

Table C.95: Filtered acceleration RMS values of the local response for bridge S089 06047.

Sensor	Filtered a_{RMS} (µg) Setup 1	Filtered a_{RMS} (µg) Setup 2
1	--	2405
2	1510	--
3	2080	2836
4	2092	2849
5	1376	--
6	--	2143

Table C.96: Peak-picking frequencies of the local response for bridge S089 06047.

Mode	Individual Sensor Frequencies (Hz)							
	Setup 1				Setup 2			
	2	**3**	**4**	**5**	**1**	**3**	**4**	**6**
1	7.41	7.41	7.41	7.53	7.40	7.39	7.39	7.40
2	9.61	9.58	9.58	10.21	9.60	9.20	9.17	9.55
3	11.97	--	--	11.97	11.75	--	--	--
4	--	12.64	12.55	--	--	--	--	12.17
5	15.55	15.55	15.55	15.55	15.33	15.33	15.33	15.33

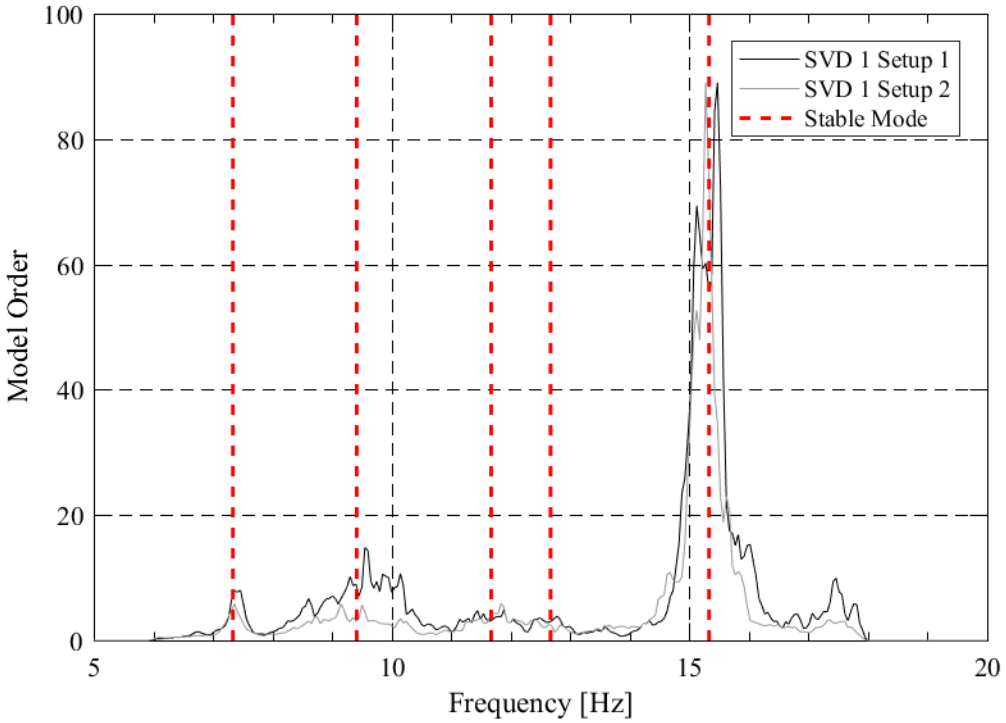

Figure C.110: SSI-UPCX method stabilization diagram of the local response for bridge S089 06047.

Table C.97: SSI-UPCX method dynamic properties of the local response for bridge S089 06047.

Mode	Frequency (Hz)	Damping (%)	Complexity (%)
1	7.34	4.01	2.72
2	9.42	8.42	3.69
3	11.67	4.58	4.21
4	12.67	5.46	27.58
5	15.33	0.96	0.33

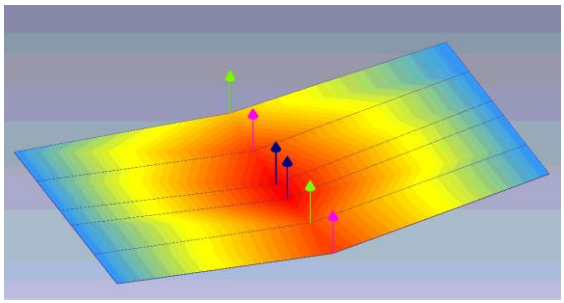

(a) Mode 1

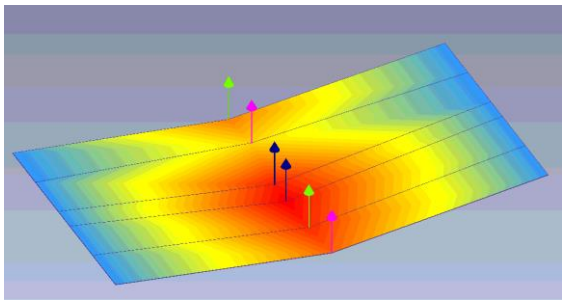

(b) Mode 2

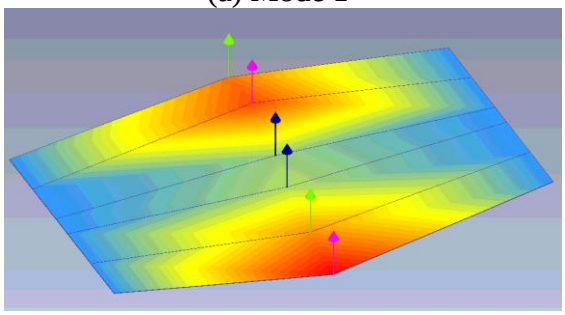

(c) Mode 3

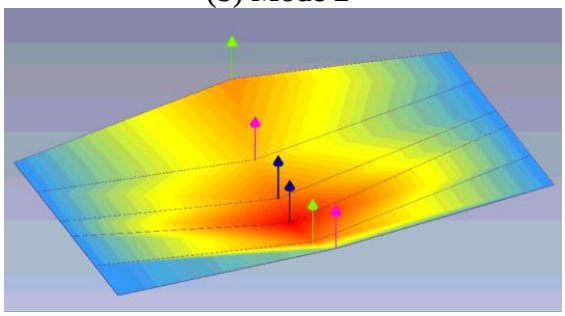

(d) Mode 4

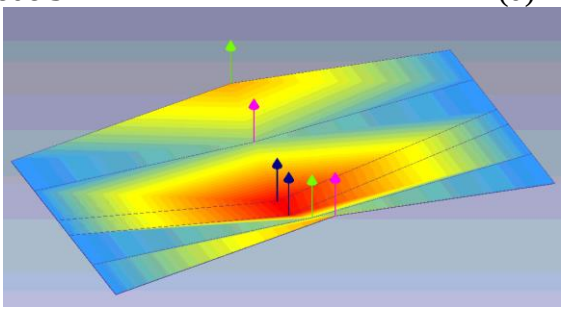

(e) Mode 5

Figure C.111: Operational deflected shapes of the local response for bridge S089 06047.

Table C.98: Operational deflected shape coordinates of the local response for bridge S089 06047.

Sensor	**ODS Coordinates**				
	Mode 1	**Mode 2**	**Mode 3**	**Mode 4**	**Mode 5**
1	0.86	0.77	1.00	0.20	-0.64
2	0.82	0.90	0.66	0.75	0.23
3	1.00	1.00	0.25	1.00	0.98
4	1.00	0.93	-0.21	0.76	1.00
5	0.87	0.52	-0.82	0.54	0.19
6	0.56	0.71	-0.72	-0.67	-0.61

Table C.99: MAC values of the local response for bridge S089 06047.

MAC	Mode 1	Mode 2	Mode 3	Mode 4	Mode 5
Mode 1	1.000	0.962	0.058	0.793	0.308
Mode 2	0.962	1.000	0.125	0.811	0.343
Mode 3	0.058	0.125	1.000	0.020	0.068
Mode 4	0.793	0.811	0.020	1.000	0.536
Mode 5	0.308	0.343	0.068	0.536	1.000

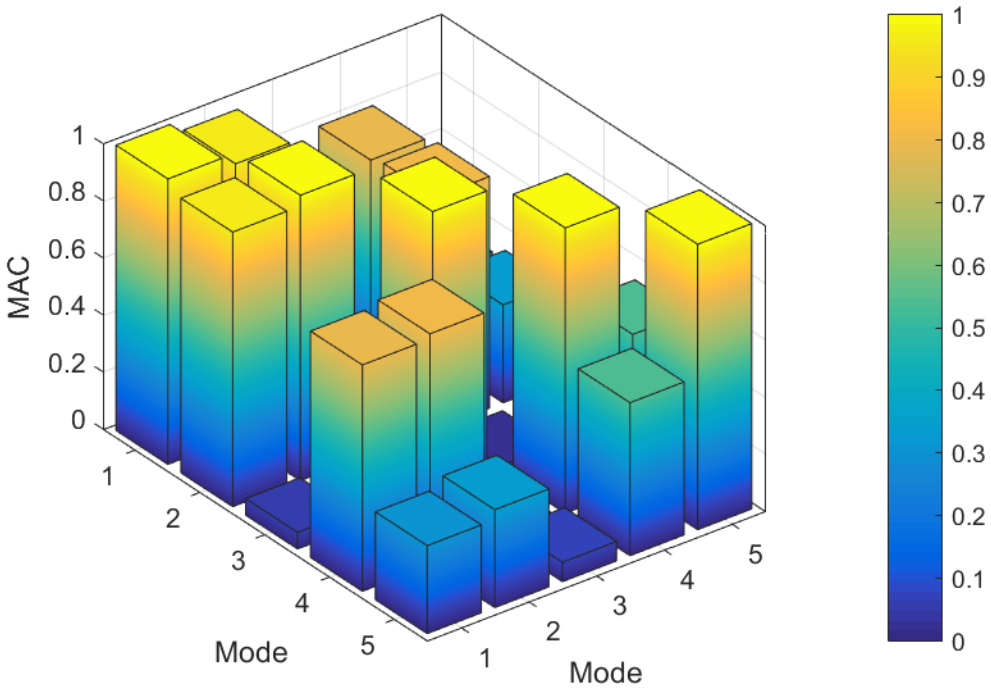

Figure C.112: MAC values of the local response for bridge S089 06047.

IT Girder Bridge C008504145:

Figure C.113: Location of bridge C008504145 (courtesy of Google Maps).

Table C.100: Bridge information summary for bridge C008504145.

Bridge ID	C008504145	**Girder Height (in [mm])**	23.63 [600]
County	Thayer	**Girder Width (in [mm])**	23.63 [600]
Year Built	2007	**Girder Spacing (in [mm])**	29.00 [737]
No. of Spans	3	**Deck Thickness (in [mm])**	6 [152]
Length Span 1 (ft)	50.75	**No. of Girders**	12
Length Span 2 (ft)	63.50	**Diaphragm**	C10x15.3
Length Span 3 (ft)	50.75	**Deck Rating**	5
Bridge Width (ft)	30.40	**Superstructure Rating**	5
Skew Angle (°)	0	**Substructure Rating**	6

Figure C.114: Photo of bridge C008504145.

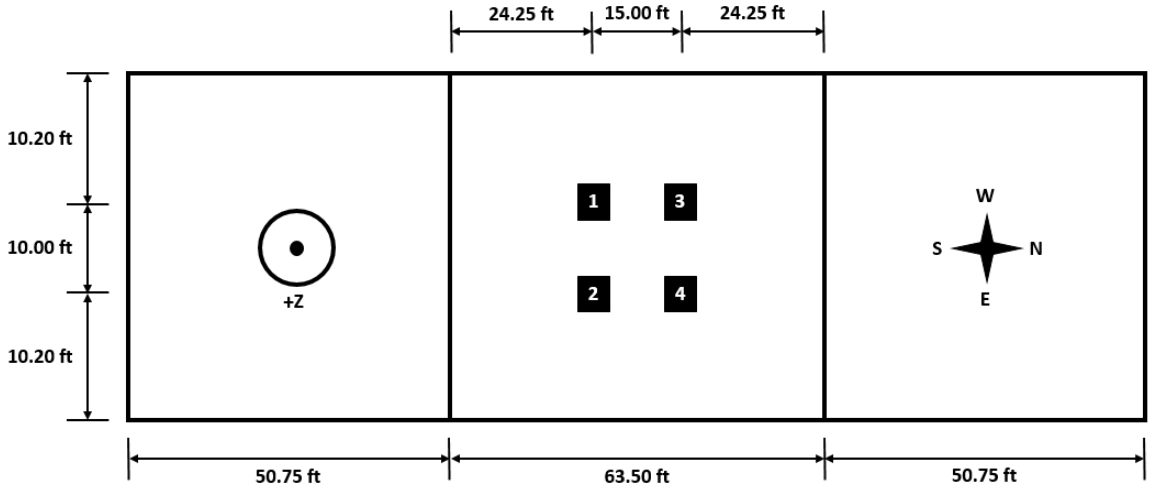

Figure C.115: Sensor locations capturing the global response for bridge C008504145.

Table C.101: Sensor information of the global response setup for bridge C008504145.

Sensor Location	Sensor Type	Sensor Id	Calibration Factor (mV/g)
1	PCB	N3	1019
2	PCB	N2	997
3	PCB	N4	1065
4	PCB	N1	1001

Date of Collection	10/7/2016
Length of Data (min)	29.30
Sampling Rate (Hz)	2048

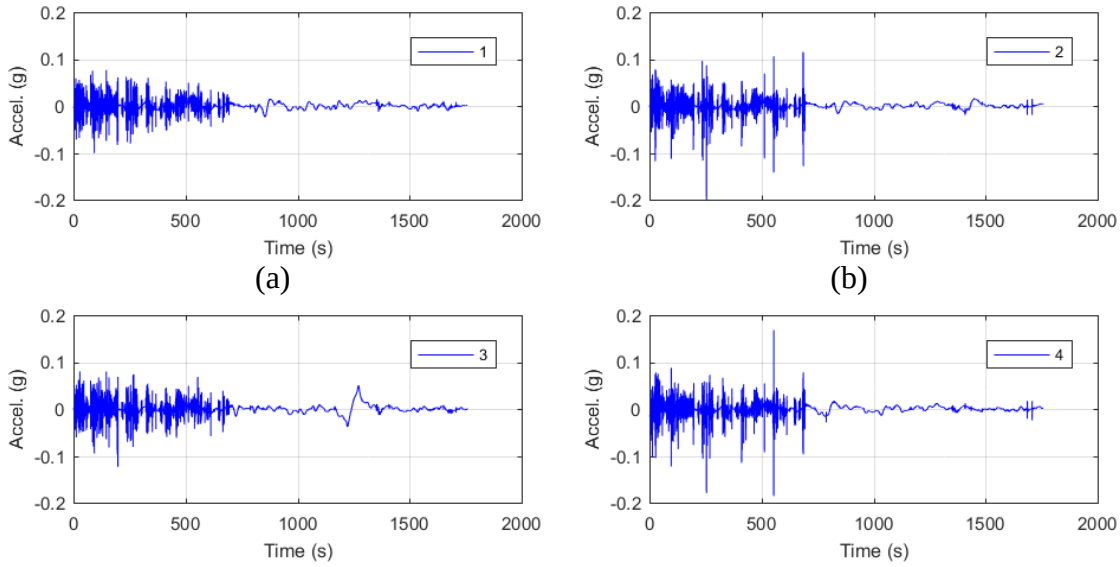

Figure C.116: Raw acceleration data of the global response for bridge C008504145.

Table C.102: Filter parameters of the global response for bridge C008504145.

Filter Parameter	Value
Hampel Identifier Order	--
FIR Bandpass Filter Order	4096
FIR Bandpass Filter Lower Cutoff Frequency (Hz)	5
FIR Bandpass Filter Upper Cutoff Frequency (Hz)	37
Tukey Averaging Window (min)	1.5

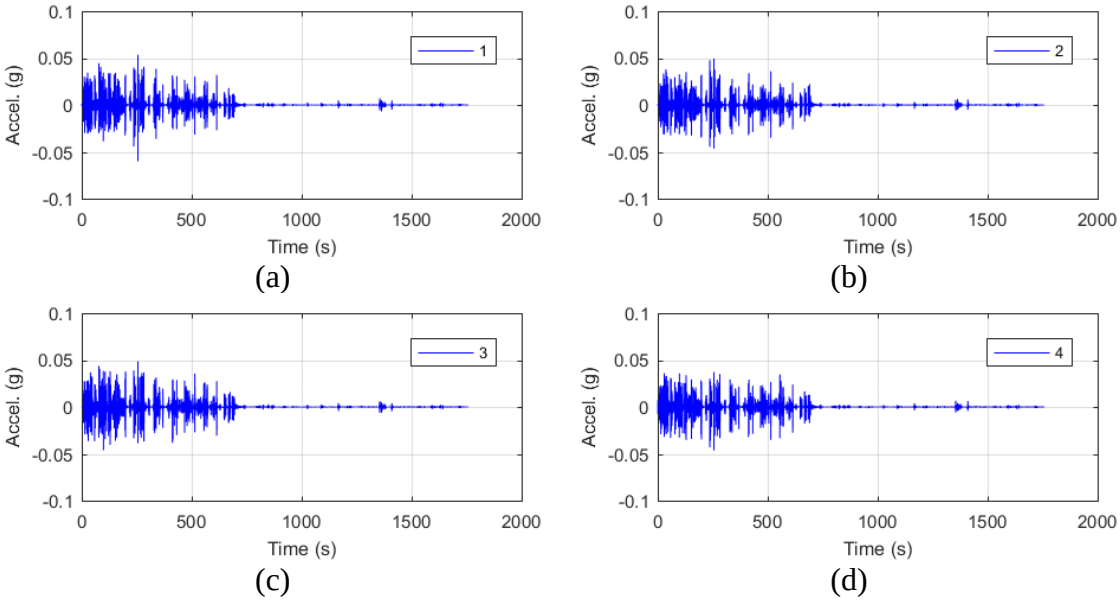

Figure C.117: Filtered acceleration data of the global response for bridge C008504145.

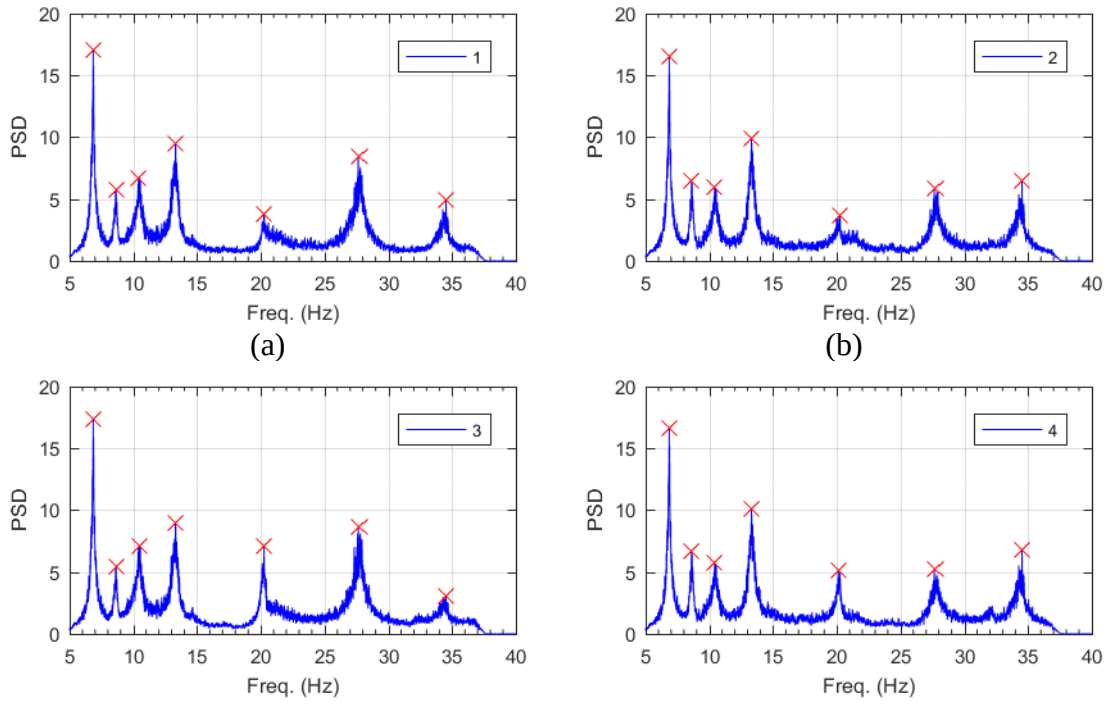

Figure C.118: Frequency content of the filtered acceleration data and peak-picking frequencies of the global response for bridge C008504145.

Table C.103: Filtered acceleration RMS values of the global response for bridge C008504145.

Sensor	**Filtered a_{RMS} (μg)**
1	2083
2	1991
3	2109
4	1979

Table C.104: Peak-picking frequencies of the global response for bridge C008504145.

Mode	**Individual Sensor Frequencies (Hz)**			
	1	**2**	**3**	**4**
1	6.85	6.85	6.85	6.85
2	8.64	8.60	8.64	8.60
3	10.41	10.41	10.52	10.41
4	13.30	13.30	13.30	13.30
5	20.23	20.25	20.25	20.11

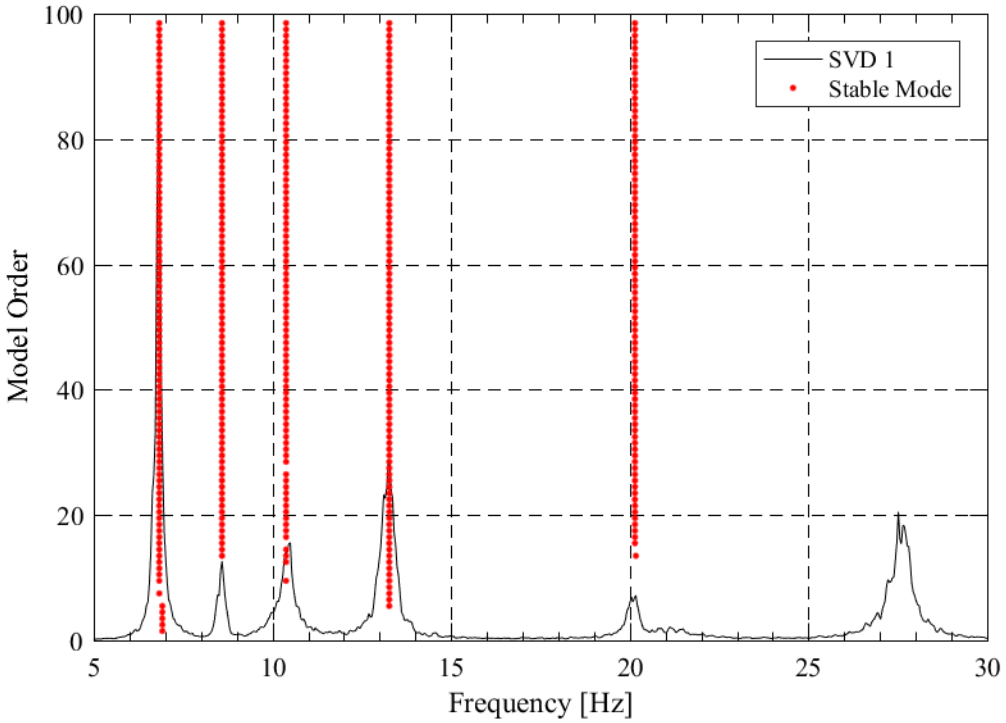

Figure C.119: SSI-UPCX method stabilization diagram of the global response for bridge C008504145.

Table C.105: SSI-UPCX method dynamic properties of the global response for bridge C008504145.

Mode	Frequency (Hz)	Damping (%)	Complexity (%)
1	6.83	1.47	0.00
2	8.59	1.23	0.12
3	10.38	2.88	0.16
4	13.27	1.46	0.12
5	20.15	0.78	0.27

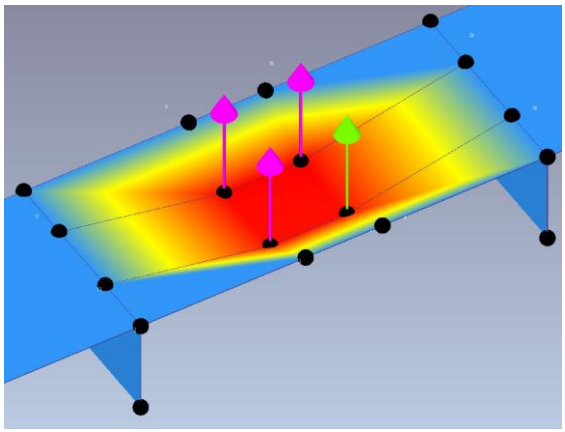

(a) Mode 1

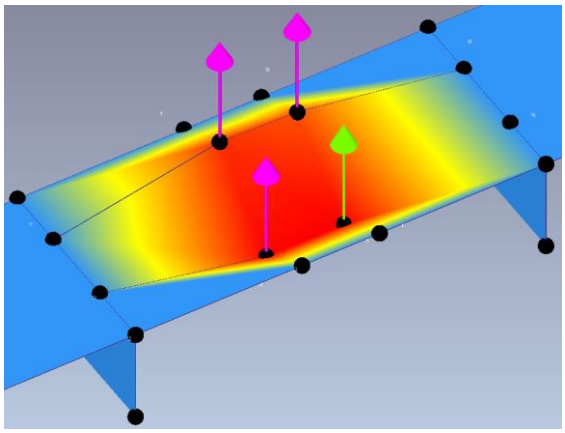

(b) Mode 2

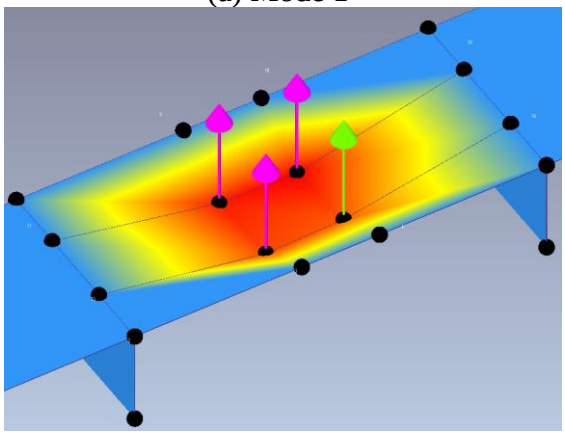

(c) Mode 3

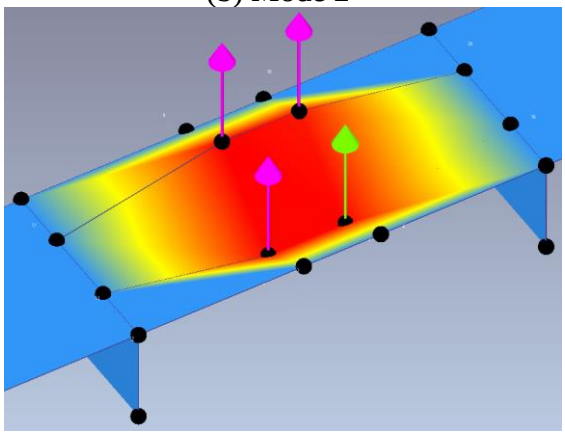

(d) Mode 4

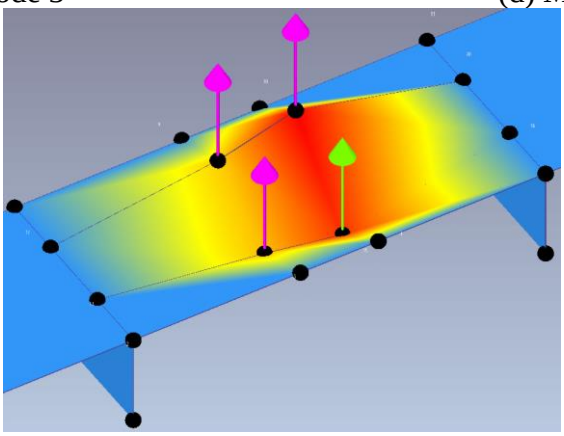

(e) Mode 5

Figure C.120: Operational deflected shapes of the global response for bridge C008504145.

Table C.106: Operational deflected shape coordinates of the global response for bridge C008504145.

Sensor	ODS Coordinates				
	Mode 1	Mode 2	Mode 3	Mode 4	Mode 5
1	0.99	-0.88	0.94	1.00	0.51
2	0.96	0.99	0.83	-0.98	-0.55
3	1.00	-0.80	1.00	0.95	1.00
4	0.96	1.00	0.78	-0.99	-0.88

Table C.107: MAC values of the global response for bridge C008504145.

MAC	Mode 1	Mode 2	Mode 3	Mode 4	Mode 5
Mode 1	1.000	0.140	0.995	0.101	0.202
Mode 2	0.140	1.000	0.100	0.996	0.951
Mode 3	0.995	0.100	1.000	0.067	0.153
Mode 4	0.101	0.996	0.067	1.000	0.935
Mode 5	0.202	0.951	0.153	0.935	1.000

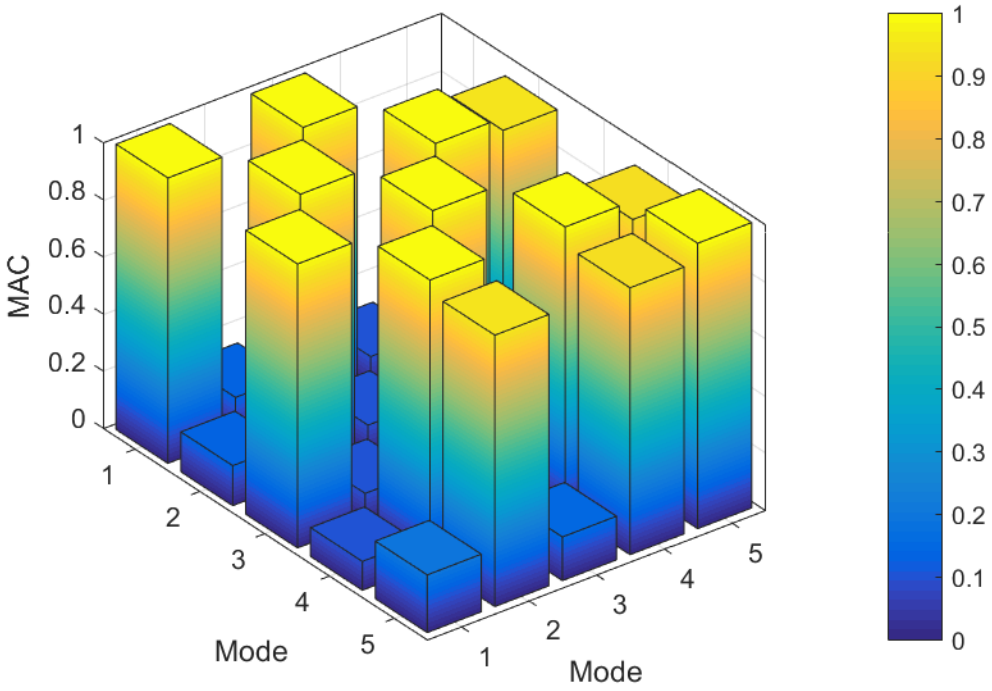

Figure C.121: MAC values of the global response for bridge C008504145.

IT Girder Bridge M011022220:

Figure C.122: Location of bridge M011022220 (courtesy of Google Maps).

Table C.108: Bridge information summary for bridge M011022220.

Bridge ID	M011022220	**Girder Height (in [mm])**	23.63 [600]
County	Sherman	**Girder Width (in [mm])**	23.63 [600]
Year Built	2012	**Girder Spacing (in [mm])**	28.38 [721]
No. of Spans	1	**Deck Thickness (in [mm])**	6 [152]
Length Span 1 (ft)	65.00	**No. of Girders**	13
Length Span 2 (ft)	--	**Diaphragm**	C8x18.75
Length Span 3 (ft)	--	**Deck Rating**	6
Bridge Width (ft)	30.40	**Superstructure Rating**	6
Skew Angle (°)	15	**Substructure Rating**	7

Figure C.123: Photo of bridge M011022220.

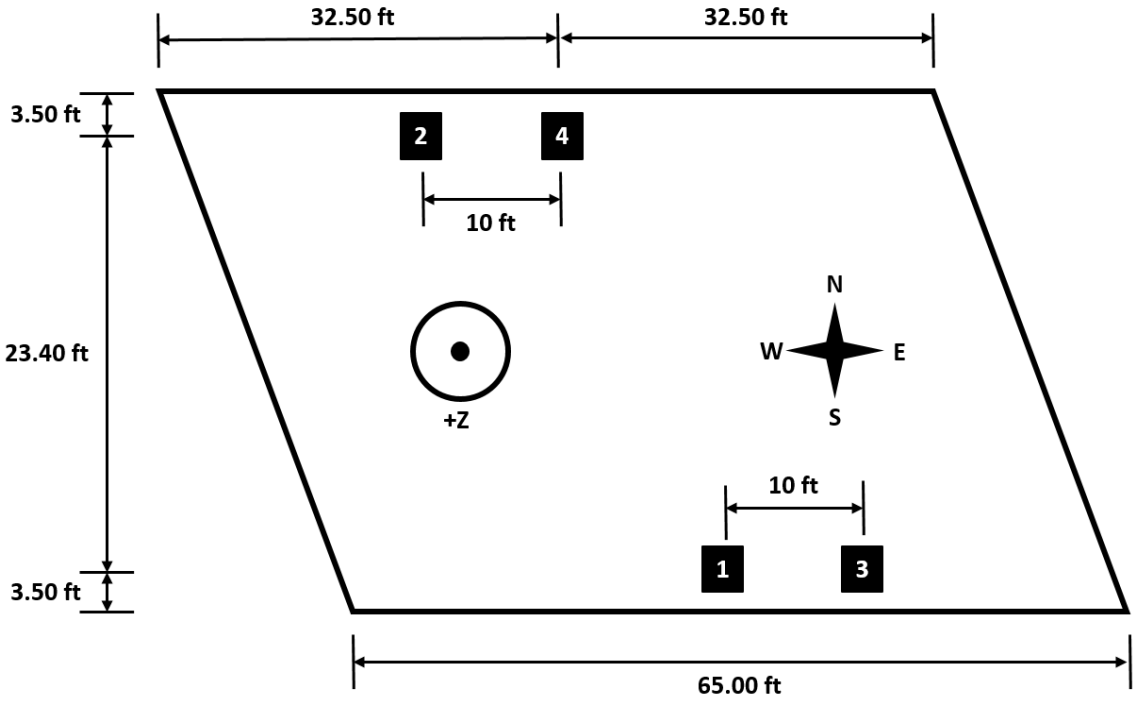

Figure C.124: Sensor locations capturing the global response for bridge M011022220.

Table C.109: Sensor information of the global response setup for bridge M011022220.

Sensor Location	Sensor Type	Sensor Id	Calibration Factor (mV/g)
1	PCB	N4	1065
2	PCB	N2	997
3	PCB	N3	1019
4	PCB	N1	1001

Date of Collection	10/21/2016
Length of Data (min)	17.58
Sampling Rate (Hz)	2048

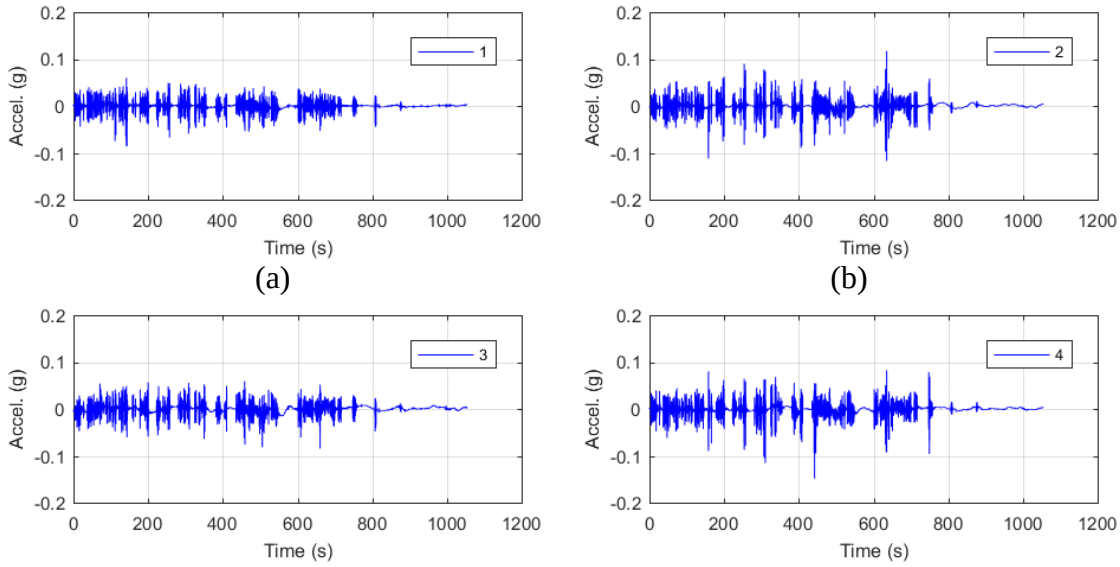

Figure C.125: Raw acceleration data of the global response for bridge M011022220.

Table C.110: Filter parameters of the global response for bridge M011022220.

Filter Parameter	Value
Hampel Identifier Order	--
FIR Bandpass Filter Order	4096
FIR Bandpass Filter Lower Cutoff Frequency (Hz)	4
FIR Bandpass Filter Upper Cutoff Frequency (Hz)	37
Tukey Averaging Window (min)	1.5

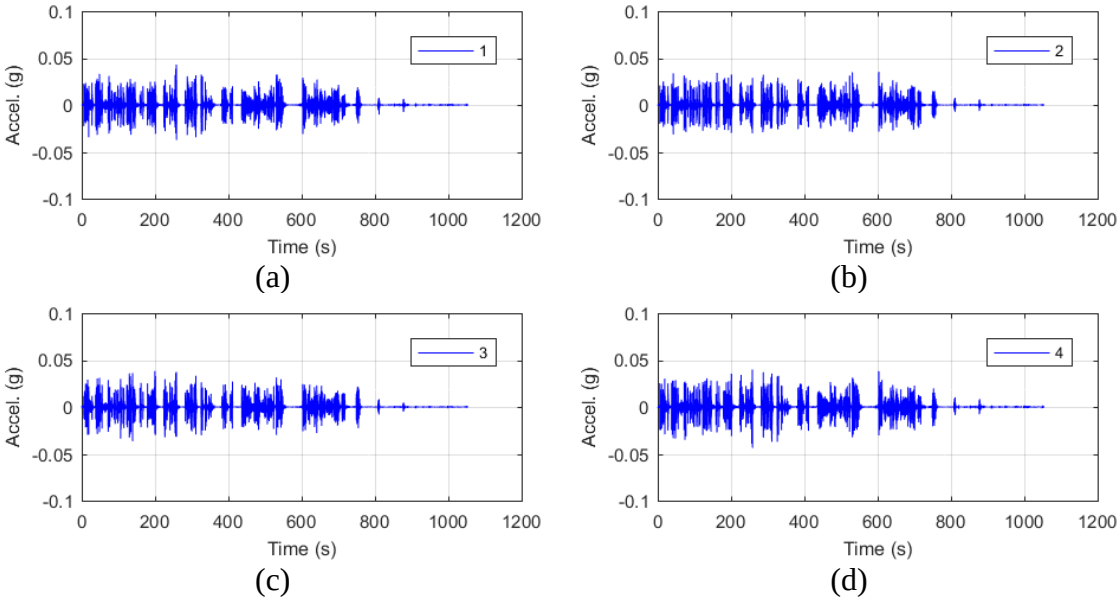

Figure C.126: Filtered acceleration data of the global response for bridge M011022220.

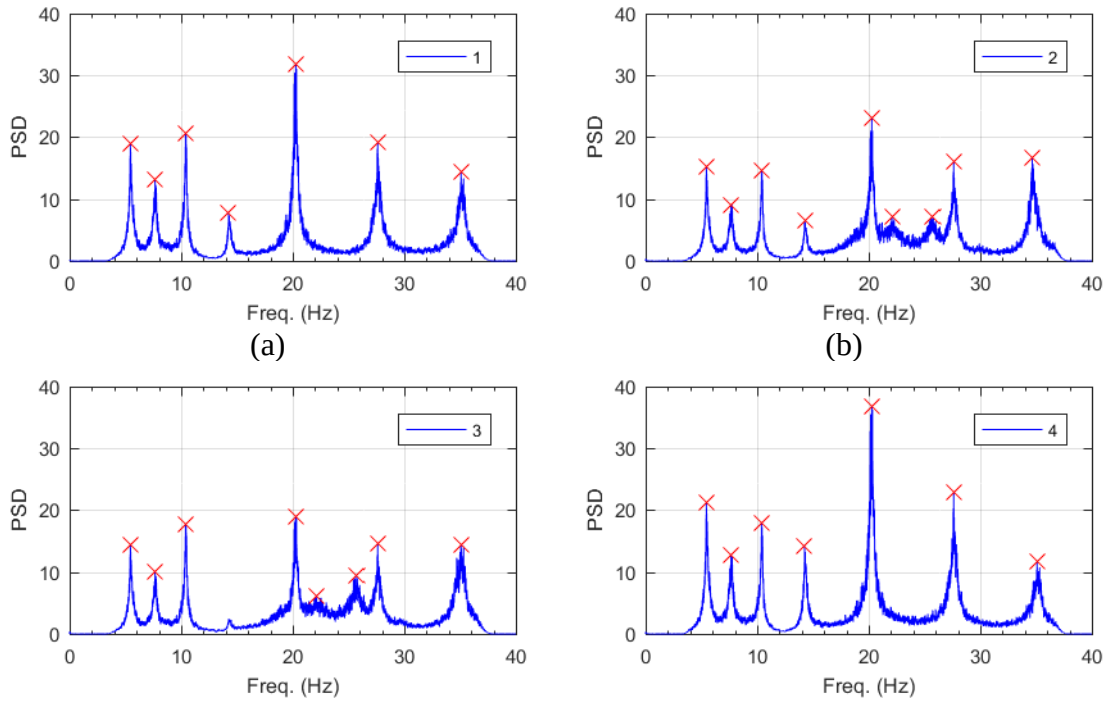

Figure C.127: Frequency content of the filtered acceleration data and peak-picking frequencies of the global response for bridge M011022220.

Table C.111: Filtered acceleration RMS values of the global response for bridge M011022220.

Sensor	**Filtered a_{RMS} (μg)**
1	3217
2	2836
3	2739
4	3519

Table C.112: Peak-picking frequencies of the global response for bridge M011022220.

Mode	**Individual Sensor Frequencies (Hz)**			
	1	**2**	**3**	**4**
1	5.45	5.45	5.45	5.45
2	7.66	7.66	7.66	7.66
3	10.39	10.39	10.39	10.39
4	14.25	14.25	--	14.25
5	20.27	20.27	20.27	20.27

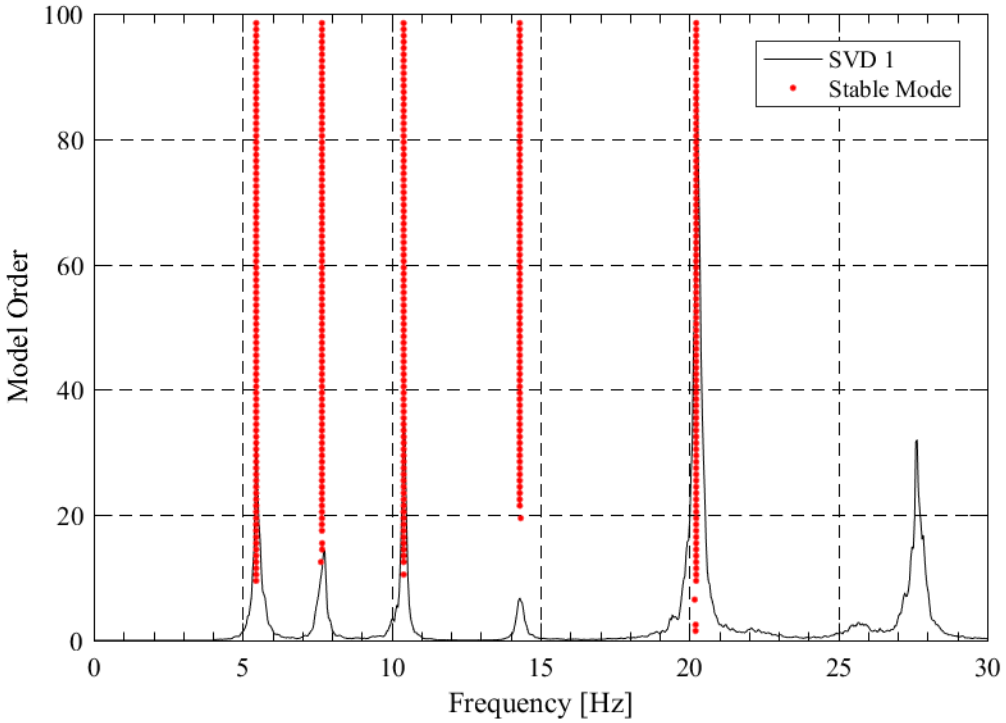

Figure C.128: SSI-UPCX method stabilization diagram of the global response for bridge M011022220.

Table C.113: SSI-UPCX method dynamic properties of the global response for bridge M011022220.

Mode	Frequency (Hz)	Damping (%)	Complexity (%)
1	5.46	1.80	0.00
2	7.66	1.71	0.07
3	10.41	0.86	0.02
4	14.31	0.83	0.04
5	20.23	0.77	0.02

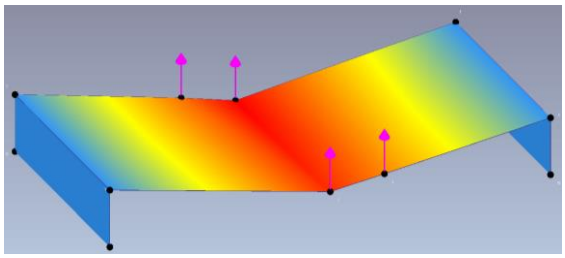

(a) Mode 1

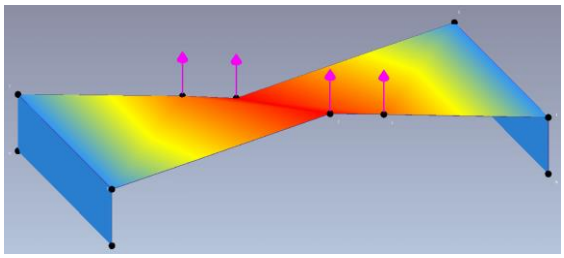

(b) Mode 2

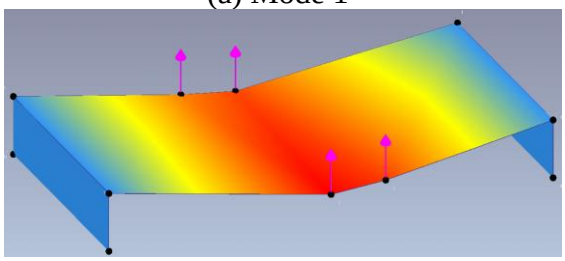

(c) Mode 3

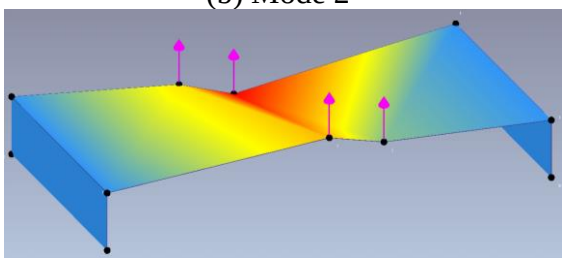

(d) Mode 4

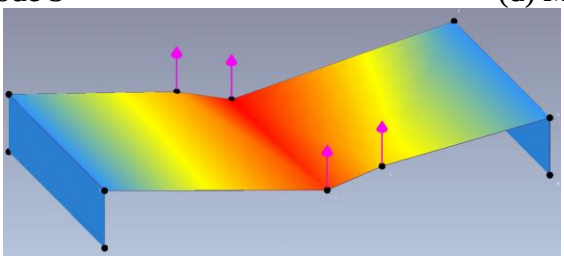

(e) Mode 5

Figure C.129: Operational deflected shapes of the global response for bridge M011022220.

Table C.114: Operational deflected shape coordinates of the global response for bridge M011022220.

Sensor	**ODS Coordinates**				
	Mode 1	**Mode 2**	**Mode 3**	**Mode 4**	**Mode 5**
1	0.89	-1.00	1.00	-0.56	0.86
2	0.73	0.72	0.69	0.46	0.60
3	0.68	-0.76	0.86	-0.17	0.50
4	1.00	1.00	0.84	1.00	1.00

Table C.115: MAC values of the global response for bridge M011022220.

MAC	**Mode 1**	**Mode 2**	**Mode 3**	**Mode 4**	**Mode 5**
Mode 1	1.000	0.208	0.989	0.082	0.988
Mode 2	0.208	1.000	0.286	0.898	0.230
Mode 3	0.989	0.286	1.000	0.126	0.971
Mode 4	0.082	0.898	0.126	1.000	0.116
Mode 5	0.988	0.230	0.971	0.116	1.000

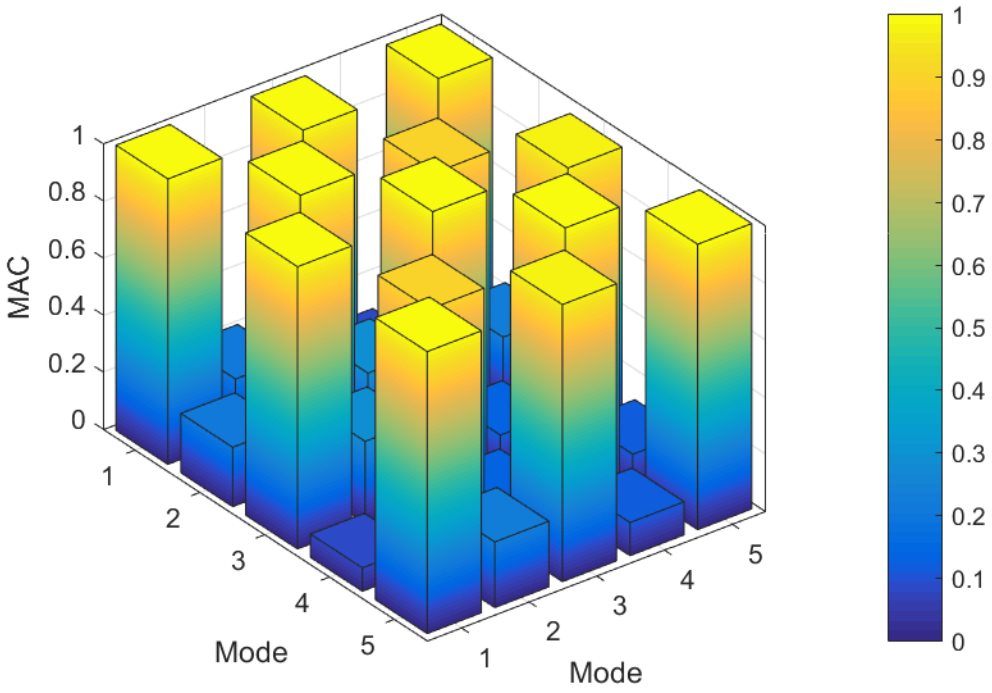

Figure C.130: MAC values of the global response for bridge M011022220.

APPENDIX D

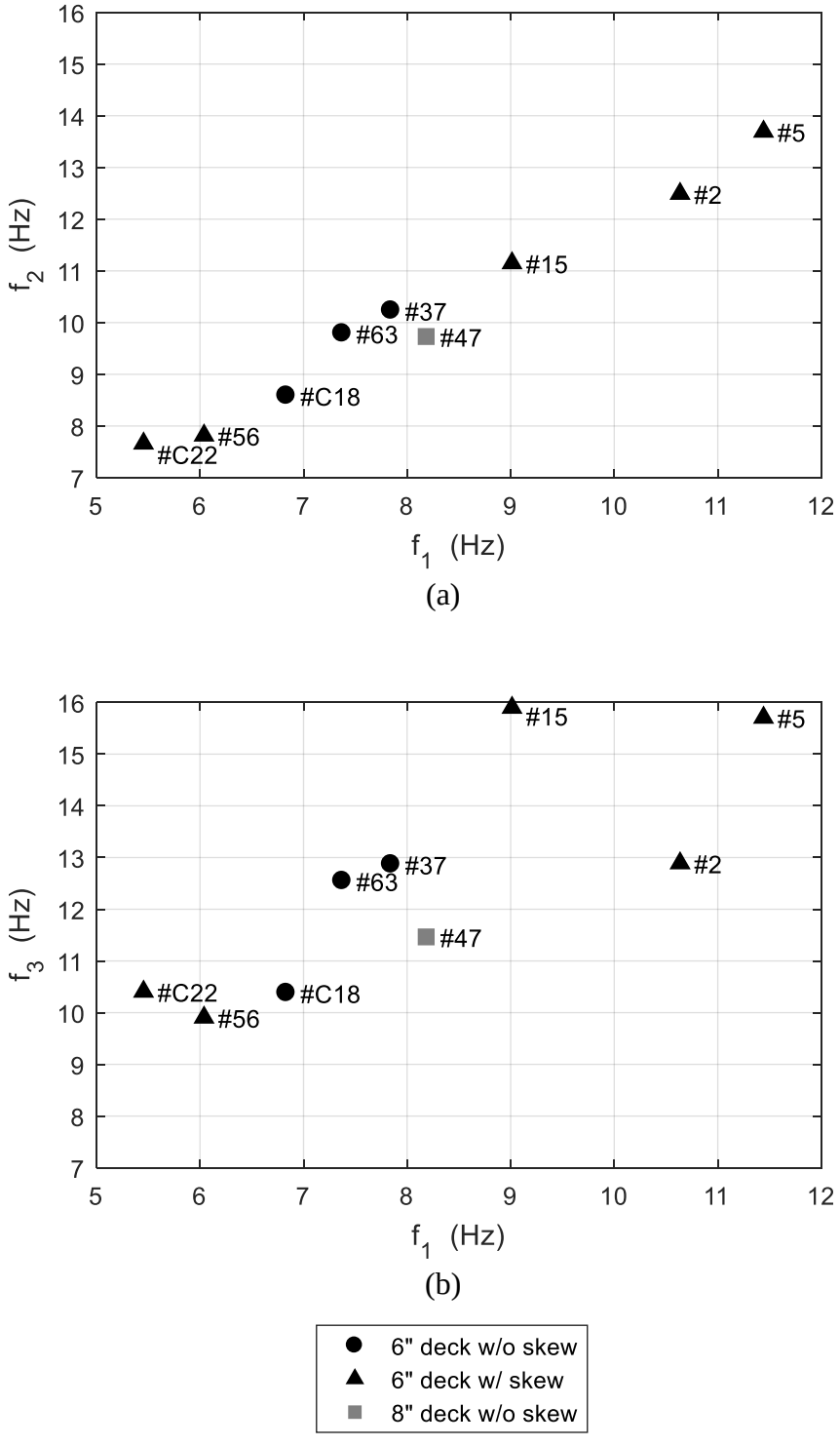

Figure D.1: System identification comparison of the modal frequencies for the instrumented IT bridges.

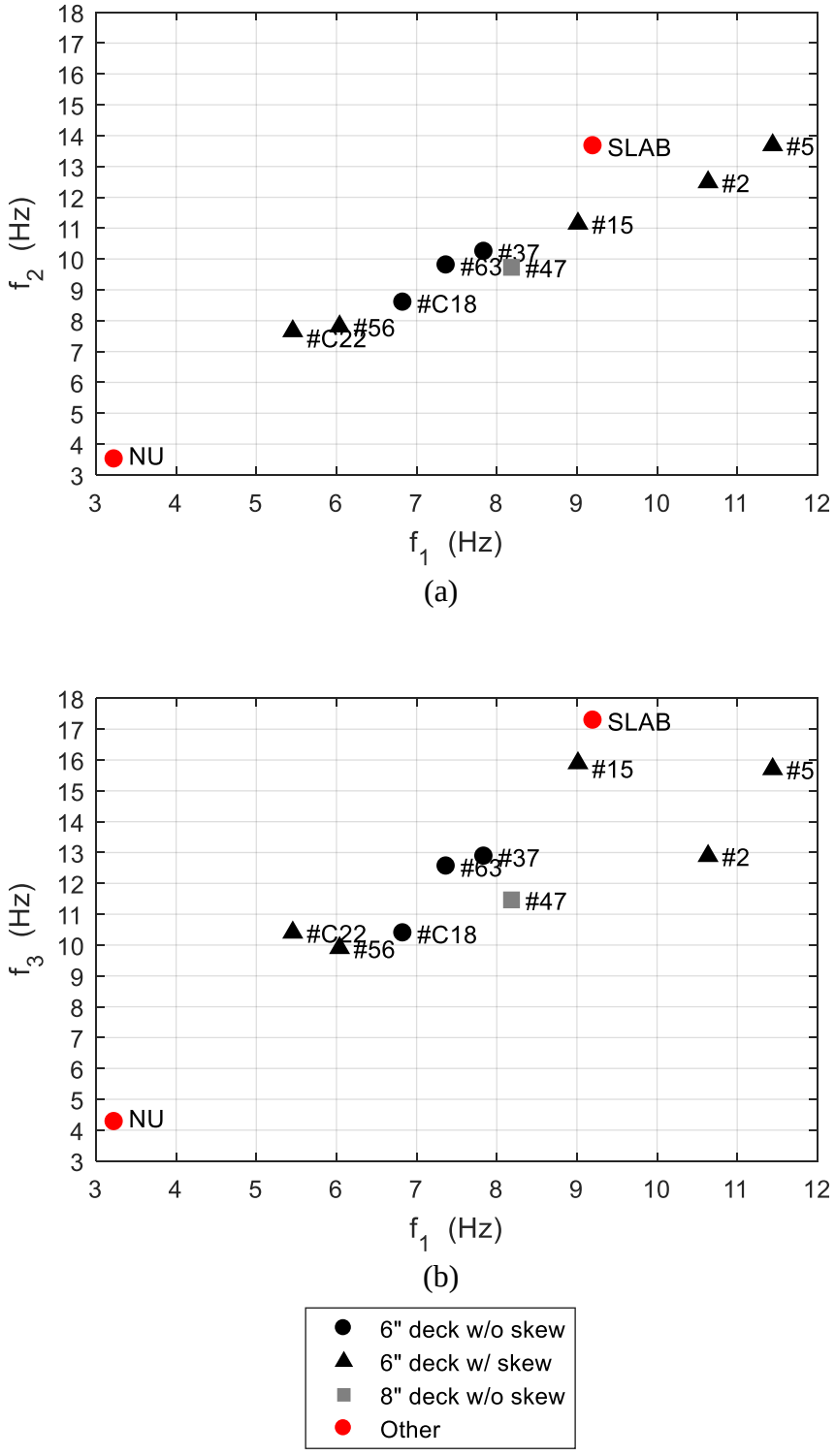

Figure D.2: System identification comparison of the modal frequencies for all instrumented bridges.

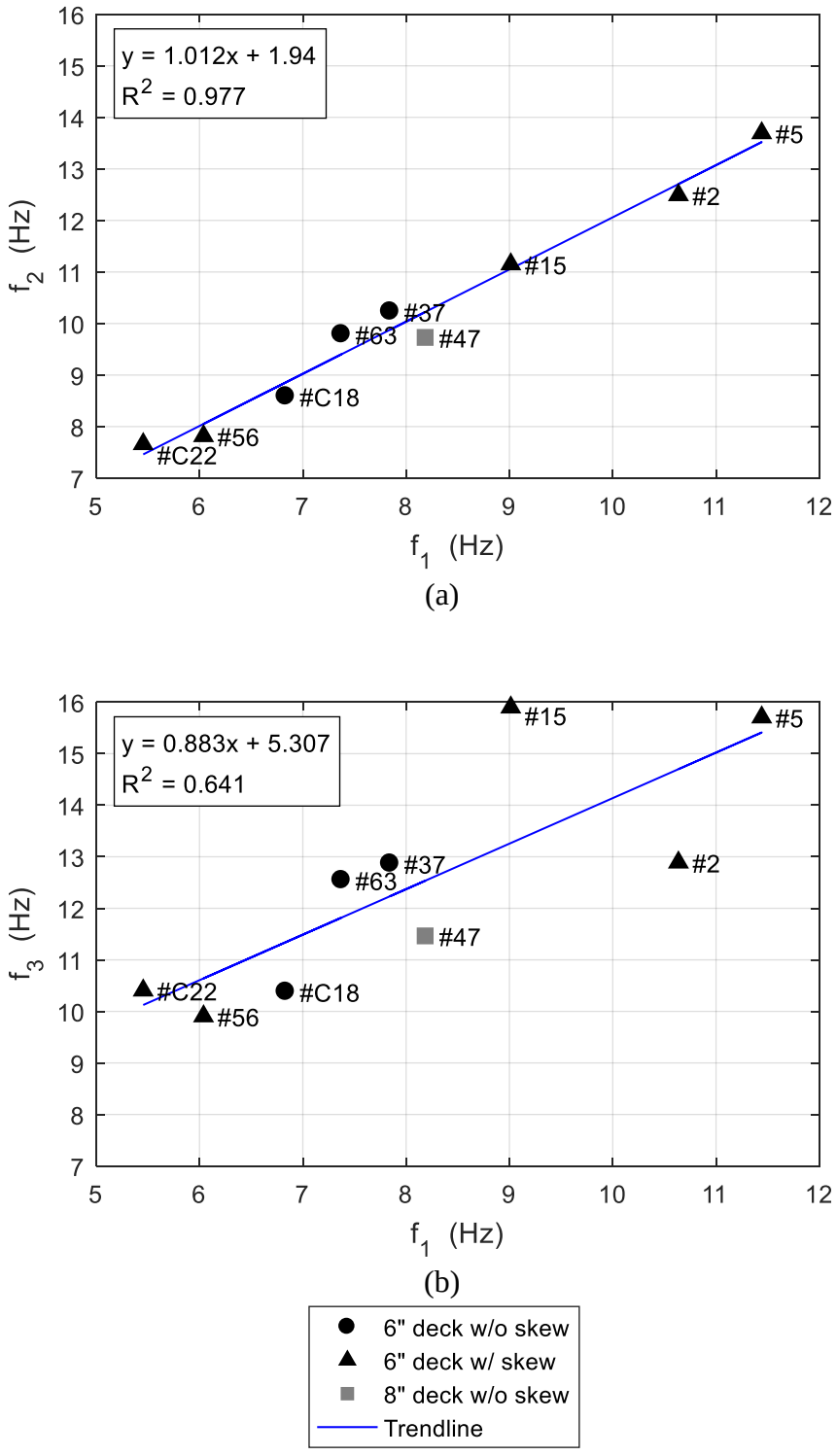

Figure D.3: System identification comparison of the modal frequencies with a trendline for the instrumented IT bridges.

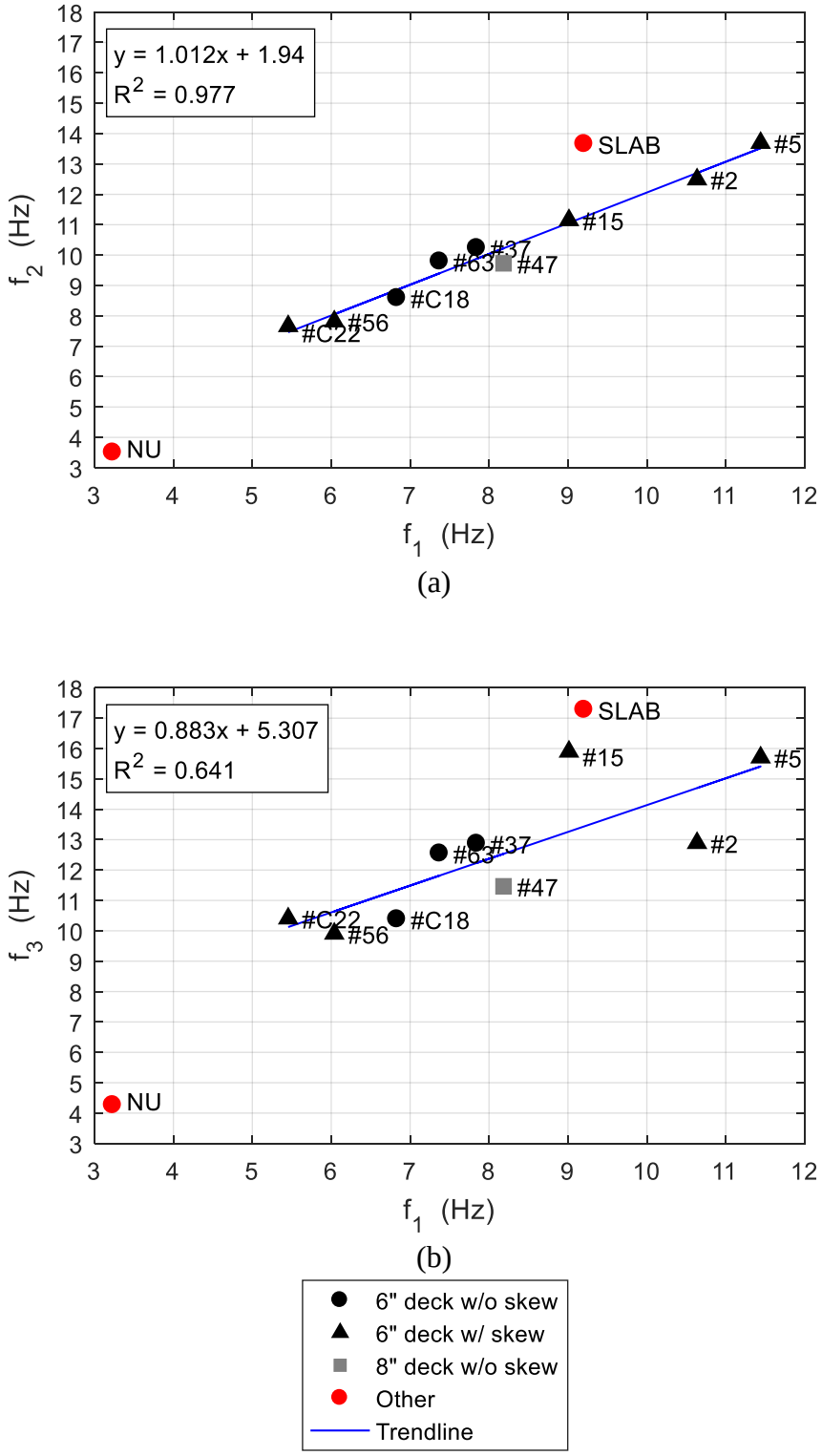

Figure D.4: System identification comparison of the modal frequencies with a trendline for all instrumented bridges.

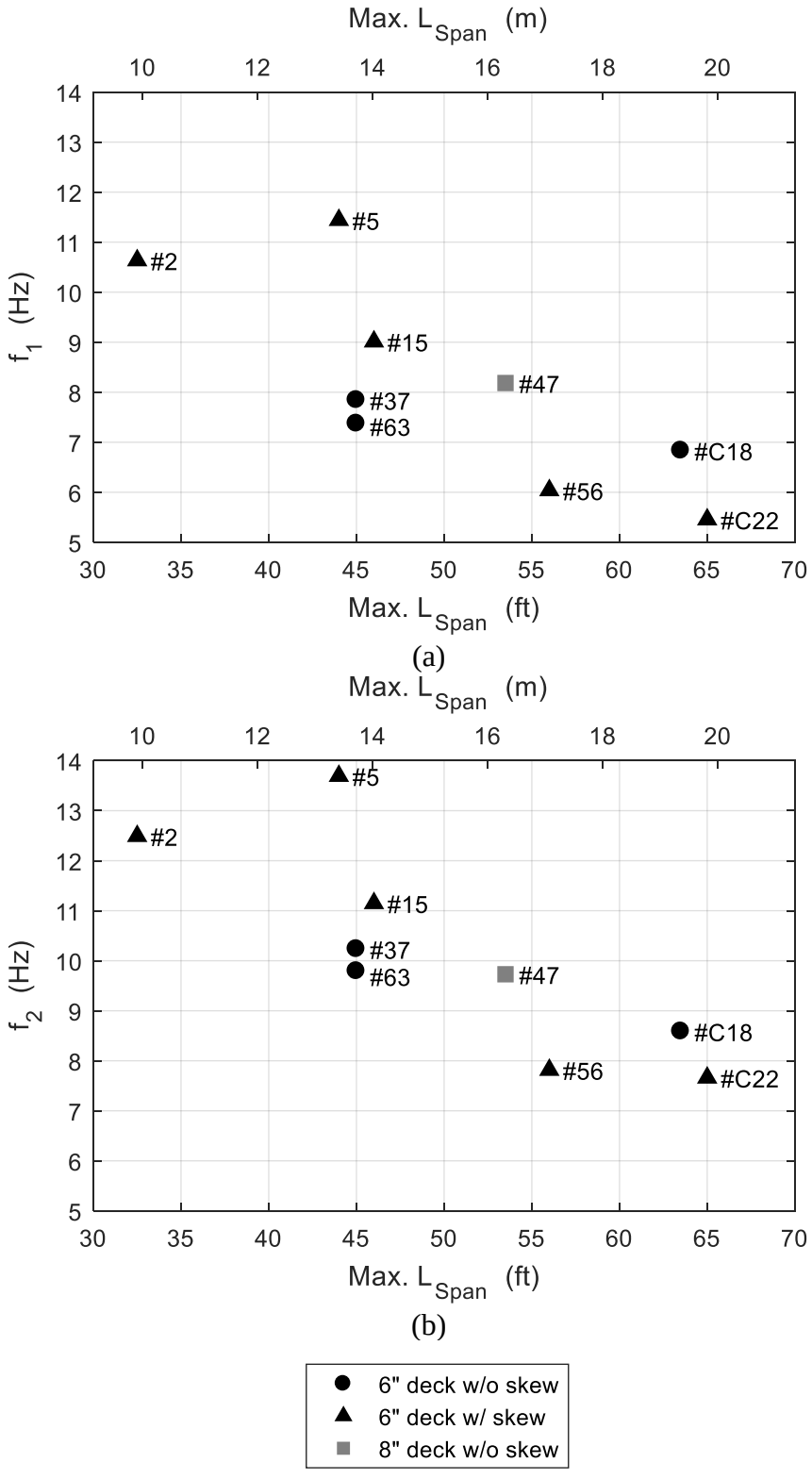

Figure D.5: System identification comparison of the maximum span length for the instrumented IT bridges.

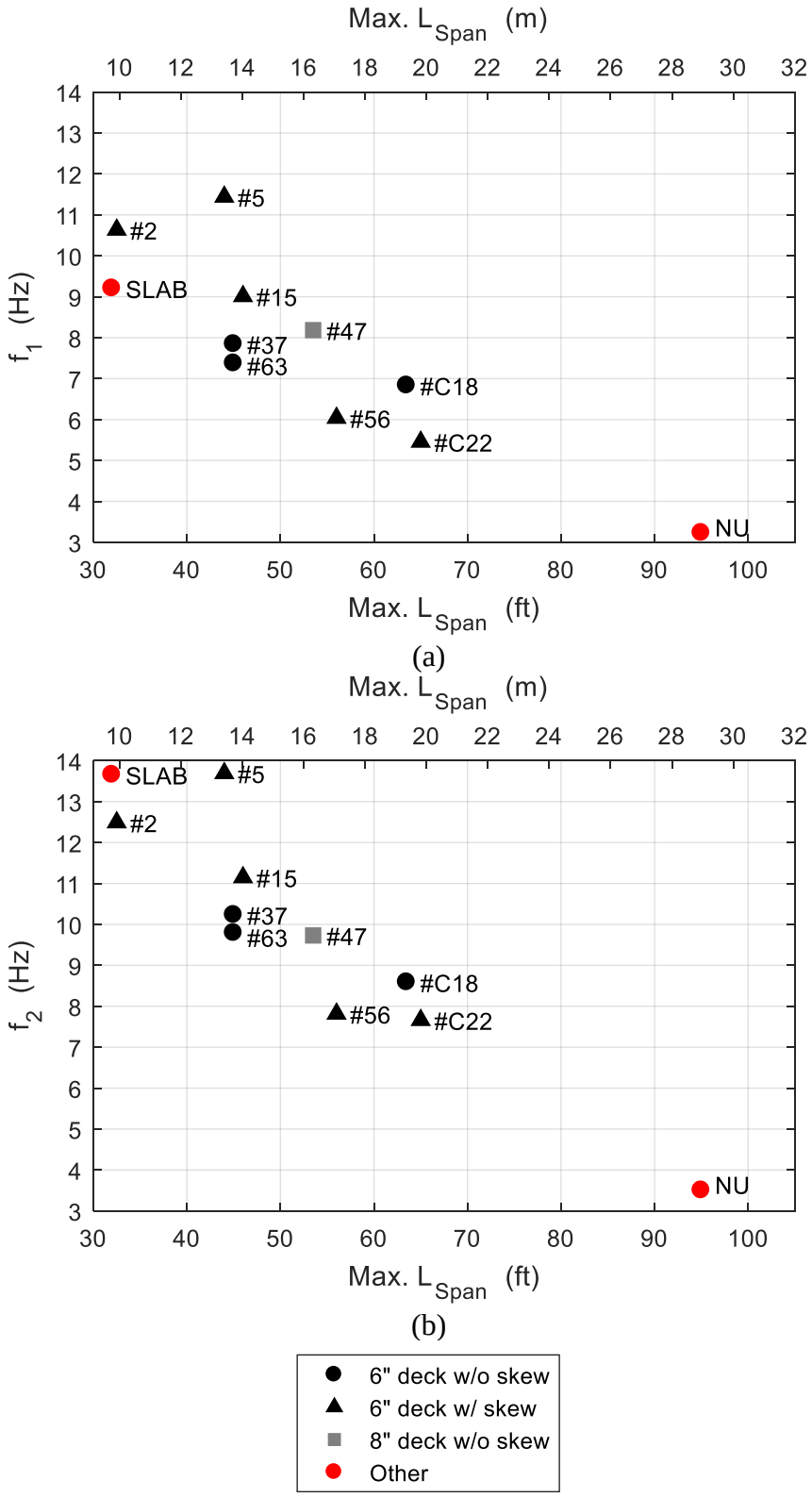

Figure D.6: System identification comparison of the maximum span length for all instrumented bridges.

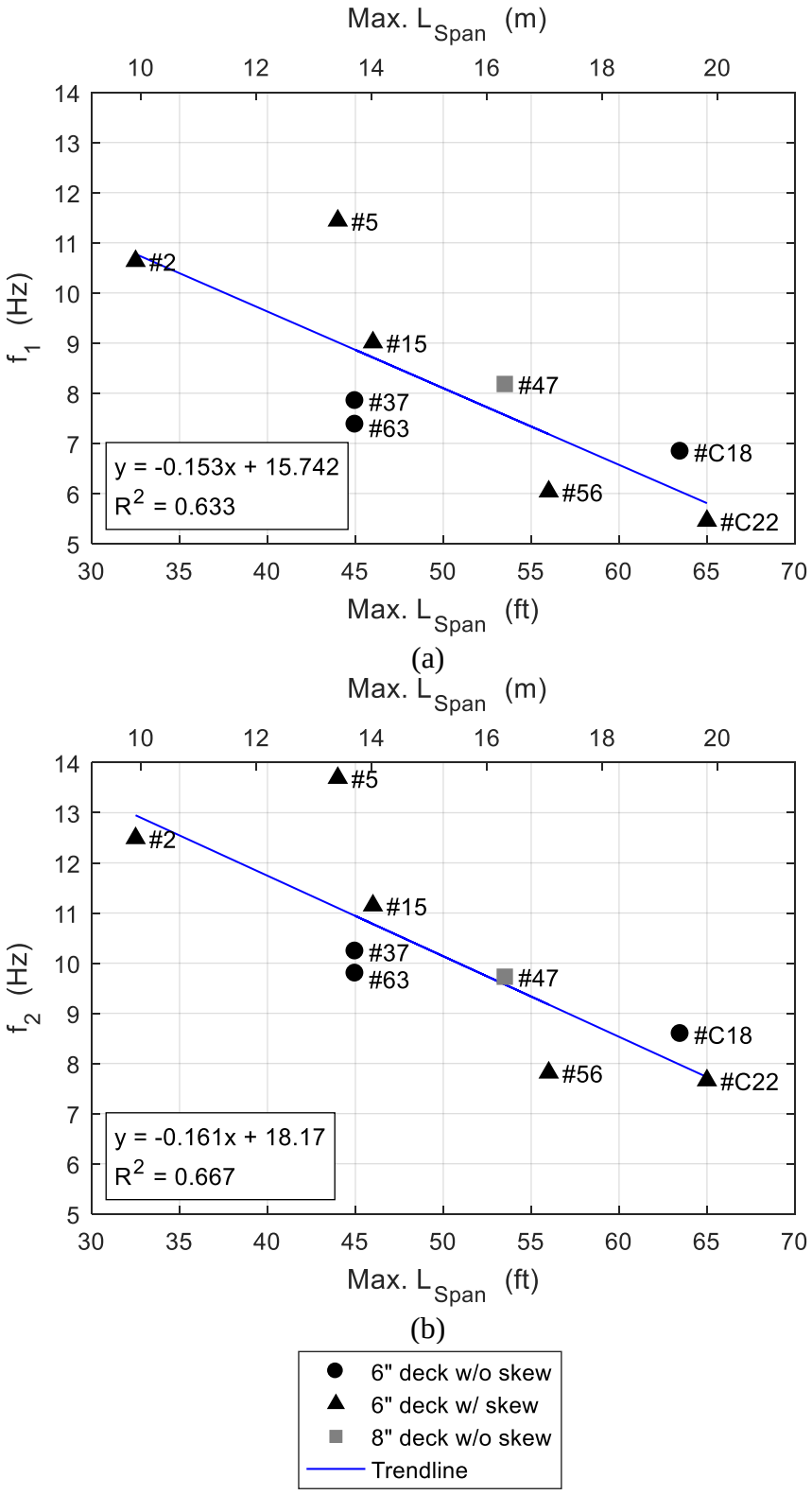

Figure D.7: System identification comparison of the maximum span length with a trendline for the instrumented IT bridges.

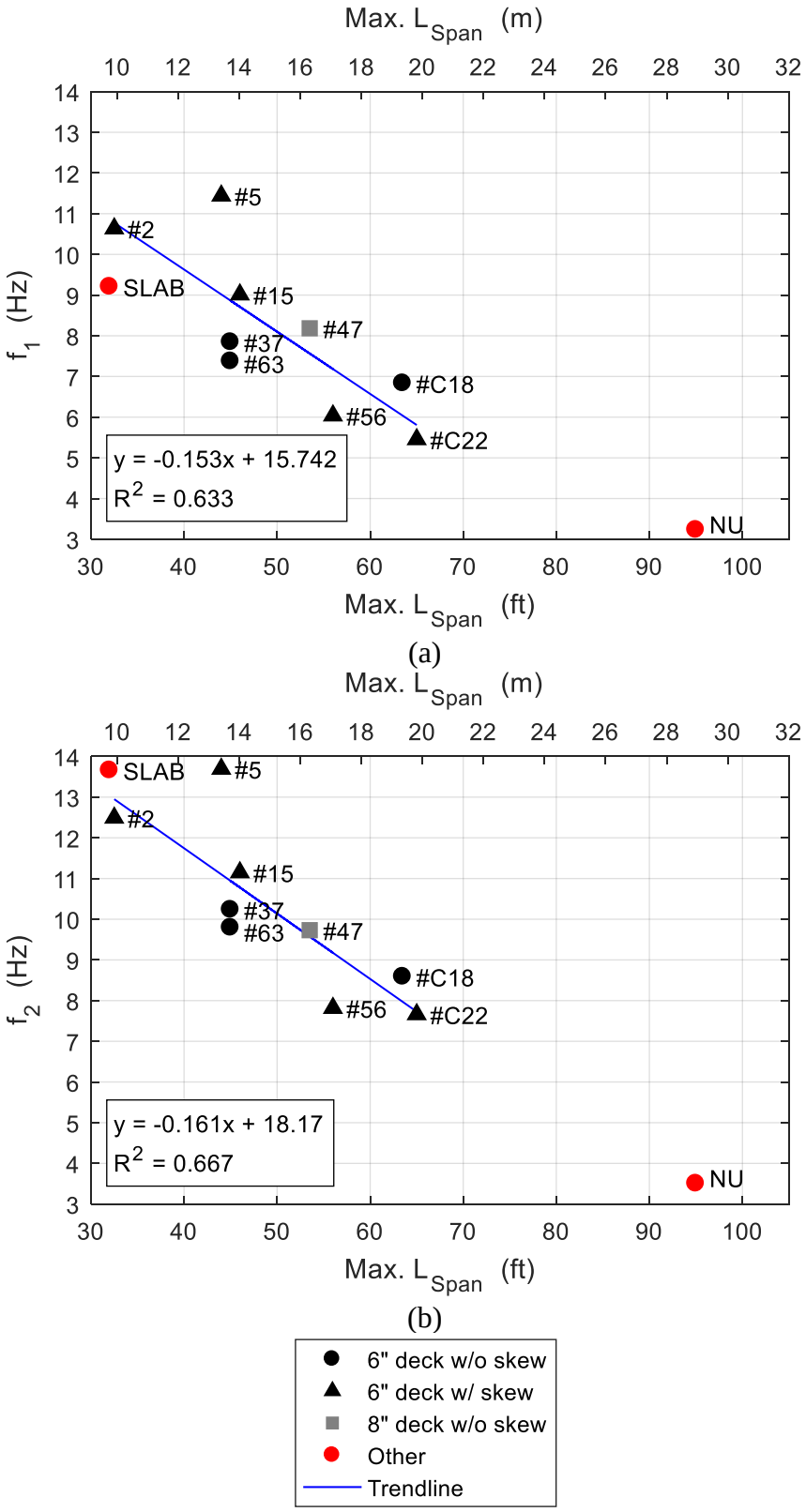

Figure D.8: System identification comparison of the maximum span length with a trendline for all instrumented bridges.

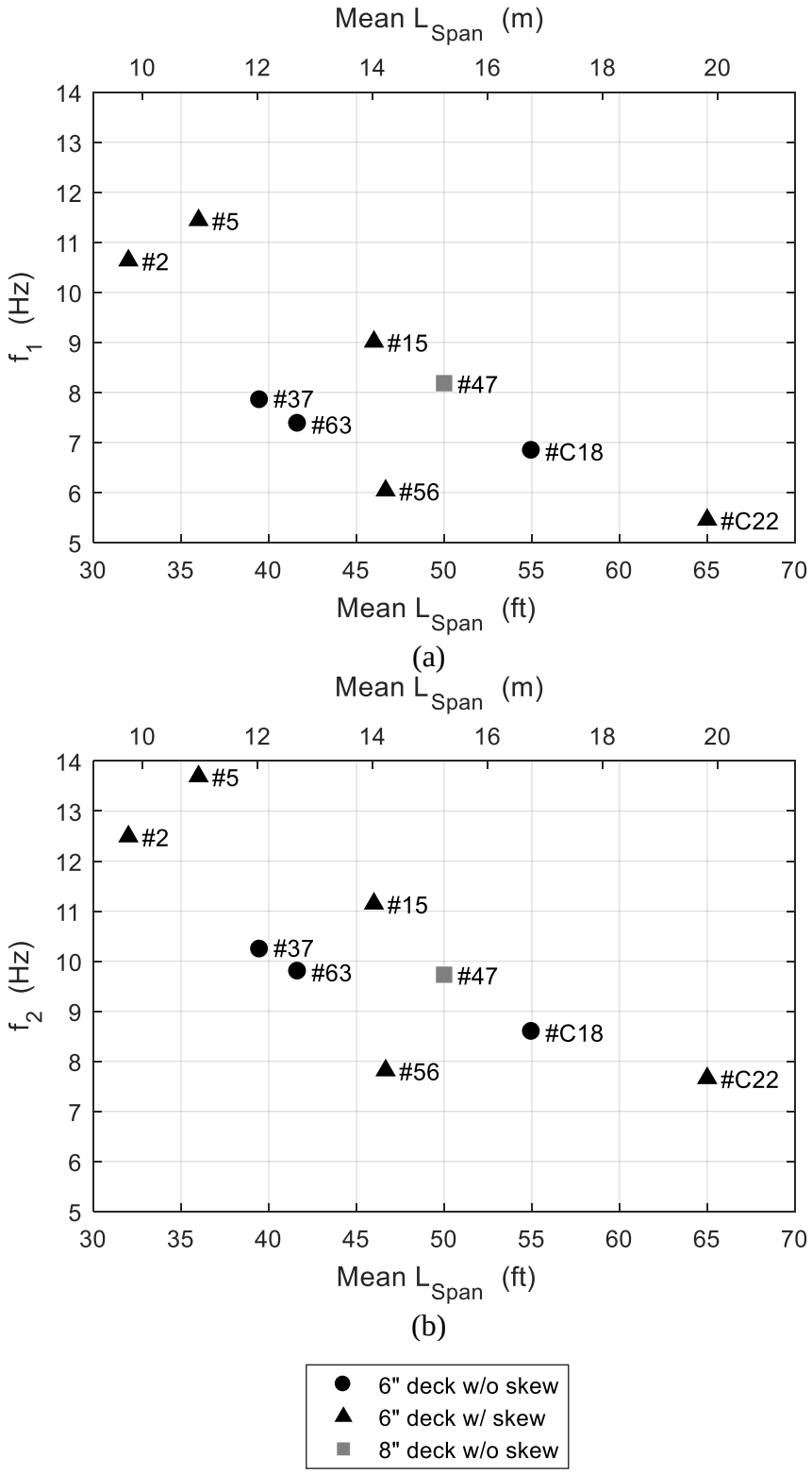

Figure D.9: System identification comparison of the mean span length for the instrumented IT bridges.

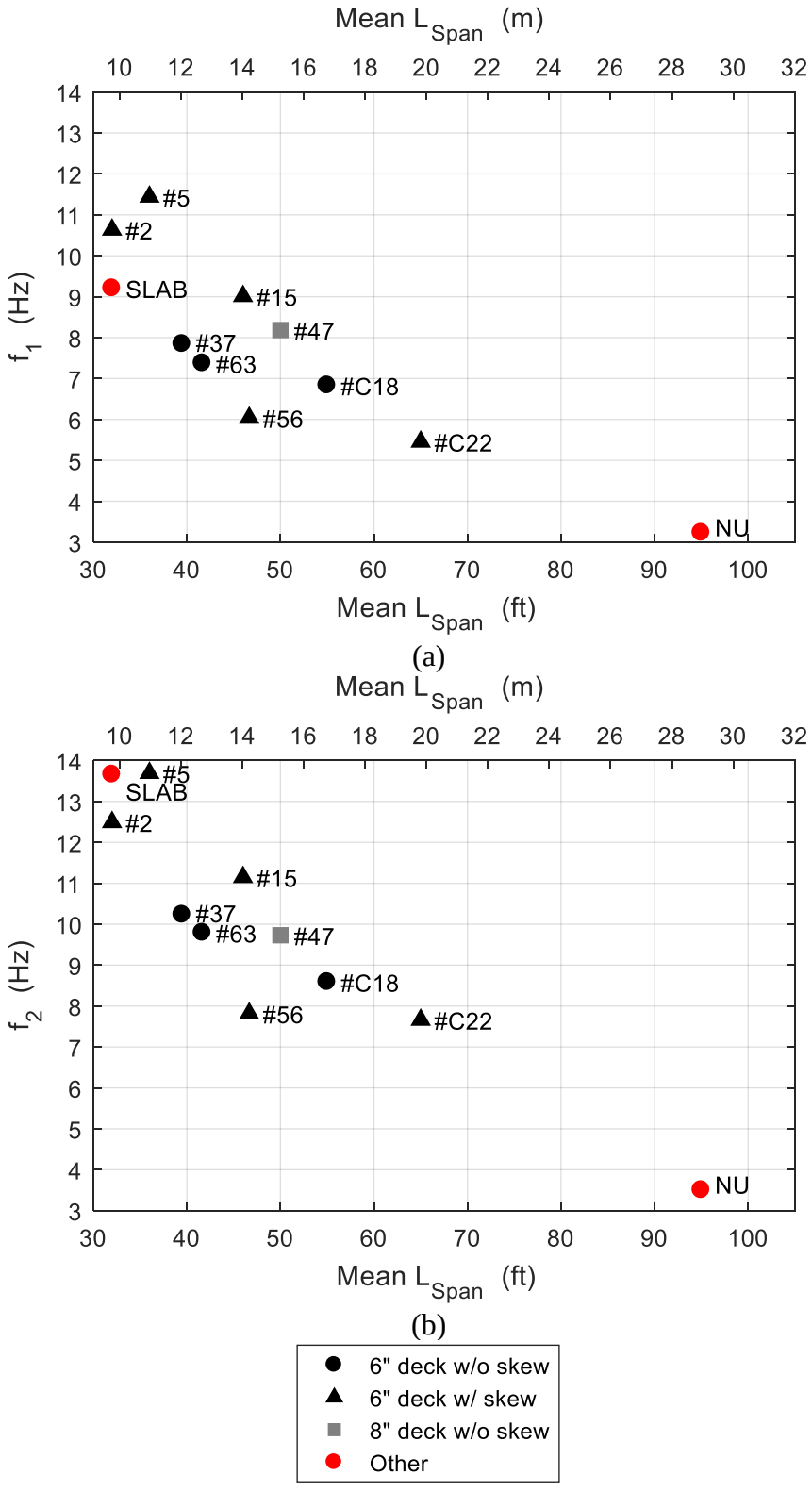

Figure D.10: System identification comparison of the mean span length for all instrumented bridges.

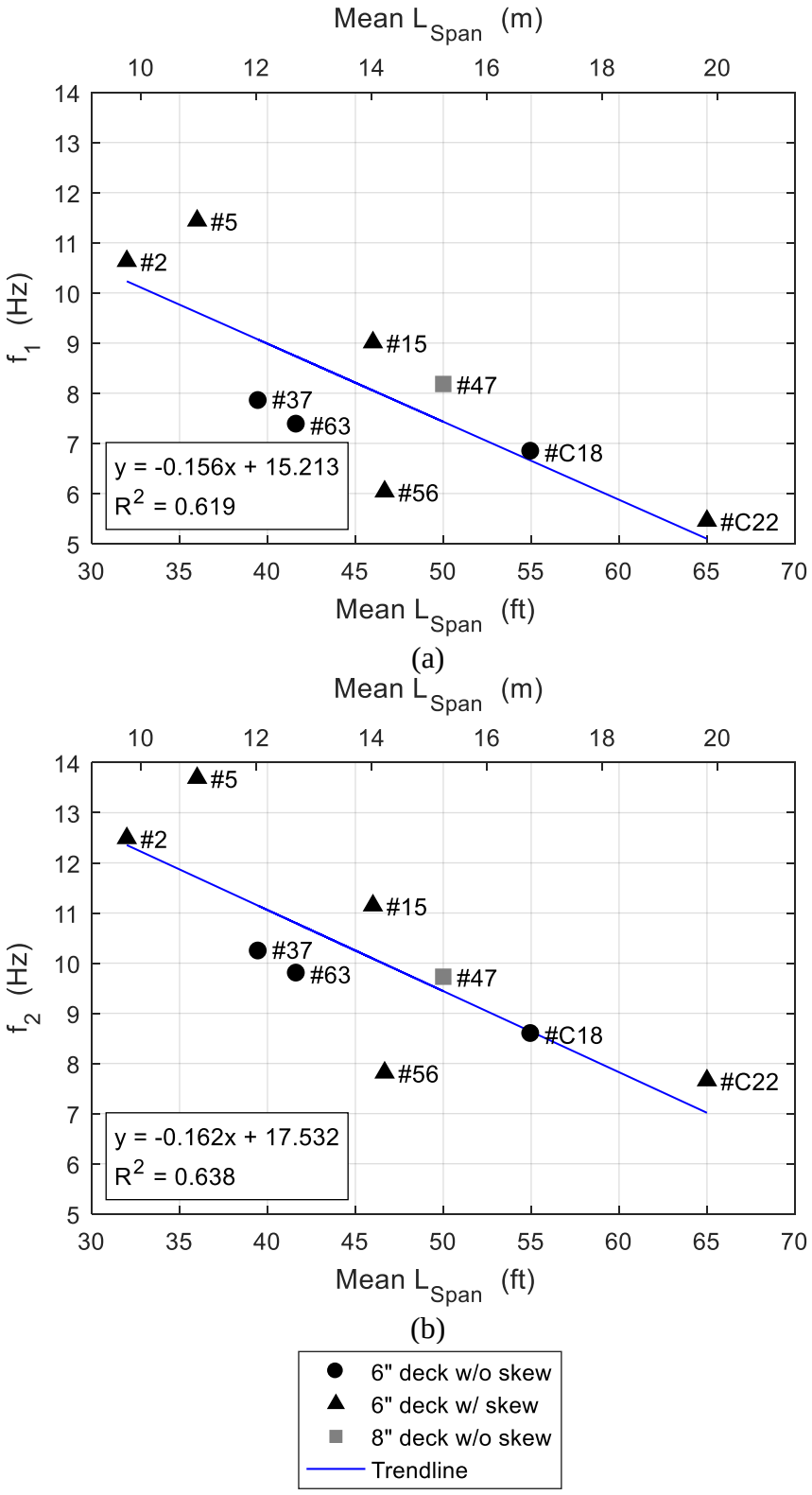

Figure D.11: System identification comparison of the mean span length with a trendline for the instrumented IT bridges.

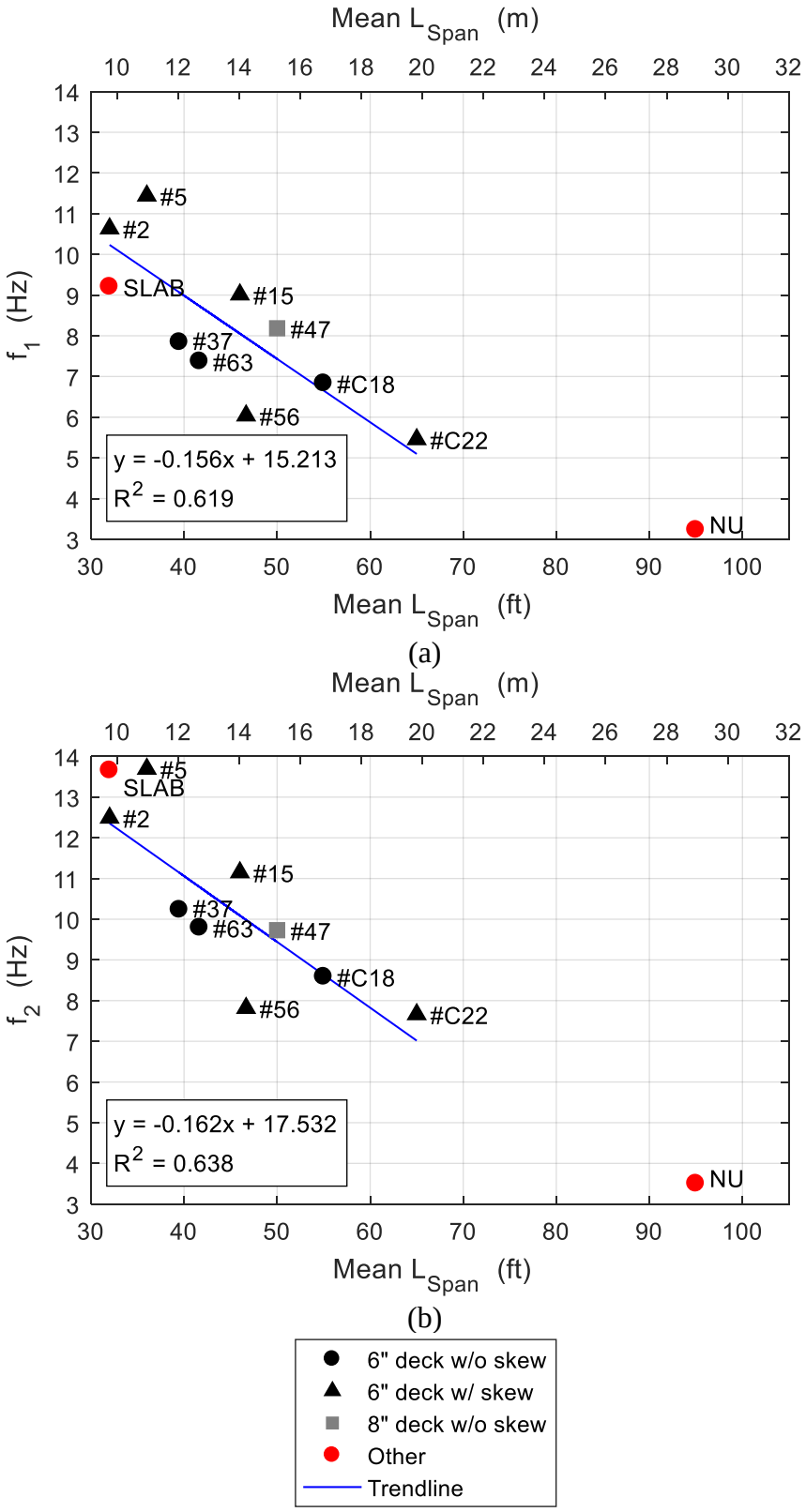

Figure D.12: System identification comparison of the mean span length with a trendline for all instrumented bridges.

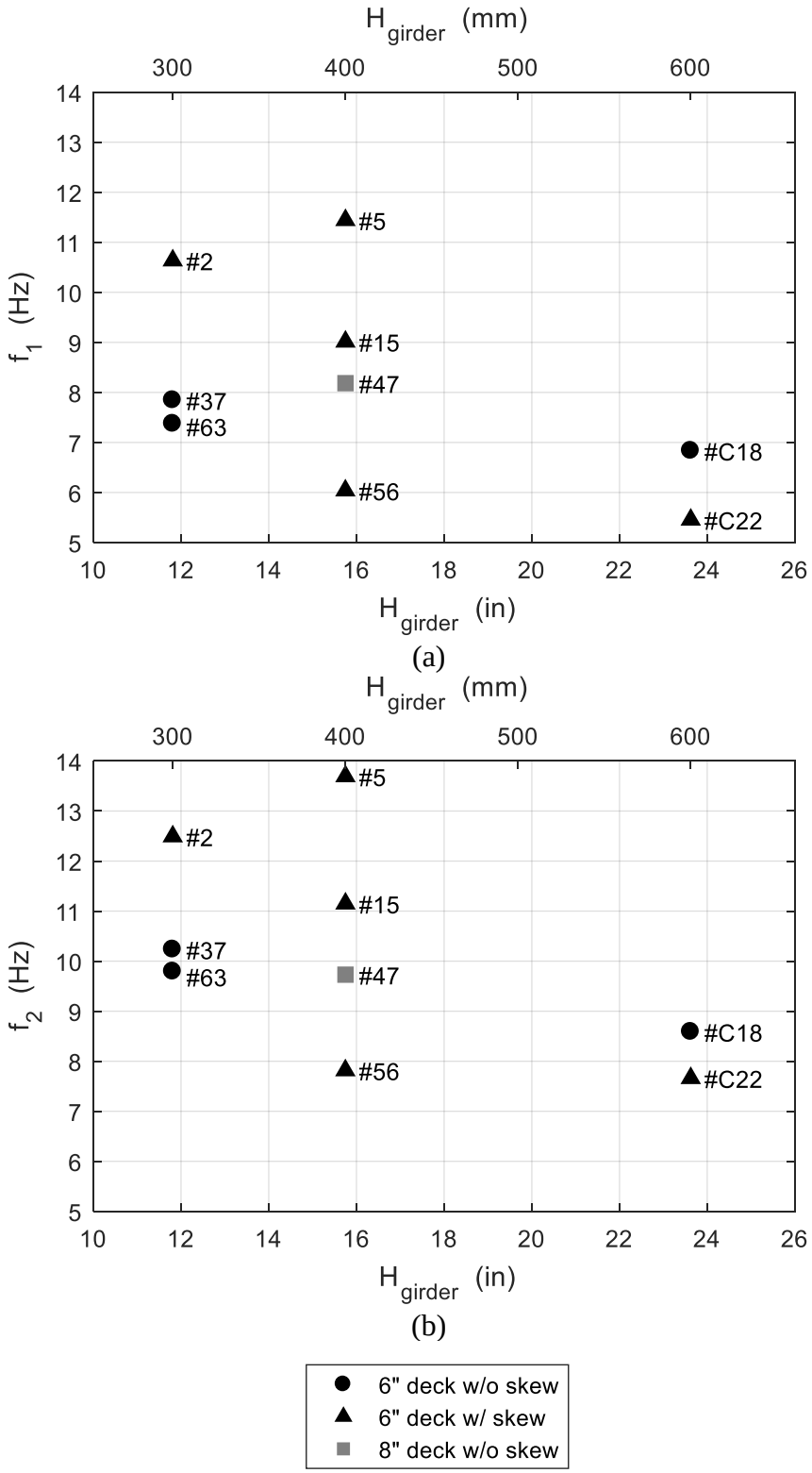

Figure D.13: System identification comparison of the girder height for the instrumented IT bridges.

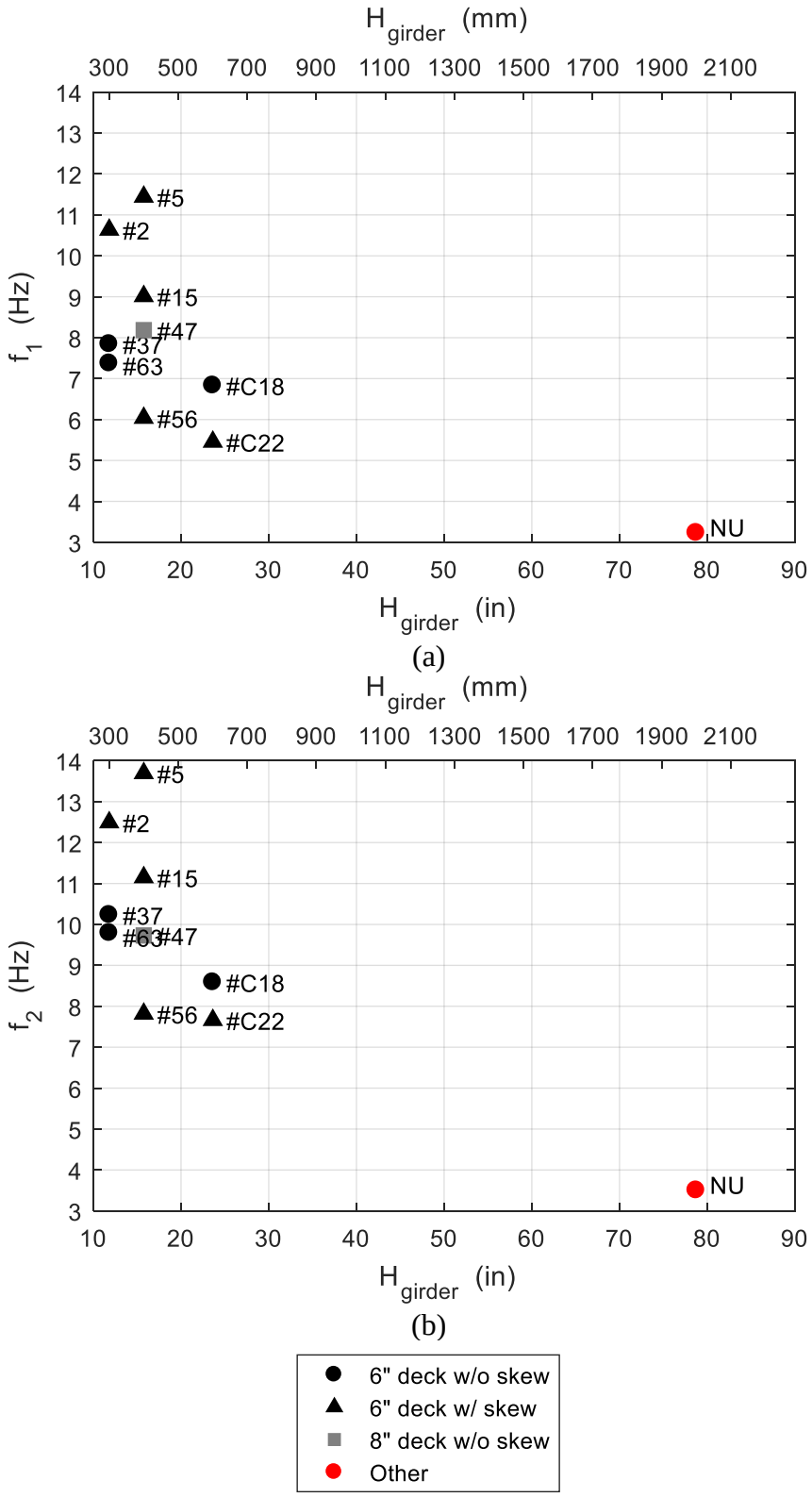

Figure D.14: System identification comparison of the girder height for all instrumented bridges.

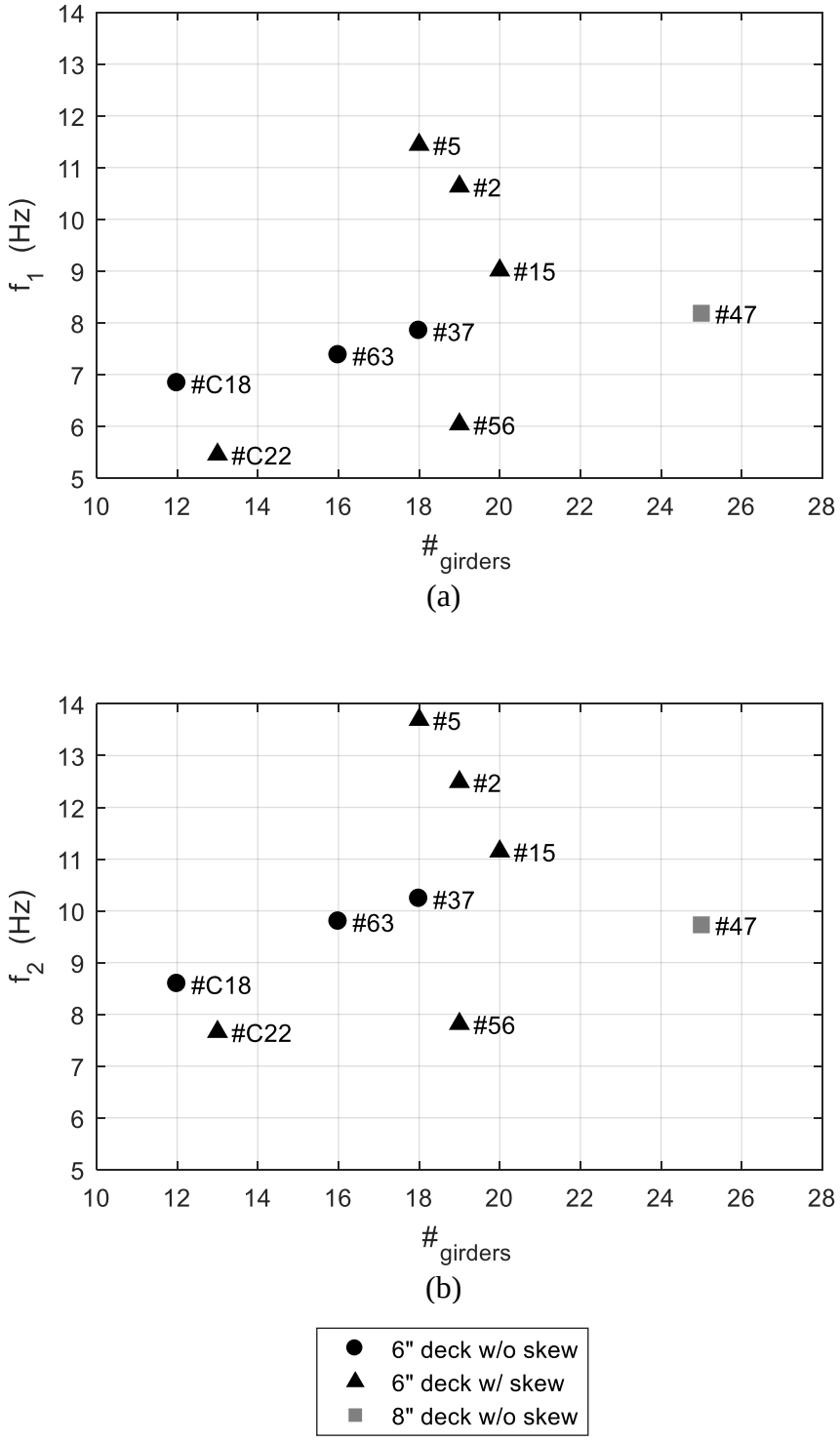

Figure D.15: System identification comparison of the number of girders for the instrumented IT bridges.

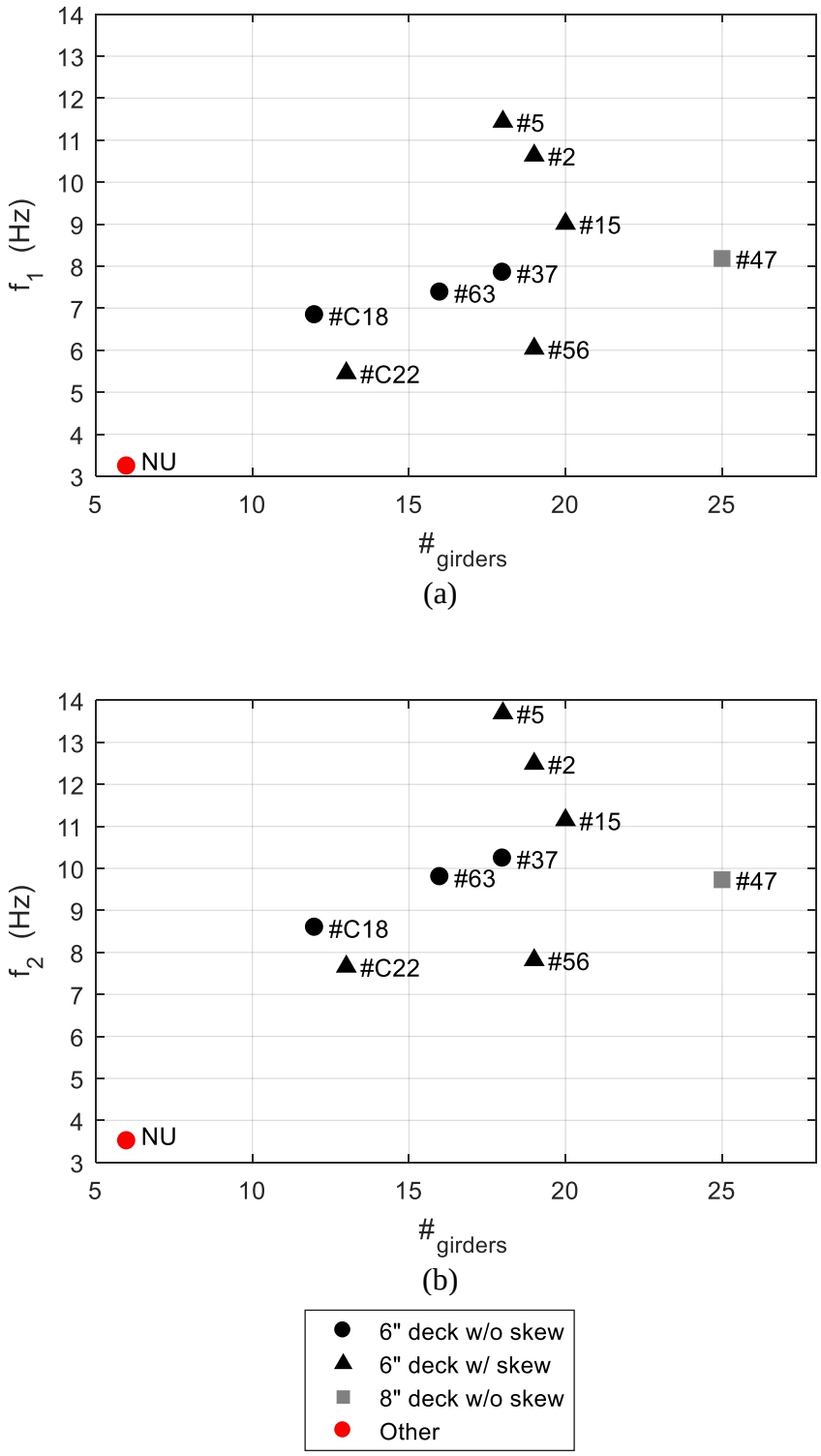

Figure D.16: System identification comparison of the number of girders for all instrumented bridges.

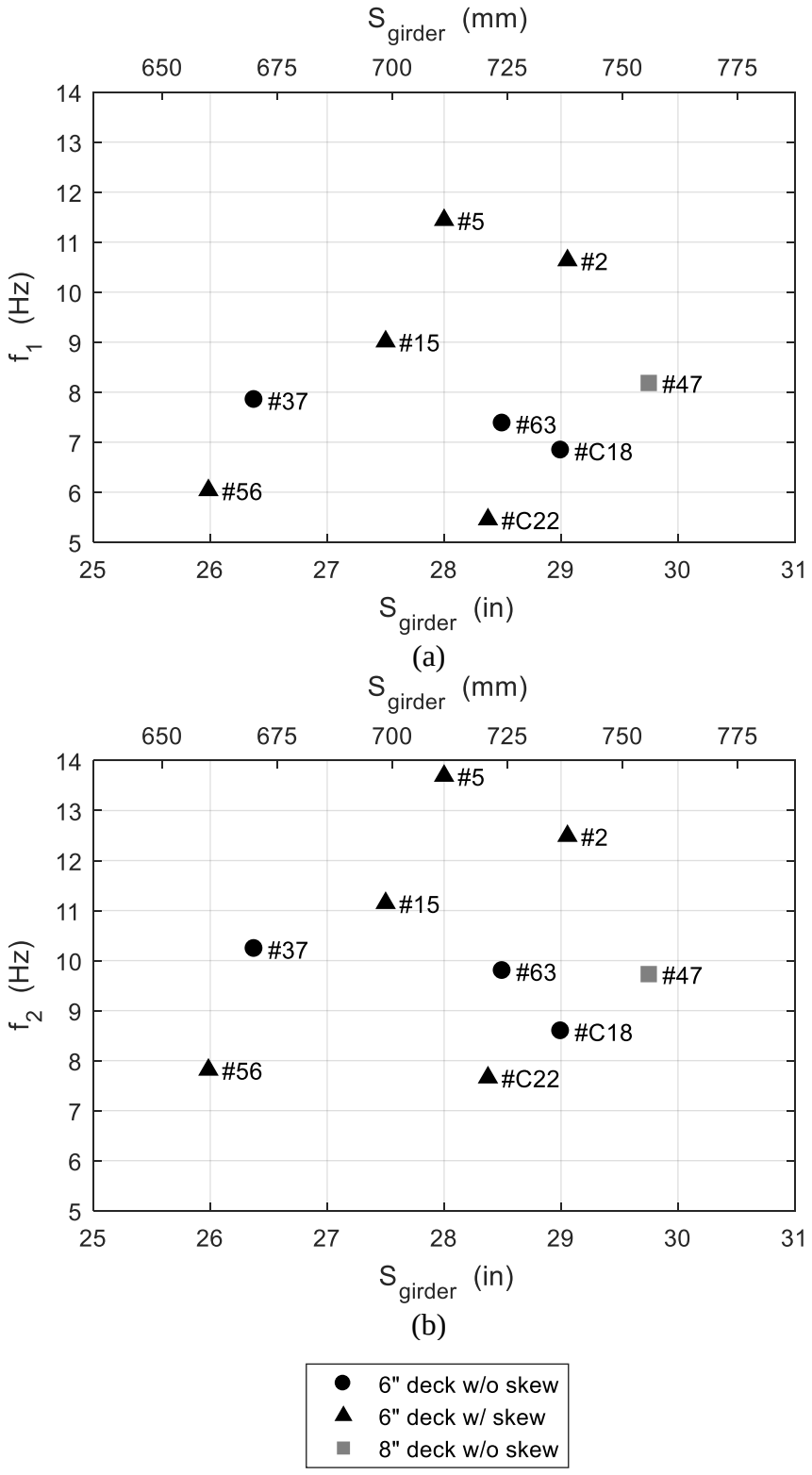

Figure D.17: System identification comparison of the girder spacing for the instrumented IT bridges.

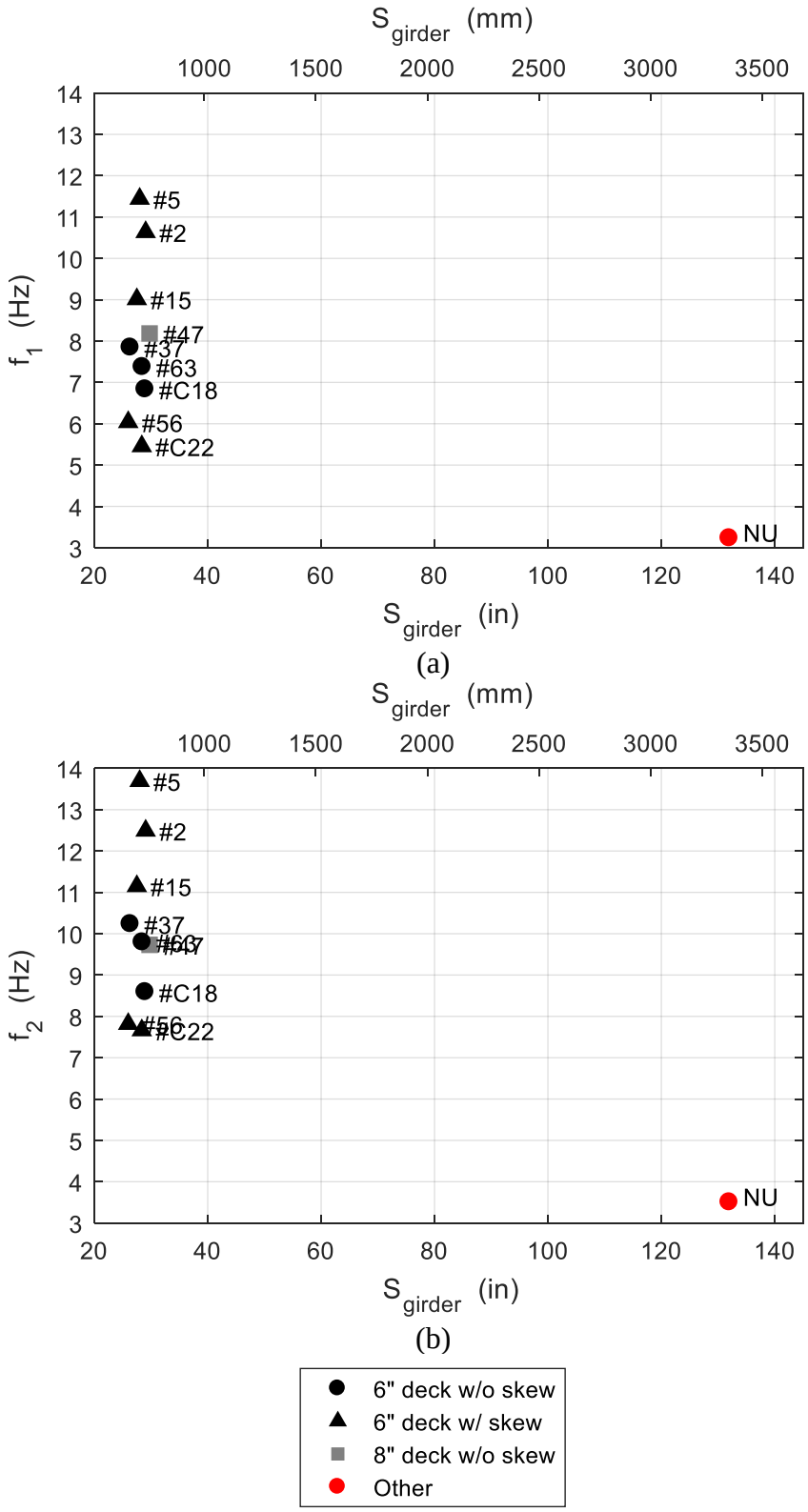

Figure D.18: System identification comparison of the girder spacing for all instrumented bridges.

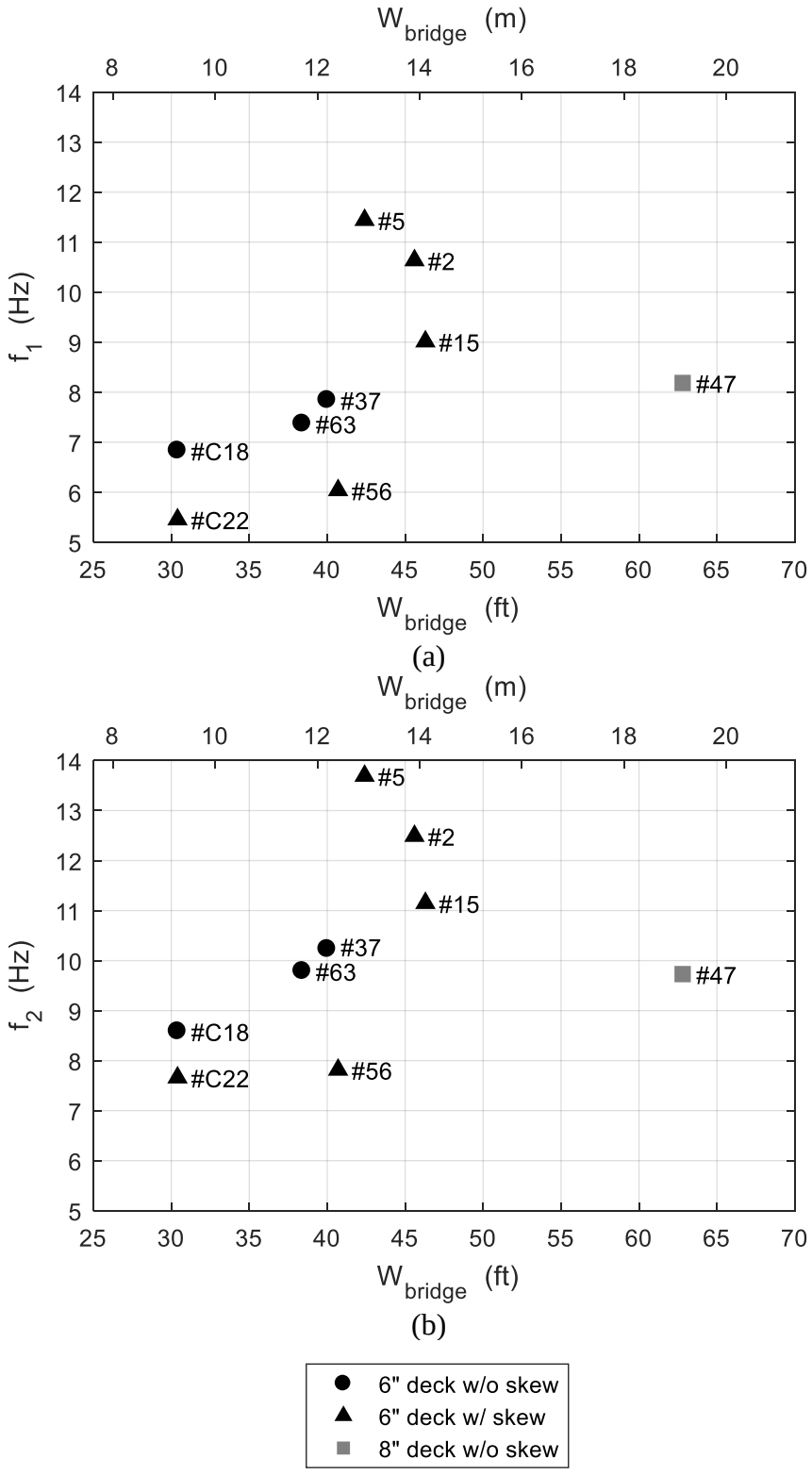

Figure D.19: System identification comparison of the bridge width for the instrumented IT bridges.

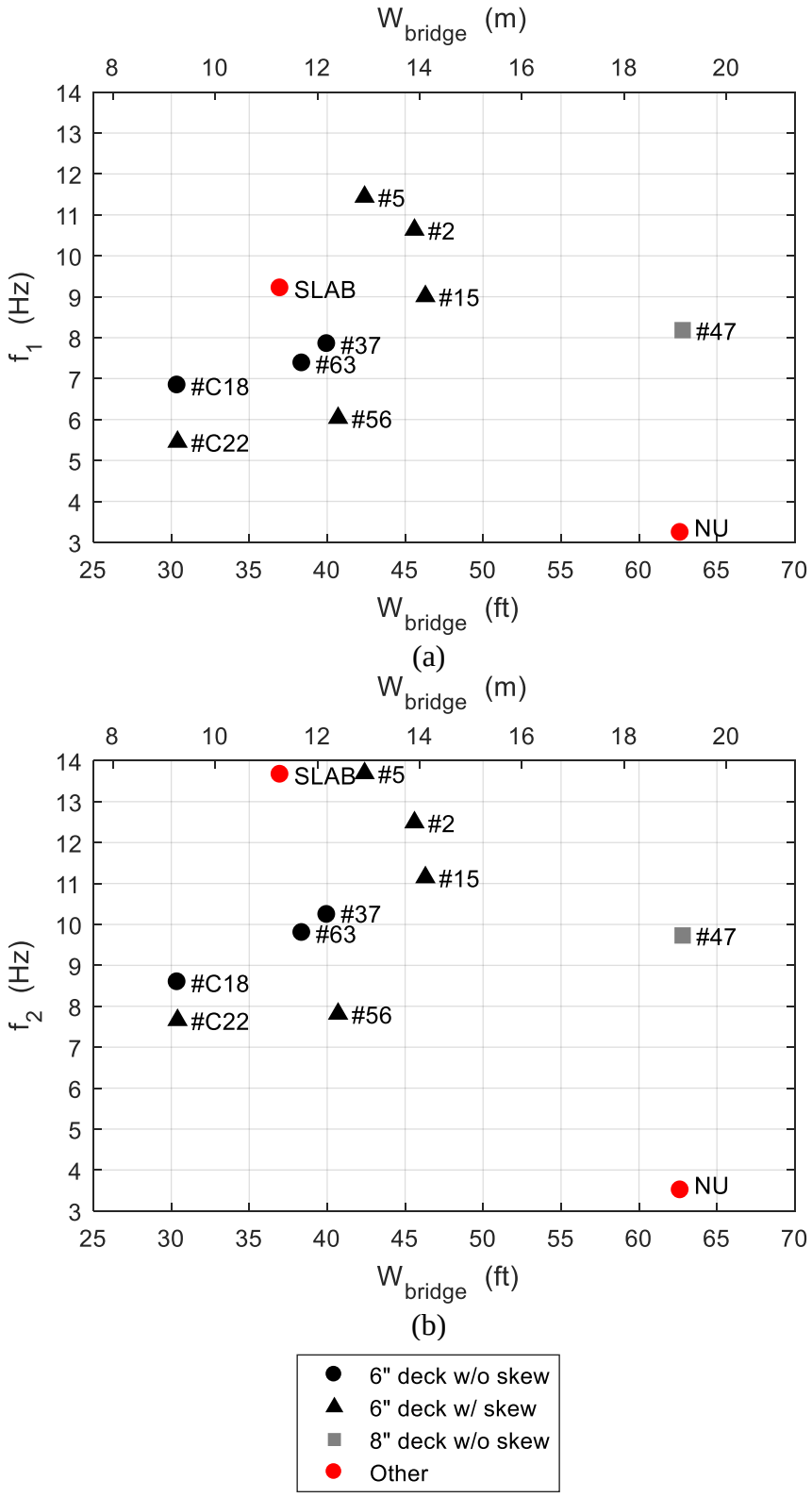

Figure D.20: System identification comparison of the bridge width for all instrumented bridges.

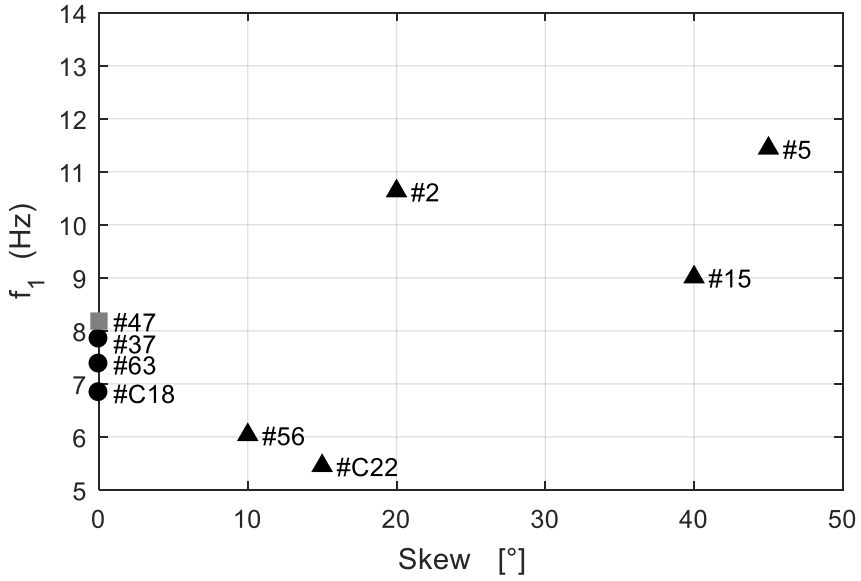

(a)

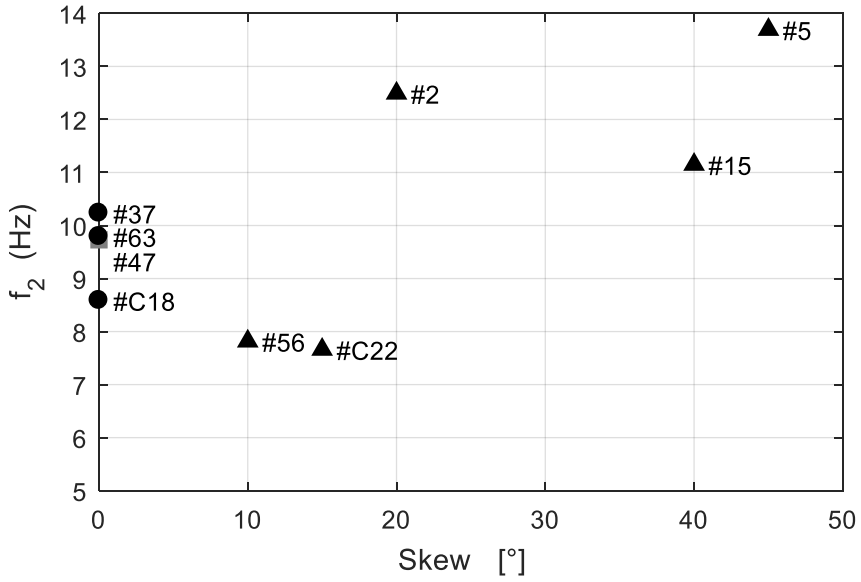

(b)

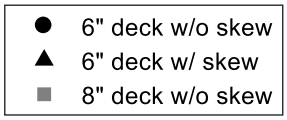

Figure D.21: System identification comparison of the skew angle for the instrumented IT bridges.

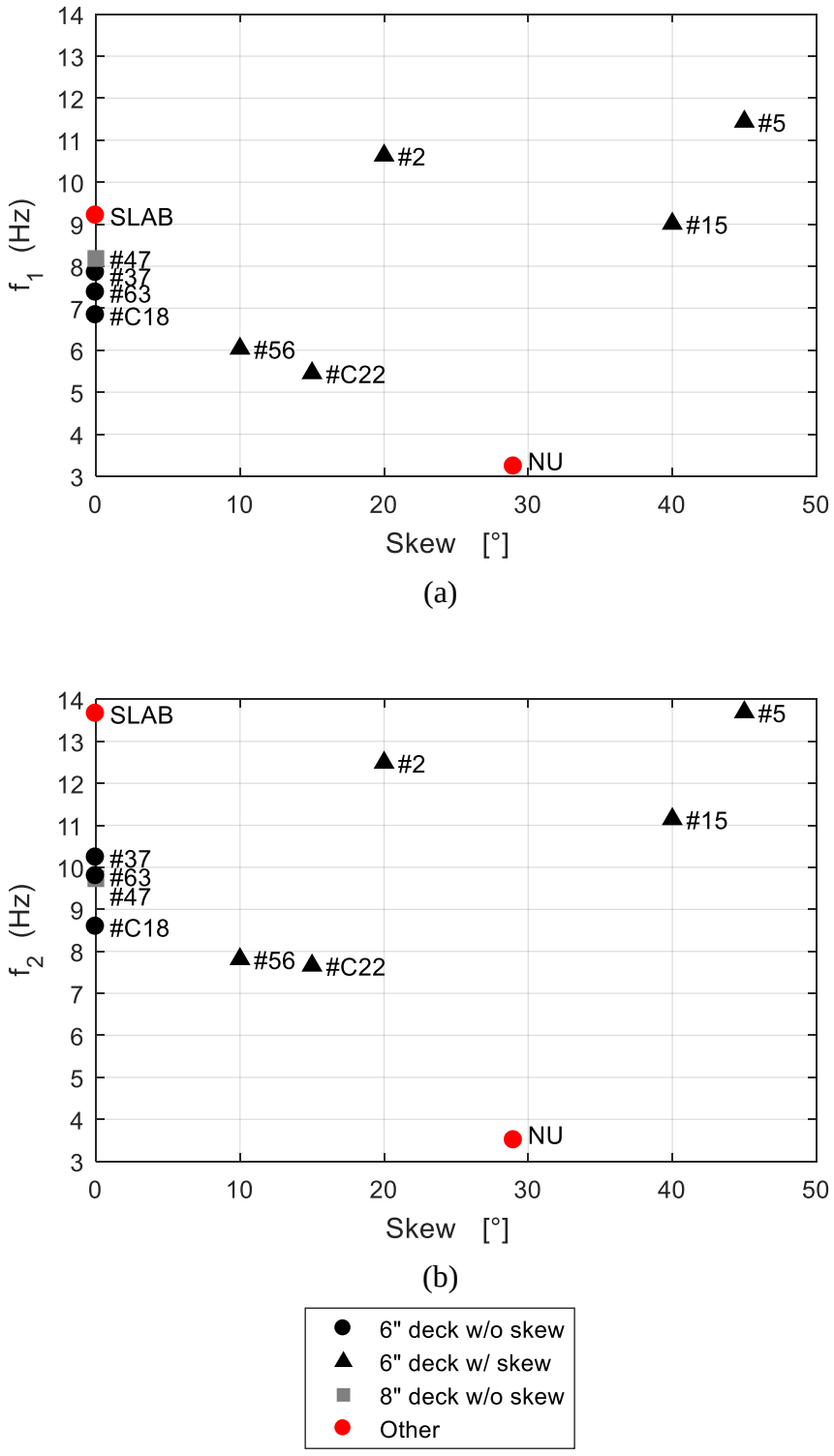

Figure D.22: System identification comparison of the skew angle for all instrumented bridges.

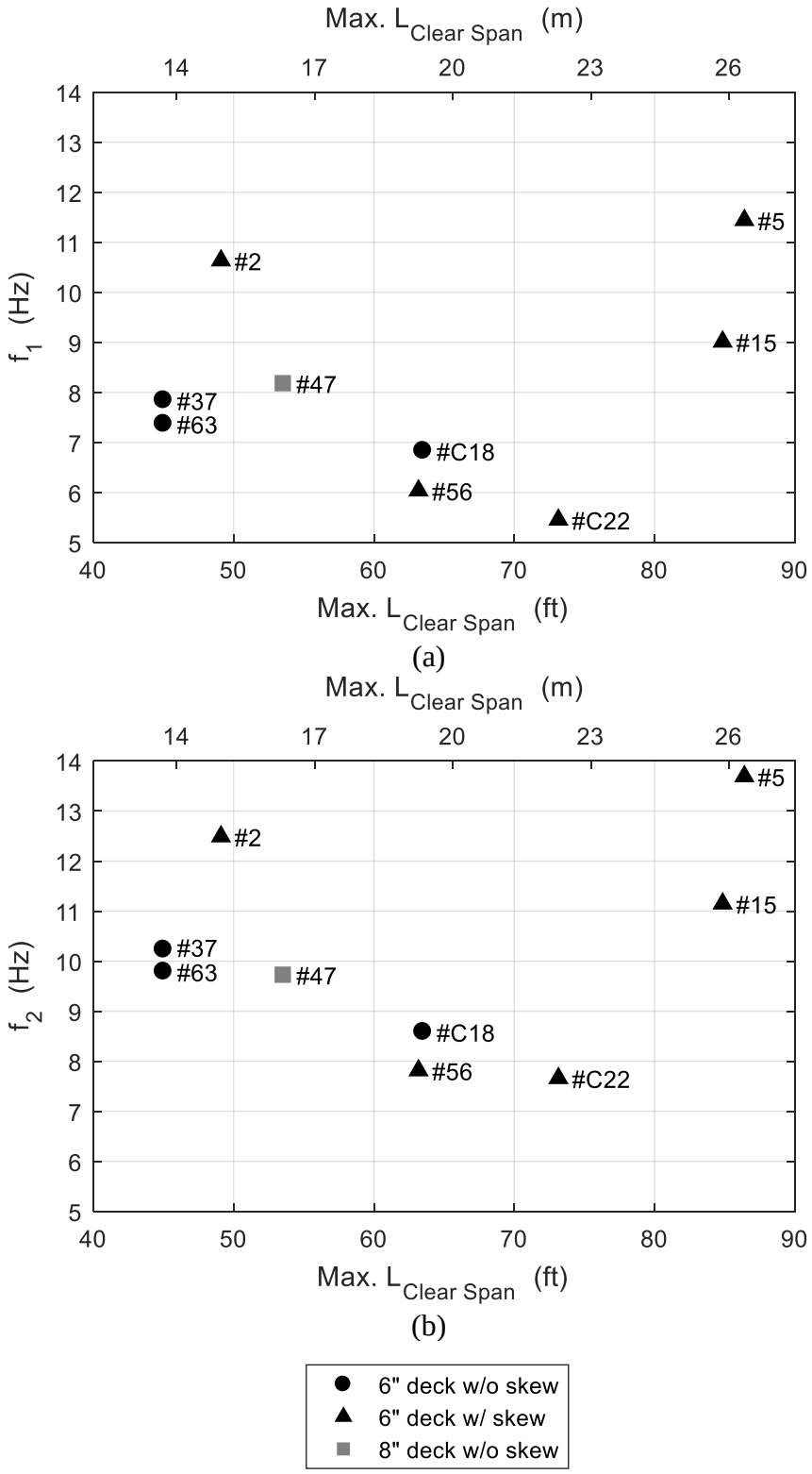

Figure D.23: System identification comparison of the maximum clear span length for the instrumented IT bridges.

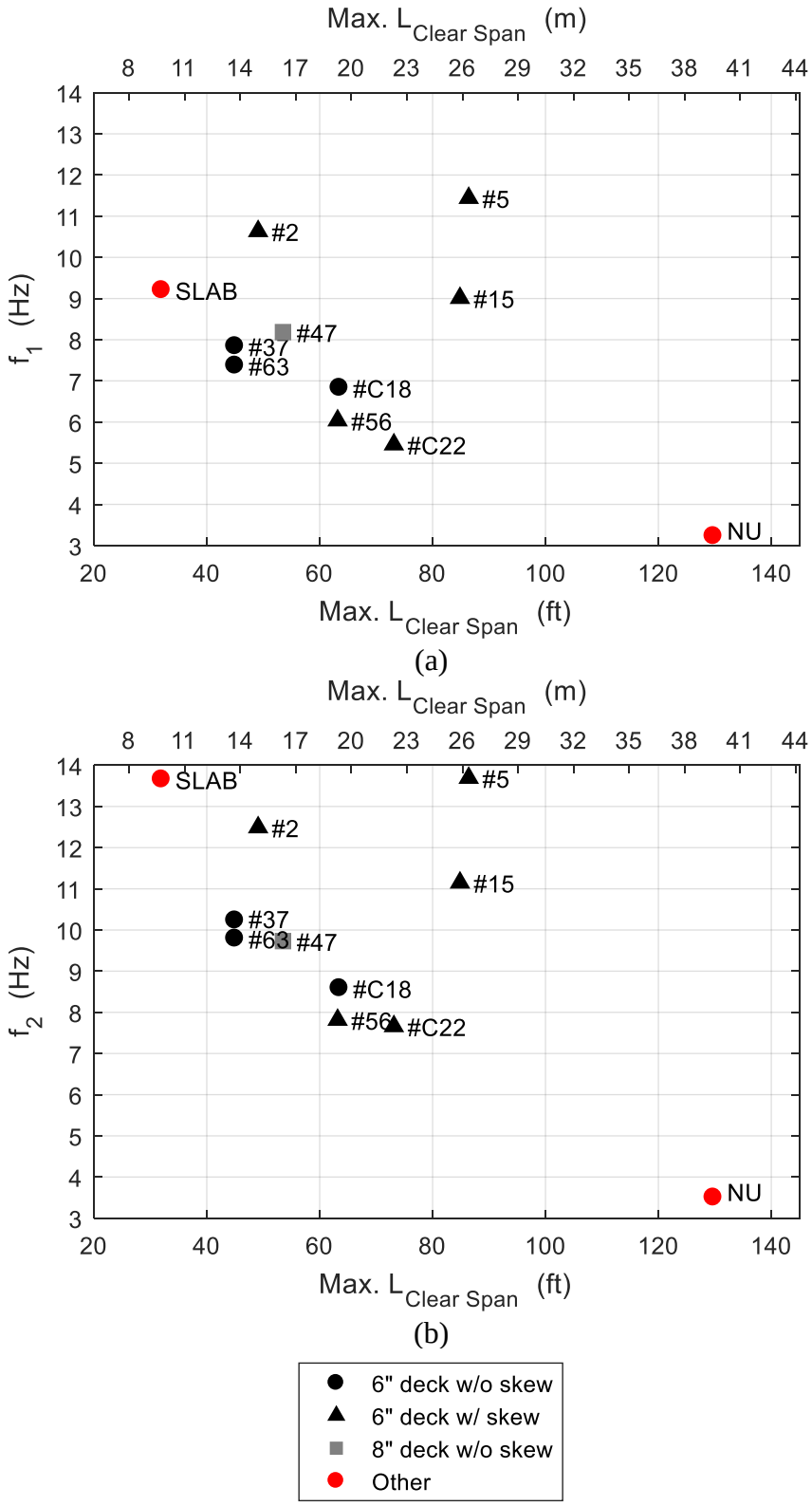

Figure D.24: System identification comparison of the maximum clear span length for all instrumented bridges.

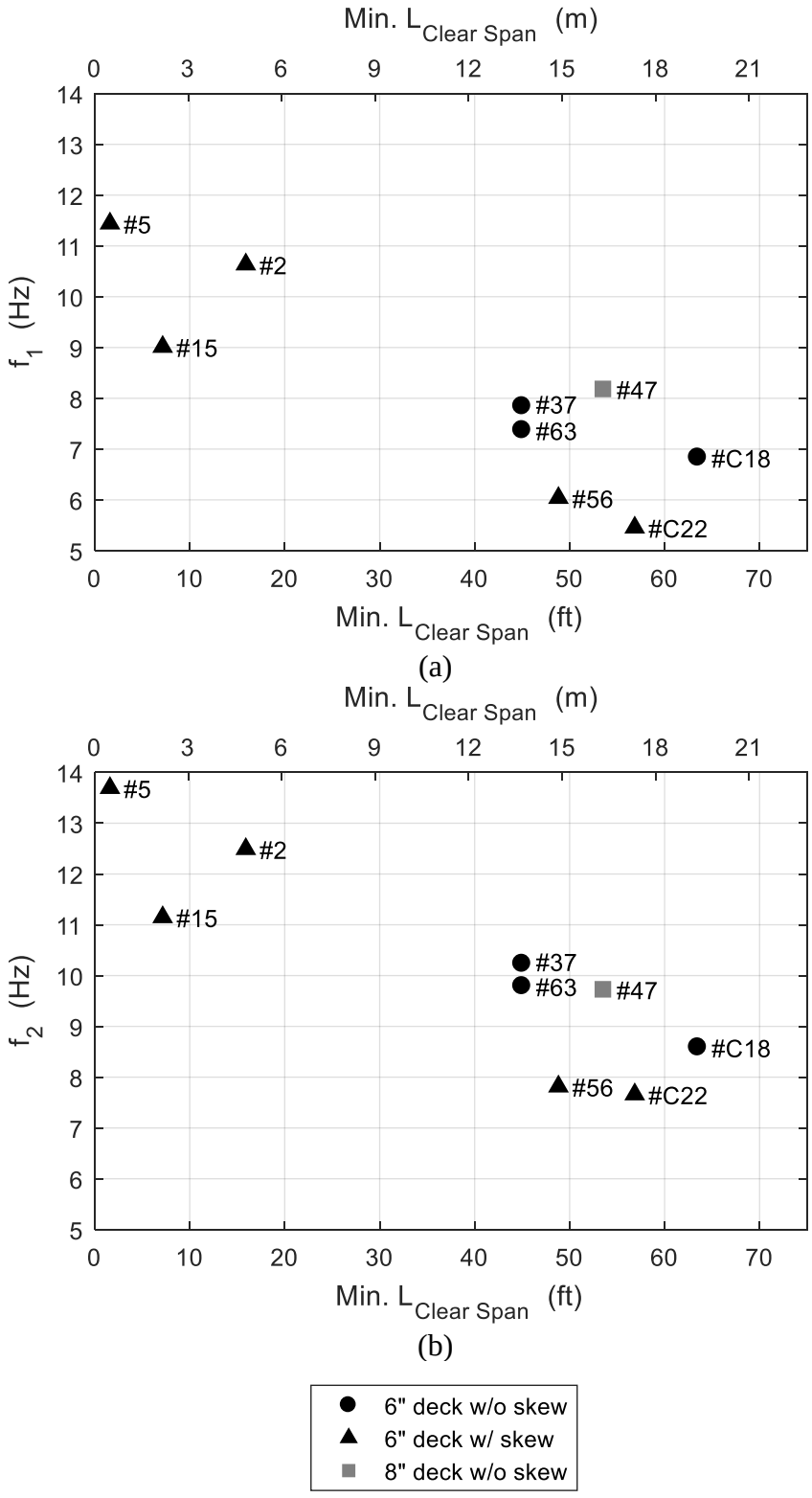

Figure D.25: System identification comparison of the minimum clear span length for the instrumented IT bridges.

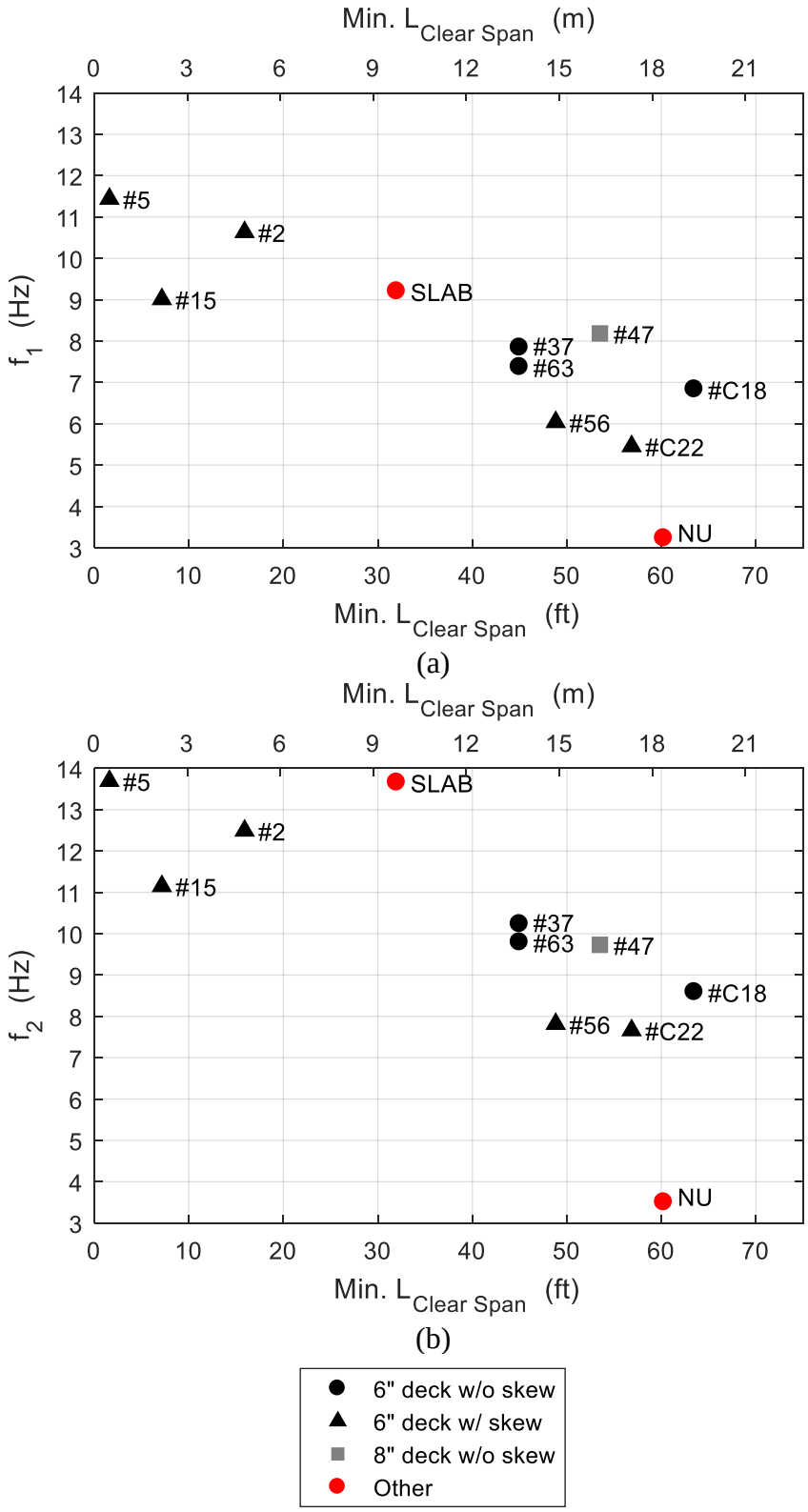

Figure D.26: System identification comparison of the minimum clear span length for all instrumented bridges.

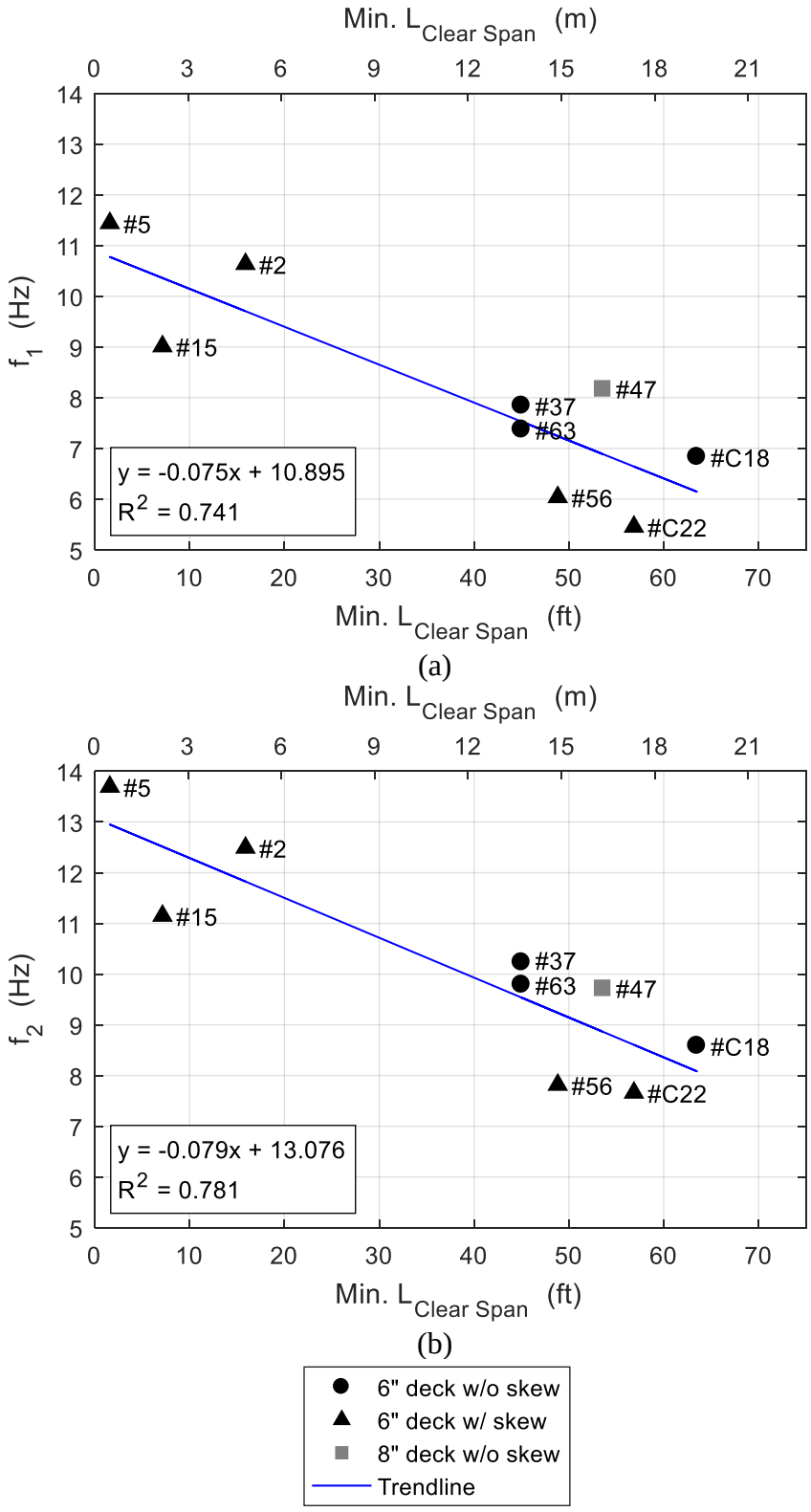

Figure D.27: System identification comparison of the minimum clear span length with a trendline for the instrumented IT bridges.

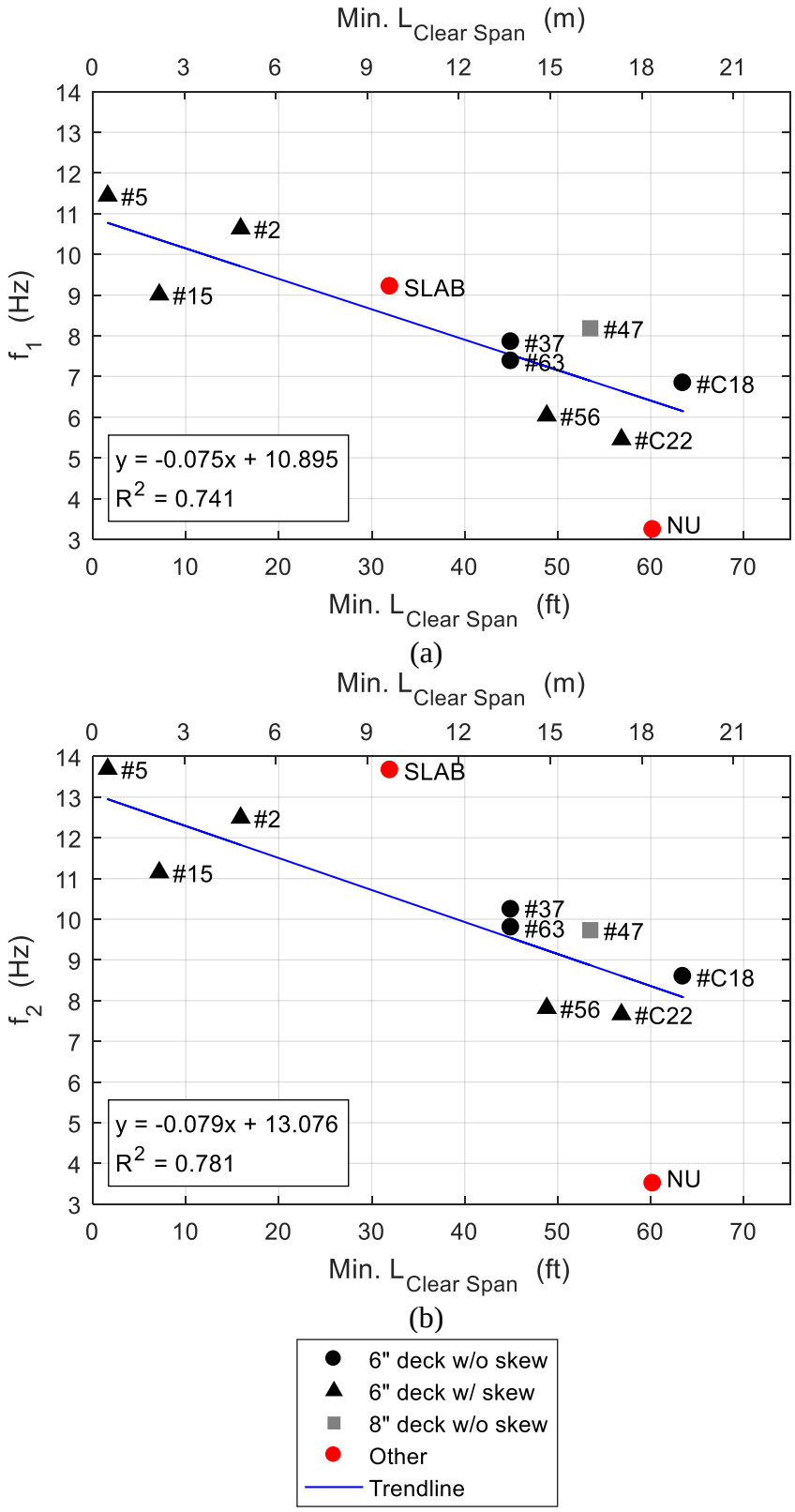

Figure D.28: System identification comparison of the minimum clear span length with a trendline for all instrumented bridges.

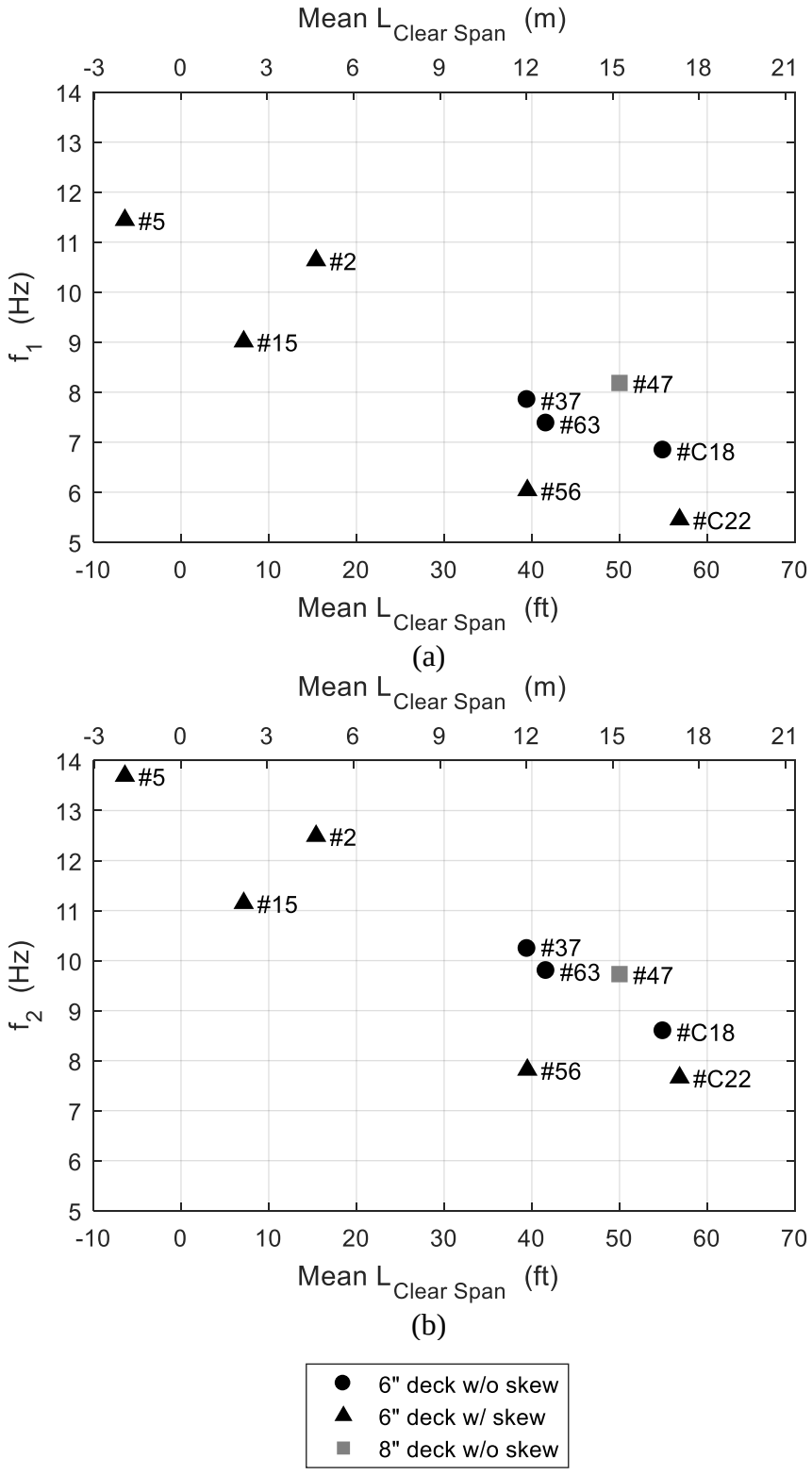

Figure D.29: System identification comparison of the mean clear span length for the instrumented IT bridges.

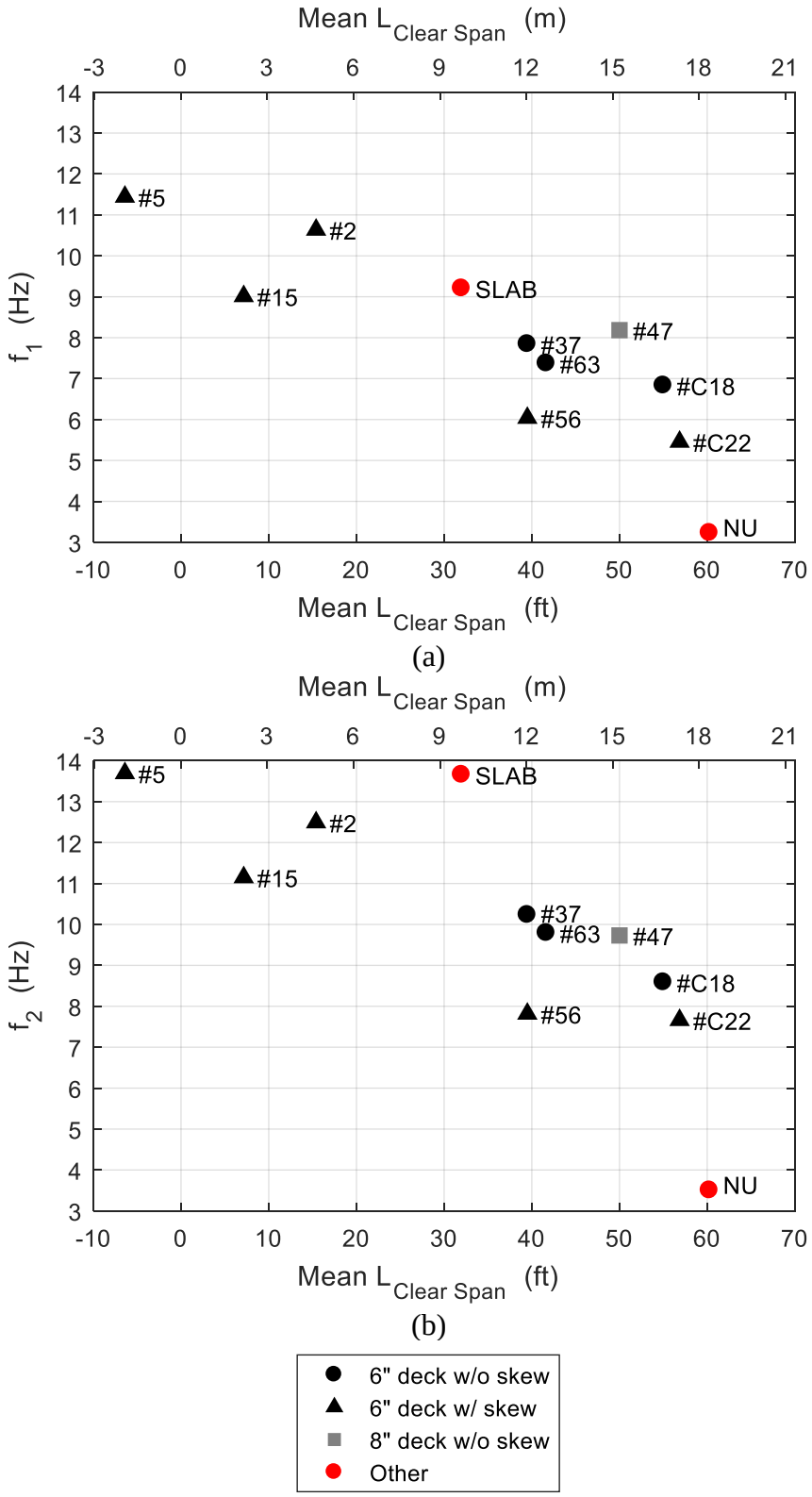

Figure D.30: System identification comparison of the mean clear span length for all instrumented bridges.

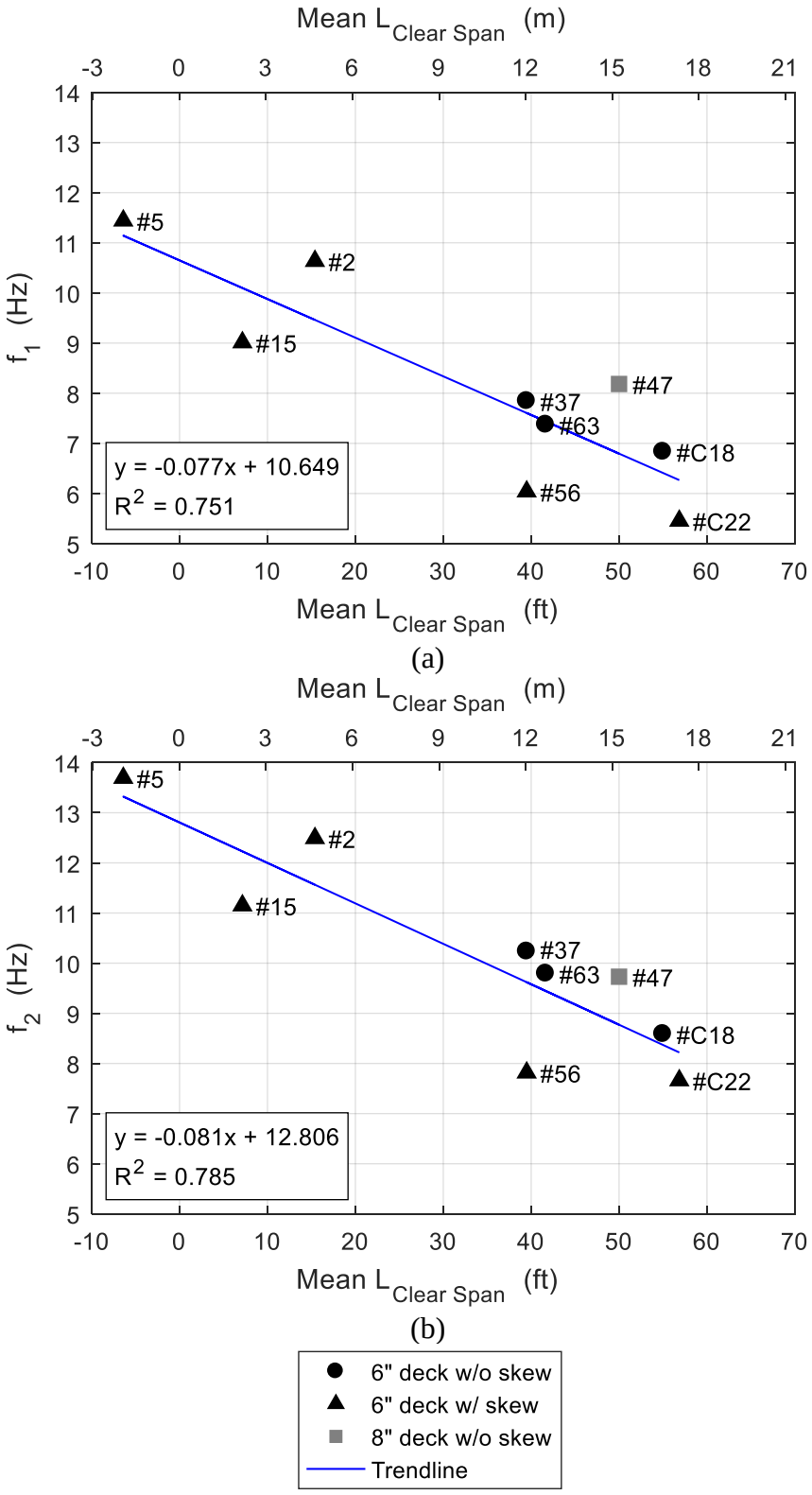

Figure D.31: System identification comparison of the mean clear span length with a trendline for the instrumented IT bridges.

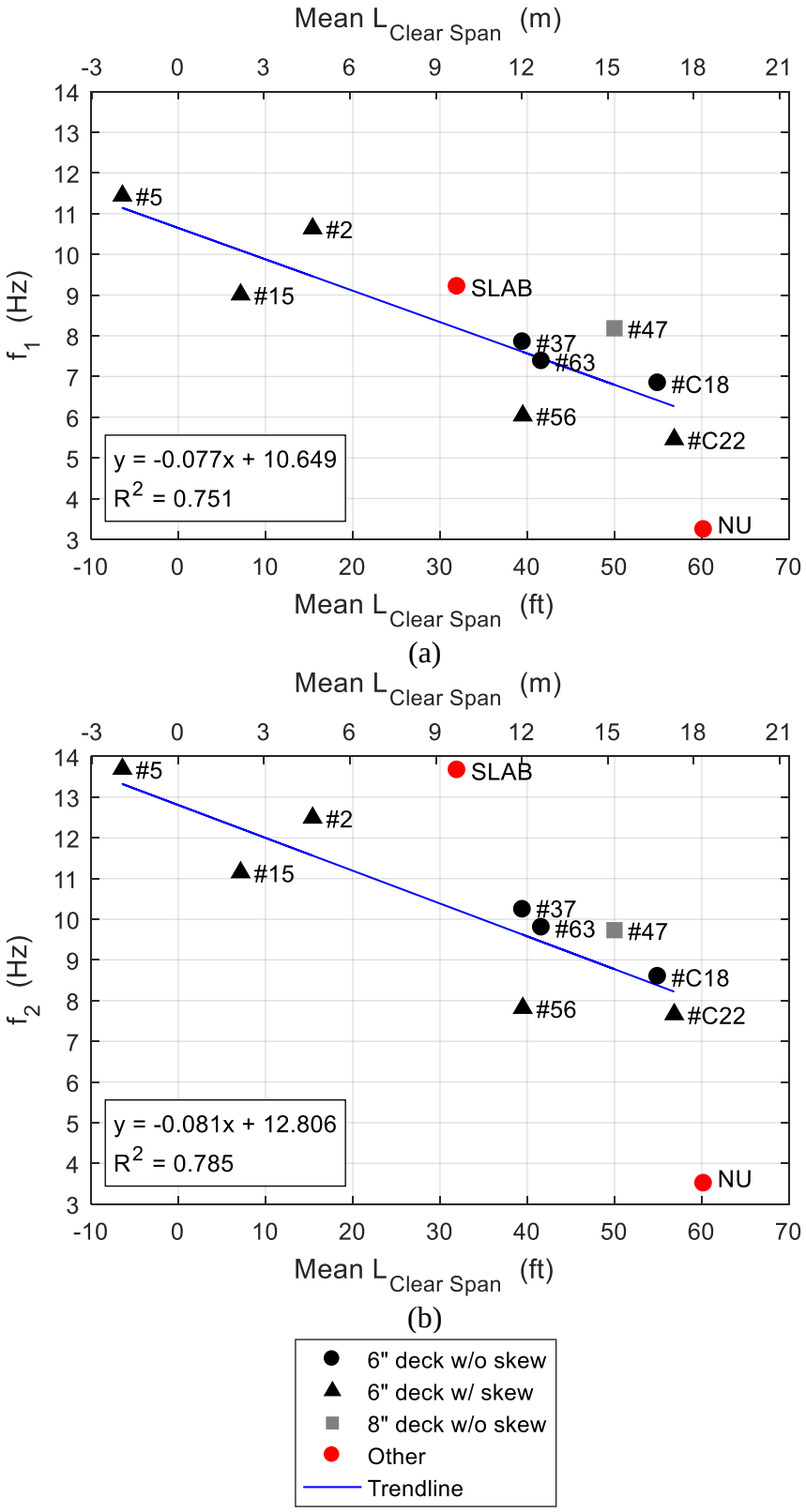

Figure D.32: System identification comparison of the mean clear span length with a trendline for all instrumented bridges.

APPENDIX E

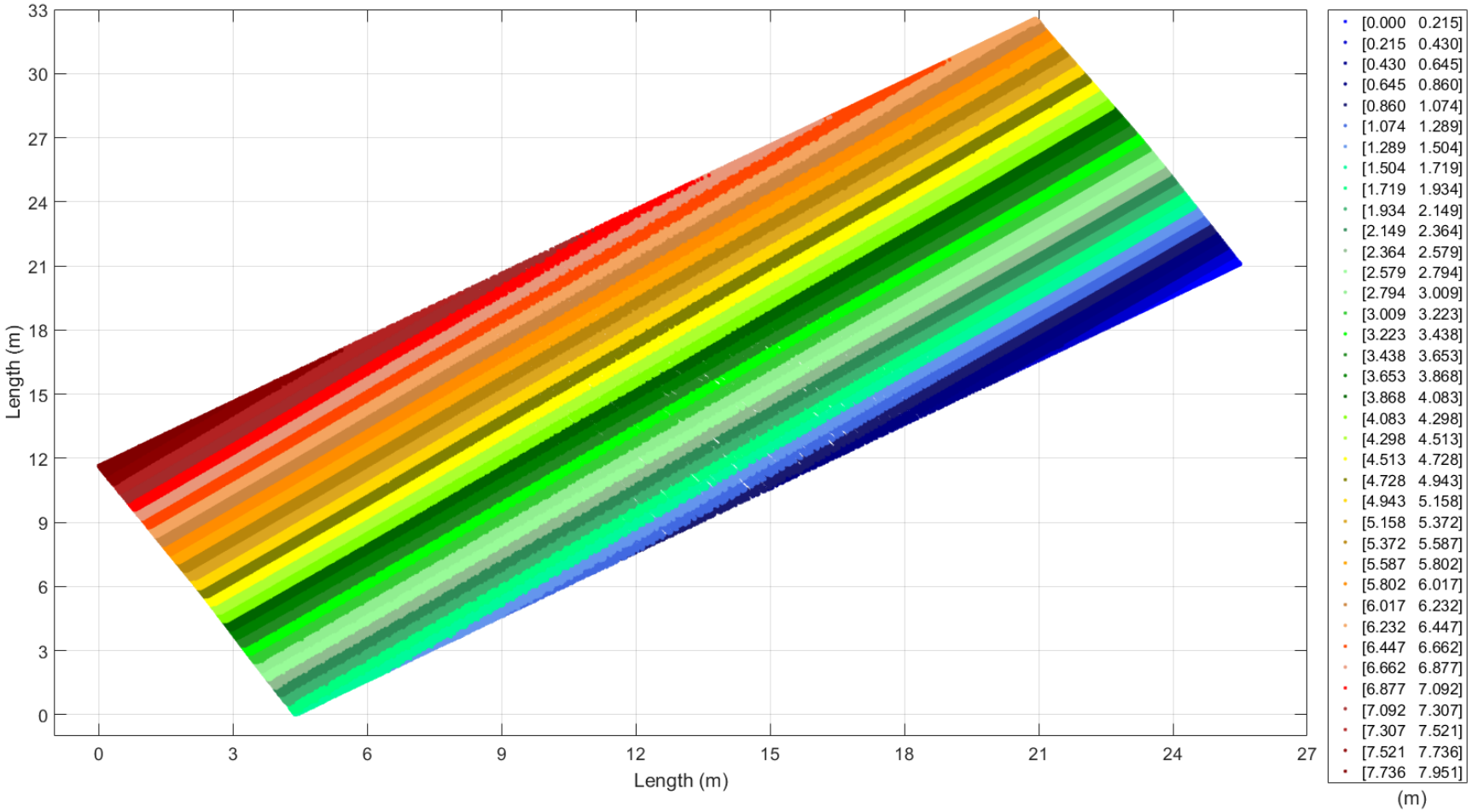

Figure E.1: Lidar depth map of the deck for bridge S006 26001.

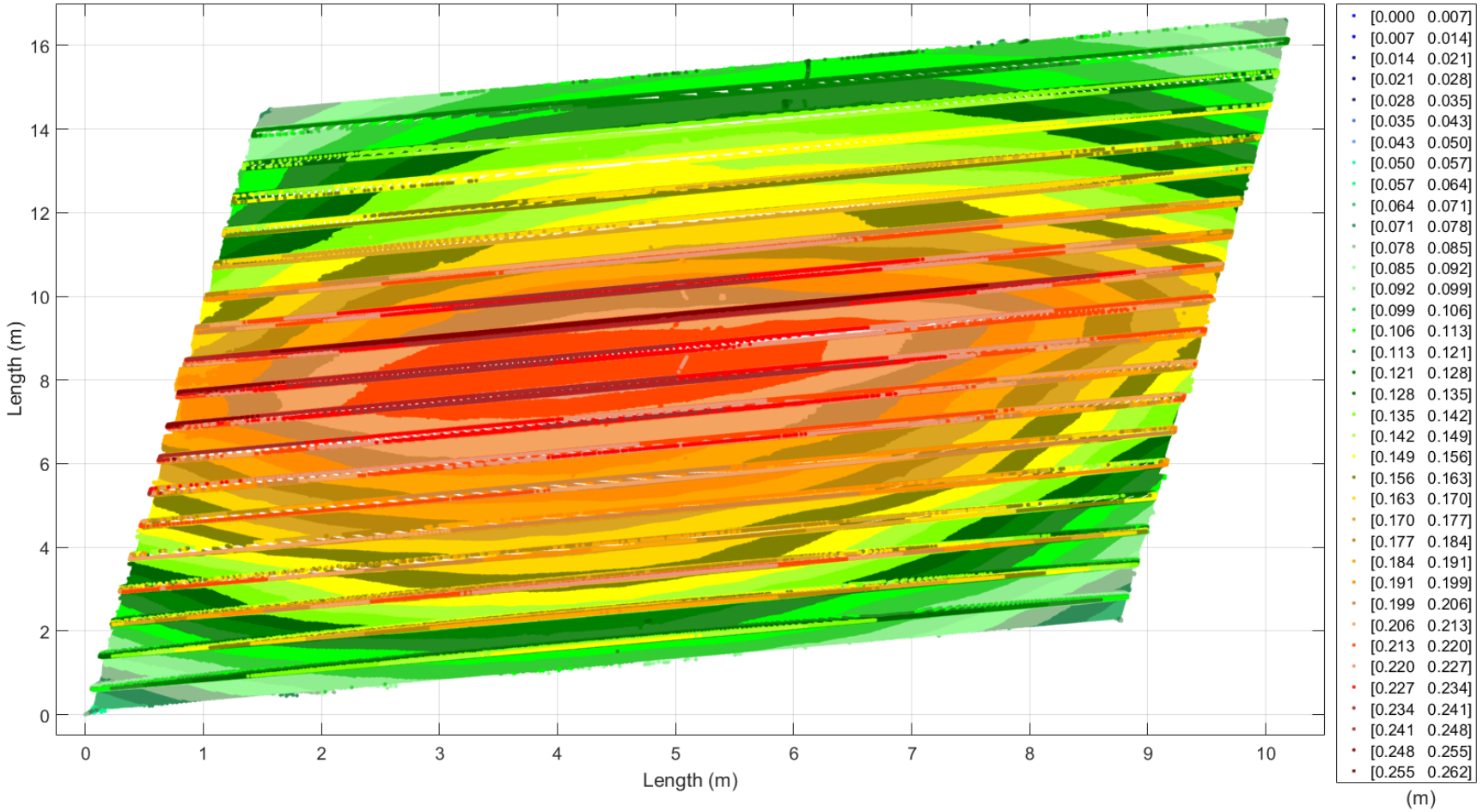

Figure E.2: Lidar depth map of the middle span girders for bridge S006 26001.

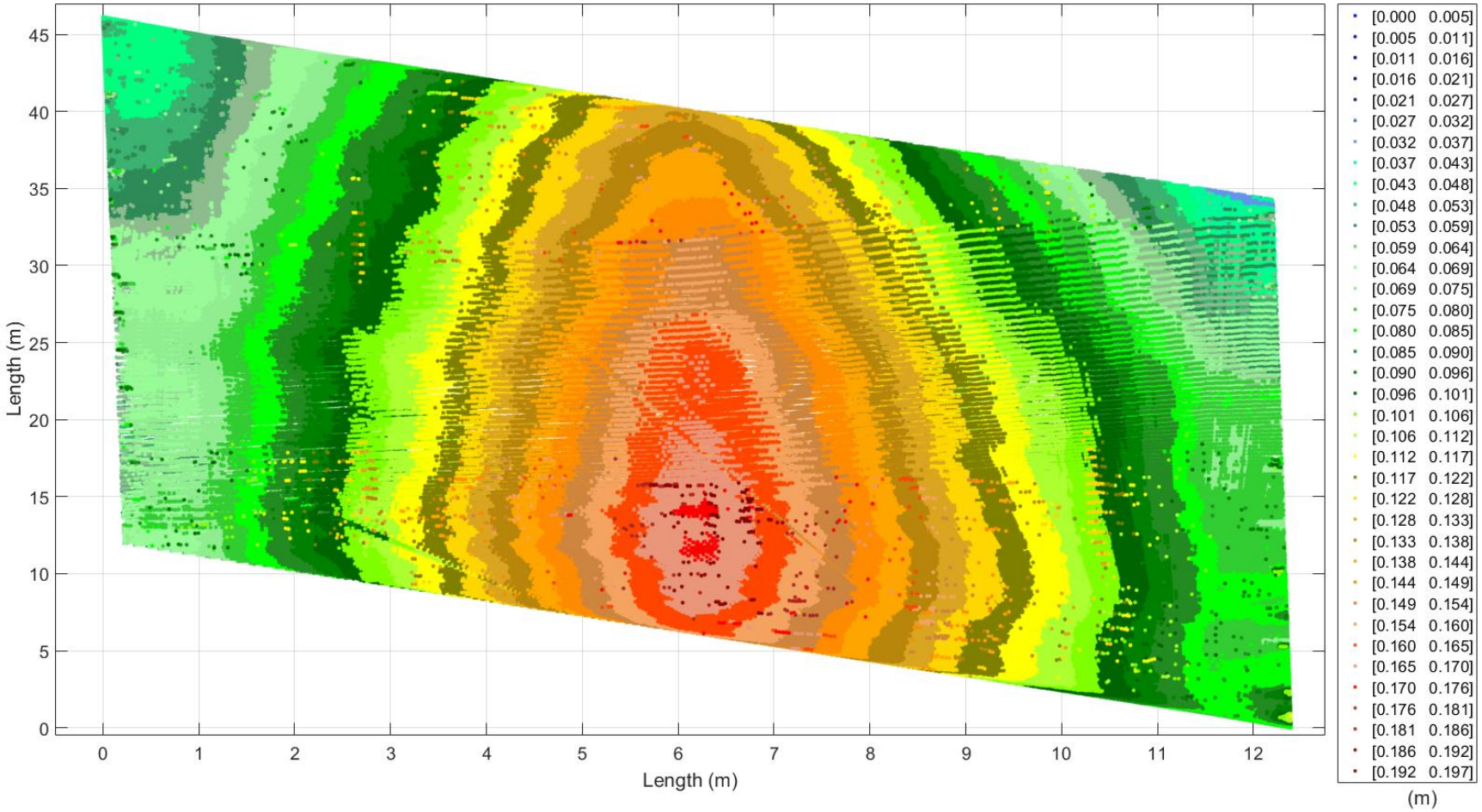

Figure E.3: Lidar depth map of the deck for bridge S009 00888.

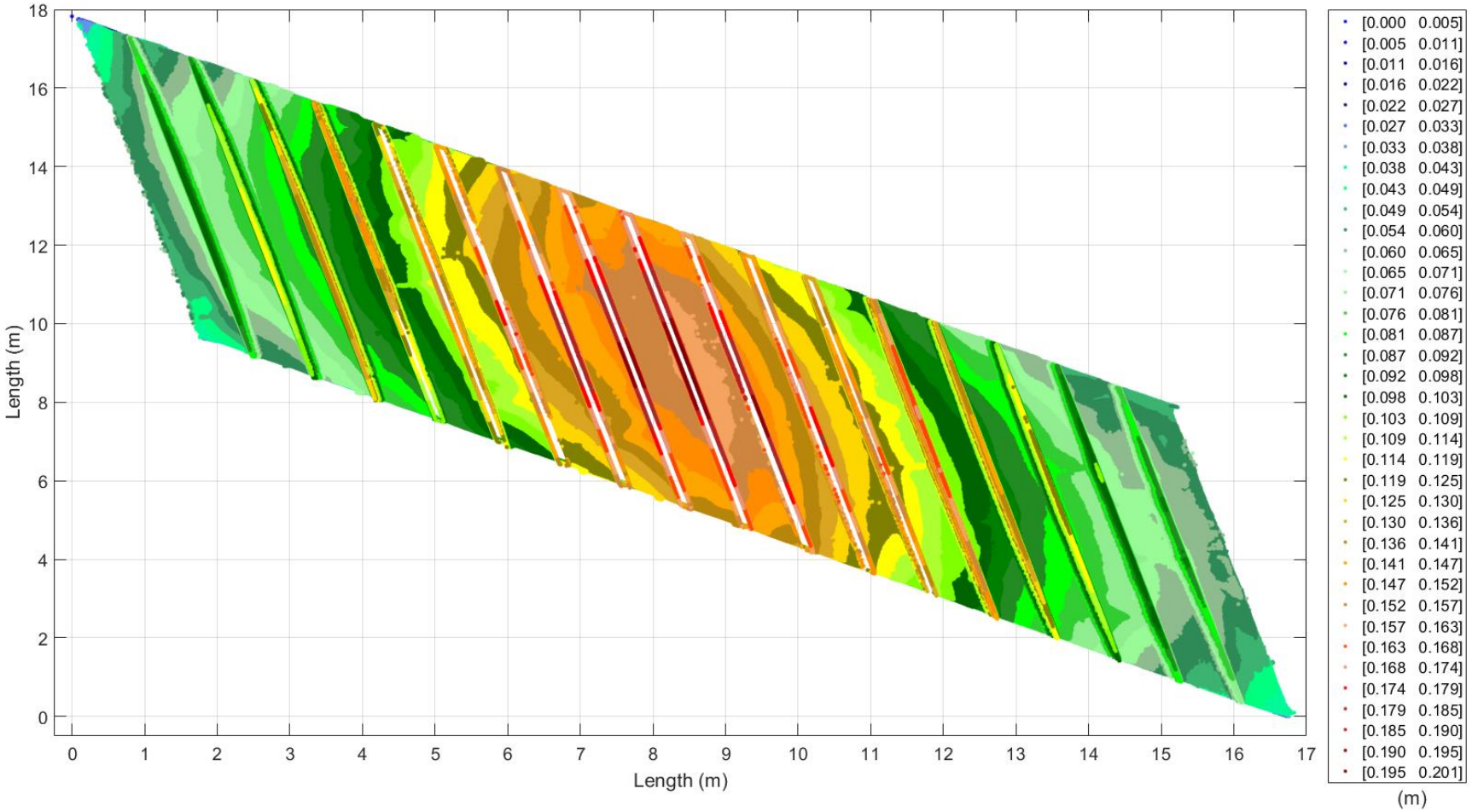

Figure E.4: Lidar depth map of the south span girders for bridge S009 00888.

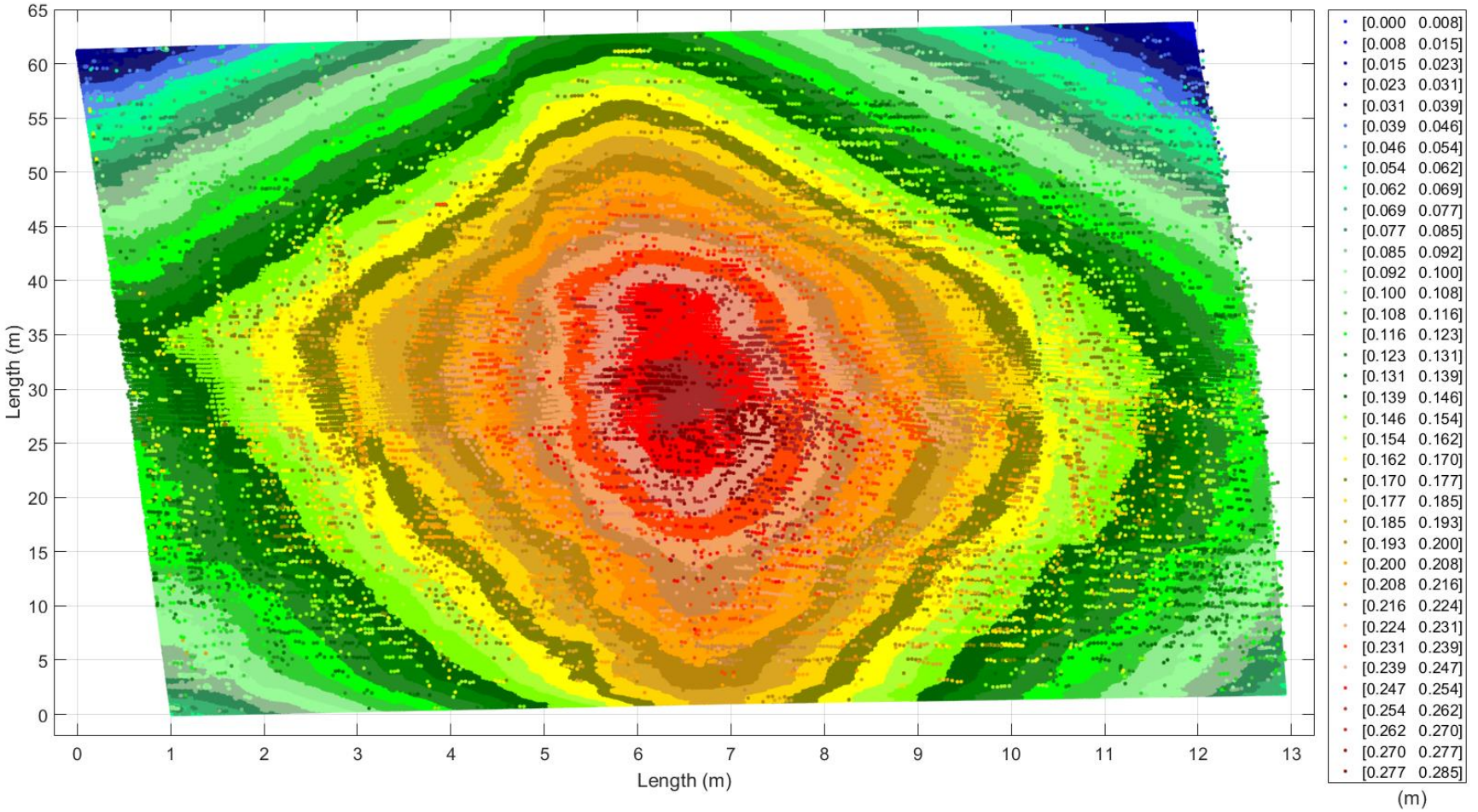

Figure E.5: Lidar depth map of the deck for bridge S050 04149.

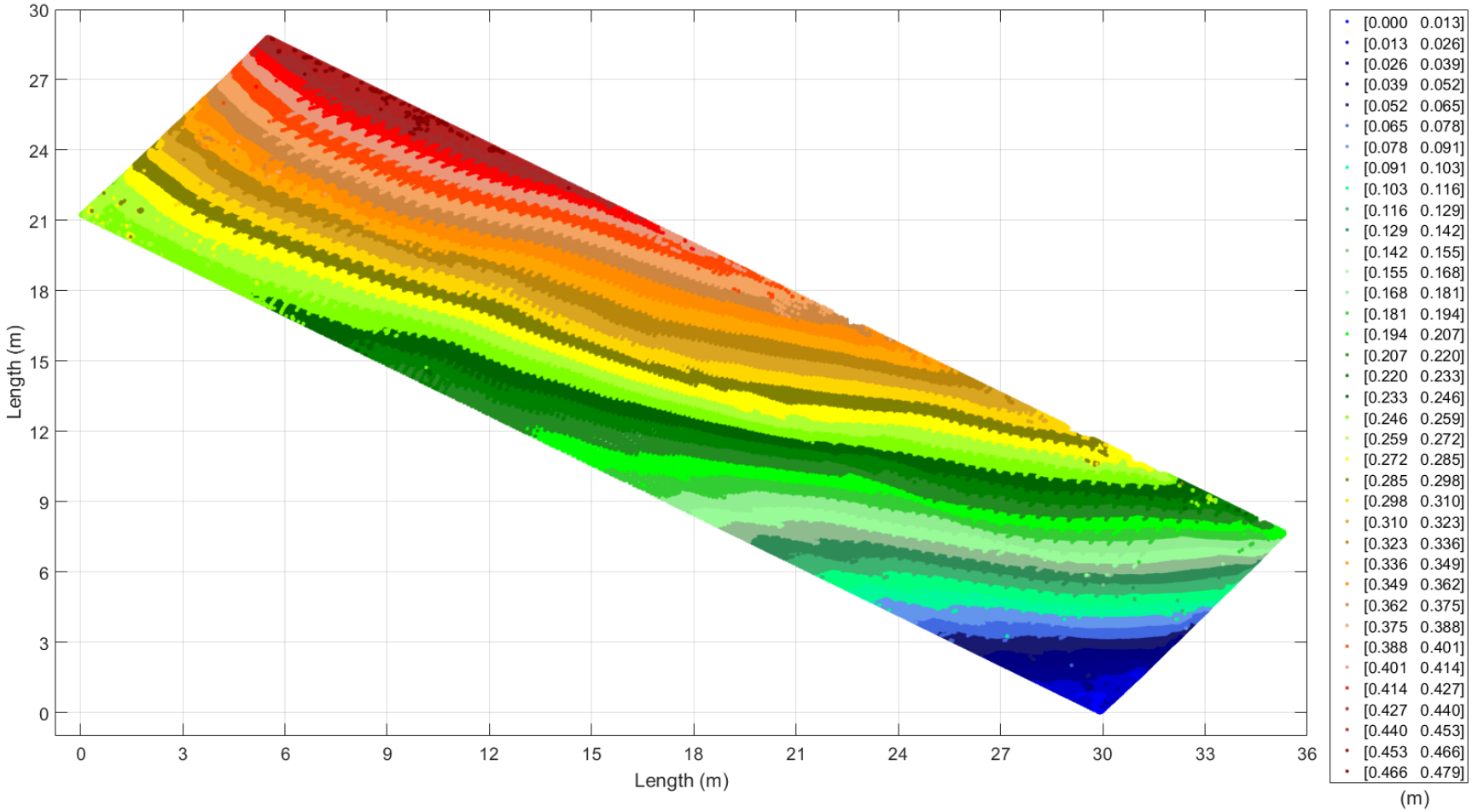

Figure E.6: Lidar depth map of the deck for bridge S058 00994.

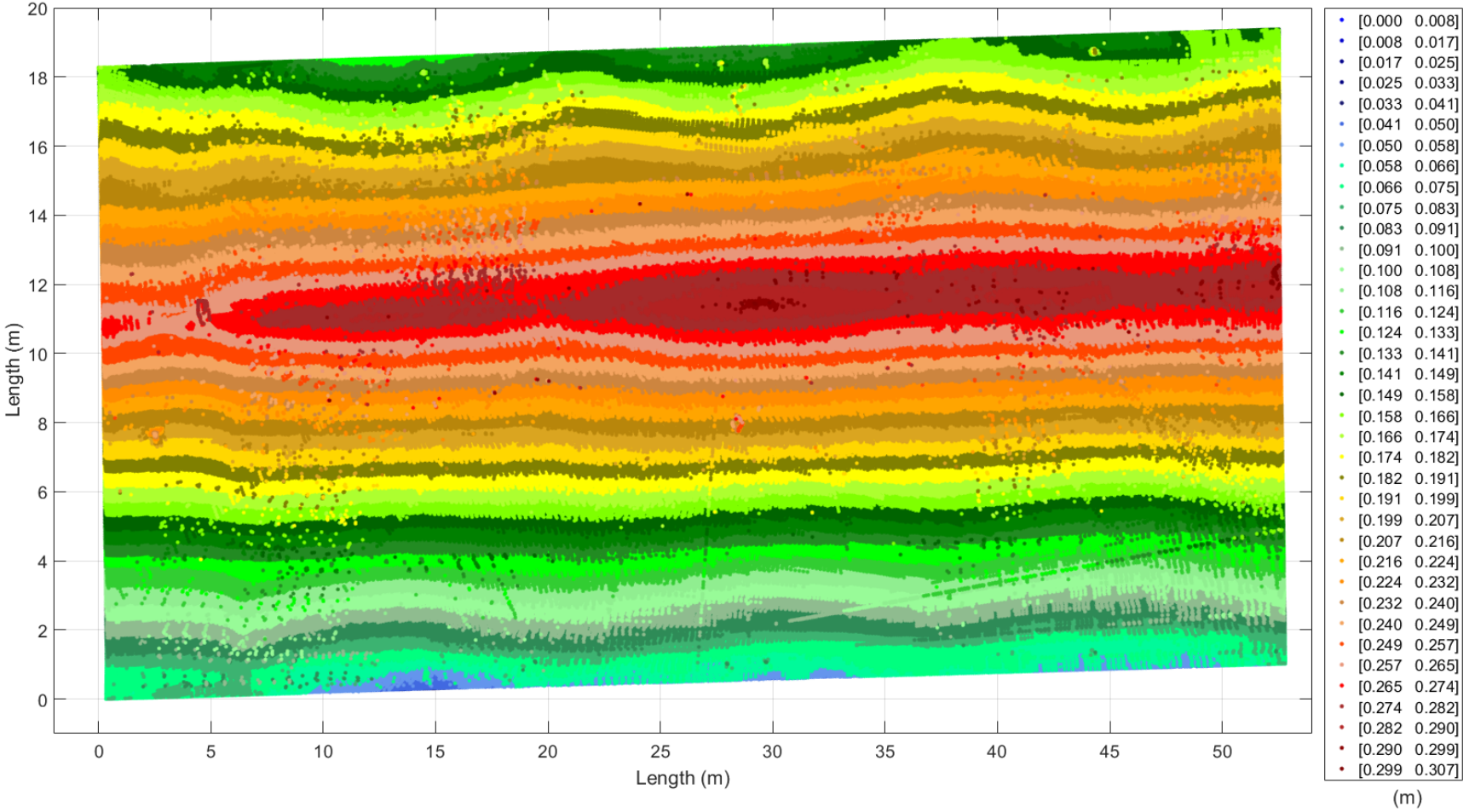

Figure E.7: Lidar depth map of the deck for bridge S080 40872R.

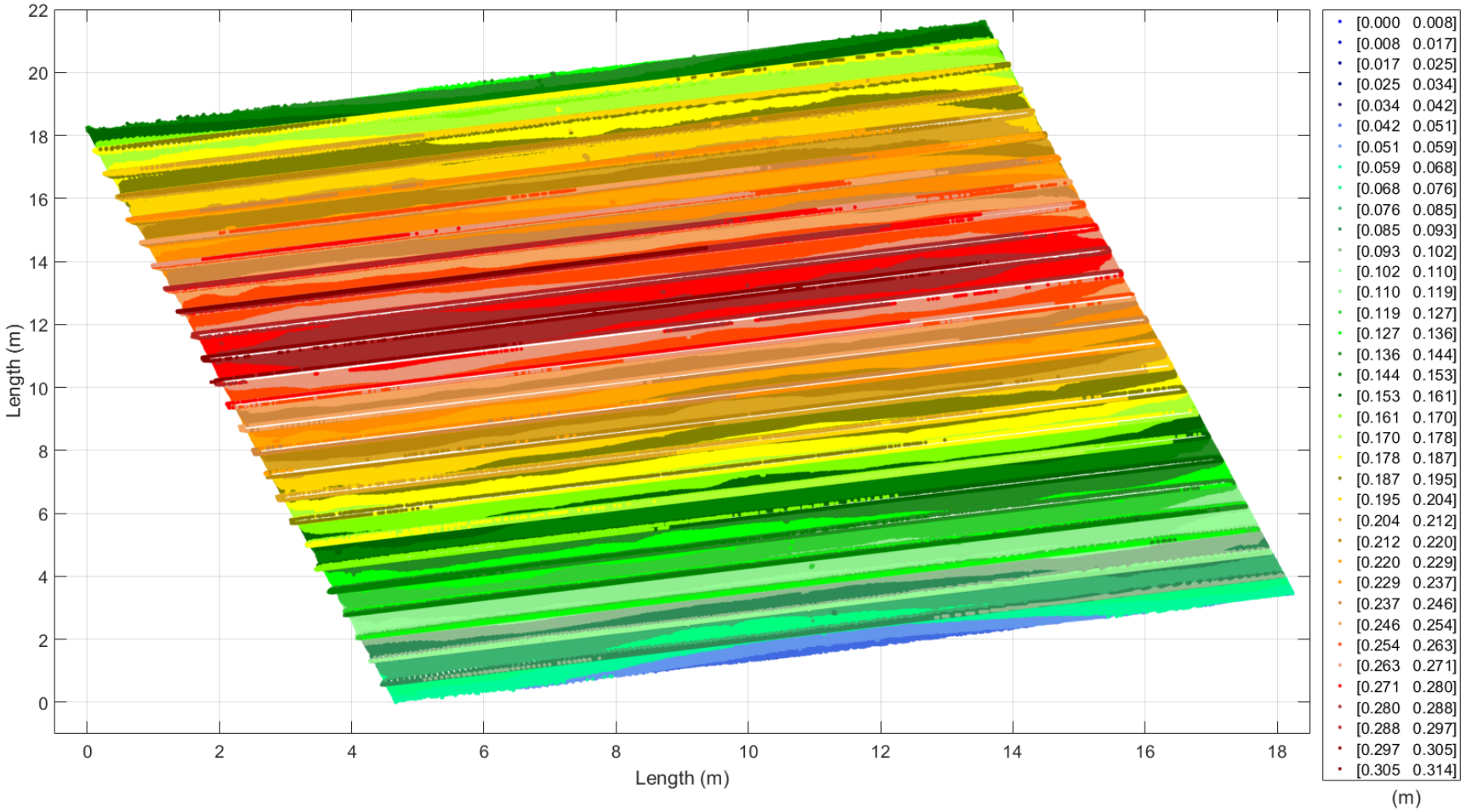

Figure E.8: Lidar depth map of the west span girders for bridge S080 40872R.

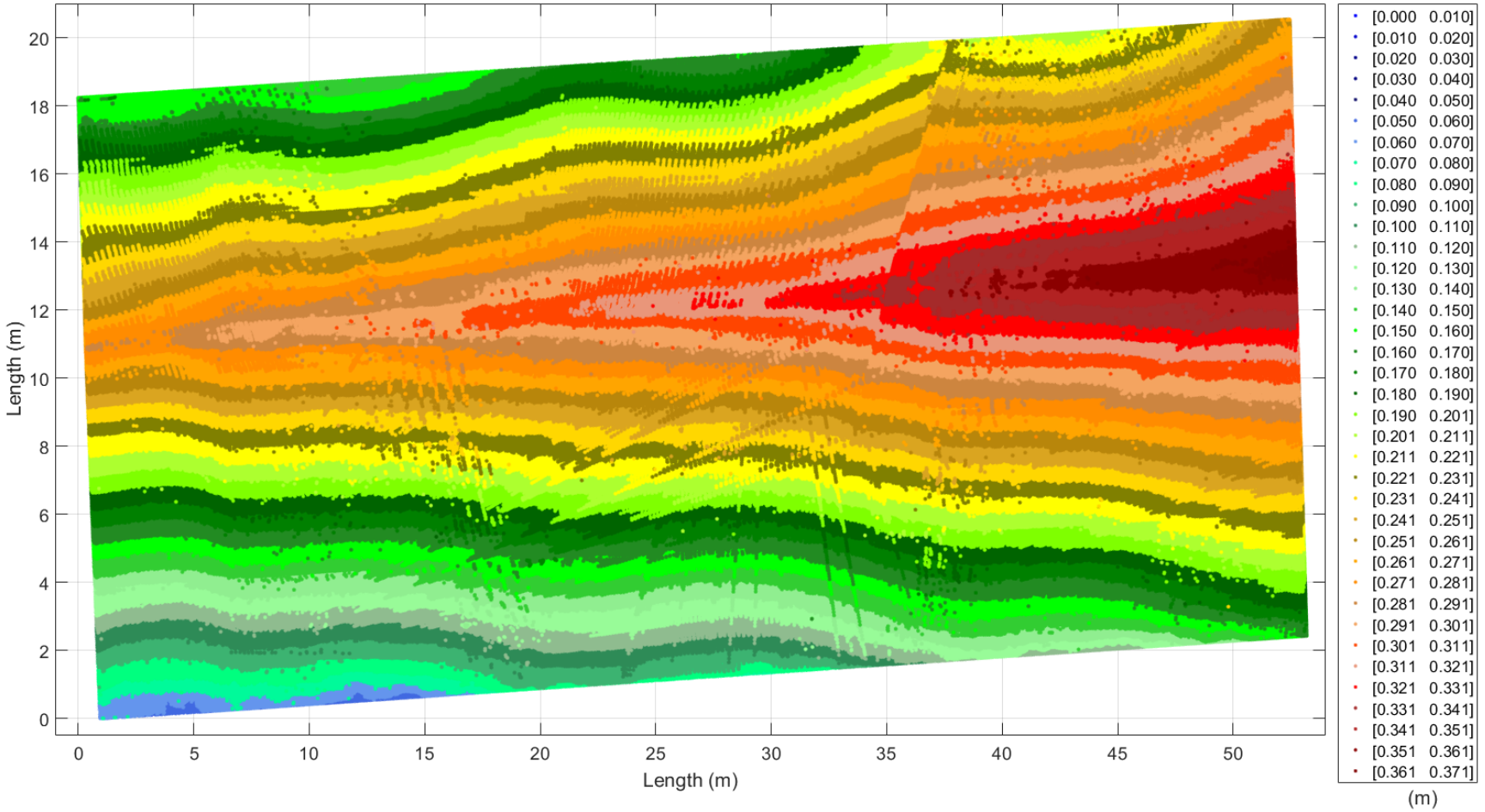

Figure E.9: Lidar depth map of the deck for bridge S080 40927R.

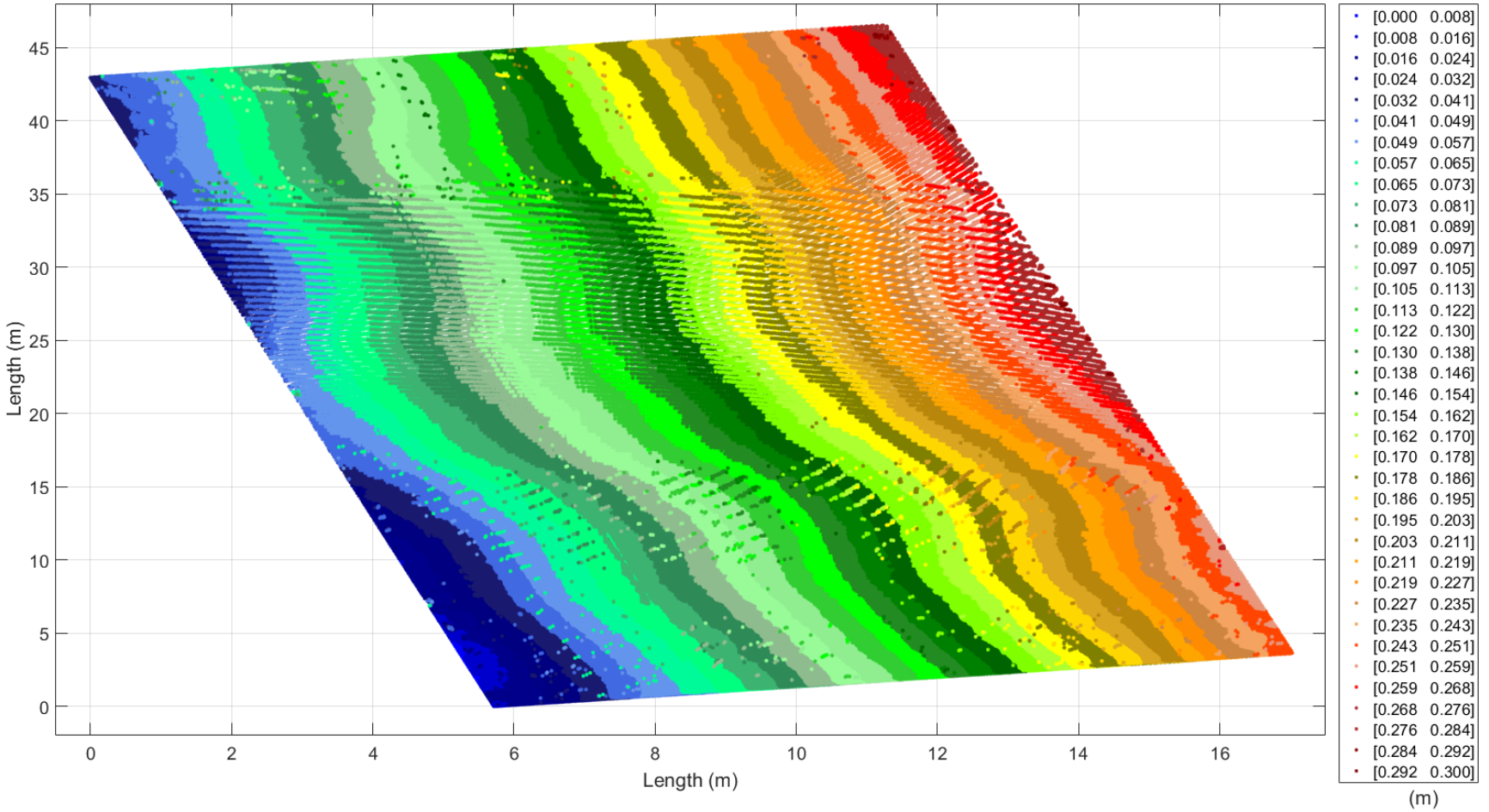

Figure E.10: Lidar depth map of the deck for bridge S081 05152L.

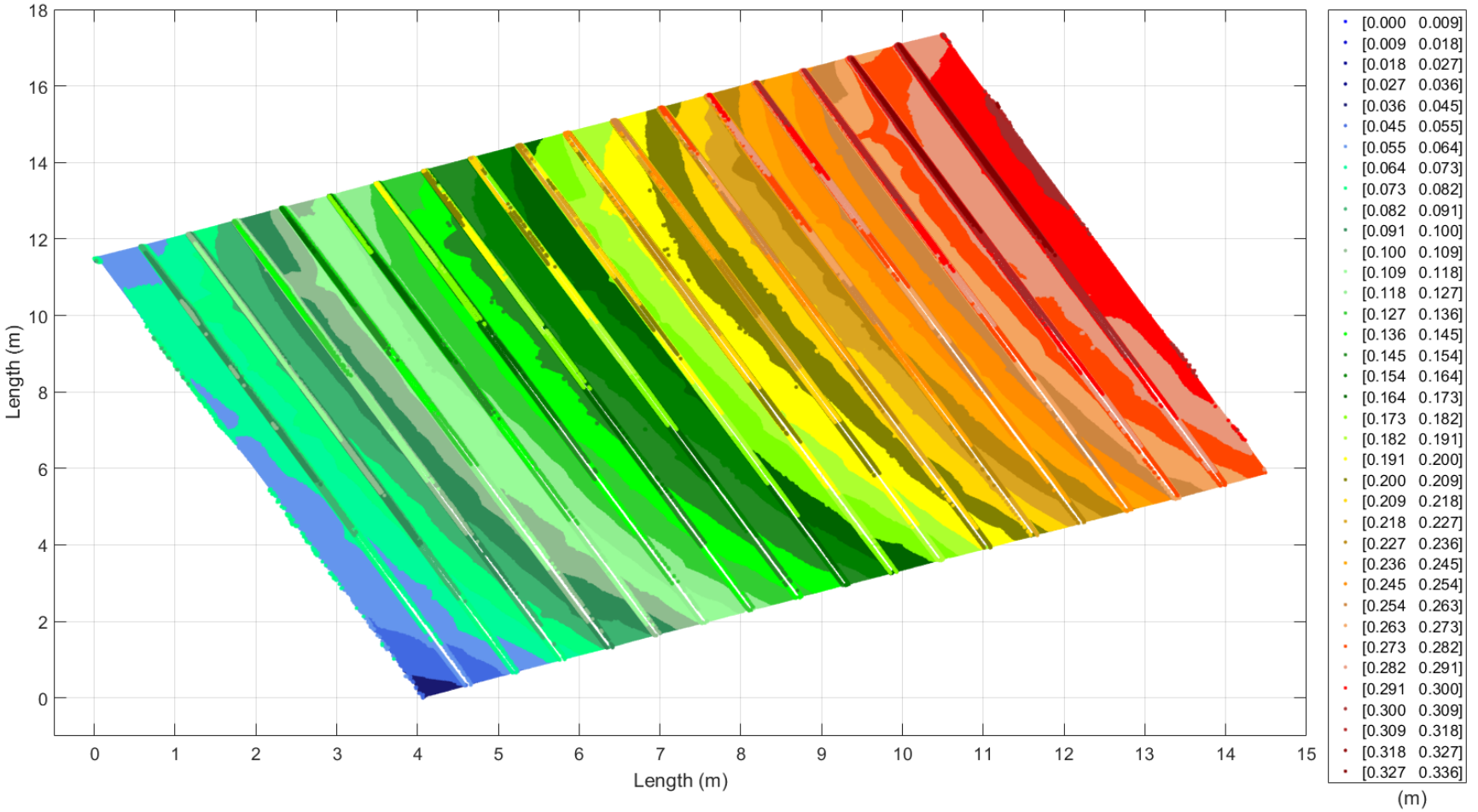

Figure E.11: Lidar depth map of the south span girders for bridge S081 05152L.

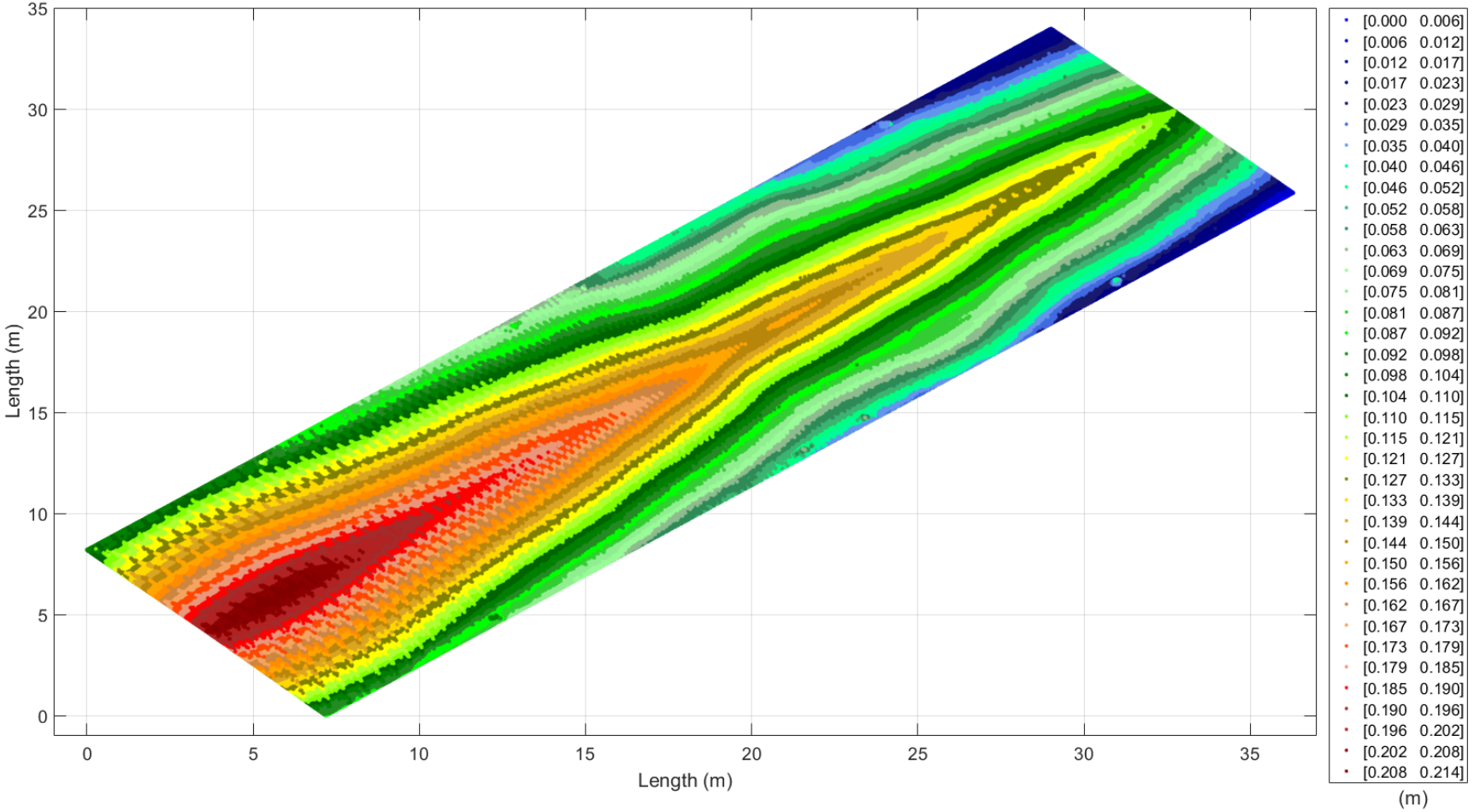

Figure E.12: Lidar depth map of the deck for bridge S089 06047.

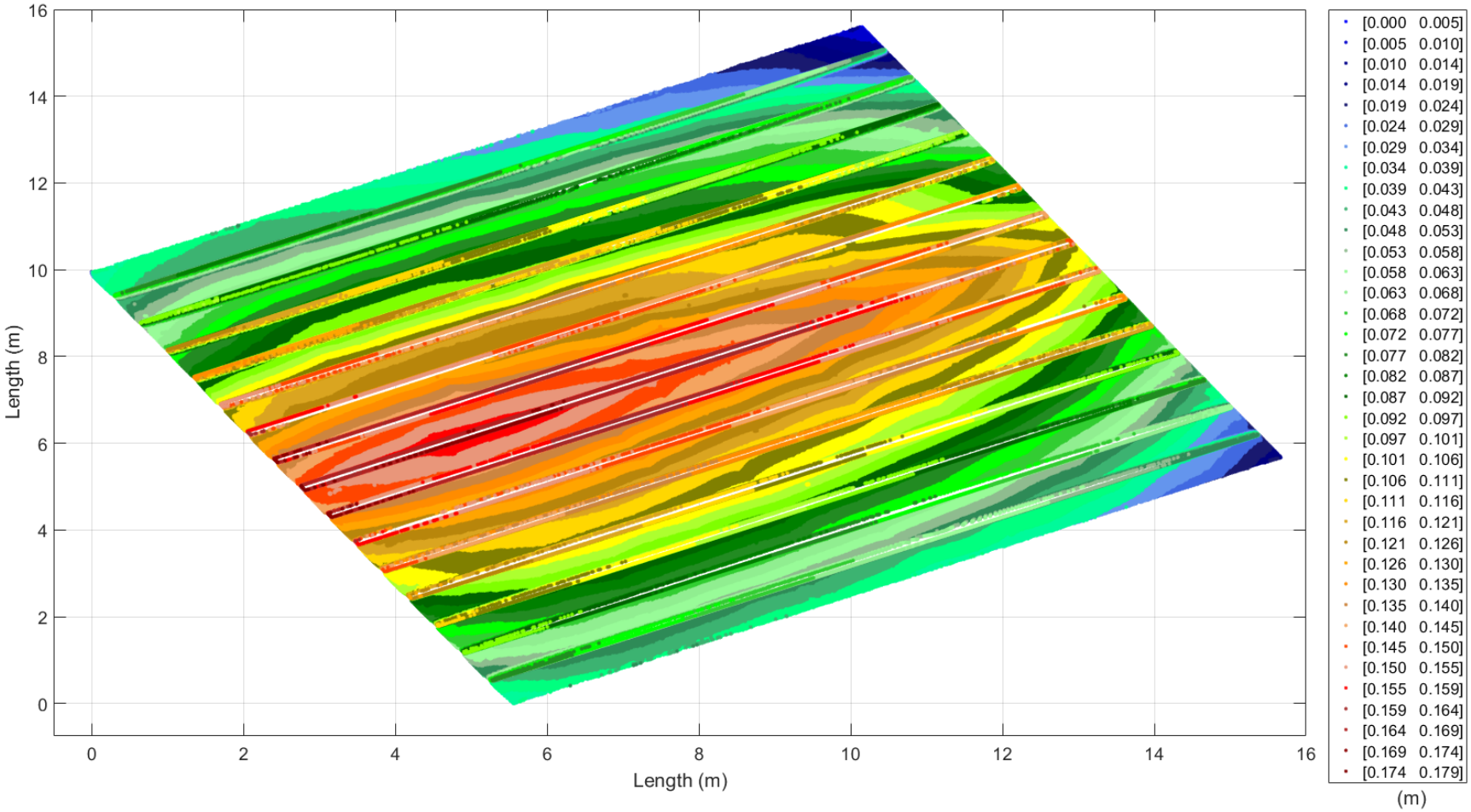

Figure E.13: Lidar depth map of the west span girders for bridge S089 06047.

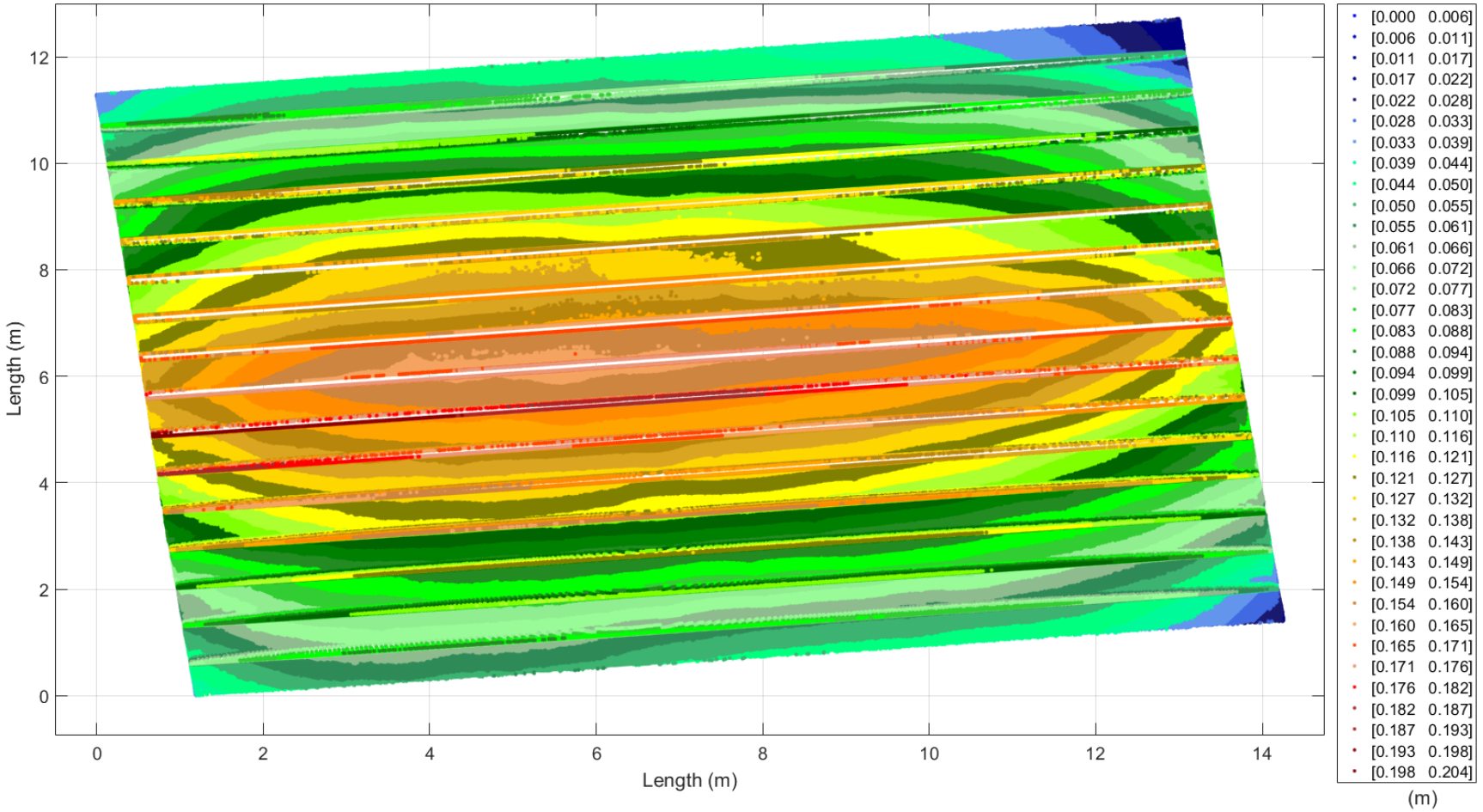

Figure E.14: Lidar depth map of the middle span girders for bridge S089 06047.

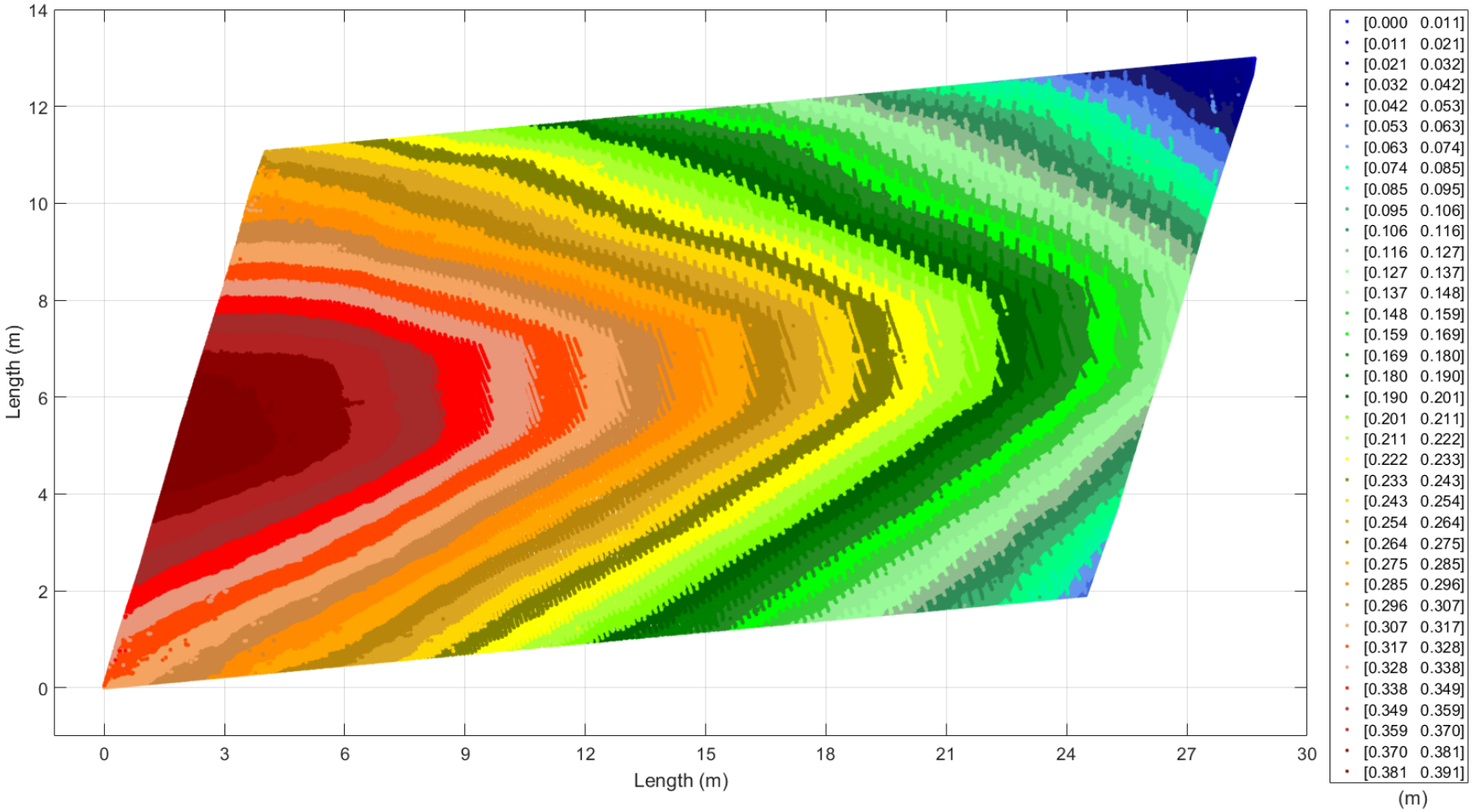

Figure E.15: Lidar depth map of the deck for bridge SS66C00220.

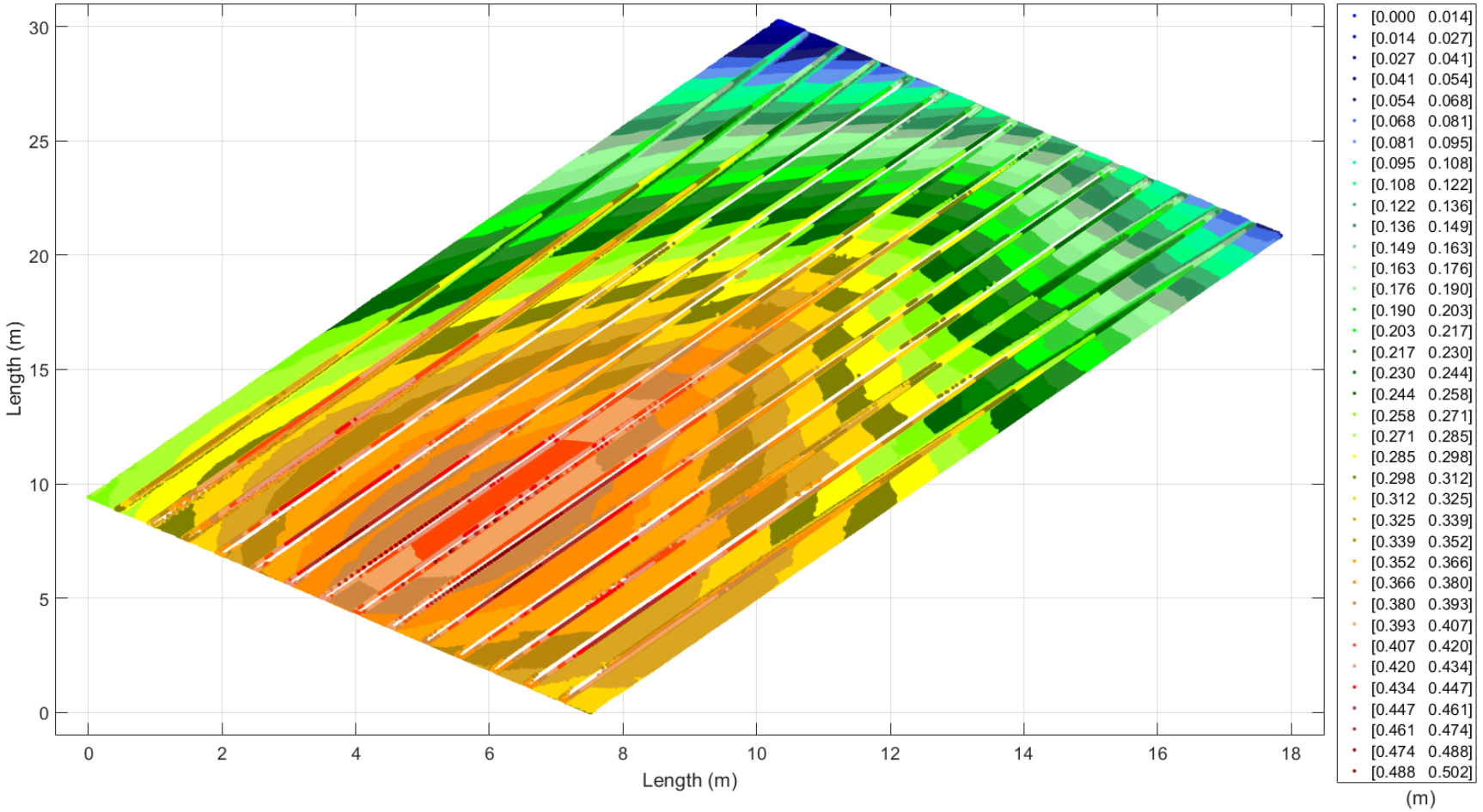

Figure E.16: Lidar depth map of the girders for bridge SS66C00220.

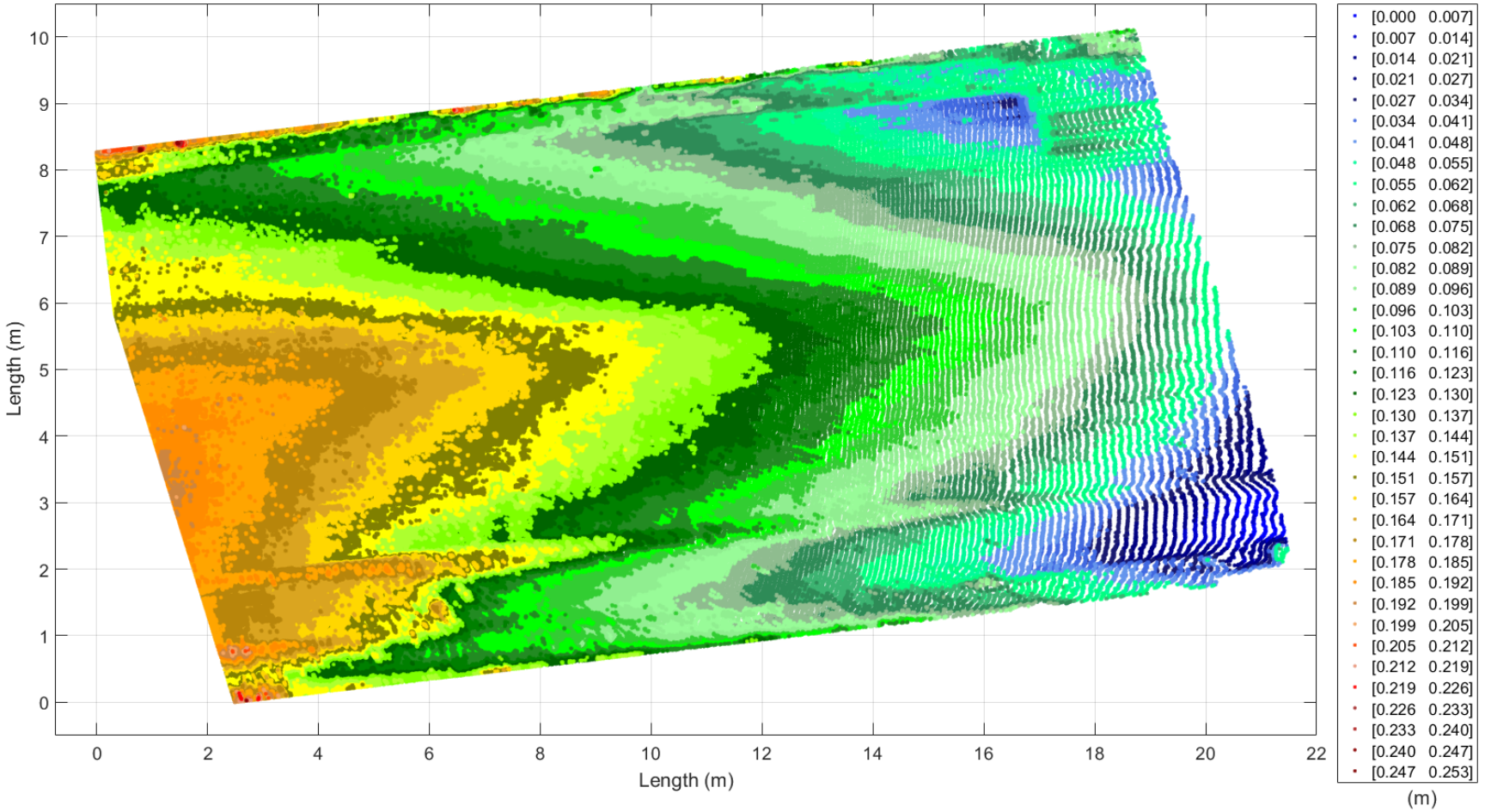

Figure E.17: Lidar depth map of the deck for bridge M011022220.

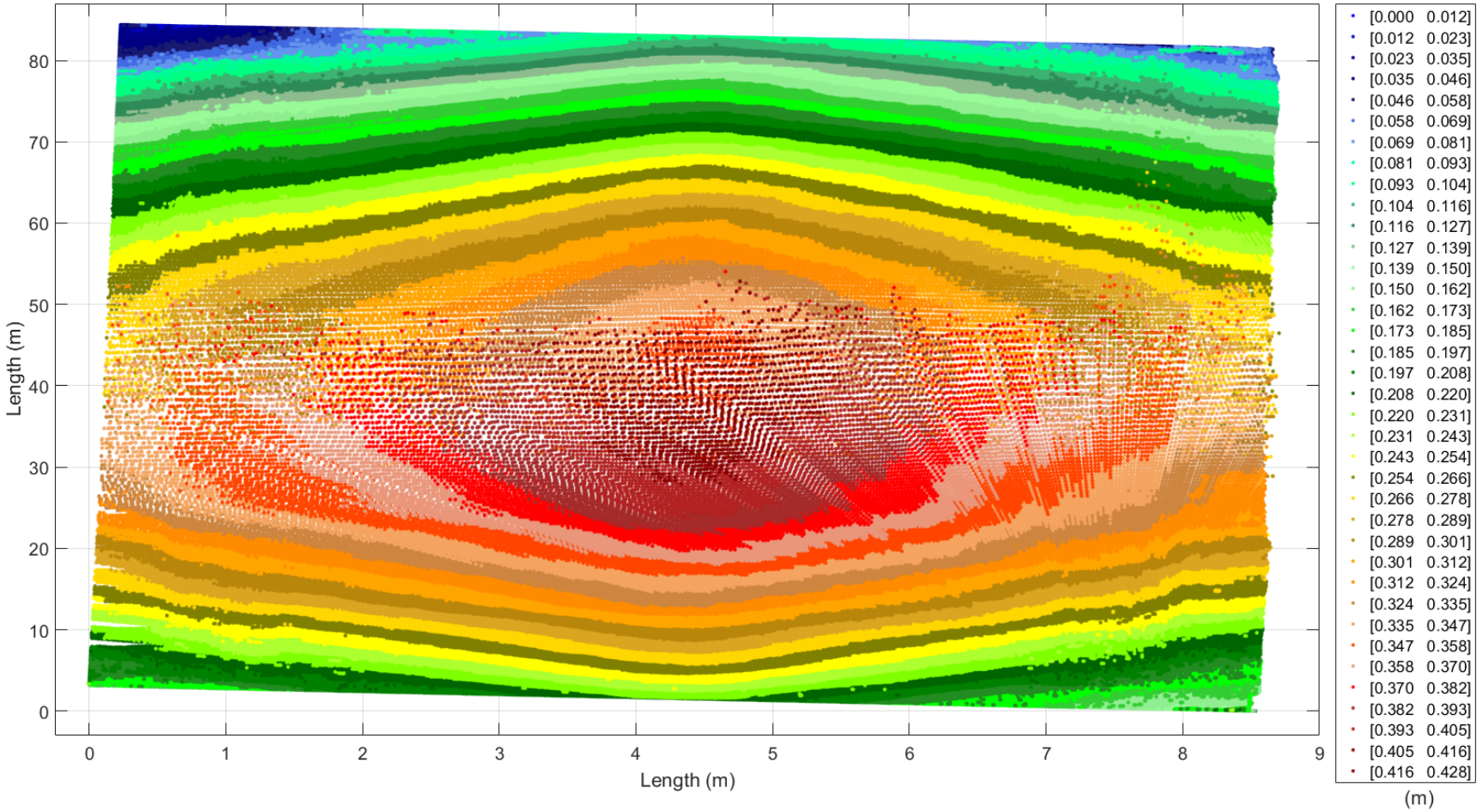

Figure E.18: Lidar depth map of the deck for bridge C004931110.

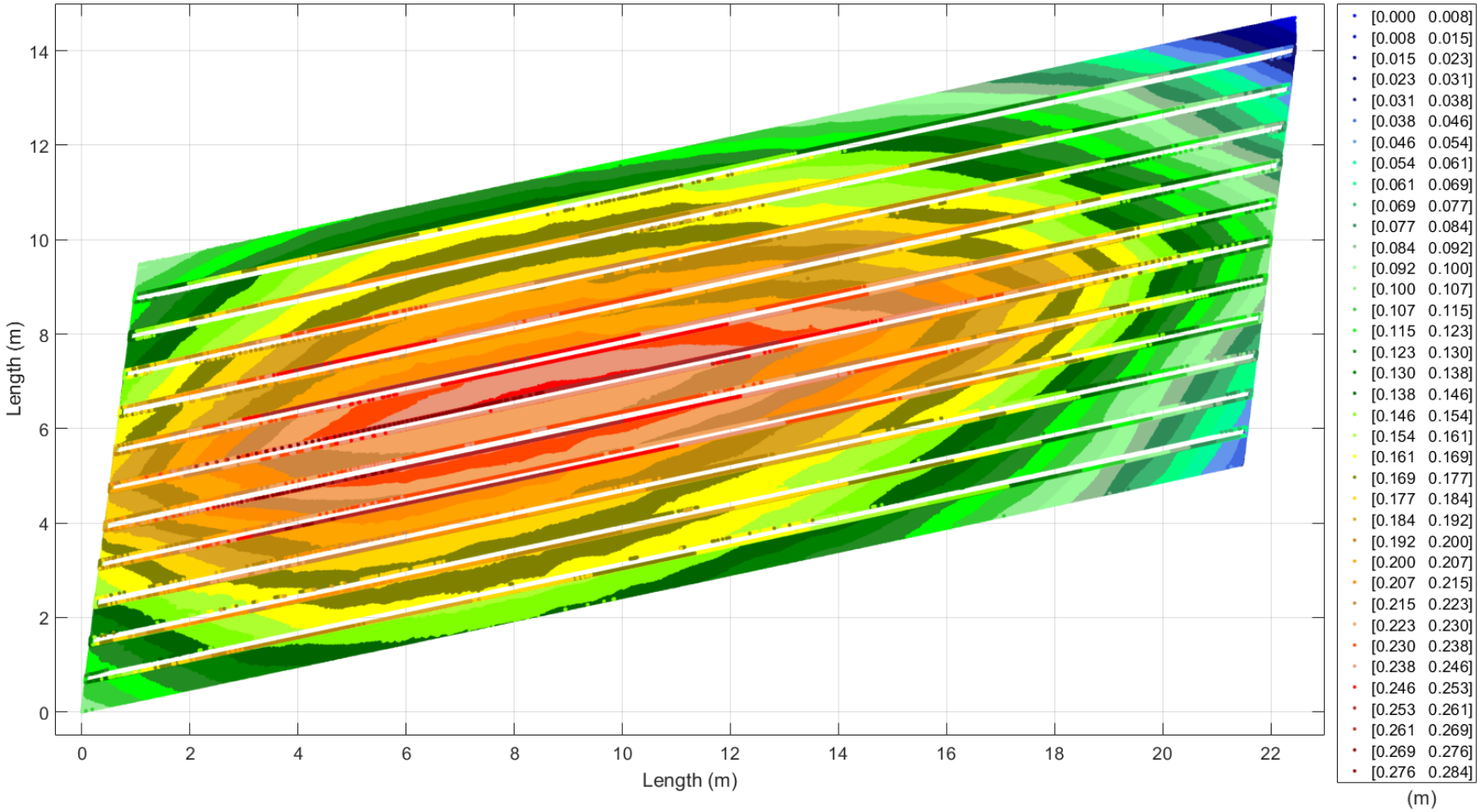

Figure E.19: Lidar depth map of the north middle span girders for bridge C004931110.

APPENDIX F

IT Girder Bridge S080 40927R:

Table F.1: Bridge information summary for bridge S080 40927R.

Bridge ID	S080 40927R	**Girder Height (in [mm])**	15.75 [400]
County	Lancaster	**Girder Width (in [mm])**	23.63 [600]
Year Built	2010	**Girder Spacing (in [mm])**	29.75 [756]
No. of Spans	3	**Deck Thickness (in [mm])**	8 [203]
Length Span 1 (ft)	48.25	**No. of Girders**	25
Length Span 2 (ft)	53.50	**Diaphragm**	C8x18.75
Length Span 3 (ft)	48.25	**Deck Rating**	8
Bridge Width (ft)	62.80	**Superstructure Rating**	9
Skew Angle (°)	0	**Substructure Rating**	9

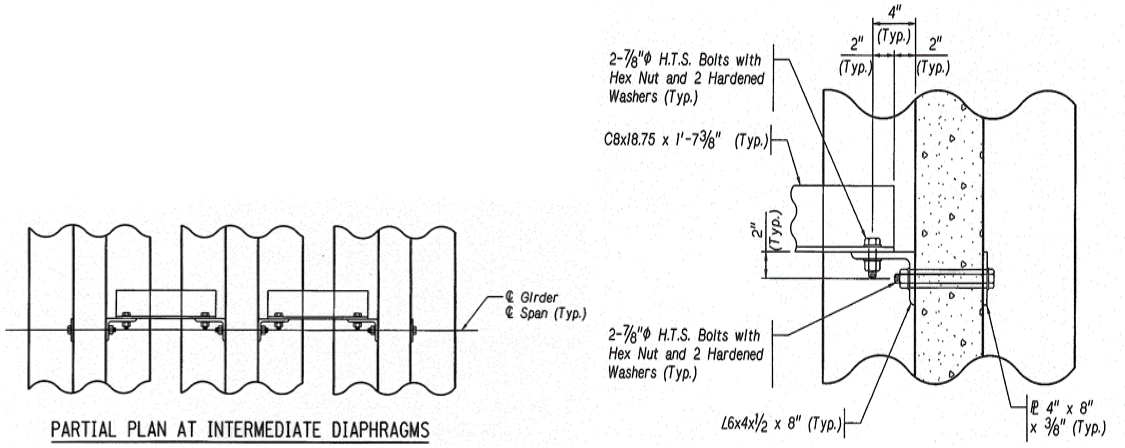

Figure F.1: Intermediate diaphragm linking girders 1, 2, and 3; 9, 10, and 11; and 23, 24, and 25 at midspan for bridge S080 40927R.

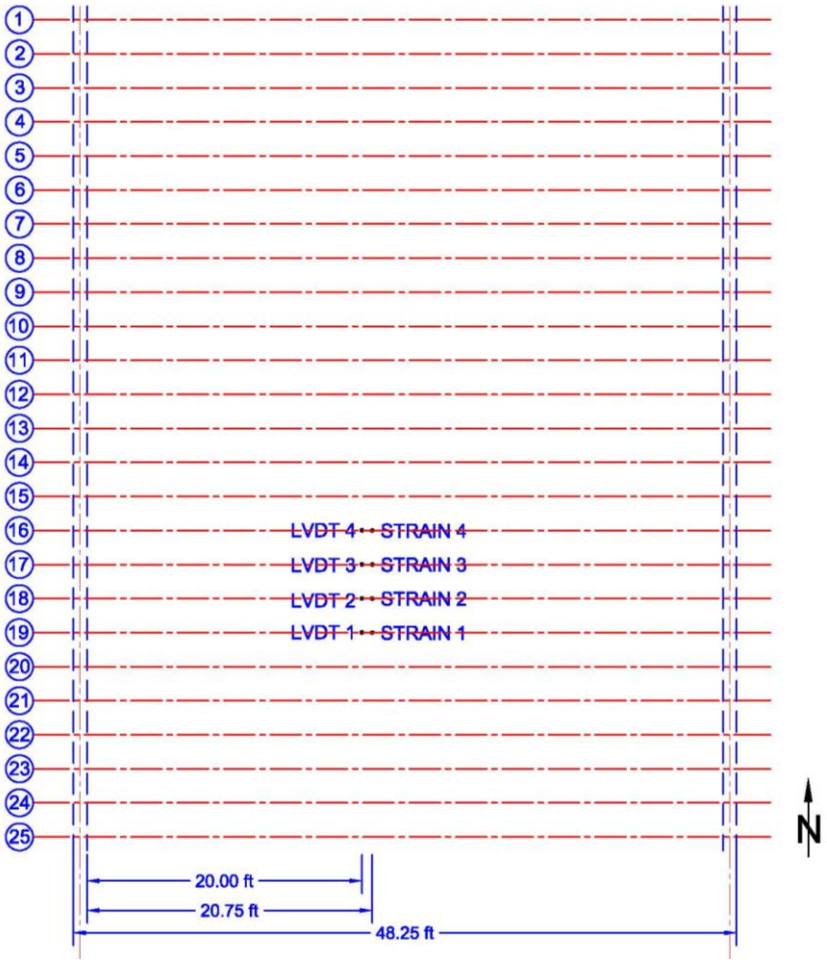

Figure F.2: LVDT and strain gauge positions for the West span of bridge S080 40927R.

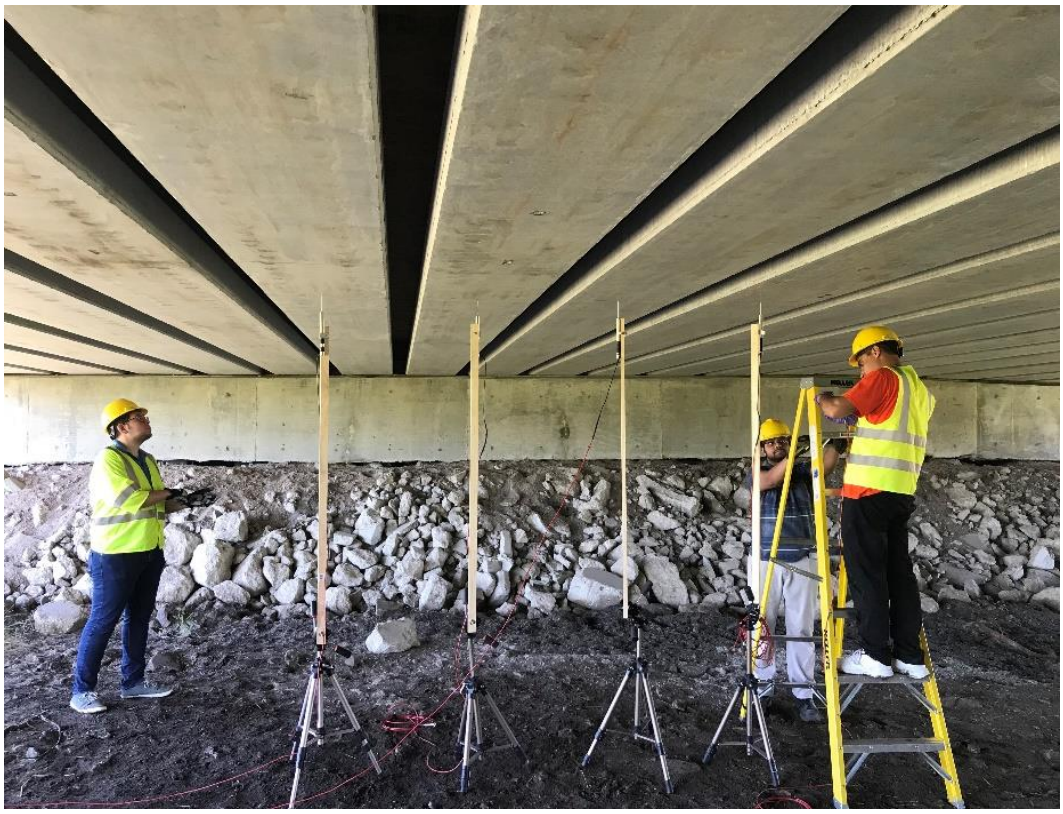

Figure F.3: LVDT and strain gauge setup for bridge S080 40927R.

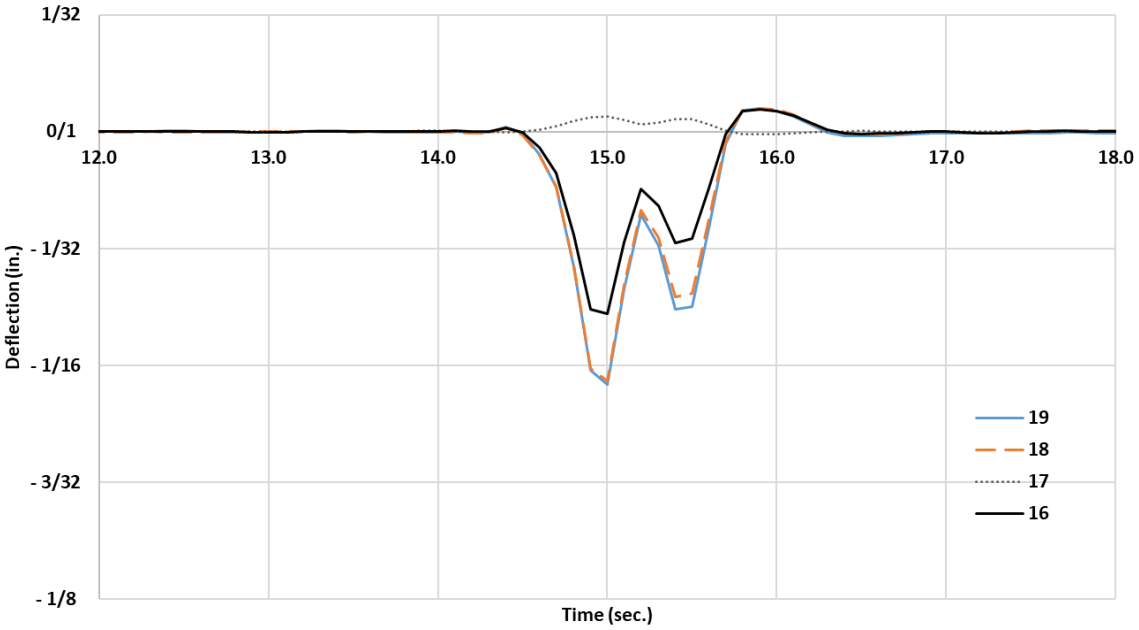

Figure F.4: Deflection-time plot for the peak truck loading for bridge S080 40927R.

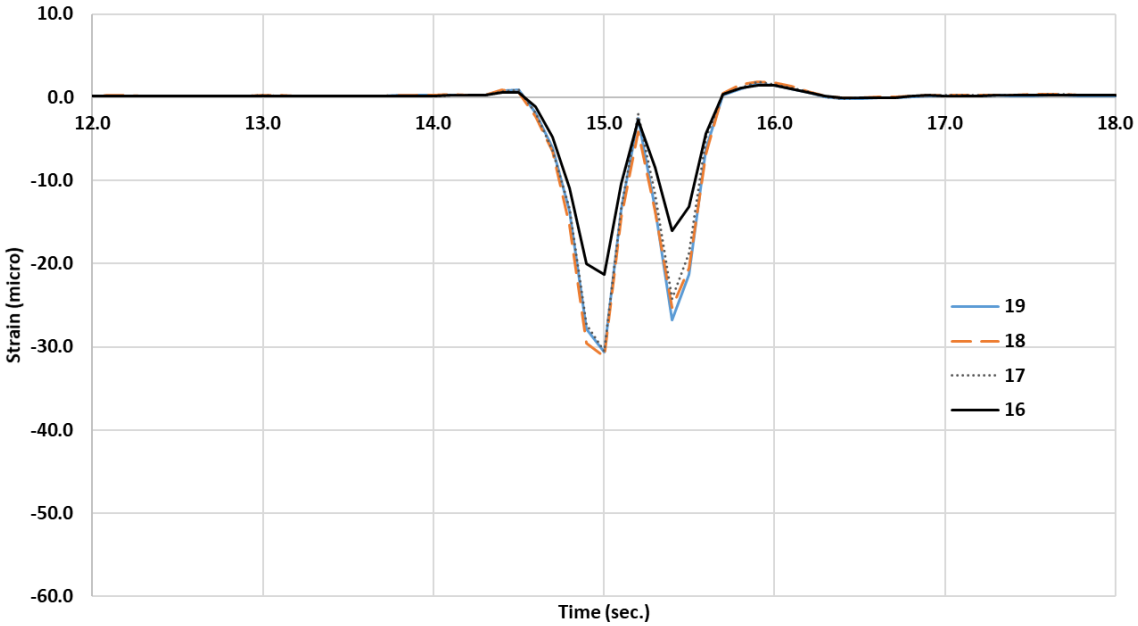

Figure F.5: Strain-time plot for the peak truck loading for bridge S080 40927R.

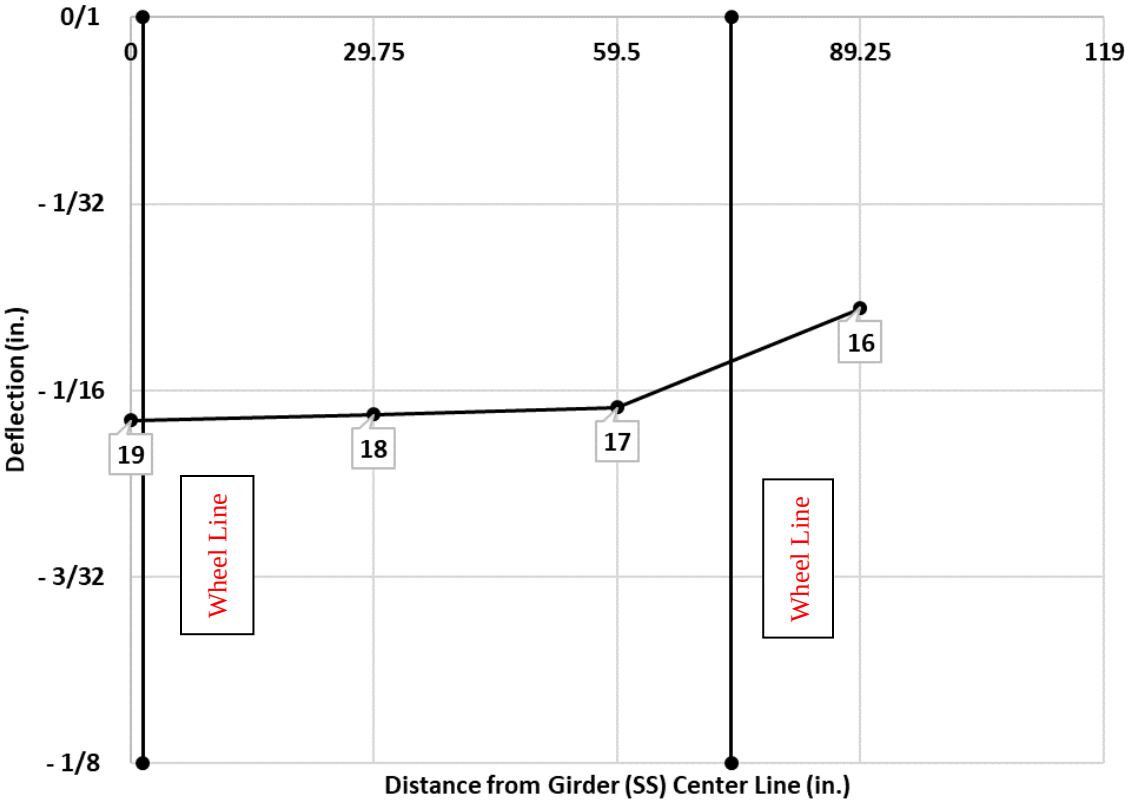

Figure F.6: Girder deflection profile at t = 15.0 seconds for bridge S080 40927R.

Bridge S050 04149

Table F.2: Bridge information summary for bridge S050 04149.

Bridge ID	S050 04149	**Girder Height (in [mm])**	23.63 [600]
County	Johnson	**Girder Width (in [mm])**	23.63 [600]
Year Built	1997	**Girder Spacing (in [mm])**	25.59 [650]
No. of Spans	3	**Deck Thickness (in [mm])**	6 [152]
Length Span 1 (ft)	66.50	**No. of Girders**	19
Length Span 2 (ft)	67.25	**Diaphragm**	Concrete
Length Span 3 (ft)	66.50	**Deck Rating**	7
Bridge Width (ft)	41.70	**Superstructure Rating**	8
Skew Angle (°)	10	**Substructure Rating**	7

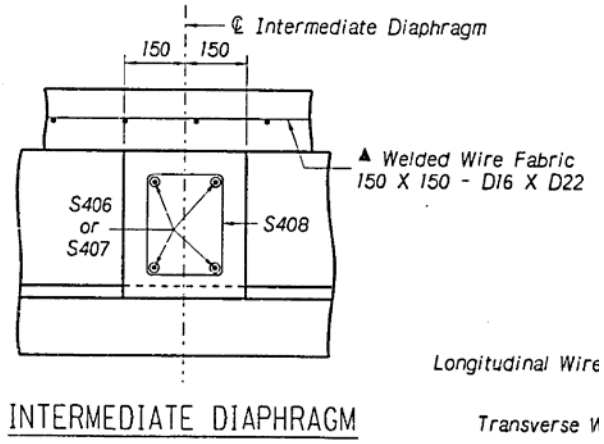

Figure F.7: Intermediate diaphragm linking all girders for bridge S050 04149.

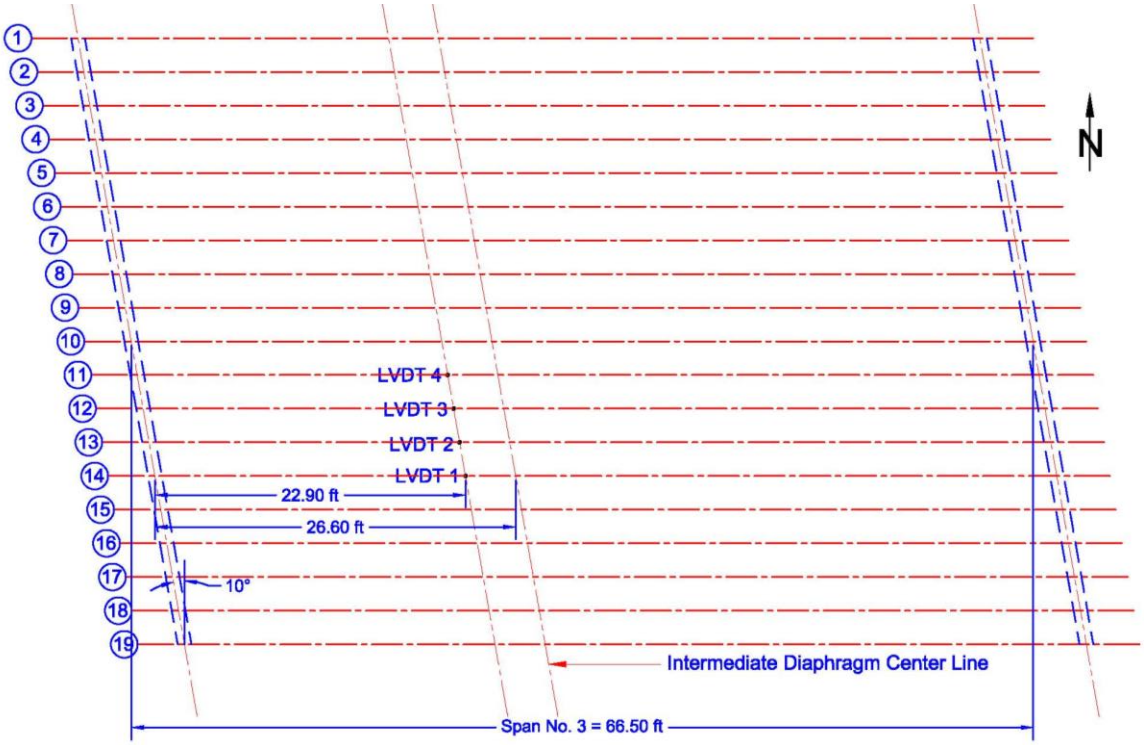

Figure F.8: LVDT positions for bridge S050 04149.

Figure F.9: LVDT setup for bridge S050 04149.

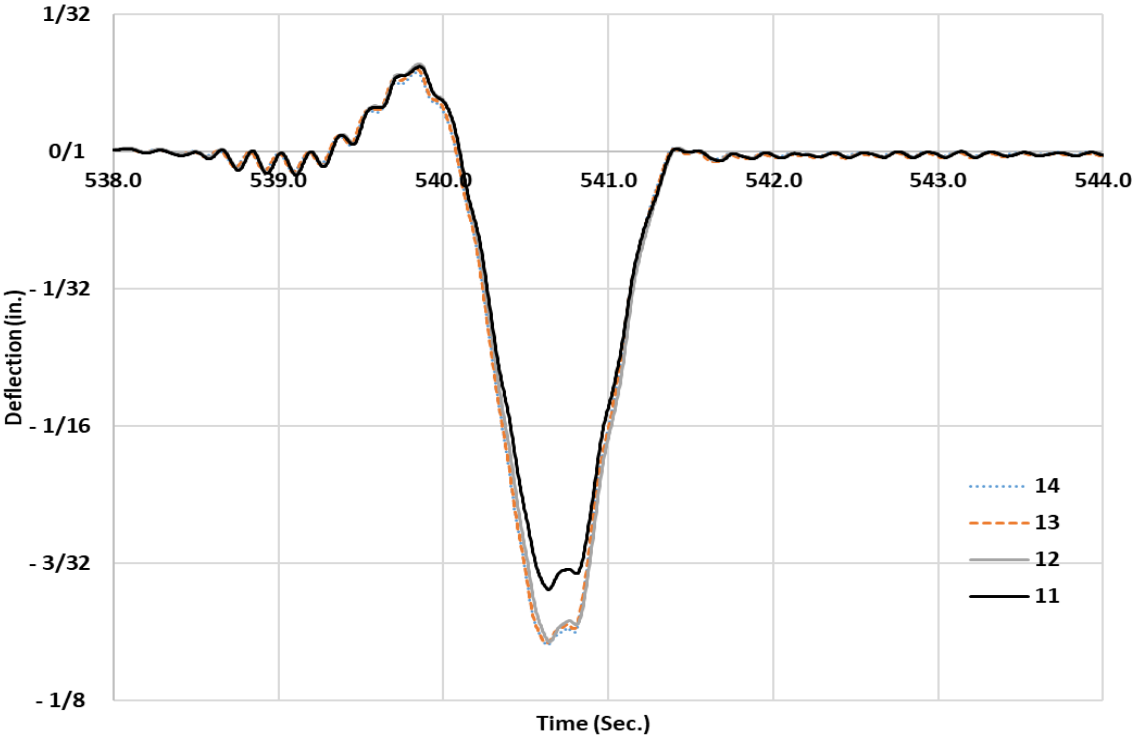

Figure F.10: Deflection-time plot for the peak truck loading for bridge S050 04149.

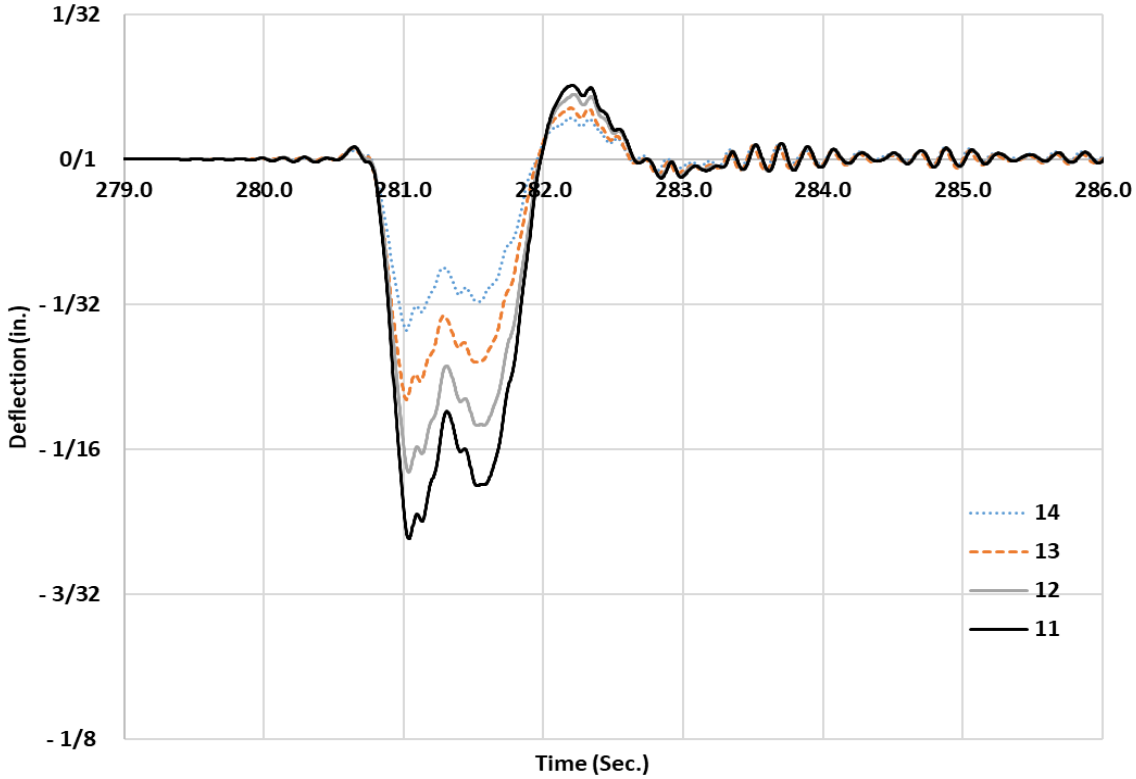

Figure F.11: Deflection-time plot at the highest recorded differential deflection for bridge S050 04149.

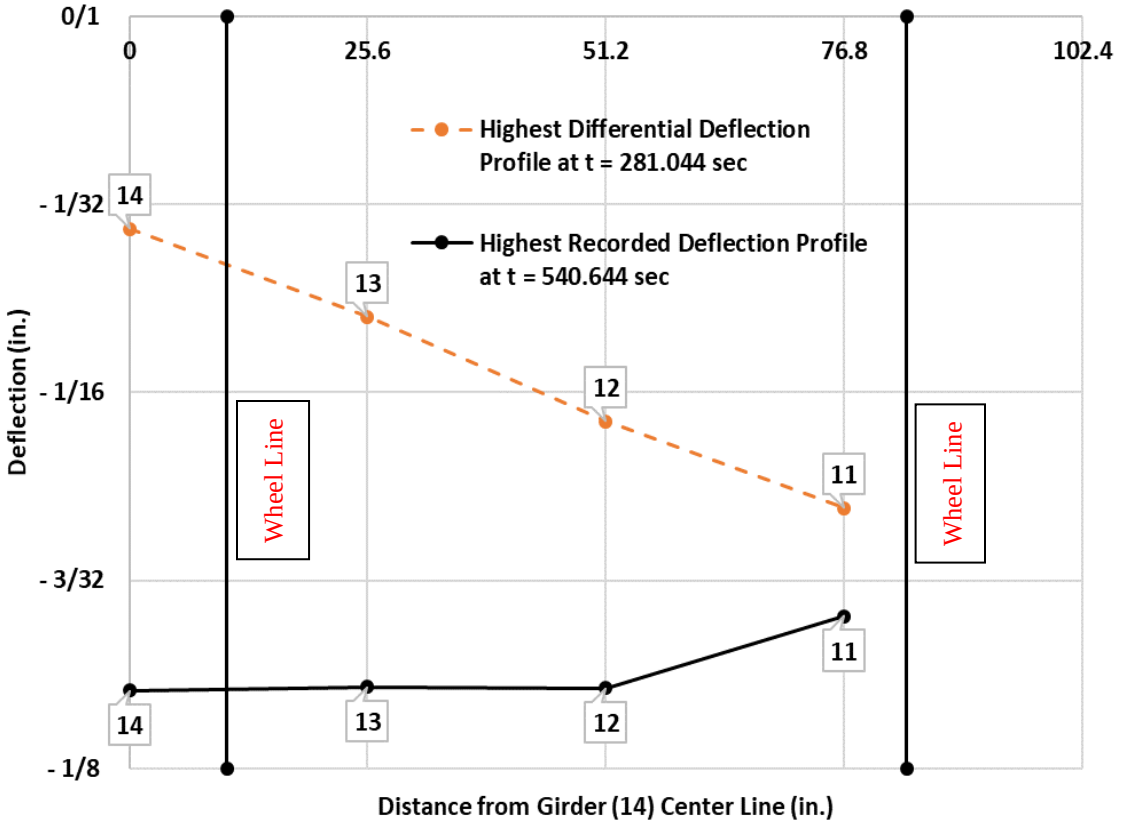

Figure F.12: Girder deflection profile at t = 281.044 seconds and t = 540.644 seconds for bridge S050 04149.

Bridge S089 06047

Table F.3: Bridge information summary for bridge S089 06047.

Bridge ID	S089 06047	**Girder Height (in [mm])**	11.81 [300]
County	Harlan	**Girder Width (in [mm])**	23.63 [600]
Year Built	2007	**Girder Spacing (in [mm])**	28.50 [724]
No. of Spans	3	**Deck Thickness (in [mm])**	6 [152]
Length Span 1 (ft)	40.00	**No. of Girders**	16
Length Span 2 (ft)	45.00	**Diaphragm**	Concrete
Length Span 3 (ft)	40.00	**Deck Rating**	8
Bridge Width (ft)	38.40	**Superstructure Rating**	9
Skew Angle (°)	0	**Substructure Rating**	9

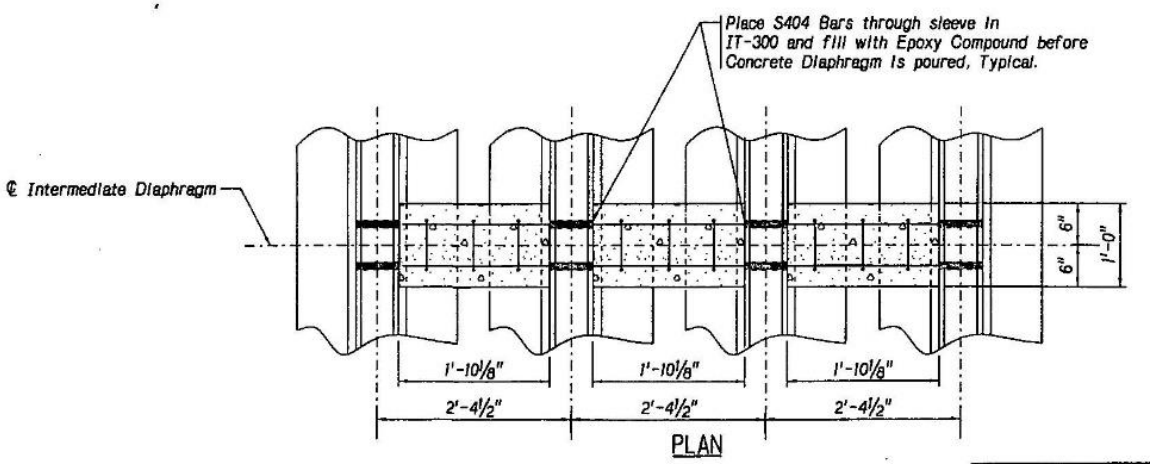

Figure F.13: Intermediate diaphragm linking the four exterior girders at midspan for bridge S089 06047.

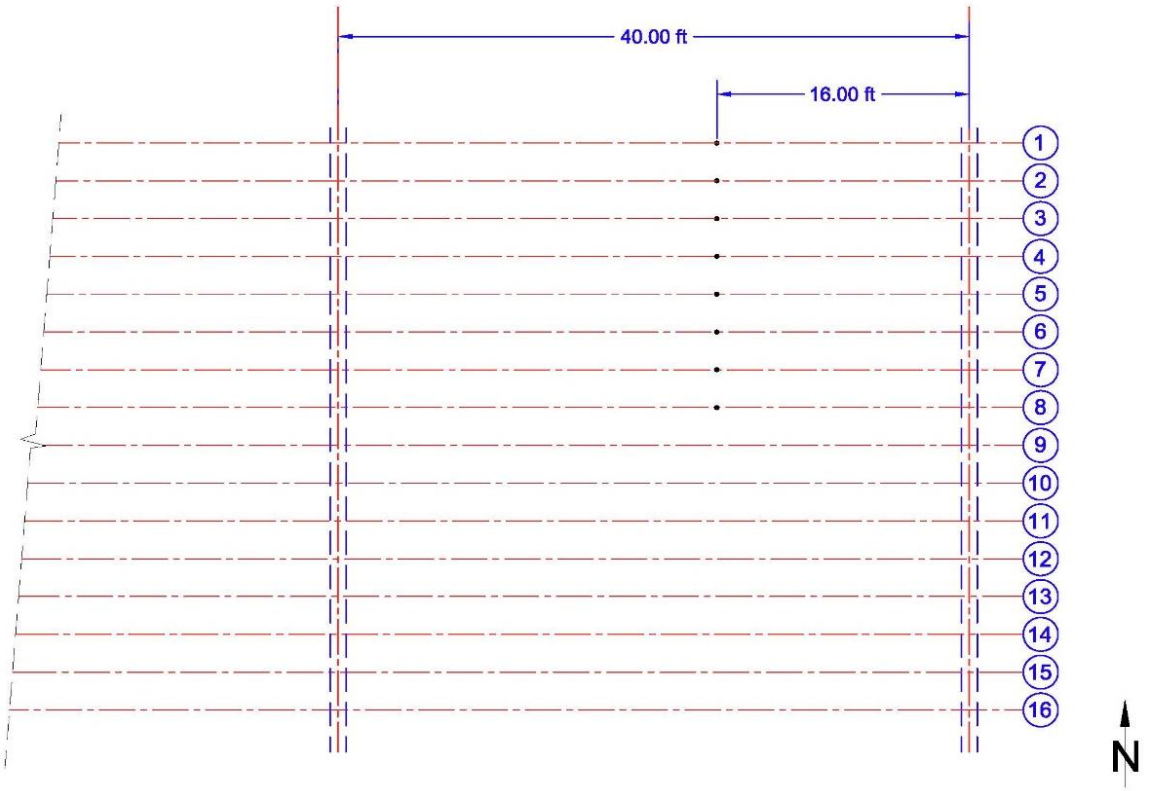

Figure F.14: LVDT and strain gauge positions for bridge S089 06047.

Figure F.15: LVDT and strain gauge setup for bridge S089 06047.

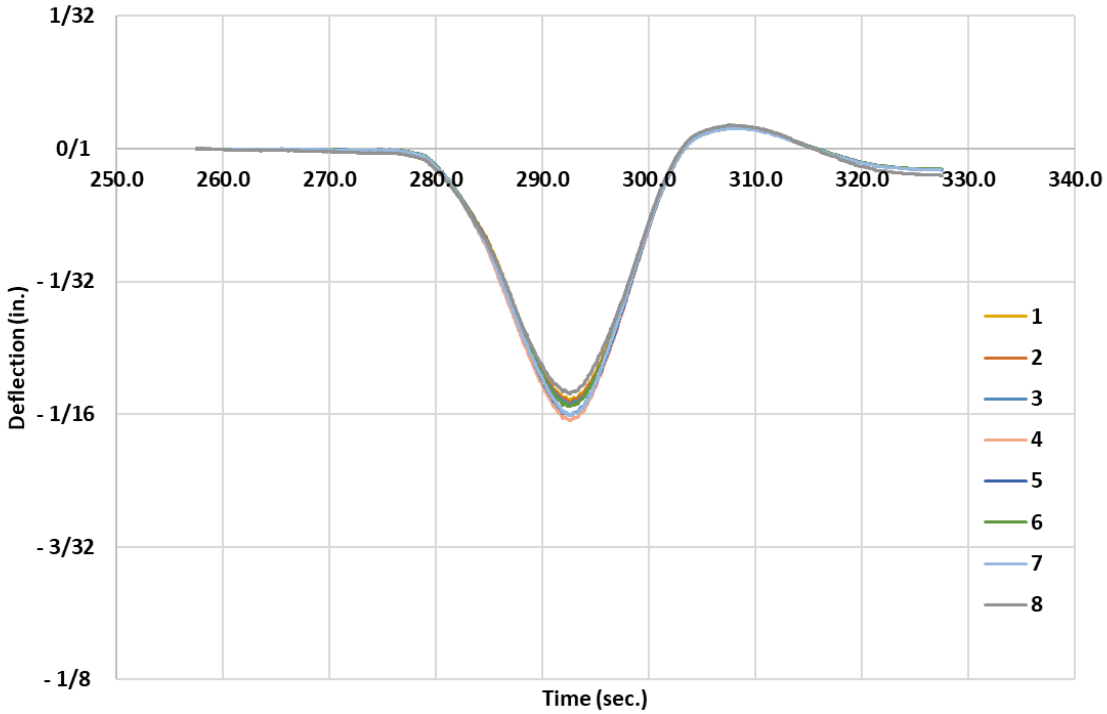

Figure F.16: Deflection-time plot for a slow truck pass resulting in the highest recorded deflection for bridge S089 06047.

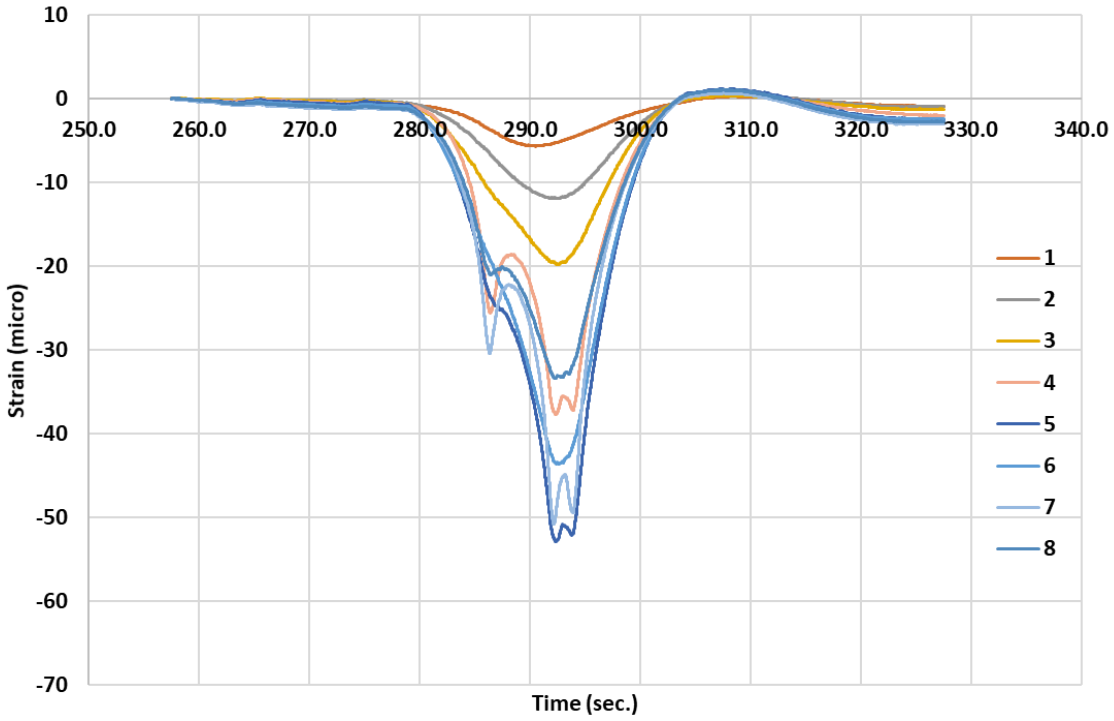

Figure F.17: Strain-time plot for a slow truck pass resulting in the highest recorded deflection for bridge S089 06047.

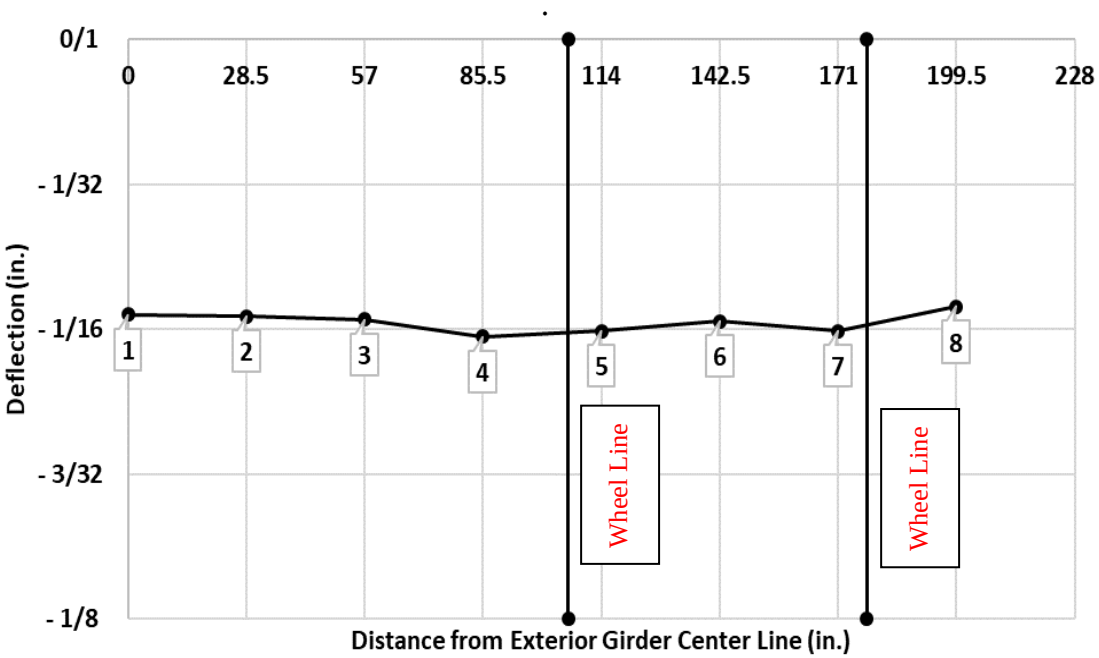

Figure F.18: Girder deflection profile at t = 292.596 seconds for bridge S089 06047.

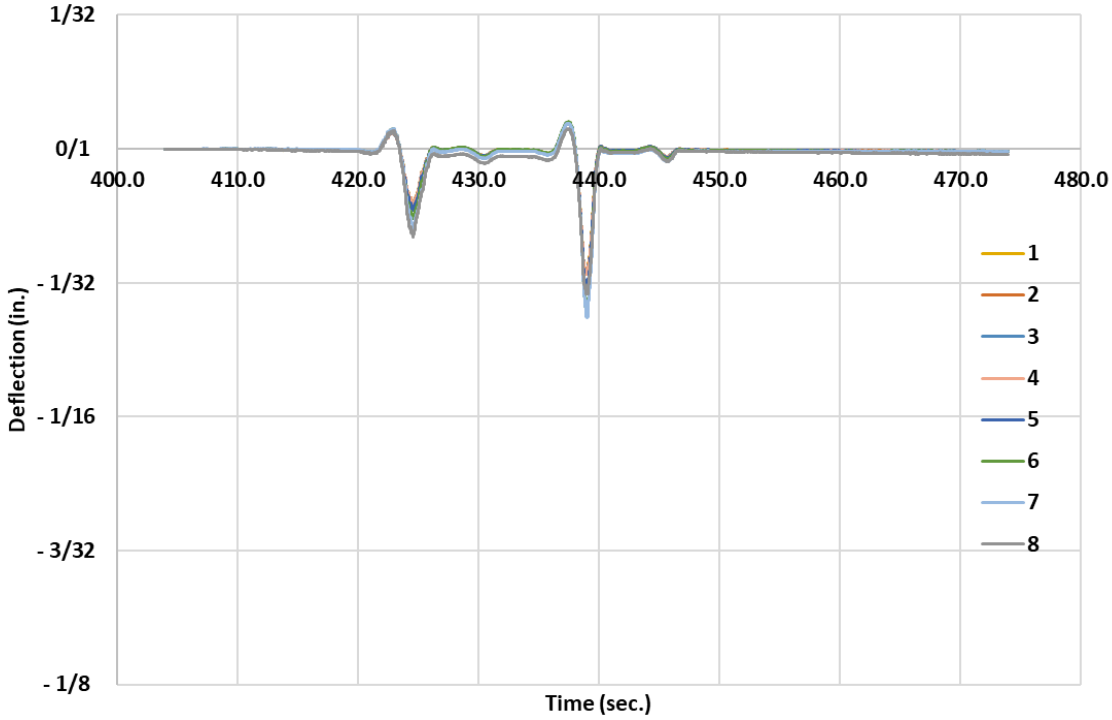

Figure F.19: Deflection-time plot for a fast truck pass resulting in the highest recorded differential deflection for bridge S089 06047.

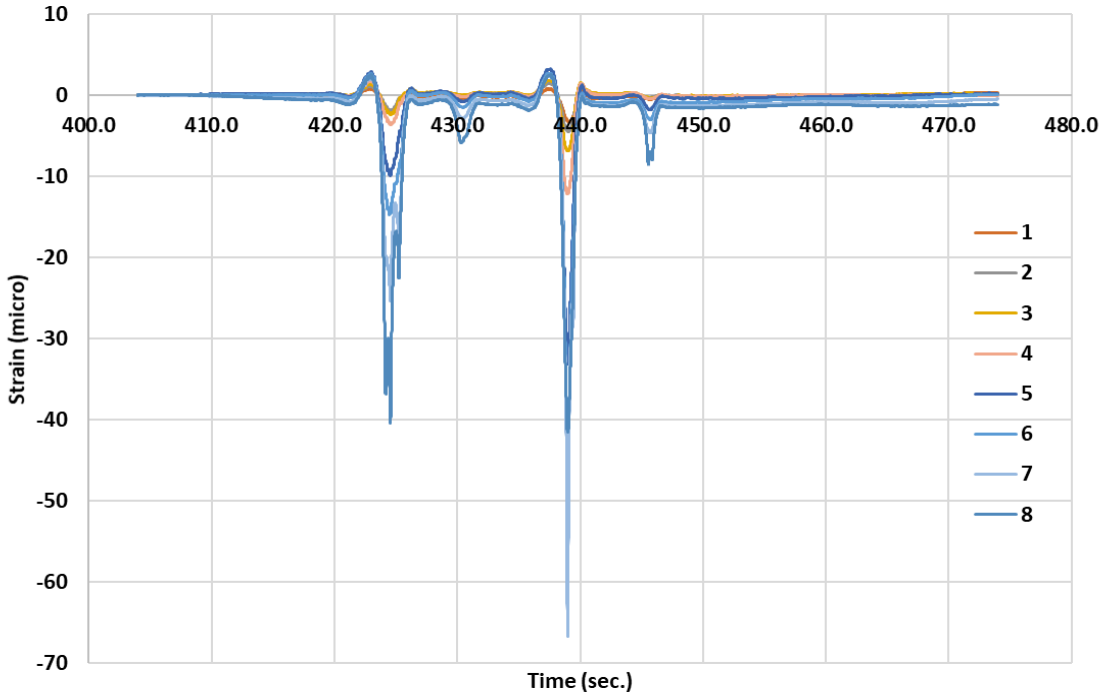

Figure F.20: Strain-time plot for a fast truck pass resulting in the highest recorded differential deflection for bridge S089 06047.

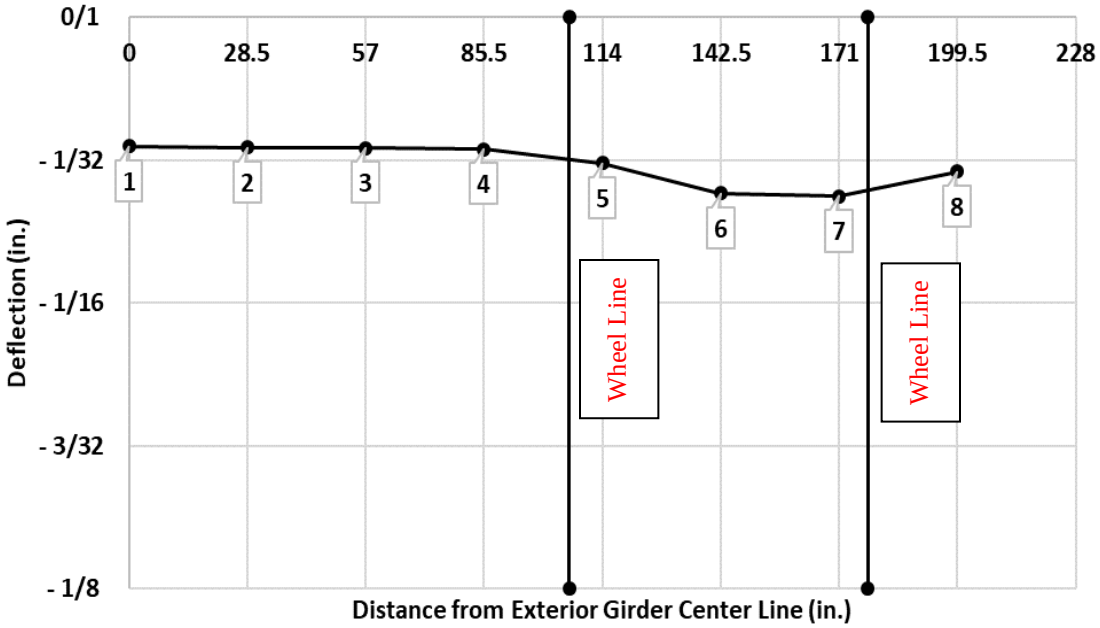

Figure F.21: Girder deflection profile at t = 438.996 seconds for bridge S089 06047.

APPENDIX G

Performance Assessment of Inverted Tee (IT) Bridge System

Questions to Bridge Contractors

Date: November 1, 2017

Contractor: [redacted]

Person Responded: [redacted]

Contact Information: [redacted]

Questions/Comments:

1) How many IT bridge projects have you completed (approximate total/average per year)? [redacted]

2) Where was the last IT bridge project? And when was it? [redacted]

3) Have you build IT bridges for states other than Nebraska? Which states? No.

4) Have you build slab bridges? If yes, how different slab from IT bridges with respect to construction duration, crew size, equipment, total cost, and easy of construction? The cost for slab bridges and IT girder bridges are relatively comparable. The avantages of the IT girders are approximately 5-6 truckloads less material needed compared to a slab, a smaller crew can be utilized, and a typical 3 span slab would take approximately 1 month longer to build than the same size IT girder bridge.

5) What are the positive and negative experience you had with IT bridge construction? Only issues we have had were regarding trying to outguess the amount of deflection of the girders when the deck and rail are poured.

6) Do you have any suggestions that would improve IT bridge construction and/or reduce its cost? Examples are stay-in-place forms, reinforcement details, overhang, etc. None.

7) If IT bridge design calls for intermediate concrete diaphragms across the bridge, how would this affect construction duration and cost? What do you suggest to reduce this effect? The pouring of a set of intermediate diaphragms takes a crew of 3-4 people approximately 2 ½ days for the forming pouring and stripping, whereas the use of steel intermediate diaphragms only takes a couple people a few hours for installation.

Other Comments or Suggestions:

Performance Assessment of Inverted Tee (IT) Bridge System

Questions to Bridge Contractors

Date: 10-30-17

Contractor: [redacted]

Person Responded: [redacted]

Contact Information: [redacted]

Questions/Comments:

1) How many IT bridge projects have you completed (approximate total/average per year)?
   [redacted]

2) Where was the last IT bridge project? And when was it?
   [redacted]

3) Have you build IT bridges for states other than Nebraska? Which states?No.

4) Have you build slab bridges? If yes, how different slab from IT bridges with respect to construction duration, crew size, equipment, total cost, and easy of construction?
   Yes. IT bridges are faster, easier, require smaller crew. Shoring is not required and need to access to waterway is reduced by using IT design as well.

5) What are the positive and negative experience you had with IT bridge construction?
   IT bridges are generally straight forward for construction. Negative is when too thick of a deck is required. Interstate 80 bridges over deflected and it is [redacted] belief this is due to deck thickness.

6) Do you have any suggestions that would improve IT bridge construction and/or reduce its cost? Examples are stay-in-place forms, reinforcement details, overhang, etc.
   Stay in place forms are a must. No other comment.

7) If IT bridge design calls for intermediate concrete diaphragms across the bridge, how would this affect construction duration and cost? What do you suggest to reduce this effect?
   Can limit added cost and duration by making diaphragms consistent and allowing tolerance in formwork at the base of the intermediate diaphragm. Allow poured prior to deck.

Other Comments or Suggestions:

Performance Assessment of Inverted Tee (IT) Bridge System

Questions to Bridge Contractors

Date: 12-14-17

Contractor: [redacted]

Person Responded: [redacted]

Contact Information: [redacted]

Questions/Comments:

1) How many IT bridge projects have you completed (approximate total/average per year)?
[redacted]

2) Where was the last IT bridge project? And when was it?
[redacted]

3) Have you build IT bridges for states other than Nebraska? Which states?
No.

4) Have you build slab bridges? If yes, how different slab from IT bridges with respect to construction duration, crew size, equipment, total cost, and easy of construction?
Yes. Not considering the substructure a slab bridge will take at least twice as long to erect and pour. It requires twice as much manpower but it seems that the permanent material cost is cheaper. IT girders are much more easier to construct and a lot less risky due to the fact that there is not falsework required.

5) What are the positive and negative experience you had with IT bridge construction?
Positive = Cost savings due to speed of girder erection and decking. Light weight girders, a large crane is not needed. IT girders eliminate a lot of the fall hazards when decking (with exception of exterior girders).
Negative = Over camber may cause thicker deck. Need to watch machine loads on exterior girder. Watch live load deflections on exterior girders while placing deck. Inability to grade bottom of deck. (although this is what makes decking quick)

6) Do you have any suggestions that would improve IT bridge construction and/or reduce its cost? Examples are stay-in-place forms, reinforcement details, overhang, etc.

Cost analysis should be done comparing spacing out the girders more to reduce the number but increasing in size. If spacing is greater stay in place plywood could not span, may have to use light SIP metal decking.
Try and bring the picking eyes closer to the center so the sling angle is reduced when picking with 1 crane.
Overhang on exterior girder needs to be minimal so live load don't effect them during placement of the deck.

7) If IT bridge design calls for intermediate concrete diaphragms across the bridge, how would this affect construction duration and cost? What do you suggest to reduce this effect?
I would suggest using metal intermediate diaphragms to speed up construction and cost.

Other Comments or Suggestions:

APPENDIX H

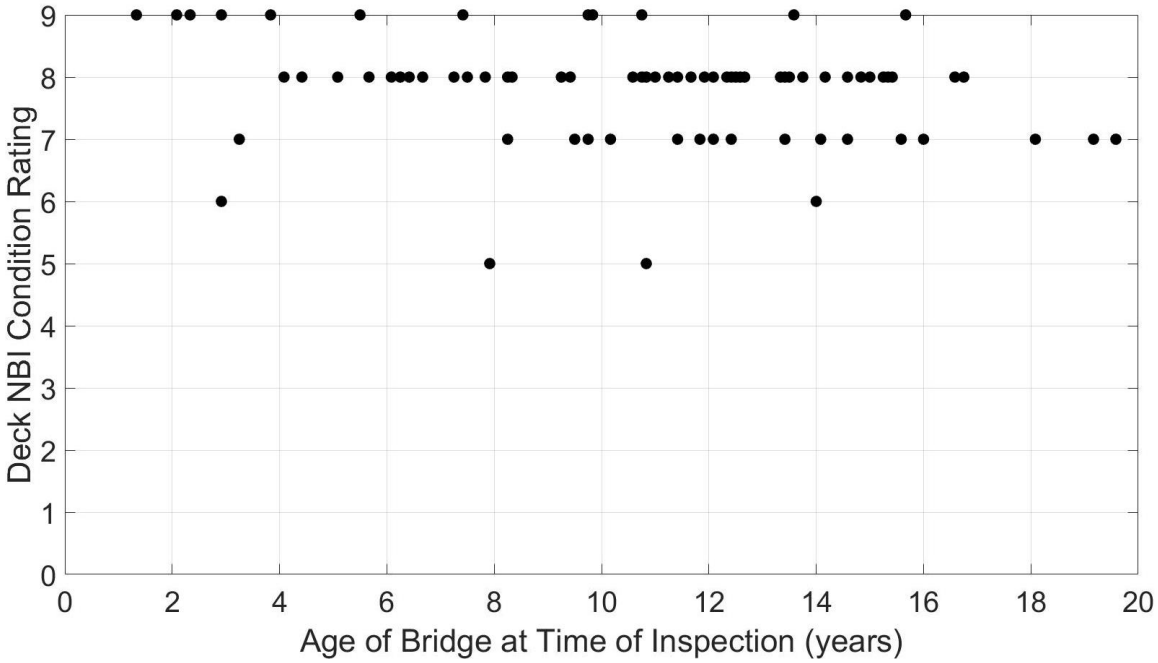

Figure H.1: Comparison of deck NBI condition rating by year.

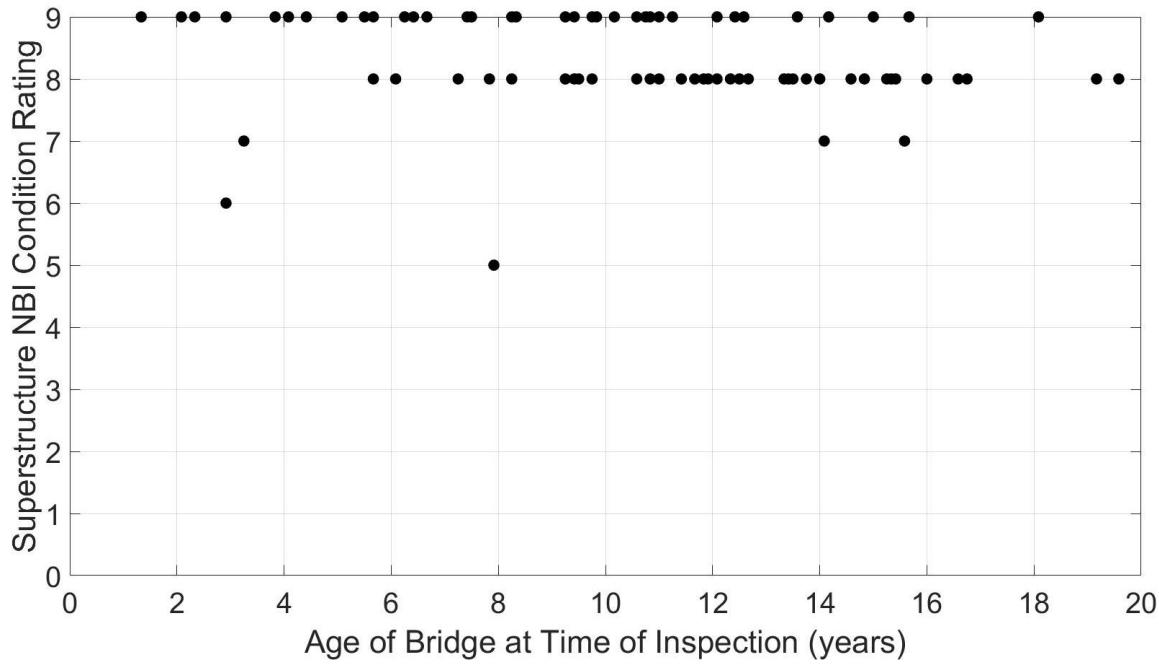

Figure H.2: Comparison of superstructure NBI condition rating by year.

Figure H.3: Comparison of substructure NBI condition rating by year.

Table H.1: Summary of NBI condition ratings.

Component	NBI condition rating				
	9	8	7	6	5
Deck	13.2%	65.1%	17.9%	1.9%	1.9%
Superstructure	46.2%	49.1%	2.8%	0.9%	0.9%
Substructure	30.2%	51.9%	16.0%	1.9%	0.0%